



The  
University  
Of  
Sheffield.

# Indole-3-Glyoxylamides as Novel Therapeutics for Prion Diseases

---

Thesis

Submitted for the Degree of Doctor of Philosophy

Jennifer Louth

Department of Chemistry

October 2015



## **Declaration**

This thesis records work carried out in the Department of Chemistry at the University of Sheffield between March 2008 and February 2015 under the supervision of Prof Beining Chen. Unless specifically stated all work was carried out by the author and has not been submitted, in whole or part, for any degree at any other educational institution.

Jennifer Louth  
February 2015



## Abstract

Transmissible spongiform encephalopathies (TSEs), also known as prion diseases, are rare but invariably fatal neurodegenerative diseases affecting both humans and animals. They are characterised by the accumulation of a misfolded form of the normal cellular prion protein, known as PrP<sup>C</sup>. No cure for these diseases currently exists, although many different compounds have been investigated as potential anti-prion therapeutics. Many have been found to be active *in vitro* but this has not been reproduced *in vivo*. The development of effective therapeutics for these diseases is therefore of crucial importance, as well as having potential implications for other protein misfolding diseases such as Alzheimer's disease.

The work outlined here details investigations into a group of around 200 indole-3-glyoxylamide compounds. These were screened in a cell line persistently infected with scrapie to establish and optimise their *in vitro* anti-prion activities, establish their structure-activity relationship and identify a lead compound. Further studies investigated the pharmacodynamic and pharmacokinetic properties of the compounds by investigating the time taken for them to exert their anti-prion effect and their curative abilities. Initial investigations into their mode of action were carried out by examining their effect on cell growth and formazan exocytosis.

Microarray and proteomics studies were carried out to investigate the molecular targets of the indole compounds, and these identified the proteasomal pathway as a possible target. Inhibition of the protein degradation systems, specifically the lysosomal proteases, resulted in a build-up of PrP<sup>Sc</sup> but this could be mitigated by co-dosing with anti-prion compounds. Targets including HSP90, caspase-12 and MTF-1 were investigated using western blotting to try and quantify changes in expression as a result of treatment, with limited variation being observed.

Finally, 3D *in vitro* models were investigated to gain further information on the potential *in vivo* activity of the compounds. Three different models were investigated with varying degrees of success and confocal microscopy was used to visualise the 3D structures. Good correlation with the published *in vivo* activities of other compounds used in the study suggests the indole compounds would be active *in vivo*, and two of the models used showed potential as high-throughput screening systems.

## Publications from This Work

Thompson, M. J., Borsenberger, V., Louth, J. C., Judd, K. E., and Chen, B. (2009) Design, synthesis and structure-activity relationship of indole-3-glyoxylamide libraries possessing highly potent activity in a cell line model of prion disease, *Journal of Medicinal Chemistry* 52, 7503-7511.

Thompson, M. J., Louth, J. C., Ferrara, S., Sorrell, F. J., Irving, B. J., Cochrane, E. J., Meijer, A. J., and Chen, B. (2011) Structure-Activity relationship refinement and further assessment of the indole-3-glyoxylamides as a lead series against prion disease, *ChemMedChem* 6, 115-130.

Thompson, M. J., Louth, J. C., Ferrara, S., Jackson, M. P., Sorrel, F. J., Cochrane, E. J., Gever, J., Baxendale, S., Silber, B. M., Roehl, H. H., and Chen, B. (2011) Discovery of 6-substituted indole-3-glyoxylamides as lead antiprion agents with enhanced cell line activity, improved microsomal stability and low toxicity, *European Journal of Medicinal Chemistry* 46, 4125-4132.

Chen, B., Thompson, M., Louth, J., and Guo, K., (2013) Prion chemical biology: On the road to therapeutics?, *Current Topics in Medicinal Chemistry* 13, 2441-64.

## Other Related Publications

Heal, W., Thompson, M. J., Mutter, R., Cope, H., Louth, J. C., Chen, B. (2007) Library synthesis and screening: 2,4-diphenylthiazoles and 2,4-diphenyloxazoles as potential novel prion disease therapeutics, *Journal of Medicinal Chemistry* 50, 1347-53.

Thompson, M. J., Louth, J. C., Greenwood, G. K., Sorrell, F. J., Knight, S. G., Adams, N. B., and Chen, B. (2010) Improved 2,4-diarylthiazole-based antiprion agents: switching the sense of the amide group at C5 leads to an increase in potency, *ChemMedChem* 5, 1476-88.

Thompson, M. J., Louth, J. C., Little, S. M., Chen, B., and Coldham, I. (2011) 2,4-diarylthiazole antiprion compounds as a novel structural class of antimalarial leads, *Bioorganic and Medicinal Chemistry Letters* 21, 3644-7.

Thompson, M. J., Louth, J. C., Little, S. M., Jackson, M. P., Boursereau, Y., Chen, B., and Coldham, I. (2012) Synthesis and evaluation of 1-amino-6-halo-beta-carbolines as antimalarial and antiprion agents, *ChemMedChem* 7, 578-86.

## Acknowledgments

Firstly I would like to offer my gratitude to my supervisor, Prof Beining Chen, for giving me the opportunity to study for a PhD, and also for the support and guidance provided over the last ten years of working with her. I would also like to thank the Departmental Managers of the Chemistry Department past and present, Richard King, Harry Adams and Louise Brown-Leng, for allowing me to pursue the PhD alongside my day-to-day technical duties.

Several people deserve thanks for their help in accumulating the data to go in this thesis. Thanks to Paul Heath and Caroline Evans for carrying out the proteomics and microarray studies, and for their patience in explaining the techniques. Thanks also to Jorge Valencia Delgadillo for his data analysis and computational skills. Thanks to Matt Jackson for help with the western blotting and for general support with the cell culture, and also for carrying out the studies into the effect of the compounds on autophagy and the *in vivo* toxicity studies. Thanks to Fiona Sorrell for doing the microsome studies, and Ron Hawley at UCSF for the ScN2a and pharmacokinetic studies. Particular thanks go to Dr Darren Robinson for his help with obtaining the confocal microscopy images, and for his patience and help with the numerous questions I had.

Thanks to all members of the Chen group, past and present, particularly Mark Thompson for being the driving force behind the initial stages of this project, for his subsequent help and for my publication record. My research technician colleague Melanie Hannah deserves a special mention as the person who has helped me through every step of this project and has been an enormous help on both a practical and emotional level. She also deserves a mention for her tireless efforts to improve the standing of technicians. On that note, thanks should go to all the support staff within the Chemistry Department, who do a fantastic job. Massive thanks also to Dr Martin Gill who has been a constant reassuring presence and an enormous help with the writing, as well as teaching me more about Welsh rugby than I ever thought I'd need to know. Thanks also to everyone who has passed through the department in my time here, who in their own way have made working life a bit brighter. Among all these people special mention goes to Youssef, Ruth, Zoe and Mike. Thanks to Dr Rhonda Snook for setting up the Women's network writing club, and for all the ladies that have attended over the past year and provided an invaluable source of support, advice and reassurance. Without writing club, getting this thesis together would have been much more difficult and taken a lot longer than it did.

Finally, thanks to all my family and friends who've endured 7 years of me trying to explain to them what exactly it is that I do. You've all been very patient. Thanks to Mum and Dad for all their support over the past 7 years, and for everything that you've done for me that has allowed me to do things I never could have done on my own. Thanks to my sister, Rosie, for entertaining me in London, the occasional motivational talk, and for the PhD survival kit that turned up on the doorstep. Thanks to all my friends for supporting me in a myriad of different ways, special mention to Mary for the holidays and subsequent outings that have been a much needed break. And last, but definitely not least, huge and heartfelt thanks to my amazing boyfriend Matt, who's been incredibly patient and done an excellent job of keeping me going both physically and emotionally. I couldn't have done it without you.

# Table of Contents

|  |           |
|--|-----------|
| Abstract .....   | iii       |
| Publications from This Work .....  | iv        |
| Acknowledgments .....  | v         |
| Table of Contents .....  | vii       |
| Table of Figures .....   | x         |
| List of Tables .....   | xxiv      |
| Abbreviations .....  | xxvii     |
| <b>1. Introduction .....</b>   | <b>1</b>  |
| 1.1. Overview of Prion Diseases .....  | 1         |
| 1.1.1. Prion Structure (PrP <sup>C</sup> ) and Function .....                                  | 2         |
| 1.1.2. Prions and Disease .....  | 5         |
| 1.1.3. Therapeutic Targets and Strategies .....  | 18        |
| 1.2. Drug Discovery and Candidate Drug Target Profiles (CDTP) .....                            | 27        |
| 1.2.1. Drug Discovery and Development Process .....  | 27        |
| 1.2.2. Pharmacokinetics and Pharmacodynamics .....   | 29        |
| 1.3. 3D Cultures .....   | 33        |
| 1.3.1. Introduction .....  | 33        |
| 1.3.2. The Advantages of a 3D System .....   | 34        |
| 1.3.3. Methods of 3D Culture .....   | 35        |
| 1.3.4. Applications for 3D Culture .....   | 41        |
| 1.4. Aims of the Thesis .....  | 43        |
| <b>2. Materials and Methods .....</b>  | <b>46</b> |
| 2.1. Materials .....   | 46        |
| 2.1.1. Cell Culture .....  | 46        |
| 2.1.2. Surface Plasmon Resonance .....   | 47        |
| 2.1.3. Microarray and Proteomics Studies .....   | 48        |
| 2.1.4. Competition Studies using Inhibitors of the Proteasome and Lysosomal<br>Proteases ..... | 48        |
| 2.1.5. Western Blotting .....  | 48        |
| 2.1.6. 3D Culture .....  | 49        |
| 2.2. Methods .....   | 50        |
| 2.2.1. Cell Culture .....  | 50        |
| 2.2.2. Compound Screening .....  | 51        |
| 2.2.3. Surface Plasmon Resonance .....   | 56        |
| 2.2.4. Additional Assays Based On The SMB Cell Line Screening Assay .....                      | 59        |
| 2.2.5. MTT-FE Assay .....  | 62        |
| 2.2.6. Microarray and Proteomics Studies .....   | 63        |
| 2.2.7. Western Blotting .....  | 66        |

|  |            |
|--|------------|
| 2.2.8. 3D Culture .....  | 69         |
| <b>3. Assay Development, Structure-Activity Relationship Optimisation and Lead Identification.....</b> | <b>77</b>  |
| 3.1. SMB Activity and Viability Screening.....   | 80         |
| 3.1.1. Results.....  | 81         |
| 3.1.2. SAR Discussion .....  | 101        |
| 3.1.3. Conclusions.....  | 107        |
| 3.2. Surface Plasmon Resonance (SPR) Binding Assay .....   | 109        |
| 3.2.1. Results.....  | 112        |
| 3.2.2. Discussion .....  | 127        |
| 3.3. Identification of the Lead Compound .....   | 129        |
| <b>4. Pharmacodynamic, Pharmacokinetic and Mode of Action Studies of the Lead Compounds .....</b>      | <b>132</b> |
| 4.1. Pharmacodynamic Studies: Curative Assay .....   | 134        |
| 4.1.1. Results.....  | 134        |
| 4.1.2. Discussion .....  | 137        |
| 4.2. Pharmacodynamic Studies: Time Course Assays .....   | 140        |
| 4.2.1. Results.....  | 141        |
| 4.2.2. Discussion .....  | 145        |
| 4.3. Mode of Action Studies: Investigations into the Effect on Cell Growth .....                       | 147        |
| 4.3.1. Results.....  | 148        |
| 4.3.2. Discussion .....  | 151        |
| 4.4. Mode of Action Study: MTT Formazan Exocytosis Assay .....   | 152        |
| 4.4.1. Introduction.....   | 152        |
| 4.4.2. Validation of Literature Compounds in the SMB Model .....                                       | 153        |
| 4.4.3. MTT-FE assay .....  | 157        |
| 4.5. Discussion .....  | 166        |
| <b>5. Mode of Action Studies: Microarray and Proteomics Studies.....</b>                               | <b>171</b> |
| 5.1. Introduction.....   | 171        |
| 5.2. Results .....   | 173        |
| 5.2.1. Sample Validation.....  | 173        |
| 5.2.2. MetaCore Pathway Analysis .....   | 176        |
| 5.3. Discussion.....   | 185        |
| 5.3.1. Proof of Concept.....   | 185        |
| 5.3.2. Can Microarray and Proteomics Studies Complement Each Other? .....                              | 188        |
| 5.3.3. 3001012 Compared to Untreated Control .....   | 190        |
| 5.3.4. 3001207 Compared to Untreated Control .....   | 194        |
| 5.3.5. 3001012 vs 3001207.....   | 196        |
| 5.4. Overall Conclusions .....   | 196        |

|   |            |
|---|------------|
| <b>6. Mode of action studies: Target elucidation .....</b>  | <b>200</b> |
| 6.1. Protein Degradation Pathways .....   | 200        |
| 6.1.1. Could These Systems be Affected by the I3GA Compounds? .....   | 204        |
| 6.2. Competition Studies Using Inhibitors of the Proteasome and Lysosomal Proteases .....                             | 205        |
| 6.2.1. Introduction .....   | 205        |
| 6.2.2. Results.....   | 209        |
| 6.2.3. Discussion .....   | 228        |
| 6.3. HSP90 Validation .....   | 232        |
| 6.3.1. Introduction .....   | 232        |
| 6.3.2. Results.....   | 233        |
| 6.3.3. Discussion .....   | 234        |
| 6.4. Target Identification and Validation using Inverse Docking and Western Blotting .....                            | 234        |
| 6.4.1. Introduction .....   | 234        |
| 6.4.2. Inverse Docking Methods .....  | 235        |
| 6.4.3. Target Identification .....  | 236        |
| 6.4.4. Target Validation Using Western Blotting.....  | 240        |
| 6.5. Overall conclusions .....  | 245        |
| <b>7. Evaluation of 3D models as high throughput screening models and predictors of <i>in vivo</i> activity .....</b> | <b>249</b> |
| 7.1. The Hanging Drop Model .....   | 251        |
| 7.1.1. Introduction .....   | 251        |
| 7.1.2. Results.....   | 253        |
| 7.1.3. Discussion .....   | 266        |
| 7.2. The Alvetex Scaffold Model .....   | 269        |
| 7.2.1. Introduction .....   | 269        |
| 7.2.2. Results.....   | 270        |
| 7.2.3. Discussion .....   | 284        |
| 7.3. The Happy Cell Model .....   | 286        |
| 7.3.1. Introduction .....   | 286        |
| 7.3.2. Results.....   | 287        |
| 7.3.3. Discussion .....   | 294        |
| 7.4. Results Summary .....  | 295        |
| 7.5. Discussion .....   | 297        |
| <b>8. Discussion and Future Work .....</b>  | <b>300</b> |
| <b>9. References .....</b>  | <b>315</b> |

# Table of Figures

**Figure 1:** The human prion protein. SP denotes the signal peptide. OR indicates the octapeptide repeats. H1 to H3 denote the three alpha helices. CD indicates the central domain and CR indicates the central region, which contain charged clusters (CC) and the hydrophobic core (HC). GPI represents the glycosylphosphatidylinositol (GPI) anchor. Crosses indicate the glycosylation residues at amino acids 180 and 196. Figure adapted from Linden *et al.* <sup>(14)</sup> .... 3

**Figure 2:** Diagrammatic representation of three of the different models proposed for the structure of PrP<sup>Sc</sup>. a. shows the  $\beta$ -helical model, with refolding of the N-terminal region of PrP<sup>C</sup> into a  $\beta$ -helix motif from residues 90 to 177. The  $\alpha$ -helical motif of PrP<sup>C</sup> is maintained. b. shows the  $\beta$ -spiral model, consisting of a spiralling core of extended sheets comprising short  $\beta$ -sheet strands, again with the maintenance of the  $\alpha$ -helical motif. c. shows the extended register  $\beta$ -sheet model, which proposes a complete refolding of PrP<sup>C</sup> into a structure composed mainly of  $\beta$ -sheets. Figure adapted from Diaz-Espinoza *et al.* <sup>(117)</sup> ..... 10

**Figure 3:** Western blot of brain homogenate from uninfected hamsters (1 and 2) and hamsters infected with scrapie (3 and 4). Lanes 2 and 4 are treated with PK, demonstrating the hydrolysis of PrP<sup>C</sup> and the presence of the PK resistant core in the infected sample known as PrP<sup>27-30</sup> or PrP<sup>res</sup>. Figure adapted from Colby and Prusiner. <sup>(12)</sup> ..... 11

**Figure 4:** Models for the conversion of PrP<sup>C</sup> to PrP<sup>Sc</sup>. The refolding model suggests that the introduction of PrP<sup>Sc</sup> starts a catalytic cascade using PrP<sup>C</sup> or an intermediate as a substrate. The seeding model suggests that PrP<sup>Sc</sup> seeds result in the subsequent conversion and aggregation of PrP<sup>C</sup>. Figure adapted from Weissmann. <sup>(128)</sup> ..... 13

**Figure 5:** Diagrammatic representation of possible sites of PrP<sup>C</sup> conversion. PrP<sup>C</sup> is synthesised in the ER before translocation to the cell surface, where it resides in the lipid rafts. After internalisation *via* clathrin-dependent endocytosis (I) or caveolin-dependent internalisation (II) PrP<sup>C</sup> can be degraded by lysosomes or recycled to the cell surface *via* recycling endosomes. PrP<sup>C</sup> conversion is thought to occur either at the cell surface or along the endolysosomal pathway, and PrP<sup>Sc</sup> can accumulate at the cell surface or in intracellular vesicles such as lysosomes. Figure adapted from Grassmann *et al.* <sup>(146)</sup> ..... 14

**Figure 6:** Forced floating method. Cells are grown on plates with a non-adhesive coating and subsequently aggregate to form spheroids. Figure adapted from Breslin and O’Driscoll. <sup>(305)</sup> ..... 35

**Figure 7:** Agitation based approaches; a. spinner flasks and b. rotating culture vessels are used to generate spheroids. Figure adapted from Breslin and O’Driscoll. <sup>(305)</sup> ..... 36

**Figure 8:** Formation of hanging drop spheroids; a. diagram depicting the method of formation. A cell suspension is pipetted through the access hole to form a drop on the bottom of the plate. The cells aggregate at the bottom of the drop, forming a spheroid after around 1 day. b. fluorescence images of live/dead staining of Cos7 (African green monkey kidney fibroblast cells) and mES (murine embryonic stem cells) spheroids over a 12 day culture. Figure adapted from Tung *et al.* <sup>(321)</sup> ..... 37

**Figure 9:** An example of a pre-engineered, biodegradable scaffold. This is a BD™ 3D open cell polylactic acid (OPLA®) scaffold. Figure adapted from Kim. <sup>(316)</sup> ..... 38

**Figure 10:** Brightfield image showing human mammary endothelial cells seeded onto microcarrier beads 133 – 215  $\mu$ m in size. Black arrows indicate cells attached to the surface of the beads (300x magnification). Figure adapted from Kim. <sup>(316)</sup> ..... 39

**Figure 11:** Schematic representation of the closed loop perfusion culture system used for 3D culture. Within the cell reservoir cells are immobilised using the micropillars, and the formation of an ECM is facilitated by laminar flow complex coacervation. This is followed by perfusion culture of the immobilised cells. Figure adapted from Toh *et al.* <sup>(327)</sup> ..... 40

**Figure 12:** I3GA parent structure. R indicates any possible substitution of the structure. .... 44

|  |     |
|--|-----|
| <b>Figure 13:</b> Example of the data for quinacrine dosed at concentrations ranging from 0.01 $\mu\text{M}$ to 20 $\mu\text{M}$ ; a. shows the original dot blot, with each concentration dosed in triplicate; b. shows the processing of the IODs for each concentration, and the calculation of averages and standard deviations; c. shows the generation of a dose-response curve and the calculated $\text{EC}_{50}$ .  | 53  |
| <b>Figure 14:</b> An example of a BSA calibration curve for calculating protein concentration. Lysis buffer containing different concentrations of BSA were measured using a Bradford assay, and the calculated slope used to calculate the protein concentration of the unknown samples. Each concentration was analysed in triplicate.   | 54  |
| <b>Figure 15:</b> Diagram showing how the gel and PVDF membrane are layered in preparation for western blotting. With the black side of the cassette down, stack upwards in the order fibre pad, filter paper, gel, membrane, filter paper, fibre pad. Figure adapted from Bio-Rad instruction manual.   | 67  |
| <b>Figure 16:</b> Structures of parent I3GA compounds, with $\text{EC}_{50}$ s of 1.5 $\mu\text{M}$ (left) and 6.4 $\mu\text{M}$ (right)   | 78  |
| <b>Figure 17:</b> Optimisation of new IgG concentrations for dot blots. Dilutions up to 1:5000 were found to give a detectable and reproducible signal, while dilutions above this gave a very weak signal. There was not found to be any significant advantage in using BSA rather than milk for blocking. The data points shown represent the mean $\pm$ SD values from a single experiment where each sample was analysed 12 times. Data is expressed as the average density of each set of dots, and is presented as the integrated optical density (IOD) value (see section 2.2.2.2).   | 82  |
| <b>Figure 18:</b> The indole structure with the substitution positions numbered. The right hand structure shows the parent structure from earlier screens. The highlighted area shows the indole component numbered with the positions used for substitutions.   | 83  |
| <b>Figure 19:</b> Example of a dot blot showing initial screen data. Dark dots show the presence of $\text{PrP}^{\text{Sc}}$ , with the absence of signal indicating absence of $\text{PrP}^{\text{Sc}}$ . The blot represents initial screens for 8 different I3GA compounds (3001064 to 3001071), as well as positive and negative controls (10 $\mu\text{M}$ curcumin and 0.5 % DMSO respectively). Each compound is screened in triplicate at 1 $\mu\text{M}$ , 10 $\mu\text{M}$ and 20 $\mu\text{M}$ . The plate is laid out as shown in the table to the right of the blot (1064 refers to compound 30010164, 1065 to 30010165 etc). All compounds were active apart from 3001068. The integrated optical density (IOD) value for each dot can be seen in the table below the blot. These values are used to calculate the amount of $\text{PrP}^{\text{Sc}}$ remaining after treatment as a percentage of the negative control. | 86  |
| <b>Figure 20:</b> Example of the layout of the data in the subsequent results tables. The indole group is described in the left hand column, with the amine group along the top. Activity data is presented for each compound, along with the lowest concentration at which that compound was active. Each result represents at least two independent experiments, and each experiment was carried out in triplicate.  | 87  |
| <b>Figure 21:</b> Example of a dot blot for $\text{EC}_{50}$ data. The data presented represent three I3GA compounds: 3001200 (columns 1-3); 3001205 (columns 4-6); 3001204 (columns 7-9); and controls (columns 10-12). In the control columns rows 1-4 were treated with 0.5 % DMSO (negative control) and rows 5-8 were treated with 10 $\mu\text{M}$ curcumin (positive control). Each compound was screened at 8 concentrations, going from low at the top to high at the bottom. The integrated optical density (IOD) value for each dot can be seen in the table. These values are used to calculate the amount of $\text{PrP}^{\text{Sc}}$ remaining after treatment as a percentage of the negative control.  | 94  |
| <b>Figure 22:</b> Example of the layout of the data in the subsequent results tables. The indole group is described in the left hand column, with the amine group along the top. Activity is expressed as the compound's $\text{EC}_{50}$ value. Each result represents at least two independent experiments, and each experiment was carried out in triplicate.   | 95  |
| <b>Figure 23:</b> Examples of substituted indoles. a. is a 1-methylindole, b. is a 2-methylindole  | 101 |

|   |     |
|---|-----|
| <b>Figure 24:</b> Figure demonstrating para-, meta- and ortho-substitutions on the amine.....   | 102 |
| <b>Figure 25:</b> Structures of some of the most active compounds, all of which contain an N-linked heterocycle at the para position of the phenyl ring (circled). a. 300994; b. 3001012; c. 3001003. ....  | 103 |
| <b>Figure 26:</b> Substituted analogues of parent compound 3000233; 3001060 (left) and 3001075 (right) .....  | 104 |
| <b>Figure 27:</b> Different modifications investigated in Library F. a. removal of one of the carbonyl groups; b. replacement of the carbonyl groups with a heterocycle; c. addition of larger groups to the 1-position of the indole ring.....   | 106 |
| <b>Figure 28:</b> Pictorial representation of the SPR technique, showing the ligand attached to the flow cell and the analyte flowing over the top. Changes in the refractive index are detected in the immediate vicinity of the surface layer of the chip. The SPR angle shifts when biomolecules bind to the surface and change the mass of the surface area. <sup>(373)</sup> .....   | 110 |
| <b>Figure 29:</b> Example sensorgram for investigating ligand-analyte interactions. Baseline represents the response from the immobilised surface only. Analyte injection causes the formation of complexes which then dissociate once the injection stops. Final removal of analyte is facilitated by regeneration solutions, returning the surface to baseline levels. Figure adapted from the Biacore sensor surface handbook. ....  | 111 |
| <b>Figure 30:</b> Immobilisation levels over 17 runs for huPrP and moPrP. Each data point represents a representative sample of baseline immobilisation levels over the course of the run, and were measured in the presence of buffer containing 6.5 % DMSO only. n = 7. Very low standard deviations for the majority of data points demonstrate the stability of the immobilisation, as does the consistency of the immobilisation level between runs. The higher error observed during the first run is thought to be due to the PrP being in a slightly different, and shifting, conformation. Protein that is not tightly bound to the chip may also be washed off during the first run, resulting in a slight decrease in immobilisation level.. | 113 |
| <b>Figure 31:</b> Response in % RU <sub>max</sub> given by quinacrine over 17 runs against huPrP and moPrP. The lower binding on the first run was attributed to limited availability of the C-terminal of PrP, where quinacrine has been shown to bind. Subsequent increases in binding are attributed to a conformational shift in the immobilised PrP during the first run, with a stable conformation being maintained thereafter.....  | 114 |
| <b>Figure 32:</b> Example of the layout of the data in the subsequent results tables. The indole group is described in the left hand column, with the amine group along the top. Observed binding at the initial screen concentration of 40 µM is expressed as the percentage of the theoretical RU <sub>max</sub> . Each result represents at least two independent experiments, and each experiment was carried out in triplicate. ....   | 116 |
| <b>Figure 33:</b> Dose response curves from SPR for the binding of compound 3001016 to huPrP, presented as the relative response (in RU) with blank data, calculated from the signal from the blank flow cell (fc1), subtracted. A steady baseline at zero is observed when buffer is injected over the chip, with a subsequent increase in signal at 51.5 seconds as the compound injection begins. The response increases as the concentration of the compound increases. Dissociation occurs once the injection stops at 112.5 seconds, as demonstrated by the decrease in signal after this point. The data is from a single injection at each concentration.....   | 121 |
| <b>Figure 34:</b> Dose response curve for compound 3000553 against huPrP. Binding at each concentration was analysed in triplicate. Binding increases with concentration up to 30 µM, at which point it decreases. The value for the goodness of fit of the curve is very low. ....   | 122 |
| <b>Figure 35:</b> Dose response curve for compound 3000534 against huPrP. Binding at each concentration was analysed in triplicate. An apparent dose-dependent increase in binding is questionable due to the high standard deviations at concentrations of 60 µM and above. ....   | 122 |

|  |     |
|--|-----|
| <b>Figure 36:</b> Dose response curve for compound 3000556 against huPrP and moPrP. Binding at each concentration was analysed in triplicate. Only very low level binding was observed, with $RU_{max}$ values peaking at less than 20 % of the expected theoretical binding, suggesting limited binding interactions. ....  | 123 |
| <b>Figure 37:</b> Dose response curve for compound 3001012 against huPrP and moPrP. Binding at each concentration was analysed in triplicate. Binding can be seen to plateau at the higher concentrations suggesting a saturation of binding, although less than 40 % of the predicted binding has occurred, suggesting limited binding interactions.....  | 123 |
| <b>Figure 38:</b> Dose response curve for compound 3000982 against huPrP and moPrP. Binding at each concentration was analysed in triplicate. Binding can be seen to plateau at very low concentrations, although only around 10 % of the predicted binding is observed, suggesting limited binding interactions. ....   | 124 |
| <b>Figure 39:</b> Dose response curve for compound 3000983 against huPrP and moPrP . Binding at each concentration was analysed in triplicate. As in <b>Figure 38</b> the binding appears to plateau at low concentrations, but only a small proportion of the expected binding is observed, suggesting limited binding interactions. ....   | 124 |
| <b>Figure 40:</b> Dose response curve for compound 3001016 against huPrP and moPrP . Binding at each concentration was analysed in triplicate. Binding increases in a dose-dependent manner although it does not reach a plateau suggesting that binding is not saturated, even though binding levels much higher than expected can be observed.....   | 125 |
| <b>Figure 41:</b> Dose response curve for compound 3001017 against huPrP and moPrP . Binding at each concentration was analysed in triplicate. Binding increases in a dose dependent manner and appears to be approaching a plateau at the higher concentrations, suggesting saturated binding at just over 100 % $RU_{max}$ . This strongly suggests specific binding to both huPrP and moPrP.....  | 126 |
| <b>Figure 42:</b> Dose response curve for compound 3001015 against huPrP and moPrP. Binding at each concentration was analysed in triplicate. Binding is increasing in a dose dependent manner but has not yet reached saturation. It is therefore not possible to determine whether this compound is binding specifically or non-specifically.....  | 126 |
| <b>Figure 43:</b> Dose response curve for compound 3001009 against huPrP and moPrP. Binding at each concentration was analysed in triplicate. Very low levels of binding were observed, although it did appear to be dose-dependent. The low levels of binding observed at the highest concentrations suggest limited binding interactions. ....   | 127 |
| <b>Figure 44:</b> Structure of 3001012, the lead compound. The compound contains an unsubstituted indole, both carbonyl groups and a N-linked heterocycle at the <i>para</i> -position of the phenyl ring. All these characteristics were found to result in optimal anti-prion activity.....  | 130 |
| <b>Figure 45:</b> Structures of the compounds used in the subsequent experiments; 3001012 (a), 3001207 (b), 3001086 (c), quinacrine (d) curcumin (e) and DMSO (f).....   | 133 |
| <b>Figure 46:</b> $EC_{50}$ curves for quinacrine (right) and curcumin (left). Cells were dosed with the compounds at a range of concentrations (as described in sections <b>2.2.2.1</b> and <b>2.2.2.2</b> ) and the amount of PrP <sup>Sc</sup> in the cell lysate was analysed using dot blotting after 5 days of exposure to the compounds. Quinacrine has an $EC_{50}$ of 0.5 $\mu$ M, while curcumin has an $EC_{50}$ of 0.7 $\mu$ M, demonstrating the concentrations at which both compounds are active in the SMB cell model..... | 135 |
| <b>Figure 47:</b> Example dot blot for 4 sets of lysate samples demonstrating the presence or absence of PrP <sup>Sc</sup> as measured by the intensity of the signal. Each row represents a different treatment, while each set of three columns represents sequential passages from left to right. The lack of signal after treatment with 3001012 at 10 nM is shown to be maintained after 4 passages.....  | 136 |

- Figure 48:** PrP<sup>Sc</sup> levels over time after dosing with either DMSO or 3001012 at 1 or 10 nM. PrP<sup>Sc</sup> levels were monitored every 4 or 5 days, with the whole experiment running for 57 days. Each time point was analysed in triplicate. .... 136
- Figure 49:** PrP<sup>Sc</sup> levels over time after treatment with either DMSO, or quinacrine at 1 or 5  $\mu$ M. Cells were either dosed once or dosed after every passage with 1  $\mu$ M quinacrine over the course of the experiment (quinacrine 1  $\mu$ M and quinacrine 1  $\mu$ M repeat dose respectively). PrP<sup>Sc</sup> levels were monitored every 4 or 5 days, with the whole experiment running for 57 days. Each time point was analysed in triplicate. .... 137
- Figure 50:** Time course data for a. quinacrine at 0.5  $\mu$ M; b. 3001012 at 1.5 nM; c. 3001207 at 20 nM. PrP<sup>Sc</sup> levels were analysed at each time point and the data is presented as the percentage of the signal from the DMSO control at the same time point. No toxicity was observed over the course of the experiment. The data points shown represent the mean  $\pm$  SD values from duplicate experiments where each sample was analysed in triplicate. .... 142
- Figure 51:** Time course data for a. quinacrine at 1.5  $\mu$ M; b. 3001012 at 4.5 nM; c. 3001207 at 60 nM. PrP<sup>Sc</sup> levels were analysed at each time point and the data is presented as the percentage of the signal from the DMSO control at the same time point. No toxicity was observed over the course of the experiment. The data points shown represent the mean  $\pm$  SD values from duplicate experiments where each sample was analysed in triplicate. .... 143
- Figure 52:** Time course data for a. quinacrine at 5  $\mu$ M; b. 3001012 at 10 nM; c. 3001207 at 100 nM; d. curcumin at 10  $\mu$ M; e. 3001086 at 1  $\mu$ M. PrP<sup>Sc</sup> levels were analysed at each time point and the data is presented as the percentage of the signal from the DMSO control at the same time point. No toxicity was observed over the course of the experiment. The data points shown represent the mean  $\pm$  SD values from duplicate experiments where each sample was analysed in triplicate. .... 144
- Figure 53:** Growth assessed by cell counting after dosing with compounds at 3 x EC<sub>50</sub>. Cells were harvested at regular time points before assessment of cell numbers using a haemocytometer. Results are expressed as the number of cells per well. The data points shown represent the mean  $\pm$  SD values from duplicate experiments where each sample was analysed 4 times. .... 148
- Figure 54:** Final cell numbers after 120 hours of growth. Analysis of statistical significance using a multiple t-test shows that the difference between cells treated with DMSO and cells treated with quinacrine is not significant (p-value 0.711) but the differences between cells treated with DMSO and 1012 or 1207 are (p values 0.001 and 0.019 respectively). The data points shown represent the mean  $\pm$  SD values from duplicate experiments where each sample was analysed 4 times. .... 149
- Figure 55:** Standard curve using the MTT assay. Cells were seeded at the specified densities, allowed to attach for 24 hours and then analysed. The data points shown represent the mean  $\pm$  SD values from a single experiment where each sample was analysed 6 times. ... 150
- Figure 56:** Growth curves for 3001012 at 10 nM, 3001207 at 100 nM and 3001086 at 1  $\mu$ M. Initial seeding density of 5,000 cells/well. The data points shown represent the mean  $\pm$  SD values from duplicate experiments where each sample was analysed 6 times. .... 150
- Figure 57:** Cells per well after 120 hours (a) and 156 hours (b). T-tests show significant differences between DMSO and 3001012 at both 120 and 156 hours (p = 0.022 and <0.001 respectively) as well as between DMSO and 3001086 at both 120 and 156 hours (p = <0.001 for both data sets). The data points shown represent the mean  $\pm$  SD values from duplicate experiments where each sample was analysed 6 times. No significant difference was found between DMSO and 3001207 at either time points. .... 151
- Figure 58:** Structures of compounds used in the screen of literature compounds. See **Table 34** for compound names. .... 155
- Figure 59:** The effect of congo red on PrP<sup>Sc</sup> levels at a range of concentrations from 0.005 nM to 10  $\mu$ M. The blot on the left shows the increased PrP<sup>Sc</sup> levels at lower concentrations of

congo red as indicated by the stronger signal. The three left hand columns are the control wells, demonstrating the normal signal for comparison. Concentrations on the blot range from 0.01  $\mu\text{M}$  at the top to 50  $\mu\text{M}$  at the bottom. The graph on the right demonstrates the effect on PrP<sup>Sc</sup> levels of a wide range of congo red concentrations, illustrating that congo red causes an increase in PrP<sup>Sc</sup> levels at concentrations as low as 5 nM. Exposure times were reduced for the blots of congo red treated cells to avoid saturation of the signal. ... 156

- Figure 60:** TS-MTT data for cells treated with 5  $\mu\text{M}$  quinacrine. Cells were treated for 5 days, with the assay being performed at 24 hour intervals. Cells were incubated with MTT-containing medium for one hour before solubilisation with 1% tween-20. The tween solution was removed and measured before solubilisation with acidic isopropanol. 6 wells were analysed for each data point. .... 158
- Figure 61:** TS-MTT data for cells treated with 3001012 (10 nM), 3001207 (100 nM) and 3001086 (1  $\mu\text{M}$ ). Cells were treated for 5 days, with the assay being performed at 24 hour intervals. Cells were incubated with MTT-containing medium for one hour before solubilisation with 1% tween-20. The tween solution was removed and measured before solubilisation with acidic isopropanol. 6 wells were analysed for each data point. .... 158
- Figure 62:** TS-MTT data for curcumin (10  $\mu\text{M}$ ) and EGCG (10  $\mu\text{M}$ ). Cells were treated for 5 days, with the assay being performed at 24 hour intervals. Cells were incubated with MTT-containing medium for one hour before solubilisation with 1% tween-20. The tween solution was removed and measured before solubilisation with acidic isopropanol. 6 wells were analysed for each data point. .... 159
- Figure 63:** TS-MTT data for congo red at 1  $\mu\text{M}$  and 10  $\mu\text{M}$ . Cells were treated for 5 days, with the assay being performed at 24 hour intervals. Cells were incubated with MTT-containing medium for one hour before solubilisation with 1% tween-20. The tween solution was removed and measured before solubilisation with acidic isopropanol. 6 wells were analysed for each data point. .... 160
- Figure 64:** TS-MTT and total MTT data for PPS at 5  $\mu\text{g}/\text{ml}$  (a), DS at 5  $\mu\text{g}/\text{ml}$  (b) and heparin at 50  $\mu\text{g}/\text{ml}$  (c). Cells were treated for 5 days, with the assay being performed at 24 hour intervals. Cells were incubated with MTT-containing medium for one hour before solubilisation with 1% tween-20. The tween solution was removed and measured before solubilisation with acidic isopropanol. 6 wells were analysed for each data point. .... 161
- Figure 65:** Cells treated for 120 hours with either DMSO (left) or quinacrine (right) and incubated for an hour with MTT. Dark spots indicate the presence of TS-MTT, with different patterns of distribution clearly visible. .... 162
- Figure 66:** Images for cells treated with either 3001012 (left), 3001207 (middle) or 3001086 (right) for 120 days and incubated for an hour with MTT. .... 163
- Figure 67:** Images for cells treated with either curcumin (left) or EGCG (right) for 120 hours and incubated for an hour with MTT. .... 163
- Figure 68:** Images for cells treated with congo red at 1  $\mu\text{M}$  (left) or 10  $\mu\text{M}$  (right) for 120 hours and incubated for an hour with MTT. .... 163
- Figure 69:** Images for cells treated with PPS (left), DS (middle) or heparin (right) for 120 hours and incubated for an hour with MTT. .... 164
- Figure 70:** PrP<sup>Sc</sup> levels in the samples used in the microarray and proteomics studies. Cells were treated for 56 hours before being harvested, and dot blots performed on a sample from each plate. A and B indicate the two biological replicates .... 174
- Figure 71:** Map of the statistically significant pathway representing apoptosis and survival – granzyme A signalling. This was the top scored map. Experimental data are represented by thermometers. Up-ward (red) thermometers indicate up-regulated signals and down-ward (blue) thermometers indicate down-regulated signals. .... 177
- Figure 72:** Map of the statistically significant pathway representing putative pathways for stimulation of fat cell differentiation by Bisphenol A. This was the second top scored map.

|  |     |
|--|-----|
| Experimental data are represented by thermometers. Up-ward (red) thermometers indicate up-regulated signals and down-ward (blue) thermometers indicate down-regulated signals. ....  | 178 |
| <b>Figure 73:</b> Map of the statistically significant pathway representing hedgehog signalling. This was the top scored map. Experimental data are represented by thermometers. Up-ward (red) thermometers indicate up-regulated signals and down-ward (blue) thermometers indicate down-regulated signals.....   | 180 |
| <b>Figure 74:</b> Map of the statistically significant pathway representing the regulation of apoptosis by mitochondrial proteins. This was the second top scored map. Experimental data are represented by thermometers. Up-ward (red) thermometers indicate up-regulated signals and down-ward (blue) thermometers indicate down-regulated signals.....  | 181 |
| <b>Figure 75:</b> Map of the statistically significant pathway representing the notch signalling pathway. This was the top scored map from the microarray data. Experimental data are represented by thermometers. Up-ward (red) thermometers indicate up-regulated signals and down-ward (blue) thermometers indicate down-regulated signals. ....  | 183 |
| <b>Figure 76:</b> Map of the statistically significant pathway representing the immune response – antigen presentation by major histocompatibility complex (MHC) class I. This was the top scored map from the microarray data. Experimental data are represented by thermometers. Up-ward (red) thermometers indicate up-regulated signals and down-ward (blue) thermometers indicate down-regulated signals. ....  | 184 |
| <b>Figure 77:</b> Representation of the different protein degradation pathways and their main substrates. ER – endoplasmic reticulum, ERAD – endoplasmic reticulum associated degradation.....   | 201 |
| <b>Figure 78:</b> Schematic diagram of the 26S proteasome, showing the 20S core and the 19S regulatory particle. Rpt and Rpn indicate subunits of the regulatory particle with or without ATPase activity respectively. Figure adapted from Deriziotis <i>et al.</i> <sup>(400)</sup> .....  | 202 |
| <b>Figure 79:</b> The process of labelling targets proteins for degradation <i>via</i> ubiquitination. E1 binds ubiquitin and transfers it to E2. The ubiquitin is transferred to E3 which covalently binds it to the target protein. E3 ligases are specific for their target protein. Figure adapted from Adams. <sup>(406)</sup> .....  | 203 |
| <b>Figure 80:</b> Structure of MG132 (left), a general inhibitor of the proteasome and the LCPs, and lactacystin (right), a specific proteasomal inhibitor. ....   | 206 |
| <b>Figure 81:</b> Structure of <i>clasto</i> -lactacystin $\beta$ -lactone, the active form of lactacystin. ....   | 206 |
| <b>Figure 82:</b> Structures of Cl3 (left), an inhibitor of cathepsins B, L, S and papain, and E64 (right), a general inhibitor of LCPs. ....  | 207 |
| <b>Figure 83:</b> Representation of the targets of the different inhibitors used in these experiments. ....  | 208 |
| <b>Figure 84:</b> Structures of 3001012 (a), 3001207 (b) and 3001086 (c). 3001012 has an EC <sub>50</sub> of 1 nM, 3001207 has an EC <sub>50</sub> of 1.5 nM (first batch) or 15 nM (second batch) and 3001086 has an EC <sub>50</sub> of 180 nM (See section 3.1).....  | 208 |
| <b>Figure 85:</b> PrP <sup>Sc</sup> levels in SMB cells after dosing with MG132 at concentrations ranging from 0.05 $\mu$ M to 20 $\mu$ M. 0.5 $\mu$ M is the lowest concentration to induce an increase in PrP <sup>Sc</sup> , and levels continue to rise in a dose-dependent manner until the amount of PrP <sup>Sc</sup> starts to decrease at 5 $\mu$ M. Toxicity was observed at concentrations higher than 5 $\mu$ M. The data points shown represent the mean $\pm$ SD values from duplicate experiments where each sample was analysed in triplicate..... | 209 |
| <b>Figure 86:</b> Data showing the effect of MG132 on 3001012 activity as measured by PrP <sup>Sc</sup> clearance. The black curve indicates 3001012 on its own at concentrations between 0.001 nM and 100 nM. The red curve indicates 3001012 at the same concentrations but co-dosed with 3 $\mu$ M MG132. Each graph shows an independent experiment, <b>Table 42</b> gives estimated   |     |

- EC<sub>50</sub> values. The data points shown represent the mean ± SD values from a single experiment where each sample was analysed in triplicate. .... 210
- Figure 87:** Statistical analysis of the data at concentrations of 5 (a), 10 (b) and 50 nM (c), comparing cells treated with 3001012 to cells treated with both 3001012 and MG132. Data from **Figure 86a** above. Statistical analysis using a multiple t-test showed statistically significant differences in all cases with *p*-values as follows; 5 nM *p* = 0.00468012, 10 nM *p* = 0.0041324, 50 nM *p* = 0.0117233. The data points shown represent the mean ± SD values from duplicate experiments where each sample was analysed in triplicate. .... 211
- Figure 88:** Effect on PrP<sup>Sc</sup> levels in SMB cells when dosed with MG132 3 μM over 128 hours (6 days). a. and b. show two independent experiments. PrP<sup>Sc</sup> levels start to rise after 48 hours. Further repeats of the time course showed PrP<sup>Sc</sup> levels beginning to rise at the same time, but the total PrP<sup>Sc</sup> accumulation observed after 128 hours varied between 300 % of control (as seen in b) and 800 % of control (as seen in a). The data points shown represent the mean ± SD values from a single experiment where each sample was analysed in triplicate. .... 212
- Figure 89:** Time course effect on PrP<sup>Sc</sup> levels in SMB cells treated with 3001012 at 10 nM co-dosed with MG132 at 3 μM. Drug treatment was assessed over a time course of 0 – 128 hours in Experiments 1 and 2. Each data point represents the mean ± SD values from a single experiment where each sample was analysed in triplicate. Data points in black show the effect of 3001012 alone; data points in red show the effect of 3001012 co-dosed with MG132. (a) Statistical analysis of Experiment 1 using multiple t-test shows that at the 96 and 104 hour time points the effect of 3001012 alone or 3001012 co-dosed with MG132 is statistically different (*p*<0.001 in both cases). (b) Statistical analysis of Experiment 2 using multiple t-test shows that at the 120 hour and 128 hour time points the effect of 3001012 alone or 3001012 co-dosed with MG132 is significantly different (*p*<0.001 in both cases). .... 213
- Figure 90:** Effect on PrP<sup>Sc</sup> levels in SMB cells when treated with a. 3001207 and b. 3001086. Black lines indicates the compound on its own, the red line indicates the compound co-dosed with 3 μM MG132. Cells were dosed for 5 days. The data points shown represent the mean ± SD values from triplicate experiments where each sample was analysed in triplicate. ... 214
- Figure 91:** Statistical analysis of the data for the lowest and highest active concentrations of 3001207 and 3001086. T-tests were carried out comparing cells dosed with the I3GA on its own to cells co-dosed with MG132 at 3 μM and a concentration gradient of the I3GA. 3001207 only showed a significant difference at 50 nM (*p* = 0.00194683, *n* = 9), while 3001086 showed a significant difference at both 1 μM and 20 μM (*p* = <0.001, *n* = 9 for both). The data points shown represent the mean ± SD values from triplicate experiments where each sample was analysed in triplicate. .... 214
- Figure 92:** Data showing the effect of a fixed concentration of 3001012, 3001207 and 3001086 on MG132 activity; a. shows the co-dosed results in comparison to MG132 on its own, while b. shows the co-dosed results only for greater clarity. The x-axis gives the concentration of MG132. The data points shown represent the mean ± SD values from duplicate experiments where each sample was analysed in triplicate. .... 215
- Figure 93:** PrP<sup>Sc</sup> levels in SMB cells after dosing with lactacystin at concentrations ranging from 0.1 μM to 20 μM. No significant effect was seen on either PrP<sup>Sc</sup> levels or cell viability. The data points shown represent the mean ± SD values from duplicate experiments where each sample was analysed in triplicate. .... 217
- Figure 94:** Data showing the effect of lactacystin on 3001012 activity as measured by PrP<sup>Sc</sup> clearance. The black curve indicates 3001012 on its own at concentrations between 0.1 nM and 10 nM. The red data indicates 3001012 at the same concentrations but co-dosed with 10 μM lactacystin – a curve could not be fitted to these data. The data points shown

- represent the mean  $\pm$  SD values from duplicate experiments where each sample was analysed in triplicate. .... 217
- Figure 95:** PrP<sup>Sc</sup> levels in SMB cells after dosing with E64 at a range of concentrations from 0.5  $\mu$ M to 25  $\mu$ M. Each concentration is dosed in triplicate. (a) demonstrates the increased amount of PrP<sup>Sc</sup> as indicated by the darker spots, while (b) shows the IOD values for those spots as a percentage of the untreated control. Figures down the left of (a) indicate the E64 concentration in  $\mu$ M. The data points shown represent the mean  $\pm$  SD values from duplicate experiments where each sample was analysed in triplicate. .... 218
- Figure 96:** The effect of two different concentrations of E64 on the activity of 3001012 (a), 3001207 (b) and 3001086 (c). Bar graphs show the data for the I3GA only, and the I3GA with 10 or 20  $\mu$ M E64 at the lowest concentration where clearance occurs when the compound is dosed on its own. Stars indicate if the difference in clearance is statistically significant. Apart from 3001207 with 10  $\mu$ M E64 ( $p = 0.00882755$ ) in all cases  $p = <0.001$ . The data points shown represent the mean  $\pm$  SD values from duplicate experiments where each sample was analysed in triplicate. .... 219
- Figure 97:** The effect of a fixed concentration of 3001012, 3001207 and 3001086 on E64 activity; a. shows the co-dosed results in comparison to E64 on its own, while b. shows the co-dosed results only for greater clarity. The x-axis gives the concentration of E64. All compounds are able to prevent the accumulation of PrP<sup>Sc</sup> induced by E64, with the activity of 3001012 being affected to the greatest degree. The data points shown represent the mean  $\pm$  SD values from duplicate experiments where each sample was analysed in triplicate. .... 220
- Figure 98:** PrP<sup>Sc</sup> levels in SMB cells after dosing with CI3 at a range of concentrations from 0.5  $\mu$ M to 25  $\mu$ M. No effect was observed on either PrP<sup>Sc</sup> levels (activity) or viability. The data points shown represent the mean  $\pm$  SD values from duplicate experiments where each sample was analysed in triplicate. .... 222
- Figure 99:** The effect of CI3 at 10  $\mu$ M on the activity of 3001012 (a), 3001207 (b) and 3001086 (c). Co-dosing with CI3 results in a decrease of the activity of 3001012 and an improvement in the activity of 3001086, but has no effect on the activity of 3001207. The data, as indicated by PrP<sup>Sc</sup> clearance, is unaffected by treatment. The data points shown represent the mean  $\pm$  SD values from duplicate experiments where each sample was analysed in triplicate. .... 223
- Figure 100:** The effect of a CI3 concentration gradient on a fixed concentration of 3001012, 3001207 and 3001086. There is no observable change in the activities of the I3GA compounds at their active concentrations. The data points shown represent the mean  $\pm$  SD values from duplicate experiments where each sample was analysed in triplicate. .... 224
- Figure 101:** PrP<sup>Sc</sup> levels in cells dosed with either 3001012 or co-dosed with 3001012 and 1  $\mu$ M congo red. At sub-active concentrations of 3001012 (<5 nM in this instance) very high levels of PrP<sup>Sc</sup> are observed, consistent with congo red dosed on its own. This rise in PrP<sup>Sc</sup> levels is reduced at higher levels of 3001012. Bar chart shows the data from the active concentrations of 3001012 for clarity. The data points shown represent the mean  $\pm$  SD values from duplicate experiments where each sample was analysed in triplicate. .... 225
- Figure 102:** Effect on PrP<sup>Sc</sup> levels when a concentration gradient of quinacrine was dosed either on its own or with MG132, E64 or CI3. Bar graphs show data for quinacrine at 1  $\mu$ M, 5  $\mu$ M and 10  $\mu$ M, with stars indicating statistically significant differences from quinacrine on its own. Statistically significant differences were found for quinacrine at 1  $\mu$ M with MG132 ( $p = 0.000221874$ ) and E64 ( $p = 0.0173923$ ) and for quinacrine at 5  $\mu$ M with MG132 ( $p = 0.000796993$ ). The data points shown represent the mean  $\pm$  SD values from duplicate experiments where each sample was analysed in triplicate. .... 226
- Figure 103:** Effect on PrP<sup>Sc</sup> levels when MG132 (a), E64 (b) and CI3 (c) were co-dosed with quinacrine. For MG132 and E64 the graph on the right shows the curve for the co-dosed cells only for clarity. The data for CI3 also includes quinacrine on its own at 5  $\mu$ M for

|   |     |
|---|-----|
| comparison. The difference between quinacrine only and quinacrine with CI3 at 25 $\mu$ M was not statistically significant (t-test, $p = 0.0673633$ ). The data points shown represent the mean $\pm$ SD values from duplicate experiments where each sample was analysed in triplicate. ....   | 227 |
| <b>Figure 104:</b> Western blots showing expression of HSP90 after a 5 day dose (a) and after a 56 hour dose (b). Graphs show HSP90 levels in treated cells from four biological replicates. Data was adjusted for loading difference and is presented as a percent of the DMSO control. ....   | 233 |
| <b>Figure 105:</b> Schematic representation of the targets identified and their possible interactions. Targets identified by inverse docking are in orange, targets identified by the microarray are in green and targets identified from a literature search are in blue. PKC was not investigated further in this study but is crucial to understanding the interactions between the other targets. Figure adapted from Jorge M Valencia Delgado. ....  | 237 |
| <b>Figure 106:</b> Western blots showing expression of MTF-1 after a 5 day dose (a) and after a 56 hour dose (b). Graphs show average MTF-1 levels in treated cells from four biological replicates ( $n = 4$ ), blots shown are representative of all replicates. Data was adjusted for loading difference and is presented as a percent of the DMSO control. ....   | 241 |
| <b>Figure 107:</b> Western blots showing expression of both forms of caspase 12 after a 5 day dose (a) and after a 56 hour dose (b). Graphs show average caspase 12 levels in treated cells from four biological replicates ( $n = 4$ ), blots shown are representative of all replicates. Data was adjusted for loading difference and is presented as a percent of the DMSO control. T-tests showed levels of cleaved protein after treatment with high doses of 3001012 and 3001207 were significantly lower than the DMSO control ( $p = 0.00535421$ and $0.043093$ respectively, $n = 4$ ). ....   | 242 |
| <b>Figure 108:</b> Picture of the Perfecta3D <sup>®</sup> hanging drop plate. The 96 well plate is on the left, and the 384 well plate is on the right. The top of the plate can be separated from the bottom to allow the water reservoirs to be filled and replenished. Image taken from <a href="http://www.3dbiomatrix.com">www.3dbiomatrix.com</a> . ....  | 252 |
| <b>Figure 109:</b> Formation of hanging drop spheroids; a diagram depicting the method of formation. A cell suspension is pipetted through the access hole to form a drop on the bottom of the plate. The cells aggregate at the bottom of the drop, forming a spheroid after around 1 day. <sup>(321)</sup> ....   | 252 |
| <b>Figure 110:</b> Dot blot of PrP <sup>Sc</sup> levels in spheroids grown under optimised conditions in 96 well plates. Each dot represents 1 spheroid. The PrP <sup>Sc</sup> levels can be seen to vary between spheroids, as demonstrated by the differing intensities of the dots and variation in absorbance levels as measured using Bio-Rad Quantity One software. This variation was attributed to problems with the efficiency of spheroid lysis, rather than genuine differences in the level of PrP <sup>Sc</sup> between spheroids. ....  | 253 |
| <b>Figure 111:</b> Optimisation of samples for dot blotting analysis. The table shows PrP <sup>Sc</sup> levels in samples prepared from lysed spheroids. Spheroids were seeded at concentrations of 500, 750 or 1,000 cells/ $\mu$ l in 40 $\mu$ l medium. They were harvested after 4 days and lysed in RIPA buffer. Spheroids were pooled together so that each sample contained either 1, 2, 3 or 4 spheroids, formed from an initial seeding density of 500, 750 and 1,000 cells/ $\mu$ l. Each sample was analysed using dot blot analysis to determine PrP <sup>Sc</sup> levels and the strength of the signal. Seeding cells at 1,000 cells/ $\mu$ l, and using two of these spheroids in each sample, was found to give the best signal. .... | 254 |
| <b>Figure 112:</b> Average PrP <sup>Sc</sup> signal from a sample containing 3 spheroids after lysis at different time points. Spheroids were lysed by the addition of RIPA, followed by shaking, at 2, 3, 4 or 7 days after seeding and the strength (as measured by the absorbance) and consistency (as measured by the error) of the PrP <sup>Sc</sup> signal compared. Spheroids lysed shortly after seeding gave a better signal than those harvested after a longer time period, although the signal  |     |

was less consistent, as indicated by the error. Spheroids harvested and lysed after 7 days gave the weakest yet most consistent signal. .... 255

**Figure 113:** Results from the spheroid lysis optimisation. PrP<sup>Sc</sup> levels were analysed by dot blot in spheroids subjected to different lysis conditions to determine the optimum lysis method. Spheroids were treated with 0.5 % DMSO and then subjected to different lysis conditions. Six replicates are presented for each treatment, and each replicate represents a sample containing 2 spheroids, lysed using the method indicated. The data in the bar chart represents the average intensity of the 6 replicates, and the standard deviation is used as a measure of the consistency of the treatment. Data is expressed as the absorbance of the signal on the blot as measured by Quantity One software (Bio-Rad). It can be clearly seen that subjecting the spheroids to freeze-thaw cycles produces the strongest, although not the most consistent, signal. .... 256

**Figure 114:** Dot blot showing PrP<sup>Sc</sup> levels in spheroids lysed using either multiple freeze-thaw cycles (top row) or digestion with collagenase (bottom two rows). Four samples were lysed with freeze-thaw cycles, 8 samples were lysed using collagenase, and each sample contained 2 spheroids. The strength of the signal was used as a measure of the successfulness of the lysis method. .... 258

**Figure 115.** Example dot blots of PrP<sup>Sc</sup> levels in spheroids dosed with 0.5 % DMSO and sonicated using the Bioruptor. Blots show results from two separate experiments. The signal is much clearer and more consistent. The blots shown in each experiment represent 6 different samples, each containing two of the DMSO treated spheroids. All samples were the same, with both blots being presented to demonstrate the consistency associated with lysing the spheroids in the Bioruptor. .... 258

**Figure 116:** PrP<sup>Sc</sup> levels for the spheroids treated with curcumin expressed as % of the DMSO treated spheroids subjected to the same lysis conditions. Only the freeze-thaw treated samples showed PrP<sup>Sc</sup> levels of less than 70% of the DMSO control (the limit for activity), and this was also the only treatment that showed a significant difference (t-test) between the DMSO treated spheroids and the curcumin treated spheroids ( $p = 0.014749$ ,  $n = 6$ ). Differences between the DMSO treated spheroids and the curcumin treated spheroids for all other treatments were non-significant. Six replicate samples were used for each lysis treatment, with each sample containing 2 spheroids treated with either 0.5 % DMSO or curcumin. .... 260

**Figure 117:** PrP<sup>Sc</sup> levels as a % of the DMSO control in spheroids treated with different compounds from the literature at a range of concentrations. PPS; Pentosan polysulfate, Amph; Amphotericin B, DS; Dextran sulfate. The data points shown represent the mean  $\pm$  SD values from duplicate experiments where each sample was analysed in triplicate. Each sample contains 2 spheroids. .... 261

**Figure 118:** PrP<sup>Sc</sup> levels as a % of the DMSO control in spheroids treated with the indole compounds 3001012 and 3001207 at a range of concentrations up 1000 x EC<sub>50</sub> in the 2D cell model. The data points shown represent the mean  $\pm$  SD values from duplicate experiments where each sample was analysed in triplicate for all treatments except 3001012 at 100 nM and 1  $\mu$ M and 3001207 at 10  $\mu$ M where the data points shown represent the mean  $\pm$  SD values from 4 experiments where each sample was analysed in triplicate. .... 262

**Figure 119:** Images of spheroids taken over a number of days after seeding. Comparison of the images shows that they do not appear to be increasing in size. .... 263

**Figure 120:** Confocal microscope image at 20 x magnification of a spheroid formed in a hanging drop plate and stained with DAPI. .... 264

**Figure 121:** Pictures demonstrating the attachment and spread of spheroids when transplanted into a 96 well plate either with or without a cell monolayer. Spread and growth of the cells from the spheroids can be clearly seen on the blank surface of the plate. Distinguishing cells from the spheroid from cells in the monolayer is more challenging. .... 265

|  |     |
|--|-----|
| <b>Figure 122:</b> Scanning electron microscopy image showing the edge of an Alvetex Scaffold (image from <a href="http://www.amsbio.com">www.amsbio.com</a> , suppliers of Alvetex scaffold). .....   | 269 |
| <b>Figure 123:</b> MTT results for SMB cells seeded onto the scaffold at densities ranging from 10,000 cells/well to 100,000 cells/well. Increased metabolic activity, suggesting increased cell numbers, can be seen for all groups. The data points shown represent the mean $\pm$ SD values from duplicate experiments where each sample was analysed in triplicate. ....   | 270 |
| <b>Figure 124:</b> Images of the Alvetex scaffold under the brightfield microscope. a. shows the scaffold containing cells at 20 x magnification. b. shows the scaffold containing cells that have been stained with neutral red, also at 20 x magnification. Although a red colour can be seen it is not possible to identify individual cells. c. shows the appearance of the wells to the naked eye with the red staining clearly visible, showing the presence of living cells within the scaffold. Staining was carried out three days after seeding, with initial seeding densities of 50,000 cells/well. ....   | 271 |
| <b>Figure 125:</b> Depth colour coded z-stack of cell free Alvetex scaffold at 40 x magnification. Frame 1 represents the top of the scaffold, frame 43 represents the bottom. Total depth is around 120 $\mu$ m with each frame 2.8 $\mu$ m apart.....  | 272 |
| <b>Figure 126:</b> Orthogonal view of a z-stack image at 40 times magnification of the Alvetex scaffold from a 12 well plate seeded with cells at an initial seeding density of 500,000 cells. Cells are stained with DAPI to visualise the nucleus, and have penetrated the scaffold to a depth of 50 $\mu$ m.....  | 273 |
| <b>Figure 127:</b> Orthogonal views of z-stack images from scaffolds harvested at different time points; 2 days (a), 4 days (b), 6 days (c) and 8 days (d). Graphs show the number of pixels in each slice of the z-stack, representing the distribution of the cells within the scaffold and the depth to which they have penetrated, which did not change much between time points. ....   | 274 |
| <b>Figure 128:</b> Orthogonal view of a z-stack image at 40 x magnification where the cells and the scaffold were stained with DAPI and Nile red respectively and imaged at different wavelengths. Total depth of the image is around 100 $\mu$ m. ....  | 275 |
| <b>Figure 129:</b> 3D representation of the z-stack shown above in <b>Figure 128</b> . Numbers are in $\mu$ m and represent the dimensions of the section. ....  | 276 |
| <b>Figure 130:</b> Orthogonal view of a z-stack image at 40 x magnification. Cell nuclei are stained with DAPI (blue), actin in the cytoskeleton is stained with phalloidin acti-stain 488 (green). The cell-cell contacts and 3D structure can be observed in all sections.....   | 276 |
| <b>Figure 131:</b> Orthogonal view of a z-stack image at 40 x magnification. Cell nuclei are stained with DAPI (blue), actin in the cytoskeleton is stained with phalloidin acti-stain 488 (green) and the scaffold is stained with Nile red (red). The red signal has slightly bled into the green channel, resulting in the yellow signal from some points of the scaffold. However, the cell nuclei, surrounded by the cytoskeleton, can be clearly seen. ....  | 277 |
| <b>Figure 132:</b> Deconstruction of <b>Figure 131</b> above. Pictures represent either cell nuclei stained with DAPI (left), actin stained green, along with bleed through from the red channel (middle) and the scaffold stained red (right). ....   | 277 |
| <b>Figure 133:</b> Image taken at 60 x magnification of scaffolds stained with DAPI and acti-stain. ...  | 278 |
| <b>Figure 134:</b> Results of initial dosing trial on cells grown in 3D within the Alvetex scaffold. PrP <sup>Sc</sup> levels are directly proportional to the integrated optical density (IOD) of the dots on the blot, as measured by Bio-Rad Quantity One software. It can clearly be seen that curcumin and 3001012 are causing reductions in the levels of PrP <sup>Sc</sup> in treated cells, although with slightly reduced efficacy compared to results in the monolayer. The results were also fairly consistent over different wells. The data points shown represent the mean $\pm$ SD values from duplicate experiments where each sample was analysed 4 times. .... | 279 |
| <b>Figure 135:</b> Comparison of the PrP <sup>Sc</sup> levels, as denoted by the signal on the dot blot, after treatment with different compounds and either 1 or 2 rounds of lysis. Two rows of an Alvetex plate were treated with either HBSS, 0.5 % DMSO, curcumin or 3001012. Eight  |     |

replicate wells, comprising 2 rows and 4 columns, were used for each treatment. Cells were lysed using RIPA buffer within the Alvetex scaffold, the lysate removed (lysis 1), and a second aliquot of RIPA buffer added to lyse any remaining cells (lysis 2). The faint signal from the second set of lysates suggests that the majority of the cells are being lysed in the initial lysis. This figure also demonstrates the activity of both curcumin and 3001012 in this model as shown by the decreased signal compared to the HBSS and DMSO control. This is more obvious in the results from the first lysis. .... 280

**Figure 136:** PrP<sup>Sc</sup> levels in cells grown in Alvetex scaffolds and treated with the I3GA compounds that have not been tested *in vivo*. Both compounds can be seen to reduce PrP<sup>Sc</sup> levels at concentrations similar to their EC<sub>50</sub>s in the 2D cellular model. The data points shown represent the mean ± SD values from duplicate experiments where each sample was analysed in triplicate. .... 281

**Figure 137:** PrP<sup>Sc</sup> levels in cells grown in Alvetex scaffolds and treated with compounds known to have *in vivo* activity (see **Table 46** for references). All compounds except amphotericin B were shown to be active. The data points shown represent the mean ± SD values from duplicate experiments where each sample was analysed in triplicate. .... 282

**Figure 138:** PrP<sup>Sc</sup> levels in cells grown in Alvetex scaffolds and treated with quinacrine and heparin. Quinacrine has been shown to be ineffective *in vivo*, while heparin has not been tested. (see **Table 46** for references). Both compounds showed activity, although in the case of quinacrine activity was reduced compared to activity in the 2D model. The data points shown represent the mean ± SD values from duplicate experiments where each sample was analysed in triplicate. .... 283

**Figure 139:** MTT viability data for cells grown in scaffolds and treated with the highest concentrations of the compounds used in the activity screening. All compounds apart from quinacrine were non-toxic at their highest concentrations. The data points shown represent the mean ± SD values from duplicate experiments where each sample was analysed in triplicate. .... 284

**Figure 140:** Pictures showing the formation of colonies and spheroid-like structures over time when SMB cells are cultured in Happy Cell matrix. Cells were seeded at 5,000 cells/well and monitored over 4 days. .... 287

**Figure 141:** Confocal image of the spheroids after transferal to a microscope slide and staining with DAPI. The right hand image shows a 3D representation of the left hand image. A strong signal can be seen from some of the spheroids, while some show a very weak signal. .... 288

**Figure 142:** Orthogonal view of a z-stack of a spheroid formed in the Happy Cell model. .... 289

**Figure 143:** PrP<sup>Sc</sup> levels in cells grown in Happy Cell matrix and treated with compounds that have not been tested *in vivo*. Both compounds can be seen to be active. The data points shown represent the mean ± SD values from duplicate experiments where each sample was analysed in triplicate. .... 290

**Figure 144:** PrP<sup>Sc</sup> levels in cells grown in Happy Cell matrix and treated with compounds known to have *in vivo* activity (see **Table 46** for references). Both compounds were shown to be active. The data points shown represent the mean ± SD values from duplicate experiments where each sample was analysed in triplicate. .... 290

**Figure 145:** PrP<sup>Sc</sup> levels in cells grown in Happy Cell matrix and treated with quinacrine, which is known not to be active *in vivo* (see **Table 46**). Quinacrine retained some activity but this was reduced compared to activity in the 2D model. The data points shown represent the mean ± SD values from duplicate experiments where each sample was analysed in triplicate. .... 291

**Figure 146:** MTT viability data for cells grown in Happy Cell matrix and treated with the highest concentrations of the compounds used in the activity screening. The data points shown represent the mean ± SD values from duplicate experiments where each sample was analysed in triplicate. .... 292

|  |     |
|--|-----|
| <b>Figure 147:</b> Cell growth within the Happy Cell medium as measured using MTT. Graph a. shows the cell numbers, as measured by absorbance levels, over time. Graph b. shows the absorbance as a factor of the control, demonstrating the effect of the different treatments on growth. The data points shown represent the mean $\pm$ SD values from duplicate experiments where each sample was analysed in triplicate..... | 293 |
| <b>Figure 148:</b> Structure of 3001012, the lead compound.....  | 300 |

## List of Tables

|   |    |
|---|----|
| <b>Table 1:</b> Prion diseases in humans and animals. <sup>(12)</sup> .....   | 2  |
| <b>Table 2:</b> Compounds exhibiting therapeutic and/or prophylactic anti-prion effects tested in cell cultures and/or bioassays. Table adapted from Trevitt and Collinge. <sup>(207)</sup> .....   | 20 |
| <b>Table 3:</b> An example of a CDTp. Table adapted from Stocks <i>et al.</i> <sup>(298)</sup> .....  | 30 |
| <b>Table 4:</b> Typical layout for initial screens. Letters A-H represent different samples at three concentrations (1, 10 and 20 $\mu$ M). Each concentration is screened in triplicate. The negative control (-ve) is 0.5 % DMSO, the positive control (+ve) is 10 $\mu$ M curcumin.....  | 52 |
| <b>Table 5:</b> Compounds and their concentrations used in the MTT-FE assay.....  | 62 |
| <b>Table 6:</b> Western blotting conditions for each of the targets. All solutions were made in TBS-T (20 ml for the block, 5 ml for the primary antibody and 10 ml for the secondary antibody) and all primary antibody incubations were done overnight at 4 °C, unless otherwise specified. ....  | 68 |
| <b>Table 7:</b> Different seeding densities and medium volumes used in the optimisation of the 96 well hanging drop plate. Figures in the table show the total number of cells per drop for each of the parameters. ....  | 69 |
| <b>Table 8:</b> Seeding conditions for the different Alvetex plate formats. ....  | 72 |
| <b>Table 9:</b> Examples of other compounds that include the I3GA pharmacophore (in red) and their proposed therapeutic function. Figure adapted from Thompson <i>et al.</i> <sup>(279)</sup> .....   | 79 |
| <b>Table 10:</b> EC <sub>50</sub> s of different compounds when probed with either 8H4 or 6H4 .....   | 82 |
| <b>Table 11.</b> Descriptions of the screening libraries used.....  | 84 |
| <b>Table 12:</b> Viability results from the initial screens. Results are given for compounds that caused cell death as measured by the MTT assay. All other compounds were classed as non-toxic. In all cases toxicity was determined at the initial screen stage, with cytotoxicity occurring at the toxic concentrations in all cases (n = 6) so no standard deviation data was available. Concentrations that were tested below the toxic concentration were not cytotoxic. ....   | 85 |
| <b>Table 13:</b> Initial screen results for library A. The compounds in library A represent a wide range of amines, in conjunction with either unsubstituted indoles (top row), 1-methylindoles (middle row) or 2-methylindoles (bottom row). ....  | 88 |
| <b>Table 14:</b> Initial screen results for library B. The compounds in library B represent optimisation of the most promising amines, as identified from library A. These were investigated in conjunction with either unsubstituted indoles (top row) or 1-methylindoles (bottom row). ....   | 89 |
| <b>Table 15:</b> Initial screen results for library C. The compounds in library C represent further optimisation of the amines identified from libraries A and B, in conjunction with unsubstituted indoles. ....   | 90 |
| <b>Table 16:</b> Initial screen results for library D. The compounds in library D represent further investigations into substitutions at the 5 and 6 position of the indole, using amine groups optimised from libraries A, B and C. The substitutions investigated were the addition of chloro groups at the 6 position (top row) and 5 position (second row), and the addition of methyl groups at the 6 position (third row) and 5 position (bottom row).....  | 91 |
| <b>Table 17:</b> Initial screen results for library E. The compounds in library E represent a continuation of the investigations into the substitutions in library D. Further investigations of the 6 chloro substitution were undertaken (top row) along with investigations into the effect of two substitutions on the indole, at the 6 position and the 1 position (second row), 6-fluoro substitutions (third row), 7-chloro substitutions (fourth row) and 7-methyl substitutions (bottom row). Amines optimised from libraries A, B and C were used..... | 92 |
| <b>Table 18:</b> Initial screen results for library F. The compounds in library F represent investigations into the effect of changes to the carbonyl groups. The effect of a monocarbonyl group was  |    |

investigated (top two rows), as was the addition of a heterocycle instead of the carbonyl groups (third row). Addition of a large group to the 1 position of the indole was also investigated (bottom row). Amines optimised from libraries A, B and C were used..... 92

**Table 19:** Initial screen results for library G. The compounds in library G represent further investigations into the effect of substitutions to the indole group using amines optimised from libraries A, B and C. The effect of the addition of a methyl bridge between the two carbonyls was examined (top row), along with the effect of <sup>i</sup>Pr substitutions at the 6 position (second row), a methyl group at the 4 position (third row), a cyano group at the 6 position (fourth row) and a nitro group at the 6 position (bottom row). ..... 93

**Table 20:** EC<sub>50</sub> results for library A ..... 96

**Table 21:** EC<sub>50</sub> results for library B..... 97

**Table 22:** EC<sub>50</sub> results for library C..... 98

**Table 23:** EC<sub>50</sub> results for library D ..... 98

**Table 24:** EC<sub>50</sub> results for library E..... 99

**Table 25:** EC<sub>50</sub> results for library F..... 99

**Table 26:** EC<sub>50</sub> results for library G ..... 100

**Table 27:** SPR screening results for library A at a concentration of 40 μM. .... 117

**Table 28:** SPR screening results for library B at a concentration of 40 μM. .... 118

**Table 29:** SPR screening results for library C at a concentration of 40 μM. .... 119

**Table 30:** SPR screening results for library D at a concentration of 40 μM ..... 119

**Table 31:** SPR screening results for library E at a concentration of 40 μM..... 120

**Table 32:** SPR screening results for library F at a concentration of 40 μM..... 120

**Table 33:** Previous EC<sub>50</sub> results compared to current EC<sub>50</sub> results for all compounds used in the time course study. .... 141

**Table 34:** Results of activity screening of anti-prion literature compounds, compared to their published activities. EGCG – Epigallocatechin gallate. See **Figure 58** for structures. .... 154

**Table 35:** An example of the raw data obtained after solubilisation of the formazan product in 1 % tween 20. Data is presented for 0.5 % DMSO and 5 μM quinacrine and the assay was performed 24 hours after dosing. The measured absorbances are averaged, the blank value is subtracted and the final result is expressed as a percentage of the DMSO control. .... 157

**Table 36:** Total amount of protein per sample as determined by Bradford assay. Each sample represents cells from one tissue culture petri dish suspended in 5 ml medium. 1 ml of this was taken for the microarray sample and 3.5 ml was taken for the proteomics sample. The final 0.5 ml was retained for analysis, and was used for the Bradford assay and dot blot analysis. More protein was required for the proteomics so a larger sample was used. .... 173

**Table 37:** Total number of DEGs found..... 174

**Table 38:** Number of DEGs grouped by up and down regulation at different cut off values. .... 175

**Table 39:** Up and down regulated proteins from the proteomic studies. The identity of the different proteins can be seen in **Table 40**. .... 175

**Table 40:** Proteins identified as up or down regulated in the proteomics studies after treatment with quinacrine, 3001012 or 3001207 and compared to the DMSO control. .... 176

**Table 41.** Genes identified as upregulated in the microarray data in cells treated with 3001012 that are involved in the proteasomal pathway. .... 193

**Table 42:** EC<sub>50</sub> values for 3001012 on its own or co-dosed with MG132 calculated from the data presented in **Figure 86**. .... 210

**Table 43:** EC<sub>50</sub> values for the I3GAs on their own or co-dosed with two different concentrations of E64 calculated from the data presented in **Figure 96**..... 220

**Table 44:** EC<sub>50</sub> values for the I3GAs on their own or co-dosed with Cl3, calculated from the data presented Estimated EC<sub>50</sub> values for the data presented **Figure 99**..... 223

**Table 45:** EC<sub>50</sub> values for quinacrine on its own or co-dosed with MG132, E64 or Cl3, calculated from the data presented in **Figure 102** ..... 226

|  |     |
|--|-----|
| <b>Table 46.</b> Compounds from the literature used in studies of activity in 3D models. Note that not all compounds were used in all studies. ....                        | 251 |
| <b>Table 47:</b> Summary of the EC <sub>50</sub> results from screening in the different 3D models. 2D results are from screens carried out alongside the 3D screens ..... | 296 |
| <b>Table 48:</b> Advantages and disadvantages of the different 3D models with relation to their potential as high-throughput drug screening systems. ....                  | 297 |

## Abbreviations

A-FABP – Fatty acid binding protein

A $\beta$  – Amyloid beta

ADME – Absorptions, distribution, metabolism and excretion

ANT – Adenine nucleotide translocator

APP – Amyloid precursor protein

AU – Absorbance units

BACE –  $\beta$ -secretase 1

BBB – Blood brain barrier

BSA – Bovine serum albumin

BSE – Bovine spongiform encephalopathy

Ca<sup>+</sup> - Calcium

CaCl<sub>2</sub> – Calcium chloride

CC<sub>1</sub>/CC<sub>2</sub> – Charged clusters 1 and 2.

CDTP – Candidate drug target profile

CI3 – Cathepsin inhibitor III

CJD – Creutzfeld-Jacob disease

Cl – Clearance

CM5 – Carboxymethylated dextran chip

CNS – Central nervous system

CWD – Chronic wasting disease

Cu – Copper

DAPI – 4',6-diamidino-2-phenylindole

DEG – Differentially expressed gene

DMEM – Dulbecco's modified eagle's medium

DMPK – Drug metabolism and pharmacokinetics

DMSO – Dimethyl sulfoxide

DS – Dextran sulfate

EAE – Experimental autoimmune encephalomyelitis

EC<sub>50</sub> – Half maximal effective concentration

ECL – Enhanced chemiluminescence  
ECM – Extracellular matrix  
EDC - 1-ethyl-3-(3-dimethylaminopropyl)carbodiimide hydrochloride  
EDTA – Ethylenediaminetetracetic acid  
EGCG - Epigallocatechin gallate  
ER – Endoplasmic reticulum  
ERAD – Endoplasmic reticulum associated degradation  
EUE – Exotic ungulate encephalopathy  
F – Oral bioavailability  
FASN – Fatty acid synthase  
FBS – Foetal bovine serum  
FDC – Follicular dendritic cells  
FFI – Fatal familial insomnia  
FIHPrP<sup>C</sup> – Full length human prion protein  
FIMoPrP<sup>C</sup> – Full length mouse prion protein  
FSE – Feline spongiform encephalopathy  
GAG – glycosaminoglycans  
GPI – Glycosylphosphatidylinositol  
GSS - Gerstmann-Straussler-Scheinker  
H1/H2/H3 – Alpha helices in PrP<sup>C</sup>  
HBS-EP – HEPES based running buffer bought from Biacore.  
HBSS – Hanks balanced salt solution  
HC – Hydrophobic core  
HCl – Hydrochloric acid  
HEPES - 4-(2-hydroxyethyl)-1-piperazineethanesulfonic acid  
HPF – hours post fertilisation  
HSP90 – Heat shock protein 90  
HTS – High throughput screening  
huPrP<sup>C</sup> – human PrP<sup>C</sup>  
I3GA – Indole-3-glyoxylamide  
IC<sub>50</sub> – Half maximal inhibitory concentration (enzymes)

IgG – Immunoglobulin antibody  
IOD – Integrated optical density  
iTRAQ – Isobaric tag for relative and absolute quantification  
 $K_2HPO_4$  – Dipotassium phosphate  
KCl – Potassium chloride  
 $K_D$  – Dissociation constant  
kDa – KiloDaltons  
KRB – Krebs ringing buffer  
Lck – Lymphocyte-specific protein tyrosine kinase  
LCP – Lysosomal cysteine proteases  
 $LD_{50}$  – Half maximal toxic concentration  
logP – Lipophilicity  
LR – Laminin receptor  
LRP – Laminin receptor precursor  
MCTS – Multicellular tumour spheroid  
 $MgSO_4$  – Magnesium sulfate  
MHC – Major histocompatibility complex  
moPrP<sup>C</sup> – mouse PrP<sup>C</sup>  
MPTP – Membrane permeability transition pore.  
MTF-1 – Metal transcription factor  
MTT - thiazolyl blue tetrazolium bromide  
MTT-FE – MTT formazan exocytosis  
NaCl – Sodium chloride  
NaOH – Sodium hydroxide  
NBCS – New born calf serum  
NHS - N-hydroxysuccinimide  
NMR – Nuclear magnetic resonance  
OR – Octapeptide repeat  
P450 – Enzymes responsible for drug metabolism  
PBS – Phosphate buffered saline  
PDTD – Potential drug target database

PK – Proteinase K

PKC – Protein kinase C

PMCA – Protein misfolding cyclic amplification

PMSF – Phenylmethanesulfonyl fluoride

PPB – Protein plasma binding

PPS – Pentosan polysulfate

*PRNP* – The human gene encoding PrP<sup>C</sup>

PrP<sup>C</sup> – The normal isoform of the prion protein

PrP<sup>res</sup>/PrP<sup>27-30</sup> – The protease resistant core of the abnormal isoform of the prion protein.

PrP<sup>Sc</sup> – The abnormal (scrapie) isoform of the prion protein.

PrPIP – Prion protein interaction partner

rhPrP – Recombinant human prion protein

PVDF – polyvinylidene fluoride

RIPA – Radioimmunoprecipitation assay

RML – Rocky mountain laboratory

RNA – Ribonucleic acid

RNAi – RNA interference

RT-PCR – Real time polymerase chain reaction

RU – Response units

RU<sub>max</sub> – Theoretical maximum response

SAR – Structure-activity relationship

ScN2a – Scrapie infected neuronal mouse brain cells

ScNB – Scrapie infected mouse neuroblastoma cells

sFI – Sporadic fatal insomnia

shRNA – Small hairpin RNA

SLS – Scientific laboratory supplies

SMB – Scrapie mouse brain

SOD – Superoxidase dismutase

SP1 – Specific protein 1

SPR – Surface Plasmon resonance

$T_{1/2}$  – Half life  
TBS – Tris buffered saline  
TBS – T Tris buffered saline with 0.1 % tween 20  
TCR – T-cell receptor  
TES – 2-[[1,3-dihydroxy-2-(hydroxymethyl)propan-2-yl]amino]ethanesulfonic acid  
TGS – Tris/glycine/SDS  
TG – Tris/glycine  
TME – Transmissible mink encephalopathy  
TI-MTT – Tween insoluble MTT  
TS-MTT – Tween soluble MTT  
TSE - Transmissible spongiform encephalopathy  
UPR – Unfolded protein response  
UPS – Ubiquitin-proteasome system  
UV – Ultra violet  
vCJD – Variant Creutzfeld-Jacob disease  
VDAC – Voltage dependent anion channel  
VHTS – Virtual high throughput screening  
VPSPr – Variably protease-sensitive prionopathy  
Vss – Volume of distribution  
Zn – Zinc



# 1. Introduction

## 1.1. Overview of Prion Diseases

Transmissible spongiform encephalopathies (TSEs), also called prion diseases, are a family of diseases affecting both animals and humans (see **Table 1**). Animal diseases include bovine spongiform encephalopathy (BSE) in cows, chronic wasting disease (CWD) in deer and elk and scrapie, the prototypic disease, in sheep and goats. <sup>(1)</sup> Human diseases include various types of Creutzfeld-Jacob disease (CJD), Gerstmann-Straussler-Scheinker disease (GSS), fatal familial insomnia (FFI) and kuru, as well as the recently identified variably protease-sensitive prionopathy (VPSPr). <sup>(2)</sup> These diseases are invariably fatal. BSE and its human counterpart CJD came to prominence in the mid-1990s when there was an outbreak of BSE among cattle. This led to the emergence of variant CJD (vCJD) in humans which is believed to be caused by the same prion strain that causes BSE, with the route of infection thought to be *via* dietary exposure to BSE prions. <sup>(1, 3-9)</sup> Despite widespread fears of an epidemic in the human population, very few people have so far been afflicted by vCJD, with 177 cases of definite or probable vCJD reported in the UK and 51 cases reported in 11 other countries (as of April 2014). <sup>(8)</sup> All these diseases are linked to an abnormal isoform of a normal cellular protein, the prion protein or PrP<sup>C</sup>. The disease causing isoform of this protein is known as PrP<sup>Sc</sup>.

Prion diseases (TSEs) can be divided into 3 etiological categories. Sporadic TSEs arise as a result of spontaneous mutations that can lead to the formation of the abnormal isoform of the protein. Inherited TSEs are caused when the mutation rendering PrP<sup>C</sup> susceptible to spontaneous conversion is passed on to offspring. A common polymorphism at residue 129 is a key determinant of susceptibility to inherited and sporadic prion diseases. <sup>(10)</sup> Dominant mutations in the gene encoding PrP<sup>C</sup> (*PRNP* in humans) can produce a mutant PrP<sup>C</sup> that more readily undergoes spontaneous transformation to PrP<sup>Sc</sup>. <sup>(11)</sup> Transmissible TSEs can also be acquired through exposure to the abnormal prion isoform. For example, iatrogenic CJD can be passed on through contaminated growth hormone taken from infected cadavers. <sup>(10)</sup> Prion diseases are generally characterised by a classical triad of histological features; spongiform vacuolation (affecting any part of the cerebral grey matter), neuronal loss and astrocytic proliferation. <sup>(1)</sup>

**Table 1:** Prion diseases in humans and animals. <sup>(12)</sup>

| Disease        | Host        | Mechanism of pathogenesis   |
|----------------|-------------|---|
| Kuru           | Humans      | Infection through ritualistic cannibalism   |
| Iatrogenic CJD | Humans      | Infection from prion-contaminated HGH, medical equipment etc.                       |
| Variant CJD    | Humans      | Believed to be infection from bovine prions   |
| Familial CJD   | Humans      | Germline mutations in the PRNP gene   |
| GSS            | Humans      | Germline mutations in the PRNP gene   |
| FFI            | Humans      | Germline mutations in the PRNP gene   |
| Sporadic CJD   | Humans      | Somatic mutation or spontaneous conversion of PrP <sup>C</sup> to PrP <sup>Sc</sup> |
| Sporadic FI    | Humans      | Somatic mutation or spontaneous conversion of PrP <sup>C</sup> to PrP <sup>Sc</sup> |
| VPSPr          | Humans      | As yet unknown  |
| Scrapie        | Sheep       | Infection   |
| BSE            | Cattle      | Infection or sporadic   |
| TME            | Mink        | Infection with prions from sheep or cattle  |
| CWD            | Deer, Elk   | Infection   |
| FSE            | Cats        | Infection with prion-contaminated bovine tissues or MBM                             |
| EUE            | Kudu, Nyala | Infection with prion-contaminated MBM   |

### 1.1.1. Prion Structure (PrP<sup>C</sup>) and Function

#### 1.1.1.1. PrP<sup>C</sup> Structure

Much recent interest has focused on determining the role of the normal isoform of the protein, PrP<sup>C</sup>. It is hoped that elucidating the role and mechanism of action of the normal isoform of the protein may give a clue as to the way the misfolded isoform affects the nervous system.

PrP<sup>C</sup> is present in a broad variety of species and is always glycosylated, membrane attached by a glycosylphosphatidylinositol (GPI) anchor and based on a common blueprint. <sup>(13)</sup> A flexible amino-terminal tail is linked to a globular carboxy-terminal domain with a strongly conserved fold which is stabilised by a disulphide bridge. The two domains are joined *via* a highly conserved hydrophobic linker. <sup>(13)</sup> PrP<sup>C</sup> is highly expressed in the nervous system but is also found in various components of the immune system, bone marrow, blood peripheral tissues and other organs. PrP<sup>C</sup> expression is affected by the maturity and cellular activation of different cell types. <sup>(14)</sup>

The mature PrP<sup>C</sup> protein, as shown in **Figure 1**, contains a well-defined c-terminal globular domain consisting of three alpha helices and two beta sheets, and a structurally less defined region containing a stretch of octapeptide repeats (the OR) and a charged cluster. The domains are linked by a hydrophobic stretch of amino acids, the hydrophobic core (HC).<sup>(14)</sup>

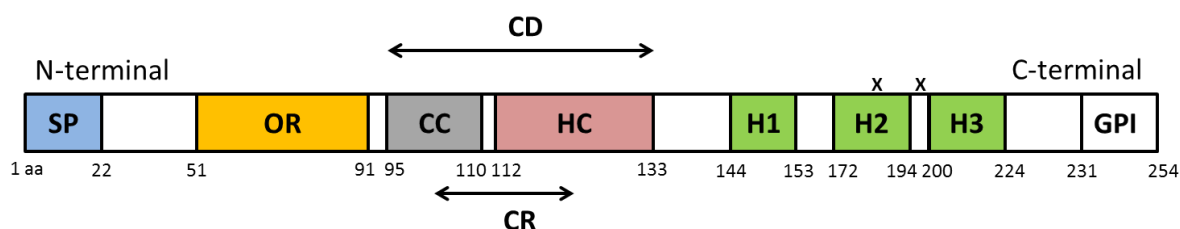


**Figure 1:** The human prion protein. SP denotes the signal peptide. OR indicates the octapeptide repeats. H1 to H3 denote the three alpha helices. CD indicates the central domain and CR indicates the central region, which contain charged clusters (CC) and the hydrophobic core (HC). GPI represents the glycosylphosphatidylinositol (GPI) anchor. Crosses indicate the glycosylation residues at amino acids 180 and 196. Figure adapted from Linden *et al.*<sup>(14)</sup>

Glycosylation occurs between residues 144-224, with glycosylation residues at amino acids 180 and 196, and one disulphide bond is present between cysteine residues 179 and 214.<sup>(14)</sup> The  $\alpha$ -helix domains are anchored to the detergent-rich areas of the membrane *via* a GPI anchor.<sup>(15)</sup> PrP<sup>C</sup> presents in three distinct topological forms: the fully extracellular form and two transmembrane isoforms known as N trans-transmembrane-PrP (<sup>Ntm</sup>PrP) and C trans-transmembrane PrP (<sup>Ctm</sup>PrP). Classification depends on their sequence orientation with relation to the lumen of the endoplasmic reticulum (ER).<sup>(16)</sup> <sup>Ctm</sup>PrP has its COOH-terminus in the ER lumen while the N-terminus is exposed to cytosolic proteases. <sup>Ntm</sup>PrP is the other way round.

### 1.1.1.2. Physiological Role of PrP<sup>C</sup>

The role of PrP<sup>C</sup> within the cell remains ambiguous, despite extensive literature on the subject. Its conservation across species suggests an important evolutionary role, with genes related to the prion protein gene (*PRNP*) having been identified in birds,<sup>(17)</sup> amphibians<sup>(18)</sup> and reptiles.<sup>(19)</sup> Comparison of the translated sequences of 40 mammalian PrP genes shows a large degree of conservation between sequences, suggesting that PrP<sup>C</sup> may have an important function,<sup>(12)</sup> and the individual glycine residues in the glycine rich area of the hydrophobic core of PrP<sup>C</sup> have also been shown to be perfectly conserved across fifteen mammalian species.<sup>(20)</sup> It was hoped that the generation of a PrP knockout mouse model would help reveal the role of PrP<sup>C</sup>. However, initial studies of PrP knockout mice did not show an overt phenotype as had been anticipated,<sup>(21, 22)</sup> although subsequent studies have revealed an abundance of more subtle phenotypes.<sup>(23)</sup> The

most striking feature of mice lacking expression of PrP<sup>C</sup> is their resistance to prion infection and their inability to replicate prions. <sup>(24)</sup> Other possible functions of PrP<sup>C</sup> suggested from mouse models include roles in sleep regulation, managing oxidative stress *via* copper binding, superoxide dismutase (SOD) and mitochondrial activities, immune system function, neuronal excitability, neuroprotection, learning and behaviour and stem cell biology. <sup>(23)</sup> Additional studies in prion knockout mice have also demonstrated a wide range of effects including disruption of olfactory behaviour, <sup>(25)</sup> iron transport, <sup>(26)</sup> tooth development, <sup>(27)</sup> glucose tolerance <sup>(28)</sup> and regeneration of adult muscle tissue. <sup>(29)</sup> Experimental autoimmune encephalomyelitis (EAE), an autoimmune disease, was shown to be more severe in PrP knockout mice. <sup>(30)</sup> This was attributed to the role of PrP<sup>C</sup> as a negative regulator of T-cell receptor signalling which is critical to the development of EAE. This suggests a critical role for PrP<sup>C</sup> in maintaining the integrity of the CNS in times of stress. <sup>(30, 31)</sup> Knockout mice were shown to have lower levels of anxiety under artificially induced stressful conditions so it is possible that PrP<sup>C</sup> also has a role in managing the response to stress at a systems level. <sup>(32)</sup>

One of the most frequently suggested cellular functions of PrP<sup>C</sup> is a survival-promoting effect on neuronal and non-neuronal cells. PrP<sup>C</sup> has been shown to have a cytoprotective function by decreasing the apoptotic rate after exposure to apoptotic stimuli. <sup>(33)</sup> It has also been suggested that PrP<sup>C</sup> protects against oxidative stress, possibly *via* its capacity to bind copper. <sup>(34-36)</sup> *In vitro* studies of rat pheochromocytoma cells showed those selected for resistance to copper toxicity or oxidative stress had higher levels of PrP<sup>C</sup>. <sup>(37)</sup> In addition, PrP<sup>C</sup> deficient primary neurons were more susceptible to agents inducing oxidative stress compared with wild type cells. <sup>(38)</sup> This was explained by a reduced level of Cu/Zn SOD activity although whether PrP<sup>C</sup> itself has SOD activity is disputed. Although it has been suggested that PrP<sup>C</sup> could have SOD-like activity, <sup>(39)</sup> this has not been reproduced *in vitro* or *in vivo*. <sup>(40-42)</sup> There is also a generally held view, which is widely supported, that PrP<sup>C</sup> is an important protein in synapses and is possibly involved in synapse formation. <sup>(43)</sup> The functional role of PrP<sup>C</sup> in the synapses has been suggested on the basis of its copper binding ability, <sup>(35)</sup> and it is thought that it can significantly modulate neuronal excitability and synaptic activity. <sup>(14)</sup> PrP<sup>C</sup> may participate in synaptic transmission by helping neurotransmitter release, controlling Ca<sup>+</sup> flux, participating in long term potentiation and altering expression of neurotransmitter receptors. <sup>(44)</sup> There are also suggestions that PrP<sup>C</sup> is involved in neurite outgrowth and maintenance of the white matter, and axonal PrP<sup>C</sup> is important in the maintenance of peripheral myelin. <sup>(45)</sup>

Various other roles for PrP<sup>C</sup> have been suggested. Down regulation was found to impair cell adhesion in the zebrafish embryo, ultimately causing developmental arrest.<sup>(46)</sup> Interactome analysis suggests a role for PrP<sup>C</sup> in lactate metabolism, and the same study verified laminin receptor precursor (LRP) as a genuine interactor.<sup>(47)</sup> PrP<sup>C</sup> can act as a marker for hematopoietic stem cells and supports their self-renewal. It may protect the stem cells from apoptosis or sustain their long term renewal.<sup>(48)</sup> PrP<sup>C</sup> also has a variety of roles in the immune system. It presents both in the innate immune system on several types of antigen presenting cells including dendritic cells, and in the adaptive immune system on T lymphocytes.<sup>(49)</sup> PrP<sup>C</sup> has been shown to modulate the responses of immune cell precursors, promote the assembly of T-cell receptor (TCR) complex components, negatively modulate phagocytosis and various aspects of peripheral inflammation and it may play an important role in the development and maintenance of the immune system.<sup>(14, 50)</sup>

## 1.1.2. Prions and Disease

### 1.1.2.1. Protein Misfolding Diseases

Prion diseases belong to a group of diseases known as proteinopathies, which are diseases associated with abnormal protein deposition.<sup>(51)</sup> The proteinopathies include Alzheimer's disease, Parkinson's disease, Huntington's disease, tauopathies and amyloid lateral sclerosis (ALS), and are thought to involve the prion-like induction of protein deposition *via* corruptive protein templating, also known as seeding.<sup>(52)</sup> This suggests that an underlying cause of many of these common neurodegenerative diseases is the seeded corruption of proteins that, under normal conditions, are harmless.<sup>(53)</sup> Although the majority of human proteopathies are thought to arise sporadically, there is evidence that some of these diseases may also be transmissible under experimental conditions.<sup>(54)</sup>

The different types of prion diseases are summarised in **Table 1** and demonstrate the range of species affected by these diseases *via* different mechanisms. Transmission of disease between species has been shown to be far less efficient than transmission within species,<sup>(55)</sup> and the slight variations between sequences result in a 'species barrier', first noted in 1965.<sup>(56)</sup> The central event in prion disease pathogenesis is the conversion of the normal cellular protein, PrP<sup>C</sup>, into an insoluble and partially protease resistant isoform known as PrP<sup>Sc</sup> which is able to propagate itself *via* further conversion of PrP<sup>C</sup> molecules.<sup>(15)</sup>

### 1.1.2.2. The 'Protein-Only' Hypothesis

The infectious nature of prion diseases was first identified when a herd of sheep were accidentally inoculated with a vaccine contaminated with the scrapie agent, with 10 % of the herd going on to develop scrapie. <sup>(57)</sup> Scrapie was subsequently transmitted successfully to mice. <sup>(58)</sup> An infectious route for the human disease Kuru was also established in the late 1960s by the demonstration that the disease could transfer from humans to monkeys. <sup>(59)</sup> The infectious agent was proposed to be a type of slow virus due to the long incubation times <sup>(60)</sup> but the finding that the infectious agent was resistant to procedures known to destroy nucleic acids cast doubt on this theory. <sup>(61)</sup> There was early speculation that the infectious particle may be a protein in the late 1960s <sup>(62)</sup> but this was not explored further until the term 'prion' was coined by Stanley Prusiner in 1982. <sup>(11)</sup> He hypothesised that the infectious agent was a 'proteinaceous infectious particle', also known as the protein-only hypothesis.

Initial evidence in favour of the protein-only hypothesis came from the identification of protease-K resistant PrP, and the finding that the concentration of this protein corresponded directly to infectivity. <sup>(63, 64)</sup> This abnormal PrP was termed PrP<sup>Sc</sup>, due to its association with scrapie, and the protease-resistant core was termed PrP<sup>res</sup> or PrP<sup>27-30</sup> due to its molecular size. Both forms of the protein were shown to be encoded by the *PRNP* gene, directly linking the infectious agent with the normal cellular form of the protein <sup>(65)</sup> and the finding that transgenic mice that did not express PrP<sup>C</sup> were resistant to infection with PrP<sup>Sc</sup> reinforced the importance of the normal cellular isoform in disease pathogenesis. <sup>(24)</sup> In addition, the discovery that infectivity could be propagated in mouse neuroblastoma cells inoculated with both brain homogenate <sup>(66)</sup> and PrP<sup>Sc</sup> derived from infected brains and spleens <sup>(67)</sup> provided further evidence to support the theory.

The experiment showing that PrP<sup>Sc</sup> was able to induce the conversion of PrP<sup>C</sup> in a cell free system <sup>(68)</sup> was a key piece of evidence in support of the protein-only hypothesis, and these initial studies have been advanced by the development of Protein Misfolding Cyclic Amplification (PMCA). <sup>(69)</sup> For many sceptics, evidence that *de novo*, infectious prions could be formed *in vitro* was an essential piece of evidence that was required for the protein-only hypothesis to be accepted. Synthetic prions which were shown to induce neurodegenerative disease in mice that overexpressed PrP<sup>C</sup> were first produced in 2004. <sup>(70)</sup> A subsequent study used PMCA to generate prions from an initial mix of PrP<sup>C</sup> and PrP<sup>Sc</sup>, and these prions were able to induce neurodegenerative disease in wild type animals. <sup>(71)</sup> The demonstration that *de novo*, infectious

prions could be generated from both PrP<sup>C</sup> <sup>(72, 73)</sup> and rPrP <sup>(74-76)</sup> without initial seeding of PrP<sup>Sc</sup> and with minimal additional factors has been suggested as a crucial piece of evidence in favour of the protein-only hypothesis. <sup>(77)</sup> The importance of co-factors has been demonstrated, with prions formed in the presence of phosphatidylethanolamine and RNA being around 1 million fold more infective than 'protein-only' prions. <sup>(78)</sup> The role of co-factors is not thought to negate the protein-only hypothesis as the main mode of disease transmission is still protein based. <sup>(77)</sup>

The identification of different prion strains within TSEs provided a further challenge to the protein-only hypothesis, as conventional wisdom dictates that different strains of infectious particles are a consequence of changes to the genetic code. <sup>(79)</sup> It has been demonstrated that the properties of each strain can be encoded into the structure of PrP<sup>Sc</sup>, resulting in different conformations and aggregation properties that can be faithfully reproduced by PrP<sup>C</sup>. <sup>(80-82)</sup> Different strains of PrP<sup>Sc</sup> have been defined using their biochemical characteristics <sup>(83)</sup> and can be structurally distinguished from each other. <sup>(84)</sup> PMCA can replicate the properties of different strains over multiple cycles, <sup>(85)</sup> and it has also been suggested that the co-factors required for the generation of *de novo* prions may encode strain properties by affecting prion conformation. <sup>(78)</sup> It can therefore be seen that there is significant evidence to suggest that the properties of different strains are encoded by the structural conformation of the specific prion.

There have been suggestions recently that the definition of the term 'prion' should be changed to make it applicable to a wider range of neurodegenerative diseases that are not conventionally thought of as infective. <sup>(86)</sup> It has therefore been suggested that the definition of prion be changed to 'proteinaceous nucleating particle', to encompass the pathological events that occur in non-infectious proteinopathies and bring all these conditions under the umbrella of the prion concept.

### **1.1.2.3. Disease Transmission and Infectivity**

As discussed in section 1.1.1.2 a unique feature of the prion diseases is their infectious nature, unlike the other proteinopathies which are not conventionally seen as infectious. PrP<sup>Sc</sup> is thought to be the main constituent of the infectious agent, based originally on the finding that PrP<sup>Sc</sup> purified from the brains of diseased animals was closely associated with infectivity. <sup>(11)</sup> The route of transmission can depend on the disease being studied. <sup>(83)</sup> Scrapie has been shown to be readily communicable between flocks although the mechanism is not understood. BSE is believed to be caused by cattle being fed meat and bone meal, and a significant body of

evidence suggests that the BSE prions were subsequently transmitted to humans *via* ingestion of contaminated meat, resulting in vCJD. <sup>(1, 3-9)</sup> CWD is thought to be spread through grazing in contaminated areas. It has been suggested that human diseases can be passed on through the use of contaminated surgical equipment, transfusion of contaminated blood or the use of contaminated human growth hormone. Under experimental conditions the fastest method to induce disease is intracerebral inoculation of PrP<sup>Sc</sup>, although intravenous and intraperitoneal injections can also be used. <sup>(83)</sup>

An interesting feature of prion diseases is the species and strain specificities of the disease. Cell free conversion assays have shown that PrP<sup>Sc</sup> is able to induce the conversion of PrP<sup>C</sup> into the abnormal form. <sup>(68)</sup> However, attempts to drive this reaction using PrP<sup>C</sup> and PrP<sup>Sc</sup> from different species have so far failed. <sup>(87-90)</sup> A correlation between the known *in vivo* transmissibility of TSE agents between species and the efficiency of the cell free conversion has been observed. <sup>(90)</sup> Analysis of sequence homology indicates that efficient PrP<sup>Sc</sup> formation depends on homology in the central third of the PrP molecule. <sup>(91-93)</sup> Inoculation of one species with PrP<sup>Sc</sup> from another species will result in prolonged incubation times or even the absence of disease pathology depending on the PrP<sup>Sc</sup> strain and host animal. The codons located between residues 90 and 130 are thought to influence transmissibility in humans and other mammals. <sup>(94)</sup> Different strains are characterised by differences in proteinase K (PK) digestion kinetics, ratios of the three principal PrP glycoforms, incubation time and PrP<sup>Sc</sup> deposition levels. <sup>(95)</sup>

The process of prion infectivity is termed neuroinvasion and is reviewed in. <sup>(83)</sup> It is thought to be a biphasic process, with the initial phase involving colonisation of lymphoreticular organs, and the second involving the somatic nervous system. The exact mechanism of transfer through the peripheral nerves is not understood. The entry of prions into neurons and subsequent transit to the CNS may occur *via* direct uptake by nerve endings in the intestine. <sup>(96)</sup> The lymphoid system has been shown to contain infectious particles <sup>(97)</sup> and a decrease in lymphocyte numbers results in a decrease in peripheral prion pathogenesis unless prions are delivered directly to the CNS. <sup>(98)</sup> Conventional dendritic cells have a critical role in initial prion capture <sup>(99)</sup> and functional follicular dendritic cells (FDCs) are crucial for peripheral prion accumulation, <sup>(100)</sup> with  $\beta$ -lymphocytes also being essential as they provide the maturation signals for the FDCs. <sup>(101)</sup> The vagal nerve and sympathetic nervous system are subsequently involved in transporting prions to the CNS. <sup>(102)</sup> Phagocytes have also been implicated in spreading infection, even though they are also thought to be a likely pathway for prion clearance, as increasing numbers of aggregates may result in

saturation of phagocytic clearance, with smaller aggregates being cleared while larger aggregates remain intact. <sup>(103)</sup> It has also been suggested that prions may hijack tunnelling nanotubes, which are possibly a conserved mechanism for cell communication, to spread from the intestinal entry site to the CNS. <sup>(104, 105)</sup> The relationship between the size of the aggregate and its infectivity has been investigated, with the most infectious particles found to be small oligomers containing between 12 and 24 monomers. <sup>(106, 107)</sup>

Investigations into the transmission of PrP<sup>Sc</sup> within cell cultures have yielded further information on the mechanism of transmission. <sup>(108)</sup> Initial uptake of a preparation of PrP<sup>res</sup> has been shown to be independent of PrP<sup>C</sup>, although uptake was affected by the PrP<sup>res</sup> preparation and aggregate size and only occurred in a subset of cells. <sup>(109)</sup> The propagation of prions within persistently infected cells has been shown to occur primarily *via* vertical transmission of prions from mother to daughter cells, <sup>(110)</sup> implying that mechanisms are in place for the partitioning of seeds during cell division. Horizontal transmission has also been documented, with PrP<sup>Sc</sup> shown to spread to adjacent, uninfected cells after its release in exosomes from infected cells, <sup>(111-113)</sup> although horizontal transmission is generally less efficient. <sup>(110)</sup>

#### **1.1.2.4. Conversion of PrP<sup>C</sup> to PrP<sup>Sc</sup>**

According to the protein-only hypothesis, discussed in section **1.1.2.2**, the central event in prion disease pathogenesis is the conversion of the normal isoform of the prion protein, PrP<sup>C</sup>, into the abnormal form, PrP<sup>Sc</sup>. PrP<sup>C</sup> is thought to be converted to PrP<sup>Sc</sup> after it is translated, glycosylated, linked to a GPI anchor and carried to the cell surface. <sup>(114)</sup> Translation of PrP<sup>C</sup> to PrP<sup>Sc</sup> results in the conversion of a predominantly  $\alpha$ -helical structure into a predominantly  $\beta$ -sheet structure. <sup>(14)</sup> PrP<sup>C</sup> is composed of 43 %  $\alpha$ -helices with no  $\beta$ -sheet structures, while PrP<sup>Sc</sup> is composed of 20 %  $\alpha$ -helices and 34 %  $\beta$ -sheets, <sup>(115)</sup> with two of the four PrP<sup>C</sup> helices being converted to  $\beta$ -sheets. <sup>(116)</sup> The exact structure of PrP<sup>Sc</sup> has not been fully determined as the insolubility of the protein renders it unsuitable for structural studies, although the high  $\beta$ -sheet content explains the tendency of PrP<sup>Sc</sup> to form protease resistant aggregates within the brain. <sup>(115)</sup> Despite this, various structural models of PrP<sup>Sc</sup> have been proposed (see **Figure 2**). <sup>(117)</sup> The  $\beta$ -helix model, as seen in **Figure 2a**, was proposed on the basis of electron crystallography data, and was based on the contention that the structure of PrP is compatible with a parallel left-handed  $\beta$ -helical fold. As these structures readily form trimers, it was suggested that they would provide a natural model for a trimeric PrP<sup>Sc</sup> molecule. <sup>(118)</sup> The  $\beta$ -spiral model, as seen in **Figure 2b** was predicted by molecular dynamic simulations, which aimed to predict the molecular basis of conversion

using a model of PrP<sup>C</sup> within an environment that is conducive to conversion.<sup>(119)</sup> In both the  $\beta$ -helix and the  $\beta$ -spiral models the formation of  $\beta$ -sheets is thought to occur within the natively unfolded N-terminal region of PrP<sup>Sc</sup>, preserving the  $\alpha$ -helices that are characteristic of PrP<sup>C</sup>. The extended register  $\beta$ -sheet model, as seen in **Figure 2c** is radically different and proposes a complete refolding of the protein, thereby removing the structural motifs of PrP<sup>C</sup>. This model was based on studies using hydrogen-deuterium exchange coupled to mass spectrometry (HX-MS) and used either recPrP<sup>(120)</sup> or brain-derived PrP<sup>Sc</sup>.<sup>(121)</sup>

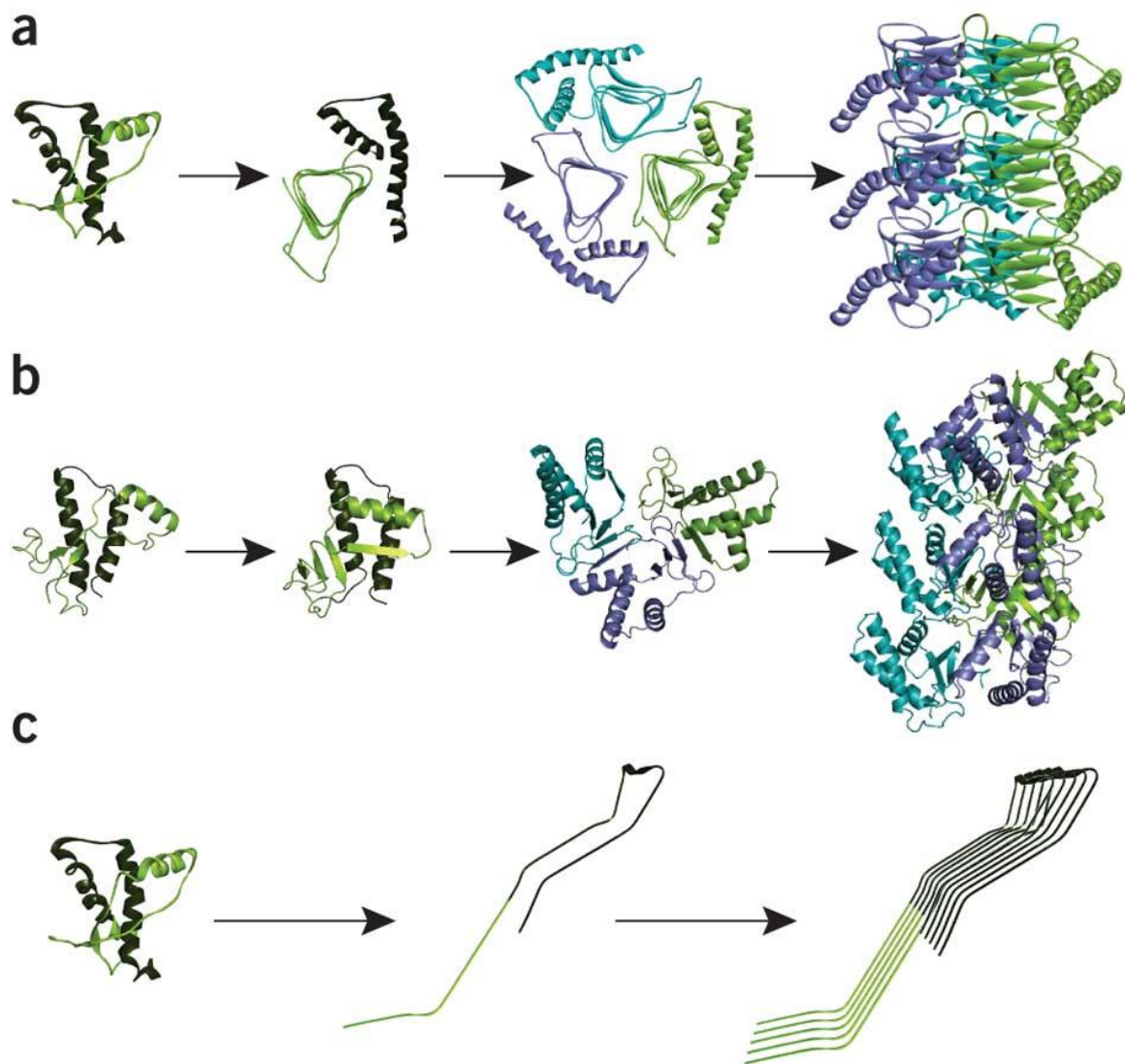


**Figure 2:** Diagrammatic representation of three of the different models proposed for the structure of PrP<sup>Sc</sup>. a. shows the  $\beta$ -helical model, with refolding of the N-terminal region of PrP<sup>C</sup> into a  $\beta$ -helix motif from residues 90 to 177. The  $\alpha$ -helical motif of PrP<sup>C</sup> is maintained. b. shows the  $\beta$ -spiral model, consisting of a spiralling core of extended sheets comprising short  $\beta$ -sheet strands, again with the maintenance of the  $\alpha$ -helical motif. c. shows the extended register  $\beta$ -sheet model, which proposes a complete refolding of PrP<sup>C</sup> into a structure composed mainly of  $\beta$ -sheets. Figure adapted from Diaz-Espinoza *et al.*<sup>(117)</sup>

A western blot of PrP<sup>C</sup> and PrP<sup>Sc</sup> can be seen in **Figure 3**. PrP<sup>Sc</sup> bands appear at a lower molecular weight after PK digestion as the PrP molecules are cleaved at the N-terminal. <sup>(115)</sup> Removal of a 12 kDa fragment results in a truncated form of PrP<sup>Sc</sup> which remains infectious and is known as PrP<sup>27-30</sup> or PrP<sup>res</sup>, and is resistant to PK digestion. <sup>(122)</sup>

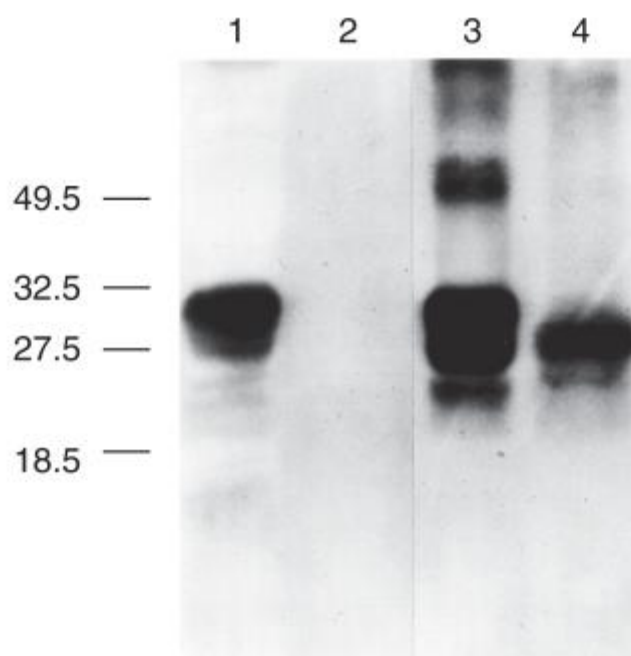


**Figure 3:** Western blot of brain homogenate from uninfected hamsters (1 and 2) and hamsters infected with scrapie (3 and 4). Lanes 2 and 4 are treated with PK, demonstrating the hydrolysis of PrP<sup>C</sup> and the presence of the PK resistant core in the infected sample known as PrP<sup>27-30</sup> or PrP<sup>res</sup>. Figure adapted from Colby and Prusiner. <sup>(12)</sup>

Following the introduction of PrP<sup>Sc</sup> from either infection or conversion from PrP<sup>C</sup>, the interaction of PrP<sup>Sc</sup> with PrP<sup>C</sup> is thought to lead to further conversion of native PrP<sup>C</sup>. This results in the accumulation of PrP<sup>Sc</sup> at the expense of PrP<sup>C</sup>, and is believed to be the main pathogenic event leading to neurodegeneration. <sup>(14)</sup> The mechanism of conversion of PrP<sup>C</sup> to PrP<sup>Sc</sup> is yet to be fully elucidated. The resistance of PrP null mice to infection has shown that PrP<sup>C</sup> expression is necessary for PrP<sup>Sc</sup> replication, <sup>(23)</sup> and dimeric PrP<sup>C</sup> has been shown to bind PrP<sup>Sc</sup> suggesting that conversion is instructed by PrP<sup>C</sup>. <sup>(123)</sup> Two theories have been suggested to explain how PrP<sup>Sc</sup> causes the misfolding of endogenous host PrP<sup>C</sup>; the template directed refolding model and the noncatalytic nucleated polymerisation model. <sup>(124)</sup> The template directed model (**Figure 4a**) suggests that the introduction of PrP<sup>Sc</sup> starts a catalytic cascade using PrP<sup>C</sup>, or an intermediate (PrP\*) as a substrate. Due to the high energy barrier it is thought unlikely that this would be a spontaneous event and would therefore require chaperone activity and energy. The involvement

of an, as yet unidentified, 'protein X' has been postulated. <sup>(125, 126)</sup> However, a recent study looking at the inhibition of PrP<sup>Sc</sup> propagation thought to be caused by competition for binding to protein X found that inhibition occurred without the need for an accessory co-factor. <sup>(127)</sup> This study also found that some mutations of the putative protein X binding site didn't inhibit the formation of PrP<sup>Sc</sup>, arguing against the involvement of protein X as a co-factor. <sup>(127)</sup>

The other model is the noncatalytic, or seeding model (**Figure 4b**), also known as the nucleation-dependent polymerisation model, which suggests that conformational change is thermodynamically controlled. Converted PrP<sup>Sc</sup> is only established once it is added to a seed or PrP<sup>Sc</sup> aggregate, with formation of the initial seed being the rate limiting step. The subsequent fragmentation of these aggregates, and the concomitant increase in aggregate numbers, results in exponential conversion rates. <sup>(128)</sup> In a cell free model PrP<sup>C</sup> can be converted to PrP<sup>Sc</sup> by incubation with PrP<sup>res</sup>. <sup>(71)</sup> Aggregation is intrinsic to conversion, supporting the nucleation theory, and the initial lag phase can be overcome by seeding with preformed aggregates. <sup>(129, 130)</sup> Protein Misfolding Cyclic Amplification (PMCA) was developed based on this seeding model of prion replication, and allows the amplification of PrP<sup>Sc</sup> by breaking up aggregates and then seeding them with PrP<sup>C</sup>, which is subsequently converted to PrP<sup>Sc</sup> with the same conformation as the original aggregate. <sup>(69, 71)</sup> A large number of cycles can cause increased amounts of *de novo* PrP<sup>Sc</sup>. <sup>(103)</sup> The use of the nucleation dependent polymerisation model as the basis for PMCA provides strong evidence that this model describes a key route by which prions are propagated, and this conclusion is further emphasised by the finding that prions in yeast and filamentous fungi propagate *via* protein aggregate fragmentation. <sup>(108)</sup>

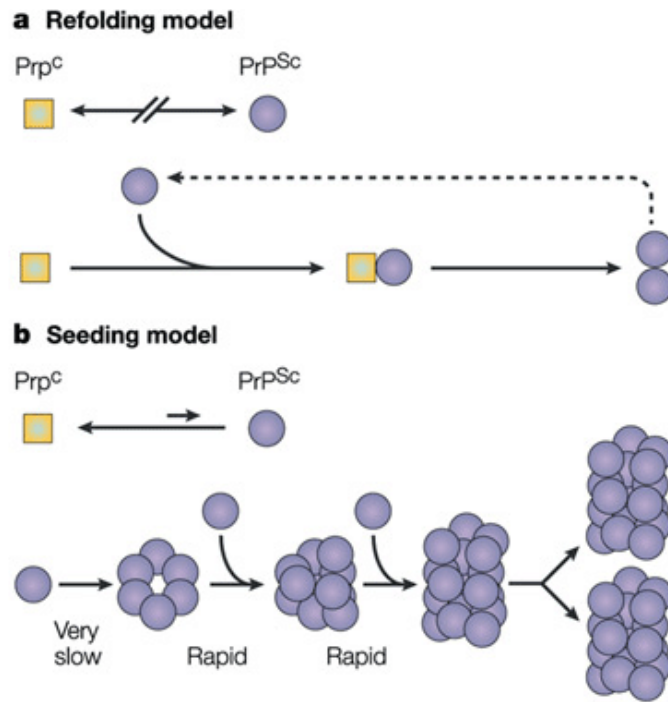


**Figure 4:** Models for the conversion of PrP<sup>C</sup> to PrP<sup>Sc</sup>. The refolding model suggests that the introduction of PrP<sup>Sc</sup> starts a catalytic cascade using PrP<sup>C</sup> or an intermediate as a substrate. The seeding model suggests that PrP<sup>Sc</sup> seeds result in the subsequent conversion and aggregation of PrP<sup>C</sup>. Figure adapted from Weissmann. <sup>(128)</sup>

Despite extensive investigations the site of PrP<sup>C</sup> conversion still remains elusive. It has been found that cholesterol is needed for the cell surface localisation of PrP<sup>C</sup>, and this in turn is essential for the formation of PrP<sup>Sc</sup>. <sup>(131, 132)</sup> Both isoforms of the protein are associated with lipid rafts <sup>(132-135)</sup> and the lipid rafts within the plasma membrane have been suggested as a possible site for conversion or interactions between the molecules. <sup>(136-139)</sup> Subsequent investigations have provided further evidence for this supposition, and the association of PrP with the lipid rafts is thought to be key to conversion. <sup>(140)</sup> The role of the lipid rafts is unclear; it is possible that they provide an optimal environment for conversion, they may contain a crucial co-factor required for conversion, or they may facilitate the co-internalisation of PrP<sup>C</sup> and PrP<sup>Sc</sup>, promoting their conversion. <sup>(141)</sup> The role of intracellular pathways in conversion has also been investigated, with PrP<sup>Sc</sup> aggregates being found along the endocytic pathway in early endosomes, the recycling compartment and the late endosomes and lysosomes. <sup>(142)</sup> The endosomal recycling compartment (ERC) has been identified as a site of PrP<sup>C</sup> conversion <sup>(143)</sup> and it has been suggested that conversion may occur as the two forms pass through the ERC together. <sup>(144)</sup> The generation of epitope-tagged PrP<sup>Sc</sup> had provided further insights, demonstrating that the initial infection of cells occurs within 1 minute of exposure, with the plasma membrane being the primary site of conversion. <sup>(145)</sup> After conversion the PrP<sup>Sc</sup> is rapidly internalised to the early

endosomes before either being recycled to the plasma membrane or being degraded by the lysosomes *via* retrograde transport to the golgi body. <sup>(144)</sup>

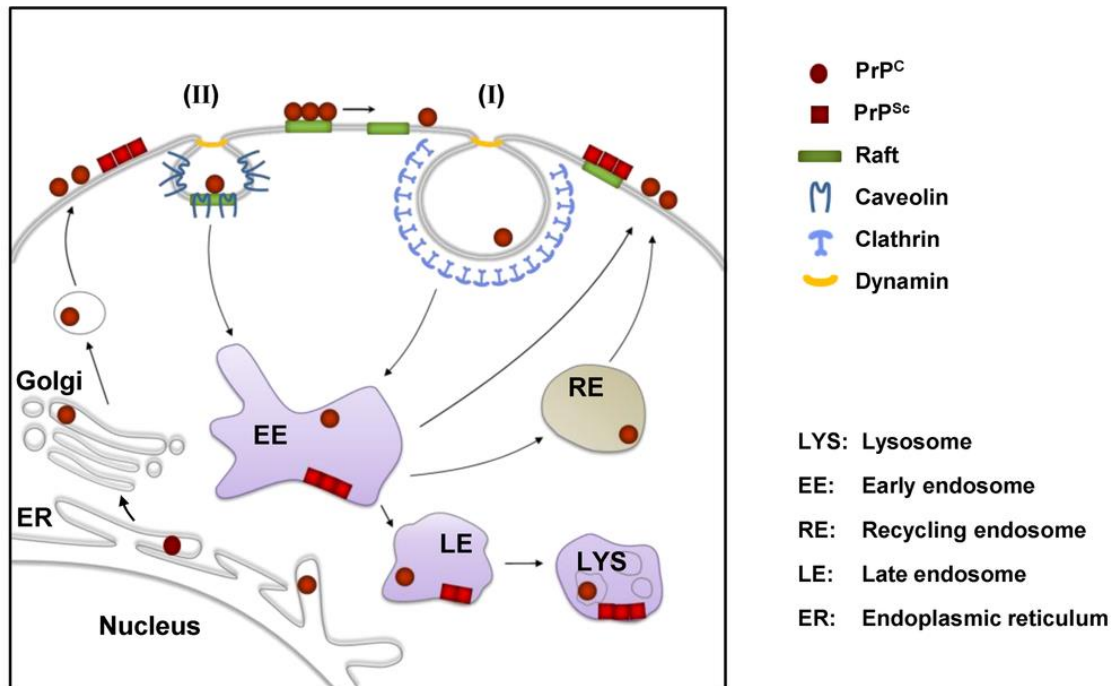


**Figure 5:** Diagrammatic representation of possible sites of PrP<sup>C</sup> conversion. PrP<sup>C</sup> is synthesised in the ER before translocation to the cell surface, where it resides in the lipid rafts. After internalisation *via* clathrin-dependent endocytosis (I) or caveolin-dependent internalisation (II) PrP<sup>C</sup> can be degraded by lysosomes or recycled to the cell surface *via* recycling endosomes. PrP<sup>C</sup> conversion is thought to occur either at the cell surface or along the endolysosomal pathway, and PrP<sup>Sc</sup> can accumulate at the cell surface or in intracellular vesicles such as lysosomes. Figure adapted from Grassmann *et al.* <sup>(146)</sup>

There are several molecules that have been implicated in the conversion of PrP<sup>C</sup> to PrP<sup>Sc</sup>. The GPI anchor is thought to be a major determinant of conversion, and enzymatic modification of the GPI anchor has been shown to reduce the capacity of PrP<sup>Sc</sup> to bind and replicate within cells. <sup>(147)</sup> The subunit of gamma-aminobutyric acid type A (GABA<sub>A</sub>) receptors known as GABA<sub>A</sub> receptor type 1 (*garbrb1*) has been found to associate with the formation of PrP<sup>Sc</sup> and inhibition of *garbrb1* dose dependently decreased levels of PrP<sup>Sc</sup>. <sup>(148)</sup> Glypican-1 has been proposed as a novel co-factor which acts by forming a scaffold which facilitates the interaction of PrP<sup>C</sup> and PrP<sup>Sc</sup> in lipid rafts. It has also been suggested that the heparin sulfate chains of glypican-1 may destabilise PrP<sup>C</sup> and therefore facilitate refolding in the presence of PrP<sup>Sc</sup>. <sup>(149)</sup> The presence of lipids and RNA was found to be required for the efficient formation of infectious prions *in vitro* using PMCA, suggesting that these co-factors may have an important role in conversion. <sup>(78)</sup> An

unidentified nucleic acid has been proposed as a catalyst for the conversion of PrP<sup>C</sup> to PrP<sup>Sc</sup>, and it was also postulated that the nucleic acid and PrP may rely on each other for propagation. <sup>(150)</sup>

The PrP<sup>Sc</sup> cleavage products are also thought to have a role in conversion. The C2 cleavage product is a C-terminal fragment about the same size as PrP<sup>res</sup>, and is the primary cleavage product in scrapie-infected brains. Decreased production of this cleavage product *via* calpain inhibitors can prevent the accumulation of PrP<sup>Sc</sup> in cell cultures. <sup>(151)</sup> On the other hand, the C1 cleavage product, which is membrane anchored, has been suggested as a dominant-negative inhibitor of PrP<sup>Sc</sup> formation by competing with PrP<sup>C</sup> for binding to PrP<sup>Sc</sup> seeds. <sup>(152)</sup> Finally, the endosomal-lysosomal system has been implicated in the formation of PrP<sup>Sc</sup>, with lysosomes being a likely site for conversion. <sup>(153)</sup>

#### **1.1.2.5. Mechanisms of Prion Neurotoxicity**

The mechanism by which PrP<sup>Sc</sup> induces a neurotoxic effect is still subject to debate, despite extensive literature on the subject. The identity of the neurotoxic molecule is also yet to be established with any certainty. Prusiner proposed PrP<sup>Sc</sup> as the infectious molecule due to the infectivity associated with PrP<sup>Sc</sup> purified from the brains of diseased animals. <sup>(11)</sup> Subsequent investigations have shown that the presence of PrP<sup>Sc</sup> does not always induce disease and *vice versa*; disease pathology has been observed without PrP<sup>Sc</sup> accumulation <sup>(154-156)</sup> while the accumulation of PrP<sup>Sc</sup> has been observed without the onset of clinical symptoms. <sup>(157, 158)</sup> PrP<sup>C</sup> is required for the development of disease, suggesting that the conversion of PrP<sup>C</sup> to PrP<sup>Sc</sup> is central to disease pathogenesis, <sup>(24, 95, 159, 160)</sup> and knockout of PrP<sup>C</sup> can reverse disease progression despite the accumulation of PrP<sup>Sc</sup>. <sup>(161, 162)</sup>

The dissociation of toxicity and infectivity was first suggested in 1993, <sup>(21, 24)</sup> with key evidence supporting this uncoupling coming with the identification of subclinical prion infections, characterised by experimental animals that were asymptomatic carriers of infection. <sup>(163)</sup> A possible explanation for the apparent uncoupling of neurotoxicity and infectivity has come from the suggestion that toxicity may be modulated by a toxic PrP intermediate. <sup>(158, 163)</sup> Studies have suggested that toxicity may be attributable to a specific toxic PrP that is distinct from PrP<sup>Sc</sup> and probably consists of small oligomers. <sup>(129, 152, 164)</sup> A general model was proposed with the rate of neurodegeneration depending on the levels of this toxic intermediate, PrP<sup>L</sup>, with the toxic effects occurring when PrP<sup>L</sup> levels crossed a hypothetical local threshold. <sup>(95)</sup> This was further developed into a model which proposed that disease progression occurs in two distinct phases;

In the first phase PrP<sup>Sc</sup> propagates exponentially, infectivity increases but no clinical disease is apparent, while in the second phase PrP<sup>Sc</sup> levels plateau, infectivity remains constant but clinical disease develops. The length of phase two was inversely proportional to PrP<sup>C</sup> levels. The results from this model suggested that PrP<sup>L</sup> may be produced by a pathway separate from, but linked to, propagation, with PrP<sup>Sc</sup> perhaps acting as a catalytic surface for PrP<sup>L</sup> production. <sup>(165)</sup>

Further insights into the nature of the toxic molecule have been revealed from the study of non-infectious PrP molecules that can induce neurodegeneration without the formation of infectious PrP<sup>Sc</sup>. <sup>(166)</sup> The residues at 105-125, in the central region (CR) of PrP, were found to be key to neurodegeneration, with mice expressing PrP with this area deleted showing a very severe neurodegenerative phenotype. A mechanism was proposed whereby a receptor molecule for PrP<sup>C</sup> is responsible for transducing a signal, with binding at two sites on PrP to this target molecule being required for normal signalling. These sites were suggested as the residues at 105-125 and an area in the C-terminal. Binding of one site only would induce a neurotoxic signal, while binding at both sites would either silence this signal or transmit a harmless signal. This theory is supported by the observation that PrP<sup>Sc</sup> may be conformationally altered in the CR, <sup>(167)</sup> and by the observed toxicity of the PrP peptide 106-126 <sup>(168-170)</sup> which would competitively inhibit binding of PrP<sup>C</sup> at both binding sites.

Along with the debate around the nature of the neurotoxic molecule, uncertainty remains over the pathways involved in inducing neurodegeneration. The requirement for PrP<sup>C</sup> to be present for neurodegeneration to occur has led to the suggestion that binding of PrP<sup>C</sup> to PrP<sup>Sc</sup> may trigger transmission of a neurotoxic signal from the extracellular milieu. <sup>(103)</sup> This is supported by the finding that antibodies that bind to PrP<sup>C</sup> and cause cross-linking of PrP<sup>C</sup> molecules can induce neurotoxicity. <sup>(171)</sup> The loss of the hypothesised PrP<sup>C</sup> neuroprotective effect, as a result of conversion to PrP<sup>Sc</sup>, is not thought to contribute to neurodegeneration, as PrP<sup>C</sup> depletion results in reversal of disease progression rather than further neurodegeneration. <sup>(83)</sup> A 'loss of function' hypothesis is therefore thought to be unlikely although the continued accumulation of PrP<sup>Sc</sup> without neurotoxicity in the absence of PrP<sup>C</sup> suggests that PrP<sup>Sc</sup> toxicity may be a PrP<sup>C</sup> dependent process. <sup>(159)</sup>

Abnormal topologies and altered trafficking of PrP<sup>Sc</sup> have also been suggested to contribute to neurodegeneration. <sup>(83)</sup> An excess of <sup>ctm</sup>PrP, a transmembrane form of PrP<sup>C</sup> with the C-terminal in the ER lumen, has been linked to neurodegeneration <sup>(16)</sup> although no direct evidence is currently

available to support this supposition. <sup>(103)</sup> A neurotoxic, cytosolic form of PrP<sup>C</sup> (PrP<sup>Cyt</sup>) has been identified that accumulates in the cytosol and forms PrP<sup>Sc</sup>-like structures, <sup>(172, 173)</sup> although, again, the role of this cytosolic PrP<sup>C</sup> has been debated. <sup>(174, 175)</sup> Endoplasmic reticulum (ER) stress, a commonly observed occurrence in prion diseases, <sup>(176)</sup> has been suggested to result in the formation of this toxic PrP species, and has therefore been suggested as a possible mechanism of toxicity. <sup>(177-179)</sup> The observation that PrP<sup>Cyt</sup> accumulated as a result of proteasomal inhibition led to further investigations into the role of the ubiquitin-proteasome system (UPS) in neurodegeneration. It was shown that propagation of PrP<sup>Sc</sup> in the presence of UPS inhibition resulted in the formation of PrP<sup>Sc</sup> aggregates that activated caspase-dependent neuronal apoptosis, suggesting that proteasomal inhibition may lead to neurodegeneration. <sup>(180)</sup> A direct relationship was also observed between prion neuropathology and UPS impairment in prion-infected mice, <sup>(181)</sup> and prion oligomers have also been shown to inhibit the proteasome <sup>(181, 182)</sup> suggesting that this may be a self-propagating cycle. It has been suggested that PrP<sup>C</sup> may mediate toxicity in conjunction with one of its interaction partners, although none of these are currently known to have any association with prion-linked neurodegeneration. <sup>(103)</sup> A final hypothesis relating to the role of PrP<sup>C</sup> is that PrP<sup>C</sup> may form transmembrane pores which could trigger neurotoxic damage. <sup>(183)</sup> However, there is currently no evidence that these pores form *in vivo* after infection.

Normal cellular pathways have also been suggested to have a role in prion induced neurodegeneration. <sup>(184)</sup> In prion infected mice the PERK/eIF2 $\alpha$  branch of the unfolded protein response (UPR), responsible for the transient shutdown of protein synthesis, was activated. This resulted in a 50 % decrease in synaptic proteins at 9 weeks post inoculation (wpi) with prions, with neuronal loss occurring a week later. <sup>(185)</sup> When prion infected mice were treated with inhibitors of this branch of the UPR at 9 wpi, global protein synthesis rates were restored and no neuronal loss in the hippocampus was observed. <sup>(186)</sup> The inhibitor mice also demonstrated dramatically increased survival. <sup>(186)</sup> There is evidence that this pathway is relevant not just in mice but also in human patients; increased UPR activation and the activation of PERK and eIF-2 $\alpha$  have been observed in the brains of patients with Alzheimer's disease, Parkinson's disease and Prion disease, suggesting that this may be a generic neurodegenerative pathway. <sup>(184)</sup>

Synaptic impairment has also been suggested to contribute to neurodegeneration. Mutant PrP has been shown to disrupt cerebellar glutamatergic neurotransmission by reducing the number

of functional channels in cerebellar granule neurons, resulting in synaptic dysfunction and neurotoxicity.<sup>(187)</sup>

### 1.1.3. Therapeutic Targets and Strategies

The majority of research into anti-prion therapeutics has targeted either the normal prion isoform (PrP<sup>C</sup>) or the abnormal isoform (PrP<sup>Sc</sup>). PrP<sup>C</sup> is a critical susceptibility factor for TSE diseases, with absence of PrP<sup>C</sup> in a host conferring resistance.<sup>(24, 159-162)</sup> The presence of PrP<sup>Sc</sup> also directly relates to TSE infectivity.<sup>(188)</sup> There are three main models for demonstrating an anti-prion effect.<sup>(189)</sup> The first *in vitro* method is to incubate PrP<sup>C</sup> with PrP<sup>Sc</sup> under particular conditions and measure the cell-free conversion of PrP<sup>C</sup> to PrP<sup>Sc</sup>.<sup>(68)</sup> This model system can be used to assess the impact of potential therapeutic compounds on conversion *in vitro*, but does not allow measurement of any effect on infectivity.<sup>(190)</sup> Protein misfolding cyclic amplification (PMCA) is widely used for these investigations and uses crude brain homogenates to achieve higher yields of PrP<sup>Sc</sup>.<sup>(191)</sup> PMCA has also been used to demonstrate the generation of *de novo* infectious prions capable of inducing disease in wild type animals.<sup>(72-74, 78)</sup> The second *in vitro* method employs infected cell cultures that persistently propagate infectious prions to screen potentially therapeutic compounds.<sup>(192, 193)</sup> In most cases prion infection does not induce any visible morphological or pathological changes to the cell cultures, meaning they can be used for this application.<sup>(108)</sup> Finally, animal models of prion disease allow the investigation of the effects of compounds in the whole organism.<sup>(189)</sup> Various compounds have been investigated although only two, quinacrine and pentosan polysulfate (PPS) have gone on to clinical trials. The quinacrine trials showed very limited success,<sup>(194)</sup> but the PPS trials were more encouraging with intraventricular administration increasing survival in patients with vCJD.<sup>(195-198)</sup> Interestingly, however, no alteration to the neuropathological changes in the brain was observed as a result of PPS treatment. An important but elusive goal is to be able to treat the disease after the appearance of symptoms, most likely by some combination of inhibiting PrP<sup>Sc</sup> formation, destabilising existing PrP<sup>Sc</sup>, blocking the neurotoxic effects of the infection and promoting the recovery of lost functions in the CNS.<sup>(199)</sup> Most efforts to date have targeted PrP<sup>Sc</sup> accumulation<sup>(200)</sup> although given the suggestion that a different molecule may be responsible for the neurotoxic effect this may not be the most effective strategy.<sup>(95, 129, 152, 158, 163, 165)</sup>

An important target in developing anti-prion therapeutics is identifying epitopes essential for the conversion of PrP<sup>C</sup> to PrP<sup>Sc</sup>, and also the identification of any co-factors that may be necessary for the reaction to occur. There has also been interest in using the immune system as a means of targeting prion diseases and work has pointed to a pivotal role for the immune system in prion infection from peripheral sites.<sup>(101, 201-204)</sup> As a result of the species and strain specificities of the disease, explained previously, it is desirable to be able to test compounds against multiple TSEs in multiple cell types.<sup>(205, 206)</sup>

#### **1.1.3.1. Anti-Prion Drug Discovery**

Several classes of anti-prion agents have been investigated (see **Table 2**). Although some of these have been successful in *in vitro* and in animal models there has been little success in clinical trials or in finding a compound that is able to reverse disease symptoms once they have first appeared. Certain compounds that show activity *in vivo* require administration at the point of infection to be effective, so would therefore be no use in 'real life' cases of prion disease. The best compounds currently available can only modestly delay disease onset or death *in vivo*, although a promising class of PERK inhibitors have been discovered that seem to be able to 'cure' infected animals.<sup>(186)</sup> These compounds work by reversing the shutdown of global protein synthesis caused by activation of the PERK/eIF-2 $\alpha$  branch of the UPR, therefore restoring synthesis of synaptic proteins and preventing neurodegeneration. Exactly how long the mice used in this study would have survived is unknown as the experiment had to be cut short due to side effects, but these initial studies showed great promise. Anti-prion compounds can exert their effect *via* a variety of different mechanisms. PrP<sup>C</sup> and/or PrP<sup>Sc</sup> can be stabilised by compounds that bind one or both isoforms, preventing conversion or aggregation. Limiting availability of PrP<sup>C</sup>, either by knocking it out or by altering the cell membrane composition to remove it from the cell surface, removes PrP<sup>C</sup> as a substrate for conversion. The cellular degradation machinery can be upregulated to increase degradation of misfolded PrP, and co factors thought to be involved in conversion can be targeted to reduce their efficacy. Other strategies include halting neuroinvasion, reducing oxidative stress and disrupting aggregates of PrP<sup>Sc</sup>, and all will be discussed in further detail.

**Table 2:** Compounds exhibiting therapeutic and/or prophylactic anti-prion effects tested in cell cultures and/or bioassays. Table adapted from Trevitt and Collinge. <sup>(207)</sup>

| Therapeutic agent class or mechanism                | Example therapeutic agents  |
|---|---|
| Glycosaminoglycans (GAGs) and GAG related compounds | Pentosan sulphate, dextran sulphate, heparin sulphate, congo red, suramin   |
| Polyamines/lipopolyamines                           | Branched polyamines, DOSPA  |
| Tricyclic derivatives of acridine and phenothiazine | Chlorpromazine, quinacrine, chloroquine   |
| Lysosomotropic compounds                            | Tyrosine kinase inhibitors  |
| Cholesterol reducing compounds                      | Mevinolin, simvastatin  |
| Polyene antibiotics                                 | Amphotericin B  |
| PrP <sup>C</sup> knockout                           | RNAi, shRNA   |
| Antibodies  | Monoclonal, polyclonal, Fab fragments   |
| Compounds targeting cellular pathways               | Trehalose, rapamycin, minocycline, phospholipase A inhibitors   |
| Compounds blocking conversion                       | Cyclic tetrapyrroles, sulfonated dyes, RNA aptamer D  |
| Miscellaneous compounds                             | DMSO, curcumin, brilliant blue, 2-aminothiazoles, 2,4-diarylthiazoles, indole-3-glyoxylamides, PrP <sup>C</sup> fragments, SOD mimetics |

The polysulfated polyanionic compounds, also known as glycosaminoglycans (GAGs), are components of the extracellular matrix and are thought to act by competing with endogenous GAGs for binding to PrP<sup>C</sup> and PrP<sup>Sc</sup>. <sup>(207)</sup> Pentosan polysulfate (PPS) is a simplified version of an endogenous GAG and has been shown to restrict the replication of PrP<sup>Sc</sup> and delay the onset of clinical disease when administered directly to the brain either before or around the time of infection in hamsters and mice. <sup>(208-210)</sup> PPS has also shown a prolongation of survival time in clinical trials when administered intraventricularly, as discussed previously. <sup>(195-198)</sup> It has been suggested to work by reducing the available concentration of PrP<sup>C</sup>, thereby limiting substrate for conversion, <sup>(211, 212)</sup> and has also been shown to compete with endogenous GAGs for binding to PrP<sup>C</sup>. <sup>(213)</sup> Other polysulfated, polyanionic compounds such as dextran sulfate and heparin have also demonstrated anti-prion activity *in vitro*, with dextran sulfate also active *in vivo*. <sup>(214-216)</sup> Congo red is an azo dye which is able to stack extensively and mimic larger sulfated polyanions, suggesting a mechanistic similarity to the GAGs. <sup>(207)</sup> Congo red and its analogues have been

extensively investigated in order to establish their anti-prion activities and determine a structure-activity relationship (SAR).<sup>(217-220)</sup> Congo red is thought to work by binding to and stabilising PrP<sup>C</sup>, and has been shown to bind non-specifically to rhPrP<sup>(221)</sup> and a carboxy-terminal domain of PrP (PrP 121-231)<sup>(222)</sup> by Surface Plasmon Resonance (SPR). It has been shown to decrease the  $\beta$ -sheet content of rhPrP and therefore increase susceptibility to PK digestion<sup>(223)</sup> as well as rendering PrP<sup>Sc</sup> resistant to denaturation, thereby stabilising the structure and reducing the potential for further conversion.<sup>(224)</sup> Additional studies have shown that congo red analogues can prevent polymerisation of PrP<sup>C</sup> in a cell free assay.<sup>(190, 218, 225)</sup> These analogues have also been suggested to work by increasing proteasomal degradation of PrP<sup>Sc</sup> by altering the rate at which PrP<sup>Sc</sup> is identified as a misfolded protein, and antagonising the inhibition of the proteasome by PrP<sup>Sc</sup>.<sup>(220)</sup> The other GAG related compound, suramin, causes the intracellular aggregation and degradation of PrP<sup>C</sup>, removing it from the cell surface.<sup>(226)</sup>

Some compounds have been found to work by rendering PrP<sup>Sc</sup> molecules protease sensitive by dissociating PrP<sup>Sc</sup> aggregates. Branched polyamines are thought to work in this manner.<sup>(227-230)</sup> Several preparations of branched polyamines were tested on prion infected neuroblastoma cells (ScN2a) and were found to eliminate all PrP<sup>Sc</sup> and cure the cells of infection.<sup>(227, 229)</sup> The branched polyamines were most effective in an acidic environment and were shown to accumulate in lysosomes, which are a known site of PrP<sup>Sc</sup> accumulation.<sup>(231)</sup> There are limitations to the efficacy of these compounds due to their size and poor bioavailability, so smaller lipopolyamines were investigated as an alternative. Some of these, such as DOSPA, were shown to effectively solubilise PrP<sup>Sc</sup> without any detrimental effects, although the problems of poor bioavailability and a limited spectrum of activity against different strains are problems that still need to be resolved.<sup>(228)</sup>

Tricyclic derivatives of acridine and phenothiazine have been investigated extensively and the lead compound from this group, quinacrine, has been taken through to clinical trials.<sup>(194)</sup> This group of compounds was originally chosen due to its ability to cross the blood-brain barrier (BBB), and quinacrine was shown to have an EC<sub>50</sub> 10 times lower than chlorpromazine or other derivatives.<sup>(232)</sup> An evaluation of quinacrine treatment showed that it can hamper *de novo* formation of PrP<sup>Sc</sup> and interact with PrP<sup>C</sup>, but also that it was ineffective *in vivo*.<sup>(233)</sup> Pharmacokinetic studies suggest that a sufficiently high concentration can be achieved in brain tissue, although it was not established how much of this was protein bound and how much was 'free'.<sup>(234)</sup> A subsequent study in sheep found that the free extracellular quinacrine

concentration was not high enough to be effective.<sup>(235)</sup> Quinacrine was used in a clinical trial in humans suffering from prion diseases but was not found to be effective, and this was thought to be down to inadequate drug concentration at crucial sites.<sup>(194)</sup>

Quinacrine and chloroquine are also reported to act in lysosomes<sup>(236)</sup> and lysosomotropic compounds are hypothesised to work *via* competitive inhibition of the GAG-PrP interaction, blocking of chaperones that aid PrP<sup>C</sup> unfolding or by destabilising PrP<sup>Sc</sup> through alteration of the lysosomal pH.<sup>(236)</sup> The tyrosine kinase inhibitor STI571 accelerated the cellular degradation of PrP<sup>Sc</sup> by triggering lysosomal degradation and these results confirm that PrP<sup>Sc</sup> can be degraded by lysosomal proteases.<sup>(131, 237)</sup> Other compounds shown to work by increasing PrP<sup>Sc</sup> degradation *via* redirection of PrP<sup>Sc</sup> to the lysosomes include chlorpromazine<sup>(238)</sup> and tamoxifen and its metabolites.<sup>(239)</sup>

The cell surface localisation of PrP<sup>C</sup> has been identified as a crucial factor in the conversion process, and cell surface localisation depends on the composition of the lipid rafts.<sup>(240)</sup> Cholesterol levels in the lipid rafts have been targeted to try and reduce the amount of PrP<sup>C</sup> on the cell surface, and interference with raft formation and association with PrP<sup>C</sup> by perturbation of cholesterol synthesis counteracted PrP<sup>Sc</sup> formation.<sup>(132, 241, 242)</sup> Treatment with Mevinolin, a HMG-CoA-reductase inhibitor that causes cholesterol depletion in cells, resulted in less cell surface PrP<sup>C</sup><sup>(243)</sup> and depletion of cholesterol through inhibition of synthesis and recycling was shown to reduce PrP<sup>Sc</sup> formation.<sup>(244)</sup> Statins have been shown to have an anti-prion effect by decreasing cellular cholesterol and reducing PrP<sup>C</sup> availability,<sup>(132)</sup> and compounds such as simvastatin and drugs that reduce cholesterol esters have been dosed synergistically with tricyclic compounds, with promising results.<sup>(245, 246)</sup> Simvastatin, quinacrine and despiramine (a tricyclic antidepressant 5 times more potent than quinacrine) dosed together were effective at concentrations at which they were ineffective individually<sup>(245)</sup> and cholesterol ester modulators decreased the EC<sub>50</sub> of quinacrine and chlorpromazine by up to 10 fold.<sup>(246)</sup> Polyene antibiotics such as amphotericin B can inhibit generation of PrP<sup>Sc</sup> in infected cell cultures and are thought to act by modifying the membrane lipid composition.<sup>(242)</sup> Glypican-1 is present in lipid rafts and is thought to aid conversion by forming a scaffold which facilitates interactions between PrP<sup>C</sup> and PrP<sup>Sc</sup>.<sup>(149)</sup> Reducing glypican-1 levels resulted in a decrease in the accumulation of PrP<sup>Sc</sup>.<sup>(149)</sup>

The development of PrP<sup>C</sup> knockout mice that were resistant to infection with PrP<sup>Sc</sup> led to investigations into the therapeutic possibilities of localised PrP<sup>C</sup> knockdown. Depleting neuronal

PrP<sup>C</sup> in mice with an established prion infection reversed early spongiform change, prevented neuronal loss and increased survival despite the extraneuronal accumulation of PrP<sup>Sc</sup>.<sup>(161)</sup> Subsequent experiments also showed that the cognitive and behavioural deficits that accompany early hippocampal spongiform pathology can be reversed by the depletion of neuronal PrP<sup>C</sup>.<sup>(162)</sup> Silencing of PrP<sup>C</sup> has been achieved using both RNAi and shRNA injections into the hippocampus, with treatment showing significant therapeutic benefit.<sup>(247, 248)</sup> A limitation to this treatment is that PrP<sup>C</sup> needs to be knocked out before neuronal loss is established, and targeting the hippocampus in the early stages of disease is an effective way of reducing the initial rate of prion propagation. With respect to human diseases it would be necessary to identify diseases at a much earlier stage than is currently possible to allow reversal of neurotoxic processes before it is too late.<sup>(249)</sup>

The use of antibodies against PrP for immunisation or therapy was not initially thought possible due to self-tolerance of PrP. However, it has been demonstrated that PrP<sup>Sc</sup> levels in infected cells can be reduced and disease onset delayed in mice by treatment with monoclonal antibodies.<sup>(250-252)</sup> The antibodies are thought to work by binding to PrP<sup>C</sup> and preventing conversion to PrP<sup>Sc</sup>, although increased endocytosis and enhanced degradation may also play a role in mediating the anti-prion effect.<sup>(253)</sup> Dimeric PrP has been successfully used to induce antibodies against cell surface PrP<sup>C</sup>, and these antibodies can decrease PrP<sup>Sc</sup> levels in prion infected cells by binding to cell surface PrP<sup>C</sup> and inhibiting conversion.<sup>(254)</sup> Adverse reactions to the Fc fragment of the whole antibody have been observed so Fab fragments have been investigated as a possible alternative.<sup>(255)</sup> Five fragments were investigated, and four of these were able to recognise cell surface PrP<sup>C</sup> and inhibit the formation of PrP<sup>Sc</sup>, probably through blocking PrP<sup>C</sup> as a substrate for conversion or stabilising the structure. Antibodies that can penetrate the blood brain barrier (BBB) or allow targeting of the immune system to PrP<sup>Sc</sup> plaques may increase efficiency.<sup>(256)</sup> The innate immune system has been implicated in the process of prion neuroinvasion and has therefore also been investigated as a possible therapeutic target. Neutralisation of the lymphotoxin- $\beta$ -receptor blocks the maturation of follicular dendritic cells which, in turn, halts scrapie neuroinvasion and prevents the spread of PrP<sup>Sc</sup> to the CNS, although this approach does require the time of peripheral prion infection to be known.<sup>(257)</sup>

Discoveries about the role of normal cellular process in disease pathogenesis have opened up new targets for anti-prion therapeutics. It has been suggested that a small decrease in the rate of PrP<sup>Sc</sup> formation could be sufficient to allow the cellular machinery to clear the remaining

misfolded protein, so total clearance of PrP<sup>Sc</sup> by any form of therapy may not be necessary. <sup>(258)</sup> Oligomers of misfolded PrP have been shown to inhibit the ubiquitin-proteasome system (UPS) <sup>(181, 182)</sup> and, in turn, inhibition of the UPS resulted in decreased degradation of PrP<sup>Sc</sup> as well as localisation of PrP<sup>C</sup> to the cell surface. <sup>(179)</sup> So far, however, there has been little progress in using compounds targeting the UPS as therapeutics. More progress has been made targeting the process of autophagy, the bulk degradation of cytosolic proteins and organelles, and a reduction of PrP<sup>Sc</sup> after treatment with drugs that induce autophagy has been shown. <sup>(259)</sup> Trehalose, an autophagy inducer, reduced PrP<sup>Sc</sup> in a time and dose dependent manner by increasing cellular degradation of the misfolded PrP <sup>(260)</sup> and similar results were obtained with rapamycin which increased the elimination of misfolded PrP before aggregation could occur. <sup>(261)</sup> Imatinib, an anti-cancer drug that activates autophagy, resulted in enhanced lysosomal degradation of PrP<sup>Sc</sup> *in vitro*. <sup>(259)</sup> Disruption of processes affecting apoptosis are thought to alter the progression of prion disease <sup>(262)</sup> and minocycline, a tetracycline with known neuroprotective activities, elicits anti-apoptotic effects against the neurotoxic activity of PrP peptides. <sup>(263)</sup> Inhibitors of intracellular signalling pathways such as phospholipase A inhibitors and glucocorticoids can reduce levels of PrP<sup>Sc</sup>, as can inhibitors of the mitogen-activated protein kinase pathways. <sup>(207)</sup>

The template assisted model of PrP<sup>Sc</sup> formation, discussed in section **1.1.2.4**, suggests that conversion of PrP<sup>C</sup> to PrP<sup>Sc</sup> requires chaperone activity, catalysed by an as yet unidentified 'protein X'. <sup>(124)</sup> Compounds that matched the spatial orientation and basic polymorphism of the proposed binding site for protein-X were found to dose-dependently inhibit the formation of PrP<sup>Sc</sup> at non-toxic concentrations of between 20 and 80  $\mu$ M. <sup>(264)</sup> There is the possibility that the anionic cyclic tetrapyrroles, sulfonated dyes, phosphorothioated oligonucleotides and sulfated glycans exert their inhibition of the formation of PrP<sup>Sc</sup> by binding to a site normally reserved for physiological ligands that are important for conversion. <sup>(199)</sup> In reference to the seeded aggregation model, RNA aptamer D reduced the formation of *de novo* synthesised PrP<sup>Sc</sup> and it is thought this might be due to its incorporation into PrP<sup>Sc</sup> aggregates, preventing the formation of high molecular weight aggregates. <sup>(265)</sup>

Various other molecules have been investigated as anti-prion compounds. Curcumin, a compound derived from turmeric, has anti-oxidative and anti-inflammatory properties as well as having anti-prion activity in both cell lines and mouse models. <sup>(266, 267)</sup> It has been shown to bind PrP<sup>Sc</sup> oligomers and fibrils and its binding site overlaps with the congo red binding site. <sup>(268)</sup> DMSO was shown to reduce PrP<sup>Sc</sup> accumulation and delay disease onset in mice when

administered at an estimated dose of 250 mg per day.<sup>(269)</sup> A high affinity was found between a cationic porphyrin and rhPrP using SPR, resonance light scattering and circular dichroism, suggesting that this could have possible uses as a therapeutic.<sup>(270)</sup> Brilliant blue is a dye with a symmetrical bifunctional structure that was thought to be likely to confer anti-prion properties.<sup>(271)</sup> Brilliant blue's role as a P2X7R antagonist was also hypothesised to confer neuroprotective properties.<sup>(271)</sup> It was found to prevent PrP<sup>Sc</sup> infectivity and accumulation *in vitro* and *in vivo* and this was attributed to specific anti-prion properties rather than P2X7R antagonism.<sup>(272)</sup> Investigations into a monocationic phenyl-furan benzimidazole found anti-prion activity in this previously untested class of compounds, with PrP<sup>Sc</sup> accumulation and infectivity inhibited.<sup>(273)</sup> 2-aminothiazoles have also been shown to be active *in vivo* and capable of accumulating at relevant concentrations in the brains of mice,<sup>(274, 275)</sup> while 2,4-diarylthiazoles<sup>(276, 277)</sup> and indole-3-glyoxylamides<sup>(278-280)</sup> have both been shown to be active *in vitro*. Fragments of PrP<sup>Sc</sup>, particularly the C1 cleavage fragment, have been suggested as dominant negative inhibitors of PrP<sup>Sc</sup> formation, probably working by competing with PrP<sup>Sc</sup> for binding sites on PrP<sup>C</sup>.<sup>(152)</sup> Finally, SOD mimetics have been tested to try and counteract the hypothesised loss of SOD-like function caused by the conformational changes to PrP<sup>C</sup>. These SOD mimetics were found to extend the incubation period, reduce nitrate and oxidative damage and reduce the brain lesion burden in treated mice.<sup>(281)</sup>

### 1.1.3.2. Cell Culture Models for Drug Discovery

Cell culture models have been used to investigate various different aspects of prion diseases, including the different biochemical properties of PrP<sup>C</sup> and PrP<sup>Sc</sup>, the nature of the infectious agent and biological markers of infection. They have also been widely used to screen drugs to assess their potential therapeutic benefit. Cell cultures were initially used to demonstrate that PrP<sup>C</sup> was the precursor to PrP<sup>Sc</sup> and also demonstrate that the PrP<sup>C</sup> endocytic pathway is crucial for the generation of the abnormal isoform.<sup>(136, 138, 282)</sup> Compounds identified in these initial *in vitro* screens can then be further investigated *in vivo* using animal models. The most widely used models are rodent models but there are also disease models in deer, sheep, cows and primates.<sup>(283)</sup>

The use of cell cultures in prion research is reviewed in Solassol *et al*<sup>(284)</sup> and Vilette.<sup>(285)</sup> The first successful attempt to establish a cell culture supporting prion replication was reported in 1970 with the establishment of the SMB cell line, a line of non-neuronal cells isolated from the brain of a mouse infected with Chandler scrapie.<sup>(286)</sup> The SMB cells are highly phagocytic and are

therefore thought to mimic cells involved in the uptake and replication of prions. <sup>(217)</sup> These cells can also be cured using PPS and then reinfected with different mouse-adapted scrapie strains including 139A (RML), 79A and 22F. <sup>(287)</sup> Subsequently, cell lines have been developed that are permissive to rodent-adapted scrapie strains, as well as cell lines that have been genetically engineered to express ovine PrP<sup>C</sup> and are therefore susceptible to two different naturally occurring scrapie isolates. <sup>(288)</sup>

The most common method of prion infection is to expose uninfected cells to an inoculum and check for formation of *de novo* PrP<sup>Sc</sup> by western blotting. Homologous cell line models express PrP<sup>C</sup> from the same species as the inoculum, while in heterologous models there is a mismatch between the species origin of the inoculum, PrP<sup>C</sup> or cell line. <sup>(284)</sup> Different cell models are susceptible to different prion strains, with some being susceptible to more than one, and some cell lines, such as the SMB cells, can be cured and then re-infected with a different strain. <sup>(287)</sup> The proportion of infected cells can range from 1 % up to 30 % so subcloning can help increase the susceptibility of cultures to infection, with cells expressing higher levels of PrP<sup>C</sup> being more susceptible to infection. <sup>(289, 290)</sup>

The development of the first cell cultures focussed on neuronal cells, and the neuroblastoma cells known as N2as are among the most extensively studied. <sup>(284)</sup> Subsequently many different types of cells have been shown to propagate PrP<sup>Sc</sup> including hypothalamic GT1 cells, pheochromocytoma cells, cholinergic neuronal cells, hippocampal derived cells, cells from the peripheral nervous system such as Schwann cells and non-neuronal cells including fibroblasts, microglia and skeletal myoblasts. <sup>(285)</sup> Epithelial cells from rabbits as well as neuroglial cells and neuronal primary cultures from mice have been developed that over express ovine PrP<sup>C</sup>, and these are susceptible to scrapie infection. <sup>(288, 291, 292)</sup>

A widespread use of cell culture has been in high-throughput drug screening programmes, where cells are dosed with different compounds and PrP<sup>Sc</sup> levels assessed by immunoblotting. <sup>(205, 217, 280, 293)</sup> This identifies compounds that can reduce PrP<sup>Sc</sup> levels, although strain specificity means that compounds which are active in a particular cell culture or against a particular strain may be ineffective in a different cell model. Investigations into the cell biology of PrP<sup>Sc</sup> using cell cultures have assessed the role of the proteasome in PrP<sup>Sc</sup> degradation, as well as investigating the involvement of the laminin receptor, heparan sulfate, lipid rafts, lysosomes and multivesicular bodies in the conversion of PrP<sup>C</sup> to PrP<sup>Sc</sup>, the intracellular accumulation of

misfolded protein and the cell to cell spreading of prions. <sup>(285)</sup> Cell lines that are particularly susceptible to infection have been used to test samples for infectivity, <sup>(294, 295)</sup> and work is ongoing to identify biochemical markers of prion disease. Investigations into the mechanisms of neurodegeneration have been limited by the absence of a cytotoxic effect of PrP<sup>Sc</sup> infection but there have been investigations into the role of SOD <sup>(296)</sup> and pro-apoptotic stimuli. <sup>(177, 180)</sup> The biological properties of cell-passaged prion strains are also an area of interest where cell culture has proved to be a powerful tool. <sup>(287)</sup> The development of cell lines that express human prions has so far been unsuccessful, although this would be a valuable tool in developing therapeutics that would be effective against human prion diseases. <sup>(297)</sup>

## **1.2. Drug Discovery and Candidate Drug Target Profiles (CDTP)**

### **1.2.1. Drug Discovery and Development Process**

The process of drug development has several stages, the aim of each one (after the initial lead discovery) being to eliminate compounds that are either not effective against the target (low efficacy) or have properties that make them unsuitable for use as a drug (unsatisfactory drug metabolism and pharmacokinetics or toxicity).

It is important to be aware of the typical phases of drug development, and the characteristics of candidate compounds that must be taken into account at each stage (all subsequent information in section 1.2 from <sup>(298)</sup> unless otherwise specified). The initial stage in drug discovery is to identify the target molecule. In this case the molecules being targeted are PrP<sup>C</sup> and PrP<sup>Sc</sup>. The relevance of the target molecule to the disease state has to be proven, as is the case in this instance. High throughput screening (HTS) can be used to identify active compounds (i.e. those showing an effect on the target molecule, whether real or hypothetical) and these 'hits' are then assessed *via* a relevant assay to find suitable lead compounds. Analogues of these lead compounds can then be synthesised to improve the potency, demonstrate a structure-activity relationship (SAR) and optimise the metabolic stability and physical properties. The desired

properties of the drug at launch can be used as a guideline to what is required. Once the lead compound has been optimised and the potency and safety proven it can move onto clinical trials.

Due to time and cost considerations, an increasingly common method of identifying potential lead compounds is by using a virtual high throughput screen (VHTS). This involves screening a large number of compounds against the target molecule using sophisticated computer systems. These systems assess the potential interactions between the compound being screened and the target based on the structures of the compound and potential binding sites on the target molecule. The Lipinski 'rule of five' is often used as a rough guide in determining whether a molecule is likely to have the desired properties to allow oral absorption. This can act as a starting point in choosing compounds for the VHTS. It proposes that poor oral absorption is likely if:

1. Molecular weight is greater than 500 (ideally should be 350 – 400)
2. Lipophilicity (as measured by LogP, see **Equation 1**) is greater than 5 (ideally should be -1 – 2.5)
3. There are more than 5 H-bond donors.
4. There are more than 10 H-bond acceptors.

Over 95% of marketed drugs adhere to at least two of these rules.

Once potential lead compounds have been identified by VHTS their activity needs to be confirmed by an appropriate assay using the compound and the target molecule. After activity is confirmed then the active compound may be confirmed as a lead compound. At this point, analogues of the lead compound can be synthesised. The aim of the analogue synthesis is to find compounds that have improved activity or pharmacokinetic properties, or reduced side effects such as toxicity. The synthesis of analogues can also allow the determination of a structure-activity relationship (SAR), in which certain substitutions at certain positions can be shown to confer improved efficacy. A quantitative SAR aims to establish the relationship between biological activity and properties such as molecular weight as well as surface and electronic properties:

1. **Lipophilicity** refers to the ability of a compound to dissolve in fats, oils, lipids and non-polar solvents. It can affect aqueous solubility, permeability, receptor binding, metabolism rate and plasma-protein binding. The logP is the intrinsic lipophilicity of the carbon skeleton and functional groups of a molecule in the absence of ionisation.

$$\log P = \log_{10} \left( \frac{[\text{solute}]_{\text{organic}}}{[\text{solute}]_{\text{aqueous}}} \right)$$

**Equation 1:** Equation for calculating the log *P* of a molecule

2. **Hydrogen bonding** is the attractive force between a hydrogen atom covalently bound to an electronegative atom (donor) and a second electronegative atom (acceptor). These bonds can be between molecules (intermolecular) or within molecules (intramolecular). They are stronger than a Van der Waals interaction but not as strong as a covalent or ionic bond. The Abrahams constant is a measure of the relative hydrogen bonding capability of functional groups. Hydrogen bonds play a vital role in determining the specificity of a compound's interaction with its target protein. <sup>(299)</sup>
3. **Electronic effects** are caused by the distribution of polarity affecting activity and distribution of compounds. Polarity will affect whether a compound will pass through the cell membrane and determine how well it will bind to its target.

## 1.2.2. Pharmacokinetics and Pharmacodynamics

### 1.2.2.1. The Candidate Drug Target Profile (CDTP) and Pharmacokinetics (PK)

The CDTP is an idea of what properties a compound would need to have to give it a good chance of reaching the market. An example of this is shown in **Table 3**. It encompasses *in vitro* and *in vivo* properties, a pharmacokinetic profile (the study of the movement of a compound within the body) and toxicity information. Quantitative pharmacokinetic measures are calculated by plotting the concentration of the drug in the blood plasma and measuring the area under the curve (AUC), also known as the integral. This can be used to describe a range of properties:

1. **Oral bioavailability (F)** is the fraction of the drug dose that is absorbed by the body and survives to general systemic circulation.
2. **Half-life (t<sub>1/2</sub>)** is the time taken for the drug concentration in the blood to reach half the original level.
3. **Volume of distribution (V<sub>ss</sub>)** is the volume that all of the drug in the body would have to occupy if present at the same concentration as that found in the blood.
4. **Clearance (Cl)** is the volume of blood from which all the drug is removed per unit time.
5. **Maximum Concentration** is the maximum concentration achieved after dosing.

6. **Plasma protein binding (PPB)** is the reversible binding of a compound to soluble proteins in the blood.

**Table 3:** An example of a CDT. Table adapted from Stocks *et al.* <sup>(298)</sup>

| Discipline                                  | Parameter                           | Preferred result                |
|---|-------------------------------------|---------------------------------|
| Biology                                     | Binding (isolated) IC <sub>50</sub> | <10 nM                          |
|   | Functional (cell) IC <sub>50</sub>  | <10 nM                          |
|   | Whole blood potency                 | <100 nM                         |
|   | Selectivity against other targets   | >100 fold                       |
|   | hERG                                | >10 μm                          |
| Drug metabolism and pharmacokinetics (DMPK) | Rat Hepatocytes Cl                  | <3 μl/min/10 <sup>6</sup> cells |
|   | Human Microsomes Cl                 | <1 μl/min/mg                    |
|   | Rat iv Cl                           | <20 ml/min/kg                   |
|   | Rat iv Vss                          | >0.5 L/Kg                       |
|   | Rat iv t <sub>1/2</sub>             | >2 hours                        |
|   | F (in two species)                  | >30%                            |
|   | P450 inhibition IC <sub>50</sub>    | >10 μM                          |
| Dose to Man prediction                      | <5 mg/kg                            |                                 |
| Physico-Chemistry                           | Molecular weight                    | <500 g/mol                      |
|   | Solubility                          | >50 μg/ml                       |
|   | PPB (Bound)                         | <98%                            |
|   | Calculated LogP                     | <5                              |

Activity at low concentrations, as demonstrated by the binding and functional IC<sub>50</sub>s, is desirable to avoid having to dose at high concentrations. The whole blood potency is important as this indicates how active the drug would be under conditions where a proportion of it may be unavailable due to binding to plasma proteins. A drug should be highly selective for its target molecule to avoid off-target effects, particularly on the hERG ion channels. Numerous structurally and functionally unrelated compounds can interfere with these channels, which are involved in cardiac action potential repolarisation. <sup>(300)</sup> Reduced function of hERG can increase the risk of potentially fatal cardiac arrhythmias so identification of compounds that may interfere with hERG channels is desirable as early as possible. High-throughput binding and functional assays can be used to measure membrane potential or Rb(+) flux, and these assays

can be combined with a more complex electrophysical investigation of compounds in cardiac myocytes to confirm inhibition of the hERG channels.

The drug metabolism and pharmacokinetic (DMPK) properties, as described previously, are significant as they give an indication of what will happen to the drug, over time, once it enters the body. It has been estimated that 40% of the failures in drug discovery are due to problems with pharmacokinetics and drug delivery. As a result of this the assessment *in vitro* of the absorption, distribution, metabolism and excretion (ADME) properties of compounds has become increasingly important in drug discovery.

Drug metabolism is routinely assessed by exposing the drug to rat hepatocytes or human microsomes and measuring the stability of the drug over time. This gives an estimate of how long it would take for a drug to be metabolised into inactive fragments and excreted. The precise duration of this process in the body cannot be directly extrapolated from microsomal stability, which is why rat *in vitro* clearance is also often measured. Low clearance rates (Cl) are desirable as if the clearance rate is too high the drug may be metabolised and excreted before it is able to work.

Pharmacokinetics measure the time course of drugs in an organism.<sup>(301)</sup> The volume of distribution (V<sub>ss</sub>) and oral bioavailability (F) are measures of how well the drug is absorbed into the body, and it is essential that these measures are high enough to allow the accumulation of active concentrations of the drug. Similarly, the half-life (t<sub>1/2</sub>) needs to be of a length which allows drug concentrations to remain high enough for long enough. Compounds with poor bioavailability and a short half-life (as estimated from microsomal stability) are unlikely to reach active concentrations, especially if the microsomal clearance rate is also high. Compounds that inhibit cytochrome P450 function may result in the accumulation of toxic levels of either the original compound, or compounds that are co-dosed, resulting in possible cytotoxic effects or adverse drug reactions. A low dose to man is desirable to limit the amount of compound that would have to be ingested and therefore reduce the possibility of off-target effects, as well as making the drug more practical to manufacture.

The physicochemical properties can be explained in terms of the Lipinski 'rule of 5' as discussed previously. Low molecular weight, good solubility and a logP below 5 are all desirable and increase the likelihood of a drug being successful. Lower levels of plasma protein binding (PPB)

are desirable as it is only the unbound fraction which can traverse cell membranes and therefore show activity.

### 1.2.2.2. *In Vitro* Drug Screening and Pharmacodynamics

Pharmacodynamics is the study of the relationship between the concentration of a given drug and the onset, intensity and duration of its pharmacological effects.<sup>(301)</sup> There are a wide range of *in vitro* tests that can be used to assess the activity of potential drug compounds. There is some debate about what is classed as an *in vitro* assay, so for convenience they can be divided into two classes; cell based assays and non-cell based assays.

Non-cell based assays use the purified target molecule to assess the activity of compounds against the target in isolation. For example, Surface Plasmon Resonance (SPR) is a technique which allows the binding interactions between the target molecule and compounds of interest to be studied directly and in real time. In terms of the CDTP (**Table 3**) the non-cell based assays are valuable in determining the binding affinity or  $K_D$  if it is not a functional assay, and this in turn can give an idea of the selectivity of a compound for its specific targets. Compounds that have very strong interactions with their targets are likely to have higher specificity than those with weaker interactions.

Cell based assays are the classic *in vitro* experiments and these assess the effects of a compound against the whole cell rather than just the isolated cellular component, allowing other properties such as toxicity to be determined. The type of cell line assay to be used depends on the target being assessed, and cell lines are often developed to provide a specific readout for the targets of interest. The efficacy of a compound is normally expressed as the concentration at which it exerts 50% of its effect. This is known as the  $EC_{50}$ , or half maximal concentration. Another common method of determining the effect of a compound is the concentration at which 50% of the cells are killed, known as cytotoxicity and expressed as  $LD_{50}$ . For assays that do not use cytotoxicity as a measure of a compound's effect a toxicity assay can be carried out in tandem. This ensures that compounds are not classified as active when they are actually toxic. A common method is to use yellow MTT (3-(4,5-Dimethylthiazol-2-yl)-2,5-diphenyltetrazolium bromide) which stains the nucleus of viable cells. This stain is converted to a purple colour by the addition of 1M HCl in isopropanol which can be quantified using a plate reader.

## 1.3. 3D Cultures

### 1.3.1. Introduction

At the beginning of the 21<sup>st</sup> century it was observed that increased chemical synthesis capabilities had resulted in large numbers of molecules being synthesised, with potential targets being identified afterwards. <sup>(302)</sup> All these compounds needed to be assessed for potential activity against the chosen target, with inactive or unsuitable compounds being identified as soon as possible. Identifying these compounds during the early stages of the drug discovery process has become a priority due to escalating costs further down the pipeline. <sup>(303)</sup> To this end, *in vitro* cell cultures have been used to carry out functional and toxicity assays on compounds identified by, for example, binding assays, and cell based testing has become a key component of drug discovery programmes. <sup>(304)</sup>

Currently, the majority of High Throughput Screening (HTS) for drug compounds is done using cells cultured in 2D monolayers, which are compatible with automated platforms and well established analytical techniques. However, there has long been a concern that these systems are not sufficiently representative of the *in vivo* situation, due to differences in cell morphology, polarity, receptor expression, oncogene expression, interaction with the extracellular matrix (ECM) and overall cellular architecture. <sup>(305)</sup> It is becoming increasingly important to identify poorly functioning compounds as early as possible, and therefore reduce the costs associated with drug failure at later stages of the drug discovery pipeline.

The potential of 3D cultures to fill this gap between 2D monolayers and *in vivo* systems is of increasing interest. The growth and function of cells in a 3D environment are noticeably different to cells grown in a monolayer, <sup>(306)</sup> and creating conditions that more accurately mimic the *in vivo* microenvironment would help increase predictive accuracy in the development of pharmaceutical compounds. Various techniques have been used to try and study cells in a more natural 3D environment, including liquid overlay and forced floating techniques, spinner flasks, artificial scaffolds including hydrogels, and spheroids in hanging drops. All of these techniques have their advantages and disadvantages, with a key problem being the lack of anything that can be successfully used in high-throughput applications.

### 1.3.2. The Advantages of a 3D System

While 2D systems are useful in terms of HTS and ease of culturing, a major problem is that they lack contact with other cells, and with the ECM. Cells grown in monolayers are typically 3 $\mu$ m thick, with the vast majority of surface area being exposed to either the growth medium or the plastic surface the cells adhere to. As a result there is very limited cell-cell contact. Conversely, their 3D counterparts tend to be ellipsoids with a diameter of 10 – 30  $\mu$ m, with nearly all the surface area being exposed to other cells or the ECM. <sup>(307)</sup>

The cell-cell and cell-ECM contacts in 3D cultures are important for a number of reasons and are central to their ability to more accurately re-create *in vivo* conditions. Cell-cell communication can occur *via* chemical-biological routes or by mechanical signalling, and also by direct contact through the cytoplasm. It occurs in its most direct form when cells adhere to each other. This requires contact over a large surface area to allow the structures to form, and therefore is more prevalent in 3D culture. This increased coupling aids cell-cell communication and is therefore important in cell function. <sup>(307)</sup>

*In vivo*, a complex, 3D ECM supports cells *via* the facilitation of communication through direct contact and by the secretion of a wide variety of cytokines and trophic factors. <sup>(308)</sup> It therefore stands to reason that careful refinement of the extracellular environment will affect the way cells behave. Interactions with the ECM are known to be important in defining cell function and mimicking *in vivo* conditions. The cell-ECM interactions work with the cell-cell signalling to maintain the homeostasis and specificity of the tissue, <sup>(309)</sup> and key processes in the cell life cycle, such as proliferation, migration and apoptosis, are regulated by organising principles determined by the ECM. <sup>(310)</sup> For example, cell-cell and cell-ECM interactions are essential for tissue morphogenesis in developing embryos. <sup>(311)</sup> In some cases the ECM can affect chromatin structure and therefore gene expression, which can differ between cells in 2D and 3D. <sup>(312)</sup> This difference in gene expression can lead to changes in phenotype in 3D culture, with it varying dramatically depending on the extracellular context. <sup>(313)</sup> Culturing cells in 3D is therefore more representative of *in vivo* conditions, and can facilitate the investigation of functional tissues rather than individual cells.

### 1.3.3. Methods of 3D Culture

Various methods have been investigated for culturing cells in 3D. As a general rule, these involve either the creation of 3D spheroids or the use of extracellular scaffolds to help the formation of 3D structures. Spheroids are the system of choice for therapeutic studies, particularly in cancer therapeutics,<sup>(314)</sup> while scaffolds have been used in tissue engineering.<sup>(315)</sup>

#### 1.3.3.1. Liquid Overlay and Forced Floating

This technique works on the principle of preventing cells adhering to a surface so they instead adhere to each other (see **Figure 6**). Typically, plates are coated with agar, causing cells to migrate towards each other, aggregate, and then form spheroids that increase in size.<sup>(316)</sup> A centrifugation step can be included if necessary to aid aggregation and spheroid formation. This method was found to be fairly reliable, particularly for tumour cell lines which tend towards aggregation. Spheroid size can be controlled to some degree by the initial seeding density, but the time involved in coating plates means that this method is not suitable for high throughput applications.<sup>(305)</sup>

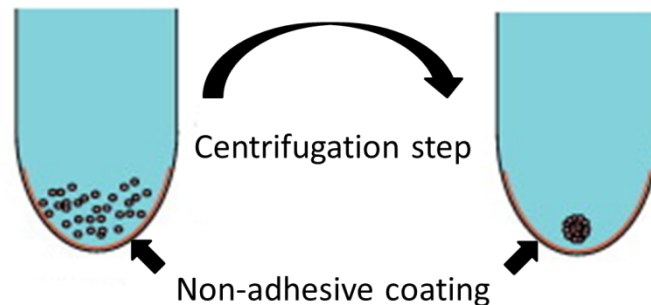


**Figure 6:** Forced floating method. Cells are grown on plates with a non-adhesive coating and subsequently aggregate to form spheroids. Figure adapted from Breslin and O'Driscoll.<sup>(305)</sup>

#### 1.3.3.2. Spinner Flasks

The spinning flask technique is similar to the liquid overlay technique in that it forces cells to aggregate and form spheroids by preventing them from adhering to the surfaces of the culture vessel. It does this by constantly mixing the cell suspension to encourage cell-cell interactions until spheroids of the required size are formed, either by gently stirring the cell suspension or by rotating the culture vessel (see **Figure 7**).<sup>(305)</sup> Depending on the bioreactor, large amount of spheroids can be produced, although they are normally of varying size.<sup>(317)</sup> Forming spheroids using the liquid overlay method and then transferring them to a spinning bioreactor to increase

in size can result in a much more homogenous population. <sup>(318)</sup> The NASA developed rotary cell culture system simulates microgravity, allowing cells to aggregate, grow three dimensionally and then differentiate. It results in cells that are similar to their *in vivo* equivalents, and through co-culturing can be used to create complex, heterologous 3D structures. <sup>(316)</sup> The primary disadvantage of spinner flasks is that the shear forces associated with stirring can alter the physiology of cells, although this can be overcome by using rotating culture vessels. <sup>(317)</sup>

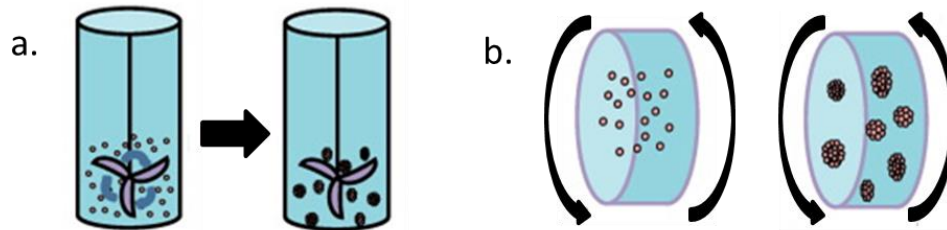


**Figure 7:** Agitation based approaches; a. spinner flasks and b. rotating culture vessels are used to generate spheroids. Figure adapted from Breslin and O’Driscoll. <sup>(305)</sup>

### 1.3.3.3. Hanging Drop Techniques

This technique promotes the formation of spheroids by culturing cells in a ‘hanging drop’ of medium. This encourages aggregation and the subsequent formation of cell-cell interactions in the bottom of the drop to form homogenous spheroids, with size being controlled through the initial seeding density (see **Figure 8**). The lack of an artificial scaffold means that concerns about the effect these may have on cell structure are mitigated, although the size of the spheroids that can be formed are limited by the amount of liquid the hanging drop can contain before succumbing to gravity. <sup>(305)</sup> This technique was originally developed to induce the formation of embryoid bodies, containing hematopoietic, endothelial, muscle and neuronal cells, from embryonic stem cells. <sup>(319)</sup> It was then modified to aid in the culture of the human hepatoma line HepG2 which failed to form spheroids in either forced floating or spinner flask methods. The hanging drop technique saw the cells accumulate at the bottom of the drop before forming a tightly packed spheroid which proceeded to display a typical solid tumour growth pattern. Structural examination of the spheroids showed them to be well organised 3D structures with a complex ECM, with the same features being found in spheroids cultured from different cell lines. <sup>(320)</sup> The use of this technique to create fast growing, homogenous spheroids led to its development for use in a 384 well, high throughput screen, that is compatible with existing instrumentation, <sup>(321)</sup> and specially designed plates in both 96 well and 384 well formats are available.

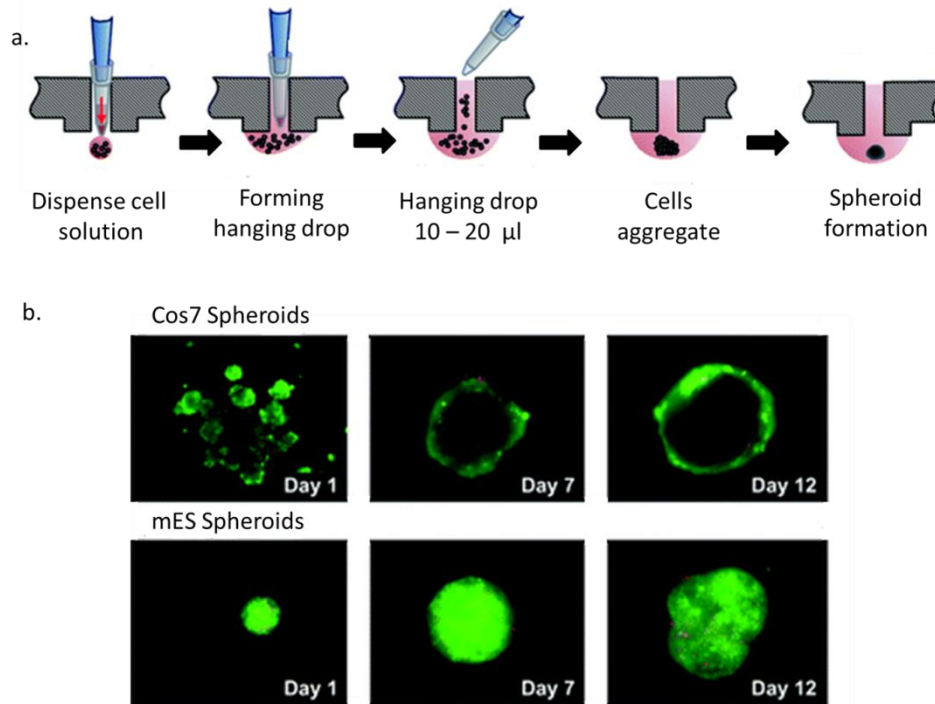


**Figure 8:** Formation of hanging drop spheroids; a. diagram depicting the method of formation. A cell suspension is pipetted through the access hole to form a drop on the bottom of the plate. The cells aggregate at the bottom of the drop, forming a spheroid after around 1 day. b. fluorescence images of live/dead staining of Cos7 (African green monkey kidney fibroblast cells) and mES (murine embryonic stem cells) spheroids over a 12 day culture. Figure adapted from Tung *et al.*<sup>(321)</sup>

#### 1.3.3.4. Scaffolds

Scaffolds work by providing a framework around which 3D structures can form. Cells attach to, and migrate along, scaffold fibres and fill the gaps of the scaffold as they divide, forming 3D structures whilst maintaining differentiation.<sup>(322)</sup> Scaffolds need to have the following characteristics: have appropriate surfaces for cell adhesion, proliferation and differentiation, be biocompatible, be highly porous with a high surface area to volume ratio, have an interconnected pore network and be resistant to mechanical *in vivo* stresses.<sup>(323)</sup> Collagen is the most commonly used scaffold, but pre-engineered scaffolds made of natural materials such as collagen composite, or synthetic polymers such as D,D-L,L polylactic acid (see **Figure 9**), have also been used to successfully grow cells including hepatocytes, neurons, endothelial cells, osteoblasts, chondrocytes, fibroblasts and smooth muscle cells.<sup>(316)</sup>

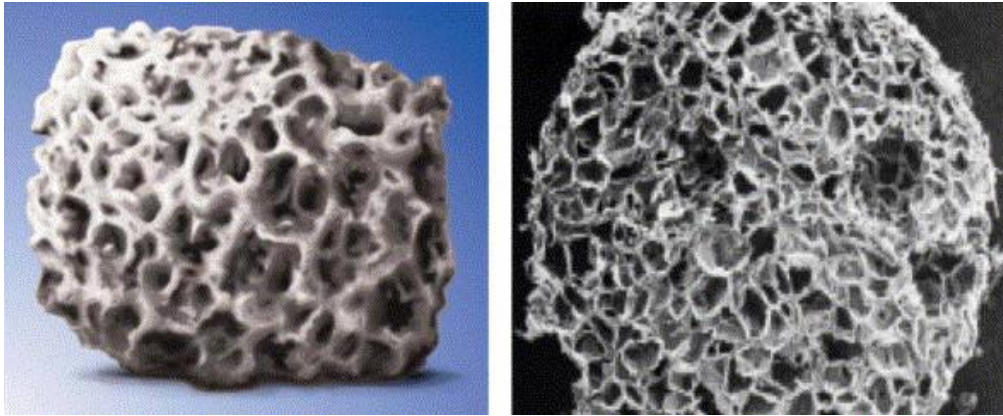


**Figure 9:** An example of a pre-engineered, biodegradable scaffold. This is a BD™ 3D open cell polylactic acid (OPLA®) scaffold. Figure adapted from Kim. <sup>(316)</sup>

Various different materials have been used as scaffolds, including natural products such as alginate and collagen, naturally derived and synthetic polymers and hydrogels formed of a cross-linked natural base material (agarose, collagen) with a high water content. <sup>(308)</sup> Problems associated with polymers (degradation) and hydrogels (expense, short shelf life, consistency), have been overcome by the development of non-degradable scaffolds made from inert materials such as polystyrene. <sup>(308)</sup> Scaffolds can allow the mechanical stress experienced by tissues *in vivo* to be replicated, and co-cultures of two or more cell types can produce complex tissues that more closely mimic the *in vivo* situation. <sup>(307)</sup> Scaffolds have also been used to culture human embryonic stem cells (hES), which hold a lot of potential for transplant therapies. So far, attempts to encourage hES cells to form viable and complex 3D structures has proved difficult, but the use of polymer scaffolds enabled their growth, differentiation and the formation of complex structures. <sup>(324)</sup>

#### **1.3.3.5. Microcarrier Beads**

Microcarrier beads were first developed in the 1960s as an alternative to 2D monoculture, and were found to support the attachment, aggregation and proliferation of a number of transformed cell lines and primary cells. <sup>(325)</sup> Microcarrier beads are small spheres 100 – 400  $\mu\text{m}$  in size and have a large surface area to volume ratio which permits a high cell density. They are also widely available. <sup>(307)</sup> They can be used to co-culture cells in close proximity <sup>(326)</sup> and are an excellent tool for studying cell-cell and cell-substratum interactions, cell differentiation and maturation and metabolic studies. <sup>(316)</sup>



**Figure 10:** Brightfield image showing human mammary endothelial cells seeded onto microcarrier beads 133 – 215  $\mu\text{m}$  in size. Black arrows indicate cells attached to the surface of the beads (300x magnification). Figure adapted from Kim.<sup>(316)</sup>

#### **1.3.3.6. Microfluidic Systems**

A microfluidic system has been described which can support 3D culture (see **Figure 11**).<sup>(327)</sup> A cell suspension is passed through the main chamber where micropillars allow the cells to attach and grow. This aids cell-cell contact, and the subsequent addition of a collagen matrix can facilitate investigation of cell-ECM interactions. It has been suggested that this might be a good platform for HTS, although it doesn't allow retrieval and characterisation of the spheroids. A 3D model of Alzheimer's disease, based on a microfluidic system, has been developed and this found that low levels of flow resulted in neurospheroids that were larger and formed more robust and complex neural networks than those formed in static flow conditions.<sup>(328)</sup>

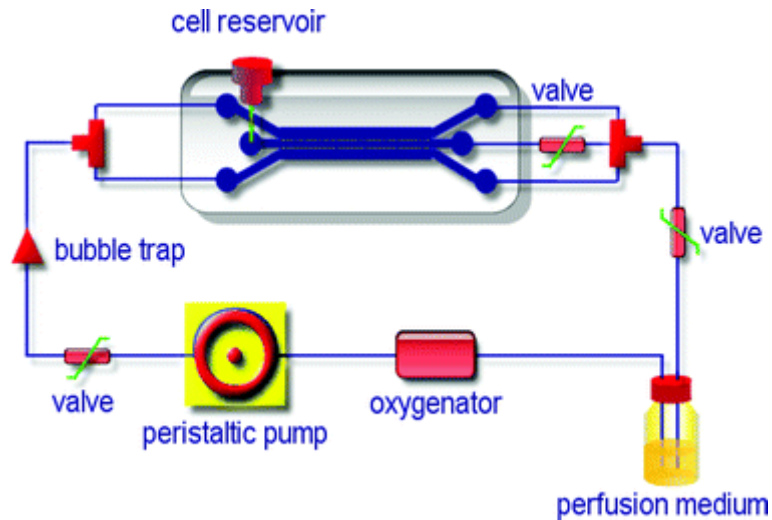


**Figure 11:** Schematic representation of the closed loop perfusion culture system used for 3D culture. Within the cell reservoir cells are immobilised using the micropillars, and the formation of an ECM is facilitated by laminar flow complex coacervation. This is followed by perfusion culture of the immobilised cells. Figure adapted from Toh *et al.* <sup>(327)</sup>

### 1.3.3.7. Organotypic Cultures

Organotypic, or explant, cultures are slightly different to the methods discussed above as they involve the transplantation of biological tissues into culture, rather than the 3D culture of individual cells, where the normal cellular function within the tissue can be maintained for a limited period of time. <sup>(329)</sup> In some cases the entire organ may be transplanted, or dissected slices of the organ may be mounted onto siliconised filter paper or porous culture membranes. This allows the sections to maintain their cytoarchitecture and pattern of cell differentiation. <sup>(307)</sup> Explant cultures have been successfully generated using tissue from lungs, small intestine, colon, brain and aorta among others. <sup>(330)</sup> For example, skin explant models have been suggested to be a useful model for wound healing, inflammation processes, autoimmune diseases, malignant transformation, stress and ageing <sup>(331)</sup> while gastrointestinal (GI) explant cultures offer a model for examining the toxic effects of xenobiotics on the GI tract and the pathogenesis of intestinal tract diseases. <sup>(332)</sup> Tissue organoids can also be formed from epithelial tissues without their corresponding stromal cells. After being freshly isolated from primary mammalian organs the organoids are typically explanted into commercially available matrices before processing. <sup>(330)</sup>

### 1.3.4. Applications for 3D Culture

The long term aim in developing 3D cultures has been to develop a system that could replicate the advantages of 2D cultures but produce data that is far more relevant to the *in vivo* situation. So far there has only been limited success in creating 3D systems that can be used in HTS, although some progress is being made in this area.<sup>(321)</sup> There are, however, some specific applications where 3D culture has been used to great advantage, and other areas where it could potentially be extremely valuable.

#### 1.3.4.1. 3D models in Cancer Research

The most widely used model in cancer research is the multicellular tumour spheroid (MCTS) model system. The use of multicellular spheroids was adapted for use in cancer research in the 1970s<sup>(333)</sup> and they were specifically manufactured for testing the effects of radiation and chemotherapeutic drugs on tumour growth. The discovery that breast cancer cells were more resistant to chemotherapeutic drugs when cultured in 3D rather than 2D emphasised the importance of 3D culture as a more relevant *in vitro* screen.<sup>(307)</sup> Their ability to replicate the *in vivo* behaviour of tumours is based on 4 important features:<sup>(334)</sup>

1. Morphological, functional and mass transport features of *in vivo* tissues can be replicated.
2. Many characteristics of tumours can be approximated with regard to growth kinetics and the effect of the microenvironment. Spheroids larger than 400-500 nm tend to have a necrotic core.
3. The spherical geometry allows direct structure-function analysis.
4. Spheroids can be used to co-culture different cells.

Due to these factors MCTS are a well-controlled 3D experimental model that can be used to assess potential chemotherapeutic strategies, with co-cultures providing the potential for studies into local penetration, distribution and efficacy of new drug candidates.

Other models have also been used to investigate different aspects of cancer biology.<sup>(335)</sup> 3D skin epidermal models have been used in studies of tissue repair and as models for cancers such as squamous cell carcinoma, melanoma or esophageal carcinoma. The early steps of metastasis have been modelled in 3D and co-cultures between normal and malignant cells used to model invasion. Angiogenesis has been investigated for its therapeutic potential as disruption of the nutrient supply to the tumour could prevent growth. Models have revealed the need for certain

factors to allow angiogenesis to occur, therefore identifying possible therapeutic targets. 3D models have also been used to investigate the tumour microenvironment.

#### **1.3.4.2. Other Models**

A number of other models have been developed to investigate the efficacy and delivery of therapeutic strategies in a more realistic setting.<sup>(336)</sup> Liver tissue models have been developed to help better understand liver diseases and drug metabolism, with the hope that they may be able to provide more relevant pharmacokinetic information. 3D models of cardiac tissue have been developed to help understand the mechanism of heart disease and also to produce implantable constructs that could help restore function in diseased hearts. Polymer scaffolds have been used to construct models of skeletal muscle and vascular smooth tissues which demonstrate similarities in morphology, contractility and differentiation to *in vivo* tissues. These have been used for drug testing and to investigate aspects of tissue repair and regeneration. Attempts have been made to model bone tissue in order to create replacements in case of injury, although refinements in cell type, cell number and scaffold material are still needed before this is successful. A model of corneal tissue has been developed for use in drug permeation and efficacy studies as the cornea is the main route of absorption for many clinically used ocular drugs. A 3D model has been developed to model the distribution and spread of adenoviruses, and epithelial raft cultures are being investigated as a model for the replication of pox and herpes viruses and to evaluate the efficacy of antiviral agents.<sup>(329)</sup> Progress has also been made recently in the development of 3D neuronal models to investigate Alzheimer's disease.<sup>(328, 337, 338)</sup> While the culturing of individual cells into 3D structures has not been used extensively in the research of anti-prion therapeutics, progress has been made using organotypic cultures. A model of prion-induced neurodegeneration has been developed using cerebellar organotypic slice cultures,<sup>(339, 340)</sup> and the prion organotypic slice culture assay allows the amplification and titration of prions under conditions that closely resemble intracerebral infection.<sup>(341, 342)</sup>

#### **1.3.4.3. Drug Safety Testing**

Current drug safety testing strategies rely on testing drugs in rats and a non-rodent species, but the predictive capability of this has been questioned. It has been suggested that 3D culture may allow the development of more relevant tissue models that could be used to test drug safety in a more accurate and reproducible way.<sup>(343)</sup> Current 2D systems don't accurately reflect the complexity of target organs and therefore make it difficult to develop relevant screens for organ toxicity. The liver is the most important organ for drug induced toxicity and, although complex

3D liver models have been created, their complexity renders them unsuitable for routine drug screening. The embryonic stem cell test uses stem cells cultured in hanging drops to test for possible developmental effects of novel drug compounds,<sup>(344)</sup> and tubular kidney cells cultured in 3D show distinct improvements in predictive ability over 2D models when tested with known kidney toxicants.<sup>(345)</sup> Microfluidic systems have also been developed to represent organs important for drug-induced adverse effects, including the liver, heart, lung, kidney and bone marrow.<sup>(346)</sup> The authors of the review conclude that although progress is being made towards an *in vitro* system for drug testing, the increased complexity of the required systems means there are still many challenges ahead.

## 1.4. Aims of the Thesis

The introduction above outlines the major pathological events associated with prion disease, and the challenges associated with developing therapeutics for these complex diseases. The breadth of compounds that have been reported as having anti-prion activity is huge, underlining once again the complexity of disease pathogenesis and making the identification of the optimum therapeutic approach very difficult. The pipeline for drug discovery is described, along with information on 3D models that have been developed in the hope that they will provide a more accurate assessment of a compound's potential to work *in vivo*.

The subsequent chapters of this thesis will outline a series of investigations into the indole-3-glyoxylamide (I3GA) compounds (**Figure 12**) as anti-prion compounds. The I3GAs were originally identified from an *in silico* screen (Mpamhanga *et al*, unpublished data), which predicted that this group of compounds would interact with PrP<sup>C</sup>. It was therefore hypothesised that the I3GAs may have anti-prion activity, and that this activity may be modulated *via* a PrP<sup>C</sup>-linked mechanism. It was further hypothesised that the I3GAs could be developed as potent anti-prion compounds through repeated rounds of analogue synthesis and screening.

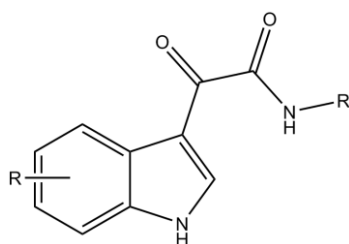


**Figure 12:** I3GA parent structure. R indicates any possible substitution of the structure.

The initial aim of the study was to establish the anti-prion activity of the I3GAs. A whole cell screening assay, using a cell line persistently infected with scrapie, was used to determine if any of the first set of I3GAs were able to reduce levels of PrP<sup>Sc</sup> *in vitro*. Results from the initial set of screening were used to develop a broad structure-activity relationship (SAR), and this in turn was used to direct the ongoing synthesis of analogues. Further rounds of screening allowed the SAR to be defined further, and the anti-prion activity of the I3GAs to be optimised. Once the anti-prion activity of the I3GAs had been established, an assay was developed to directly measure the binding between the I3GAs and PrP. This was done using SPR, which allowed interrogation of the real-time interaction between the I3GAs and recombinant PrP. I3GAs shown to be active in the cell line screen were investigated in this assay, but very few of the compounds showed an interaction with PrP, suggesting that their anti-prion activity was not the result of direct interaction with PrP<sup>C</sup>.

The discovery that the I3GAs were not binding to PrP<sup>C</sup> necessitated the development of a new hypothesis regarding the mode of action of these compounds. In the absence of any clues, further investigations were undertaken to define the pharmacodynamic and pharmacokinetic properties of the I3GAs. This data, taken in conjunction with data from microarray and proteomics studies, led to the proposal that the compounds work by upregulating the proteasomal degradation pathway, increasing the degradation of misfolded aggregates and reducing the burden of infection in the cells. Investigation of this hypothesis did not produce any conclusive results, although it is thought that an effect of the I3GAs on protein degradation may be part of their mode of action. Work was also carried out to validate the results of the microarray and proteomics studies using Western Blotting, and this technique was also used to investigate potential cellular targets of the I3GAs identified from an *in silico* screen.

The primary aim of this thesis was to establish the anti-prion activity of the I3GAs and determine their mode of action in this context. As many anti-prion compounds show promise *in vitro* but

fail to show activity *in vivo* it was also thought desirable to obtain some data pertaining to the potential *in vivo* activity of these compounds. To this end, 3D cell culture models were developed which, it was hypothesised, would be able to predict which of the novel compounds may be active *in vivo*. Based on the pharmacokinetic data it was hypothesised that the I3GAs may be active *in vivo*, and the data from the 3D models support this supposition. The potential of the 3D models to be used in a high throughput context was also assessed. It was proposed that routinely using 3D models for screening for anti-prion compounds could result in the identification of potential therapeutics that were more likely to have *in vivo* activity. These models therefore have the potential to reduce the inefficiencies and false positives associated with the anti-prion drug discovery pipeline.

## 2. Materials and Methods

The information outlined below relates to the materials and methods used to conduct the studies outlined in this thesis. The information on cell culture and compound screening describes the work carried out in section **3.1**, as well as being the basis for the work carried out in sections **4.1, 4.2, 4.3, 4.4.2** and **6.2**.

### 2.1. Materials

#### 2.1.1. Cell Culture

SMB cells (see section **1.1.3.2** for more information) were obtained from the TSE centre at the Institute of Animal Health, now based at the Roslin Institute at the University of Edinburgh. Medium 199 without phenol red, foetal bovine serum (FBS), new born calf serum (NBCS), phosphate buffered saline (PBS) and Hank's balanced salt solution (HBSS) were from Invitrogen. Medium 199 with phenol red, penicillin-streptomycin solution and trypsin-EDTA solution were from Sigma Aldrich. Tissue culture treated petri dishes were from BD Falcon (through SLS) and Nunc, tissue culture treated flasks were from Greiner. 96, 24 and 12 well plates were from Corning and Greiner, with other cell culture consumables purchased from Fisher Scientific and Starlab.

Reagents for the MTT and Bradford assays were obtained from Sigma Aldrich and the plate reader was from BioTek instruments. All reagents for dot blot analysis were purchased from Sigma Aldrich with the exception of guanadine thiocyanate (Fisher Scientific) and some of the antibodies. The primary antibodies were 6H4 (Prionics through Celtic Foods) and 8H4 (Sigma Aldrich) and the secondary antibody was anti-mouse IgG (GE Healthcare and Santa Cruz *via* Insight Biotechnology). Nitrocellulose was from Amersham *via* Fisher Scientific. Blots were visualised using chemiluminescent solutions (GE Healthcare and Geneflow). Imaging was done using either hyperfilm from GE Healthcare, developed using Kodak developing solutions (Sigma Aldrich) or by using the ChemiDoc system from Bio-Rad. The haemocytometer was from bright line through Fisher Scientific and the microscope was from Olympus.

Solutions were made as follows. Reagents were from Sigma Aldrich:

- **Nonidet P40 (NP40) lysis buffer** - 10 mM Tris HCl, 100 mM NaCl, 0.5 % v/v nonidet P40, 0.5 % w/v sodium deoxycholate and 10 mM EDTA at pH 7.4
- **Radioimmunoprecipitation assay (RIPA) buffer** - 50 mM Tris HCl, 150 mM NaCl, 1 % Triton-X, 1 % sodium deoxycholate and 0.1 % SDS at pH 8.
- **10 x tris buffered saline (TBS)** – 200 mM Tris, 9 % NaCl at pH 7.4
- **Acidic isopropanol** – 8.33 ml HCl in 1 litre isopropanol (final concentration 0.1 M HCl)

The library of small molecules used in these experiments were synthesised by Chen *et al.* Other compounds, including the positive controls and those used in the screen of literature compounds, were purchased from Sigma Aldrich with the exception of Amphotericin B, which was purchased from Fluka. All compounds were solubilised in either HBSS or DMSO and stored as 10 mM stock solutions.

## 2.1.2. Surface Plasmon Resonance

The SPR binding experiments were carried out using a Biacore 3000 instrument. Chips, reagents and consumables were purchased from Biacore through GE Healthcare. The 50 mM sodium hydroxide and 10 mM sodium acetate solutions were prepared using chemicals from Sigma Aldrich. DMSO was also purchased from Sigma Aldrich. Bacterially expressed recombinant PrP was obtained from the TSE resource centre, based at the Roslin Institute at the University of Edinburgh.

Buffers were made as follows and were filtered and degassed before use:

- **HBS-EP buffer** - 0.01 M HEPES pH 7.4, 0.15 M NaCl, 3 mM EDTA and 0.005 % v/v surfactant P20 at pH 7.4
- **Running buffer** - 150 mM NaCl, 10 mM Sodium Phosphate, 3 mM EDTA and 0.05% v/v Surfactant P20.

### **2.1.3. Microarray and Proteomics Studies**

All samples were prepared from SMB cells cultured and passaged using materials described in section **2.1.1**. Proteomic analysis was carried out using an iTRAQ based proteomic workflow. RNA was prepared for the microarray using the RNeasy method from Qiagen and quality assessed using the Agilent Bioanalyser 2100. The microarray was carried out using the Gene Chip IVT express kit from Affymetrix.

### **2.1.4. Competition Studies using Inhibitors of the Proteasome and Lysosomal Proteases**

All experiments were carried out using SMB cells, cultured and analysed using materials described in section **2.1.1**. MG132 and E64 were purchased from Sigma Aldrich, lactacystin was from Enzo Life Sciences and cathepsin inhibitor III was from Calbiochem. All were stored as a 10 mM solution in DMSO, with all solutions except MG132 stored as 10 or 200 µl aliquots at – 20 °C.

### **2.1.5. Western Blotting**

Cells were cultured in 6 well plates from Greiner with all other culture consumables and Bradford reagent as in section **2.1.1**. Protease inhibitor tablets were from Roche. 5 x lamelli sample buffer was made up in-house. Any Kd Mini-protean gels were purchased from Bio-Rad, ColorPlus protein marker was from New England Biolabs and the TGS buffer (10x) was from National Diagnostics *via* SLS. Both the electrophoresis tank and the blotting tank were from Bio-Rad. Immobilon-P transfer membrane (PVDF) was purchased from Fisher Scientific and the filter paper purchased from Bio-Rad. The 10 x TG buffer used to make up the transfer buffer was from National Diagnostics *via* SLS. Dried milk powder and BSA were from Sigma Aldrich, and TBS stock was made as before. Antibodies against HSP90, Lck and caspase 12 were from Cell Signalling *via* New England Biolabs, antibodies against beta actin and Sp1 were from Abcam and the MTF-1 antibody, as well as the secondary antibodies, were from Santa Cruz *via* Insight Bioscience. Blots were imaged using a Bio-Rad ChemiDoc and analysed using the Image Lab software.

## 2.1.6. 3D Culture

Compound screening, SMB cell culture and MTT and Bradford assays were all carried out using the materials described in section 2.1.1. Unless otherwise stated the same medium was used as is used for the routine screening.

**The Hanging Drop Model** - 96 well hanging drop plates were purchased from 3DBiomatrix *via* Sigma Aldrich after trials using samples of both plates from 3D Biomatrix. Collagenase and TES were purchased from Sigma Aldrich.

**The Alvetex Scaffold Model** - The Alvetex plates were purchased from Amsbio. Neutral red was from Sigma Aldrich.

**The Happy Cell Model** - The Happy Cell medium in DMEM was obtained from Biocroi Ltd, and low binding plates for use with the matrix were from Greiner Bio-One. DMEM was purchased from Sigma and L-glutamine purchased from Fisher Scientific.

**Confocal Microscopy** – Confocal microscopy studies were carried out using a Nikon A1 confocal microscope which is based in the light microscopy facility in the Biomedical Sciences department of Sheffield University. Slides and coverslips were from Gerhard Menzel *via* Fisher Scientific. Vectashield mounting medium containing DAPI was from Vector Laboratories, Nile red was from Sigma Aldrich and Acti-stain 488 fluorescent phalloidin (henceforth referred to as acti-stain) was from Cytoskeleton Inc *via* Bioquote Ltd. Images were analysed using ImageJ open source software.

## **2.2. Methods**

### **2.2.1. Cell Culture**

The information below outlines the methods for routine culture, dosing, lysing and analysis of the SMB cells (see section **1.1.3.2** for further information on the SMB cells). Due to the nature of the materials being used all work was carried out in a class two containment lab

#### **2.2.1.1. Initial Cell Culture**

Cells received from the Institute for Animal Health were defrosted and re-suspended in medium warmed to 37 °C. Medium was composed of medium 199 supplemented with 10% NBCS, 5% FBS and 0.5% Penicillin-Streptomycin. The cells were spun down for 5 minutes at 150 x g and the supernatant removed and replaced with fresh pre-warmed medium to remove all DMSO. The cells were then transferred to a tissue-culture treated plastic dish or T75 flask and incubated at 37°C, 5% CO<sub>2</sub> for 24 hours to allow the cells to attach. After 24 hours the medium was replaced to remove any dead cells and residual DMSO. The cells were then incubated for a further six days (making seven days in total) with a medium change after three or four days. Under normal culturing conditions the cells would be confluent at this time.

#### **2.2.1.2. Passaging and Seeding Cells for Experiments**

To passage the cells all medium was removed and replaced with 5 ml of a solution containing 0.05 % trypsin and 0.002 % EDTA, made up by diluting a 10 x solution in HBSS. The cells were incubated at 37 °C for around 5 minutes or until they were observed to have detached from the surface of the dish. Medium was added to the plate to stop the trypsin-EDTA and the cells were removed from the plate and spun down for 5 minutes at 150 x g. The supernatant was removed and the pellets re-suspended in fresh medium before the cells were counted using a haemocytometer. Five fresh culture dishes or 3 T75 flasks were plated out with  $5 \times 10^5$  cells or  $1 \times 10^6$  cells respectively to maintain cell stocks. Sterile 96 well plates were also seeded with the cell suspension, with between  $1 \times 10^4$  and  $1.5 \times 10^4$  cells per well, depending on passage and growth rate. These plates were then left overnight to allow the cells to attach before being dosed with compounds of interest. Cell stocks were passaged once a week and the medium was changed after 3 or 4 days.

### **2.2.1.3. Cell Storage**

On occasion it was necessary to put the cell stocks into storage. This was to maintain stocks and was also necessary during periods of inactivity in the cell culture laboratory. Cells were detached from the plate or flask using trypsin-EDTA as in section **2.2.1.2** before being spun down for 5 minutes at 150 x g. The supernatant was removed and replaced with a storage solution composed of FBS containing 10 % DMSO. 2 ml of this solution was added for each flask of cells, and 1 ml aliquots of this solution were transferred into cryovials. These were frozen at a rate of -1 °C/minute in a -80 °C freezer before being transferred to a cryostorage unit where they were stored long term in the vapour phase of liquid nitrogen.

## **2.2.2. Compound Screening**

### **2.2.2.1. Dosing and Initial Screens**

After 24 hours the cells in the 96 well plates were checked to ensure they had attached and were ready for dosing. The initial screens for each compound were carried out in triplicate at three concentrations; 1 µM, 10 µM and 20 µM. There were also 12 wells for negative controls (0.5 % DMSO) and 12 wells for the positive controls (10 µM curcumin) (see **Table 4**). DMSO stock solutions of each of the compounds were prepared by weighing out approximately 2 mg of the compound and then dissolving it in DMSO to give a final concentration of 10 mM. The 10 mM stock was diluted to 200 times the required concentration in DMSO. This was then diluted 10 times in HBSS (5 µl DMSO dilution into 45 µl HBSS) before being added to the medium at a 20 times dilution (5 µl HBSS dilution into 100 µl medium) to give a final DMSO concentration of 0.5 %. Once dosing was complete the cells were incubated at 37 °C for five days.

**Table 4:** Typical layout for initial screens. Letters A-H represent different samples at three concentrations (1, 10 and 20  $\mu$ M). Each concentration is screened in triplicate. The negative control (-ve) is 0.5 % DMSO, the positive control (+ve) is 10  $\mu$ M curcumin.

|   | 1       | 2       | 3       | 4       | 5       | 6       | 7       | 8       | 9       | 10      | 11      | 12      |
|---|---------|---------|---------|---------|---------|---------|---------|---------|---------|---------|---------|---------|
| 1 | -ve     | -ve     | -ve     | C<br>1  | C<br>1  | C<br>1  | -ve     | -ve     | -ve     | G<br>1  | G<br>1  | G<br>1  |
| 2 | +ve     | +ve     | +ve     | C<br>10 | C<br>10 | C<br>10 | +ve     | +ve     | +ve     | G<br>10 | G<br>10 | G<br>10 |
| 3 | A<br>1  | A<br>1  | A<br>1  | C<br>20 | C<br>20 | C<br>20 | E<br>1  | E<br>1  | E<br>1  | G<br>20 | G<br>20 | G<br>20 |
| 4 | A<br>10 | A<br>10 | A<br>10 | D<br>1  | D<br>1  | D<br>1  | E<br>10 | E<br>10 | E<br>10 | H<br>1  | H<br>1  | H<br>1  |
| 5 | A<br>20 | A<br>20 | A<br>20 | D<br>10 | D<br>10 | D<br>10 | E<br>20 | E<br>20 | E<br>20 | H<br>10 | H<br>10 | H<br>10 |
| 6 | B<br>1  | B<br>1  | B<br>1  | D<br>20 | D<br>20 | D<br>20 | F<br>1  | F<br>1  | F<br>1  | H<br>20 | H<br>20 | H<br>20 |
| 7 | B<br>10 | B<br>10 | B<br>10 | -ve     | -ve     | -ve     | F<br>10 | F<br>10 | F<br>10 | -ve     | -ve     | -ve     |
| 8 | B<br>20 | B<br>20 | B<br>20 | +ve     | +ve     | +ve     | F<br>20 | F<br>20 | F<br>20 | +ve     | +ve     | +ve     |

#### 2.2.2.2. EC<sub>50</sub> Analysis

Cells were sub-cultured and seeded into 96 well plates as described in section 2.2.1.2. Cells were dosed as described in section 2.2.2.1, except that 8 concentrations of each compound were used instead of three. Results from the initial screens were used to determine the concentrations for EC<sub>50</sub> screening. For example, if the compound was active at 10  $\mu$ M but not 1  $\mu$ M it would be screened at concentrations ranging from 0.5  $\mu$ M to 20  $\mu$ M. Each concentration was dosed in triplicate and each plate contained 12 positive control wells and 12 negative control wells. Plates were incubated at 37 °C for 5 days after dosing. Concentration curves were created and the EC<sub>50</sub> calculated using the graphing programme GraphPad Prism 5.0. Results were plotted on a log axis and the EC<sub>50</sub> value determined using a non-linear regression of the dose response curve.

$$Y = \text{Bottom} + (\text{Top} - \text{Bottom}) / (1 + 10^{((\text{LogIC50} - X) * \text{HillSlope})})$$

**Equation 2:** Equation for calculating the non-linear regression of the dose response curve.

Data was obtained and processed as shown in **Figure 13** below. Dot blot images were analysed to convert the image into numbers, by expressing the relative density of each dot as the Integrated Optical Density (IOD). The IOD was then expressed as a percentage of the untreated control. An average and a standard deviation was calculated from the data in triplicate, before the fitting of a nonlinear curve and the calculation of an EC<sub>50</sub> value.

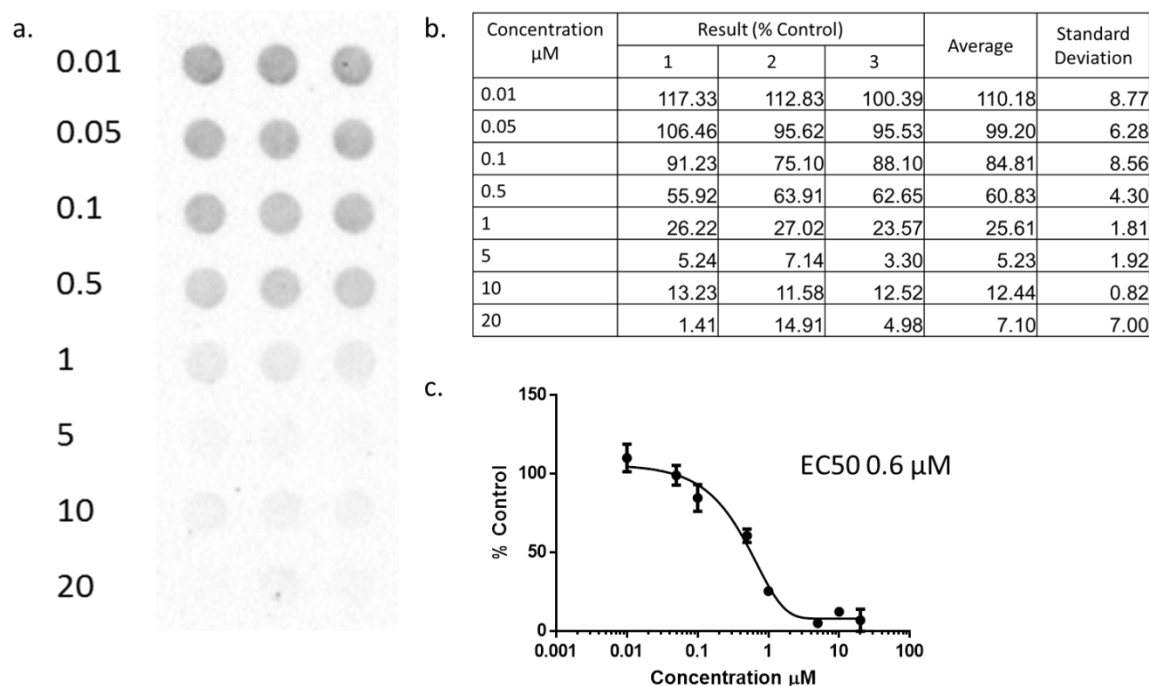


**Figure 13:** Example of the data for quinacrine dosed at concentrations ranging from 0.01  $\mu\text{M}$  to 20  $\mu\text{M}$ ; a. shows the original dot blot, with each concentration dosed in triplicate; b. shows the processing of the IODs for each concentration, and the calculation of averages and standard deviations; c. shows the generation of a dose-response curve and the calculated  $\text{EC}_{50}$ .

All compound screens were repeated at least twice to confirm the  $\text{EC}_{50}$  value and the results in section 3.1.1.3 are the average of the screens along with the standard deviation, in  $\mu\text{M}$ . Compounds that showed activity in the initial screen but showed no activity in the  $\text{EC}_{50}$  screen were classed as false positives and therefore inactive.  $\text{EC}_{50}$  values were also calculated for quinacrine and curcumin to validate the results of the compounds with unknown anti-prion activity.

### 2.2.2.3. Viability Assay

Viability assays using MTT (thiazolyl blue tetrazolium bromide) were carried out in duplicate alongside the activity assays. After the five day incubation 10  $\mu\text{l}$  of the MTT stock solution at 5 mg/ml was added to the medium and the solution incubated for 2 hours. After two hours the medium was removed and 30  $\mu\text{l}$  or 60  $\mu\text{l}$  of acidic isopropanol (propan-2-ol with 0.1 M HCl) was added. This was then measured on a UV plate reader at 570 nm with a background subtraction at 690 nm. Viability was calculated as a percentage of the untreated control.

#### 2.2.2.4. Cell Lysis

Once the five day incubation period was over the cells were lysed. This released the content of the cells so the amount of PrP<sup>Sc</sup> could be measured. The plates were examined by eye before lysis to ensure that the cells were healthy and alive and to identify any abnormal wells. Medium was removed from the plates and 50  $\mu$ l of either NP40 or RIPA lysis buffer was added. 25  $\mu$ l of benzonase at 0.2  $\mu$ l/ml in lysis buffer was added to the lysate to remove all nucleic acids from the protein samples. The plates were shaken for one hour on an orbital shaker after the addition of lysis buffer and benzonase to ensure that all the cells had lysed before the protein determination was carried out.

#### 2.2.2.5. Protein Determination

A Bradford assay was used to determine the concentration of protein in the cell lysate. The protein concentration, as determined by the Bradford assay, was used to determine the relative quantity of cell lysate to load onto the membrane for the dot blot. Ideally between 30  $\mu$ g and 40  $\mu$ g of protein was loaded in each well of the dot blot manifold.

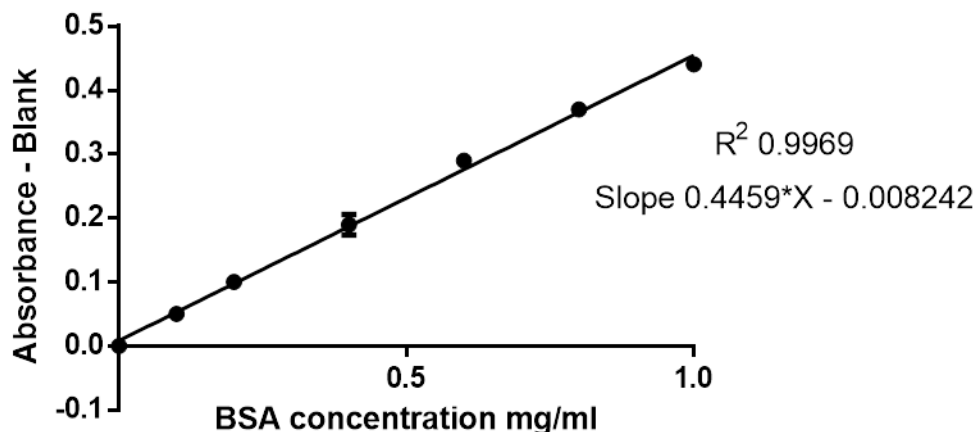


**Figure 14:** An example of a BSA calibration curve for calculating protein concentration. Lysis buffer containing different concentrations of BSA were measured using a Bradford assay, and the calculated slope used to calculate the protein concentration of the unknown samples. Each concentration was analysed in triplicate.

For both the calibration standards and the cell lysates 250  $\mu$ l of Bradford reagent was added to 5  $\mu$ l of the sample, followed by incubation for 5 minutes at room temperature. Absorbance was then measured at 570 nm using a plate reader. BSA standards were used to create a linear concentration gradient, using concentrations of 0.1 to 1.0 mg/ml (see **Figure 14**). The net absorbance was plotted against the protein concentration of each standard to construct a standard curve. The protein concentration of the unknown samples was then determined by

interpolation of the net absorbance values. The average concentration of protein was used to determine how much of each well should be applied to the nitrocellulose membrane.

#### **2.2.2.6. Dot Blot Analysis**

A 96 well manifold under vacuum was used to immobilise the cell lysate onto a nitrocellulose membrane, which then underwent a series of washes and treatments. This resulted in a final photographic image which allowed identification of wells in which PrP<sup>Sc</sup> levels had been reduced.

A piece of nitrocellulose membrane was clamped into the manifold on top of two pieces of filter paper the same size and shape. A vacuum of around 350 mmHg was applied to the manifold and the lysate from the 96 well plates loaded onto the manifold. Samples were transferred directly so the arrangement of compounds on the membrane was the same as the arrangement on the plate. Once all the liquid had been pulled through, the membrane was removed and left to dry for at least an hour. This was to ensure that the protein was fully immobilised on the membrane. This process was repeated for all plates with the top and bottom parts of the manifold being cleaned with 10% ethanol in water between each plate.

Once the membranes were dry they were subjected to a series of washes to isolate, unfold and tag the PrP<sup>Sc</sup> so it could be measured *via* chemiluminescence. All washes were done using tris buffered saline with 0.1 % Tween 20 (TBS-T) or without (TBS). A working solution of TBS was made up fresh for each set of blots by diluting 100 ml of a 10 times stock in 900 ml water. TBS was used to make up reagent solutions unless stated otherwise, and 25 ml or 30 ml of each solution was prepared which could be used on one or two blots.

Blotting was done using a series of washes as detailed below. Where two concentrations are shown these are for pre- and post-optimisation protocols:

- Proteinase K at 75 µg/ml or 150 µg/ml for one hour at 37 °C. 1.5 ml aliquots of the stock solution at 1.5 mg or 3 mg were diluted into 28.5 ml TBS to make the working solution. The stock solution was prepared in advance and stored in the freezer
- 1 mM phenylmethylsulfonyl (PMSF) fluoride for 10 minutes at 37 °C. 150 µl of a 200 mM stock solution in ethanol was added to 30 ml water to make the working solution.
- 3 x 5 minute washes in TBS-T. All steps from this point onwards were done at room temperature with shaking at 100 rpm.

- 1.8 M guanidine thiocyanate for 10 minutes. 5.32 g guanidine thiocyanate was dissolved in 25 ml TBS.
- 3 x 5 minute washes in TBS-T.
- 5% fat free milk solution for 1 hour. 1.5 g fat free milk powder was mixed with 30 ml PBS.
- 3 x 5 minute washes in TBS-T.
- 6H4 or 8H4 for 1 hour. A 0.2 µg/ml solution was made up in TBS-T and could be used repeatedly.
- 3 x 5 minute washes in TBS-T.
- Secondary antibody (anti-mouse IgG) for 1 hour. A 1:4,000 dilution was prepared in TBS-T, and was only used once.
- 1 x 15 minute washes in TBS-T
- 2 x 5 minute washes in TBS (Tween can interfere with the ECL solutions).
- 3 minute wash with 5 ml ECL solution. This is made up of equal amount of solutions A and B, which should be mixed together at least 5 minutes before use.

Once all the washes were complete the blots were visualised using either hyperfilm which was developed and fixed after exposure to the blot, or by using the Bio-Rad ChemiDoc system. The relative density of the dots was measured and quantified using either Labworks (UVP) or Quantity One (Bio-Rad) software. These software packages calculated the relative density of each of the dots and expressed it as the Integrated Optical Density (IOD). Results from the compounds were described as a percentage of the untreated controls to quantify changes in PrP<sup>Sc</sup> levels, and the MTT and dot blot data was analysed to assess the effects of the compounds on PrP<sup>Sc</sup> levels and cell viability.

### **2.2.3. Surface Plasmon Resonance**

All studies were carried out using a Biacore 3000 instrument using a protocol developed and optimised by the Chen group, which is outlined in detail below.<sup>(221)</sup>

#### **2.2.3.1. Immobilisation Protocol**

PrP was immobilised onto a CM5 chip using a standard Biacore amine coupling protocol. A new CM5 chip was docked and primed three times with the HBS-EP buffer used for the

immobilisation. Once the chip had been primed the first flow cell on the chip was prepared as a blank reference cell. The surface was activated using an equal mixture of EDC and NHS. This was injected for 7 minutes at a flow rate of 5  $\mu$ l/minute. The activated sites were then blocked with a 7 minute injection of 1 M ethanolamine-HCl pH 8.5 solution at the same flow rate.

Once the blank flow cell had been prepared, subsequent flow cells were used to immobilise the huPrP and moPrP. The cell surface was activated using the same method as above. Just before immobilisation the PrP was diluted to a concentration of around 20  $\mu$ g/ml in sodium acetate pH 5.5 buffer and this was injected manually at a flow rate of 5  $\mu$ l/ml. These parameters provided a solution that was concentrated enough to obtain the desired immobilisation level, whilst at the same time allowing control to be maintained over the immobilisation to ensure the immobilisation level was not too high. An immobilisation level of between 3000 and 4000 RU was targeted and this was usually achieved with two injections. After the protein injection the chip surface was blocked with ethanolamine as before and then regenerated using a solution composed of 25 mM NaOH and 1 M NaCl to ensure that any unbound protein was washed off the chip. The flow rate was increased to 30  $\mu$ l/minute followed by 3 injections of 5  $\mu$ l regeneration solution. After immobilisation the flow of HBS-EP buffer was continued overnight to allow the chip to equilibrate.

Once the immobilisation was complete the immobilisation level was calculated by subtracting the baseline level after the EDC-NHS injection from the baseline level after the immobilisation. This calculation was performed straight after the immobilisation, and also at the start of each run, to ensure consistency (see **Figure 30**). This provided confidence that the PrP was firmly bound and wasn't dissociating from the chip, resulting in a decrease in immobilisation level, or aggregating, resulting in an increase in the immobilisation level. Checking the immobilisation before each run also ensured that the regeneration steps described in section **2.2.3.2** were working properly by demonstrating that none of the analytes used were still bound to the PrP.

#### **2.2.3.2. Compound Runs**

Initially, compounds were assessed at 40  $\mu$ M to allow comparison with previous studies.<sup>(221)</sup> Any compounds that showed binding were run at a range of concentrations to try and establish a mode of binding.

Compounds were diluted to 0.61 mM in DMSO and were then diluted in running buffer so the final compound concentration was 40  $\mu$ M and the final DMSO concentration was 6.5%. 6.5% DMSO was added to the running buffer for compound runs and DMSO solutions of 5.5%, 6%, 6.5%, 7% and 7.5% were run alongside the samples which allowed a correction to be made for the presence of DMSO in the samples. Two regeneration solutions were used; the NaOH/NaCl solution used during the immobilisation, supplemented with 1% SDS and a glycine pH 2 solution supplemented with 1% ethylene glycol. These solutions forced the dissociation of any bound compound from the protein to ensure that all the binding sites were available at the beginning of each run. The running buffer, containing 6.5 % DMSO, was used as a sample blank and quinacrine at 40  $\mu$ M was used as the positive control. Quinacrine has been shown to specifically bind to PrP<sup>(221, 233, 347)</sup> with a *kD* of 15  $\mu$ M.<sup>(221)</sup>

To screen the compounds, runs were set up to automatically perform the following series of injections; Compounds were injected for 1 minute at a flow rate of 30  $\mu$ l/min, followed by a 3 minute wait to allow for dissociation. The regeneration solutions were then injected at a flow rate of 35  $\mu$ l/min, with a 20 second injection of the NaCl/NaOH solution (as used in the immobilisation step) being followed by a 20 second injection of the pH 2 glycine solution. These ensured that any analyte that remained bound to the ligand was removed. This was followed by 1 minute of stabilisation time before the end of the run. Each compound was run in triplicate, and each set of triplicate runs was separated by a run during which only buffer was injected. A set of five DMSO calibration standards were injected at the start, in the middle and at the end of each set of compounds, with each of the five concentrations being injected in triplicate at each stage. Quinacrine in triplicate was also included at the start and the end of each set of compound runs. Data was analysed using a macro set up in excel, which automatically calculated results and presented them as % RU<sub>max</sub>, (see section 3.2) taking into account the DMSO calibration.

## 2.2.4. Additional Assays Based On The SMB Cell Line Screening Assay

All assays outlined below used SMB cells routinely cultured as described in **2.2.1**.

### 2.2.4.1. Curative Assay

These experiments were carried out using cells seeded into 24 well plates. Cells were seeded at 50,000 cells per well in 400  $\mu$ l medium into two separate 24 well plates using 12 wells of each. The cells were incubated for 24 hours to allow attachment before the medium was changed and the cells dosed with the appropriate compounds at the following concentrations:

3001012 – 1 nM and 10 nM ( $EC_{50}$  1 nM). See **Figure 45** for structure.

Positive control – 1  $\mu$ M quinacrine or 10  $\mu$ M curcumin. See **Figure 45** for structures.

Negative control – 0.5 % DMSO

The compounds were prepared using the same dilutions as in section **2.2.2.6** for the initial dilution of the stock solution into DMSO. 10  $\mu$ l of the DMSO dilution was added to 90  $\mu$ l of HBSS and 20  $\mu$ l of this was added to each well, giving a 20 times dilution into the medium as before. Unless stated otherwise the cells were dosed once at the start of the assay.

Once the cells reached confluence they were passaged and samples taken for dot blot analysis. This was performed routinely every 5 or 6 days depending on the confluence of the cells. The medium was removed and the cells washed with 400  $\mu$ l of pre-warmed HBSS. Cells were detached using 200  $\mu$ l of trypsin-EDTA solution in HBSS (as in section **2.2.1.2**) which was stopped with 200  $\mu$ l medium. A 200  $\mu$ l aliquot was taken from each well (12 in total for each plate) and stored prior to being lysed and analysed. The remaining cells for each treatment were then pooled together (1 sample per treatment, 4 samples per plate.) to be counted and re-plated in triplicate. All samples were spun down at 150 x g for 5 minutes.

The cells for re-plating were re-suspended in 1.2 ml of medium. One of the four samples was counted, since all samples were found to have similar cell counts, and from this the amount needed to plate the cells out at 50,000 cells per well was calculated. All samples were plated out in triplicate so the same plate template was used after each split. The aliquots for analysis were re-suspended in 100  $\mu$ l of lysis buffer and 50  $\mu$ l of benzonase per aliquot. These samples were then shaken on an orbital shaker for one hour. A protein determination using Bradford reagent

was carried out as described in section **2.2.2.5** prior to the samples being frozen at -80°C for analysis at a later date.

#### **2.2.4.2. Time Course Assays**

Cells were seeded into 96 well plates following the same protocol as described in section **2.2.1.2**. EC<sub>50</sub>s were run alongside the time course assays to ensure that there was no change in activity due to the use of new stock solutions and a different passage of cells. Compounds were prepared using the same dilutions as described in section **2.2.2.1**. Each compound was dosed in triplicate and the entire experiment was carried out at least twice for each treatment.

Cells were seeded at 10,000 cell/well and incubated for 24 hours before dosing to allow attachment. Dosing was applied at this point, and the first set of compounds in triplicate lysed immediately. Medium was removed using a multi-channel pipette and replaced with 50 µl lysis buffer or RIPA. This process was carried out again at 8 or 16 hour intervals and repeated over 6 days giving 12 time points for a 128 hour incubation.

Once a plate had been completely lysed, 25 µl of benzonase at 0.2 µl/ml was added to each well and the plate was shaken at 200 rpm for one hour. At this point a Bradford assay was carried out, using the protocol described in section **2.2.2.5** and the plate stored until analysis. Cell viability was not measured as it was well established in previous screens that the compounds were being used at non-toxic concentrations. PrP<sup>Sc</sup> levels were assessed using dot blot analysis as described in section **2.2.2.6**.

#### **2.2.4.3. Growth Curve Analysis**

To assess cell numbers using the haemocytometer the cells were grown in 24 well plates with an initial seeding density of 20,000 cells/well in 400 µl medium. Each compound was dosed in triplicate, with the first harvest and count done immediately after dosing. The next count was done 8 hours after dosing, with the same pattern being repeated for the next 6 days. The three wells were combined into one sample for counting, and for the earlier time points were spun down and re-suspended in a third of the amount of medium to concentrate the sample and improve the accuracy of the count. Cell numbers were determined by aspirating the sample and taking two 20 µl aliquots which were pipetted into either side of the haemocytometer. Four of the five sampling squares were then counted giving a total of 8 counts for each sample. As far as

possible, counting was done as soon as the samples were ready, although there was not found to be any problems with counting them a day later.

For the MTT assays the cells were seeded into 96 well plates at a density of 5,000 cells/well. The outer rows of the plate were not used so were filled with medium to reduce variability in growth caused by evaporation. One plate represented one time point and six wells were dosed per treatment. The experiment was repeated in duplicate on each plate. At 24 hour intervals the medium on the seeded wells was removed and replaced with 100  $\mu$ l medium containing 0.5 mg/ml MTT solution. After incubation for 2 hours at 37°C the medium was removed and the cells re-suspended in 50  $\mu$ l acidic isopropanol. The absorbance of the wells was then measured at 570 nm with a background subtraction of 690nm using a plate reader. A calibration curve was created by seeding a plate with different concentrations of cells (5,000 to 40,000 cells/well) and then analysing the plate as described above. (see **Figure 55**). While MTT measures metabolic activity which is not directly proportional to cell number it was thought that the assay would be sufficiently sensitive for this application, and this proved to be the case.

#### **2.2.4.4. Screening of Literature Compounds**

Compounds for testing were either made up in DMSO as 10 mM stocks, or in HBSS as 5 mg/ml stocks depending on the solubility of particular compound. Compounds in HBSS stock solutions were diluted to 20 times the desired concentration and then diluted 1:20 into the culture medium. The effect of the compounds on PrP<sup>Sc</sup> levels was determined by dot blot analysis as described in section **2.2.2.6**.

#### **2.2.4.5. Competition Studies Using Inhibitors of the Proteasome and Lysosomal Proteases**

Cells were seeded into 96 well plates as before, at a density of 8,000 cells per well. Initial experiments investigated the inhibitors on their own, and the results of these initial experiments were used to determine the concentration of the inhibitors to be used in subsequent competition experiments. All inhibitors were diluted from the 10 mM stock solution following the same dilution scheme as for the compounds, giving a final DMSO concentration of 0.5% as for the routine screening. Cells were dosed with either the I3GA at a range of concentrations with a fixed concentration of inhibitor, of the inhibitor at a range of concentrations with a fixed concentration of the I3GA. For co-dosing experiments all compounds were prepared in DMSO at twice the desired concentration (400 times working concentration rather than 200 times). The

two compounds were then mixed 1:1 before being diluted in HBSS and then dosed into the culture medium. A time course study was also undertaken, to try and determine how long it took for protein levels to rise after treatment with MG132, and how this would be affected by co-dosing with 3001012. The time course assay was carried out as before, with two time points per day being taken over 5 days (0 – 128 hours). All end-point assays were carried out over 5 days. MTT assays were used to determine cell viability and were carried out as before. PrP<sup>Sc</sup> levels were determined by dot blot analysis as described in section **2.2.2.6**.

## 2.2.5. MTT-FE Assay

Cells were seeded into 96 well plates at 10,000 cells/well and left to attach overnight. The following day the cells were dosed with the compounds of interest at concentrations determined as a result of the screen described in section **4.4.2**. The wells round the edge of the plate were not used in order to reduce the amount of noise in the data.

The compounds tested and the concentrations used are detailed in **Table 5**.

**Table 5:** Compounds and their concentrations used in the MTT-FE assay

| 13GA compounds    | Literature compounds                    |
|-------------------|---|
| 3001012 10 nM     | Quinacrine 5 $\mu$ M                    |
| 3001207 100 nM    | Pentosan polysulfate (PPS) 5 $\mu$ g/ml |
| 3001086 1 $\mu$ M | Dextran sulphate (DS) 5 $\mu$ g/ml      |
|                   | Heparin 50 $\mu$ g/ml                   |
|                   | Congo red 1 and 10 $\mu$ M              |
|                   | EGCG 10 $\mu$ M                         |

Dosing was performed as in section **2.2.2.1**, with compounds being diluted to 20 times working concentration before being dosed onto the cells. Compounds with stock solutions made up in DMSO (3001012, 3001207, 3001086, quinacrine and congo red) were diluted to 200 times working concentration in DMSO to ensure a final DMSO concentration of 0.5 %. This was thought important to maintain consistency with previous assays. As before the negative control was 0.5 % DMSO.

The assays were carried out as a time course, with the MTT-FE assay being carried out every day for 5 days (120 hours in total). All compounds were known to be active within this timeframe. The assay protocol was modified from Hong *et al.* <sup>(348)</sup> Medium was removed from the cells and replaced with 100  $\mu$ l culture medium containing 0.5 mg/ml MTT (diluted from a 5 mg/ml stock in PBS as before). The plate was incubated at 37 °C for an hour, at which point the medium was removed and replaced with 50  $\mu$ l 1 % tween 20. After 10 minutes incubation at 37 °C the tween solution was transferred to a clean plate and then read in a plate reader at 570 nm with a 690 nm background subtraction. This is referred to as tween-soluble MTT (TS-MTT). The remaining MTT, known as tween-insoluble MTT (TI-MTT), was solubilised in 50  $\mu$ l acidic isopropanol before being read using the same parameters.

## 2.2.6. Microarray and Proteomics Studies

### 2.2.6.1. Sample Preparation

Samples for the proteomics and microarray assays needed to be carefully prepared to ensure that the results were reproducible within, and comparable between, the two studies. The number of samples to be analysed was limited by the iTRAQ which was only able to multiplex 8 samples. Biological replicates were needed for each sample so only 4 samples could be analysed. Cells treated with 0.5 % DMSO were used as the untreated control, and this was the baseline against which the treated cells were compared. The compounds were dosed at 3 x EC<sub>50</sub>, ensuring that the concentration would be high enough to clear the PrP<sup>Sc</sup> but hopefully avoid any off-target side effects. Quinacrine was dosed at 1.5  $\mu$ M, 3001012 at 4.5 nM and 3001207 at 6 nM with concentrations based on EC<sub>50</sub>s determined using the same passage of cells and stock solutions as used in the sample preparation.

Time course experiments (as described in section 4.2) were used to determine the time point at which the cells would be lysed. These optimisation steps ensured that the compounds had time to exert their anti-prion effect whilst, again, minimising possible off-target side effects that could confuse results. Although quinacrine exerted its anti-prion effect much more quickly at higher concentrations, it showed a similar time course to the I3GA compounds at the concentrations used in this study. 56 hours was therefore chosen as the point at which maximum clearance had occurred for all three compounds.

The samples were prepared in tissue culture treated petri-dishes, using two dishes per compound to provide the biological replicates. Culture conditions were the same as for all other experiments. The cells were left to attach overnight and the medium changed before dosing. The plates were dosed at the appropriate concentrations with a final DMSO concentration of 0.5 %. After 56 hours the medium was removed and the plates washed 3 times with HBSS. It was vital to ensure that all medium was removed so that the proteomics study was not contaminated with protein from the medium. A 0.02 mg/ml EDTA solution was used to remove the cells from the bottom of the plate. Trypsin is usually used for this step but was avoided as it can interfere with the downstream analysis. The cells were removed fully from the plate with a cell scraper and samples taken for protein determination and dot blot analysis to confirm the protein concentration and the presence or absence of PrP<sup>Sc</sup>. The samples were split into two (3.5 ml for proteomics, 1 ml for microarray), spun down for 5 minutes at 12,000 x g, the supernatant removed, and the pellets stored at -80 °C.

Protein determination and dot blot analysis were carried out as per sections **2.2.2.5** and **2.2.2.6** respectively.

#### **2.2.6.2. Proteomic Analysis**

The prepared samples were compared in a multiplex format to determine changes in the protein expression profile resulting from treatment with the compounds. An 8-plex isobaric tag for relative and absolute quantification (iTRAQ) based proteomic workflow was used for the experiments. The iTRAQ technology is based on the chemical labelling of peptides with a series of isobaric reagents after enzymatic digestion of the proteins. The isobaric reagents have the same mass but are distinct from each other, producing different reporter ions when fragmented. Labelled samples were combined, fractionated by nano liquid chromatography and fragmented and analysed by tandem mass spectrometry. Proteins were simultaneously identified and relatively quantified in this approach. It was possible to analyse 8 different samples at once due to the availability of 8 different iTRAQ reagents, so in this study two biological replicates were carried out for each of the four compounds. Data processing and downstream statistical analysis were performed using the well-established pipeline developed at the Chemical Engineering at the Life Science Interface (ChELSI) Institute at Sheffield University.

### **2.2.6.3. Microarray Analysis**

DNA microarrays were used to measure the expression levels of a large number of genes simultaneously. Total RNA was extracted from the cell pellets and the quantity and quality assessed. Once this had been confirmed the RNA was processed using the Gene Chip IVT express kit from Affymetrix. 15 µg of the biotin-labelled antisense RNA produced was fragmented and applied to the Mouse 430 plus 2 Gene Chip arrays, which allowed analysis of over 34,000 well characterised mouse genes (information from [www.affymetrix.com](http://www.affymetrix.com)). After 16 hours incubation at 45 °C with rotation at 60 rpm the arrays were washed and the fluorescent signal developed using a streptavidin-phycoerythrin conjugate. The arrays were then scanned and following quality control using the Expression console package the data was available for downstream analysis.

### **2.2.6.4. Network Analysis**

The data from both the proteomics and the microarray studies were combined, analysed and compared using the MetaCore software. Cellular level biological networks were built for all conditions. Gene and protein expression in treated cells were compared to gene and protein expression in cells that had been treated with DMSO only to determine which pathways were affected by treatment with either quinacrine or the I3GAs. Networks were built detailing pathways that may be altered as a result of treatment. Separate networks were built for the proteomics and microarray data individually, and then a third network was built using a combination of both data sets.

Microarray data was analysed using the GeneSpring GX software, and the normalisation of the data was carried out using the PLIER 16 to standardise changes in gene expression attributed to biological variation instead of technical variation. Differentially expressed genes (DEGs) with an absolute fold change of  $\geq 1.0$  were determined by a paired Student's T-test using  $p$  value  $<0.05$ , and the false discovery rate was determined at this  $p$  value according to the Benjamini and Hochberg method.<sup>(349)</sup>

The proteomics data was originally expressed as an iTRAQ ratio, with up regulated proteins having a number greater than one and down regulated proteins having a number lower than one. In order to make these data comparable to the microarray data a transformation was necessary. This was achieved by taking the value of the lowest ratio of a group of data and

subtracting it from the selected microarray cut off point. This was added to all the values in the data set, and all down regulated proteins were transformed into negative values.

The reports produced by MetaCore contained several different sets of data. Pathway maps were constructed based on the data sets, both individually and combined. The pathway maps represent a set of signalling and metabolic maps covering the human system in a comprehensive way. Experimental data is visualised on the map as blue (for down regulation) and red (for up regulation) histograms, with the height of the histogram corresponding to the relative expression level for a particular gene or protein. Enrichment analysis consisted of matching gene IDs of possible targets with functional ontological entities in MetaCore. The probability of a random intersection is estimated in a *p*-value of hypergeometric intersection, with a lower *p*-value indicating higher relevance of the entity to the dataset. Process networks were suggested on the basis of each set of data, with each process representing a pre-set network of protein interactions characteristic for the process. Metabolic networks were also suggested.

### **2.2.7. Western Blotting**

Cells were cultured as in section **2.2.1.2** and seeded into 6 well tissue-culture treated plates at a density of 150,000 cells/well in 1.5 ml medium. After an overnight incubation to allow attachment, they were dosed according to the protocol in section **2.2.2.1**. Cells were dosed with either 3001012 at 5 or 10 nM or 3001207 at 50 or 100 nM, and 75  $\mu$ l of the 20 times HBSS dilution was added to the medium to give a final DMSO concentration of 0.5%. Cells were then incubated for either 56 hours or 5 days before harvesting, at which point all medium was removed from the cells and they were harvested from the plate using a 0.5 ml trypsin-EDTA solution (see section **2.2.1.2**). After the addition of 0.5 ml of medium the samples were spun down at 150 x g for 5 minutes before the supernatant was removed and the pellet re-suspended in 1 ml HBSS. These were spun down at 11,300 x g for 5 minutes, after which the pellet was washed twice with sterile HBSS to remove any traces of medium. The pellets were then lysed on ice in 250  $\mu$ l of RIPA buffer supplemented with protease inhibitors, spun down for 1 minute at 1,700 x g to remove cellular debris, and a Bradford assay carried out to determine protein concentration (see section **2.2.2.5**). Samples for analysis were diluted in RIPA if required to give a final protein concentration of 1  $\mu$ g/ $\mu$ l (40  $\mu$ g protein in total). 10  $\mu$ l lamelli buffer at 5 times working concentration was added to give a final sample volume of 50  $\mu$ l. The samples were then

heated at 75 °C for 5 minutes and loaded onto the gel. To avoid problems with degradation the samples were kept on ice at all times and prepared and loaded onto the gel as quickly as possible.

After heating, 40 µl of each sample was loaded onto the gel, which had been placed in the tank and the gasket filled with 1 x TGS buffer. Marker was loaded onto either one or both of the outside lanes, depending on how many samples were being run. The tank was filled with TGS up to the appropriate level and the gel run at 300 V for 5 minutes to move the samples into the stacking layer of the gel. It was then run for 30 minutes at 180 V. All gels were run using the same conditions.

While the gel was running, appropriate size pieces of PVDF were activated in methanol and then soaked in transfer buffer (100 ml methanol, 100 ml 10 x TG buffer, 800 ml water) for half an hour. Once the gel was run it was removed from the case and briefly soaked in transfer buffer, before being layered with the PVDF membrane and filter paper according to the order shown in

**Figure 15**

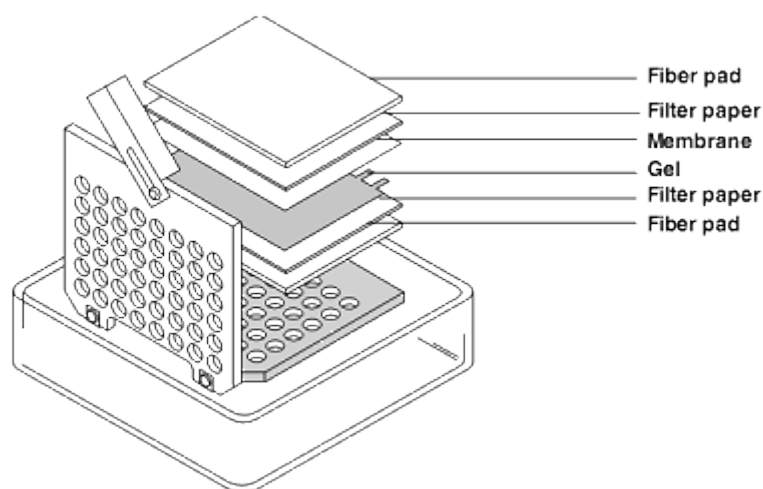


**Figure 15:** Diagram showing how the gel and PVDF membrane are layered in preparation for western blotting. With the black side of the cassette down, stack upwards in the order fibre pad, filter paper, gel, membrane, filter paper, fibre pad. Figure adapted from Bio-Rad instruction manual.

The cassette was then placed into the tank with the black side of the cassette next to the black side of the tank. An ice pack was placed in the gap and the tank filled to the brim with transfer buffer. This was run for 30 minutes at 180 mA.

Once the transfer was complete the PVDF was checked and if marker could be seen then the transfer had been successful. The edges were trimmed and it was placed into a centrifuge tube containing 25 ml TBS-T (see section **2.2.2.6** for composition). A series of washes were then performed as follows (at room temperature unless otherwise specified):

- TBS-T, 15 minutes
- Block, 1 hour
- Primary antibody, overnight at 4 °C or 1 hour at room temperature
- TBS-T, 3 x 5 minutes
- Secondary antibody, 1 hour
- TBS-T, 1 x 15 minutes
- TBS, 2 x 5 minutes
- ECL solutions, 3 minutes.

Blocking and primary antibody conditions were optimised for each antibody individually, as can be seen in **Table 6**.

**Table 6:** Western blotting conditions for each of the targets. All solutions were made in TBS-T (20 ml for the block, 5 ml for the primary antibody and 10 ml for the secondary antibody) and all primary antibody incubations were done overnight at 4 °C, unless otherwise specified.

| Target     | Supplier              | Block conditions | Primary conditions                            | Secondary      |
|------------|-----------------------|------------------|---|----------------|
| HSP90      | NEB – 4875S           | 5 % BSA          | 1:1,000 in 5% BSA                             | Rabbit 1:4,000 |
| Sp1        | AbCam - ab77440       | 5 % BSA          | 4 ug/ml in 5% BSA                             | Mouse 1:4,000  |
| Lck        | NEB - 2752            | 5 % BSA          | 1:500 in 5% BSA                               | Rabbit 1:4,000 |
| MTF-1      | Santa Cruz - sc-48775 | 5% milk          | 1:200 in 5 % milk                             | Rabbit 1:4,000 |
| Caspase 12 | NEB - 2202            | 5% milk          | 1:2,000 in 5% milk                            | Rabbit 1:4,000 |
| Beta-actin | Abcam - ab8227        | 5 % BSA          | 1:2,000 in 5% BSA, 1 hour at room temperature | Rabbit 1:4,000 |

Once the washes were complete the blots were visualised using the Bio-Rad ChemiDoc system, and the resulting bands analysed using the image lab software.

## 2.2.8. 3D Culture

The SMB cells, cultured routinely as in section 2.2.1, were used in all experiments.

### 2.2.8.1. The Hanging Drop Model

#### 2.2.8.1.1. Optimisation of Spheroid Formation and Culture

Initial optimisation was carried out using the 384 well plates to prove that the SMB cells would form spheroids. Drops were formed from 20  $\mu\text{l}$  medium, with initial seeding densities of 300, 1,500 and 7,500 cells per drop, as per the manufacturer's recommendation. 10  $\mu\text{l}$  medium was added to each drop 2 days after seeding, with a further 5  $\mu\text{l}$  being added every two or three days subsequently. Spheroid formation was observed in the hanging drops and monitored by eye.

Further optimisation was carried out using the 96 well hanging drop plate to identify the optimal drop size and seeding density (see **Table 7**).

**Table 7:** Different seeding densities and medium volumes used in the optimisation of the 96 well hanging drop plate. Figures in the table show the total number of cells per drop for each of the parameters.

| Cells/ $\mu\text{l}$ | Medium volume ( $\mu\text{l}$ ) |        |        |
|----------------------|---------------------------------|--------|--------|
|                      | 25                              | 35     | 50     |
| 250                  | 6,250                           | 8,750  | 12,500 |
| 375                  | 9,375                           | 13,125 | 18,750 |
| 500                  | 12,500                          | 17,500 | 25,000 |

Cell suspensions of the required seeding density were prepared and the appropriate amount (25  $\mu\text{l}$ , 35  $\mu\text{l}$  or 50  $\mu\text{l}$ ) gently pipetted into the well to allow the formation of the hanging drop. 2 ml of water was added to the wells round the edges of both the upper and lower sections of the plate to reduce evaporation from the drops. This was replenished at the same time as the medium. Cells were monitored over 7 days, and 25 % of the original volume of medium was added every two or three days. Additional optimisation used the same protocol but investigated higher seeding densities of 500, 750 or 1,000 cells/  $\mu\text{l}$ . Spheroids were harvested by pipetting the whole drop up from the top of the plate. If harvesting was problematic due to the spheroid getting lodged in the top of the well then the well was flushed with HBSS to dislodge the spheroid and remove it from the plate. To facilitate downstream processing the spheroids were

spun down to allow the removal of medium. If required the spheroids were rinsed with HBSS before being re-suspended in the lysis buffer.

A variety of methods were used to lyse the spheroids. Two different lysis buffers were used during the optimisation process; 100  $\mu$ l NP40 buffer and 100  $\mu$ l RIPA buffer (see section 2.1.1 for composition of both). To facilitate lysis of the spheroids in the lysis buffer additional techniques were employed. These included incubating the spheroids at 70 °C for 30 minutes, as well as carrying out freeze-thaw cycles and passing the spheroids through narrow gauge needles. Freeze-thaw cycles were carried out by allowing the samples to freeze completely, before thawing in a water bath at 37 °C. This was repeated 4 times. Lysing the spheroids by passing them through a small gauge needle used a 21 g.a. needle and a 500  $\mu$ l syringe, with the solution containing the spheroid being passed through the needle multiple times. It should be noted that the spheroids that were subjected to this treatment were re-suspended in 200  $\mu$ l lysis buffer as 100  $\mu$ l was found to be impractical. The efficacy of each technique was determined using spheroids that had been dosed with 0.5 % DMSO, with two spheroids being combined into one sample. A total of 48 spheroids were combined into 24 samples, which were divided into 4 groups of 6 and subjected to one of the above lysis methods after being suspended in RIPA lysis buffer.

Collagenase digestion was carried out using a variety of different buffers and concentrations. Stock solutions at 10 mg/ml were made up in TESCA buffer (50 mM TES, 0.36 mM  $\text{CaCl}_2$ ) and stored in the freezer until required. Three different buffers were used for the digestion, including TESCA as well as high calcium TESCA (containing 5 mM  $\text{CaCl}_2$  rather than 0.36mM) and krebs-ringer buffer (135 mM NaCl, 5 mM KCl, 1 mM  $\text{MgSO}_4$ , 0.4 mM  $\text{K}_2\text{HPO}_4$ , 1 mM  $\text{CaCl}_2$ , 5.5 mM glucose, 20 mM HEPES, pH 7.4). Each spheroid was digested in 100  $\mu$ l of each of the buffers containing either 0.5, 1 or 2.5 mg/ml collagenase. Spheroids were incubated at 37 °C and were monitored at 30 minute intervals to determine if dissociation was occurring. After 3 hours of incubation the spheroids were removed from the collagenase solution, either by spinning the solution down at 13,400 rpm for 5 minutes and removing the supernatant or by removing the spheroid with a pipette and placing it in a clean tube. In both cases the spheroid would finally be re-suspended in 100  $\mu$ l RIPA.

Sonication of the sample in the bioruptor was carried out by first re-suspending the spheroids in 100  $\mu$ l RIPA, before decontaminating the outside of the tubes by exposing them to 1 M sodium

hydroxide for 1 hour. The tubes were then transferred to the bioruptor, which could accommodate 6 tubes at a time. Each batch of 6 tubes was subjected to 5 x 30 second bursts of sonication, with a gap of 30 seconds between each burst. The water bath attached to the bioruptor maintained the temperature within the sonicator at 4 °C.

#### **2.2.8.1.1. Compound Screening and Additional Investigations**

Cells were seeded into 96 well hanging drop plates at a density of 1,000 cells/ $\mu$ l in 40  $\mu$ l medium. 5  $\mu$ l medium was added to each well every two or three days to counteract evaporation and medium depletion. Compounds were prepared for dosing as described in section 2.2.2.1 for compounds in DMSO, and as in section 2.2.4.4 for compounds in HBSS. 2  $\mu$ l of the 20 x dilution in HBSS was added to each hanging drop. Compounds were initially screened at 10 times EC<sub>50</sub> with concentrations subsequently being increased. Concentrations for the literature compounds were calculated from their EC<sub>50</sub> in the cell line model (see **Table 34**) as well as their reported activities *in vivo*. The spheroids were incubated for 5 days and then harvested by pipetting the entire drop up from the top of the plate. The drops were transferred to microcentrifuge tubes, with two drops (and therefore two spheroids) per tube. The tubes were spun down at 13,400 rpm for 5 minutes, the medium removed, the spheroids rinsed with 50  $\mu$ l HBSS and re-suspended in 100  $\mu$ l RIPA and 50  $\mu$ l 0.2  $\mu$ l/ml benzonase. Each sample was then subjected to 5 30 second cycles in the bioruptor, with 30 seconds between cycles. Dot blot analysis was carried out as described in section 2.2.2.6.

Investigations into the viability of the spheroids by seeding them into 96 well plates were carried out by culturing the spheroids as normal for 3 days, and then transferring them into a 96 well plate. Wells were either blank or pre-seeded to establish a 2D monolayer, which was done the day before transferal. Plates were then monitored and images captured to demonstrate how the spheroids behaved. Spheroids were lysed in the 96 well plate by removing the medium and replacing it with 100  $\mu$ l RIPA and 50  $\mu$ l 0.2  $\mu$ l/ml benzonase.

MTT assays were carried out by harvesting the spheroid from the hanging drop plate and re-suspending it in 100  $\mu$ l medium containing 0.5 mg/ml MTT. After 2 hours incubation, the spheroid was spun down, rinsed with HBSS, re-suspended in 50  $\mu$ l acidified isopropanol and the resultant solution measured in a plate reader.

### 2.2.8.2. The Alvetex Scaffold Model

Cell seeding in all formats was carried out according to the manufacturers' recommendations, with the initial seeding density determined by the specific application and plate format.

3 different plate types were used with different seeding conditions, but in all cases the scaffolds needed to be activated using a wash of 70 % ethanol, followed by 3 washes with medium. Cells were seeded into the 96 well plates in the full volume of medium, but in the case of the 24 and 12 well plates the cells were seeded onto the scaffold in a small amount of medium, left to attach for two or three hours, with the wells subsequently being flooded with the required final volume, shown below. All parameters can be seen in **Table 8**.

**Table 8:** Seeding conditions for the different Alvetex plate formats.

| Well number | Ethanol volume (µl) | Initial seeding density (cells) | Seeding volume (µl) | Final volume (µl) |
|-------------|---------------------|---------------------------------|---------------------|-------------------|
| 12          | 1000                | 500,000                         | 150                 | 3000              |
| 24          | 500                 | 250,000                         | 75                  | 1500              |
| 96          | 50                  | 50,000                          | 200                 | 200               |

The optimum seeding density for the 96 well plates was based on the initial growth data as determined by MTT. Based on the manufacturer recommendation, cells were seeded at initial densities of 10,000, 25,000, 50,000 and 100,000 cells/well in 200 µl medium. Growth was monitored using an MTT assay. The medium was removed from the well and replaced with 200 µl medium containing 0.5 mg/ml MTT. This was incubated for two hours before the medium was removed and the formazan product solubilised using 50 µl acidic isopropanol. The resulting solution was transferred to a clean 96 well plate for measurement. The four different seeding densities were monitored over the course of 7 days. MTT assays done on the 24 well plates were carried out in the same way, with 1 ml of medium containing 0.5 mg/ml MTT being added to each well and 200 µl acidic isopropanol used for solubilisation.

Visualisation of the cells using neutral red was carried out according to the Alvetex protocol. A 0.5 % Neutral Red solution was made up in HBSS and sterile filtered. The medium was removed from the scaffold and 2 washes with 200 µl HBSS carried out. 100 µl of Neutral Red solution was added to each well and incubated for 5 minutes at room temperature. The stain was removed and the scaffolds washed for 5 minutes on the shaker with 200 µl HBSS. This was repeated once

before the wash buffer was removed and replaced with 100  $\mu$ l HBSS, rendering the scaffolds ready for visualisation.

Initial compound screens were carried out by dosing 8 wells with either HBSS only, 0.5 % DMSO, 10  $\mu$ M curcumin or 10 nM 3001012. Subsequent studies used the same compounds as were used in the hanging drop studies (see **Table 46**). Dosing was carried out as for the 2D screens (see section **2.2.2.1**) In the cases where the stock solution was prepared in HBSS, a 20 x dilution of the compound was prepared in HBSS, before being diluted into the culture medium as normal. 96 well plates were dosed with 10  $\mu$ l of the compound into 200  $\mu$ l medium, 24 well plates were dosed with 75  $\mu$ l of the compound into 1.5 ml medium. Initial experiments used all wells of the 96 well plate, but due to a pronounced edge effect subsequent experiments only used the inner wells of the plate.

Cell lysis in the 96 well plates was carried out by removing the medium, washing the wells with 100  $\mu$ l HBSS and then adding 100  $\mu$ l RIPA. The plates were then placed on an orbital shaker at 200 rpm for as long as possible (minimum 1 hour) and the RIPA aspirated within the wells at regular intervals. 50  $\mu$ l benzonase at 0.2  $\mu$ l/ml was then added, the plate shaken for a further 15 minutes and then the lysate transferred to a clean 96 well plate. In the initial study a second round of lysis was carried out to see if all the cells had been lysed. This gave a very weak signal, suggesting it was not beneficial and was therefore not repeated in subsequent studies. The cells grown and dosed in the 24 well plates were removed from the scaffolds before lysis. Once again the medium was removed and the wells washed with 500  $\mu$ l HBSS, before the addition of 500  $\mu$ l of a solution containing 0.05 % trypsin and 0.002% EDTA as used in the routine cell culture (see section **2.2.1.2**). After 15 minutes incubation at 37 °C the plates were shaken for 15 minutes, before the addition of 500  $\mu$ l medium to stop the enzymatic digestion. The whole well was transferred to a microcentrifuge tube and spun down at 12,000 x g for 5 minutes. The resultant pellet was re-suspended in 100  $\mu$ l RIPA and 50  $\mu$ l 0.2  $\mu$ l/ml benzonase solution. To try and retrieve as many cells as possible this was repeated 2 more times, and the three samples combined in the same 150  $\mu$ l of lysis buffer. This was found to give a good enough signal on the blot but was very labour intensive. In both cases, dot blot analysis was carried out as described in section **2.2.2.6**.

### **2.2.8.3. The Happy Cell Model**

As per the manufacturer's instructions the Happy Cell suspension solution was mixed 1:1 with DMEM containing 10 % NBCS, 5 % FBS, 2 mM L-glutamine and 1% Penicillin-Streptomycin. The concentrations used were taken from the literature where DMEM had been used for routine culture of SMB cells. <sup>(350)</sup> Initially the cells were seeded at four different concentrations; 1,000, 2,500, 5,000 and 10,000 cells/well. Aliquots of cells suspension containing the appropriate number of cells in Medium 199 were spun down and re-suspended in the Happy Cell matrix, with 100 µl of this being added to each well of the low-binding 96 well plate. These were specifically used to encourage the formation of 3D structures. The plate was then monitored by eye to confirm the optimum seeding density. The successful formation of spheroids was confirmed in this study, with subsequent experiments using initial seeding densities of 5,000 or 10,000 cells/well.

As initial attempts to harvest the cells for MTT and dot blot analysis were unsuccessful, an inactivation solution supplied by the manufacturer was used with the matrix. The 2 mg/ml stock solution was diluted to 0.6 mg/ml in HBSS, and 20 µl of this working solution was added to each well. The plate was incubated for an hour at 37 °C, allowing the cells to sediment out of the matrix. Careful aspiration of the majority of the medium left the spheroids in the bottom of the well, and washes could be carried out by adding 100 µl HBSS, aspirating, leaving the spheroids to sediment for 10 minutes and then removing the majority of the liquid as before. The cells were then either re-suspended in 50 µl RIPA and 25 µl 0.2 % benzonase, or 100 µl medium containing 0.5 mg/ml MTT. MTT assays were carried out using the same basic protocol as before. The only change was that after removal of the medium containing MTT the cells were washed with 100 µl HBSS to remove excess medium and avoid any interference with the assay. After this wash step the cells were re-suspended in 50 µl acidified isopropanol to solubilise the formazan product, and the absorbance measured in a plate reader. Growth curve assays were carried out using MTT assays as detailed above, with assays carried out at 4 time points (0 hours, 24 hours, 48 hours and 120 hours).

Images of the spheroids were obtained by either capturing images while the spheroids were still within the plate using a brightfield microscope, or by staining and mounting the cells and then examining them using confocal microscopy (see section **2.2.8.4**)

#### **2.2.8.4. Confocal Microscopy**

The preparation of the 3D structures for confocal microscopy involved the harvesting and fixing of the 3D structures followed by staining and visualisation. Slightly different approaches were used for each of the models as protocols had to be optimised for each of the 3D structures. Vectashield mounting media containing DAPI was used to visualise the nuclei of the cells in all cases, with other stains used as described subsequently.

Spheroids from the hanging drop model and the happy cell model were prepared according to the same protocol. Hanging drop spheroids were harvested as described in section **2.2.8.1**, and the happy cell spheroids were retrieved after inactivation of the matrix using the inactivation solution as described in section **2.2.8.3**. All spheroids were rinsed with HBSS, and to try and maintain the morphology of the spheroids they were allowed to sediment to the bottom of the tube before the HBSS was removed and replaced with 500  $\mu$ l 4% paraformaldehyde solution. Fixation was done over 24 hours, before rinsing with HBSS and permeabilisation with 0.1 % Triton-X for 15 minutes. After further HBSS rinses the spheroids were re-suspended in a drop of Vectashield mounting medium with DAPI and mounted on a slide. The slide was sealed using clear nail varnish to prevent contamination of the microscope with biohazardous material. The nuclei of the cells in the spheroids were then visualised at 405 nm using confocal microscopy.

The Alvetex scaffolds to be visualised were prepared in 12 well plates as it was possible to remove the scaffolds for fixation and mounting. Scaffolds were initially seeded as discussed in section **2.2.8.2**, and then incubated for 6 days before harvesting. In order to visualise the proliferation of the cells, scaffolds were harvested, fixed and mounted at 2 day, 4 day, 6 day and 8 day time points. To fix the scaffolds they were removed from the plate using forceps and subjected to 3 x 3 minutes washes in HBSS. The cells were fixed using an excess of a 1:1 mixture of ice cold methanol and acetone for twenty minutes at 4 °C, before the scaffolds were washed again in HBSS as before. A drop of mounting medium containing DAPI was placed on the slide, the scaffold was placed on top of it and another drop of mounting medium placed on top of the scaffold. A cover slip was placed on top and then sealed with clear nail varnish.

Where required, Nile red staining was carried out after fixation. A 1 mg/ml stock solution was prepared in methanol, and then diluted 1:2000 into HBSS. Scaffolds were incubated in this working solution for 10 minutes at room temperature. This was followed by 3 x 3 minute HBSS washes before mounting as above. Where required, acti-stain was used at a concentration of

100 nM by diluting 3.5  $\mu$ l of stock into 500  $\mu$ l HBSS. The stock was made up at 14  $\mu$ M in methanol. Each scaffold was fixed as above before being incubated with 500  $\mu$ l of the working solution at room temperature for 30 minutes in the dark. 3 x 3 minute HBSS washes were then carried out before any further staining was carried out. Where both Nile red and Acti-stain incubations were carried out the Nile red incubation was carried out first, followed by the Acti-stain incubation and mounting. Activation of DAPI with ultraviolet light and subsequent detection of the blue emission at 405 nm allowed the visualisation of the nuclei of the cells within the scaffold. Nile red emitted at 525 nm and the Acti-stain emitted at 488 nm, allowing all three channels to be collected at the same time.

### 3. Assay Development, Structure-Activity Relationship Optimisation and Lead Identification

The development of small drug-like molecules as anti-prion compounds was started by the Chen group when virtual high throughput screening (VHTS) was used to identify potential anti-prion compounds. VHTS was carried out on 1.3 million compounds. They were computationally docked to the proposed protein X binding site<sup>(126)</sup> that was identified from a 3D NMR structure of recombinant human PrP (PDB structure entry 1qm3).<sup>(351, 352)</sup> Those that showed a strong predicted binding affinity based on hydrogen bonding and lipophilic interactions between the compound and the binding pocket were clustered into structurally similar groups. These groups were then narrowed down based on solubility, cLogP (less than 6), GOLD score (greater than 60) and availability from suppliers. A library of commercially sourced compounds was purchased, based on the results from the VHTS screening. These were then screened using Surface Plasmon Resonance (SPR) to evaluate their binding to PrP,<sup>(221)</sup> before those that showed promise were evaluated for their anti-prion activity in the SMB cell line model.<sup>(351, 353)</sup>

Hits from both assays were analysed and active compounds from three different structural groups were identified as potentially interesting; pyridine dicarbonitriles, aminothiazoles and indole-3-glyoxylamides (I3GAs). The pyridine dicarbonitriles and aminothiazoles were initially investigated, with these structural groups showing both binding to PrP<sup>Sc</sup> and micromolar activity in the cell line.<sup>(221, 351, 354, 355)</sup> The initial VHTS screen, as well as the preliminary validation work was carried out by Chen *et al* before the experimental work presented in this thesis was begun.

The experimental work in this thesis focusses on the I3GAs, a structural group that showed promise as the parent structures were shown to have EC<sub>50s</sub> of less than 10 µM (see **Figure 16**).

<sup>(280)</sup>

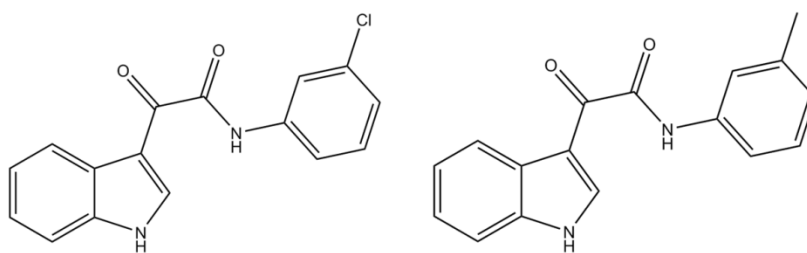


**Figure 16:** Structures of parent I3GA compounds, with  $EC_{50}$ s of 1.5  $\mu$ M (left) and 6.4  $\mu$ M (right)

The I3GAs were chosen due to the good activity of the parent compounds and their potential for modification. The I3GA structural motif is also known to be medically significant, and is included in phospholipase inhibitors, <sup>(356-359)</sup> antibiotics, <sup>(360)</sup> p38 $\alpha$  MAPK inhibitors, <sup>(361-364)</sup> tubulin polymerisation inhibitors <sup>(365-367)</sup> and compounds for the treatment of HIV <sup>(368)</sup> (see **Table 9**).

**Table 9:** Examples of other compounds that include the I3GA pharmacophore (in red) and their proposed therapeutic function. Figure adapted from Thompson *et al.* <sup>(279)</sup>

| Name           | Structure | Function   |
|----------------|-----------|--|
| Varespladib    |           | Secretory phospholipase inhibitor, for acute coronary syndrome                                 |
| Methyl indoxam |           | General phospholipase inhibitor, for treatment of obesity                                      |
| Indibulin      |           | Tubulin polymerisation inhibitor, for treatment of solid tumours and breast cancer             |
| BMS-488043     |           | HIV-1 attachment indicator, for treatment of HIV   |
| SC10-469       |           | Selective p38α MAPK inhibitor for dental pain, multiple myeloma and fracture and wound healing |
| Various        |           | A range of antibiotics, depending on substitution, for systemic infections                     |

The cell line screening assay was established and optimised to test the anti-prion activity of a series of I3GAs that were synthesised by Chen *et al.* The results from these experiments were used to refine the structure-activity relationship (SAR), and to subsequently identify a lead compound. Structural optimisation focussed on improving activity in the cell line assay. Surface

Plasmon Resonance (SPR) was used as a high-throughput screening tool, based on a protocol developed by Touil *et al.*,<sup>(221)</sup> to test the binding of the compounds to full length human recombinant PrP, (recPrP) as an initial investigation into the mode of action. A full explanation of SPR can be found in section 3.2 and the protocol is outlined in detail in section 2.2.3. All compounds used were synthesised by Chen *et al.* The majority were synthesised by Mark Thompson while Vinciane Borsenberger, Katy Judd and Steve Ferrara are also acknowledged for their role in the synthesis.

### 3.1. SMB Activity and Viability Screening

Screens of the I3GA compounds were carried out in the SMB cells to determine their anti-prion activity, and this information was subsequently used to determine the SAR. Initial screens were carried out to evaluate the ability of the I3GAs to reduce PrP<sup>Sc</sup> levels in the SMB cells at concentrations of 1  $\mu$ M, 10  $\mu$ M and 20  $\mu$ M. MTT assays were carried out in parallel to assess any cytotoxic effects of the compounds by measuring the activity of living cells *via* mitochondrial dehydrogenases. Viable cells convert the water-soluble MTT to an insoluble purple formazan, which can be solubilised and measured.<sup>(369)</sup> Determination of toxicity was crucial because cells that were dead gave the same readout in the activity screen as cells with reduced levels of PrP<sup>Sc</sup>, therefore raising the possibility of false positives in the activity screen. Positive and negative controls were included in all screens. Curcumin was chosen as the positive control as it has been shown to be a potent anti-prion agent.<sup>(266)</sup> The negative control was 0.5 % DMSO as it had no impact on cell viability or PrP<sup>Sc</sup> levels (data not shown). Stock solutions for all the I3GA compounds were made up in DMSO so this also accounted for any off-target effects of the 0.5 % DMSO remaining after dilution. Once the initial screens were carried out and satisfactory results obtained any compounds showing activity were analysed to determine their EC<sub>50</sub> value. A dose-response curve was generated for each compound, allowing the calculation of an EC<sub>50</sub> value *via* nonlinear regression of the curve. The EC<sub>50</sub> value is a measure of the anti-prion activity of the compound, and the term half maximal effective concentration (EC<sub>50</sub>) refers to the concentration of the drug at which 50 % of its effect is observed. This is measured as the halfway point between the baseline (no effect) and the maximum effect after a specified exposure time.

After lysis, a Bradford assay was used to determine the protein concentration of the lysate and therefore calculate the amount to be used in the dot blot analysis. The Bradford assay uses the binding of Coomassie Brilliant Blue to protein to determine protein concentration. Binding causes a shift in absorbance from 465 nm to 595 nm which can be measured spectroscopically. <sup>(370)</sup> Dot blot analysis was used to quantify the amount of PrP<sup>Sc</sup> in the cell lysate, and the dot blot protocol that was used was optimised from a protocol developed and reported by Rudyk *et al.* <sup>(217)</sup> Dot blot analysis works on a similar principle to western blotting, in that the target protein is bound by a primary antibody which, in turn, is bound to a secondary antibody with a chemiluminescent tag. This allows visualisation of the protein of interest. Rather than using electrophoresis the cell lysate is loaded directly onto the membrane, and a PK digestion is then used to remove all protein except the protease resistant core of PrP<sup>Sc</sup>. PMSF is used to stop the PK digestion, before the protein is denatured using a concentrated guanidine thiocyanate solution. The membrane is then blocked with milk before being probed with antibodies and visualised. An example of a dot blot can be seen in **Figure 19**. The darker dots show where the primary antibody had bound and could therefore be used to quantify the amount of PrP<sup>Sc</sup> in that particular sample. This, combined with the MTT data, could then be used to determine the anti-prion potency and possible toxic effects of the compounds of interest. Materials and methods are detailed in full in sections **2.1.1**, **2.2.1** and **2.2.2**.

### **3.1.1. Results**

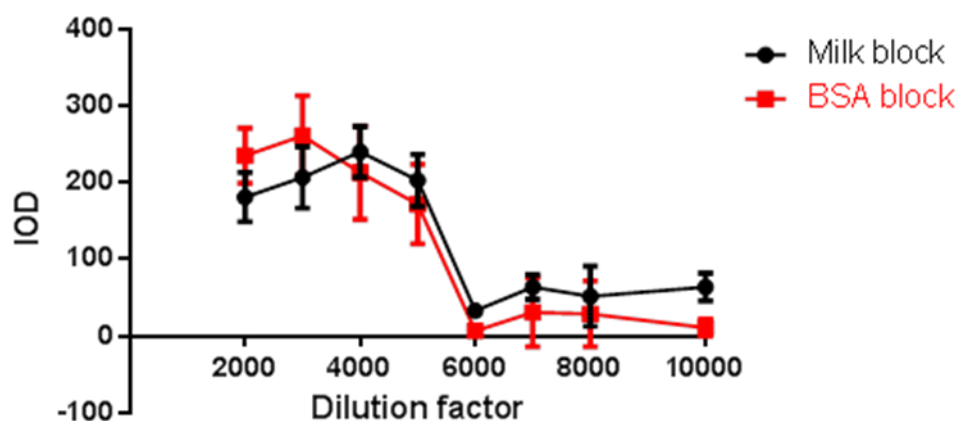
#### **3.1.1.1. Optimisation**

Two different primary antibodies were used over the course of these studies. To ensure that results using these two different antibodies would be comparable, the new antibody was tested using compounds with known anti-prion activity. Although the new antibody (8H4) maps to the region between residues 145 and 180 while 6H4 maps to residues 144-152, the results for the two antibodies were found to be comparable (see **Table 10**).

**Table 10:** EC<sub>50</sub>s of different compounds when probed with either 8H4 or 6H4

| Compound   | EC <sub>50</sub> 8H4 (μM) | EC <sub>50</sub> 6H4 (μM) |
|------------|---------------------------|---------------------------|
| Quinacrine | 0.25                      | 0.4 ± 0.232               |
| Curcumin   | 1                         | 0.95 ± 0.208              |
| 3001012    | 0.001                     | 0.000123 ± 0.000351       |

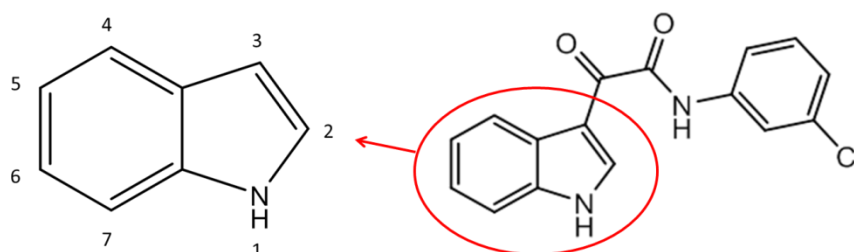
Optimisation of the secondary antibody concentration was also performed, along with investigations into whether a BSA block might be preferable to a milk blot. A blot of an untreated 96 well plate was carried out, and different sections of the blot were exposed to increasing concentrations of the secondary antibody. The minimum concentration of secondary antibody required to give an adequate signal was assessed. This experiment was carried out in duplicate with one membrane blocked with 5% milk in TBS-T, and the other membrane blocked with 5% BSA in TBS-T. This aimed to determine whether BSA resulted in more efficient blocking which may, in turn, allow a better signal to be obtained with lower concentrations of the secondary antibody. BSA did not result in an improvement in the strength of the dot blot signal as shown in **Figure 17**.



**Figure 17:** Optimisation of new IgG concentrations for dot blots. Dilutions up to 1:5000 were found to give a detectable and reproducible signal, while dilutions above this gave a very weak signal. There was not found to be any significant advantage in using BSA rather than milk for blocking. The data points shown represent the mean ± SD values from a single experiment where each sample was analysed 12 times. Data is expressed as the average density of each set of dots, and is presented as the integrated optical density (IOD) value (see section 2.2.2.2).

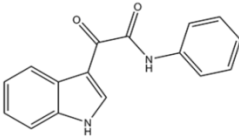
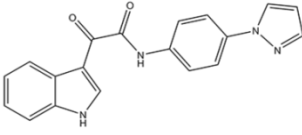
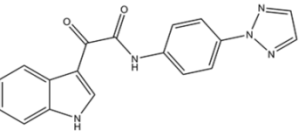
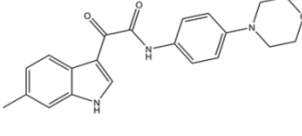
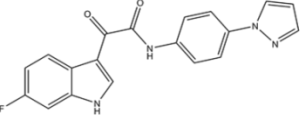
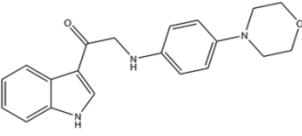
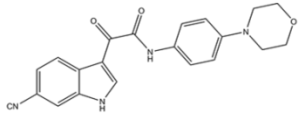
### 3.1.1.2. Initial Screen Results

Analysis of the initial screen results was facilitated by splitting the compounds up into libraries. To a certain extent these libraries are chronological, with library A being the first to be synthesised and screened. Later libraries are grouped depending in the particular structural features being investigated, and this is outlined in **Table 11**. The numbering on the indole ring is shown in **Figure 18**



**Figure 18:** The indole structure with the substitution positions numbered. The right hand structure shows the parent structure from earlier screens. The highlighted area shows the indole component numbered with the positions used for substitutions.

**Table 11.** Descriptions of the screening libraries used.

| Library | Description  | Example structure  | Number of compounds | Active compounds |
|---------|--|--|---------------------|------------------|
| A       | Unsubstituted indoles, 1-methylindoles and 2-methylindoles with different amines.                    |     | 66                  | 12               |
| B       | Optimisation of compounds identified from library A using unsubstituted indoles and 1-methylindoles. |    | 43                  | 29               |
| C       | Optimisation of compounds identified from libraries A and B using only unsubstituted indoles.        |    | 12                  | 9                |
| D       | Indoles substituted at the 5 and 6 position with amines optimised from previous libraries.           |   | 26                  | 22               |
| E       | Indoles substituted at the 6 and 7 position with amines optimised from previous libraries.           |  | 16                  | 16               |
| F       | Monocarbonyls and other analogues with amines optimised from previous libraries.                     |  | 21                  | 4                |
| G       | Further investigation of indoles substituted at the 5 and 6 position and other modifications.        |  | 13                  | 9                |

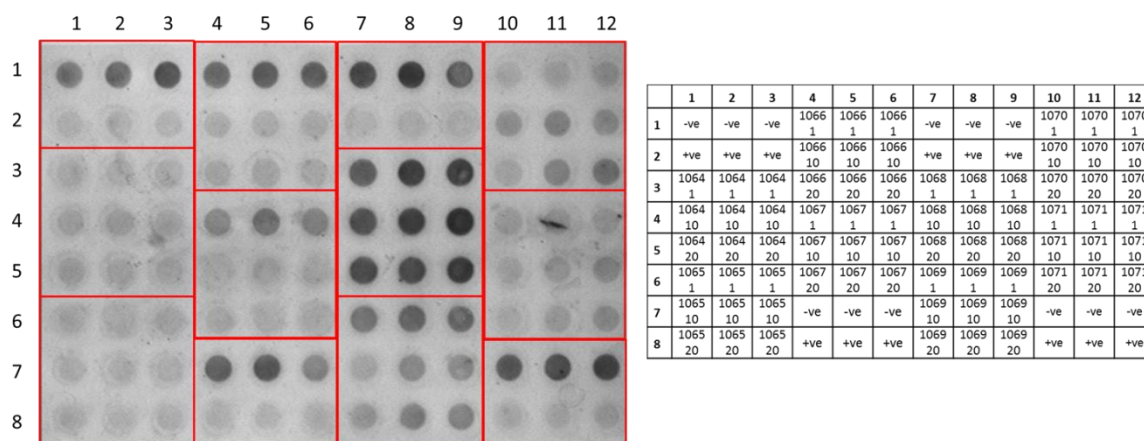
The majority of the I3GA compounds that were screened were found to be non-toxic apart from the compounds shown in **Table 12**.

**Table 12:** Viability results from the initial screens. Results are given for compounds that caused cell death as measured by the MTT assay. All other compounds were classed as non-toxic. In all cases toxicity was determined at the initial screen stage, with cytotoxicity occurring at the toxic concentrations in all cases (n = 6) so no standard deviation data was available. Concentrations that were tested below the toxic concentration were not cytotoxic.

| Library | Compound | Toxic concentration ( $\mu\text{M}$ ) |
|---------|----------|---------------------------------------|
| A       | 3000282  | 20                                    |
|         | 3000684  | 20                                    |
|         | 3000688  | 20                                    |
|         | 3000667  | 20                                    |
|         | 3000736  | 20                                    |
|         | 3000650  | 20                                    |
|         | 3000737  | 20                                    |
| B       | 3000916  | 20                                    |
| C       | 3001162  | 1                                     |
| D       | 3000786  | 20                                    |
| F       | 3001014  | 10                                    |
|         | 3001018  | 20                                    |
|         | 3001021  | 20                                    |
|         | 3001024  | 20                                    |

Although the majority of toxic compounds were only toxic at the highest concentration used in the initial screen, 3001162 induced cell death at all concentrations, making it unusually toxic for this group of compounds. 3001162 was the only compound with a sulphur-containing heterocycle, suggesting that this particular structural moiety cannot be tolerated by the SMB cells. No well-defined pattern was observed in the other toxic molecules, although the higher proportion of toxic molecules in library F suggests that the cells are particularly sensitive to changes to the carbonyl groups. All toxic molecules from the other libraries, with the exception of 3001196, had substitutions on the indole group, suggesting that for certain amine groups substitution to the indole group may confer toxicity onto otherwise non-toxic molecules.

The results of the initial activity screens are shown below. An example of the raw data obtained for the initial screens can be seen in **Figure 19**.



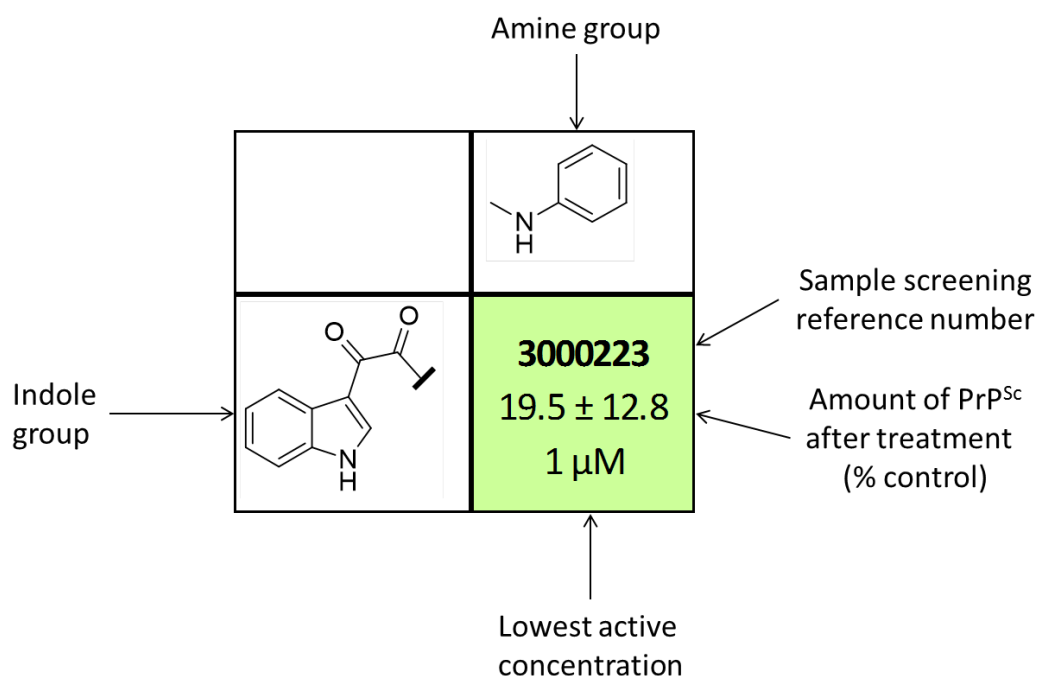
|   | 1       | 2       | 3       | 4       | 5       | 6       | 7       | 8       | 9       | 10      | 11      | 12      |
|---|---------|---------|---------|---------|---------|---------|---------|---------|---------|---------|---------|---------|
| 1 | 161.87  | 206.43  | 293.957 | 200.247 | 245.183 | 224.925 | 299.681 | 384.645 | 206.661 | 32.9075 | 38.7051 | 53.425  |
| 2 | 27.7626 | 34.6133 | 31.953  | 38.2996 | 39.4837 | 34.2095 | 15.4453 | 26.447  | 19.8282 | 80.7555 | 114.569 | 82.3133 |
| 3 | 28.5143 | 32.8425 | 28.5227 | 37.5517 | 38.7514 | 38.4906 | 214.223 | 361.212 | 335.312 | 36.8271 | 102.691 | 144.953 |
| 4 | 36.1061 | 37.3226 | 24.4594 | 77.2328 | 130.305 | 82.0851 | 238.214 | 334.102 | 432.257 | 41.3732 | 116.897 | 42.118  |
| 5 | 41.8676 | 26.7176 | 25.5641 | 11.743  | 30.9645 | 24.7749 | 274.495 | 266.167 | 365.951 | 35.0783 | 50.9335 | 71.0364 |
| 6 | 25.9055 | 10.3869 | 26.5873 | 21.9945 | 19.709  | 19.1026 | 135.82  | 186.268 | 177.953 | 25.2584 | 47.9989 | 72.5898 |
| 7 | 29.8064 | 29.0705 | 23.8175 | 212.123 | 244.783 | 111.449 | 41.7967 | 96.5833 | 91.724  | 245.805 | 283.932 | 320.783 |
| 8 | 26.7999 | 18.8558 | 28.8387 | 24.027  | 29.299  | 26.1714 | 60.9312 | 113.173 | 108.988 | 33.6009 | 32.2041 | 39.231  |

**Figure 19:** Example of a dot blot showing initial screen data. Dark dots show the presence of PrP<sup>Sc</sup>, with the absence of signal indicating absence of PrP<sup>Sc</sup>. The blot represents initial screens for 8 different I3GA compounds (3001064 to 3001071), as well as positive and negative controls (10 μM curcumin and 0.5 % DMSO respectively). Each compound is screened in triplicate at 1 μM, 10 μM and 20 μM. The plate is laid out as shown in the table to the right of the blot (1064 refers to compound 30010164, 1065 to 3001065 etc). All compounds were active apart from 3001068. The integrated optical density (IOD) value for each dot can be seen in the table below the blot. These values are used to calculate the amount of PrP<sup>Sc</sup> remaining after treatment as a percentage of the negative control.

All initial screen results were processed and expressed as a percentage of the PrP<sup>Sc</sup> signal relative to the untreated control (0.5 % DMSO). The value for the untreated control was the average of the 12 wells on each plate that were dosed with 0.5 % DMSO. Any compound that reduced PrP<sup>Sc</sup> by ≤ 70 % of the DMSO control, as measured by the IOD, were considered active. This cut off value was established by previous studies <sup>(278-280, 353, 355)</sup> and was used where appropriate throughout this thesis as a method of determining which compounds should be investigated further in the secondary assay. Each compound was assessed individually to determine if further analysis was required. Other publications reporting high-throughput screening programmes have used a cut off of 50 %. <sup>(205, 371)</sup> The higher cut off value of 70 % was used in this study due to the relatively small number of compounds involved, as identifying all compounds with anti-prion activity, even at low levels, was essential. This approach did result in false positives, as 11 out of

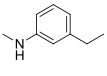
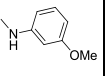
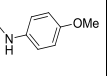
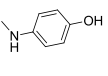
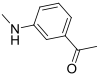
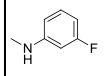
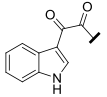
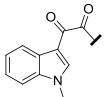
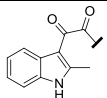
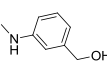
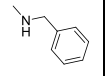
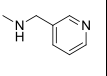
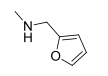
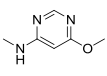
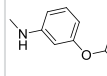
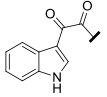
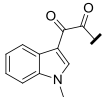
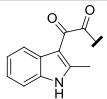
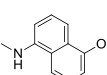
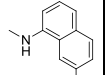
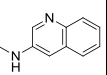
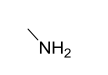
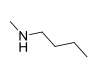
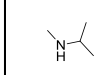
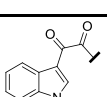
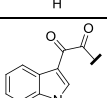
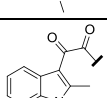
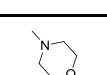
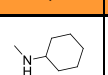
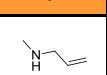
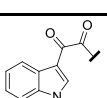
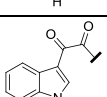
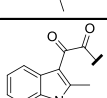
121 compounds identified as active in the initial screen were found to be inactive in the dose response screening. The majority of compounds, however, had their activity confirmed in the dose response screening, validating the approach that was used.

Initial screen data is presented as shown in **Figure 20** with the indole structure on the left hand side (with different substitutions) and the amine group along the top. Active compounds are highlighted in green. The activity data for the initial screen is presented as the amount of PrP<sup>Sc</sup>, as a percentage of the negative control, remaining after treatment with the lowest active concentration of compound. The lowest active concentration is stated below the activity data as an indicator of compound activity.

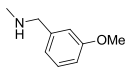
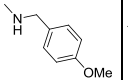
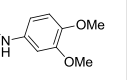
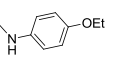
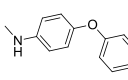
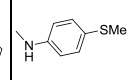
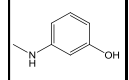
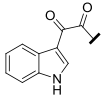
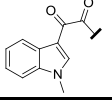
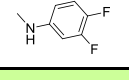
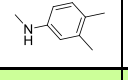
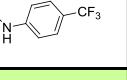
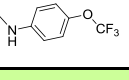
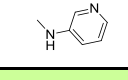
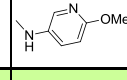
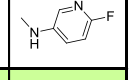
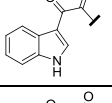
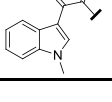
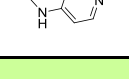
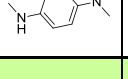
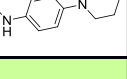
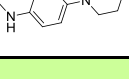
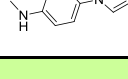
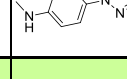
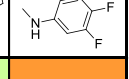
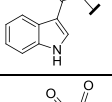
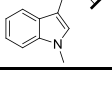
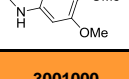
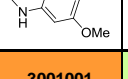
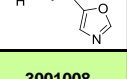
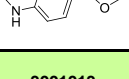
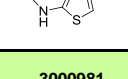
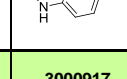
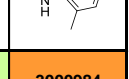
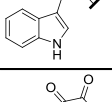
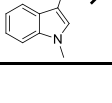
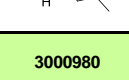
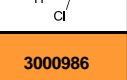
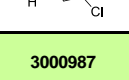
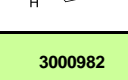
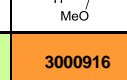
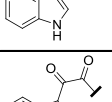
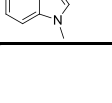


**Figure 20:** Example of the layout of the data in the subsequent results tables. The indole group is described in the left hand column, with the amine group along the top. Activity data is presented for each compound, along with the lowest concentration at which that compound was active. Each result represents at least two independent experiments, and each experiment was carried out in triplicate.

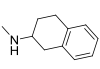
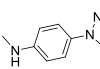
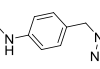
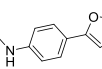
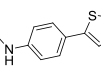
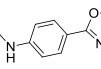
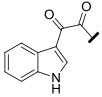
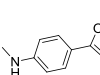
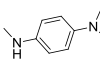
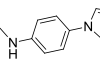
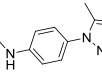
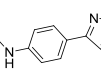
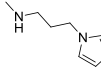
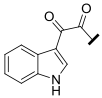
**Table 13:** Initial screen results for library A. The compounds in library A represent a wide range of amines, in conjunction with either unsubstituted indoles (top row), 1-methylindoles (middle row) or 2-methylindoles (bottom row).

|   |   |   |   |   |   |  |   |
|---|---|---|---|---|---|--|---|
|   |    |    |    |    |    |    |    |
|    | <b>3000223</b><br>19.5 ± 12.8<br>1 μM   | <b>3000553</b><br>37.9 ± 23<br>10 μM  | <b>3000259</b><br>17.5 ± 7<br>10 μM   | <b>3000260</b><br>6.7 ± 8.2<br>1 μM   | <b>3000234</b><br>17.8 ± 8.6<br>1 μM  | <b>3000235</b><br>98.8 ± 22<br>20 μM   | <b>3000530</b><br>27.1 ± 8.9<br>1 μM  |
|    | <b>3000556</b><br>68.5 ± 15.3<br>20 μM  | <b>3000662</b><br>132 ± 38.5<br>20 μM   | <b>3000663</b><br>61.8 ± 8<br>20 μM   | <b>3000664</b><br>11.6 ± 1.4<br>1 μM  | <b>3000656</b><br>47.3 ± 16.1<br>10 μM  | <b>3000732</b><br>157 ± 58.8<br>20 μM  | <b>3000665</b><br>114 ± 20.7<br>20 μM   |
|    | <b>3000557</b><br>41.6 ± 15<br>10 μM  | <b>3000651</b><br>78.8 ± 22.5<br>20 μM  | <b>3000648</b><br>44 ± 14.6<br>20 μM  | <b>3000649</b><br>49.8 ± 36.8<br>20 μM  | <b>3000645</b><br>83.1 ± 13.7<br>20 μM  | <b>3000646</b><br>84.4 ± 13.2<br>20 μM   | <b>3000652</b><br>64 ± 18.2<br>20 μM  |
|   |    |    |    |    |    |    |    |
|    | <b>3000529</b><br>70.1 ± 28.9<br>20 μM  | <b>3000258</b><br>17.6 ± 10.1<br>10 μM  | <b>3000255</b><br>90 ± 24.9<br>20 μM  | <b>3000522</b><br>107 ± 18.9<br>20 μM   | <b>3000230</b><br>95.2 ± 18.2<br>10 μM  | <b>3000554</b><br>23 ± 16.5<br>1 μM  | <b>3000261</b><br>98.3 ± 15.7<br>20 μM  |
|   | <b>3000686</b><br>91.2 ± 13.2<br>20 μM  | <b>3000733</b><br>137 ± 59.5<br>20 μM   | <b>3000283</b><br>148 ± 57.1<br>10 μM   | <b>3000684</b><br>117 ± 36.1<br>20 μM   | <b>3000685</b><br>109 ± 1.7<br>20 μM  | <b>3000739</b><br>86.4 ± 11.5<br>10 μM   | <b>3000688</b><br>169 ± 77.6<br>10 μM   |
|  | <b>3000738</b><br>78.5 ± 24.6<br>20 μM  | <b>3000734</b><br>80.8 ± 10.7<br>20 μM  | <b>3000284</b><br>76.7 ± 25.4<br>10 μM  | <b>3000647</b><br>73.7 ± 10<br>20 μM  | <b>3000709</b><br>83 ± 8.7<br>20 μM   | <b>3000735</b><br>69.7 ± 31.4<br>20 μM   | <b>3000650</b><br>103 ± 10.3<br>10 μM   |
|   |  |  |  |  |  |  |  |
|  | <b>3000531</b><br>135 ± 31.5<br>20 μM   | <b>3000532</b><br>101 ± 42.3<br>20 μM   | <b>3000533</b><br>115 ± 21.2<br>20 μM   | <b>3000534</b><br>41.3 ± 14.8<br>1 μM   | <b>3000232</b><br>63.2 ± 14.7<br>20 μM  | <b>3000251</b><br>80.8 ± 14.3<br>20 μM   | <b>3000249</b><br>74.9 ± 8.2<br>20 μM   |
|  | <b>3000689</b><br>121 ± 28.8<br>20 μM   | <b>3000690</b><br>114 ± 33.5<br>20 μM   | <b>3000666</b><br>111.29 ± 1.9<br>20 μM   | <b>3000667</b><br>102 ± 25.2<br>10 μM   |   | <b>3000691</b><br>124 ± 46.2<br>20 μM  |   |
|  | <b>3000653</b><br>96.3 ± 18<br>20 μM  |   | <b>3000654</b><br>112.7 ± 19.7<br>20 μM   | <b>3000655</b><br>87.6 ± 14.1<br>20 μM  |   | <b>3000737</b><br>129 ± 36.7<br>10 μM  |   |
|   |  |  |  |  |   |  |   |
|  | <b>3000245</b><br>112 ± 18.6<br>20 μM   | <b>3000246</b><br>80.3 ± 14.3<br>20 μM  | <b>3000250</b><br>83.1 ± 16.1<br>20 μM  | <b>3000248</b><br>158 ± 17.3<br>20 μM   |   |  |   |
|  |   | <b>3000740</b><br>100 ± 14.9<br>20 μM   | <b>3000736</b><br>131 ± 62.5<br>10 μM   |   |   |  |   |
|  |   | <b>3000711</b><br>81.9 ± 25.4<br>20 μM  | <b>3000710</b><br>102 ± 14.7<br>20 μM   |   |   |  |   |

**Table 14:** Initial screen results for library B. The compounds in library B represent optimisation of the most promising amines, as identified from library A. These were investigated in conjunction with either unsubstituted indoles (top row) or 1-methylindoles (bottom row).

|   |    |    |    |    |    |    |    |
|---|---|---|---|---|--|---|---|
|    | <b>3000914</b><br>104 ± 15.3<br>20 µM   | <b>3000915</b><br>104 ± 3.7<br>20 µM  | <b>3000918</b><br>19.3 ± 12.2<br>1 µM   | <b>3000979</b><br>6.5 ± 3.8<br>1 µM   | <b>3000993</b><br>56 ± 1<br>10 µM  | <b>3000991</b><br>5.6 ± 1.5<br>1 µM   | <b>MT609</b><br>52.4 ± 12.3<br>1 µM   |
|    |   |   |   |   | <b>3001085</b><br>31.5 ± 8.13<br>20 µM   |   |   |
|   |    |    |    |    |    |    |    |
|    | <b>3000985</b><br>1.4 ± 2<br>1 µM   | <b>3000978</b><br>48.7 ± 2.03<br>1 µM   | <b>3001002</b><br>6.1 ± 0.8<br>1 µM   | <b>3000999</b><br>6.7 ± 0.2<br>1 µM   | <b>3000996</b><br>8 ± 3.2<br>10 µM   | <b>3000998</b><br>4.9 ± 0.6<br>1 µM   | <b>3000997</b><br>52.3 ± 3.2<br>1 µM  |
|    |   |   |   |   |  |   |   |
|   |   |   |   |   |   |   |   |
|  | <b>3000983</b><br>26.99 ± 7.88<br>1 µM  | <b>3000992</b><br>7.2 ± 1<br>1 µM   | <b>3000995</b><br>6.5 ± 2.7<br>1 µM   | <b>3000994</b><br>4.6 ± 1.5<br>1 µM   | <b>3001003</b><br>17.1 ± 4.9<br>1 µM   | <b>3001012</b><br>6.98 ± 3.18<br>1 µM   | <b>3001007</b><br>62.46 ± 11.4<br>20 µM   |
|  |   |   |   | <b>3001088</b><br>15.73 ± 5<br>1 µM   | <b>3001086</b><br>12.56 ± 5.19<br>1 µM   | <b>3001087</b><br>17.73 ± 5.94<br>1 µM  | <b>3001083</b><br>103.87 ± 30.91<br>20 µM   |
|   |  |  |  |  |  |  |  |
|  | <b>3001000</b><br>143 ± 10.6<br>20 µM   | <b>3001001</b><br>75.4 ± 10.9<br>20 µM  | <b>3001008</b><br>16.8 ± 8.1<br>10 µM   | <b>3001013</b><br>16.77 ± 4.23<br>1 µM  | <b>3000981</b><br>41.6 ± 14.49<br>1 µM   | <b>3000917</b><br>10.3 ± 13.16<br>1 µM  | <b>3000984</b><br>93.78 ± 29.65<br>20 µM  |
|  |   |   | <b>3001082</b><br>110.82 ± 2.03<br>20 µM  | <b>3001006</b><br>19.88 ± 13.41<br>1 µM   |  | <b>3001005</b><br>82.51 ± 11.45<br>20 µM  | <b>3001084</b><br>94.32 ± 13.73<br>20 µM  |
|   |  |  |  |  |  |  |   |
|  | <b>3000980</b><br>21.7 ± 15.51<br>10 µM   | <b>3000977</b><br>4.13 ± 1.71<br>1 µM   | <b>3000986</b><br>85.35 ± 19.96<br>20 µM  | <b>3000987</b><br>40 ± 10.45<br>10 µM   | <b>3000982</b><br>5.85 ± 1.19<br>1 µM  | <b>3000916</b><br>139.69 ± 0.004<br>10 µM   |   |
|  |   |   |   |   |  |   |   |

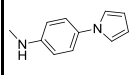
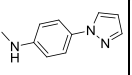
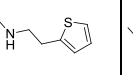
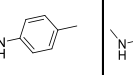
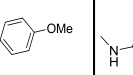
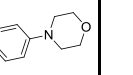
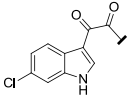
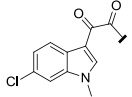
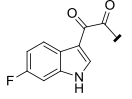
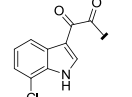
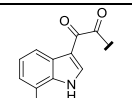
**Table 15:** Initial screen results for library C. The compounds in library C represent further optimisation of the amines identified from libraries A and B, in conjunction with unsubstituted indoles.

|   |   |   |   |   |   |   |
|---|---|---|---|---|---|---|
|   |  |  |  |  |  |  |
|  | <b>3001136</b><br>53.59 ± 5.48<br>20 μM   | <b>3001137</b><br>16.24 ± 3.08<br>1 μM  | <b>3001138</b><br>19.59 ± 9.83<br>1 μM  | <b>3001142</b><br>8 ± 2.46<br>1 μM  | <b>3001162</b><br>toxic<br>1 μM   | <b>3001165</b><br>6.26 ± 2.82<br>1 μM   |
|   |  |  |  |  |  |  |
|  | <b>3001166</b><br>11.27 ± 5.16<br>1 μM  | <b>3001164</b><br>12.94 ± 0.94<br>10 μM   | <b>3001143</b><br>9.36 ± 4.21<br>1 μM   | <b>3001144</b><br>8.16 ± 0.64<br>1 μM   | <b>3001163</b><br>18.88 ± 7.43<br>1 μM  | <b>3001167</b><br>99.82 ± 7.54<br>1 μM  |

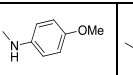
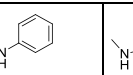
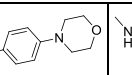
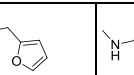
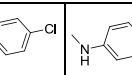
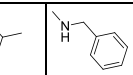
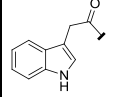
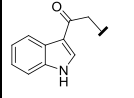
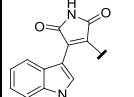
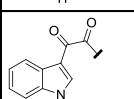
**Table 16:** Initial screen results for library D. The compounds in library D represent further investigations into substitutions at the 5 and 6 position of the indole, using amine groups optimised from libraries A, B and C. The substitutions investigated were the addition of chloro groups at the 6 position (top row) and 5 position (second row), and the addition of methyl groups at the 6 position (third row) and 5 position (bottom row).

|   |  |  |  |  |  |
|---|---|---|---|---|--|
|    | <b>3001060</b><br>10.53 ± 2.4<br>1 μM   | <b>3001058</b><br>59.35 ± 4.68<br>1 μM  | <b>3001063</b><br>22.14 ± 9.63<br>1 μM  | <b>3001061</b><br>17.84 ± 0.74<br>1 μM  | <b>3001059</b><br>13.93 ± 6.32<br>1 μM   |
|    | <b>3001066</b><br>14.61 ± 1.08<br>10 μM   | <b>3001064</b><br>11.73 ± 0.98<br>1 μM  | <b>3001069</b><br>30.02 ± 11.87<br>10 μM  | <b>3001067</b><br>37.79 ± 11.48<br>10 μM  | <b>3001065</b><br>8.2 ± 3.59<br>1 μM   |
|    | <b>3001072</b><br>19.51 ± 2.29<br>1 μM  | <b>3001070</b><br>16.31 ± 4.14<br>1 μM  |   | <b>3001073</b><br>13.92 ± 2.27<br>1 μM  | <b>3001071</b><br>26.15 ± 16.98<br>1 μM  |
|    | <b>3001075</b><br>31.44 ± 9.61<br>20 μM   | <b>3001080</b><br>17.15 ± 10.17<br>10 μM  |   | <b>3001077</b><br>15.07 ± 0.77<br>10 μM   | <b>3001081</b><br>15.08 ± 2.93<br>1 μM   |
|   |  |  |  |  |  |
|  | <b>3001062</b><br>48.87 ± 7.94<br>20 μM   | <b>3000641</b><br>7.9 ± 6.97<br>1 μM  | <b>3000785</b><br>11.01 ± 7.17<br>1 μM  | <b>3000786</b><br>120.19 ± 12.04<br>10 μM   | <b>3000787</b><br>45.27 ± 4.53<br>1 μM   |
|  | <b>3001068</b><br>118.29 ± 21.67<br>20 μM   |   |   |   |  |
|  | <b>3001074</b><br>37.22 ± 8.66<br>20 μM   |   |   |   |  |
|  | <b>3001076</b><br>115.79 ± 15.56<br>20 μM   |   |   |   |  |

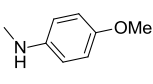
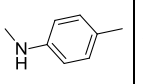
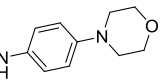
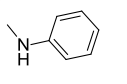
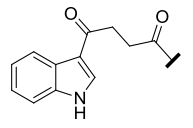
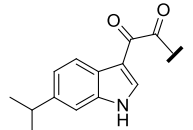
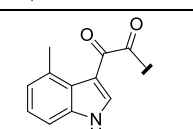
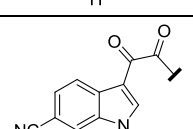
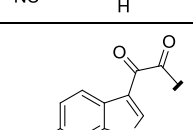
**Table 17:** Initial screen results for library E. The compounds in library E represent a continuation of the investigations into the substitutions in library D. Further investigations of the 6 chloro substitution were undertaken (top row) along with investigations into the effect of two substitutions on the indole, at the 6 position and the 1 position (second row), 6-fluoro substitutions (third row), 7-chloro substitutions (fourth row) and 7-methyl substitutions (bottom row). Amines optimised from libraries A, B and C were used.

|  |  |  |  |  |  |  |
|--|---|---|---|---|---|---|
|   | <b>3001123</b><br>7.42 ± 4.23<br>1 μM   | <b>3001124</b><br>42.72 ± 10.13<br>1 μM   | <b>3001125</b><br>5.46 ± 3.68<br>1 μM   |   |   |   |
|   | <b>3001127</b><br>17.54 ± 6.90<br>1 μM  | <b>3001128</b><br>9.33 ± 1.19<br>1 μM   |   |   | <b>3001130</b><br>22.89 ± 4.23<br>1 μM  | <b>3001129</b><br>11.02 ± 1.58<br>1 μM  |
|   | <b>3001139</b><br>37.86 ± 8.08<br>10 μM   | <b>3001140</b><br>11.73 ± 3.03<br>1 μM  |   |   | <b>3001126</b><br>5.55 ± 5.78<br>1 μM   |   |
|   |   |   |   | <b>3001181</b><br>24.47 ± 2.73<br>1 μM  | <b>3001180</b><br>7.78 ± 3.6<br>1 μM  | <b>3001141</b><br>15.58 ± 4.51<br>1 μM  |
|  |   |   |   | <b>3001184</b><br>15.45 ± 9.25<br>10 μM   | <b>3001183</b><br>7.28 ± 2.2<br>1 μM  | <b>3001182</b><br>29.13 ± 8.78<br>1 μM  |

**Table 18:** Initial screen results for library F. The compounds in library F represent investigations into the effect of changes to the carbonyl groups. The effect of a monocarbonyl group was investigated (top two rows), as was the addition of a heterocycle instead of the carbonyl groups (third row). Addition of a large group to the 1 position of the indole was also investigated (bottom row). Amines optimised from libraries A, B and C were used.

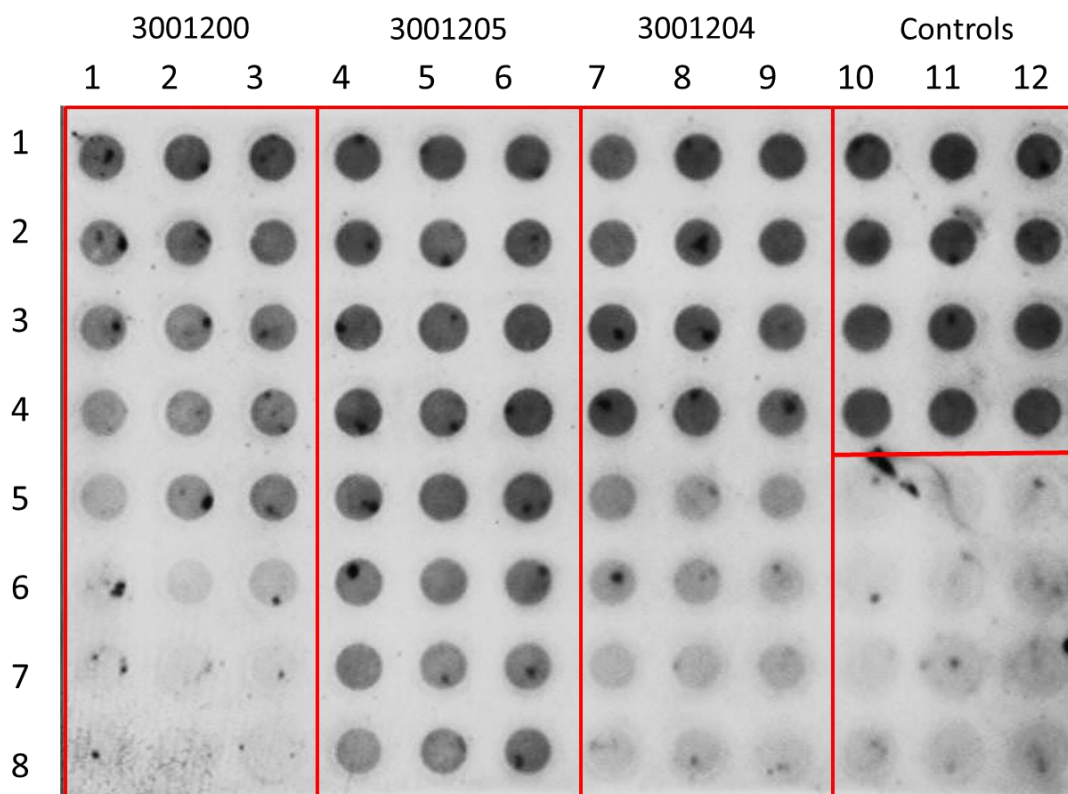
|   |  |  |  |  |  |  |  |
|---|---|---|---|---|--|---|---|
|  | <b>3000525</b><br>97.26 ± 14.8<br>20 μM   | <b>3000520</b><br>112.81 ± 0.00<br>20 μM  | <b>3001010</b><br>46.61 ± 15.52<br>10 μM  | <b>3001011</b><br>78.04 ± 14.21<br>20 μM  | <b>3001009</b><br>37.8 ± 6.44<br>20 μM   |   | <b>3000527</b><br>109.26 ± 7.38<br>20 μM  |
|  | <b>3001015</b><br>5.16 ± 2.48<br>1 μM   | <b>3001016</b><br>5.63 ± 0.23<br>1 μM   | <b>3001017</b><br>4.82 ± 2.48<br>1 μM   |   |  |   | <b>3001014</b><br>128.69 ± 4.52<br>10 μM  |
|  | <b>3001018</b><br>98.18 ± 4.08<br>20 μM   | <b>3001019</b><br>120.16 ± 2.83<br>20 μM  | <b>3001057</b><br>116.39 ± 20.24<br>20 μM   |   | <b>3001021</b><br>91.86 ± 9.22<br>20 μM  | <b>3001020</b><br>104.17 ± 19.21<br>20 μM   | <b>3001056</b><br>96.80 ± 19.41<br>20 μM  |
|  | <b>3001022</b><br>44.29 ± 12.17<br>20 μM  | <b>3001023</b><br>87.88 ± 2.5<br>20 μM  |   |   | <b>3001026</b><br>44.5 ± 3.28<br>20 μM   | <b>3001025</b><br>43.82 ± 6.48<br>20 μM   | <b>3001024</b><br>77.73 ± 6.62<br>20 μM   |

**Table 19:** Initial screen results for library G. The compounds in library G represent further investigations into the effect of substitutions to the indole group using amines optimised from libraries A, B and C. The effect of the addition of a methyl bridge between the two carbonyls was examined (top row), along with the effect of <sup>i</sup>Pr substitutions at the 6 position (second row), a methyl group at the 4 position (third row), a cyano group at the 6 position (fourth row) and a nitro group at the 6 position (bottom row).

|   |  |  |  |  |
|---|---|---|--|---|
|    | <b>3001192</b><br>102.73 ± 0.41<br>20 μM  | <b>3001203</b><br>110.22 ± 1.33<br>20 μM  | <b>3001193</b><br>79.23 ± 11.47<br>20 μM   | <b>3001202</b><br>119.52 ± 2.61<br>20 μM  |
|    | <b>3001199</b><br>14.44 ± 2.98<br>1 μM  | <b>3001206</b><br>5.52 ± 0.39<br>20 μM  |  |   |
|    | <b>3001204</b><br>11.59 ± 1.74<br>10 μM   | <b>3001205</b><br>46.42 ± 11.27<br>20 μM  | <b>3001194</b><br>31.03 ± 6.68<br>1 μM   |   |
|   | <b>3001207</b><br>18.04 ± 4.58<br>1 μM  | <b>3001208</b><br>12.35 ± 3.36<br>1 μM  |  |   |
|  | <b>3001209</b><br>10.63 ± 3.55<br>1 μM  | <b>3001210</b><br>7.23 ± 2.72<br>1 μM   |  |   |

### 3.1.1.3. EC<sub>50</sub> Activity Screening

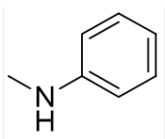
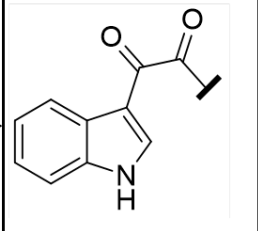
The tables below show the calculated EC<sub>50</sub> values for the I3GA compounds that were found to have anti-prion activity in the initial screen, as outlined in section 3.1.1.2. An example of the raw data obtained for the EC<sub>50</sub> screens can be seen in **Figure 21**.



|   | 1       | 2       | 3       | 4       | 5       | 6       | 7       | 8       | 9       | 10      | 11      | 12      |
|---|---------|---------|---------|---------|---------|---------|---------|---------|---------|---------|---------|---------|
| 1 | 190.169 | 214.032 | 231.836 | 223.823 | 219.235 | 205.509 | 172.248 | 244.789 | 232.935 | 267.558 | 285.982 | 269.271 |
| 2 | 166.73  | 178.909 | 170.784 | 216.331 | 172.824 | 216.375 | 170.219 | 246.508 | 209.87  | 243.283 | 242.581 | 237.606 |
| 3 | 135.015 | 141.849 | 154.41  | 203.157 | 169.721 | 203.781 | 222.23  | 223.473 | 175.778 | 205.278 | 227.694 | 228.556 |
| 4 | 90.209  | 114.549 | 144.028 | 211.898 | 178.568 | 226.27  | 227.848 | 185.696 | 170.896 | 198.885 | 219.44  | 200.393 |
| 5 | 47.1789 | 134.712 | 127.216 | 180.736 | 162.581 | 184.062 | 85.9292 | 66.111  | 74.8507 | 8.25455 | 27.5897 | 28.3772 |
| 6 | 54.6134 | 27.015  | 49.6441 | 167.574 | 125.892 | 154.734 | 93.5612 | 66.3625 | 47.0727 | 16.5015 | 15.8718 | 29.4331 |
| 7 | 27.5581 | 16.4854 | 18.4838 | 119.33  | 96.5173 | 116.653 | 38.5544 | 35.384  | 44.6966 | 10.5622 | 18.9116 | 14.322  |
| 8 | 23.9875 | 18.0305 | 7.49379 | 84.2115 | 118.507 | 150.89  | 25.3707 | 33.1261 | 20.9215 | 30.0885 | 19.3461 | 30.415  |

**Figure 21:** Example of a dot blot for EC<sub>50</sub> data. The data presented represent three I3GA compounds: 3001200 (columns 1-3); 3001205 (columns 4-6); 3001204 (columns 7-9); and controls (columns 10-12). In the control columns rows 1-4 were treated with 0.5 % DMSO (negative control) and rows 5-8 were treated with 10  $\mu$ M curcumin (positive control). Each compound was screened at 8 concentrations, going from low at the top to high at the bottom. The integrated optical density (IOD) value for each dot can be seen in the table. These values are used to calculate the amount of PrP<sup>Sc</sup> remaining after treatment as a percentage of the negative control.

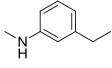
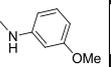
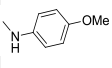
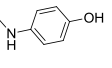
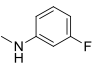
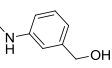
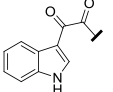
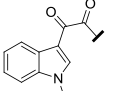
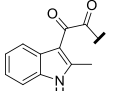
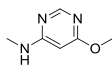
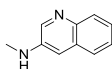
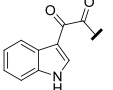
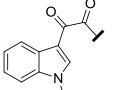
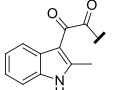
Data is presented as shown in **Figure 22**, with the stated values representing the EC<sub>50</sub> value of the particular compound. This value is a measure of the compound's anti-prion activity, and is the concentration at which the compound exerts 50% of its anti-prion effect. See section **3.1.1.2** for detailed explanations of each library.

|  |  |   |
|--|--|---|
|  | Amine group<br> |   |
| Indole group<br> | <b>3000233</b><br><b>0.32 ± 0.02</b><br><b>μM</b>  | ← Sample screening reference number<br>← EC <sub>50</sub> value |

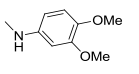
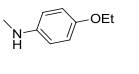
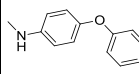
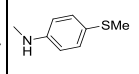
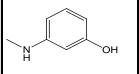
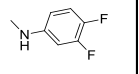
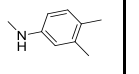
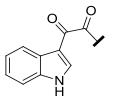
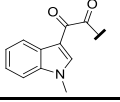
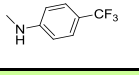
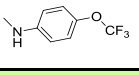
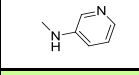
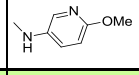
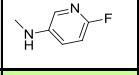
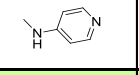
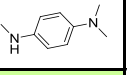
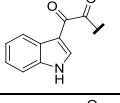
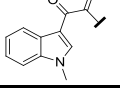
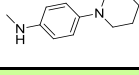
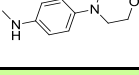
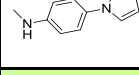
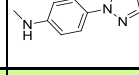
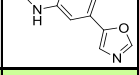
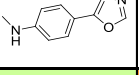
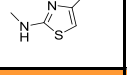
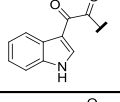
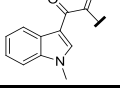
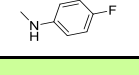
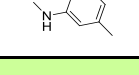
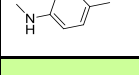
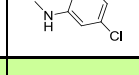
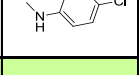
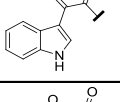
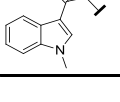
**Figure 22:** Example of the layout of the data in the subsequent results tables. The indole group is described in the left hand column, with the amine group along the top. Activity is expressed as the compound's EC<sub>50</sub> value. Each result represents at least two independent experiments, and each experiment was carried out in triplicate.

Screens of compounds with known activity in prion infected cell lines were carried out alongside the I3GA screens. Quinacrine gave an EC<sub>50</sub> of 0.31 ± 0.2 μM (literature value in ScN2a cells 0.3 μM<sup>(232)</sup>) and the value for curcumin was 0.87 ± 0.15 μM (literature value in ScNB cells 10 nM<sup>(266)</sup>). These values are in good agreement with the literature and validate the screening strategy.

**Table 20:** EC<sub>50</sub> results for library A

|   |  |  |  |  |  |  |  |
|---|---|---|---|---|--|---|---|
|    | <b>3000233</b><br>0.32 ± 0.02<br>μM   | <b>3000553</b><br>12.1 ± 2.4 μM   | <b>3000259</b><br>0.232 ± 0.002<br>μM   | <b>3000260</b><br>0.011 ± 0.006<br>μM   | <b>3000234</b><br>0.24 ± 0.12<br>μM  | <b>3000530</b><br>0.64 ± 0.04<br>μM   | <b>3000258</b><br>Inactive  |
|    | <b>3000556</b><br>6.9 ± 0.85 μM   |   | <b>3000663</b><br>4.7 ± 5.5 μM  | <b>3000664</b><br>0.068 ± 0.018<br>μM   | <b>3000656</b><br>3.77 ± 1.69<br>μM  |   |   |
|    | <b>3000557</b><br>Inactive  |   | <b>3000648</b><br>Inactive  | <b>3000649</b><br>Inactive  |  |   |   |
|   |  |  |   |   |  |   |   |
|    | <b>3000554</b><br>0.68 ± 0.13<br>μM   | <b>3000534</b><br>0.17 ± 0.07 μM  |   |   |  |   |   |
|    |   |   |   |   |  |   |   |
|  |   |   |   |   |  |   |   |

**Table 21:** EC<sub>50</sub> results for library B

|   |   |   |   |   |  |   |   |
|---|---|---|---|---|--|---|---|
|   |    |    |    |    |    |  |  |
|    | <b>3000918</b><br>0.52 ± 0.15 μM  | <b>3000979</b><br>0.06 ± 0.000 μM   | <b>3000993</b><br>1.03 ± 0.07 μM  | <b>3000991</b><br>0.04 ± 0.035 μM   | <b>MT609</b><br>0.82 ± 0.03 μM   | <b>3000985</b><br>0.22 ± 0.2 μM   | <b>3000978</b><br>1.2 ± 0.56 μM   |
|    |   |   | <b>3001085</b><br>Inactive  |   |  |   |   |
|   |    |    |    |    |    |  |  |
|    | <b>3001002</b><br>0.29 ± 0.13 μM  | <b>3000999</b><br>0.38 ± 0.09 μM  | <b>3000996</b><br>1.66 ± 0.51 μM  | <b>3000998</b><br>0.12 ± 0.03 μM  | <b>3000997</b><br>1.21 ± 0.18 μM   | <b>3000983</b><br>0.79 ± 0.34 μM  | <b>3000992</b><br>0.026 ± 0.03 μM   |
|    |   |   |   |   |  |   |   |
|   |    |    |    |    |    |  |  |
|   | <b>3000995</b><br>0.072 ± 0.027 μM  | <b>3000994</b><br>0.009 ± 0.002 μM  | <b>3001003</b><br>0.006 ± 0.003 μM  | <b>3001012</b><br>0.001 ± 0.0004 μM   | <b>3001008</b><br>0.53 ± 0.08 μM   | <b>3001013</b><br>0.019 ± 0.005 μM  | <b>3000981</b><br>Inactive  |
|  |   | <b>3001088</b><br>0.019 ± 0.005 μM  | <b>3001086</b><br>0.17 ± 0.05 μM  | <b>3001087</b><br>0.018 ± 0.003 μM  |  | <b>3001006</b><br>0.037 ± 0.018 μM  |   |
|   |  |  |  |  |  |   |   |
|  | <b>3000917</b><br>0.064 ± 0.009 μM  | <b>3000980</b><br>6.4 ± 2.3 μM  | <b>3000977</b><br>0.13 ± 0.02 μM  | <b>3000987</b><br>1.51 ± 0.15 μM  | <b>3000982</b><br>0.065 ± 0.035 μM   |   |   |
|  |   |   |   |   |  |   |   |

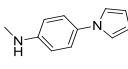
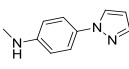
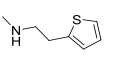
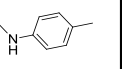
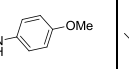
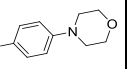
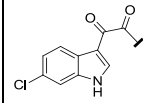
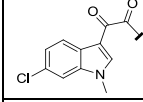
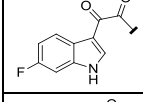
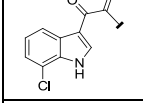
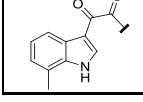
**Table 22:** EC<sub>50</sub> results for library C

|  |                                    |                                       |   |                                  |   |
|--|------------------------------------|---------------------------------------|---|----------------------------------|---|
|  |                                    |                                       |   |                                  |   |
|  | <b>3001136</b><br>Inactive         | <b>3001137</b><br>0.003 ± 0.000<br>μM | <b>3001138</b><br>0.6 ± 0.4 μM          | <b>3001142</b><br>0.02 ± 0.00 μM | <b>3001165</b><br>0.00095 ±<br>0.00005 μM |
|  |                                    |                                       |   |                                  |   |
|  | <b>3001166</b><br>0.035 ± 0.015 μM | <b>3001164</b><br>0.12 ± 0.03 μM      | <b>3001143</b><br>0.0013 ± 0.0003<br>μM | <b>3001144</b><br>0.11 ± 0.06 μM | <b>3001163</b><br>0.006 μM                |

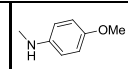
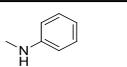
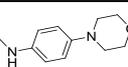
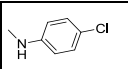
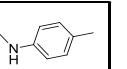
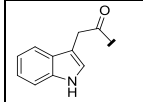
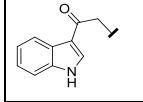
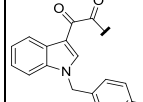
**Table 23:** EC<sub>50</sub> results for library D

|  |                                       |                                       |                                       |                                       |                                    |
|--|---------------------------------------|---------------------------------------|---------------------------------------|---------------------------------------|------------------------------------|
|  |                                       |                                       |                                       |                                       |                                    |
|  | <b>3001060</b><br>0.074 ± 0.009<br>μM | <b>3001058</b><br>0.009 ± 0.001<br>μM | <b>3001063</b><br>0.1 ± 0.02 μM       | <b>3001061</b><br>0.1 ± 0.03 μM       | <b>3001059</b><br>0.007 ± 0.000 μM |
|  |                                       |                                       |                                       |                                       |                                    |
|  | <b>3001066</b><br>1.63 ± 0.81 μM      | <b>3001064</b><br>0.47 ± 0.04 μM      | <b>3001069</b><br>0.074 ± 0.005<br>μM | <b>3001067</b><br>0.56 ± 0.12 μM      | <b>3001065</b><br>0.068 ± 0.004 μM |
|  |                                       |                                       |                                       |                                       |                                    |
|  | <b>3001072</b><br>0.06 ± 0.006<br>μM  | <b>3001070</b><br>0.012 ± 0.003<br>μM |                                       | <b>3001073</b><br>0.045 ± 0.007<br>μM | <b>3001071</b><br>0.005 ± 0.004 μM |
|  |                                       |                                       |                                       |                                       |                                    |
|  | <b>3001075</b><br>13 ± 2.8 μM         | <b>3001080</b><br>0.87 ± 0.31 μM      |                                       | <b>3001077</b><br>0.9 ± 0.3 μM        | <b>3001081</b><br>0.12 ± 0.06 μM   |
|  |                                       |                                       |                                       |                                       |                                    |
|  | <b>3001062</b><br>Inactive            | <b>3000641</b><br>0.16 ± 0.06 μM      | <b>3000785</b><br>0.14 ± 0.06<br>μM   | <b>3000787</b><br>0.41 ± 0.23 μM      |                                    |
|  |                                       |                                       |                                       |                                       |                                    |
|  | <b>3001074</b><br>6.2 ± 2.1 μM        |                                       |                                       |                                       |                                    |
|  |                                       |                                       |                                       |                                       |                                    |

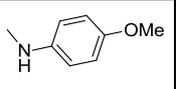
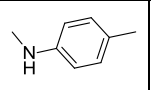
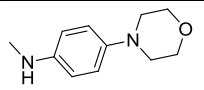
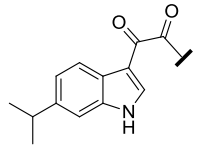
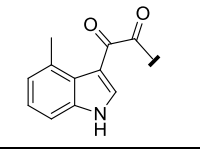
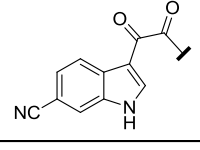
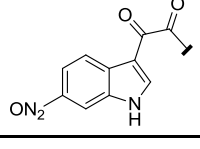
**Table 24:** EC<sub>50</sub> results for library E

|   |  |  |  |  |  |  |
|---|---|---|---|--|---|---|
|  | <b>3001123</b><br>0.012 ± 0.003<br>μM   | <b>3001124</b><br>0.007 ± 0.003<br>μM   | <b>3001125</b><br>0.44 ± 0.2 μM   |  |   |   |
|  | <b>3001127</b><br>0.27 ± 0.01 μM  | <b>3001128</b><br>0.15 ± 0.02 μM  |   |  | <b>3001130</b><br>2.7 ± 0.42 μM   | <b>3001129</b><br>0.15 ± 0.02 μM  |
|  | <b>3001139</b><br>0.008 ± 0.002<br>μM   | <b>3001140</b><br>0.0015 ± 0.0005<br>μM   |   |  | <b>3001126</b><br>0.01 ± 0.004<br>μM  |   |
|  |   |   |   | <b>3001181</b><br>0.45 ± 0.16 μM   | <b>3001180</b><br>0.024 ± 0.017<br>μM   | <b>3001141</b><br>0.008 ± 0.000 μM  |
|  |   |   |   | <b>3001184</b><br>1.4 ± 0.14 μM  | <b>3001183</b><br>0.14 ± 0.035 μM   | <b>3001182</b><br>0.0145 ± 0.0005<br>μM   |

**Table 25:** EC<sub>50</sub> results for library F

|   |  |  |  |  |  |
|---|---|---|---|--|---|
|  |   |   | <b>3001010</b><br>3.9 ± 1.9 μM  | <b>3001009</b><br>Inactive   |   |
|  | <b>3001015</b><br>0.36 ± 0.12 μM  | <b>3001016</b><br>1.40 ± 0.5 μM   | <b>3001017</b><br>0.11 ± 0.02 μM  |  |   |
|  |   |   |   | <b>3001026</b><br>Inactive   | <b>3001025</b><br>Inactive  |

**Table 26:** EC<sub>50</sub> results for library G

|   |  |  |  |
|---|---|---|--|
|  | <b>3001199</b><br>0.33 ± 0.06 μM  | <b>3001206</b><br>0.6 ± 0 μM  |  |
|  | <b>3001204</b><br>2.75 ± 0.35 μM  | <b>3001205</b><br>10 ± 0 μM   | <b>3001194</b><br>0.68 ± 0.11 μM   |
|  | <b>3001207</b><br>0.0022 ± 0.0028 μM  | <b>3001208</b><br>0.011 ± 0.0014 μM   |  |
|  | <b>3001209</b><br>0.011 ± 0.00141 μM  | <b>3001210</b><br>0.035 ± 0.01 μM   |  |

### 3.1.2. SAR Discussion

The ultimate aim of this stage of the project was to determine if there was a relationship between the structure of I3GAs and their potency in the cell based assay. This was done by analysing the activity data from the first round of the screening programme to determine structures that were beneficial to the anti-prion effect. Analogues of these active compounds were then synthesised and screened to try and further increase the potency.

#### 3.1.2.1. Library A

The compounds in library A consisted of amines attached to an unsubstituted indole, a 1-methylindole or a 2-methylindole and were based originally on the parent compound, an m-chloro substituted phenyl ring attached to an unsubstituted indole *via* a glyoxylamide linker (see **Figure 16**). One trend that is immediately obvious is that a methyl substitution at the 1 or 2 position of the indole (see **Figure 23**) is detrimental to activity.

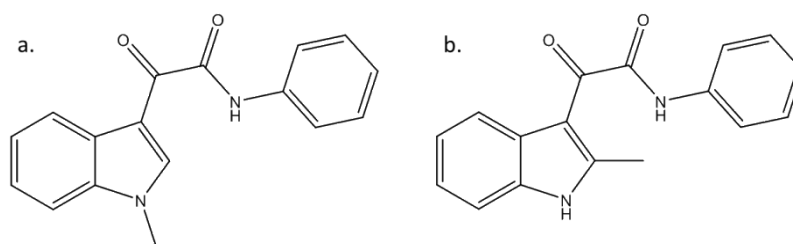


**Figure 23:** Examples of substituted indoles. a. is a 1-methylindole, b. is a 2-methylindole

All compounds containing the 2-methylindole were inactive. Although three showed activity in the initial screens this was not confirmed in the EC<sub>50</sub> screens so they were classed as inactive. Substitution at the 1 position also reduced activity although there were a few compounds that retained some activity (3000556, 3000663, 3000664 and 3000656). In all these cases, however, activity was reduced when compared to the unsubstituted analogue. Compare 3000233 (EC<sub>50</sub> 0.32 μM) with 3000556 (EC<sub>50</sub> 6.9 μM) or 3000234 (EC<sub>50</sub> 0.24 μM) with 3000656 (EC<sub>50</sub> 3.77 μM). As a general rule the substituted indoles were at least an order of magnitude less active than their unsubstituted equivalent.

There was also a clear pattern in the activity of the unsubstituted compounds. Only compounds derived from aromatic amines were active, while those derived from aliphatic, benzylic or secondary amines were largely inactive. The only exception was the 3-aminoquinolyl compound

3000534 ( $EC_{50}$  0.7  $\mu$ M), which was the only bicyclic compound to show activity. One of the most active compounds was the unsubstituted phenyl ring (3000233) and only substitution at the para-position improved on this activity. Meta-substituted compounds retained a degree of activity although they didn't improve on the activity of the unsubstituted phenyl. Substitution at the ortho-position resulted in a complete loss of activity. Compare the p-methoxy derivative (3000260,  $EC_{50}$  0.011  $\mu$ M) with its m-methoxy equivalent (3000259,  $EC_{50}$  0.23  $\mu$ M). It can therefore be seen that primary aromatic amines with a para-substituent give the most potent anti-prion effect, while substitution of the indole at the 1 position reduces activity and substitution at the 2 position is not tolerated.

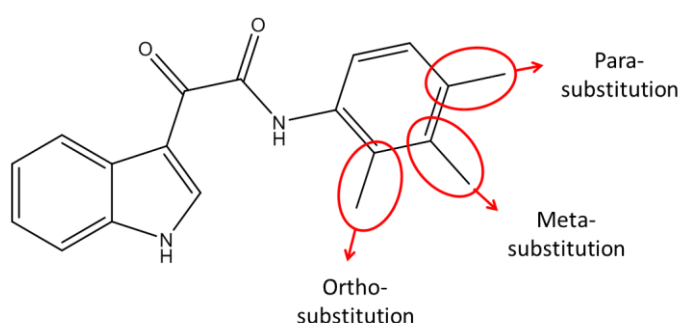


**Figure 24:** Figure demonstrating para-, meta- and ortho-substitutions on the amine.

### 3.1.2.2. Library B

Using the information gleaned from the first library the second library was made up of unsubstituted indoles and 1-methyl indoles. Again a preference for para-substituted amines was seen, with p-OEt (3000979,  $EC_{50}$  0.06  $\mu$ M) and p-SMe (3000991,  $EC_{50}$  0.04  $\mu$ M) showing better activity than the unsubstituted parent compound (3000233), although neither were as active as the p-Me substitution (3000260). The most effective compounds were those possessing a p-amino substituent. Three of these compounds gave  $EC_{50}$  values of less than 10 nM (3000994, 9 nM; 3001003, 6 nM; 3001012, 1 nM) and all these contained an N-linked heterocycle at the para-position of the phenyl ring (see **Figure 25**). It can therefore be seen that a heterocycle containing at least one hydrogen bond acceptor should be present in the para-position for optimal activity.

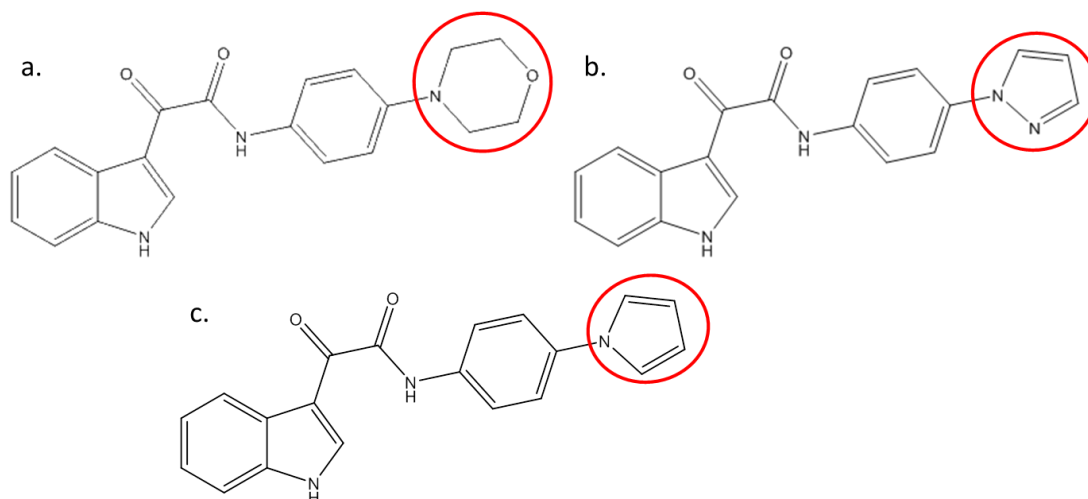


**Figure 25:** Structures of some of the most active compounds, all of which contain an N-linked heterocycle at the para position of the phenyl ring (circled). a. 300994; b. 3001012; c. 3001003.

Analogues of these compounds containing a 1-methyl substituted indole were also screened, and although these generally retained good activity they were not as potent as their unsubstituted equivalent.

Compounds that were substituted at both the meta and para-positions were found to have either activity that was comparable to the meta-substituted analogue or to be inactive. For example, the 3,4-dimethoxy derivative (3000918,  $EC_{50}$  0.52  $\mu$ M) had a similar activity to the m-methoxy analogue (3000259,  $EC_{50}$  0.23  $\mu$ M) and a lower activity than the p-methoxy analogue (3000260,  $EC_{50}$  0.01  $\mu$ M). There is therefore no additive effect of substituting at two positions. This was further emphasised by the complete loss of activity seen in the 3,4,5-trisubstituted compounds. Activity was also lost on insertion of a methyl bridge between the amide nitrogen and the phenyl ring as can be seen in compounds 3000914 and 3000915, which were from m- or p-methoxybenzylamides. The incorporation of a nitrogen at the 3 position of the phenyl ring was shown to reduce the activity of a compound, for example 3000997 had an  $EC_{50}$  of 1.21  $\mu$ M compared to the same compound without the nitrogen, 3000917, which had an  $EC_{50}$  of 0.064  $\mu$ M. A nitrogen at the 4-position of the phenyl ring also resulted in a drop in activity.

### 3.1.2.3. Library C

Library C was based on the most active compounds from library 2, particularly 3001012 ( $EC_{50}$  1 nM). Only three compounds showed comparable or better activity than the parent compound – 3001137 ( $EC_{50}$  3 nM), 3001165 ( $EC_{50}$  0.95 nM) and 3001143 ( $EC_{50}$  1.3nM). In compound 3001137 the addition of an additional nitrogen into the p-pyrazol-1-yl substituent caused a very slight

decrease in activity. Changing the position of the nitrogen molecules, as in 3001143, and adding an oxygen molecule to the p-pyrazol-1-yl substituent, as in 3001165, resulted in comparable activity.

All other changes to the para substituent on the phenyl ring resulted in a decrease or complete loss of activity. Adding a methylene bridge between the phenyl ring and the heterocycle led to a decrease in activity of two orders of magnitude (3001138,  $EC_{50}$  0.6 $\mu$ M). Adding a 3,5-dimethyl substitution to the pyrazole ring caused a similar drop in activity. The only substituted compound with activity comparable to the lead compounds was the 1-methylpyrazol-1-yl derivative (3001163,  $EC_{50}$  6nM). Apart from this compound all other substitutions were very detrimental to activity. Unusually one of these compounds (3001162) was highly toxic to the cells, suggesting the use of a sulphur-containing heterocycle can't be tolerated.

#### 3.1.2.4. Library D

This library aimed to investigate the effect of different substitutions on the indole ring at the 5 and 6 positions. Amines with proven activity on the unsubstituted indole were used to determine whether activity could be improved with indoles that had either a chloro or methyl substitution at the five or six position.

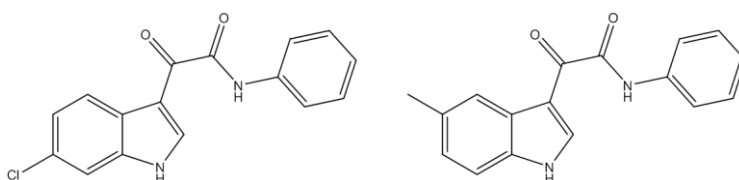


**Figure 26:** Substituted analogues of parent compound 3000233; 3001060 (left) and 3001075 (right)

Comparing the results from the substituted indoles with the results from the unsubstituted indoles shows a clear pattern. In all cases the 5-methyl substitution caused a decrease in activity. Compare the unsubstituted 3000233 ( $EC_{50}$  0.32  $\mu$ M) with the 5-methyl substituted 3001075 ( $EC_{50}$  13  $\mu$ M), and the unsubstituted 3000260 ( $EC_{50}$  0.011  $\mu$ M) with the 5-methyl substituted 3001080 ( $EC_{50}$  0.87  $\mu$ M). The 5-chloro substituted indoles also caused a decrease in activity although not by as much as the 5-methyl substitution. Compare again 3000233 with the 5-chloro substituted 3001066 ( $EC_{50}$  1.63  $\mu$ M). This is an order of magnitude better than the 5-methyl substituted indole but still nearly an order of magnitude worse than the unsubstituted analogue.

Compounds 3001069 ( $EC_{50}$  0.074  $\mu$ M) and 3001067 ( $EC_{50}$  0.56  $\mu$ M) gave results closer to their unsubstituted analogue, respectively 3000982 ( $EC_{50}$  0.065  $\mu$ M) and 3000977 ( $EC_{50}$  0.13  $\mu$ M).

Substitution at the 6-position appears to be more beneficial to activity, with the 6-chloro substituted indole generally giving an increased or comparable activity to the unsubstituted analogue. Compound 3001060 ( $EC_{50}$  0.074  $\mu$ M) in particular shows a notable increase in activity compared to its unsubstituted analogue (3000233,  $EC_{50}$  0.32  $\mu$ M). In most other cases results were comparable, see 3001059 ( $EC_{50}$  7 nM) compared to 3000994 ( $EC_{50}$  9 nM) and 3001058 ( $EC_{50}$  9 nM) compared to 3000260 ( $EC_{50}$  11 nM). The methyl substitution at the 6 position gave the most beneficial effect, with four out of five compounds showing increased activity compared to the unsubstituted analogue. Compare 3001073 ( $EC_{50}$  0.045  $\mu$ M) with 3000977 ( $EC_{50}$  0.13  $\mu$ M). The 6-methyl N-benzyl compound 3001074 ( $EC_{50}$  6.2  $\mu$ M) is active but all other N-benzyl compounds (3000255, 3001062, 3001068 and 3001076) are inactive. It can therefore be seen that substitution at the 6 position is advantageous (or not detrimental) to activity, while substitution at the 5 position causes a decrease (or no change) in activity compared to the unsubstituted analogue. It is also clear that the 6-methyl substitution is more advantageous than the 6-chloro substitution.

### 3.1.2.5. Library E

This library continued the theme of the previous library but looked at substitutions in some additional positions on the indole. More compounds were synthesised with a 6-chloro substitution but none of these showed any improvement in activity over the unsubstituted analogue. As seen before there was comparable activity, with any decreases in activity being fairly small. Compare 3001123 ( $EC_{50}$  12 nM) with 3001003 ( $EC_{50}$  6 nM). Addition of a methyl group at the 1- position of the indole ring caused a drop in activity of around one order of magnitude compared to the 6-chloro substituted indole. Compare 3001128 ( $EC_{50}$  0.15  $\mu$ M) to 3001124 ( $EC_{50}$  7 nM). A 6-fluoro substitution gave results very similar to the unsubstituted analogues suggesting that this had no effect on activity. Compare the 6-fluoro substituted compounds 3001139 ( $EC_{50}$  8 nM) and 3001126 ( $EC_{50}$  10 nM) with their unsubstituted analogues, respectively 3001003 ( $EC_{50}$  6 nM) and 3000260 ( $EC_{50}$  11 nM).

Substitution at the 7 position did not improve on the activity of the unsubstituted analogues. For the 7-methyl substitution results were at least an order of magnitude worse than the unsubstituted analogues. Compare the 7-methyl substituted compounds 3001184 ( $EC_{50}$  1.4  $\mu$ M)

and 3001183 ( $EC_{50}$  0.14  $\mu$ M) with their unsubstituted analogues, respectively 3000977 ( $EC_{50}$  0.13  $\mu$ M) and 3000260 ( $EC_{50}$  11 nM). The 7-chloro substituted compounds retained more activity compared to the unsubstituted analogues than the 7-methyl compounds. However, their activity was still less or comparable to the unsubstituted analogues, and in no case was there a beneficial effect on activity. It can therefore be seen that none of the substitutions to the indole ring in this library were beneficial to activity compared to the unsubstituted analogue.

### 3.1.2.6. Library F

This library investigated the effect of removing one of the carbonyl groups or replacing the carbonyl groups with a heterocycle. It also investigated the addition of larger groups to the 1-position of the indole ring.

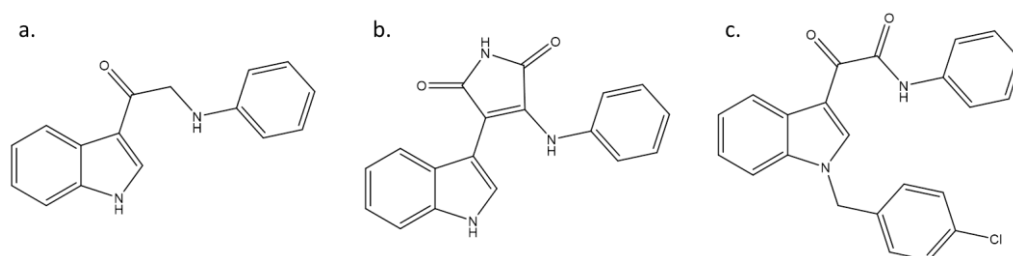


**Figure 27:** Different modifications investigated in Library F. a. removal of one of the carbonyl groups; b. replacement of the carbonyl groups with a heterocycle; c. addition of larger groups to the 1-position of the indole ring.

It can be seen that the addition of the large group to the 1 position of the indole was not tolerated in terms of cell line activity, suggesting that while the substitution of small groups may be tolerated there is a steric limit to retaining activity. Removal of one or other of the carbonyl groups resulted in a large decrease or total loss of activity, while replacing the carbonyl group with a heterocycle was not tolerated and resulted in total loss of activity. Removal of the carbonyl group adjacent to the indole ring was only tolerated in one instance, 3001010 ( $EC_{50}$  3.9  $\mu$ M). However, the activity was very low compared to the compound with the other carbonyl group removed (3001017,  $EC_{50}$  0.11  $\mu$ M), which in turn showed low activity when compared to the analogue with both carbonyl groups (3000994,  $EC_{50}$  9 nM). Removal of the carbonyl group furthest away from the indole ring was better tolerated, resulting in a decrease in activity of around one order of magnitude. Compare 3001015 ( $EC_{50}$  0.36  $\mu$ M) to its analogue containing both carbonyl groups, 3000260 ( $EC_{50}$  0.011  $\mu$ M).

### 3.1.2.7. Library G

Having established in previous libraries that a substitution at the 6-position was the most beneficial for anti-prion activity the effect of substitutions at this position was further investigated. The effect of a methyl bridge between the carbonyl groups and a methyl substitution at the 4-position of the indole ring was also investigated.

The effect of the methyl bridge was to remove any activity from the compound while the 4-methyl substituted compounds showed a decreased activity of around two degrees of magnitude compared to the unsubstituted compound. Compare 3001204 ( $EC_{50}$  2.75  $\mu$ M) to its unsubstituted analogue 3000260 ( $EC_{50}$  0.011  $\mu$ M), or 3001205 ( $EC_{50}$  10  $\mu$ M) to its unsubstituted analogue 3000977 ( $EC_{50}$  0.13  $\mu$ M).

With respect to the substitutions at the 6 position, there were varied results. Derivatives with an isopropyl group at the 6 position showed a large decrease in activity compared to the unsubstituted analogues and to similar compounds with different substitutions at the 6-position. Compare 3001199 ( $EC_{50}$  0.33  $\mu$ M) with the unsubstituted analogue 3000260 ( $EC_{50}$  0.011  $\mu$ M), or the 6-chloro analogue 3001058 ( $EC_{50}$  0.009  $\mu$ M). The modifications that proved the most effective were the addition of a 6-cyano or 6-nitro group. The former reduced the  $EC_{50}$  by nearly an order of magnitude from the previous best in one case, compare 3001207 ( $EC_{50}$  0.0022  $\mu$ M) with the 6-chloro analogue 3001058 ( $EC_{50}$  0.009  $\mu$ M). The 6-nitro analogues showed similar or improved activity to the unsubstituted analogue, compare 3001210 ( $EC_{50}$  0.035  $\mu$ M) with the unsubstituted analogue 3000977 ( $EC_{50}$  0.13  $\mu$ M), although none of the 6-nitro compounds gave better activity than the 6-cyano analogues.

### 3.1.3. Conclusions

From this screening programme it is possible to draw detailed conclusions on two things, namely the effect on activity of substitutions on the indole ring and the effect on activity of different amines. The effect on activity of removing one of the carbonyl groups was also examined but in far less detail.

In conclusion it can be seen that in the majority of cases the unsubstituted indole is as potent as any of its substituted analogues. The only exception to this is substitutions at the 6-position. The

6-methyl and 6-nitro substitutions resulted in slight increases in activity, while the 6-cyano substitution resulted in an increase in activity, with an increase of an order of magnitude observed in one case. However, in terms of the activity of the lead compound, substitutions on the indole ring did not result in an increase in activity. A methyl group at the 2 position rendered the compound inactive while substitution at the 1 position caused a notable decrease in activity compared to the unsubstituted equivalent. Substitution at the 6 position was beneficial or had no effect on activity, and the 6-methyl substitution was advantageous. A 6-cyano substituted analogue of the lead compound was not synthesised although the SAR data from library G suggests that this may be optimal. Substitution at the 5 position caused a decrease or had no effect on activity. Substitution at the 7 position had no effect on activity compared to the unsubstituted equivalent.

With respect to the effect of different amines there was also a clear pattern. Only aromatic amines showed activity. Phenyl rings substituted at the para-position showed a clear improvement in activity over the unsubstituted phenyl ring. Substitutions at the meta-position showed no improvement in activity while substitution at the ortho-position caused total loss of activity. A heterocycle containing at least one hydrogen bond acceptor needed to be present at the para-position for optimal activity. Compounds substituted at both the meta and para-positions had activity similar or worse than the meta-substituted equivalent and the trisubstituted compounds were all inactive. There was therefore no additive effect of multiple substitutions on the phenyl ring. Insertion of a methyl bridge between the amide nitrogen and the phenyl ring reduced activity, as did incorporation of a nitrogen group at the 3- or 4-position of the phenyl ring.

Strikingly, removal of one or other of the carbonyl groups caused a large decrease in, or total loss of, activity compared to compounds containing both groups.

An interesting observation was that in the majority of the screens the total removal of PrP<sup>Sc</sup> was not observed. Even at the highest concentrations of the most potent compounds, 5 to 20 % of the PrP<sup>Sc</sup> remained. This can be seen in the example data presented in **Figure 13**, and faint spots are still visible on the dot blots presented in **Figure 19** and **Figure 21**. The initial screen data presented in **3.1.1.2** also demonstrates the residual PrP<sup>Sc</sup> that remained after treatment. This raises the question of whether the cells are cured, and whether they still retain infectivity. It is possible that that PrP<sup>Sc</sup> levels have been lowered to such a degree that accumulation to pre-

treatment levels would be prevented by normal cellular processes, and in this context the cells could be considered cured. However, if the residual PrP<sup>Sc</sup> was still infective then to refer to the cells as cured would perhaps be erroneous. Further work is required to show the long term effects of treatment on PrP<sup>Sc</sup> levels, and also to determine whether the cells are still infectious.

Validation of the dot blot analysis using western blotting was carried out by Mark Thompson and Matthew Jackson using a selection of the most active compounds. The reduction in PrP<sup>Sc</sup> levels and the activity of the compounds was reproduced using western blotting, therefore validating the dot blot protocol for use in this application.

### **3.2. Surface Plasmon Resonance (SPR) Binding Assay**

SPR is a technique widely used to monitor biomolecular interactions in real time. It has been used in a wide range of applications such as ligand fishing, microbiology, virology and epitope mapping as well as studying host-pathogen, protein-protein, protein-nucleic acid, protein-membrane and protein-cell interactions. <sup>(372)</sup> The approach involves attaching one of the interaction partners, known as the ligand, to the surface of a sensor chip. Solution containing the hypothesised interaction partner, known as the analyte, is passed over the surface of the chip. Binding interactions at the sensor surface generate a response which is proportional to the bound mass, allowing identification of interaction partners and elucidation of their mode of binding. The strength of the interaction can be determined by monitoring dissociation, and the surface can then be regenerated to remove any remaining analyte, allowing the immobilised ligand to be used multiple times (see **Figure 28**).

There are various methods of immobilisation available but one of the most commonly used is amine coupling using a CM5 chip. The gold coated surface of the chip is covered with carboxymethylated dextran which is then activated using a combination of EDC (1-ethyl-3-(3-dimethylaminopropyl)carbodiimide hydrochloride) and NHS (N-hydroxysuccinimide). This produces reactive succinimide esters which react spontaneously with amine and other nucleophilic groups allowing direct immobilisation of proteins. Any active sites that aren't used for immobilising protein are blocked using ethanolamine to ensure that they don't form interactions with the analyte. Each sensor chip has four flow channels. At least one of these acts

as the blank control, where the surface of the chip is activated and blocked without any protein bound to it. This ensures that any binding seen is between the analyte and the ligand, rather than the analyte and the surface of the chip. Direct binding to the surface can cause high non-specific binding so needs to be accounted for. The remaining flow cells can be immobilised with different proteins or the same protein at different levels as required.

Once the ligand has been immobilised the analyte of interest is flowed over the surface of the chip and interactions between the two are calculated from changes in the refractive index, measured in response units (RU). SPR occurs in thin conducting films at the interface between two media of different refractive indexes, in this case the glass of the sensor chip and the sample solution. The layer of gold on the surface of the chip acts as the conducting film.

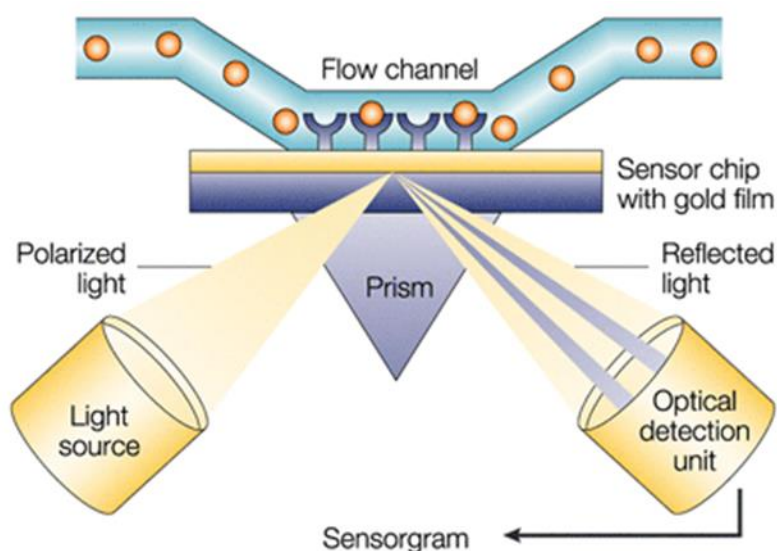


**Figure 28:** Pictorial representation of the SPR technique, showing the ligand attached to the flow cell and the analyte flowing over the top. Changes in the refractive index are detected in the immediate vicinity of the surface layer of the chip. The SPR angle shifts when biomolecules bind to the surface and change the mass of the surface area. <sup>(373)</sup>

Binding is calculated using the shift from the baseline signal (immobilised ligand only), subtracting the signal from the reference cell and then expressing the shift as a percentage of what would be expected if all the binding sites had been occupied 1:1. This is known as the  $RU_{max}$  and is calculated as from the molecular weight of the ligand, the molecular weight of the analyte and the immobilisation level (see **Equation 3**). The immobilisation level is the difference, in response units, between the signal after the EDC/NHS activation and the signal after immobilisation of the ligand and regeneration of the surface:

$$\left(\frac{\text{Immobilisation level}}{\text{MW of ligand}}\right) \times \text{MW of analyte}$$

**Equation 3:** Method for calculating the  $\text{RU}_{\text{max}}$  of a compound

An analyte showing binding of around 100%  $\text{RU}_{\text{max}}$  would have a specific 1:1 interaction with the ligand, while the detection of a much higher  $\text{RU}_{\text{max}}$  value would suggest non-specific binding. If there was very little variation from baseline during the analyte injection then that would indicate that there was no interaction between the two molecules.

The nature of the interaction between ligand and analyte can also be examined by investigating the dissociation constant ( $kD$ ). This measures how long it takes for the ligand-analyte complex to dissociate and uses this as a measure of the strength of the interaction. With SPR there is a dissociation period after the analyte injection, where nothing but running buffer is passed over the surface of the chip. Any decrease in signal during this phase can then be used to monitor the dissociation. To ensure that all the analyte is removed from the chip the final step in the SPR run is to use regeneration solutions to dislodge any remaining bound analyte. After this the chip is ready to be injected with a new analyte (see **Figure 29**).

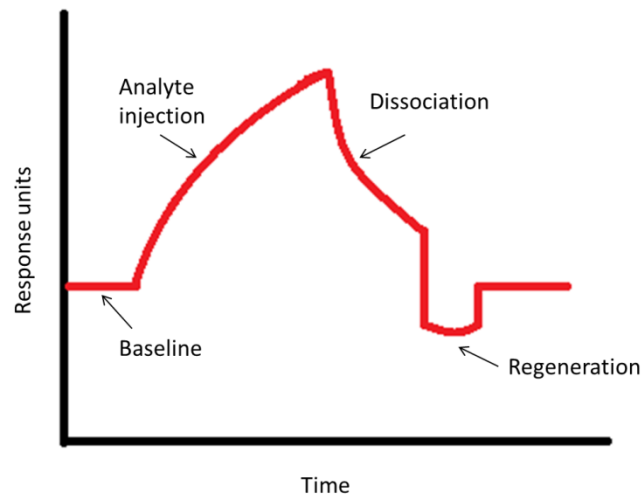


**Figure 29:** Example sensorgram for investigating ligand-analyte interactions. Baseline represents the response from the immobilised surface only. Analyte injection causes the formation of complexes which then dissociate once the injection stops. Final removal of analyte is facilitated by regeneration solutions, returning the surface to baseline levels. Figure adapted from the Biacore sensor surface handbook.

SPR, using a Biacore 3000 instrument, was used to determine if there was a binding interaction between one of two forms of bacterially expressed recombinant PrP (full length human, huPrP, and full length mouse, moPrP) and the I3GAs. The moPrP was used to provide a comparison with the cell line assay, which was carried out in murine brain cells. Previous work had also used truncated human recombinant PrP (t-huPrP) <sup>(221, 351)</sup> to try and identify the region of PrP that the compounds might be binding to, but unfortunately there was none available for this study. It was thought that if binding affinities similar to the EC<sub>50</sub>s were demonstrated in the SPR assay then it may be possible to conclude that the compounds exert their *in vitro* anti-prion effect through binding to PrP<sup>C</sup>. Weak interactions may suggest a different mode of action.

Previous work within the group had optimised the protocol for binding recombinant PrP to a gold sensor chip coated with carboxymethylated dextran (CM-dextran). <sup>(221)</sup> This method was chosen because PrP<sup>C</sup> is a known binder to heparin <sup>(213)</sup> and heparin resembles CM-dextran structurally, with binding of heparin to PrP occurring *via* the N-terminal. I3GAs were passed over the immobilised protein and the response analysed to determine if any of the compounds were interacting with the PrP. For these experiments the focus was on the shift in baseline after the analyte injection rather than the dissociation phase. It was decided to look at the binding event itself rather than the strength of the interaction, as this was the initial parameter of interest. This was because proof of an interaction, regardless of the strength, was required to demonstrate that the compounds may be working through direct interaction with PrP. Further elucidation of the interaction, through calculation of the *kD* and therefore the strength of the binding, was planned if any of the compounds showed significant, specific binding. Any compounds that showed binding were run at a series of concentrations to determine the shape of the binding curve and reveal further the mechanism of binding.

Materials and methods are discussed in full in sections **2.1.2** and **2.2.3** respectively.

## **3.2.1. Results**

### **3.2.1.1. Optimisation**

The SPR binding experiments using the Biacore 3000 instrument were carried out according to a protocol developed by the Chen group for previous work, as detailed in <sup>(221)</sup> and section **2.2.3**. As such it didn't require any optimisation although some small changes were made. Previous work

had used a chip for 5 runs before discarding it. It was thought that it might be possible to use the chip for longer, saving both time and money and allowing more of a comparison between runs. <sup>(221)</sup> The immobilisation levels and binding by quinacrine (the positive control) were monitored over time and were found to be stable after 17 runs carried out over a period of 4 weeks (see **Figure 30** and **Figure 31**). The stability of the immobilisation levels and the quinacrine binding also suggest that the PrP is bound to the chip surface in a stable confirmation and that aggregation of PrP on the chip surface, as indicated by an increase in the baseline immobilisation level, does not seem to occur. Changes in the conformation of immobilised PrP over time were suggested to result in increased exposure of the C-terminal. <sup>(221)</sup> As quinacrine has been shown to bind to the C-terminal of PrP <sup>(347)</sup> it was suggested that fluctuations in quinacrine binding could be due to changes in the conformation of the immobilised PrP. As can be seen in **Figure 31**, quinacrine binding during the initial run is significantly lower than subsequent runs, suggesting that less of the C-terminal may be exposed. However, quinacrine binding increases by the second run, and is subsequently consistent, suggesting that the conformation of the immobilised PrP has stabilised and the binding site on the C-terminal is available.

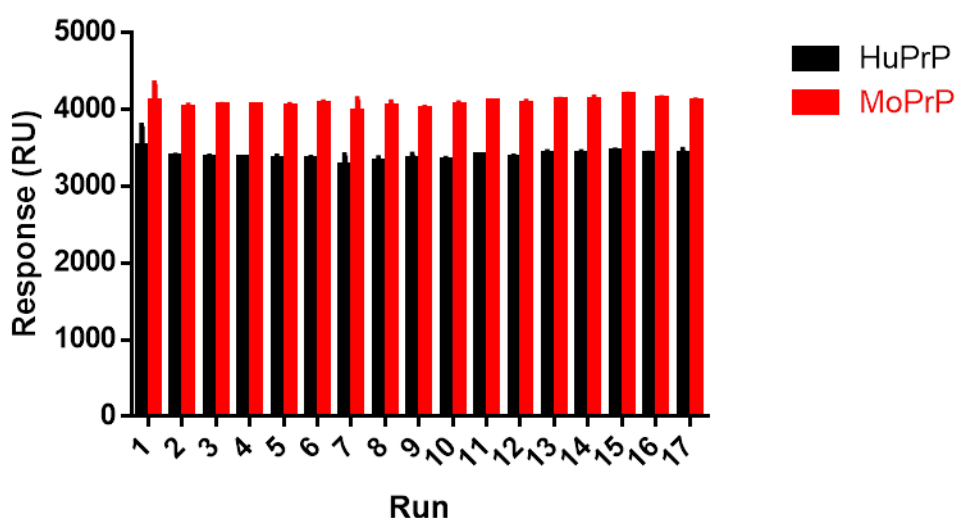


**Figure 30:** Immobilisation levels over 17 runs for huPrP and moPrP. Each data point represents a representative sample of baseline immobilisation levels over the course of the run, and were measured in the presence of buffer containing 6.5 % DMSO only. n = 7. Very low standard deviations for the majority of data points demonstrate the stability of the immobilisation, as does the consistency of the immobilisation level between runs. The higher error observed during the first run is thought to be due to the PrP being in a slightly different, and shifting, conformation. Protein that is not tightly bound to the chip may also be washed off during the first run, resulting in a slight decrease in immobilisation level.

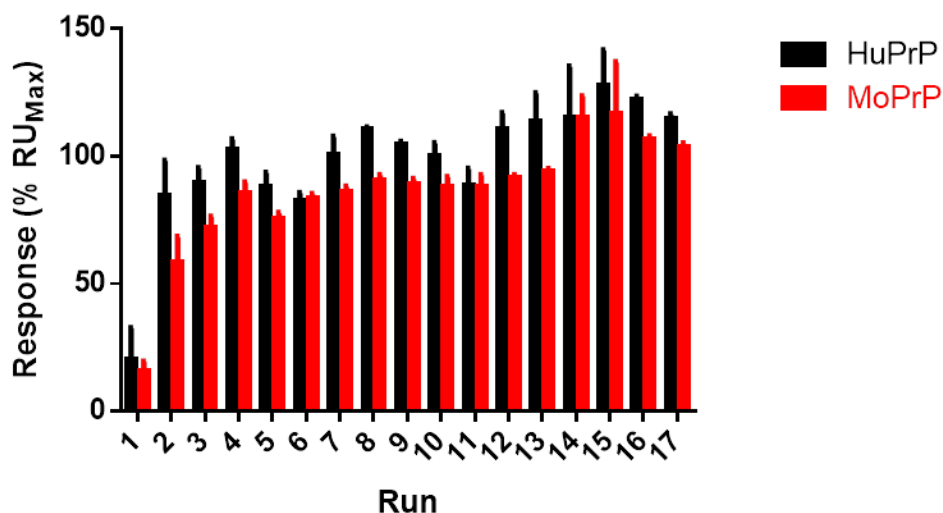


**Figure 31:** Response in % RU<sub>max</sub> given by quinacrine over 17 runs against huPrP and moPrP. The lower binding on the first run was attributed to limited availability of the C-terminal of PrP, where quinacrine has been shown to bind. Subsequent increases in binding are attributed to a conformational shift in the immobilised PrP during the first run, with a stable conformation being maintained thereafter.

### 3.2.1.2. Initial Screens

All compounds were initially screened at 40  $\mu$ M and the results expressed as % RU<sub>max</sub>. Theoretical RU<sub>max</sub> was calculated as described in **Equation 3** and the observed binding response of the compound was expressed as a percentage of this theoretical value. Compounds that showed over 100% RU<sub>max</sub> binding were not likely to be specific binders. It was thought that these compounds were either interacting with the surface of the chip or were non-specifically binding to the ligand. Compounds showing a high interaction with flow cell, as assessed by their interaction with the blank flow cell one, were likely to be binding to the surface of the chip rather than the protein so reliable binding data for these compounds could not be obtained. Non-specific binders were thought to be binding to all areas of the protein rather than the specific binding site that had been identified, and were therefore discounted. The use of a PrP peptide containing the hypothetical protein X binding site was suggested to determine whether the compounds were binding in this region as predicted, and truncated PrP had been used in previous studies,<sup>(221, 351)</sup> but neither the peptide nor the truncated PrP were available at the time these studies were carried out.

Quinacrine was the positive control as it is known to bind to PrP and was used in previous experiments by the group.<sup>(221, 233)</sup> In the majority of cases it gave a result of 100 % RU<sub>max</sub>  $\pm$  5% (see **Figure 31**). Low levels of quinacrine binding shown by the first run, and the subsequent

increase to theoretical levels, are thought to be due to small shifts in the conformation of the immobilised protein for a limited period after the immobilisation is carried out. This shift exposes more of the C-terminal which is where quinacrine is thought to bind. <sup>(221)</sup>

Most of the compounds that were screened by SPR were also active in the SMB cell line. A few inactive compounds were included to allow for comparison. The results have been divided into the same libraries as used for the SMB screening. Results have been assigned to one of four categories:

**Orange** = non-binders, results < 5 %  $RU_{max}$ .

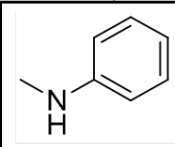
**Yellow** = low level binders, results >5 %  $RU_{max}$  but <20 %  $RU_{max}$ .

**Green** = Binders, results >20 %  $RU_{max}$

**Blue** = Inconclusive results.

The majority of screens were carried out in duplicate (at least) to ensure the reliability of results. Where confirmed the initial result was used. If the repeat differed significantly from the initial result then the compound was repeated again and the result shown is the result confirmed by the third screen. Compounds considered to be binders were then screened at a range of nine concentrations and the results analysed using a one-phase association linear fit.

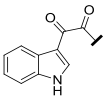
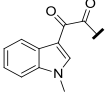
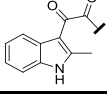
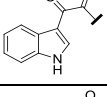
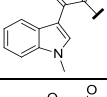
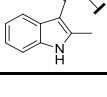
As in section **3.1.1** the results of the SPR experiments are presented here in libraries based on compound structure (see **Table 11** and section **3.1.1.2** for detailed explanations of each library) The data is presented as outlined in **Figure 32** with the indole structure on the left and the amine structure along the top. Each box contains the compound screening number along with the percentage of the theoretical binding ( $RU_{max}$ ) that was observed at a concentration of 40  $\mu$ M.

|   |  |
|---|--|
|   | <br>Amine group |
| <br>Indole group | <b>3000233</b><br><b>13.9 ± 5.7 %</b>  |

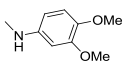
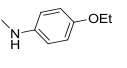
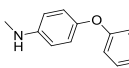
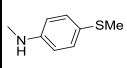
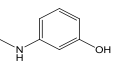
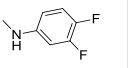
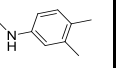
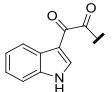
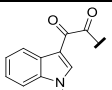
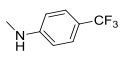
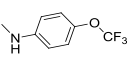
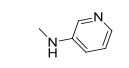
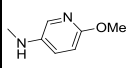
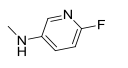
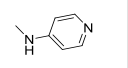
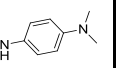
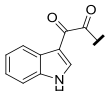
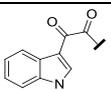
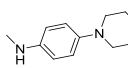
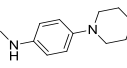
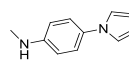
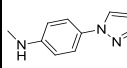
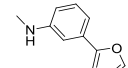
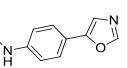
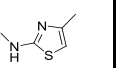
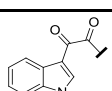
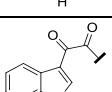
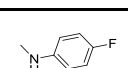
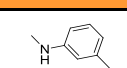
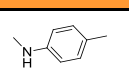
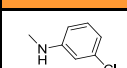
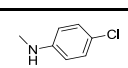
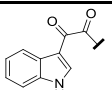
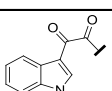
Sample screening reference number  
 % RU<sub>max</sub>

**Figure 32:** Example of the layout of the data in the subsequent results tables. The indole group is described in the left hand column, with the amine group along the top. Observed binding at the initial screen concentration of 40  $\mu\text{M}$  is expressed as the percentage of the theoretical RU<sub>max</sub>. Each result represents at least two independent experiments, and each experiment was carried out in triplicate.

**Table 27:** SPR screening results for library A at a concentration of 40  $\mu$ M.

|  |  |  |  |  |  |  |  |
|--|---|---|---|---|--|---|---|
|   | <b>3000233</b><br>13.9 $\pm$ 5.7 %  | <b>3000553</b><br>45.7 $\pm$ 4.2 %  | <b>3000259</b><br>19.3 $\pm$ 27.8 %   | <b>3000260</b><br>21.4 $\pm$ 26.1 %   | <b>3000234</b><br>31.61 $\pm$ 2.41 %   | <b>3000530</b><br>-0.34 $\pm$ 3.16 %  | <b>3000258</b><br>33.48 $\pm$ 2.04 %  |
|   | <b>3000556</b><br>34.84 $\pm$ 2.48 %  |   | <b>3000663</b><br>1.2 $\pm$ 1.8 %   | <b>3000664</b><br>-1.6 $\pm$ 1 %  | <b>3000656</b><br>28.2 $\pm$ 1.8 %   |   |   |
|   | <b>3000557</b><br>19.18 $\pm$ 0.51 %  |   | <b>3000648</b><br>23.2 $\pm$ 1.2 %  | <b>3000649</b><br>4.13 $\pm$ 0.5 %  |  |   |   |
|  |  |  |   |   |  |   |   |
|   | <b>3000554</b><br>1.68 $\pm$ 0.61 %   | <b>3000534</b><br>43.36 $\pm$ 17.40 %   |   |   |  |   |   |
|   |   |   |   |   |  |   |   |
|  |   |   |   |   |  |   |   |

**Table 28:** SPR screening results for library B at a concentration of 40  $\mu$ M.

|   |   |   |   |   |  |   |   |
|---|---|---|---|---|--|---|---|
|   |    |    |    |    |    |  |  |
|    | <b>3000918</b><br>33.25 $\pm$ 5.05 %  | <b>3000979</b><br>-0.62 $\pm$ 1.25 %  | <b>3000993</b><br>0.96 $\pm$ 5.21 %   | <b>3000991</b><br>-3.8 $\pm$ 1.9 %  | MT609<br>not screened  | <b>3000985</b><br>-3.66 $\pm$ 0.92 %  | <b>3000978</b><br>-10.42 $\pm$ 0.32 %   |
|    |   |   | <b>3001085</b><br>170.92 $\pm$ 99.64 %  |   |  |   |   |
|   |    |    |    |    |    |  |  |
|    | <b>3001002</b><br>-1.94 $\pm$ 1.69 %  | <b>3000999</b><br>-2.98 $\pm$ 1.85 %  | <b>3000996</b><br>0.92 $\pm$ 0.33 %   | <b>3000998</b><br>-7.68 $\pm$ 0.46 %  | <b>3000997</b><br>1.27 $\pm$ 3.65 %  | <b>3000983</b><br>26.61 $\pm$ 9.12 %  | <b>3000992</b><br>7.3 $\pm$ 3.3 %   |
|    |   |   |   |   |  |   |   |
|   |    |    |    |    |    |  |  |
|   | <b>3000995</b><br>18.53 $\pm$ 8.98 %  | <b>3000994</b><br>-4.7 $\pm$ 0.4 %  | <b>3001003</b><br>-13.24 $\pm$ 0.92 %   | <b>3001012</b><br>53.37 $\pm$ 1.53 %  | <b>3001008</b><br>-1.29 $\pm$ 4.56 %   | <b>3001013</b><br>-2.86 $\pm$ 17.13 %   | <b>3000981</b><br>21.76 $\pm$ 2.14 %  |
|  |   | <b>3001088</b><br>-1.24 $\pm$ 2.14 %  | <b>3001086</b><br>-0.86 $\pm$ 4.56 %  | <b>3001087</b><br>-1.84 $\pm$ 4.6 %   |  | <b>3001006</b><br>17.9 $\pm$ 4 %  |   |
|   |  |  |  |  |  |   |   |
|  | <b>3000917</b><br>-0.59 $\pm$ 8.56 %  | <b>3000980</b><br>-6.18 $\pm$ 1.41 %  | <b>3000977</b><br>-0.88 $\pm$ 2.43 %  | <b>3000987</b><br>1.1 $\pm$ 4.1 %   | <b>3000982</b><br>22.52 $\pm$ 3.64 %   |   |   |
|  |   |   |   |   |  |   |   |

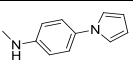
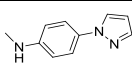
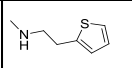
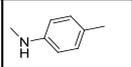
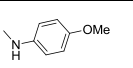
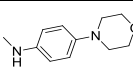
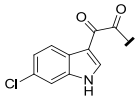
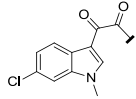
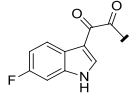
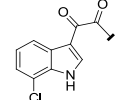
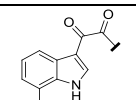
**Table 29:** SPR screening results for library C at a concentration of 40  $\mu$ M.

|  |                                      |  |                                       |  |  |
|--|--------------------------------------|--|---------------------------------------|--|--|
|  |                                      |  |                                       |  |  |
|  | <b>3001136</b><br>-7.01 $\pm$ 4.85 % | <b>3001137</b><br>-92.52 $\pm$ 77.02 % | <b>3001138</b><br>24.99 $\pm$ 53.62 % | <b>3001142</b><br>-0.13 $\pm$ 7.83 %     | <b>3001165</b><br>116.27 $\pm$ 40.09 % |
|  |                                      |  |                                       |  |  |
|  | <b>3001166</b><br>5.55 $\pm$ 4.73 %  | <b>3001164</b><br>7.31 $\pm$ 11.54 %   | <b>3001143</b><br>44.13 $\pm$ 37.31 % | <b>3001144</b><br>-117.72 $\pm$ 462.96 % | <b>3001163</b><br>6.33 $\pm$ 4.26 %    |

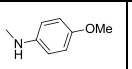
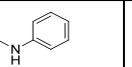
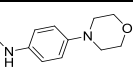
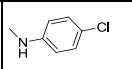
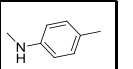
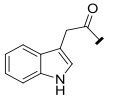
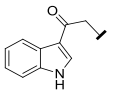
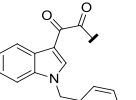
**Table 30:** SPR screening results for library D at a concentration of 40  $\mu$ M

|  |                                      |                                       |                                      |                                       |                                      |
|--|--------------------------------------|---------------------------------------|--------------------------------------|---------------------------------------|--------------------------------------|
|  |                                      |                                       |                                      |                                       |                                      |
|  | <b>3001060</b><br>32.3 $\pm$ 7.9 %   | <b>3001058</b><br>-10.98 $\pm$ 0.92 % | <b>3001063</b><br>-1.81 $\pm$ 0.93 % | <b>3001061</b><br>-1.73 $\pm$ 1.36 %  | <b>3001059</b><br>-9.44 $\pm$ 1.14 % |
|  | <b>3001066</b><br>-17.43 $\pm$ 1.1 % | <b>3001064</b><br>-4.07 $\pm$ 1.19 %  | <b>3001069</b><br>1.23 $\pm$ 0.65 %  | <b>3001067</b><br>3.28 $\pm$ 0.7 %    | <b>3001065</b><br>-6.45 $\pm$ 1 %    |
|  | <b>3001072</b><br>-3.59 $\pm$ 0.7 %  | <b>3001070</b><br>-18.28 $\pm$ 9.55 % |                                      | <b>3001073</b><br>-10.92 $\pm$ 1.47 % | <b>3001071</b><br>-9.91 $\pm$ 6.24 % |
|  | <b>3001075</b><br>-6.68 $\pm$ 0.46 % | <b>3001080</b><br>1.78 $\pm$ 5.89 %   |                                      | <b>3001077</b><br>-27.65 $\pm$ 7.51 % | <b>3001081</b><br>3.98 $\pm$ 2.42 %  |
|  |                                      |                                       |                                      |                                       |                                      |
|  | <b>3001062</b><br>-5.55 $\pm$ 1.94 % | <b>3000641</b><br>27.15 $\pm$ 3.14 %  | <b>3000785</b><br>2.9 $\pm$ 1.1 %    | <b>3000787</b><br>4.4 $\pm$ 6.5 %     |                                      |
|  |                                      |                                       |                                      |                                       |                                      |
|  | <b>3001074</b><br>16.77 $\pm$ 0.64 % |                                       |                                      |                                       |                                      |
|  |                                      |                                       |                                      |                                       |                                      |

**Table 31:** SPR screening results for library E at a concentration of 40  $\mu$ M

|   |  |  |  |  |  |  |
|---|---|---|---|---|--|---|
|  | <b>3001123</b><br>-4.58 $\pm$ 6.67 %  | <b>3001124</b><br>20.73 $\pm$ 16.42 %   | <b>3001125</b><br>-3.40 $\pm$ 10.37 %   |   |  |   |
|  | <b>3001127</b><br>-3.32 $\pm$ 3.58 %  | <b>3001128</b><br>-5.42 $\pm$ 8.87 %  |   |   | <b>3001130</b><br>-10.17 $\pm$ 9.72 %  | <b>3001129</b><br>-1.9 $\pm$ 4.96 %   |
|  | <b>3001139</b><br>-3.21 $\pm$ 14.58 %   | <b>3001140</b><br>68.03 $\pm$ 28.41 %   |   |   | <b>3001126</b><br>0.1 $\pm$ 1.12 %   |   |
|  |   |   |   | <b>3001181</b><br>11.28 $\pm$ 3.56 %  | <b>3001180</b><br>-1.57 $\pm$ 4.87 %   | <b>3001141</b><br>-1.95 $\pm$ 7.25 %  |
|  |   |   |   | <b>3001184</b><br>-1.05 $\pm$ 9.89 %  | <b>3001183</b><br>-2.5 $\pm$ 9.89 %  | <b>3001182</b><br>-4.94 $\pm$ 6.75 %  |

**Table 32:** SPR screening results for library F at a concentration of 40  $\mu$ M.

|   |  |  |  |  |  |
|---|---|---|---|--|---|
|  |   |   | <b>3001010</b><br>-1.47 $\pm$ 4.88 %  | <b>3001009</b><br>29.6 $\pm$ 17.66 %   |   |
|  | <b>3001015</b><br>31.48 $\pm$ 0.13 %  | <b>3001016</b><br>118.15 $\pm$ 1.2 %  | <b>3001017</b><br>76.41 $\pm$ 1.08 %  |  |   |
|  |   |   |   | <b>3001026</b><br>0.8 $\pm$ 3 %  | <b>3001025</b><br>45 $\pm$ 12.8 %   |

### 3.2.1.3. Dose response Analysis

Binding studies were carried out at a range of concentrations to obtain dose-response curves for compounds that showed binding to PrP in the initial screens. The same chip that was used in the initial screens was also used for the dose-response analysis. A sensorgram such as the one in **Figure 33** would be expected for a compound showing good binding and a dose response. Injection of the compound of interest occurs at 51 seconds, at which point an increased response can be observed if binding occurs. This injection continues for 1 minute, after which the signal can be seen to drop off dramatically. The 3 minute dissociation period allows the unforced dissociation of the analyte from the ligand, with regeneration solutions being injected after this period to ensure that all the analyte has been removed. The injection of the regeneration solutions is not shown in **Figure 33**.

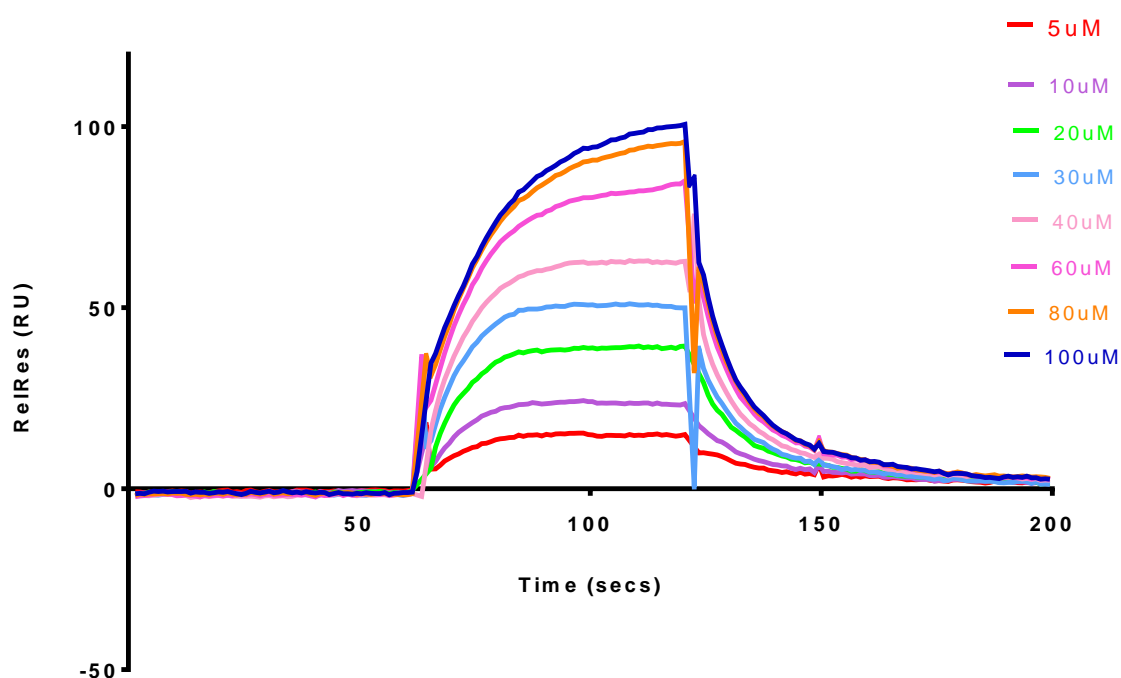


**Figure 33:** Dose response curves from SPR for the binding of compound 3001016 to huPrP, presented as the relative response (in RU) with blank data, calculated from the signal from the blank flow cell (fc1), subtracted. A steady baseline at zero is observed when buffer is injected over the chip, with a subsequent increase in signal at 51.5 seconds as the compound injection begins. The response increases as the concentration of the compound increases. Dissociation occurs once the injection stops at 112.5 seconds, as demonstrated by the decrease in signal after this point. The data is from a single injection at each concentration.

The data in the following figures is the data from the time point at 112.5 seconds, which represents the end of the analyte injection. This point is therefore the maximum increase in RU from baseline that would be observed if the analyte was binding to the ligand.

### 3.2.1.3.1. Library A

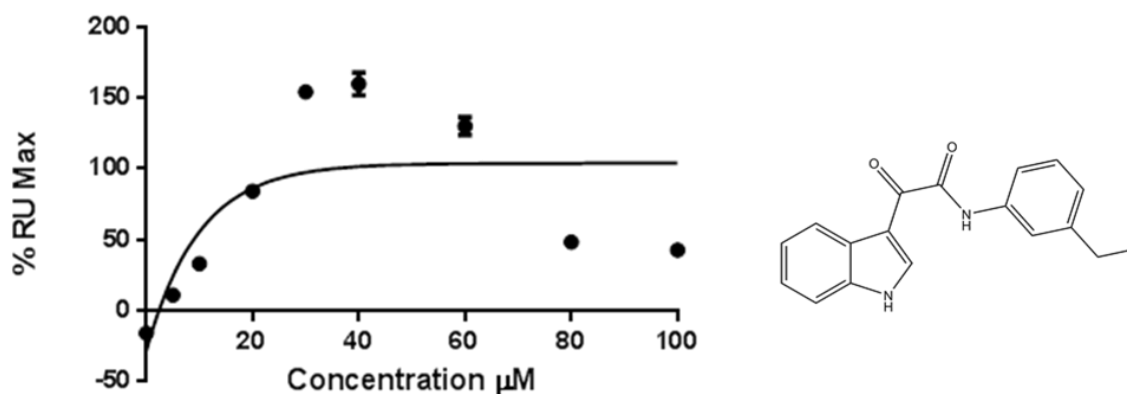


**Figure 34:** Dose response curve for compound 3000553 against huPrP. Binding at each concentration was analysed in triplicate. Binding increases with concentration up to 30  $\mu\text{M}$ , at which point it decreases. The value for the goodness of fit of the curve is very low.

The curve fitting in **Figure 34** suggests that this compound is a specific binder although the goodness of fit ( $R^2$ ) value is very low. The repeat of this compound produced a similar result.

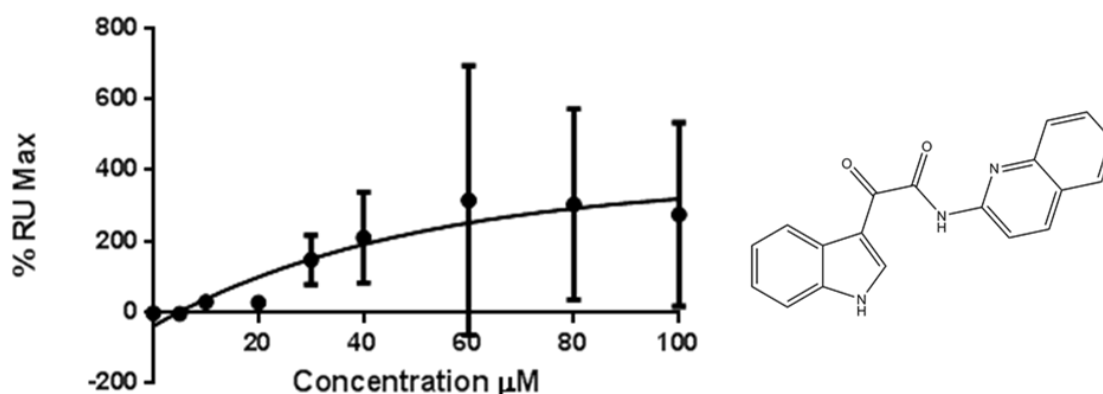


**Figure 35:** Dose response curve for compound 3000534 against huPrP. Binding at each concentration was analysed in triplicate. An apparent dose-dependent increase in binding is questionable due to the high standard deviations at concentrations of 60  $\mu\text{M}$  and above.

The high standard deviations seen in **Figure 35** suggest that 3000584 may be a non-specific binder. At higher concentrations the first injection was very high with the subsequent two injections being much lower, resulting in the very high standard deviations observed at concentrations from 60  $\mu\text{M}$  and above.

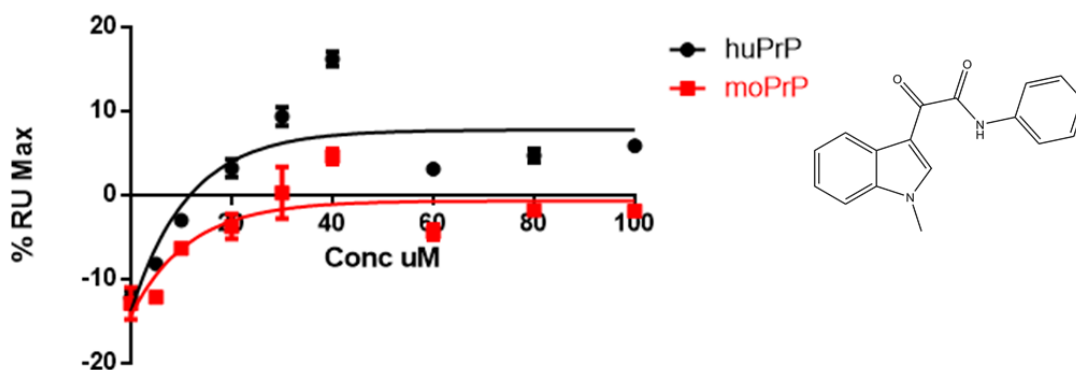


**Figure 36:** Dose response curve for compound 3000556 against huPrP and moPrP. Binding at each concentration was analysed in triplicate. Only very low level binding was observed, with  $RU_{max}$  values peaking at less than 20 % of the expected theoretical binding, suggesting limited binding interactions.

After dose response analysis this compound was re-classified as a non-binder. Although it appears to show a dose response it can be seen in **Figure 36** that it is at such low levels that there is no clear evidence of any binding to the protein.

### 3.2.1.3.1. Library B

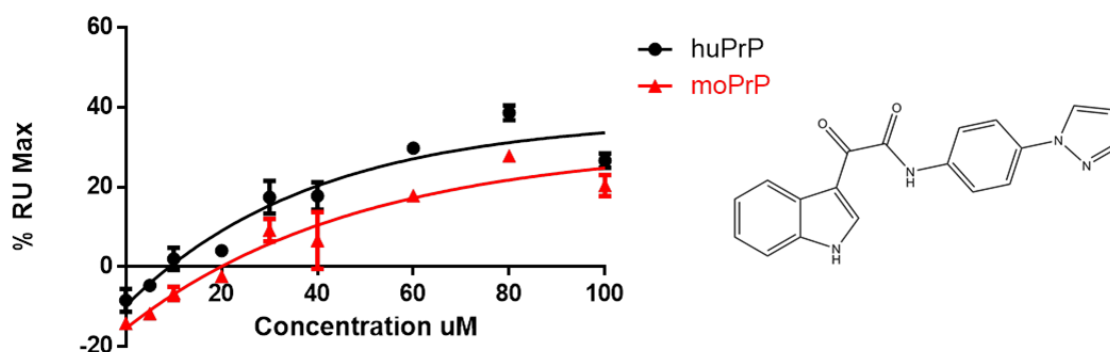


**Figure 37:** Dose response curve for compound 3001012 against huPrP and moPrP. Binding at each concentration was analysed in triplicate. Binding can be seen to plateau at the higher concentrations suggesting a saturation of binding, although less than 40 % of the predicted binding has occurred, suggesting limited binding interactions.

This is the lead compound from the SMB screening and **Figure 37** does seem to show some degree of binding. As with other compounds the binding seems to reach a plateau before the theoretical  $RU_{max}$  is reached. The concentration at which binding is observed is much higher than the cellular  $EC_{50}$ .

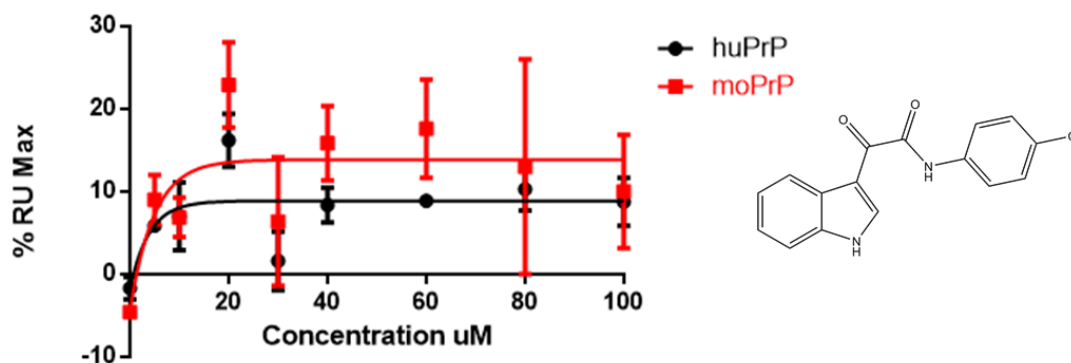


**Figure 38:** Dose response curve for compound 3000982 against huPrP and moPrP. Binding at each concentration was analysed in triplicate. Binding can be seen to plateau at very low concentrations, although only around 10 % of the predicted binding is observed, suggesting limited binding interactions.

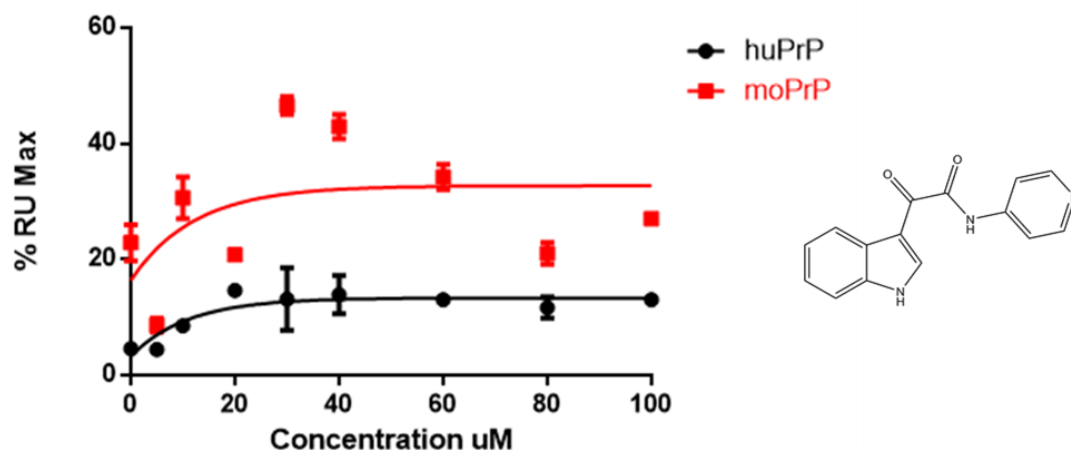


**Figure 39:** Dose response curve for compound 3000983 against huPrP and moPrP. Binding at each concentration was analysed in triplicate. As in **Figure 38** the binding appears to plateau at low concentrations, but only a small proportion of the expected binding is observed, suggesting limited binding interactions.

**Figure 38** and **Figure 39** show that for these two compounds the response was not increased with higher concentrations of compound, and the maximum response that was seen was well below the theoretical  $RU_{max}$ .

3001085 failed to show a dose response so was re-classified as a non-binder.

### 3.2.1.3.1. Library C

3001165 was the only compound to show any binding activity although with high standard deviations which suggested it was interacting with flow cell 1 rather than with the protein.

### 3.2.1.3.1. Library D

3001060 failed to show a dose response or binding response over the range of concentrations. A dose response was not carried out on 3000641 as there was none of the compound left.

### 3.2.1.3.1. Library E

3001124 and 3001140 were run at a range of concentrations but at higher concentrations showed a very large interaction with flow cell 1. This meant that it was impossible to determine if there was any binding occurring between the compound and PrP<sup>C</sup> at these concentrations as explained previously. The high standard deviations at the lower concentrations also cast doubt upon the validity of the original allocation of these compounds as binders, as there was likely to be interaction with flow cell 1 at the lower concentrations as well.

### 3.2.1.3.1. Library F

These compounds were the most interesting as they give the nearest to a specific binding dose response curve of any of the I3GAs. Compound 3001017 (**Figure 41**) in particular reached a plateau at around 150 % RU<sub>Max</sub>, with very low standard deviation, suggesting specific binding.

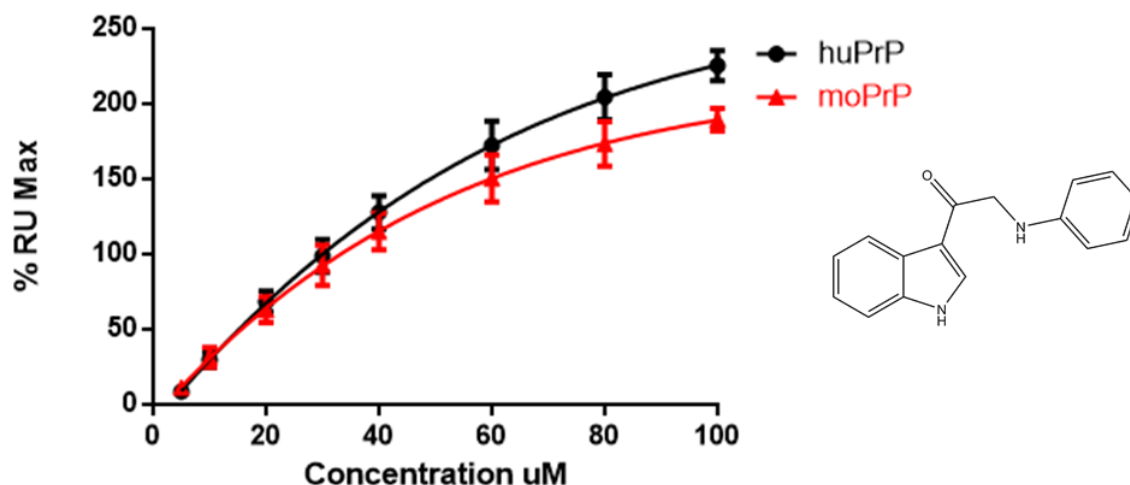


**Figure 40:** Dose response curve for compound 3001016 against huPrP and moPrP . Binding at each concentration was analysed in triplicate. Binding increases in a dose-dependent manner although it does not reach a plateau suggesting that binding is not saturated, even though binding levels much higher than expected can be observed.

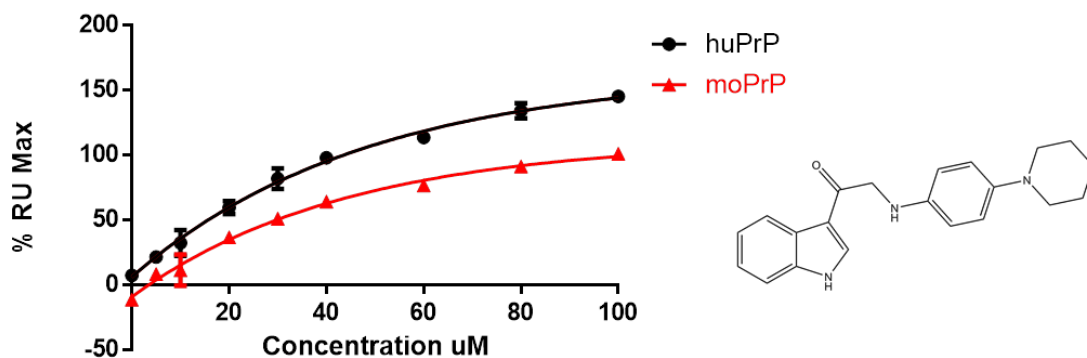


**Figure 41:** Dose response curve for compound 3001017 against huPrP and moPrP . Binding at each concentration was analysed in triplicate. Binding increases in a dose dependent manner and appears to be approaching a plateau at the higher concentrations, suggesting saturated binding at just over 100 %  $RU_{max}$ . This strongly suggests specific binding to both huPrP and moPrP.

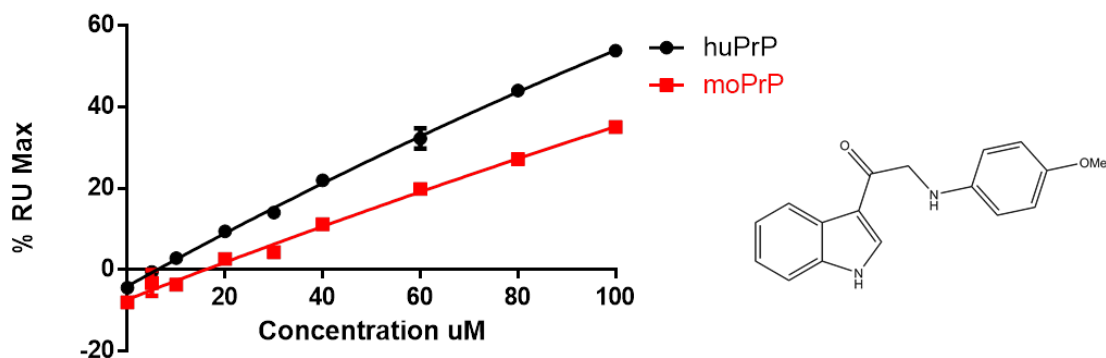


**Figure 42:** Dose response curve for compound 3001015 against huPrP and moPrP. Binding at each concentration was analysed in triplicate. Binding is increasing in a dose dependent manner but has not yet reached saturation. It is therefore not possible to determine whether this compound is binding specifically or non-specifically.

The dose response for 3001015, as shown in **Figure 42**, was almost linear, although it is not known if it would have reached a plateau if higher concentrations had been used. It is therefore hard to say with any confidence whether this is a specific or non-specific binder, although up to 100  $\mu$ M it does look like a non-specific binder. 3001016 reaches a plateau at around 200 %  $RU_{max}$ , suggesting that the binding may be non-specific (see **Figure 40**).

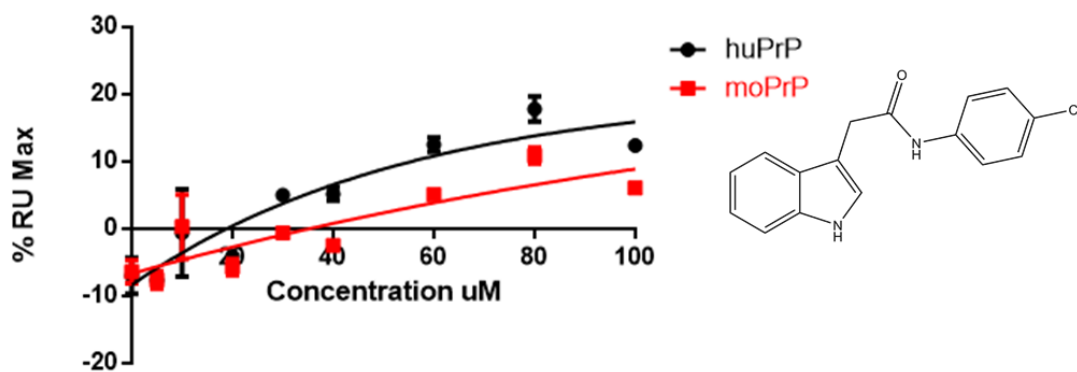


**Figure 43:** Dose response curve for compound 3001009 against huPrP and moPrP. Binding at each concentration was analysed in triplicate. Very low levels of binding were observed, although it did appear to be dose-dependent. The low levels of binding observed at the highest concentrations suggest limited binding interactions.

As can be seen in **Figure 43**, 3001009 only showed very low level binding. 3001025 did not show any dose response and the binding levels from the initial screen were not replicated so this was reclassified as a non-binder.

### 3.2.2. Discussion

It was hoped that the SPR data might go some way to elucidating the method by which the I3GAs exert their effect. The original hypothesis suggested that the I3GAs may be acting by binding to PrP<sup>C</sup> and preventing conversion of the normal isoform to PrP<sup>Sc</sup>. The I3GAs clearly reduced PrP<sup>Sc</sup> levels in the cells in a dose dependent manner, although it has not been determined whether this was done through inhibiting conversion of PrP<sup>C</sup> or *via* some other mechanism.

It is quite clear from the results above that the majority of the I3GAs tested do not bind to PrP, and those that do are binding at concentrations much lower than their EC<sub>50</sub> in the cell line. This makes it highly unlikely that they are exerting their anti-prion effect through binding to PrP<sup>C</sup>. Compounds from library F (3001015, 1016 and 1017) were the only ones that showed a response that suggested they might be specific binders. The explanation for the failure of these compounds to bind to recombinant PrP is unknown, but seems counterintuitive as the *in silico* screen initially identified them as potential interaction partners with the prion protein. Another possibility is that the binding site was unavailable due to the conformation of the PrP on the

chip. The PrP was thought to be bound to the CM5 chip *via* the N-terminal due to the structural similarity of CM-dextran to heparin. <sup>(221)</sup> Heparin has been shown to bind to the N-terminal of PrP <sup>(374)</sup> and heparin binding was shown to be prevented by immobilisation of PrP onto the chip. <sup>(221)</sup> The hypothesised protein-X binding pocket is thought to be between residues 167 and 218 <sup>(126)</sup> so it is therefore thought unlikely that this would be compromised due to the interaction of PrP with the chip. However, it is possible that the binding site may have been inaccessible due to the conformation adopted by PrP, as the positive control that was used was not a compound known to bind to this specific area. It is therefore not possible to entirely rule out an interaction of the I3GAs with PrP<sup>C</sup> however from the evidence presented here it appears unlikely that this would be the primary mode of action. A final possible explanation for the observed lack of binding is that the NMR model used in the *in silico* screen was not very well defined, and therefore may not have been an accurate enough model to predict binding with a high level of accuracy (personal correspondence from Prof Chen). The reasons outlined above may explain the paradox that these compounds bind to PrP *in silico*, but don't appear to bind to PrP *in vitro*.

Both 3001016 and 3001017 gave dose-response curves of the required shape for binders, although 3001016 in particular had reached 200 % RU<sub>max</sub> and not reached a definite plateau. 3001017 reached a plateau at around 150 % RU<sub>max</sub>. This was the only compound to show anything resembling a specific 1:1 binding curve. Again though, there is the discrepancy between the response seen in the SPR assay and the activity from the cell based assay as 3001017 had an EC<sub>50</sub> of 0.1µM.

3001015 showed a strong response with very low standard deviations but was a straight line response that showed no sign of reaching a plateau. This suggests that this compound is a non-specific binder but, unlike other compounds, isn't interacting with the chip surface. It is thought that this compound was probably interacting with the protein but not with a specific binding site as the binding doesn't appear to reach saturation point. These three compounds all have the same monocarbonyl structure (and were the only three to have this structure) so it's possible that this may be particularly suited to interacting with the PrP.

Some of the compounds, including the three mentioned above, were assessed for their tendency to form aggregates. Aggregation based effects have often been responsible for producing false positive results in binding studies so it was thought important to see if this may be responsible for the 'binding' seen in the SPR studies. <sup>(375)</sup> All compounds showing evidence of binding to PrP<sup>C</sup>

were assessed for their tendency to form aggregates using the dynamic light scattering technique.<sup>(278)</sup> The main compounds of interest were 3001015, 3001016 and 3001017 as these showed what appeared to be a strong binding affinity with the PrP. 3001016 and 3001017, which showed the strongest binding, were both found to form large aggregates at the concentrations used in the SPR screening. The data for 3001016 and 3001017 appears to be reaching a plateau at the higher concentrations, suggesting the covering of the available protein surface by these aggregates. 3001015 was also shown to aggregate, although not to the same extent, and this is reflected in the lower binding affinity seen in the SPR data. The data for 3001015 did not appear to reach a plateau, but this may also be due to the formation of aggregates at a lower rate. It is possible that a plateau may have been reached if higher concentrations or longer injections of 3001015 had been used. Aggregation of the compounds was observed on the blank flow cell, suggesting that aggregation was responsible for the observed signal. The data presented above, however, has this data subtracted, suggesting that either a certain amount of the aggregation is dependent on PrP, or that some genuine binding may be occurring. As the general aggregation tendency of these compounds matches their observed PrP<sup>C</sup> binding affinities it must be concluded that this is caused by the aggregation of the compounds rather than a genuine interaction with the protein, however some form of PrP dependent interaction may be a possibility.

### 3.3. Identification of the Lead Compound

After careful consideration of all the SPR and cell line screening data, compound 3001012 (**Figure 44**) was chosen as the lead compound. This compound was chosen on the basis of its nanomolar activity, and also because the synthesis of this compound was less problematic than the synthesis of some of the other I3GA compounds (personal correspondence from Mark Thompson). A relatively large amount of the compound had been synthesised and tested for purity, meaning that an adequate amount of high purity compound was available for the subsequent experiments.

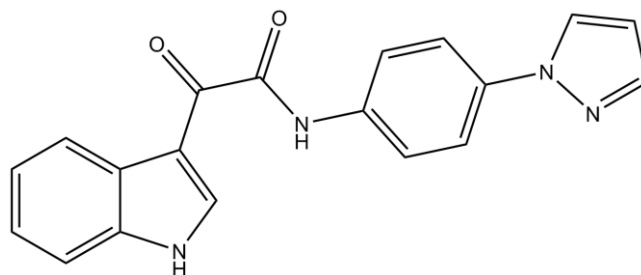


**Figure 44:** Structure of 3001012, the lead compound. The compound contains an unsubstituted indole, both carbonyl groups and a N-linked heterocycle at the *para*-position of the phenyl ring. All these characteristics were found to result in optimal anti-prion activity.

All 3 compounds from library B containing an N-linked heterocycle at the *para*-position of the phenyl ring had activities of less than 10 nM, and 3001012 was chosen as it was the most active. Substitutions to the indole ring didn't increase the activity, and in certain cases decreased the activity, and as this was a key feature of the SAR it was decided to use the unsubstituted indole.

It can be seen from the data presented in section 3.1.1 that the I3GAs represent an extremely potent group of anti-prion compounds with a tightly defined SAR. Substitution of the indole was not found to have a significant benefit in terms of activity, and aromatic amines with phenyl rings substituted at the *para*-position were most beneficial. A heterocycle with at least one hydrogen bond acceptor is required for optimal activity, as are both carbonyl groups. The significance of this discovery is substantial – although many anti-prion compounds have been described there are none that are active at such low concentrations. Investigations within the group into other groups of compounds have not found anything with nearly the same nanomolar activity as the I3GAs. Work within the group has shown quinacrine and curcumin to have  $EC_{50}$ s of 0.5  $\mu$ M and 0.7  $\mu$ M (see **Figure 46**) while investigations into thiazoles<sup>(276, 355)</sup> and pyridine dicarbonitriles<sup>(354)</sup> have only identified compounds with micromolar activities. Other promising groups of compounds to have been tested in the SMB model include benzamides,<sup>(376)</sup> which only showed weak inhibition at 20  $\mu$ M, and the 2-aminothiazoles<sup>(275)</sup> which were generally active around 1  $\mu$ M, although the most active had an  $EC_{50}$  of 81 nM. However, none of these match the activity of the I3GA compounds or have such a well characterised SAR, making them a unique, interesting and promising anti-prion therapeutic.

It is quite clear from the SPR data that this compound does not exert its anti-prion effect through binding. This has led to the original rationale for investigating these compounds, namely their identification as potential binders to PrP<sup>C</sup> in the *in silico* screen, being questioned. As

discussed in section **3.2.2** there are explanations that could be offered to explain the observed lack of binding, specifically the use of recombinant PrP instead of PrP<sup>C</sup>, the possibility that the binding site was inaccessible and possible inadequacies associated with the model of PrP that was used in the *in silico* screen. Despite this contradiction, the excellent activity exhibited by the I3GAs and their well-defined SAR were felt to justify further investigations into their anti-prion properties. Although the compounds do not appear to interact with PrP, they do have a clearly defined effect on PrP<sup>Sc</sup> levels in the SMB cells, suggesting the mode of action is unrelated to PrP<sup>C</sup>. The original hypothesis, that the I3GAs exert their anti-prion activity *via* direct interaction with PrP<sup>C</sup>, has not been supported and therefore a new hypothesis was required. The breadth of anti-prion compounds in the literature, and the wide variation in their mode of action made formulating a new hypothesis challenging. The SAR that was established for these compounds does not match the SAR established for these compounds in their role as tubulin polymerisation inhibitors, <sup>(365-367)</sup> meaning that this data did not provide any clues as to what the mode of action might be. The next challenge, therefore, was to try and show what the mode of action might be. Two possible modes of action were hypothesised. The first was that the I3GAs may be working by increasing cell growth, resulting in increased levels of PrP<sup>Sc</sup> dilution and subsequent reductions in steady state levels. The second was that the compounds may be working by influencing the aggregation of PrP<sup>Sc</sup>. Both these hypotheses are explored further in the subsequent chapter.

## 4. Pharmacodynamic, Pharmacokinetic and Mode of Action Studies of the Lead Compounds

Chapter 3 investigated the anti-prion properties of a large number of I3GA compounds. A high throughput cell based screening assay was used to determine the effect of these compounds on both cell viability and PrP<sup>Sc</sup> levels, and these data in turn were used to establish a structure-activity relationship (SAR). Further investigation of the SAR led to the development of I3GA compounds with nanomolar activities which subsequent rounds of optimisation failed to significantly improve upon. The most potent I3GA compounds were found to be unsubstituted indoles with an N-linked heterocycle at the para-position of the phenyl ring while the most advantageous substitution to the indole group was the addition of a cyano or nitro group at the 6-position.

In order to reveal further information about the properties and activity of the I3GAs, three of the compounds were investigated in more detail. 3001012, the most potent of the unsubstituted N-linked heterocycle compounds, was identified as the lead compound (see section 3.3) and was therefore selected. Other compounds investigated in some, but not all, of the experiments detailed in this chapter were 3001207 and 3001086, also I3GA compounds. 3001207 was chosen as the most potent of the I3GA compounds with a 6-cyano substitution, with an EC<sub>50</sub> close to that of 3001012. 3001086 was used in experiments carried out by another member of the group and so was included to allow direct comparison with studies that had already been carried out. The inclusion of both I3GA compounds allowed conclusions to be drawn about this structural group. Quinacrine was investigated for comparative purposes as a compound suspected to have a different mode of action to the I3GAs, due to its ability, unlike the I3GAs, to bind PrP (see **Figure 31** and **Figure 37**). Curcumin was used due to its use in the activity screening as a positive control. A series of compounds from the literature were also investigated, these are discussed in more detail in section 4.4.2.

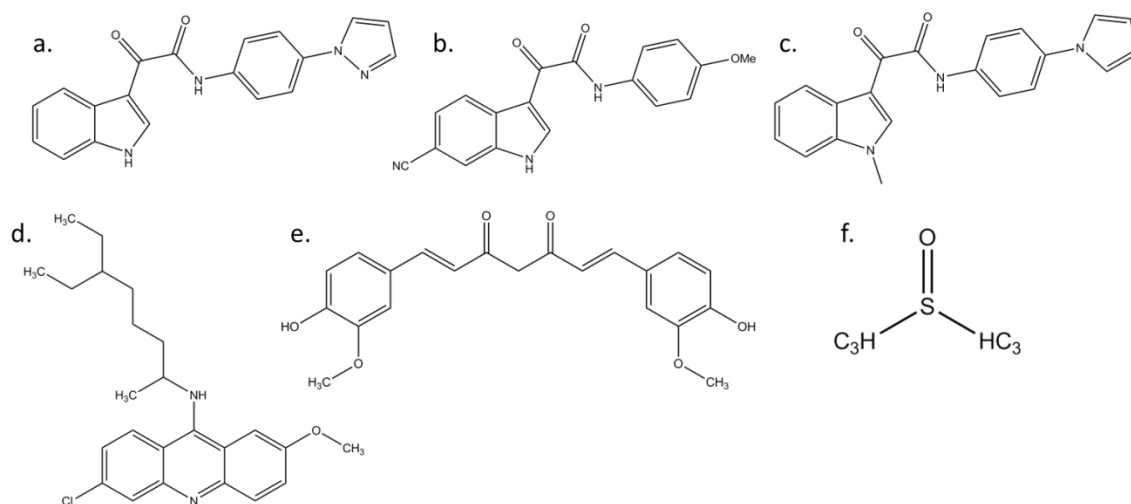


**Figure 45:** Structures of the compounds used in the subsequent experiments; 3001012 (a), 3001207 (b), 3001086 (c), quinacrine (d) curcumin (e) and DMSO (f).

In order to gain more insight into the lead compounds a series of experiments were carried out, focussing on 3001012 and 3001207. All were examining the pharmacodynamic properties of the I3GA compounds, i.e. the effect of the drug on the cells.

- **The curative assay** - The ability of the compounds to ‘cure’ the cells was investigated by monitoring PrP<sup>Sc</sup> levels in the cells for a prolonged period after treatment with the compounds. Testing the residual infectivity of the cells was not possible so it was hoped that this assay would give reassurance that the absence of PrP<sup>Sc</sup> was not simply a transient effect of treatment with these compounds.
- **Time course assays** – These were carried out to determine how long the compounds took to exert their anti-prion effect, allowing elucidation of further information about the mode of action of the I3GAs. These assays were carried out with the I3GA compounds as well as with quinacrine and curcumin for comparison.

There will also be discussion in this chapter of preliminary mode of action studies that were carried out, examining the effect of treatment on cell growth and MTT formazan exocytosis. The effect of the I3GAs and quinacrine on cell growth was investigated to determine if growth was being affected by any of the compounds. These studies were undertaken to try and glean information about the mode of action of the I3GAs compared to quinacrine and curcumin. Other groups had suggested that growth rate may affect the anti-prion activities of compounds<sup>(110, 377)</sup> and so an effect on growth rate could therefore be part of the mode of action. Another study is also outlined here, using the MTT formazan exocytosis (MTT-FE) assay. This assay uses the exocytosis by cells of the formazan formed during the MTT assay as a marker for the presence of

aggregated protein in cells. <sup>(348)</sup> It was hypothesised that disaggregation of protein aggregates may be a potential mode of action for the I3GAs, and that MTT formazan exocytosis (MTT-FE) could be used as an indirect readout of protein disaggregation. Compounds from the literature were also used in this study to allow comparison of the I3GAs with compounds whose mode of action had been investigated and reported.

## **4.1. Pharmacodynamic Studies: Curative Assay**

The curative assay was carried out using 3001012 and quinacrine. Quinacrine was used because a long term study on this compound had been carried out, investigating its effects in different cell lines. <sup>(233)</sup> This study showed that quinacrine caused the clearance of PrP<sup>Sc</sup> for 15 weeks. Both quinacrine and 3001012 were investigated at concentrations close to their respective EC<sub>50</sub>s and the effect of repeat dosing compared to single dosing was also considered. Materials and methods for this study are outlined in detail in sections **2.1.1** and **2.2.4.1**.

### **4.1.1. Results**

In order to confirm that the correct concentrations were being used for the positive controls, EC<sub>50</sub> curves for these compounds were run. Results were found to be comparable to those obtained previously (see **Figure 46** and **Table 10**).

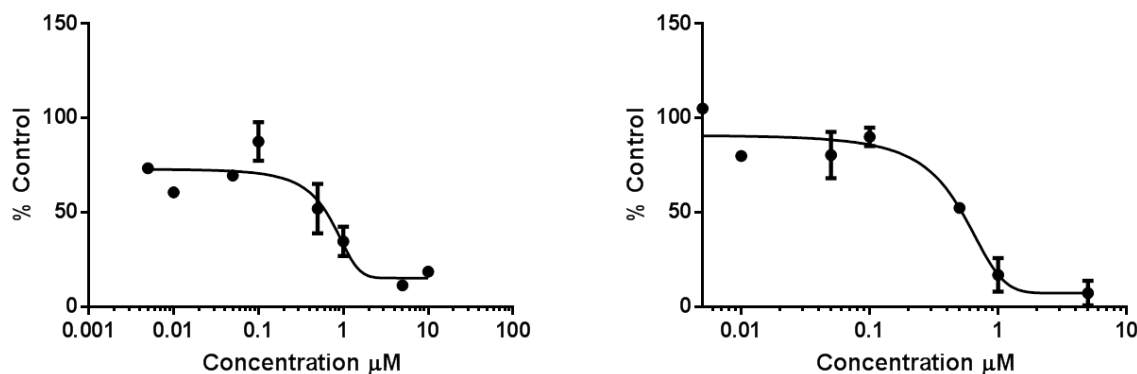


**Figure 46:** EC<sub>50</sub> curves for quinacrine (right) and curcumin (left). Cells were dosed with the compounds at a range of concentrations (as described in sections 2.2.2.1 and 2.2.2.2) and the amount of PrP<sup>Sc</sup> in the cell lysate was analysed using dot blotting after 5 days of exposure to the compounds. Quinacrine has an EC<sub>50</sub> of 0.5 μM, while curcumin has an EC<sub>50</sub> of 0.7 μM, demonstrating the concentrations at which both compounds are active in the SMB cell model.

The curative assay was subsequently run four times:

1. The first run was to ensure that the protocol that had been proposed worked. This was run for 4 passages and resulted in the cell number and the time between passages being reduced to allow the assay to continue for longer. Apart from these minor adjustments the assay was successful (data not shown).
2. The second run used the refined protocol and was run for 7 passages. Curcumin was used as the positive control (data not shown).
3. The third run was maintained for 8 passages. Quinacrine was used as the positive control instead of curcumin (data not shown).
4. The fourth run was for 12 passages. As before 3001012 was run at 1 nM and 10 nM. Quinacrine was run at 1 μM, 5 μM and also at 1 μM with repeated dosing after each passage.

Lysates of treated cells were prepared and analysed in groups of 4 passages, as shown in **Figure 47**. Results presented here are from the fourth run, as this was the longest running and therefore the most significant in terms of the possible reappearance of PrP<sup>Sc</sup>.

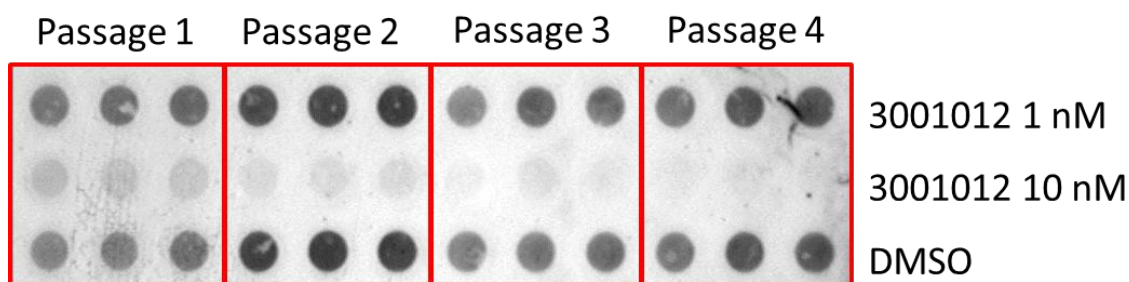


**Figure 47:** Example dot blot for 4 sets of lysate samples demonstrating the presence or absence of PrP<sup>Sc</sup> as measured by the intensity of the signal. Each row represents a different treatment, while each set of three columns represents sequential passages from left to right. The lack of signal after treatment with 3001012 at 10 nM is shown to be maintained after 4 passages.

Results from the longest running assay are shown below. 3001012 was again run at 1 nM and 10 nM. Quinacrine was run at 1  $\mu$ M and 5  $\mu$ M, and also at 1  $\mu$ M with repeat dosing after every split to see how this might affect results. The cells were passaged every four or five days depending on how confluent the cells were.

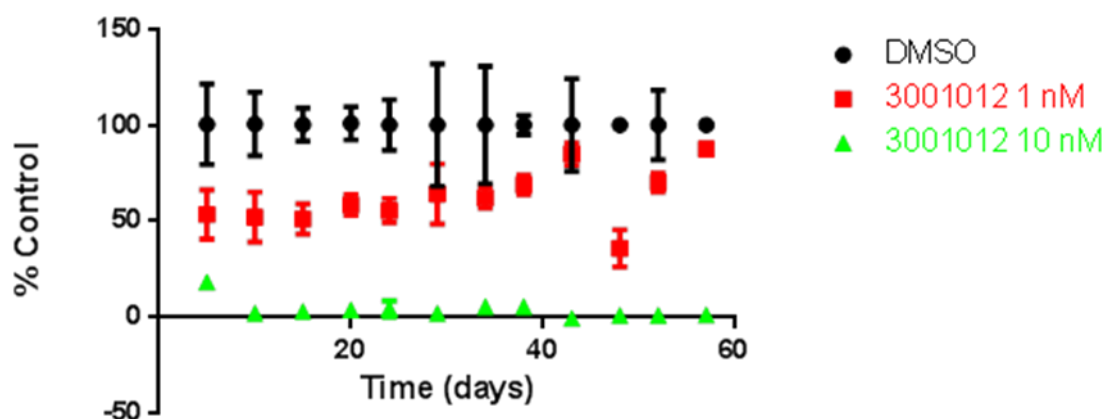


**Figure 48:** PrP<sup>Sc</sup> levels over time after dosing with either DMSO or 3001012 at 1 or 10 nM. PrP<sup>Sc</sup> levels were monitored every 4 or 5 days, with the whole experiment running for 57 days. Each time point was analysed in triplicate.

Complete clearance of PrP<sup>Sc</sup> over the time period, as shown in **Figure 48**, was seen when the cells were dosed with 3001012 at 10 nM. Clearance at 1 nM was generally around 50 %, as would be expected as the EC<sub>50</sub> is 1 nM, although it did fluctuate between 40 and 57 days.

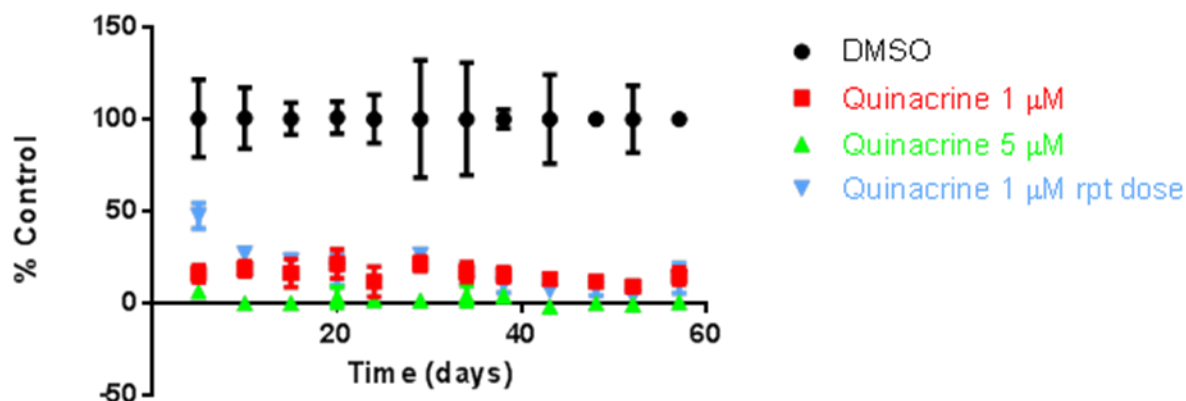


**Figure 49:** PrP<sup>Sc</sup> levels over time after treatment with either DMSO, or quinacrine at 1 or 5 μM. Cells were either dosed once or dosed after every passage with 1 μM quinacrine over the course of the experiment (quinacrine 1 μM and quinacrine 1 μM repeat dose respectively). PrP<sup>Sc</sup> levels were monitored every 4 or 5 days, with the whole experiment running for 57 days. Each time point was analysed in triplicate.

**Figure 49** shows quinacrine to be effective at clearing PrP<sup>Sc</sup> at a concentration of 1 μM when the cells were dosed once. No toxic effect was observed under the microscope at any point of the assay. An interesting observation was that for the first two splits after initial dosing the cell pellets had a yellow colour that disappeared after two passages. This was not seen in the cells that were dosed after every split.

#### 4.1.2. Discussion

The aim of the curative assay was to determine how long it would take for the cells to re-start production of PrP<sup>Sc</sup> after being 'cured' to give a measure of the long term efficacy of the anti-prion activity of the I3GAs. It can be seen that treatment with compounds at concentrations higher than their EC<sub>50</sub> results in the reduction of PrP<sup>Sc</sup> signal for up to 57 days.

Quinacrine was dosed at 1 μM and 5 μM and both treatments showed the complete clearance of PrP<sup>Sc</sup> over the duration of the assay (see **Figure 49**). Dosing at 5 μM showed a complete clearance of PrP<sup>Sc</sup> (levels of <5 % of the blank) whereas dosing at 1 μM showed slightly higher levels (generally between 10 and 20 % of the blank). 1 μM is the lowest concentration shown to cause complete clearance of PrP<sup>Sc</sup> and as such slight variations in the assay might cause this to be slightly less effective. Changes in stock solution and cell passage might be enough to shift the

EC<sub>50</sub> slightly and reduce efficacy at 1 μM. Even though the clearance is not complete it is highly significant.

Compound 3001012 for the most part behaved exactly as expected (see **Figure 48**). Routine screening had shown this compound to have an EC<sub>50</sub> of 1 nM and so this concentration was used to see if partial clearance of the PrP<sup>Sc</sup> resulted in reappearance of the protein faster than total clearance. For comparison a 10 nM solution was also used to ensure total clearance of PrP<sup>Sc</sup>. Cells treated with 10 nM 3001012 showed complete clearance of PrP<sup>Sc</sup> with no recurrence over the 57 day period of the assay, suggesting that at this concentration the cells are 'cured'. Initial results for cells treated with 1 nM 3001012, up to 38 days, showed PrP<sup>Sc</sup> levels gradually rising from around 50 % blank to around 60 % blank. After this point levels fluctuated but then settled at around 70 % of the blank. The data point at 57 days suggests that PrP<sup>Sc</sup> levels have returned to pre-treatment levels (around 100 % of the blank). The significance of this is not clear - if found not to be an artefact it may be indicative of PrP<sup>Sc</sup> starting to return to pre-treatment levels, with the lag phase perhaps due to PrP<sup>Sc</sup> levels being low enough to prevent conversion and aggregation for a limited period of time. A repeat of this study would be required to rule out the possibility of experimental artefacts and help elucidate this matter further.

The discrepancies in the 1 nM data could possibly be explained by the ageing of the cells over the course of the assay, which may have affected results. Under normal conditions the cells are passaged every 7 days, and passaging them every 4 days caused them to grow more slowly and become more likely to undergo apoptosis. Longer running assays were only possible due to the close monitoring of the cells, ensuring they were passaged in good time. The lower than expected activity from 1 nM 3001012 may also be the result of dilution error. A fresh 10 mM stock solution of 3001012 was made up for these assays and it's possible that this may have produced a small shift in the EC<sub>50</sub>. Similarly the large dilutions required to obtain concentrations low enough to be used in this assay were inherently prone to error. Small errors in dilution may have been enough to result in an inactive concentration - 3001012 at 0.5 nM was shown to have no effect on the amount of PrP<sup>Sc</sup> while 5 nM caused almost total clearance. Experience has shown that this compound in particular is fairly consistent across different assays, with variation generally within the range found during the initial screen and EC<sub>50</sub> calculation. However, the potential for small errors in dilution are thought to be the most likely explanation for the lack of activity from 3001012 at 1 nM.

The results from these experiments show clearly that 3001012 caused complete clearance of PrP<sup>Sc</sup> with no return of infection within the time frame of the assay. A previous paper suggested that cells cured of quinacrine started to produce PrP<sup>Sc</sup> after around 3 months. <sup>(233)</sup> Without running the assay for longer it is not possible to say whether PrP<sup>Sc</sup> may have returned, and the data obtained does not suggest that PrP<sup>Sc</sup> levels are starting to rise. Rather, these data are consistent with a prolonged period of PrP<sup>Sc</sup> absence which was observed after treatment with both compounds. However, previous papers that have carried out these kinds of studies have suggested that the lack of detectable PrP<sup>Sc</sup> may be due to a dilution effect rather than an actual absence of the protein. <sup>(377)</sup> The authors concluded that the continued growing and splitting of the cells means that PrP<sup>Sc</sup> levels never return to a detectable level although it is still being produced, as it was being diluted by the dividing cells. It was proposed that dosing cells and then arresting growth resulted in PrP<sup>Sc</sup> returning much more quickly, within around two weeks in the case of quinacrine. It is obviously important in determining the potency of lead compounds to establish whether the prolonged reduction of PrP<sup>Sc</sup> is due to the cells being 'cured' or whether residual PrP<sup>Sc</sup> could result in levels eventually starting to increase. It would be a good idea, therefore, to try and carry out the experiment where the cell growth is arrested and see if PrP<sup>Sc</sup> levels do return to pre-treatment levels more quickly. While it's questionable whether the effect of compounds on growth-arrested cells is relevant to the *in vivo* potential of prospective therapeutic compounds, this would add to the body of knowledge about these compounds.

An interesting observation was that PrP<sup>Sc</sup> levels appeared to be reduced almost completely during the curative assay, with clearance of PrP<sup>Sc</sup> appearing more complete than was observed in the screens carried out over 5 days. This was observed from the second passage onwards at the highest concentrations of both 3001012 and quinacrine, suggesting that the normal 5 day duration of the screening experiments may not be long enough to allow total reduction of PrP<sup>Sc</sup>. The increased efficiency of PrP<sup>Sc</sup> clearance after 10 days, along with the failure of PrP<sup>Sc</sup> levels to rise again, provides persuasive evidence that the cells are cured of infection. As discussed in section 3.3 a measure of infectivity would be desirable, but the data presented here suggests it may be valuable to look at the residual infectivity over a longer time frame than 5 days.

In conclusion, 3001012 seemed to be a potent inhibitor of PrP<sup>Sc</sup> over a long period of time, with just one dose at ten times the EC<sub>50</sub> value appearing to cure the cells for at least eight weeks. However, there is a suggestion that PrP<sup>Sc</sup> production may still occur, albeit at undetectable levels, which would require further investigation. The same applies to quinacrine at 1 and 5 µM,

although the repeat dosing experiments with 1 $\mu$ M quinacrine show that this compound is not toxic to the cells at this concentration, even after prolonged exposure.

## 4.2. Pharmacodynamic Studies: Time Course Assays

Time course assays were carried out to identify how long it took for compounds to exert their anti-prion effect. These experiments were initially suggested to help determine the optimum protocol for preparing samples for the microarray and proteomics studies detailed in section 5. Choosing the correct concentrations and duration of dosing was seen as important to avoid any off-target effects that the compounds may be having – longer dosing times and higher concentrations were thought more likely to confuse the results by increasing background noise and changes unrelated to the compound's anti-prion functions. Initially it was suggested dosing should be done at the EC<sub>50</sub> concentration, however subsequently this was revised to dosing at 3 times EC<sub>50</sub> as it was not possible to guarantee 50% clearance of PrP<sup>Sc</sup>. In order to confirm the time course for these compounds these experiments were also carried out at higher concentrations of between 5 and 10 times EC<sub>50</sub>.

The initial focus of these experiments was on the compounds to be used in the microarray and proteomic studies, namely 3001012 and 3001207. 3001207 was selected for the microarray and proteomics studies as it was the most active of the two compounds featuring a 6-cyano substitution to the indole. The 6-cyano substitution was beneficial to activity (see section 3.1.2.7) in contrast to the majority of substitutions to the indole, so these compounds, and 3001207 in particular, were of interest. Quinacrine was used in the microarray and proteomics studies and for that reason is included in these studies. Time course assays were also carried out on curcumin and 3001086 for comparative purposes. These assays were only carried out at the higher concentrations. See **Figure 45** for structures of all compounds

All concentrations were based on the previously calculated EC<sub>50</sub> values which were confirmed as part of these experiments. Materials and methods for this study are outlined in detail in sections 2.1.1 and 2.2.4.2..

## 4.2.1. Results

### 4.2.1.1. Confirmation of EC<sub>50</sub> Values

To ensure that the correct concentrations were being used the EC<sub>50</sub> curves were repeated to check that the results could be replicated in a different passage of cells. Encouragingly the results were found to be comparable to previous experiments for all compounds.

**Table 33:** Previous EC<sub>50</sub> results compared to current EC<sub>50</sub> results for all compounds used in the time course study.

| Compound   | Previous EC <sub>50</sub> result | Current EC <sub>50</sub> result |
|------------|----------------------------------|---------------------------------|
| Quinacrine | 0.31 ± 0.2 μM                    | 0.65 μM                         |
| Curcumin   | 0.87 ± 0.15 μM                   | 1.2 μM                          |
| 3001012    | 1 ± 0.4 nM                       | 1 nM                            |
| 3001207    | 2.2 ± 2.8 nM                     | 1.7 nM                          |
| 3001086    | 0.17 ± 0.05 μM                   | 0.25 μM                         |

Some variability was observed between runs, although this is almost within the range of error found in the previous screens. Overall it was thought that the results are very reassuring as the compounds are not differing much in activity across different stock solutions and cell passages, especially given the dilutions involved. The EC<sub>50</sub> screens carried out at this point were for conformation only and so were not repeated. Consequently, there are no standard deviation data for these values.

### 4.2.1.2. Time Course Screen for Activity at EC<sub>50</sub>

Initial time course investigations looked at the effect over time of three compounds, quinacrine, 3001012 and 3001207, when they were dosed at their EC<sub>50</sub> concentrations.

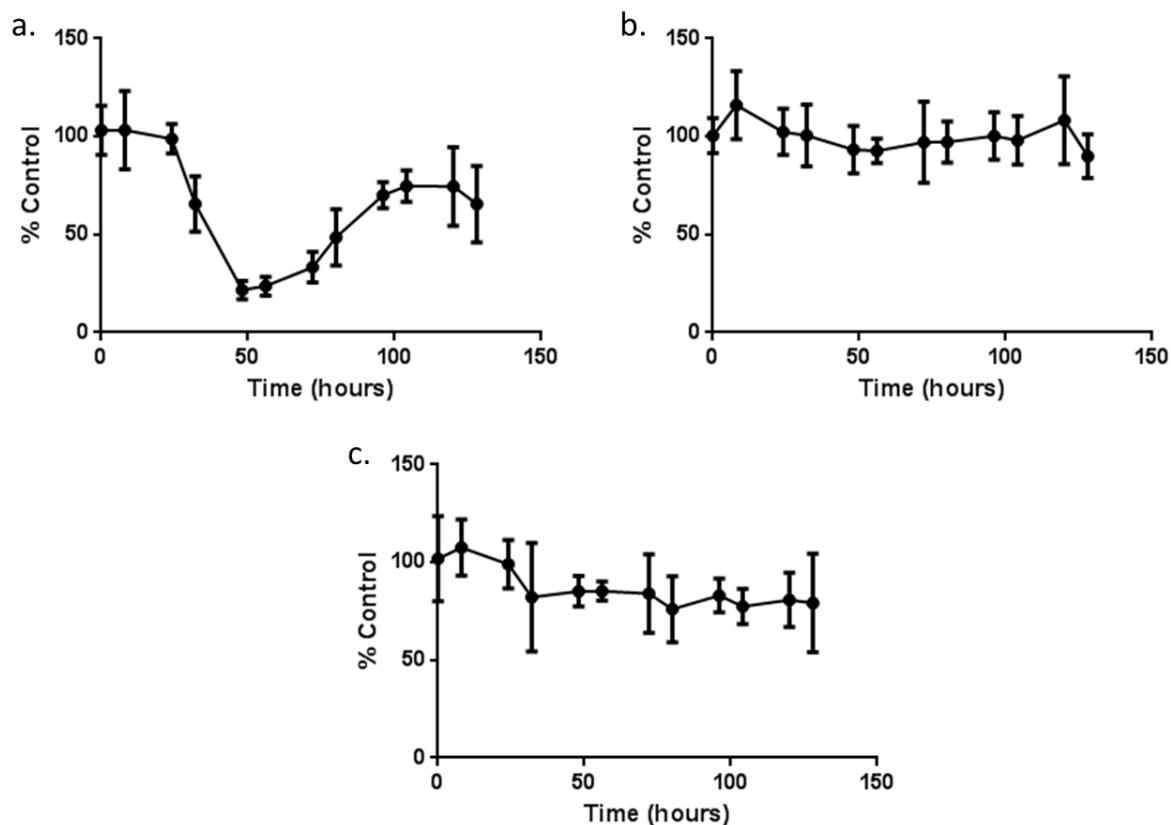


**Figure 50:** Time course data for a. quinacrine at 0.5  $\mu\text{M}$ ; b. 3001012 at 1.5 nM; c. 3001207 at 20 nM. PrP<sup>Sc</sup> levels were analysed at each time point and the data is presented as the percentage of the signal from the DMSO control at the same time point. No toxicity was observed over the course of the experiment. The data points shown represent the mean  $\pm$  SD values from duplicate experiments where each sample was analysed in triplicate.

The data in **Figure 50** shows that 3001012 and 3001207 did not show a decrease in PrP<sup>Sc</sup> levels over time when dosed at their EC<sub>50</sub> concentration. Quinacrine at 0.5  $\mu\text{M}$  showed a different pattern, with an initial decrease in PrP<sup>Sc</sup> levels up to 48 hours, after which time PrP<sup>Sc</sup> levels increased again to around 75% of the original level. Previous screens had established that the compounds were being used at non-toxic concentrations so toxicity as assessed by the MTT assay was not measured. Plates were monitored by eye and no toxic effects were observed.

#### 4.2.1.3. Time Course Screen for Activity at 3 times EC<sub>50</sub>

Further investigations were subsequently undertaken into the activity of the compounds investigated in **Figure 50** when they were dosed at 3 times their EC<sub>50</sub>.

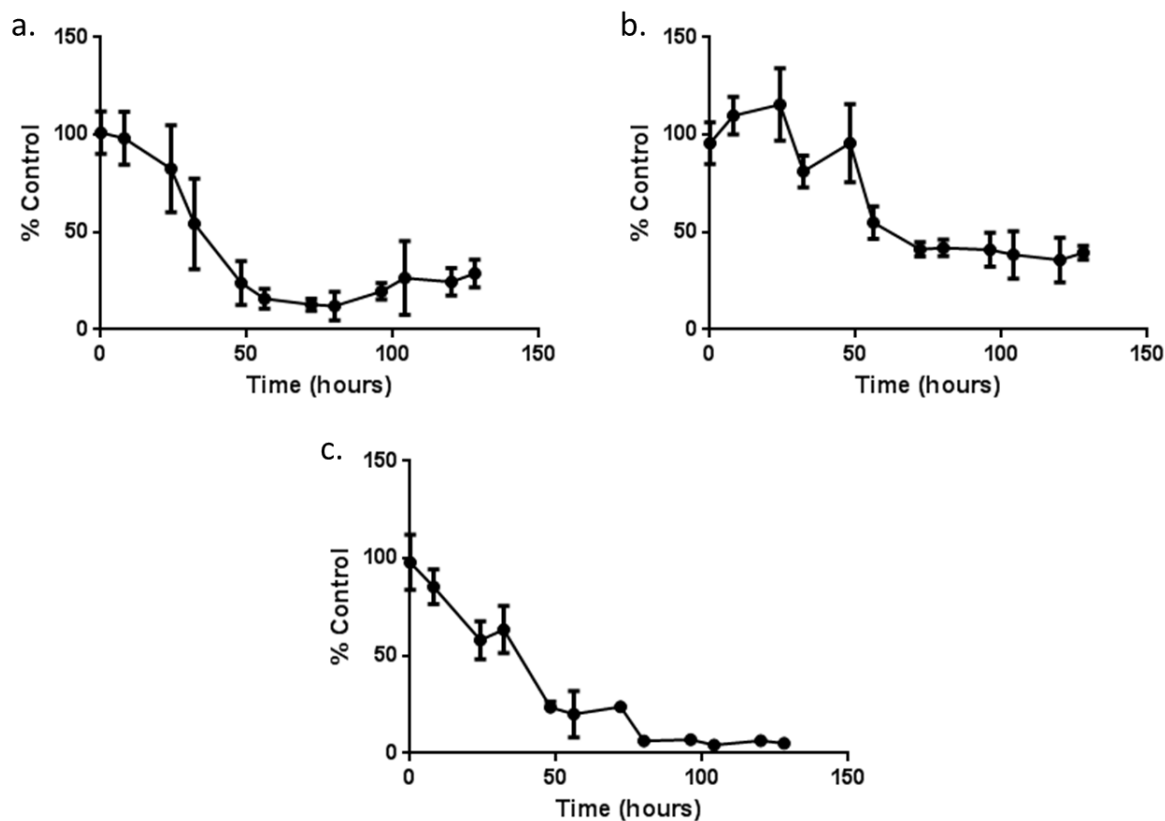


**Figure 51:** Time course data for a. quinacrine at 1.5  $\mu\text{M}$ ; b. 3001012 at 4.5 nM; c. 3001207 at 60 nM. PrP<sup>Sc</sup> levels were analysed at each time point and the data is presented as the percentage of the signal from the DMSO control at the same time point. No toxicity was observed over the course of the experiment. The data points shown represent the mean  $\pm$  SD values from duplicate experiments where each sample was analysed in triplicate.

It can be seen in **Figure 51** that quinacrine at 1.5  $\mu\text{M}$  showed full clearance by 56 hours, with no subsequent rise in PrP<sup>Sc</sup> levels as observed when quinacrine was dosed at 0.5  $\mu\text{M}$ . 3001012 at 4.5 nM showed a steady decrease to around 40 % of original PrP<sup>Sc</sup> levels by 72 hours and 3001207 at 60 nM showed a decrease of PrP<sup>Sc</sup> levels to around 20 % by 48 hours, with virtually full clearance being achieved by 80 hours.

#### 4.2.1.4. Time Course Activity at 5 – 10 times EC<sub>50</sub>

Finally, the compounds investigated in **Figure 50** and **Figure 51** were investigated at concentrations equivalent to between 5 and 10 times their EC<sub>50</sub>. 3001086 and curcumin were also investigated at these concentrations.

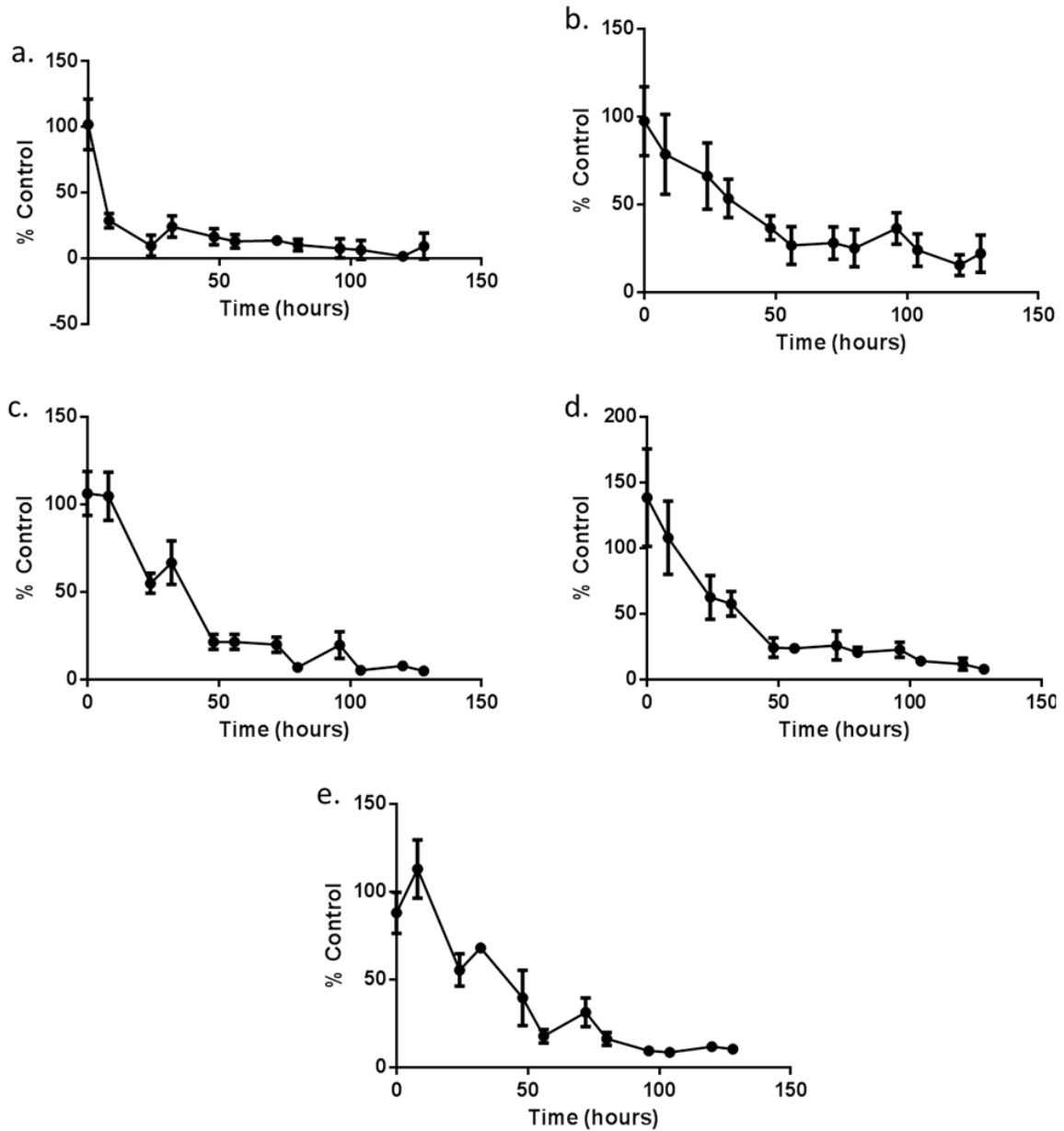


**Figure 52:** Time course data for a. quinacrine at 5  $\mu$ M; b. 3001012 at 10 nM; c. 3001207 at 100 nM; d. curcumin at 10  $\mu$ M; e. 3001086 at 1  $\mu$ M. PrP<sup>Sc</sup> levels were analysed at each time point and the data is presented as the percentage of the signal from the DMSO control at the same time point. No toxicity was observed over the course of the experiment. The data points shown represent the mean  $\pm$  SD values from duplicate experiments where each sample was analysed in triplicate.

The data in **Figure 52** shows that quinacrine at 5  $\mu$ M showed full PrP<sup>Sc</sup> clearance by 24 hours. 3001012 at 10 nM showed a steady decrease to around 30 % of original PrP<sup>Sc</sup> levels by 56 hours, while 3001207 at 100 nM showed a decrease of PrP<sup>Sc</sup> levels to around 20 % by 48 hours, with virtually full clearance being achieved by 80 hours. Curcumin at 10  $\mu$ M gave good clearance by

48 hours and 3001086 at 1  $\mu\text{M}$  followed the same pattern as the other I3GAs and resulted in clearance to around 20 % of original levels by 56 hours.

## 4.2.2. Discussion

Compounds were run over 128 hours at different concentrations to determine how long it took for each compound to exert its anti-prion effect. Quinacrine was found to clear  $\text{PrP}^{\text{Sc}}$  rapidly at higher concentrations (5  $\mu\text{M}$ ), but more slowly at lower concentrations (1.5  $\mu\text{M}$ ). The I3GA compounds were consistent in the time it took to clear  $\text{PrP}^{\text{Sc}}$  at the higher concentrations, with no effect when dosed at  $\text{EC}_{50}$  concentrations. When dosed at the highest concentration the main difference was that the final level of clearance was lowered, compared to dosing at 3 x  $\text{EC}_{50}$ . Curcumin at 10  $\mu\text{M}$  showed a similar pattern to the I3GA compounds as did 3001086, with maximum clearance at 48 and 56 hours respectively. All compounds were used at concentrations known to be non-toxic from previous screens, and this was confirmed by observation of the cells over the course of the experiment. No toxic effects were observed at any point.

Quinacrine, at high concentrations, clearly acts much more quickly than the in-house compounds (see **Figure 52a**). In all repeats of this experiment  $\text{PrP}^{\text{Sc}}$  was nearly cleared after 8 hours and totally cleared after 24 hours. For both 3001012 and 3001207, even at the highest concentration, it takes 56 hours and 48 hours respectively to clear  $\text{PrP}^{\text{Sc}}$  down to baseline levels (see **Figure 52b** and **c**). 3001086 adhered to the same pattern as the other I3GA compounds with clearance taking 56 hours (see **Figure 52e**). Whilst the I3GA compounds are significantly more active than quinacrine (3001012 is 333 x more active, 3001207 is 250 x more active, 3001086 is approximately twice as active) they take up to 7 times longer to clear the  $\text{PrP}^{\text{Sc}}$  from the cells.

Quinacrine, despite at high concentrations clearing  $\text{PrP}^{\text{Sc}}$  from the cells very quickly, is not as efficient at lower concentrations, taking up to 48 hours to exert its full effect (see **Figure 51a**). It is the only compound to show this increased speed of activity at higher concentrations, and this may be due to its mode of action. Quinacrine is known to interact with  $\text{PrP}^{\text{C}}$  and is also able to inhibit the formation of *de novo*  $\text{PrP}^{\text{Sc}}$ ,<sup>(233)</sup> with binding to  $\text{PrP}$  likely to be crucial to its mode of action. Whilst curcumin is known to bind to  $\text{PrP}$  fibrils<sup>(268)</sup> its mode of action has not been fully characterised, and the results presented here suggest it does not share a mode of action with

quinacrine (see **Figure 52d**). As demonstrated in section **3.2** none of the I3GA compounds with both carbonyl groups were shown to interact with PrP, suggesting that these compounds are not exerting their anti-prion effect *via* direct interaction with PrP. It therefore seems likely that the difference in the time taken for quinacrine to clear PrP<sup>Sc</sup>, compared to curcumin and the I3GAs, is related to their differing modes of action.

The failure of the two I3GA compounds to show any activity at their EC<sub>50</sub> concentrations (see **Figure 50b** and **c**) suggests a similar scenario to that seen in the curative assay. It would be expected that a reduction of PrP<sup>Sc</sup> to around 50% of starting levels should be seen by the end point of the time course, at the 5 day time point which is used in the routine screens. It is thought that some of the same problems experienced in the curative assay may also have a role here, such as the potential problems with dilution error, and furthermore there may be a narrow window between no clearance and total clearance. The error associated with the EC<sub>50</sub> screening may make determining the EC<sub>50</sub> with the required accuracy more challenging, especially at the very low concentrations at which these compounds are active. It is also possible that looking for more subtle changes in PrP<sup>Sc</sup> levels is problematic due to the occasional lack of clarity in the blots. This was a particular problem during the first few time points due to the lower numbers of cells and the weaker signal which was obtained as a result. It was concluded that doing these assays at such low protein concentrations was perhaps not practical, although results from the higher concentrations gave adequately conclusive results.

The results for quinacrine at EC<sub>50</sub> concentration were also not as expected. As quinacrine was dosed at much higher concentrations it is unlikely that this is due to dilution error, although the problems with clarity may still play a part. The pattern seen does seem to be reproducible for all quinacrine experiments at this concentration. An initial decrease in PrP<sup>Sc</sup> hits its lowest point at around 48 hours, with PrP<sup>Sc</sup> levels at 20 – 30 % of control levels. PrP<sup>Sc</sup> levels then gradually increase to around 80 – 90 % by the end of the assay. It is possible that at these low concentrations the conversion of PrP<sup>C</sup> to PrP<sup>Sc</sup> is initially prevented, but there may not be enough of the compound to maintain this. As a result, after a certain period of time the conversion of PrP<sup>Sc</sup> is able to recommence. This would fit in with the idea that this compound is working by binding to either PrP<sup>C</sup> or PrP<sup>Sc</sup>.

The discussions in sections **3.1.3** and **4.1.2** have both raised the question of whether the cells are genuinely cured or not by questioning whether PrP<sup>Sc</sup> is still present within the cells. Analysing

PrP<sup>Sc</sup> levels after 5 days appeared to show that residual PrP<sup>Sc</sup> was still present, while the curative assay data suggest that analysis of PrP<sup>Sc</sup> levels at a later time point results in almost total clearance. It was hoped that the time course assays might provide further insights into this question. It can be seen that for all compounds the majority of the reduction in PrP<sup>Sc</sup> levels has occurred by 56 hours, after which PrP<sup>Sc</sup> levels remain low. In most cases the data corresponding to a 5 day dose do not show total clearance, corresponding to the data from the endpoint studies. It is possible that running these studies for longer would result in further decreases in PrP<sup>Sc</sup> levels, although any subsequent decrease in PrP<sup>Sc</sup> would be occurring at a much slower rate than the initial decrease. While the data from the curative assay supports the supposition that the cells are cured, a reliable measure of residual infectivity at different time points would be required to provide more conclusive evidence of this.

Although this data doesn't provide any more information about how the I3GA compounds are working, it does suggest that they have a different mode of action to quinacrine at least. This reinforces the SPR data suggesting that this group of compounds, unlike quinacrine, do not bind to PrP<sup>C</sup>.

### **4.3. Mode of Action Studies: Investigations into the Effect on Cell Growth**

Cell growth has been shown to be important in maintaining steady state levels of PrP<sup>Sc</sup>,<sup>(110, 377)</sup> so the effect of the I3GA compounds on cell growth was investigated. It was hypothesised that the compounds might be working by increasing cellular proliferation which, in turn, would further dilute and decrease PrP<sup>Sc</sup> levels. Growth curve analysis was carried out using two different methods, either counting the cells using a haemocytometer or by monitoring growth using the MTT assay described in section **2.2.2.3**. Experiments were initially carried out using the compounds studied in the microarray and proteomics studies (quinacrine, 3001012, 3001207) when conditions for the sample preparation were being optimised. Curcumin and 1086 were also examined for their effect on growth, but only *via* the MTT assay. As before, cells treated with 0.5% DMSO were used as the negative control against which the treated samples were compared. Materials and methods for this study are outlined in sections **2.1.1** and **2.2.4.3**.

## 4.3.1. Results

### 4.3.1.1. Monitoring Cell Growth Using a Haemocytometer

Initial analysis of cell growth was carried out using a haemocytometer. The cells were treated with different compounds and then harvested and counted at the specified time points.

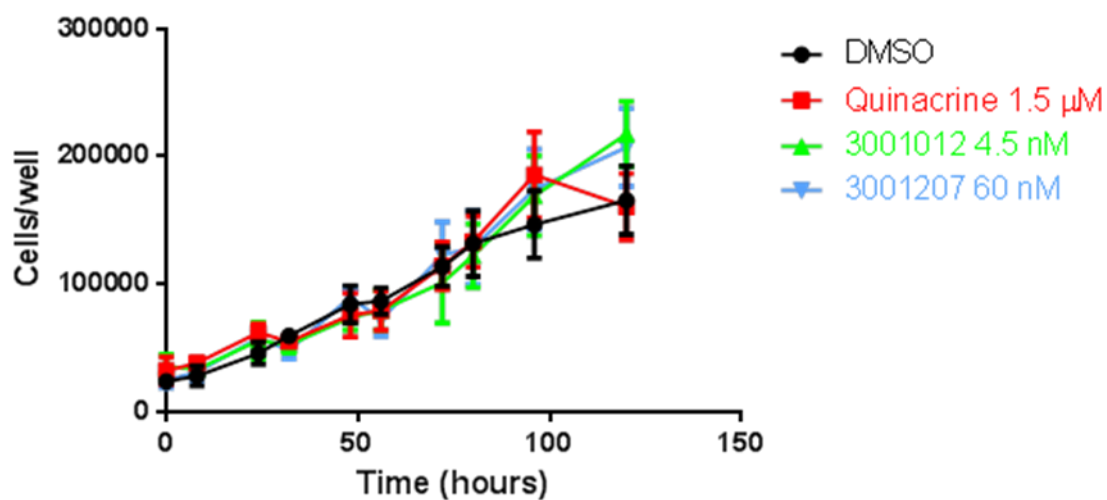


**Figure 53:** Growth assessed by cell counting after dosing with compounds at  $3 \times EC_{50}$ . Cells were harvested at regular time points before assessment of cell numbers using a haemocytometer. Results are expressed as the number of cells per well. The data points shown represent the mean  $\pm$  SD values from duplicate experiments where each sample was analysed 4 times.

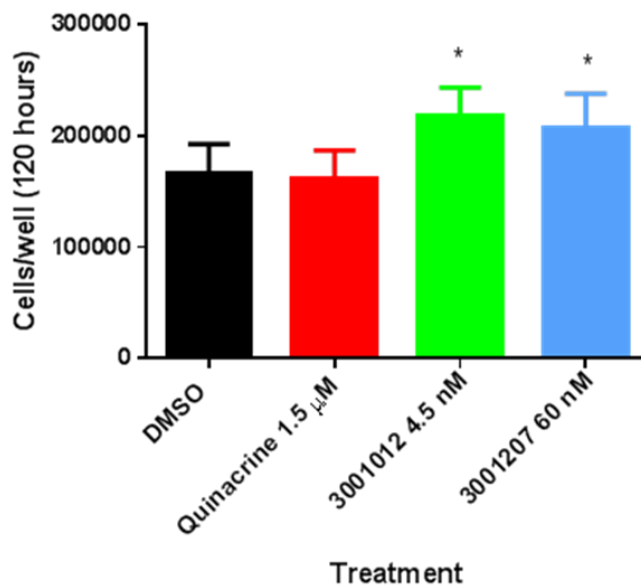


**Figure 54:** Final cell numbers after 120 hours of growth. Analysis of statistical significance using a multiple t-test shows that the difference between cells treated with DMSO and cells treated with quinacrine is not significant (p-value 0.711) but the differences between cells treated with DMSO and 1012 or 1207 are (p values 0.001 and 0.019 respectively). The data points shown represent the mean  $\pm$  SD values from duplicate experiments where each sample was analysed 4 times.

The data in **Figure 53** and **Figure 54** demonstrate that growth up to 80 hours appears fairly consistent with growth dropping off after this point in the DMSO treated cells but not those treated with the I3GA compounds. Growth in cells treated with quinacrine dropped off more dramatically at 96 hours suggesting that apoptosis is starting to be induced at this time point for cells treated with quinacrine but not cells treated with the I3GAs.

#### 4.3.1.2. Monitoring Cell Growth Using the MTT Assay

In addition to the direct cell counting, growth was also monitored using the MTT assay. In this case metabolic activity, as determined by production of the purple formazan product, was used as a marker for cell numbers. In order to extrapolate cell numbers from that absorbance values obtained from the MTT assay a calibration curve was created (see **Figure 55**).

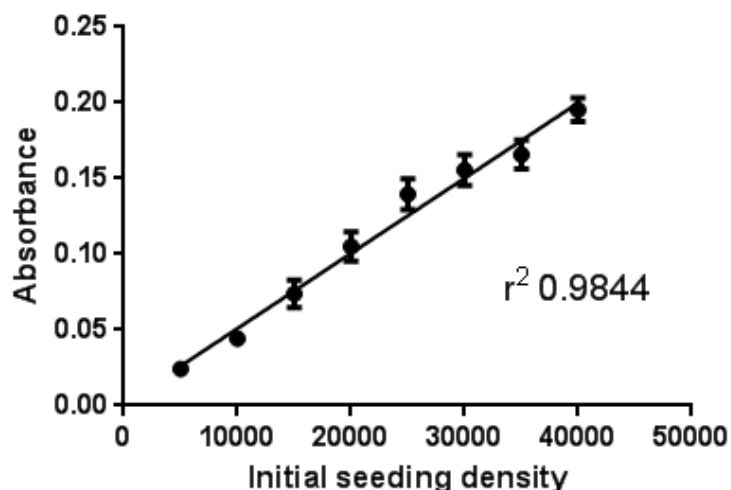


**Figure 55:** Standard curve using the MTT assay. Cells were seeded at the specified densities, allowed to attach for 24 hours and then analysed. The data points shown represent the mean  $\pm$  SD values from a single experiment where each sample was analysed 6 times.

Subsequently, experiments were run using DMSO as the negative control, 3001012 at 10 nM, 3001207 at 100 nM and 3001086 at 1  $\mu$ M. Each compound was dosed in replicates of 6, and the two sets of data combined for analysis. Absorbance data was converted to cell/well using the calibration curve above. Although some proliferation may have occurred during the 24 hours between seeding and analysis it was not thought that this would have significantly altered the curve, although no experimental evidence was obtained to support this supposition.

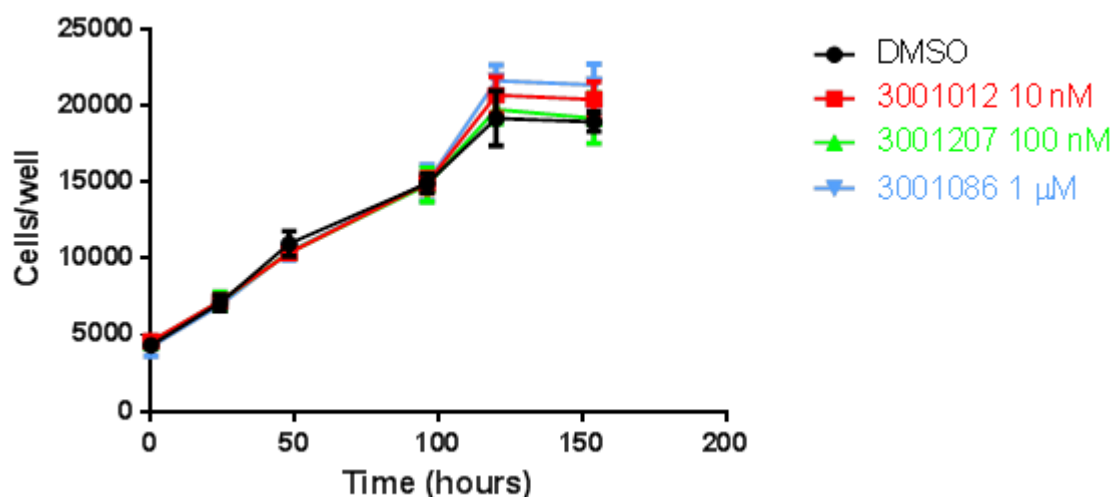


**Figure 56:** Growth curves for 3001012 at 10 nM, 3001207 at 100 nM and 3001086 at 1  $\mu$ M. Initial seeding density of 5,000 cells/well. The data points shown represent the mean  $\pm$  SD values from duplicate experiments where each sample was analysed 6 times.

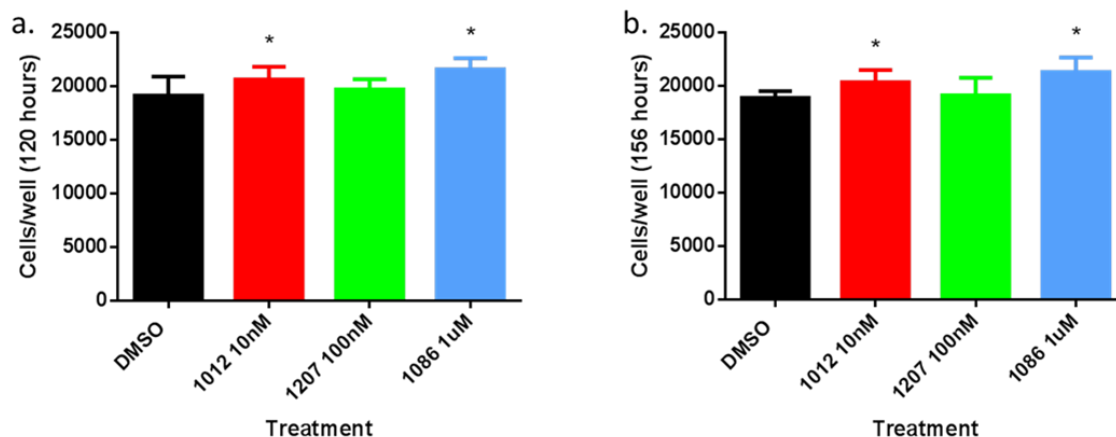


**Figure 57:** Cells per well after 120 hours (a) and 156 hours (b). T-tests show significant differences between DMSO and 3001012 at both 120 and 156 hours ( $p = 0.022$  and  $<0.001$  respectively) as well as between DMSO and 3001086 at both 120 and 156 hours ( $p = <0.001$  for both data sets). The data points shown represent the mean  $\pm$  SD values from duplicate experiments where each sample was analysed 6 times. No significant difference was found between DMSO and 3001207 at either time points.

It can be seen from the data in **Figure 56** and **Figure 57** that growth is consistent for all treatments up to 96 hours. At this point the growth curves diverge slightly, with cells treated with 3001012 and 3001086 showing significantly higher growth than the cells treated with DMSO and 3001207. After 120 hours, growth for all treatments reaches a plateau, suggesting that the cells have reached confluence. Comparison of cell numbers after treatment with 0.5 % DMSO to cell numbers after treatment with 3001012 or 3001086 showed statistically significant differences, although this was not observed after treatment with 3001207.

### 4.3.2. Discussion

The results obtained suggest that compounds 3001012 and 3001086 are increasing the growth rate of cells to a statistically significant degree. Data for 3001207 from the haemocytometer counts is contradicted by the data from the MTT screens and is therefore inconclusive. The reduced error in the MTT assays suggests that these data may be more reliable, and therefore that it is more likely that 3001207 is not affecting growth rate. It is quite clear, however, that the increases in growth rate, although statistically significant, are relatively small. The differences between the different treatments only become obvious after 96 hours of treatment.

It had been suggested that part of the anti-prion effect may come from increasing cell growth and therefore reducing levels of PrP<sup>Sc</sup> by a simple dilution effect. This was suggested in response to a study showing that cell division leads to a predictable reduction in PrP<sup>Sc</sup> levels to a steady state, although not to total clearance. <sup>(110)</sup> Similarly, 'cured' cells that had their growth arrested showed a reappearance of PrP<sup>Sc</sup> after a few days, <sup>(377)</sup> rather than the three months seen in other studies. <sup>(233)</sup> As noted previously, although the increase in growth was significant it was still relatively small, and nowhere near the increase in growth necessary to cause the aforementioned dilution effect. The importance of this dilution effect can also be questioned as a result of the information gleaned from the time course assays carried out previously (see section 4.2). The finding that different compounds take different amounts of time to clear PrP<sup>Sc</sup> from cells, without having a dramatic effect on cell growth, suggests that the dilution factor may not play a large role in this case. It is interesting to note that growth is very similar for all treatments up to the final time points, at which point differences between the treatments can be observed. This could suggest that treatment with the I3GA compounds ameliorates the decreased growth and initiation of apoptosis that occur as the cells reach confluence. It could therefore be hypothesised that they have a survival promoting effect.

## **4.4. Mode of Action Study: MTT Formazan Exocytosis Assay**

### **4.4.1. Introduction**

The MTT formazan exocytosis (MTT-FE) assay described here is based on an assay described by Hong *et al.* <sup>(348)</sup> The authors reported that extracellularly applied amyloid-beta (A $\beta$ ) oligomers caused the exocytosis of formazan formed during the standard MTT assay, which appeared as needle-like structures. This could be distinguished from the intracellular granules of formazan by using a different method of solubilisation - granules could be solubilised using 1 % tween, with the extracellular 'needles' remaining intact. The needles could then be solubilised using acidic isopropanol as per the standard MTT assay protocol. Hong *et al* used this assay to identify small molecule compounds which could affect the toxicity or structure of A $\beta$  oligomers by measuring, among other things, the effect of the compounds on MTT-FE. <sup>(348)</sup> A $\beta$  aggregates were shown to dose-dependently increase MTT-FE, while compounds such as congo red and curcumin inhibited

A $\beta$  induced MTT-FE and increased levels of tween-soluble MTT (TS-MTT). The authors reached the conclusion that if compounds are causing an increase in the level of TS-MTT then they may be working by causing the disaggregation of toxic A $\beta$  oligomers.

It was hypothesised that this assay could be deployed to investigate the mode of action of the I3GA compounds, by monitoring changes in TS-MTT levels over time when dosed with the I3GA compounds. If they were working *via* disaggregation of PrP<sup>Sc</sup> oligomers then, hypothetically, an increase in TS-MTT would be expected. As it was not possible to verify the assay by monitoring changes in MTT-FE after exposure to extracellularly applied PrP<sup>Sc</sup>, anti-prion compounds from the literature were also investigated. By comparing compounds with a known mode of action to our unknown I3GAs it was hoped that more information could be gleaned regarding the anti-prion mechanism of the I3GAs.

#### **4.4.2. Validation of Literature Compounds in the SMB Model**

Several compounds that were reported to have anti-prion activity were chosen from the literature to be used in the MTT-FE assay to provide a comparison with the I3GA compounds. Where possible compounds with a reported mode of action were chosen to facilitate comparison with the I3GAs, whose mode of action is unknown. In order to ensure that the compounds were used at the correct concentrations in the MTT-FE assay, anti-prion activity and EC<sub>50</sub> values were confirmed for the compounds in the SMB model. By validating the reported anti-prion activities of these compounds in the SMB model it was also hoped to provide confidence that results obtained for the I3GA compounds could be confidently compared to other small molecule compounds reported in the literature. Screening was carried out using the same protocol as was used for the screening of the I3GA compounds (see sections **2.1.1**, **2.2.1**, **2.2.2** and **2.2.4.4** for materials and methods).

##### **4.4.2.1. Results**

The selected compounds were screened in the SMB cell line assay using the same protocols as were used for the screening of the I3GA compounds (see **3.1**). Initial screens established whether the compounds were active, before screening at a range of concentrations to determine the EC<sub>50</sub> value. Although these compounds had all been reported as active anti-prion compounds in the literature this was often in different cell lines or against different prion

strains. The calculated EC<sub>50</sub> value for each compound in the SMB model, and how they compare to the reported literature values, can be seen in **Table 34**. Overall, good correlation was observed between the reported values and the values calculated in the SMB cells.

**Table 34:** Results of activity screening of anti-prion literature compounds, compared to their published activities. EGCG – Epigallocatechin gallate. See **Figure 58** for structures.

| Compound             | EC <sub>50</sub>    | LD <sub>50</sub> | Literature value   | Reference  | Structure |
|----------------------|---------------------|------------------|--|------------|-----------|
| Pentosan polysulfate | 0.175 ± 0.025 µg/ml | >25 µg/ml        | 0.16 µg/ml in ScN2a cells, 0.001 – 0.01 µg/ml in ScMNB cells | (214, 238) | a.        |
| Dextran sulfate      | 0.483 ± 0.275 µg/ml | >25 µg/ml        | 10-100 ng/ml in ScMNB cells                                  | (214)      | b.        |
| Heparin              | 5.3 ± 2.658 µg/ml   | >25 µg/ml        | 1 µg/ml in ScMNB cells                                       | (214)      | c.        |
| Amphotericin B       | 6.25 ± 0.768 µM     | > 20 µM          | 4.5 µg/ml (4.87 µM) in ScGTI-7 and Sc512 cells               | (242)      | d.        |
| EGCG                 | 7.5 ± 2.041 µM      | > 20 µM          | 50 µM in ScN2a cells   | (378)      | e.        |
| Chlorpromazine       | 2.83 ± 2.021 µM     | 20 µM            | 3 µM in SMB cells, 10 µM in ScN2a cells                      | (232, 238) | f.        |
| Congo red            | Inactive at 50 µM   | > 20 µM          | 1-100 µM in SMB cells  | (217)      | g.        |



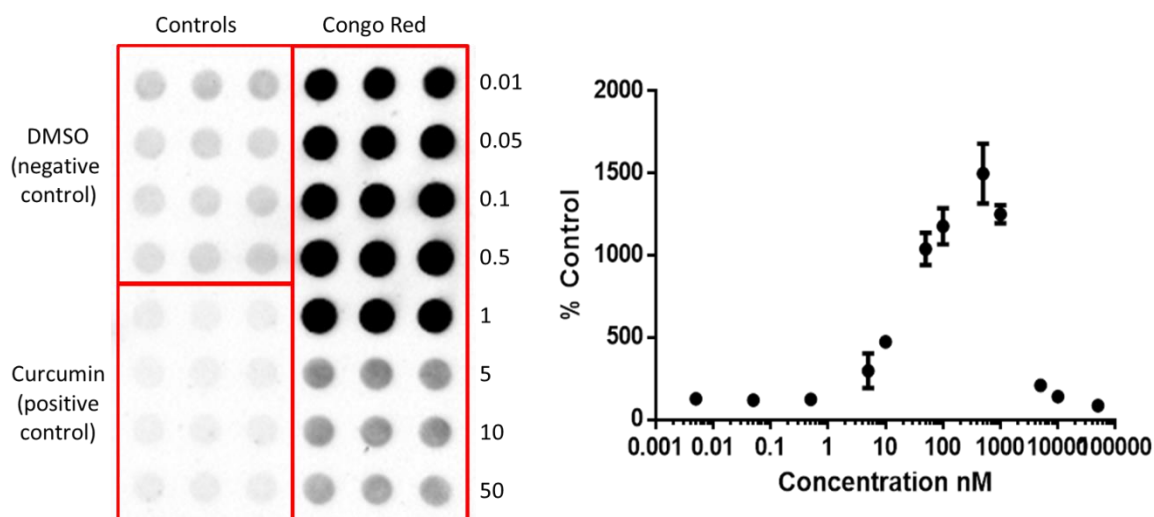


**Figure 59:** The effect of congo red on PrP<sup>Sc</sup> levels at a range of concentrations from 0.005 nM to 10  $\mu$ M. The blot on the left shows the increased PrP<sup>Sc</sup> levels at lower concentrations of congo red as indicated by the stronger signal. The three left hand columns are the control wells, demonstrating the normal signal for comparison. Concentrations on the blot range from 0.01  $\mu$ M at the top to 50  $\mu$ M at the bottom. The graph on the right demonstrates the effect on PrP<sup>Sc</sup> levels of a wide range of congo red concentrations, illustrating that congo red causes an increase in PrP<sup>Sc</sup> levels at concentrations as low as 5 nM. Exposure times were reduced for the blots of congo red treated cells to avoid saturation of the signal.

#### 4.4.2.2. Discussion

Overall it was felt that there was good correlation between reported values for the compounds investigated and those achieved in the SMB model. The main exception to this was congo red, which was not found to be active in the SMB cells. On the contrary, at certain concentrations it actually caused a 15-fold increase in PrP<sup>Sc</sup> levels (see **Figure 59**). This increase in PrP<sup>Sc</sup> with congo red at low concentrations (0.1  $\mu$ M) is something that has been observed and reported previously.<sup>(217)</sup> In this respect our data are in agreement with the literature. However, the same study reported that treatment with 1 $\mu$ M congo red resulted in 50 % PrP<sup>Sc</sup> clearance, and 100  $\mu$ M congo red gave near total PrP<sup>Sc</sup> clearance, and this was not observed. Furthermore the magnitude of the increase in PrP<sup>Sc</sup> levels (to approximately 1500 % control) is much greater in this study than has been reported in the literature (maximum increase of 250 %).

It has been suggested that the reason for the increase in PrP<sup>Sc</sup> levels at lower concentrations is because at concentrations below 5  $\mu$ M congo red exists as a monomer, while above 5  $\mu$ M it exists as a filamentous aggregate.<sup>(379)</sup> It has been suggested that the monomer may stimulate PrP<sup>Sc</sup> formation by binding to only one site on PrP<sup>C</sup>, while at higher concentrations it may form a supramolecular complex which could sequester PrP<sup>C</sup> and PrP<sup>Sc</sup> and prevent interactions and conversion.<sup>(380)</sup>

### 4.4.3. MTT-FE assay

As described in section 4.4.1 this assay uses changes in the ratio of the two different products of the MTT assay to determine whether protein aggregation is occurring. Increased protein aggregation is associated with increased MTT formazan exocytosis, which results in increased levels of the tween-insoluble formazan product (TI-MTT) at the expense of the intracellular, tween-soluble formazan product (TS-MTT). Decreased protein aggregation, or increased protein disaggregation, was hypothesised to result in an increase in TS-MTT at the expense of TI-MTT. As TS-MTT and TI-MTT are interlinked, the total amount of product formed (referred to henceforth as total MTT) would be equivalent to the amount in a conventional MTT assay. It was thought that this should stay relatively consistent, with changes represented by differences in the ratio of the two products. It was hypothesised that if compounds were working *via* some effect on protein aggregates then this would be expressed by changes in the ratio of TS-MTT to TI-MTT. Materials and methods are outlined in detail in sections 2.1.1 and 2.2.5.

#### 4.4.3.1. Results

All results are presented as the amount of TS-MTT as a percentage of the DMSO control. Total MTT was calculated from the addition of TS-MTT and TI-MTT – results were found to be similar to those obtained *via* conventional MTT assays (data not shown). Raw data was obtained as a print out from the plate reader and was transferred into an excel spreadsheet for analysis. Absorbances were converted to a percentage of the average of the blank wells (6 in total). An example of the raw data and the calculations performed can be seen in **Table 35**.

**Table 35:** An example of the raw data obtained after solubilisation of the formazan product in 1 % tween 20. Data is presented for 0.5 % DMSO and 5  $\mu$ M quinacrine and the assay was performed 24 hours after dosing. The measured absorbances are averaged, the blank value is subtracted and the final result is expressed as a percentage of the DMSO control.

| Treatment | Absorbance |       |       |       |       | Average | Blank sub | % DMSO   |
|-----------|------------|-------|-------|-------|-------|---------|-----------|----------|
| DMSO      | 0.063      | 0.058 | 0.06  | 0.063 | 0.065 | 0.0618  | 0.0571    |          |
| Quin 5uM  | 0.081      | 0.072 | 0.082 | 0.084 | 0.076 | 0.079   | 0.0743    | 120.2265 |

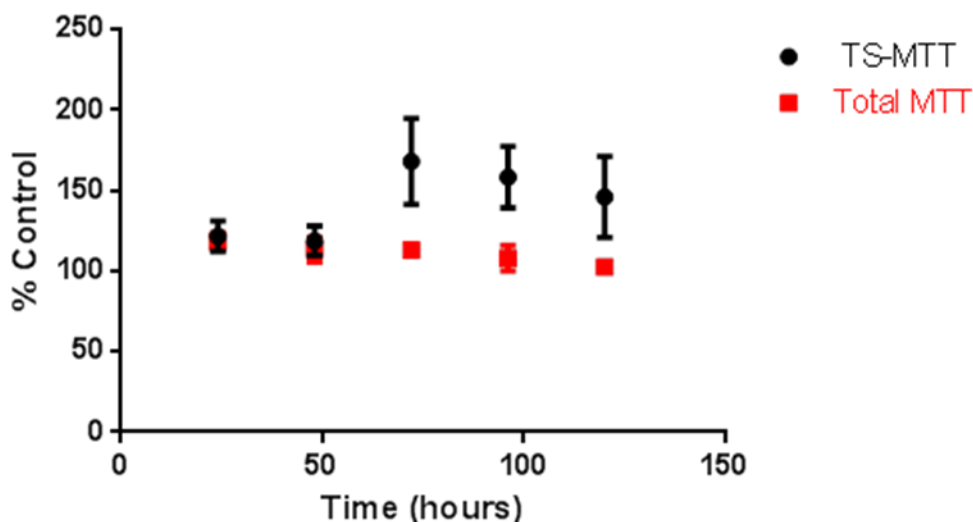


**Figure 60:** TS-MTT data for cells treated with 5  $\mu$ M quinacrine. Cells were treated for 5 days, with the assay being performed at 24 hour intervals. Cells were incubated with MTT-containing medium for one hour before solubilisation with 1% tween-20. The tween solution was removed and measured before solubilisation with acidic isopropanol. 6 wells were analysed for each data point.

The data for quinacrine at 5  $\mu$ M, as shown in **Figure 60**, demonstrates an increase in the proportion of TS-MTT that can be observed over time, without any significant change in the overall MTT levels.

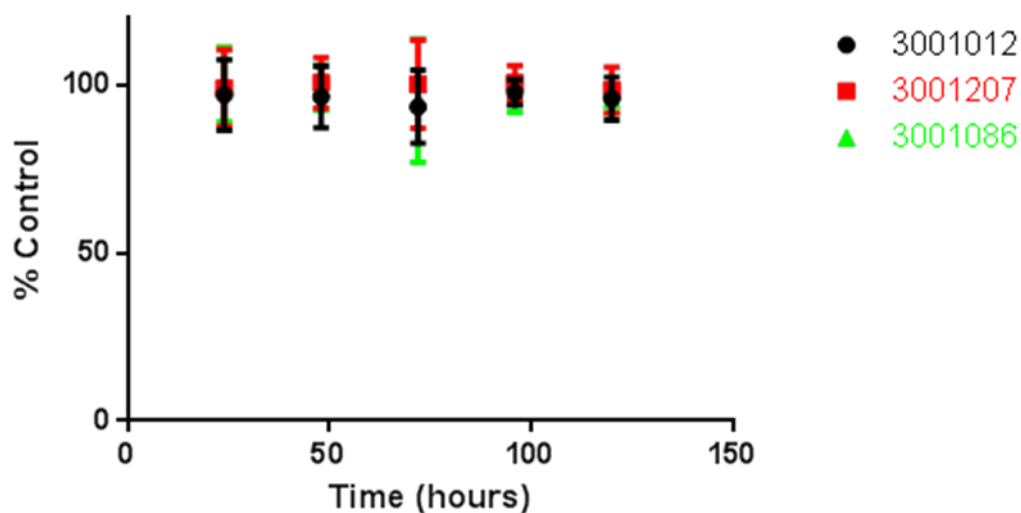


**Figure 61:** TS-MTT data for cells treated with 3001012 (10 nM), 3001207 (100 nM) and 3001086 (1  $\mu$ M). Cells were treated for 5 days, with the assay being performed at 24 hour intervals. Cells were incubated with MTT-containing medium for one hour before solubilisation with 1% tween-20. The tween solution was removed and measured before solubilisation with acidic isopropanol. 6 wells were analysed for each data point.

It can be seen in **Figure 60** that no significant difference in TS-MTT levels or total MTT levels (data not shown) was observed over the course of the assay as a result of treatment with any of the I3GA compounds.

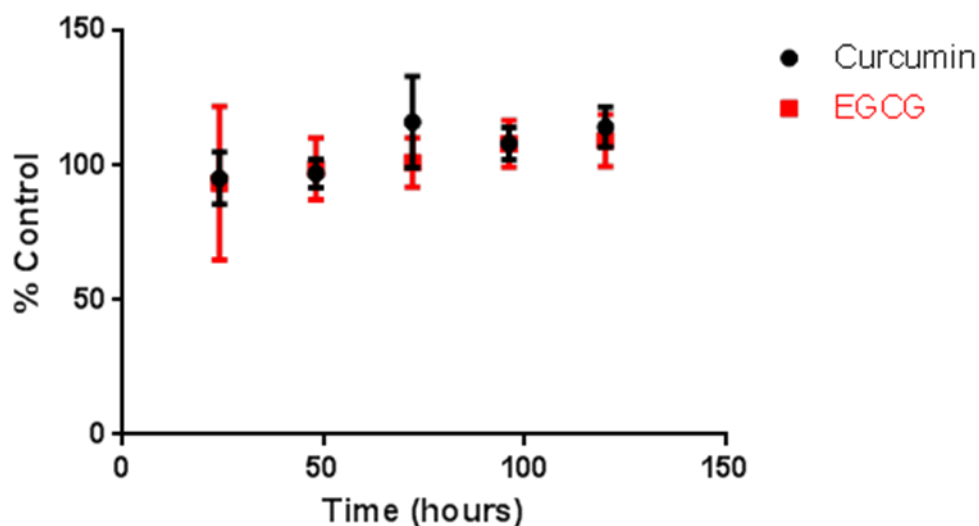


**Figure 62:** TS-MTT data for curcumin (10  $\mu$ M) and EGCG (10  $\mu$ M). Cells were treated for 5 days, with the assay being performed at 24 hour intervals. Cells were incubated with MTT-containing medium for one hour before solubilisation with 1% tween-20. The tween solution was removed and measured before solubilisation with acidic isopropanol. 6 wells were analysed for each data point.

The data in **Figure 62** shows no significant difference in TS-MTT levels or total MTT levels (data not shown) was observed over the course of the assay as a result of treatment with curcumin or EGCG.

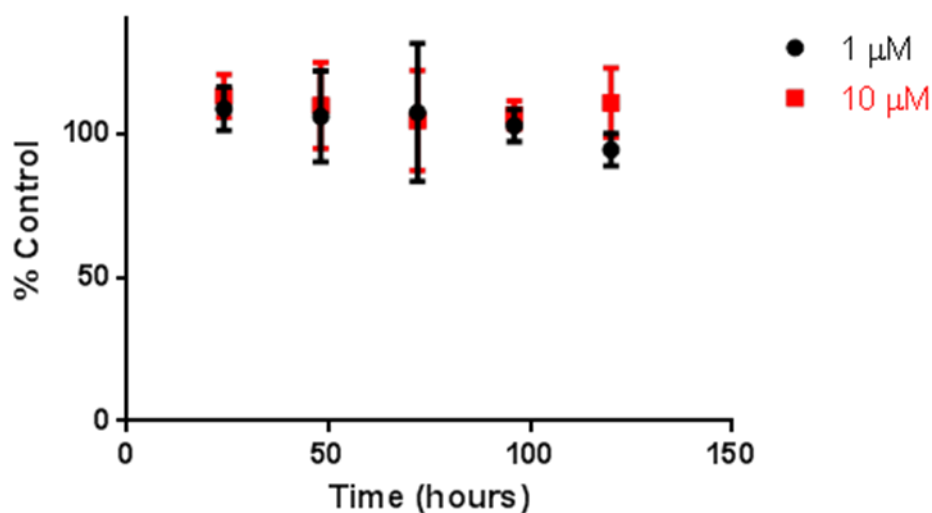


**Figure 63:** TS-MTT data for congo red at 1  $\mu\text{M}$  and 10  $\mu\text{M}$ . Cells were treated for 5 days, with the assay being performed at 24 hour intervals. Cells were incubated with MTT-containing medium for one hour before solubilisation with 1% tween-20. The tween solution was removed and measured before solubilisation with acidic isopropanol. 6 wells were analysed for each data point.

As can be seen in **Figure 63**, no significant difference in TS-MTT levels or total MTT levels (data not shown) was observed over the course of the assay as a result of treatment with either 1  $\mu\text{M}$  or 10  $\mu\text{M}$  congo red. It had been hypothesised that since the different concentrations of congo red showed markedly different effects on PrP<sup>Sc</sup> levels in the cells, that they may have different effects on levels of TS-MTT. This was not found to be the case.

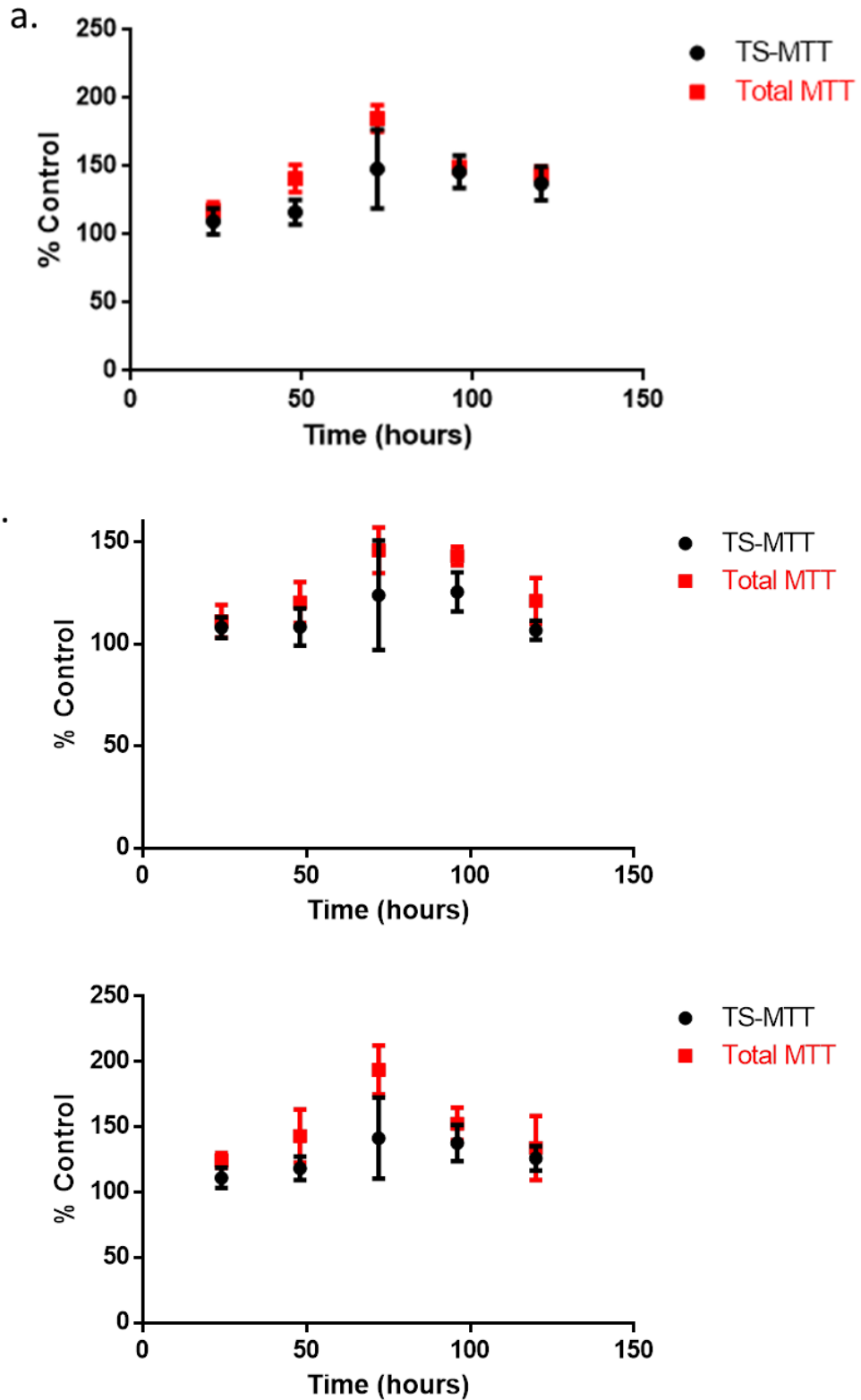


**Figure 64:** TS-MTT and total MTT data for PPS at 5 µg/ml (a), DS at 5 µg/ml (b) and heparin at 50 µg/ml (c). Cells were treated for 5 days, with the assay being performed at 24 hour intervals. Cells were incubated with MTT-containing medium for one hour before solubilisation with 1% tween-20. The tween solution was removed and measured before solubilisation with acidic isopropanol. 6 wells were analysed for each data point.

It can be seen from the data in **Figure 64** that a different pattern was observed after treatment with PPS, DS and heparin. Levels of TS-MTT were shown to rise over the course of the experiment, but levels of total MTT also rose, following a similar pattern. This suggests that these compounds are having an effect on increasing cell growth or metabolism, rather than promoting the production of TS-MTT at the expense of TI-MTT.

The cells were also observed under the microscope so that the 'granules' and 'needles' could be observed and photographed. Unfortunately the resolution and magnification of the microscopes were not sufficient to visualise the TI-MTT, although spots of granular MTT could be observed. A very distinct pattern was observed in the cells treated with quinacrine. It appeared that the granular MTT was localising at the edges of the cells, producing a distinctive 'leopard print' pattern (see **Figure 65**). This was not observed as a result of treatment with any of the other compounds (see **Figure 66**, **Figure 67**, **Figure 69** and **Figure 68**).

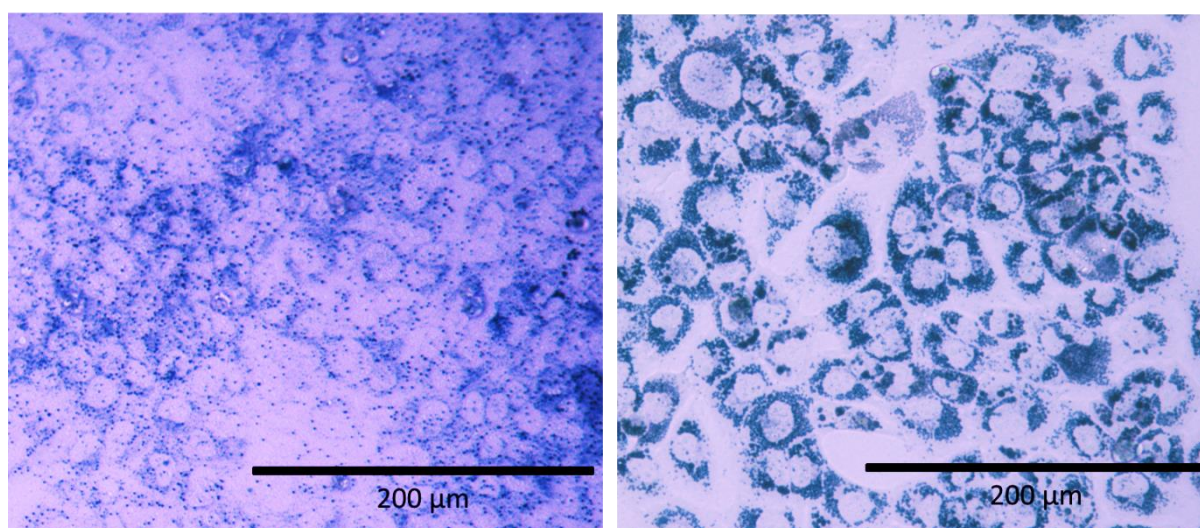


**Figure 65:** Cells treated for 120 hours with either DMSO (left) or quinacrine (right) and incubated for an hour with MTT. Dark spots indicate the presence of TS-MTT, with different patterns of distribution clearly visible.

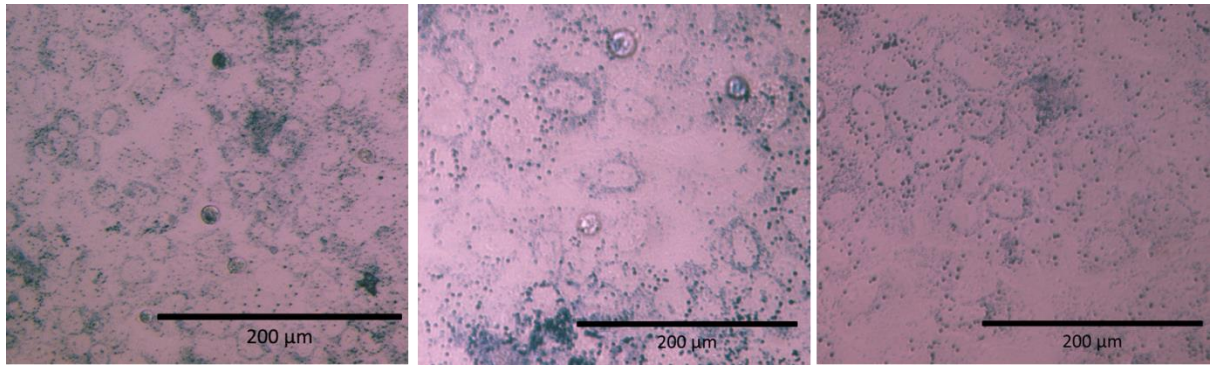


**Figure 66:** Images for cells treated with either 3001012 (left), 3001207 (middle) or 3001086 (right) for 120 days and incubated for an hour with MTT.

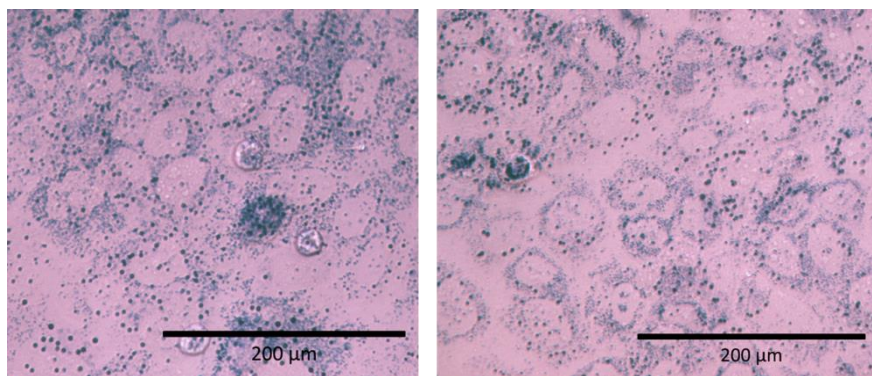


**Figure 67:** Images for cells treated with either curcumin (left) or EGCG (right) for 120 hours and incubated for an hour with MTT.

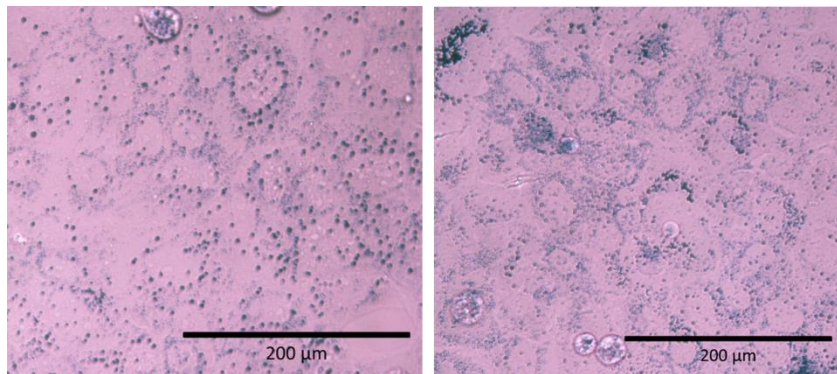


**Figure 68:** Images for cells treated with congo red at 1 μM (left) or 10 μM (right) for 120 hours and incubated for an hour with MTT.

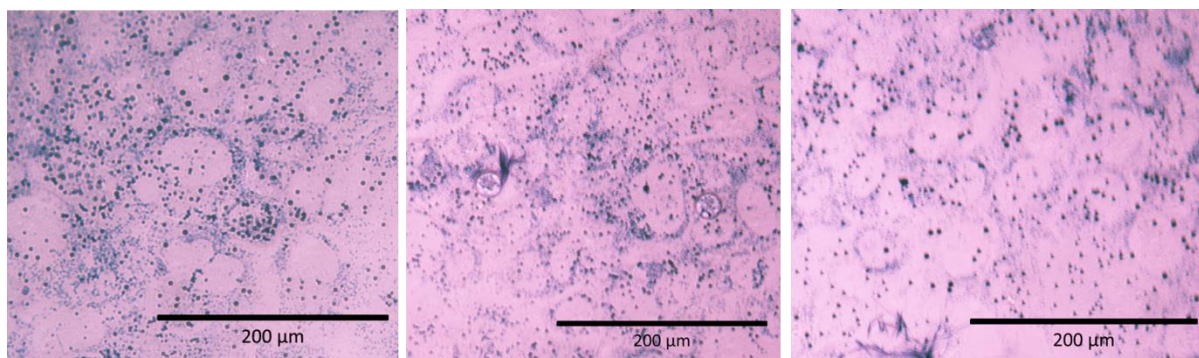


**Figure 69:** Images for cells treated with PPS (left), DS (middle) or heparin (right) for 120 hours and incubated for an hour with MTT.

#### 4.4.3.2. Discussion

A common problem with the treatment of prion diseases is the inability of the majority of anti-prion compounds to reverse the disease following the onset of the clinical symptoms. This is possibly due, at least in part, to the failure of most anti-prion compounds to disaggregate PrP<sup>Sc</sup> that has already formed, with it being more likely they are somehow preventing the conversion of PrP<sup>C</sup> to PrP<sup>Sc</sup>. The only compounds that have been shown to disaggregate PrP<sup>Sc</sup> are the complex polyamines,<sup>(228)</sup> and unfortunately none were available for this study.

Against this backdrop, on one hand it's unsurprising to find that the I3GA compounds, nor the majority of the literature compounds, had any effect on TS-MTT levels. The only compound to have any effect on TS-MTT levels, independent of total MTT levels, was quinacrine. The effect of quinacrine on TS-MTT levels suggests either some disaggregating effect of this compound that has not yet been explored, or another mechanism by which the proportion of TS-MTT may be affected. Quinacrine is known to bind to PrP<sup>C</sup> and is thought to work by interacting with PrP<sup>C</sup> and hampering the *de novo* formation of PrP<sup>Sc</sup>.<sup>(233)</sup> It has a  $K_D$  of 15 μM<sup>(221)</sup> and binding is thought to induce a conformational change that renders PrP<sup>C</sup> resistant to conversion and aggregation, as well as increasing the α-helical content.<sup>(223)</sup> The polyanionic compounds (PPS, DS and heparin) are thought to act by competitive inhibition of interactions between endogenous GAGs and PrPs<sup>(207)</sup> or by reducing the effective concentration of PrP<sup>C</sup>.<sup>(211, 212)</sup> It may be that quinacrine's role in rendering PrP<sup>C</sup> resistant to aggregation may produce a similar effect to that seen in the original paper, therefore suggesting that both the disaggregation of toxic oligomers, and changes in the aggregation propensity of existing protein, can produce changes in the products of the MTT assay.

Congo red was included in this experiment due to its unique ability, among these compounds, to increase levels of PrP<sup>Sc</sup>. It was hypothesised that if disaggregating compounds could cause an increase in the proportion of TS-MTT, then compounds known to increase levels of PrP<sup>Sc</sup> might have the opposite effect. To test this hypothesis congo red was tested at two concentrations – one at which it caused an increase in PrP<sup>Sc</sup>, and another at which it had no effect. As can be seen in **Figure 63** there was no effect of congo red on TS-MTT levels at either concentration, suggesting that although PrP<sup>Sc</sup> levels are increasing, they may not be forming aggregates. The inability of congo red to cure the cells in this model probably explains the lack of effect seen at the concentrations that do not result in increased levels of PrP<sup>Sc</sup>.

The results from PPS, DS and heparin suggest that although treatment increases the amount of TS-MTT this is due to a proportional increase in total cell number (as measured by total MTT) rather than production of TS-MTT at the expense of TI-MTT. MTT levels have been used previously in this chapter as a measure of cell growth (see section **4.3**), and the results presented here appear to suggest that PPS, DS and heparin may be accelerating cell growth. Studies into cell growth were carried out using the same initial seeding densities as these studies and found that cell numbers, as measured by MTT, plateaued at around 3 days after dosing, suggesting that at this point the cells had reached maximum confluence. The subsequent slight decrease was attributed to apoptosis due to limited space and resources. It is thought that this could explain the pattern seen in the results here.

The results for curcumin were in some ways surprising as this was a compound that was shown to cause the disaggregation of A $\beta$  oligomers in the original paper. <sup>(348)</sup> However, due to differences in the conditions used (persistently infected cells compared to cells challenged with oligomers) as well as different proteins (PrP<sup>Sc</sup> compared to A $\beta$ ) it is perhaps not surprising that it didn't cause changes in this case. Results from the time course assays (see **Figure 52**) suggest that quinacrine and curcumin may not share a mode of action, and this is further confirmed by the results from this assay. The time course assays also suggested a mode of action for the I3GA compounds that was distinct from quinacrine, with the clearance pattern being more reminiscent of curcumin than quinacrine. This assay provides further evidence that the I3GAs are working *via* a different method to quinacrine, although it doesn't shed any further light on what the mode of action might be.

Every attempt was made to ensure that this assay was as accurate and as reproducible as possible but examination of the data in **Table 35** reveals that the absolute differences in absorbance were quite small, even when a large difference was observed on conversion of the absorbance into a percentage. As discussed previously, a positive control, such as a complex polyamine, was not available for this assay and it is therefore not possible to say what absolute change in absorbance would be expected from a compound that was genuinely disaggregating PrP<sup>Sc</sup>. Some reassurance can be taken from the limited dynamic range of this assay, as the maximum signal obtained from one well of a confluent 96 well plate was found to be around 0.1 units. However, the lack of validation from a positive control calls into question both the significance of the changes observed during this assay and whether the assay was suitably optimised.

The experiments performed in this section were carried out on the basis that a disaggregating effect of the I3GAs would help clear the cells of infection. The original hypothesis was that the fragmentation of large aggregates would facilitate PrP<sup>Sc</sup> degradation through normal cellular pathways. Alternatively this hypothetical disaggregating effect can also be looked at in the context of the nucleation-dependent polymerisation model of prion conversion. Both this model and PMCA rely on the disaggregation of prion seeds and subsequent cycles of growth and fragmentation to explain the exponential increase in PrP<sup>Sc</sup> levels. In this context compounds that cause protein disaggregation may actually increase PrP<sup>Sc</sup> levels, rather than reducing them. This alternative perspective suggests that increased fragmentation would increase the number of seeds available and therefore facilitate conversion of PrP<sup>C</sup> to PrP<sup>Sc</sup>. It is therefore possible that compounds with a disaggregating effect could do more harm than good. The well documented ability of quinacrine to reduce PrP<sup>Sc</sup> levels suggests that this effect is not occurring in this case, supporting the hypothesis that quinacrine may prevent PrP aggregation rather than breaking up existing aggregates.

## 4.5. Discussion

From the data presented above it can be seen that further insights have been gained into the effect of the I3GA compounds but also into some of the well-established anti-prion compounds, particularly quinacrine.

The curative assay has shown that the I3GA compounds prevent the reappearance of 'normal' levels of PrP<sup>Sc</sup> for up to 57 days after just one dose at concentrations close to the calculated EC<sub>50</sub>. Quinacrine and curcumin also caused this long term reduction in PrP<sup>Sc</sup> levels. Other published data suggest that the lack of an increase in PrP<sup>Sc</sup> levels is not due to the cells being cured, rather that PrP<sup>Sc</sup> is still being produced but is rendered undetectable *via* dilution as the cells divide and multiply. If this is the case then that suggests the curative effect is not a direct, specific effect related to the compound itself, rather a more general effect caused by the multiplication of cells. However, this data does show that the effect of the I3GA compounds is not transitory i.e. they are not simply causing a temporary reduction in PrP<sup>Sc</sup>. This is obviously an extremely important property for the I3GAs to possess. The curative assays also provided evidence that full clearance of PrP<sup>Sc</sup> can be achieved by treatment with the I3GAs. Complete clearance was not observed after the standard 5 day dosing period but was observed to have occurred after 10 days as seen in the data for the curative assay, when the higher concentrations of compound were used. This therefore suggests that full clearance of PrP<sup>Sc</sup> from the cells can be achieved with a slightly longer dosing period than is currently used.

The time course assays that were carried out identified differences between the times taken for the I3GA compounds to be fully effective compared to quinacrine. At the highest concentrations of 5 to 10 times EC<sub>50</sub> quinacrine had reduced PrP<sup>Sc</sup> levels to their cured baseline within 24 hours, while the I3GA compounds (and curcumin) took up to 56 hours to exert their full effect. At lower concentrations (3 times EC<sub>50</sub>) the pattern seen for the I3GA compounds was similar with 56 hours of treatment required to reduce PrP<sup>Sc</sup> levels to the cured baseline. Quinacrine, however, took almost twice as long to reduce PrP<sup>Sc</sup> at lower concentrations. These data, taken as a whole, support the hypothesis that the I3GA compounds do not share a mode of action with quinacrine. This was suggested on the basis that quinacrine is known to bind to PrP<sup>C</sup>, while the I3GAs do not, at least not at concentrations that match their activity in the cell line assay. It would appear that quinacrine activity is, at least in part, controlled by concentration. This is further suggested by the data from quinacrine at the lowest concentration (0.5 µM) where an initial decrease in PrP<sup>Sc</sup> levels is reversed after around 48 hours, with PrP<sup>Sc</sup> levels returning to almost pre-treatment levels. It would appear that the amount of quinacrine is not sufficient to maintain the curative effect that is seen initially. This concentration dependent effect was not seen as a result of treatment with the I3GA compounds. It was hypothesised that the decrease seen after treatment with 1 µM quinacrine might simply be as a result of the cells dividing at a higher rate due to not being at confluence – this had been demonstrated in the literature. <sup>(110)</sup> It was

thought, however, that if this was the explanation for the initial decrease and subsequent increase of PrP<sup>Sc</sup> then this is something that should have been seen both in the I3GA compounds at low concentrations and in the DMSO controls. This was not something that was observed.

The time course data was also analysed with respect to the finding that residual PrP<sup>Sc</sup> remained after 5 days of dosing, but was totally eliminated after 10 days in the curative assay. The time course data showed that PrP<sup>Sc</sup> levels appeared to plateau after the initial decrease which occurred within 56 hours. There was no overwhelming evidence to suggest that levels were still decreasing in a consistent manner. A key difference between the 10 day point in the curative assay and the 5 day endpoint assays was that the cells were passaged during the curative assays. As cell division has been suggested to lead to a predictable reduction in PrP<sup>Sc</sup> (110) it is possible that the passaging of the cells, followed by an period of cell growth and division, was enough to dilute the already low levels of PrP<sup>Sc</sup> and render it undetectable. It is possible that cell division is responsible for a second phase of PrP<sup>Sc</sup> reduction, which proceeds at a much slower rate than the initial decrease seen up to 56 hours. There is no evidence from the growth curve analysis to suggest that cell growth occurs at a faster rate immediately after passaging, or that cell growth declines towards the end of the 5 day period, but that does not rule out the possibility that cell division has a role in eliminating the remaining PrP<sup>Sc</sup>. As mentioned before, the key to determining if PrP<sup>Sc</sup> is still present is determining whether the cells retain any infectivity at different time points.

Growth curve assays were carried out to further investigate the suggestion that PrP<sup>Sc</sup> levels are simply maintained at low levels as a result of cell division. It was hypothesised that if the compounds were affecting cell growth then reduction in PrP<sup>Sc</sup> levels may result from an enhancement of growth and subsequent increase of this dilution effect. Although statistically significant differences were seen in the growth rate of treated cells compared to untreated cells, these were relatively small. As a result it was not thought that this might be the mechanism by which any of the compounds were causing reductions in PrP<sup>Sc</sup> levels. The differences between the treatments were also more prevalent at the final time points, suggesting that the increased growth may be a result of some kind of protection against apoptosis.

Results from the MTT-FE assay again reinforce the idea that the mode of action of the I3GA compounds is distinct from that of quinacrine. Whilst quinacrine causes an increase in levels of TS-MTT this was not seen as a result of treatment with any of the other compound. The changes

in TS-MTT as a result of treatment with quinacrine are hypothesised to be a result of quinacrine affecting the aggregation propensity of PrP<sup>Sc</sup>, and therefore preventing the formation of aggregates rather than disaggregating those that already exist. This suggests a possible new application for this assay. The lack of effect of the I3GA compounds on TS-MTT levels is unsurprising for many reasons, from the general - very few compounds are able to reverse disease progression after the appearance of clinical signs - to the specific - the lack of interaction between PrP<sup>C</sup> and the I3GA compounds makes it unlikely that the compounds are working by interacting directly with PrP<sup>Sc</sup> aggregates.

Further insights into the pharmacodynamic and pharmacokinetic properties of the I3GAs were gained from experiments carried out by Chen *et al*, as well as by collaborators external to the University. The aim of these studies was to gain further insights into the potential of the compounds to work *in vivo*. Work carried out within the group investigated the toxicity of a selection of the I3GA compounds towards zebrafish larvae. Larvae at 48 hours post fertilisation (hpf) were dosed with the compounds at 5 µM, and the survival after 5 days recorded. Both 3001207 and 3001012 were found to have no effect on zebra fish survival, and acridine orange staining showed that the embryos were developmentally normal with a general absence of acute toxic effects. <sup>(279)</sup> The stability of the compounds in the presence of mouse liver microsomes was also tested. The extent of compound degradation by microsomes was used as a measure of the potential *in vivo* stability of the compounds, with limited degradation being desirable to prevent the compound being metabolised before reaching its target. Compounds were exposed to the microsomes for 30 minutes, before the amount of the compound that had not been metabolised was analysed using HPLC. Both 3001012 and 3001207 showed good stability in the presence of microsomes, suggesting an *in vitro* half-life of several hours. <sup>(279)</sup> These results were thought to be very promising in terms of the *in vivo* properties of the I3GA compounds.

Further pharmacokinetic investigations were carried out by Ronald Hawley at the University of California San Francisco (UCSF). In these experiments CD-1 mice were fed 3001012 in a liquid chocolate diet at a concentration of 50 mg/kg. 3001012 was found to reach a brain concentration of 16 nM suggesting favourable pharmacokinetic properties and the ability to cross the blood-brain barrier (BBB) (Personal correspondence from Ronald Hawley). This was thought to be a key finding as the ability of the compound to enter the brain is likely to be crucial for *in vivo* activity. In addition to the pharmacokinetic studies the anti-prion activity of

the compounds was assessed in the ScN2a cell line, a scrapie-infected neuroblastoma cell line. Proof of compound efficacy in these neuronal cells was suggested to provide further evidence of the compound's *in vivo* potential by demonstrating activity in both neuronal and non-neuronal cells. For all compounds tested there was found to be good correlation between activity in the SMB cells and activity in the ScN2a cells ( $P < 0.0001$ , Pearson  $r = 0.9731$ ). Activity was reduced in the ScN2a cells by around one order of magnitude, with  $EC_{50}$ s of  $0.014 \mu\text{M}$  and  $0.011 \mu\text{M}$  for 3001012 and 3001207 respectively. <sup>(279)</sup> Despite this, all the compounds tested retained good activity.

Overall, it can be seen that the data presented here have further confirmed the SPR data suggesting that the I3GA compounds are not interacting directly with  $\text{PrP}^{\text{C}}$  or  $\text{PrP}^{\text{Sc}}$ . Quinacrine is thought to act by preventing the formation of *de novo*  $\text{PrP}^{\text{Sc}}$  by binding to  $\text{PrP}^{\text{C}}$  and rendering it resistant to aggregation and conversion, and from the data presented here it would seem unlikely that this is how the I3GA compounds are working. Unfortunately the data so far has not shed any further light on what the mode of action is; only what it is not. However, the additional data that have been obtained are promising – lack of *in vivo* toxicity, good microsomal stability, good *in vivo* pharmacokinetics and activity in different cell lines – and all suggest that these compounds have potential as compounds that may be active *in vivo*.

# 5. Mode of Action Studies: Microarray and Proteomics Studies

## 5.1. Introduction

Systems biology is an emerging approach to studying complex biological systems. It is based on the holistic idea that by looking at a system in its entirety, individual processes can be understood in the wider context of the system they exist in. Rather than focussing on individual genes or proteins, a systems biology approach looks at the properties of cells, tissues and organisms and their role in a relevant system's structure and dynamics.<sup>(381)</sup>

Proteomics and microarray studies are examples of a 'top down' approach to systems biology, where large amounts of information are obtained on the protein and gene expression of the system of interest. This approach has been used by Leroy Hood *et al* to investigate changes in the protein and gene expression of mice infected with different strains of scrapie, with data from an infected system being compared to data from an uninfected system to try and identify pathways that might be altered.<sup>(382)</sup> However, this approach has never been used to identify the molecular targets of anti-prion compounds. By carrying out these studies on cells that had been treated with the lead compounds it was hoped to reveal their mode of action, as well as demonstrating the validity of this approach in deconvoluting the targets of small, drug-like molecules. There was also interest in whether there would be any crossover between the results from the proteomics and the microarray, thereby validating their use as complimentary techniques.

It was initially hoped that data could be generated from the cell lines that would be directly comparable to the data from the Leroy Hood paper, however, this was not possible due to the fact that the Leroy Hood paper used a whole animal model rather than a cell line and was comparing treated animals to untreated animals. There was no uninfected cell line available to use as a control so instead untreated, infected cells were used as a baseline against which to measure changes.

At the start of the study it was hoped that the results would help answer several questions:

1. Can proteomics and microarray studies be used to identify the targets of small, drug like molecules?
2. Are the techniques complementary to each other?
3. What are the molecular targets of the I3GA anti-prion compounds?
4. Are all the I3GA compounds working in the same way?

It was anticipated that the results from the quinacrine-treated sample could be used as a proof of concept by comparing the results from the study with known targets of quinacrine from the literature, as well as providing data for a compound thought to have a different mode of action to the I3GAs. Chapter 4 provided further information about the mode of action of 3001012 and 3001207, without enabling any definitive conclusions to be drawn. The results from the microarray and proteomics studies would be examined to try and identify the pathways that were affected as a result of treatment. 3001012, as the lead compound, was the obvious candidate for this study. 3001207 was chosen as it was the lead compound from the group with substitutions at the 6-position, with an  $EC_{50}$  very close to that of 3001012. Comparison of results using the two different techniques could be carried out to identify crossover between the two, and similarly comparison of results from the two different I3GAs could be carried out to see if they had targets in common.

Proteomics and microarray studies were carried out by Paul Heath in the Sheffield Institute for Translational Neuroscience (SITraN) (microarray) and Caroline Evans in the Department of Chemical and Biological Engineering (proteomics). As the primary researcher, I was responsible for designing the experiments, choosing the compounds to be studied, preparing the cell pellets for analysis and the subsequent analysis and interpretation of the data once it had been processed through MetaCore.

Materials and methods for this study are outlined in detail in sections **2.1.3** and **2.2.6**.

## 5.2. Results

### 5.2.1. Sample Validation

Bradford assays and dot blot analyses were carried out on the samples prepared for the microarray and proteomics studies to check protein levels and ensure treatment had been successful.

**Table 36:** Total amount of protein per sample as determined by Bradford assay. Each sample represents cells from one tissue culture petri dish suspended in 5 ml medium. 1 ml of this was taken for the microarray sample and 3.5 ml was taken for the proteomics sample. The final 0.5 ml was retained for analysis, and was used for the Bradford assay and dot blot analysis. More protein was required for the proteomics so a larger sample was used.

| Treatment                      | Microarray sample ( $\mu\text{g}$ ) | Proteomics sample ( $\mu\text{g}$ ) |
|--------------------------------|-------------------------------------|-------------------------------------|
| DMSO A                         | 269.920                             | 944.71                              |
| DMSO B                         | 284.362                             | 995.267                             |
| Quinacrine 1.5 $\mu\text{M}$ A | 217.926                             | 762.742                             |
| Quinacrine 1.5 $\mu\text{M}$ B | 200.595                             | 702.083                             |
| 3001012 4.5 nM A               | 290.139                             | 1015.486                            |
| 3001012 4.5 nM B               | 269.919                             | 944.718                             |
| 3001207 6 nM A                 | 295.916                             | 1035.706                            |
| 3001207 6 nM B                 | 206.372                             | 722.303                             |

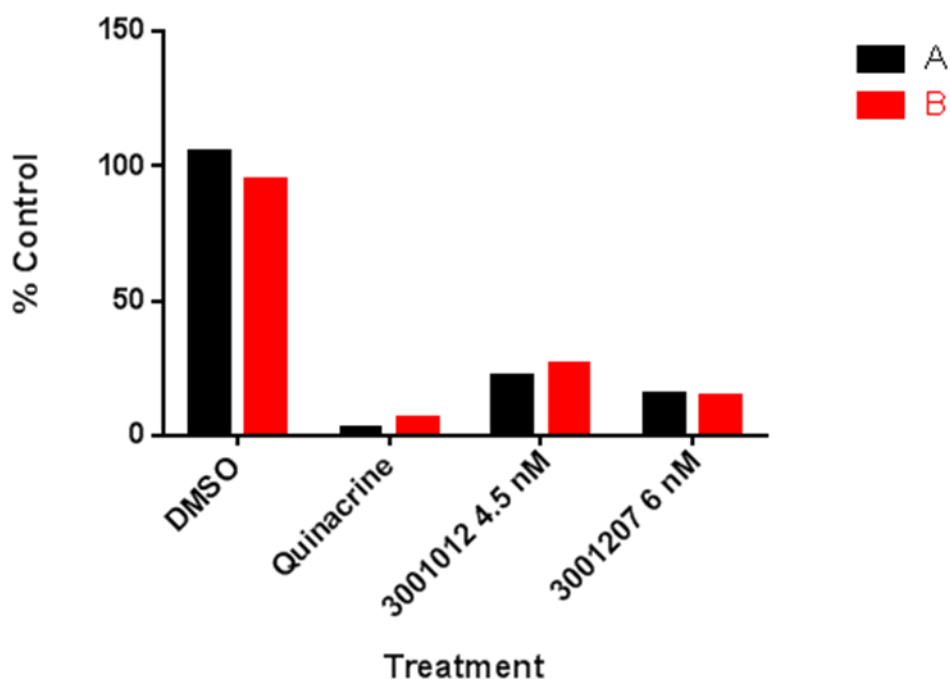


**Figure 70:** PrP<sup>Sc</sup> levels in the samples used in the microarray and proteomics studies. Cells were treated for 56 hours before being harvested, and dot blots performed on a sample from each plate. A and B indicate the two biological replicates

### 5.2.1.1. DEGs and Up and Down Regulated Proteins

**Table 37:** Total number of DEGs found

| Comparison                | Quinacrine vs DMSO | 1012 vs DMSO | 1207 vs DMSO | 1012 vs 1207 | 1012 vs quinacrine | 120 vs quinacrine |
|---------------------------|--------------------|--------------|--------------|--------------|--------------------|-------------------|
| DEGs with an AFC $\geq 1$ | 3519               | 4406         | 4802         | 3053         | 3757               | 5078              |

The lists of genes were separated into groups depending on whether they were up or down regulated and then filtered using absolute fold cut off values of  $\geq 1.5$ ,  $\geq 2$ , or  $\geq 2.5$ .

**Table 38:** Number of DEGs grouped by up and down regulation at different cut off values.

| Absolute fold change | Quinacrine vs DMSO |      | 1012 vs DMSO |      | 1207 vs DMSO |      |
|----------------------|--------------------|------|--------------|------|--------------|------|
|                      | Up                 | Down | Up           | Down | Up           | Down |
| ≥ 1.5                | 11                 | 7    | 241          | 27   | 20           | 7    |
| ≥ 2                  | -                  | -    | 59           | 1    | 1            | -    |
| ≥ 2.5                | -                  | -    | 5            | -    | -            | -    |

On the basis of this information it was decided to use an absolute fold cut off of  $\geq 1.5$  for the microarray data due to the very small number of genes with an absolute fold change of  $\geq 2$  or above.

**Table 39:** Up and down regulated proteins from the proteomic studies. The identity of the different proteins can be seen in **Table 40**.

| Quinacrine vs DMSO |      | 1012 vs DMSO |      | 1207 vs DMSO |      |
|--------------------|------|--------------|------|--------------|------|
| Up                 | Down | Up           | Down | Up           | Down |
| 2                  | 7    | 9            | 9    | 10           | 8    |

**Table 40:** Proteins identified as up or down regulated in the proteomics studies after treatment with quinacrine, 3001012 or 3001207 and compared to the DMSO control.

|                    | Up   | Down   |
|--------------------|--|--|
| Quinacrine vs DMSO | Histone H2B<br>RNA-binding, signal transduction-associated protein 1<br>MCG68069<br>Histone H1.2 [CHAIN 0]<br>Putative uncharacterized protein<br>Pre-mRNA-processing factor 19 [ISOFORM 3]<br>Vimentin [CHAIN 0]  | Fatty acid synthase<br>6-phosphogluconate dehydrogenase  |
| 3001012 vs DMSO    | Putative uncharacterized protein<br>ATP synthase subunit alpha<br>40S ribosomal protein S16 [CHAIN 0]<br>ADP/ATP translocase 2 (ANT 2) [CHAIN 0]<br>ADP/ATP translocase 1 (ANT 1) [CHAIN 0]<br>60S ribosomal protein L10 [CHAIN 0]<br>Cad protein<br>60S ribosomal protein L27 [CHAIN 0]<br>Putative uncharacterized protein | Hsp90 co-chaperone Cdc37<br>Shugoshin-like 2 (Sgo2)<br>Adenosine kinase (AK) [ISOFORM Short]<br>60S ribosomal protein L36<br>Filamin, alpha<br>60S ribosomal protein L29 [CHAIN 0]<br>AHNAK nucleoprotein<br>Protein disulfide-isomerase (PDI)<br>Triosephosphate isomerase (TIM) [CHAIN 0]            |
| 3001207 vs DMSO    | Heat shock protein HSP 90-beta (HSP 84)<br>Histone H2B<br>ATP synthase subunit alpha<br>40S ribosomal protein S16 [CHAIN 0]<br>ADP/ATP translocase 2 (ANT 2) [CHAIN 0]<br>Putative uncharacterized protein<br>60S ribosomal protein L27 [CHAIN 0]<br>Uncharacterized protein   | Shugoshin-like 2 (Sgo2)<br>Uncharacterized protein<br>60S ribosomal protein L17 [CHAIN 0]<br>Heterogeneous nuclear ribonucleoprotein A/B,<br>Transaldolase<br>Uncharacterized protein<br>Protein disulfide-isomerase<br>Filamin, alpha<br>AHNAK nucleoprotein<br>B-cell receptor-associated protein 31 |

## 5.2.2. MetaCore Pathway Analysis

The data generated from the network analysis in MetaCore is presented below. The two most statistically significant pathway maps are presented for each treatment, along with a summary of the key proteins or genes from the microarray and proteomics studies around which the pathways have been generated. These key elements of the pathways are also marked in the maps with a blue or red thermometers; a blue thermometer indicates down regulation while a red thermometer indicates up regulation. The height of the thermometer indicates the extent of the up or down regulation. While no statement is made about whether the identified pathways were up or down regulated, this is inferred by the up or down regulation of the component targets from the microarray and proteomics studies. The role of the up and down regulated components can be used to determine what the effect on the pathway as a whole is likely to be, and this is discussed in section 5.3.

### 5.2.2.1. Quinacrine Compared to Untreated Control

The MetaCore analysis of both microarray and proteomics data combined resulted in two statistically significant pathway maps; granzyme A signalling (**Figure 71**) and pathways for the stimulation of fat cell differentiation by Bisphenol A (**Figure 72**).

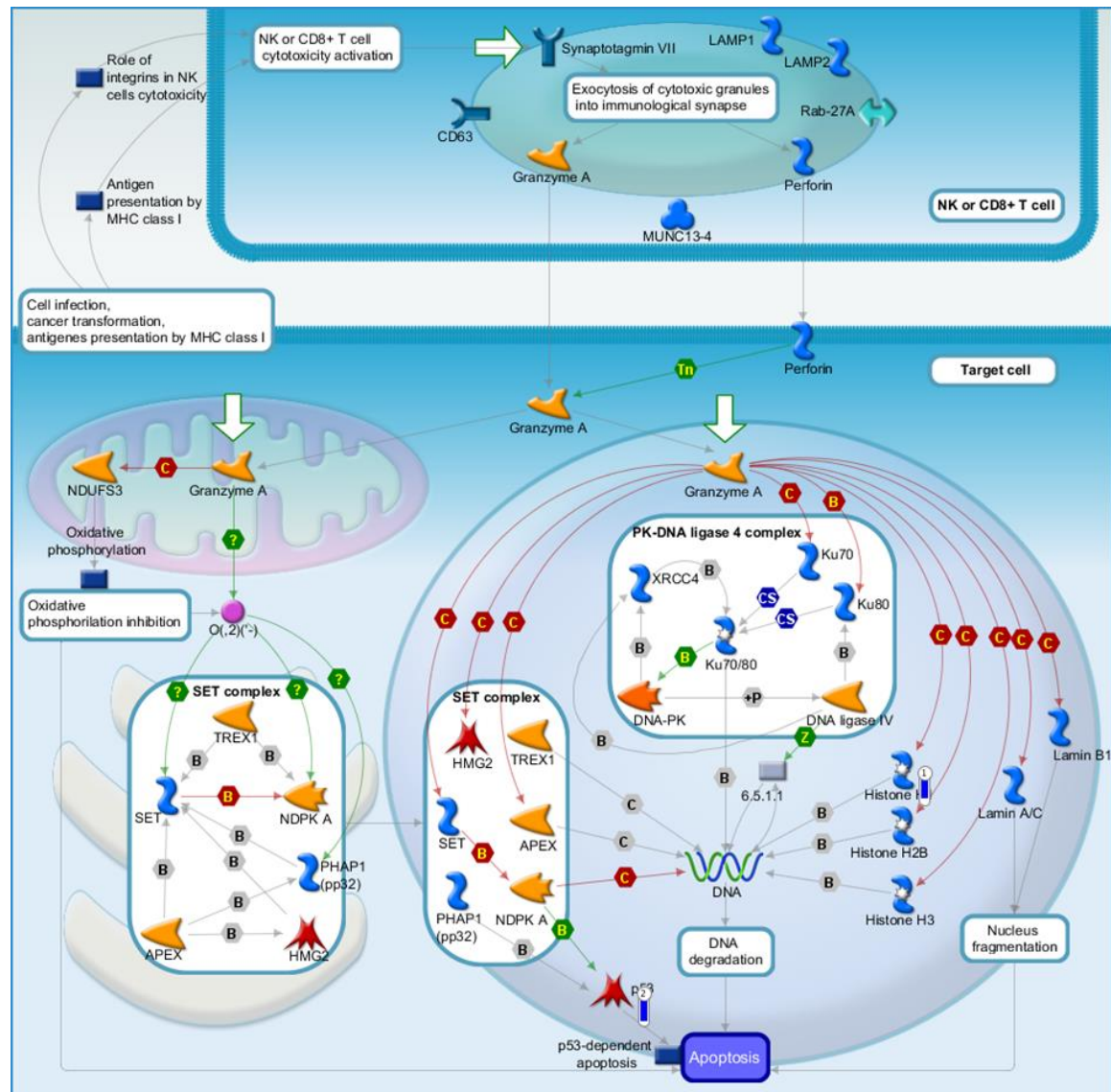


**Figure 71:** Map of the statistically significant pathway representing apoptosis and survival – granzyme A signalling. This was the top scored map. Experimental data are represented by thermometers. Up-ward (red) thermometers indicate up-regulated signals and down-ward (blue) thermometers indicate down-regulated signals.

Down regulated: Histone H2A and p53

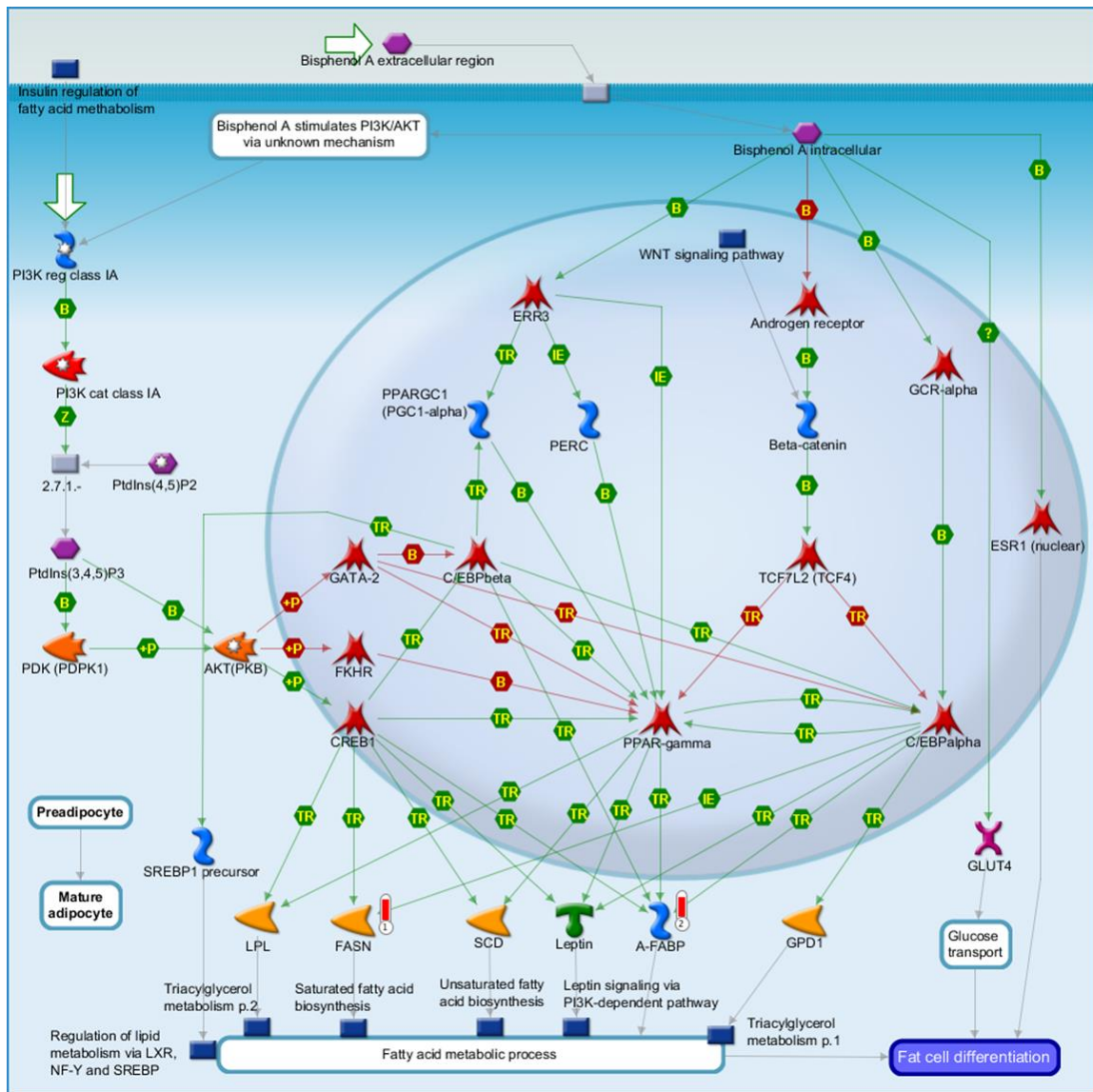


**Figure 72:** Map of the statistically significant pathway representing putative pathways for stimulation of fat cell differentiation by Bisphenol A. This was the second top scored map. Experimental data are represented by thermometers. Up-ward (red) thermometers indicate up-regulated signals and down-ward (blue) thermometers indicate down-regulated signals.

Up regulated: A-FABP and FASN

These two pathways were the only ones identified from analysis of the combined data sets. The data sets were also analysed separately and each analysis produced the top 5 statistically significant pathways for that data set. The pathways identified from the microarray data were as follows (in order of statistical significance, most significant first):

- DNA damage – ATM/ATR regulation of G1/S checkpoint
- Cholesterol biosynthesis

- DNA damage – DNA damage induced responses
- DNA damage – Role of NFBFD1 in DNA damage response
- Apoptosis and survival – DNA damage induced apoptosis.

Pathways identified from the proteomics data were as follows (in order of statistical significance, most significant first):

- Regulation of lipid metabolism – Regulation of fatty acid synthase activity in hepatocytes.
- Cell cycle – Chromosome condensation in prometaphase
- Cell cycle – Sister chromatid cohesion
- Cell cycle – Initiation of mitosis
- Cytoskeleton remodelling – neurofilaments.

The DEGs from the DMSO vs quinacrine data set were also compared with the data from the Hood paper.<sup>(382)</sup> There was crossover in the case of three genes; histone H2B, histone H1.2 and vimentin.

#### **5.2.2.2. 3001012 Compared to Untreated Control**

Microarray and proteomics data were combined and analysed using MetaCore. The top two statistically significant pathway maps were related to hedgehog signalling (see **Figure 73**) and the regulation of apoptosis by mitochondrial proteins (see **Figure 74**). These pathways were also identified by MetaCore analysis of the proteomics and microarray data sets individually.

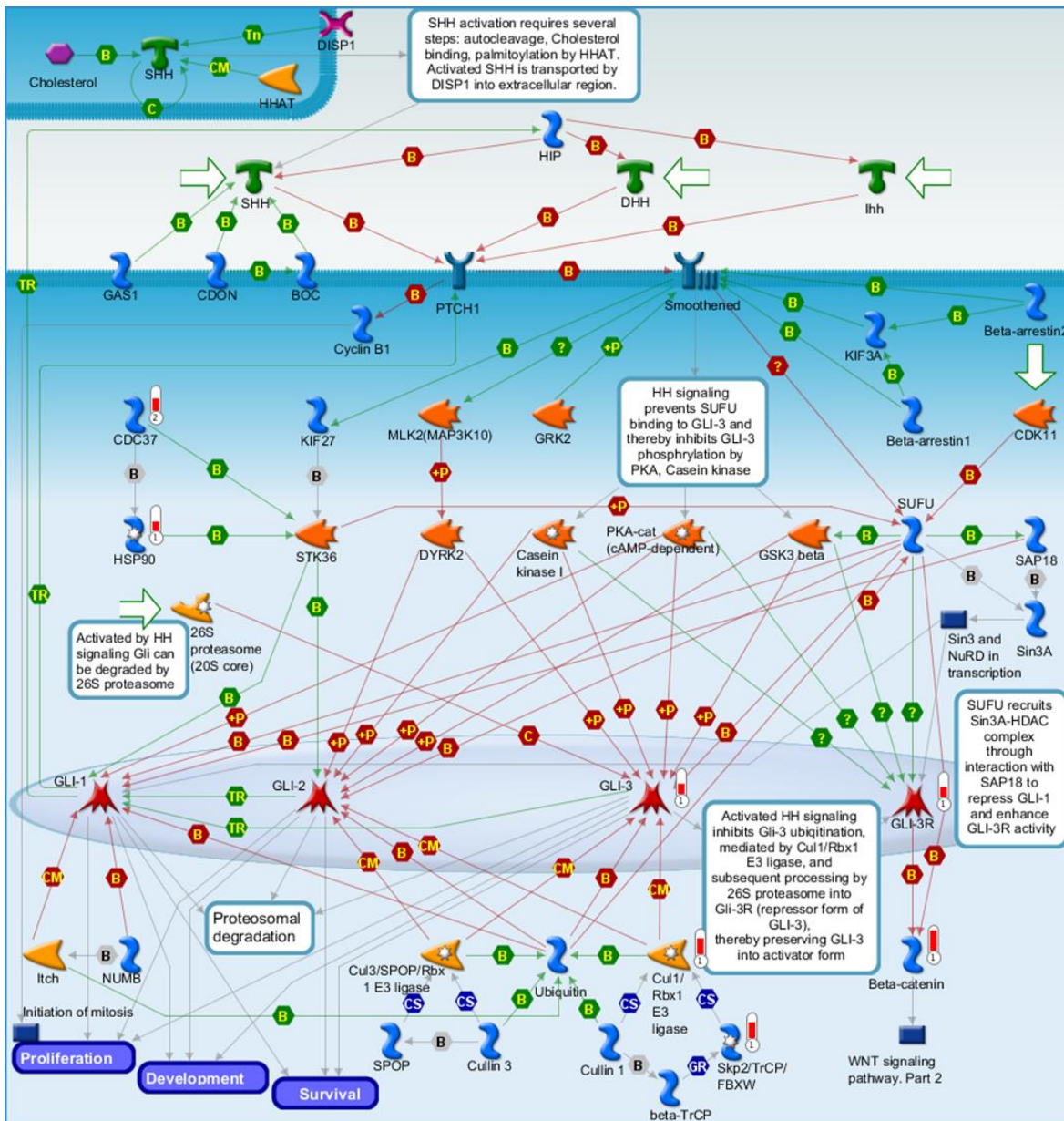


**Figure 73:** Map of the statistically significant pathway representing hedgehog signalling. This was the top scored map. Experimental data are represented by thermometers. Up-ward (red) thermometers indicate up-regulated signals and down-ward (blue) thermometers indicate down-regulated signals.

Up regulated: CDC37, HSP90, GLI-3, GLI-3R, beta-catenin, Skp2/TrCP/FBXW and Cul1/Rbx1 E3 ligase

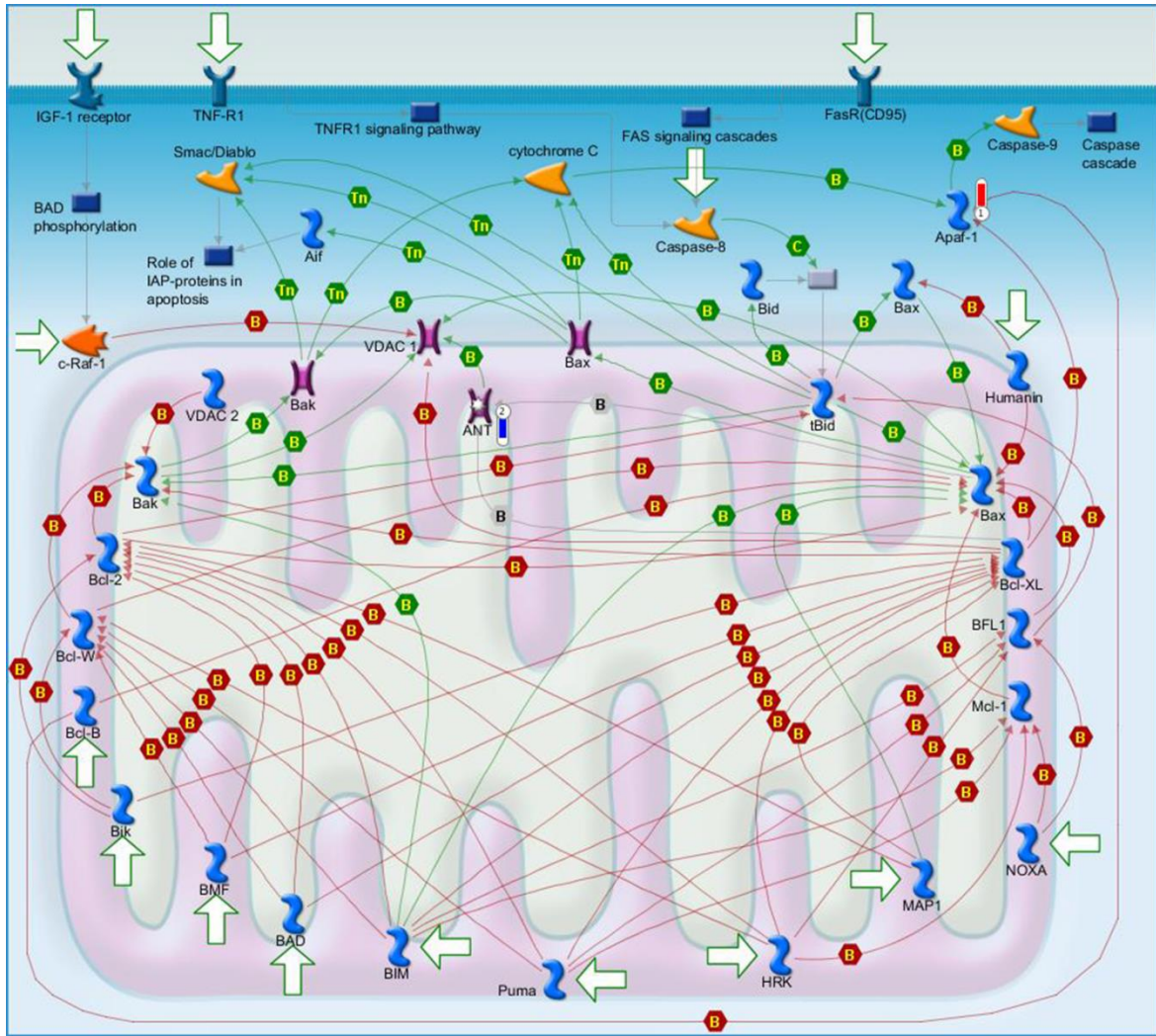


**Figure 74:** Map of the statistically significant pathway representing the regulation of apoptosis by mitochondrial proteins. This was the second top scored map. Experimental data are represented by thermometers. Up-ward (red) thermometers indicate up-regulated signals and down-ward (blue) thermometers indicate down-regulated signals.

Up regulated: Apaf-1

Down regulated: ANT

The pathways shown above represent the two most statistically significant pathways. The MetaCore analysis ranks the top five statistically significant pathways (where these can be identified) and the other pathways identified from the combined data set as a result of treatment with 3001012 were (in order of statistical significance, most significant first):

- G-protein signalling – RhoA regulation pathway.
- Cell adhesion – Ephrin signalling
- Neurophysiological processes – Receptor-mediated axon growth repulsion.

The microarray and proteomics data sets were also analysed individually to identify pathways affected by treatment with 3001012. As would be expected, the separate analyses identified some of the pathways that were identified by the combined analysis. Analysis of the microarray data identified the hedgehog signalling pathway, while analysis of the proteomics data identified both the regulation of apoptosis by mitochondrial proteins and the RhoA signalling pathway. Pathways identified from the microarray data also include (in order of statistical significance, most significant first):

- Regulation of cystic fibrosis transmembrane conductance regulator (CFTR) activity
- Development – growth hormone signalling *via* P13K/AKT and MAPK cascades
- G-protein signalling – Ras family GTP-ases in kinase cascades
- Development – A2B receptor: action *via* G-protein alpha s

Pathways identified from the proteomics data also include:

- Glycolysis and gluconeogenesis

Only three pathways, including those mentioned above, were identified from the proteomics data, with glycolysis and gluconeogenesis having the greatest statistical significance.

### **5.2.2.3. 3001207 Compared to Untreated Control**

No pathways were matched to the combined data from the microarray and proteomics studies for 3001207. The number of DEGs with a fold change of  $\geq 1.5$  identified from treatment with 3001207 was much smaller compared to the number identified from treatment with 3001012 (27 compared to 268, see **Table 38**) which may explain why no pathways were identified for the combined data set. Analysis of the separated data sets identified 5 pathways for each of the data sets, and the top ranked pathways for each set of data are shown below. Pathways identified from the microarray data feature either histone H3 or p73 (both of which were up regulated), while the pathways identified from the proteomics data feature ANT, HSP90 and HSP90 beta.

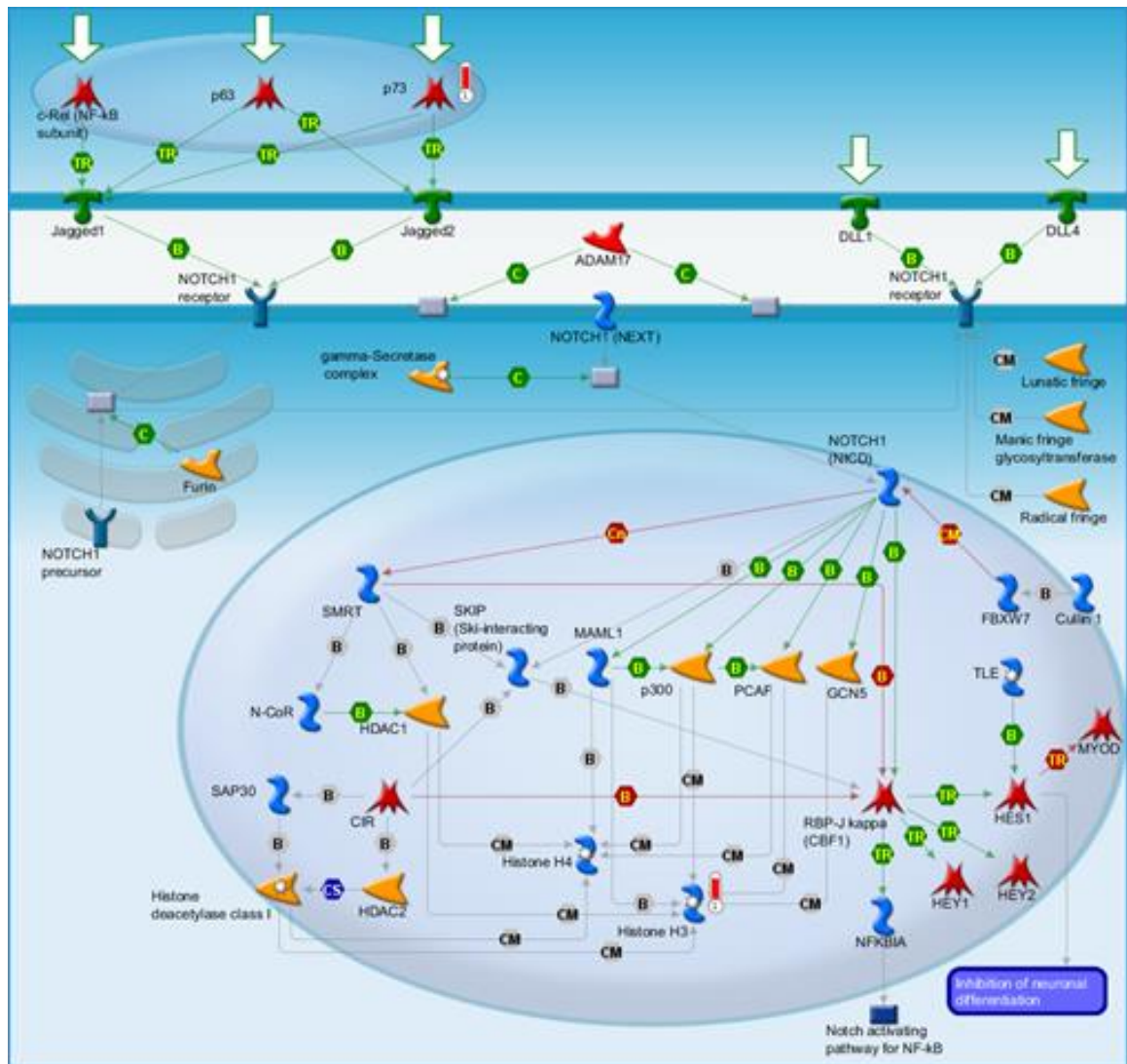


**Figure 75:** Map of the statistically significant pathway representing the notch signalling pathway. This was the top scored map from the microarray data. Experimental data are represented by thermometers. Up-ward (red) thermometers indicate up-regulated signals and down-ward (blue) thermometers indicate down-regulated signals.

Up regulated: P73 and Histone H3

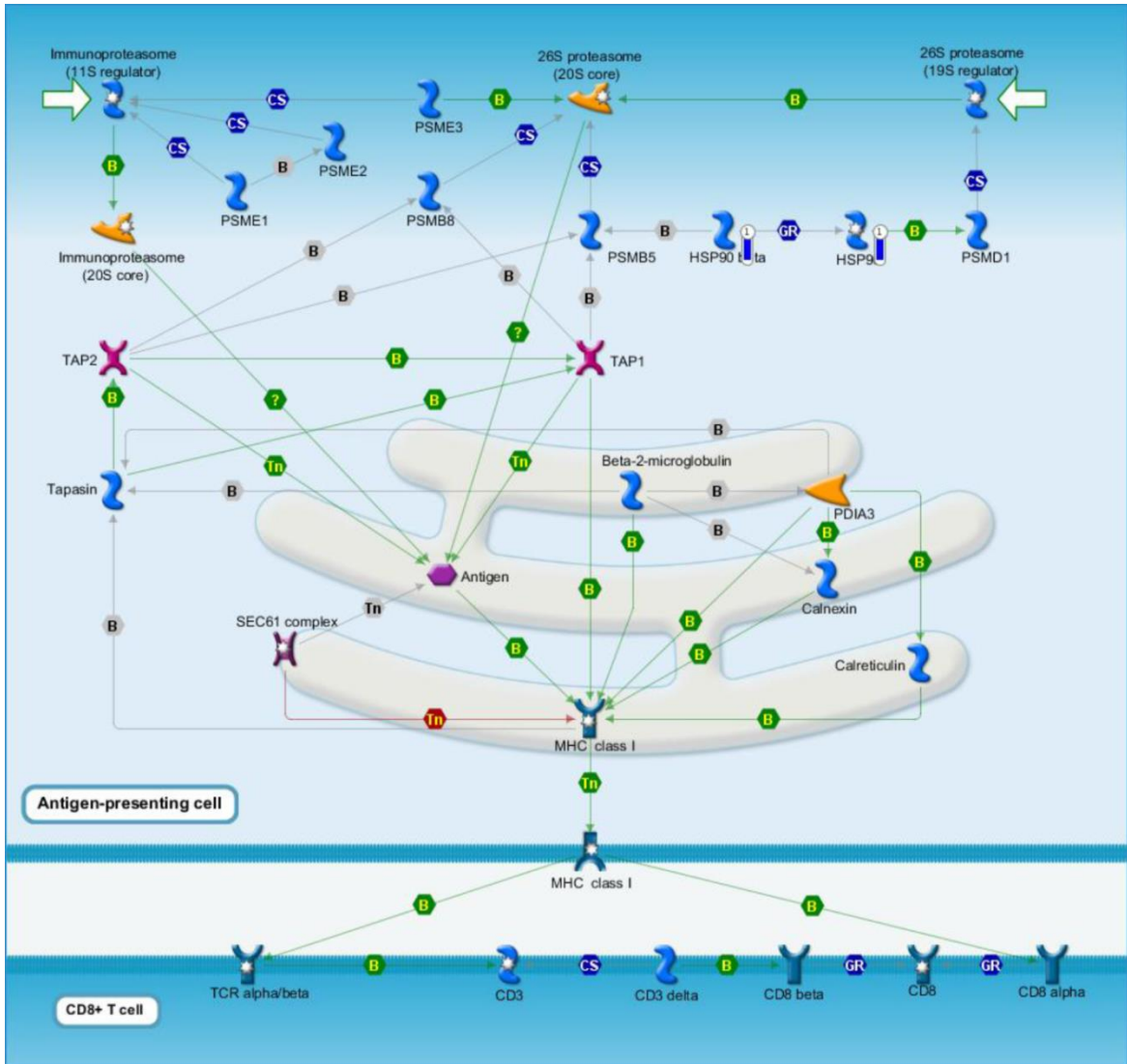


**Figure 76:** Map of the statistically significant pathway representing the immune response – antigen presentation by major histocompatibility complex (MHC) class I. This was the top scored map from the microarray data. Experimental data are represented by thermometers. Up-ward (red) thermometers indicate up-regulated signals and down-ward (blue) thermometers indicate down-regulated signals.

Down regulated; HSP90 and HSP90 beta

The other pathways identified from the microarray data (in order of statistical significance, most significant first) were;

- DNA damage – Inhibition of telomerase activity and cellular senescence
- Cell cycle – Chromosome condensation in prometaphase
- Cell cycle – Sister chromatid cohesion
- Transcription – Role of heterochromatin protein 1 (HCP1) family in transcriptional silencing.

The other pathways identified from the proteomics data (in order of statistical significance, most significant first) were;

- Mechanisms of CFTR activation by S-nitroglutathione (normal and CF)
- CFTR folding and development (normal and CF)
- Development – glucocorticoid receptor signalling
- Apoptosis and survival – regulation of apoptosis by mitochondrial proteins.

Of possible interest is the fact that two of the pathways identified include links to Sp1 (inhibition of telomerase activity and CFTR activation by S-nitrosoglutathione, microarray data and proteomics data respectively). Sp1 is a transcription factor and is involved in the copper dependent regulation of PrP<sup>C</sup> (see section 6.4.3.2 for more information).

#### **5.2.2.4. Comparison of 3001012 and 3001207**

As previously mentioned there was a 10-fold difference in the number of DEGs with a fold change of  $\geq 1.5$  identified after treatment with 3001012 compared to 3001207, although the total number of DEGs identified was comparable (4406 for 3001012 and 4802 for 3001207, see **Table 37**). Comparison of the pathways identified by MetaCore does show a certain amount of crossover, specifically in the identification of the regulation of apoptosis by mitochondrial proteins as a pathway affected by both compounds and the down regulation, in both cases, of ANT. Pathways with links to HSP90 were also identified for both compounds, though while HSP90 is up regulated after treatment with 3001012, it is down regulated after treatment with 3001207. It is thought, however, that the crossover between the data sets is limited and ambiguous in places, particularly in the case of the contradictory effects on HSP90, casting doubt on the hypothesis that these two compounds work in the same way.

## **5.3. Discussion**

### **5.3.1. Proof of Concept**

As discussed earlier, it was hoped to compare the quinacrine results with the literature to provide confidence that these techniques could be used to deconvolute the molecular targets of small molecule anti-prion drug compounds. Possible targets for quinacrine were identified from

the literature and then compared to the results from both the microarray and proteomics studies.

A paper published by Fasano *et al* compared the gene expression profile of infected scGT1 cells to cells which had been cured with quinacrine. <sup>(383)</sup> They compared the expression of around 15,000 genes and found that the gene for laminin was down regulated as a result of the clearance of PrP<sup>Sc</sup> from the cell by quinacrine. Other possible targets included the genes encoding EGF-like repeats and discoidin I-like domains protein 3 precursor and LIM and SH3 domain protein 1, which were up regulated. Endothelin-1 receptor and neogenin were down regulated. Other work suggests that the specific binding shown by quinacrine towards PrP<sup>C</sup> may be responsible for the anti-prion effect. <sup>(223, 233)</sup> Quinacrine had also been proposed to work in lysosomes by inhibiting the GAG-PrP interaction. <sup>(236)</sup> Other hypotheses include destabilisation of the cell membrane by recycling cholesterol into the endosomal compartments <sup>(245)</sup> and blocking channels formed by PrP. <sup>(384)</sup>

**Figure 71** shows processes related to histones and p53 dependent apoptosis being down regulated. Histones are involved with facilitating the formation of chromatin in cells, and act as a spool around which DNA can wind. They are also thought to have a role in transcription regulation, DNA repair and replication and chromosomal stability. p53 is known as the tumour suppressor protein and is essential for the prevention of human cancers – all human cancers are associated with the suppression of either the gene or up and downstream signalling. <sup>(385)</sup> p53 can induce growth arrest or apoptosis depending on physiological conditions, and has a role in Alzheimer's disease. <sup>(386)</sup> The down regulation of p53 suggests that apoptosis may be inhibited, although whether this is linked to a general down regulation of the granzyme A signalling pathway is unclear. Granzymes are serine proteases that act by cleaving caspases which in turn activate caspase-activated DNase which degrades DNA and induces an apoptotic cascade. The main function of granzyme A signalling is to induce apoptosis in infected cells, and elevated levels of granzyme A have been found in patients with an infectious disease or in a pro-inflammatory state. <sup>(387)</sup> Granzyme A can also cause the release of cytochrome C and other proteins which suppress inhibitor of apoptosis proteins.

It is thought that the down regulation of histones and p53 in the granzyme A signalling pathway may be due to the cells being 'cured' and therefore returning to their normal, uninfected state. As this pathway is implicitly associated with the immune response it would seem reasonable to

assume that the observed down regulation is actually the pathways within the cured cells returning to their baseline levels as PrP<sup>Sc</sup> levels reduce, with it being likely that this pathway is activated during infection. Unfortunately it's not possible to confirm this without an uninfected control which is something that was not available for this study. Down regulation of p53 may also be related to the cells recovering from infection as it can promote cell growth, although quinacrine is known to up regulate p53 in cancer cells to increase the apoptosis of cancerous cells. AKT, which is involved in the fatty acid metabolic process (see **Figure 72**) is also part of a system including p53 that is affected by quinacrine in its anti-cancer role. <sup>(388)</sup>

**Figure 72** shows the effect on metabolic processes of the plastic monomer Bisphenol A (BPA). BPA is a key component of many plastics and epoxy resins and as a result is present in a significant amount of food packaging and plastic bottles. Environmental exposure to BPA has been linked to weight gain as it is thought to have an impact on fat cell formation by disrupting adipogenesis and lipid accumulation. <sup>(389)</sup> Elements of the fatty acid metabolic process, specifically fatty acid synthase (FASN) and fatty acid binding proteins (A-FABP) are upregulated. FASN is an enzyme system which catalyses fatty acid synthesis, while A-FABP is a transport protein for fatty acids and facilitates the transfer of fatty acids between the extra- and intracellular membranes. The up regulation of these two components suggests an up regulation of fatty acid metabolic processes and fat cell differentiation, both of which are key elements of this pathway. It is possible that up-regulation of A-FABP may increase recycling of cholesterol into the endosomal compartment, due to its role in facilitating the transfer of fatty acids between extra and intracellular membranes. However, this is contradicted by the up-regulation of fatty acid synthase which, hypothetically, would mitigate this type of cell membrane destabilisation.

The identification of several pathways associated with DNA damage and cell cycle were thought to be interesting due to the suggested involvement of cell cycle proteins in neurodegeneration. <sup>(390)</sup> The increased expression of cell cycle proteins has been observed in post-mitotic neurons from patients with Alzheimer's disease, and it has been suggested that re-entry into the cell cycle may promote Alzheimer's pathology, with failure to complete the cell cycle resulting in neurodegeneration, also termed 'abortosis'. <sup>(391)</sup> The down regulation of cell cycle pathways, as observed in the MetaCore analysis, could therefore be suggested as possibly protective against neurodegeneration. However, cell cycle proteins have also been observed in healthy post-mitotic neurons, and it has been suggested that they may fulfil essential physiological functions

such as facilitating DNA repair and neuroplasticity.<sup>(390)</sup> Further to this, the key elements of the down regulated cell cycle pathways were related to DNA repair rather than being classical markers of cell cycle. Another important consideration that undermines this suggestion is that the cells being used in this study were still replicating and so were progressing through the cell cycle. It is therefore thought more likely that the prevalence of these cell cycle pathways is due to changes in normal cellular processes as a result of the reduction of the infectious burden.

Although there was some crossover between DEGs identified by the Hood paper and the MetaCore analysis this was limited, especially since the Hood paper identified 333 DEGs. However, they had identified genes that differed between infected and uninfected mouse models, with the aim of identifying genes that may contribute to disease pathogenesis. It was hypothesised that curing the cells may result in the down regulation of genes that were up regulated in the disease state, however in reality the models are very different and do not withstand detailed comparison to each other. Neither the system, (mouse model, *in vivo* compared to cell model, *in vitro*), or the comparison (infected vs uninfected compared to infected vs cured) are directly comparable.

Overall the data from the microarray and proteomics studies are not conclusive. It is thought that there is enough crossover between the pathways identified as being altered by quinacrine and the modes of action proposed in the literature to be confident of the validity of the technique, although the crossover is limited. The suggestion that quinacrine is affecting fatty acid synthesis and cholesterol recycling is particularly interesting.

### **5.3.2. Can Microarray and Proteomics Studies Complement Each Other?**

Another aim of this project was to investigate the extent to which the two techniques can complement each other. It was hypothesised that changes in gene expression, as identified by the microarray, would be represented in the proteomics data by changes in the expression of the related proteins. This was not found to be the case – as far as could be determined there was no correlation between the DEGs from the microarray and proteins identified as being up and down regulated in the proteomics. Similarly, comparison of the pathways identified by the two different techniques shows limited crossover, although in the case of 3001012 and

quinacrine there was enough correlation between the data sets for MetaCore to be able to identify pathways from the shared data set.

The lack of crossover between the microarray and proteomics data was more pronounced when there were fewer DEGs and proteins to form pathways around. For example, with the quinacrine data there were only 18 DEGs and 9 differentially expressed proteins (see **Table 38** and **Table 39**). For each data set there was one key gene which dominated the top ranked pathways. In the microarray data 3 out of the 5 top ranked pathways, all related to DNA damage, were associated with the down-regulation of p53. In the proteomics data, 3 out of the top 5 pathways, all associated with cell cycle, were associated with the down-regulation of histone H1. A brief glance at the data would suggest that quinacrine exerts its effect through one of these mechanisms, but the lack of supporting evidence perhaps casts doubt on this assumption. On the other hand, both data sets identified pathways related to cholesterol biosynthesis, which has been proposed as a target for quinacrine. <sup>(245)</sup>A similar pattern can be seen in the data for 3001207, which also had a smaller number of DEGs and proteins to form pathways around. Microarray pathways were dominated by p73 and histone H3, and the proteomics pathways dominated by HSP90 and HSP90 beta

The data set for 3001012, by comparison, is much larger and therefore the pathways are not as dominated by a single factor. When analysed separately, both data sets identified pathways involved in g-protein signalling, either related to the up-regulation of mitogen activated protein kinases (microarray) or the down-regulation of ephrin A receptors (proteomics), but examination of the pathways reveals no crossover between the two. There was further crossover between the two techniques with the microarray data identifying HSP90 as upregulated while the proteomics identified CDC37, a HSP90 chaperone, as upregulated.

In conclusion it is difficult to say from this study whether proteomics can be used to validate the results of microarray experiments and vice versa. The translation of changes in gene expression to changes in protein expression was not observed, although the complexity of the relationship between gene and protein expression may explain this to a certain extent. However, gaining useful information from MetaCore depends on having enough data to put into it in the first place, and for this purpose it was useful to be able to combine the two sets of data. If the assumption is made that gene expression does not directly relate to protein expression then having measures of changes in both the genome and the proteome makes the resulting data set

far more powerful. It can therefore be concluded that although the two sets of data may not be able to validate each other, the two together are greater than the sum of their parts.

### 5.3.3. 3001012 Compared to Untreated Control

The MetaCore analysis of the microarray and proteomics data for 3001012 does not show any obvious trend in the areas that are affected by treatment. The two top scored pathways suggest that 3001012 may have an effect either on development *via* the hedgehog signalling pathway, or on apoptosis regulation by mitochondria.

In embryos the hedgehog signalling pathway is involved in development, and controls a diverse range of developmental processes.<sup>(392)</sup> In adults the hedgehog (Hh) family of proteins control cell growth, survival and fate, with the cellular response depending on the type of receptor cell, the dose and the time of exposure. Hh proteins are divided into three subgroups known as desert hedgehog (Dhh), indian hedgehog (Ihh) and sonic hedgehog (Shh), with the latter being broadly expressed and the best studied and understood in humans. All the subgroups have similar physiological effects, with different effects due to differences in expression. The binding of Hh to the receptor (Patched) activates a signalling cascade, which in turn activates a zinc-finger transcription factor known as Gli-3, which is upregulated in the MetaCore study. Gli-3 functions primarily as a repressor of the pathway. In the absence of Hh, Gli-3 is truncated, *via* the proteasome, into its repressor form. Introduction of Shh leads to this processing being inhibited and the full length form of Gli-3 accumulating. Various cancers have been linked to the activation of hedgehog signalling, and it can directly promote cancer by regulating cell growth and survival.

The complexity of the pathway and the number of upregulated components make elucidating whether the whole pathway is up or down regulated more difficult. The up regulation of Gli3, along with up regulation of E3 ligases and the repressor form of Gli3 (Gli3R) all suggest that the pathway is being inhibited. The inhibition of Wnt signalling *via* antagonism of beta-catenin by Gli3R suggests a knock-on effect on Wnt signalling, although the up regulation of beta-catenin may be able to counteract this increased antagonism. Contradicting this data is the effect of HSP90 and CDC37 which are upregulated. The role of these two proteins within this pathway appear to be the activation of the STK36 kinase, which in turn activates Gli2. This could therefore

result in activation of the pathway, possibly counteracting the repression by Gli3R. It is therefore difficult, in this instance, to determine whether the pathway is up or down regulated.

The link between this pathway and the mechanism by which the compounds are working is not immediately obvious, and the literature does not suggest any direct links between hedgehog signalling and prion diseases. The up-regulation of both the Gli3 gene and genes related to the proteasome suggest that reducing the burden of infection results in repression of the Hh signalling pathway as a result of an increase in the truncated form of Gli3. However, there is no evidence of any of the other key elements of the pathway (Shh, Ihh, Dhh and their receptors) being affected by treatment, and the up regulation of HSP90, in this case, would appear to be contributing to pathway activation. While inhibition of the hedgehog signalling pathway can be lethal in embryos, down regulation in adult tissues is tolerated, with this being targeted as a potential treatment for cancers resulting from over-activation of the pathway.<sup>(392)</sup> It is therefore hard to suggest why this pathway should be affected by treatment with anti-prion compounds, although it does provide a potentially interesting new area of investigation.

Mitochondria are the central organelle involved in the intrinsic apoptotic pathway which is governed by the pro- and anti-apoptotic Bcl family.<sup>(393)</sup> Apoptosis is regulated by controlling membrane permeability and the release or retention of cytochrome C, and the apoptotic pathway is initiated by the formation of a cytosolic apoptosome. This is comprised of Apaf-1 (upregulated in this study), procaspase-9 and cytochrome C. The apoptotic process is executed by caspases, which are cysteine proteases that cleave substrates at aspartic acid residues. Mitochondrial permeability is regulated *via* the voltage dependent anion channel (VDAC) which forms a permeability transition pore, with increased permeability being associated with apoptosis. This is a transmembrane channel between the VDAC on the outer mitochondrial membrane and the adenine nucleotide translocator (ANT) on the inner mitochondrial membrane. ANT was downregulated after treatment with both 3001012 and 3001207, suggesting that treatment with I3GAs may decrease mitochondrial membrane permeability. The up regulation of Apaf-1 suggests that treatment may be leading to increased apoptosis, while a reduction in membrane permeability suggests decreased apoptosis, again making elucidation of the effect on the whole pathway difficult.

The effect of treatment ANT was thought to be potentially interesting. Increased opening of the mitochondrial permeability transition pore (MPTP) has been implicated in neurodegeneration

<sup>(394)</sup> with pore opening being triggered by, among other things, an excess of  $\text{Ca}^{2+}$ , <sup>(395)</sup> stress in the endoplasmic reticulum (ER) <sup>(396)</sup> and oxidative stress caused by an increase in copper. <sup>(397)</sup> It is therefore possible that the compounds may be able to prevent neurodegeneration by contributing to the maintenance of the mitochondrial membrane integrity. Opening of the MPTP has been shown to cause the mitochondria to swell and burst, releasing cytochrome C and initiating the apoptotic cascade. <sup>(398)</sup> Reducing the formation of the MPTP could therefore potentially reduce neuronal apoptosis and degeneration. This is counteracted, however, by the up regulation of Apaf-1, which may be contributing to apoptosis. It could therefore be hypothesised that the decrease in infection was due to treatment inducing the apoptosis of infected cells although, as discussed before, there is no evidence for either increased apoptosis or decreased growth rates in treated cells. It is therefore thought unlikely that this is a primary mode of action of 3001012.

Examination of the pathways does reveal components known to be related to prion diseases. The top ranked pathway (**Figure 71**), shares links to the proteasomal pathway, which has been shown to play a role in the pathogenesis of prion disease. <sup>(179)</sup> A number of genes have also been identified from both the microarray data and the MetaCore data that are either involved in, or share links to, the proteasomal pathway (see **Table 41**). Around 10% of the DEGs are involved in either ubiquitination or proteasomal processes and all of these were upregulated.

**Table 41.** Genes identified as upregulated in the microarray data in cells treated with 3001012 that are involved in the proteasomal pathway.

| Gene               | Function  |
|--------------------|---|
| ANAPC              | E3 ubiquitin ligase   |
| ASB8               | Substrate recognition component of an E3 ubiquitin ligase complex |
| BRCA1              | E3 ubiquitin ligase   |
| CDC23              | E3 ubiquitin ligase   |
| CDC27              | E3 ubiquitin ligase   |
| Cul/Rbx1 E3 ligase | E3 ubiquitin ligase   |
| DTL                | Substrate specific adapter of an E3 ubiquitin ligase complex      |
| FBXL3              | Substrate recognition component of an E3 ubiquitin ligase complex |
| FBXW11             | Substrate recognition component of an E3 ubiquitin ligase complex |
| HSP90              | Role in maintaining proteasome activity                           |
| KEAP1              | Substrate adaptor protein for an E3 ubiquitin ligase complex      |
| Skp2/TRcP/FBXW     | E3 ubiquitin ligase   |
| TOPORS             | E3 ubiquitin ligase   |
| UBR1               | E3 ubiquitin ligase   |
| VHL                | Target recruitment subunit in the E3 ubiquitin ligase complex     |

The proteasome, also known as the ubiquitin-proteasome system (UPS) is responsible for tagging and degrading misfolded proteins as part of the unfolded protein response (UPR) and has been implicated in various neurodevelopmental and neurodegenerative diseases including prion diseases. <sup>(399)(400)</sup> Infected mouse brains have been shown to have increased levels of ubiquitin conjugates, with toxic prion oligomers inhibiting the UPS both *in vitro* and *in vivo*. <sup>(181, 182)</sup> Accumulation of PrP<sup>C</sup> in the cytosol as a consequence of retrograde transportation *via* endoplasmic reticulum associated degradation (ERAD) can aid conversion if it exceeds the degradative capacity of the UPS, and transient proteasome inhibition has been shown to initiate PrP conversion. It is also thought that UPS impairment may allow for the accumulation of PrP into toxic aggregates. Another effect of the UPR is the inhibition of global protein synthesis, and this inhibition has been shown to cause a critical decline in key synaptic proteins, leading to neurodegeneration. Restoration of protein synthesis was shown to completely cure prion infected mice. <sup>(186)</sup> It is therefore possible that this pathway has multiple roles in the neurodegeneration associated with prion disease.

As shown above, a significant proportion of the genes and proteins affected by treatment with 3001012 were related to the proteasomal pathway, and all of them were upregulated. It would be reasonable to conclude that 3001012 may be working, at least in part, by upregulating the UPS and therefore increasing ubiquitination and degradation of PrP<sup>Sc</sup>. This corresponds with the finding that the I3GAs don't seem to be interacting with PrP<sup>C</sup> or PrP<sup>Sc</sup> directly, suggesting that a different pathway may be involved. The UPS will be examined in more detail in a section **6.1**.

### **5.3.4. 3001207 Compared to Untreated Control**

The data set for 3001207 was much smaller than the data set for 3001012 and therefore it is harder to draw conclusions from the limited data available. One of the key proteins in the microarray data is p73, which is related to p53 and is also considered a tumour suppressor. P73 is involved in cell cycle regulation and the initiation of apoptosis, and can control cell cycle and regulation *via* mechanisms previously ascribed to p53. <sup>(401)</sup> P73 also has a role in neural development, and is a positive regulator of embryonic and adult neural stem cells. <sup>(386)</sup> The other key protein from the microarray studies is histone H3, which is part of the family of histone proteins that play a central role in transcription regulation, DNA repair and replication and chromosomal stability.

Notch signalling was identified as the top rated pathway based on the microarray data from treatment with 3001207. The up regulation of p73, resulting in the increased activation of Notch1, suggests that this pathway is up regulated. Notch itself is a receptor with four isoforms, and the notch signalling pathway is involved in regulating cell fate during development and also maintaining tissue homeostasis in adults. Notch is also a key regulator of adult neural stem cells, with roles in the regulation of migration, morphology, synaptic plasticity and the survival of immature and mature neurons. <sup>(402)</sup> The involvement of notch signalling in neuronal survival suggests that it may have a role in prion disease pathology, but there does not appear to be any information among the literature to suggest a link. There is a clear link between the notch signalling pathway and Alzheimer's disease as  $\gamma$ -secretase, the protease complex responsible for cleaving the amyloid precursor protein (APP) to produce amyloid-beta (A $\beta$ ), is also responsible for activating notch signalling *via* cleavage of the notch receptor. <sup>(403)</sup> The multiple substrates of  $\gamma$ -secretase has hampered the development of therapies targeted at the cleavage of APP due to the off target effects on the notch signalling pathway. However, as there is no role for  $\gamma$ -

secretase in the conversion of PrP<sup>C</sup> to PrP<sup>Sc</sup> there is not the same link between prion diseases and notch.

The top rated pathway based on the proteomics data was related to the immune response, specifically the presentation of antigens by the major histocompatibility complex (MHC) class 1. This pathway features links to the proteasomal pathway *via* HSP90, as with the pathways from the 3001012 data, but in this case HSP90 is down-regulated. As the presentation of antigens by MHC class I is designed to alert the immune system to cells that are infected, it's possible that the down regulation of elements of this pathway is due, as with quinacrine treatment, to cells returning to normal baseline levels after the removal of infection. As such, this may not be the mechanism by which the cells have been cured, rather a secondary effect relating to the removal of the burden of infection. The time course data for the 3001207 treated cells showed that full clearance was not achieved until 56 hours, which was the point at which the cells were harvested. It is possible, however, that the down-regulation of this pathway began at the point at which the infection started to decrease, so it's possible that these off target effects may also be observed in the 3001207 treated cells.

As with the quinacrine data, pathways related to cell cycle were identified as being affected by treatment with 3001207. Unlike the quinacrine data these pathways appear to be upregulated, as indicated by the up regulation of histone H3. For the reasons outlined in section 5.3.1 it is thought unlikely that changes to cell cycle are behind the anti-prion activity of the compounds. It is interesting, however, that there was this crossover between quinacrine and 3001207, but not 3001012.

Overall there do not seem to be any obvious links between 3001207 and any of the pathways known to be involved with prion diseases. This raises the possibility of a novel mode of action *via* a pathway that has yet to be identified. A possibility is that up regulation of the apoptotic pathways helps clear cells that are infected, however as excess cell death was not observed in any of the treated cultures (compared to the untreated control) this would seem doubtful. The lack of a large difference in growth also casts doubt on this hypothesis. The involvement of the notch signalling pathway in neuronal maintenance makes this pathway a possible candidate for intervention, although there is no literature precedent to support this at this time.

### 5.3.5. 3001012 vs 3001207

As previously mentioned it was hypothesised that 3001012 and 3001207 would share a mode of action due to their similar structures and activities. The only crossover that was observed was that, in both cases, ANT was downregulated, suggesting that the compounds may be working by decreasing mitochondrial permeability and therefore affecting apoptotic processes. Direct comparison of the top 5 pathways identified by MetaCore using the combined data sets was not possible as this data was not available for 3001207. Comparison of the pathways identified for the individual data sets does show crossover in the pathways identified from the proteomics data, with the regulation of apoptosis by mitochondrial proteins featuring in both lists. This, again, suggests that both compounds may be working by affecting apoptosis *via* mitochondrial processes.

However, there was no effect on the proteasomal pathway observed after treatment with 3001207, nor was there any effect on the hedgehog signalling pathway. The limited crossover seen in these studies leads to the conclusion that these two compounds are not exerting their anti-prion effect in the same way, even though they are structurally similar and have almost equivalent activities in the cell line assay. Interestingly the key proteins identified for 3001207 were much more closely related to the key proteins identified for quinacrine – p53 and p73 are part of the same family and have related but distinct functions as tumour suppressors. Similarly, the histones H2 and H3 are part of the same family and have related functions. However, the pathways that were identified were different (notch signalling for 3001207 and granzyme A signalling for quinacrine) and to add to the confusion p73 and histone H3 were upregulated after treatment with 3001207, while p53 and histone H2 were down-regulated after treatment with quinacrine. This suggests that while similar proteins may be affected by treatment with these compounds, the downstream effect is quite different.

## 5.4. Overall Conclusions

As laid out at the beginning of this chapter, four questions were asked. It was hoped that by answering these questions, insights could be gained into the suitability of systems biology techniques for elucidating the targets of small drug-like molecules, as well as identifying

potential targets of the I3GA compounds and elucidating further whether they have a common mode of action.

In order to answer these questions, cells were treated with DMSO, quinacrine, 3001012 or 3001207. Microarray and proteomics analyses were carried out, and the results analysed using MetaCore to identify pathways affected by treatment. Quinacrine was included in the study as a positive control due to the information available in the literature on its mode of action – quinacrine would be used to validate the technique for use with compounds where the mode of action was unknown. DMSO was the negative control, and all treated cells were compared to the results from DMSO in order to determine the differences between treated and untreated cells.

The quinacrine results were thought to be hopeful, as pathways that were identified could be explained either in terms of a published mode of action, or as a consequence of the changes in immune response due to treatment and subsequent reduction of the infectious burden. The down regulation of the histones and p53 was thought to be an example of this. Up-regulation of A-FABP and fatty acid synthase suggested a role for quinacrine in altering cholesterol homeostasis, something that has been reported.<sup>(245)</sup> The importance of laminin, as reported by the authors of a study into the effect of quinacrine on gene expression in ScGT1 cells,<sup>(383)</sup> was not reproduced in this study. However, it is thought that the quinacrine results can be used to validate the results obtained for the I3GAs.

The second aim of this study was to determine if microarray and proteomics studies could be used to complement each other. This was based on the hypothesis that changes in gene expression would be confirmed by the concomitant changes in protein expression, as detected by the proteomics studies. The specific validation of certain DEGs *via* identification of changes in their respective protein levels was not found to be possible, and this was attributed to the complex relationship between gene and protein expression, as well as the smaller number of proteins that could be identified in the proteomics studies. However, combining the two sets of data resulted in more powerful MetaCore analysis, with enough data available for 3001012 and quinacrine to allow pathways to be identified from the combined data set. If the assumption that gene expression does not necessarily correlate to protein expression is used, then having both sets of data is clearly beneficial and, although they may not complement each other directly, they do provide more information together than either would provide on its own.

Analysis of the MetaCore data for 3001012 identified roles for the compound either in altering hedgehog signalling or apoptosis as regulated by mitochondria. The link to hedgehog signalling was potentially interesting as this is not a pathway with known links to prion diseases, but did not provide any further insights into how 3001012 might be working. Increased mitochondrial permeability is associated with neurodegeneration, so decreased permeability as indicated by the down regulation of ANT may therefore be part of 3001012's curative effect. No treatment-induced apoptosis was observed in treated cells, suggesting that apoptosis of infected cells is not part of the mode of action. Further study of the top ranked MetaCore pathways (5 in total) revealed that around 10 % of DEGs were related to protein degradation pathways, with the majority being upregulated E3 ubiquitin ligases. As this is a pathway with established links to prion diseases it was decided that this was a potentially interesting avenue of investigation.

The data set for 3001207 was much smaller, with none of the pathways identified by MetaCore having established links to prion disease. Again there was the suggestion that the induction of apoptosis, possibly as a consequence of changes in notch signalling, may have a role to play in clearing the cells of infection. However, as mentioned previously, no additional apoptosis was observed in treated cells compared to untreated cells. As with quinacrine, the changes in the immune system were attributed to the down regulation of these effects as the cells were relieved of their infectious burden. As with the effect of 3001012 on hedgehog signalling, it's possible that the effects of 3001207 on notch signalling represent a novel involvement of these pathways in prion diseases. It is also possible that these changes represent off-target effects of the compounds, which are unrelated to their anti-prion activity.

The inclusion of two I3GA compounds in this study aimed to show whether the two compounds were working in the same way. Their structural similarity, along with the tightly defined SAR for this group of compounds (see section **3.1.3**) suggested that they would share a mode of action, and would therefore identify the same, or related, pathways in the MetaCore analysis. This was not found to be the case. There was no distinct effect of 3001207 on the proteasomal pathway, with the exception of its down-regulation of HSP90, contradicting the data from 3001012. Analysis of the proteomics data identified the regulation of apoptosis by mitochondrial processes as being affected by both compounds, although as discussed previously the relevance of this to the mode of action of the compounds is unknown. An interesting observation was that 3001207 was shown to affect a much smaller set of genes than 3001012, perhaps suggesting that it has fewer off target effects. However, the limited crossover between the data sets does

seem to suggest that the two compounds are working in different ways, despite their structural similarity and their comparative activities in the cell line.

In summary, it is thought that the use of microarray and proteomics is a valid approach for elucidating the targets of small drug-like molecules. Although the two techniques were not found to complement each other directly, the two sets of data together were thought to be more than the sum of their parts. Although no obvious mode of action has been identified for the I3GA compounds it has revealed links to the proteasomal pathway, known to have links with prion disease. It was therefore hypothesised that the I3GA compounds may be working through some modulation of the protein degradation system, resulting in increased degradation of PrP<sup>Sc</sup>. There was limited crossover in the data for 3001012 and 3001207, leading to the initial conclusion that these two compounds do not share a mode of action. However, this is questionable due to their structural similarity and tightly defined SAR and therefore warrants further investigation.

## 6. Mode of action studies: Target elucidation

A key finding from the microarray and proteomics studies, discussed in section 5.3.3, was that treatment of the SMB cells with the I3GA compound 3001012 resulted in the upregulation of multiple components of the proteasomal pathway. Due to the up-regulation of several E3 ubiquitin ligases, as well as HSP90, it was hypothesised that 3001012 may be working *via* up-regulation of protein degradation systems. The studies outlined in this chapter were designed to validate and further reveal the possible effect of the I3GAs on the UPS, as well as investigating possible changes to targets of the I3GAs identified through other methods.

### 6.1. Protein Degradation Pathways

Within cells there are two major pathways that facilitate protein degradation: The ubiquitin-proteasome system (UPS) and autophagy (see **Figure 77**). The UPS primarily degrades soluble intracellular proteins and transmembrane proteins that have been translocated from the membrane into the cytosol. Lysosomes primarily degrade membrane proteins in addition to degrading cytosolic proteins through autophagy. The two pathways are not entirely separate and therefore it is not possible to consider one without the other. The proteasome, also known as the UPS, is a multicatalytic enzyme which is expressed in the nucleus and cytoplasm of eukaryotic cells. Its primary function is to degrade proteins that are incomplete or misfolded. Autophagy is more of a bulk process, responsible for degrading unwanted cellular components. It is generally mediated by lysosomes, which contain lysosomal cysteine proteases (also known as cathepsins) that are also involved in protein degradation. Autophagy is a catabolic process whereby proteins are delivered to the lysosomal compartment for degradation, and several lines of evidence point to autophagy and the proteasomal pathway being interrelated, having shared substrates and regulatory molecules as well as showing co-ordinated and sometimes compensatory functions. <sup>(404)</sup>

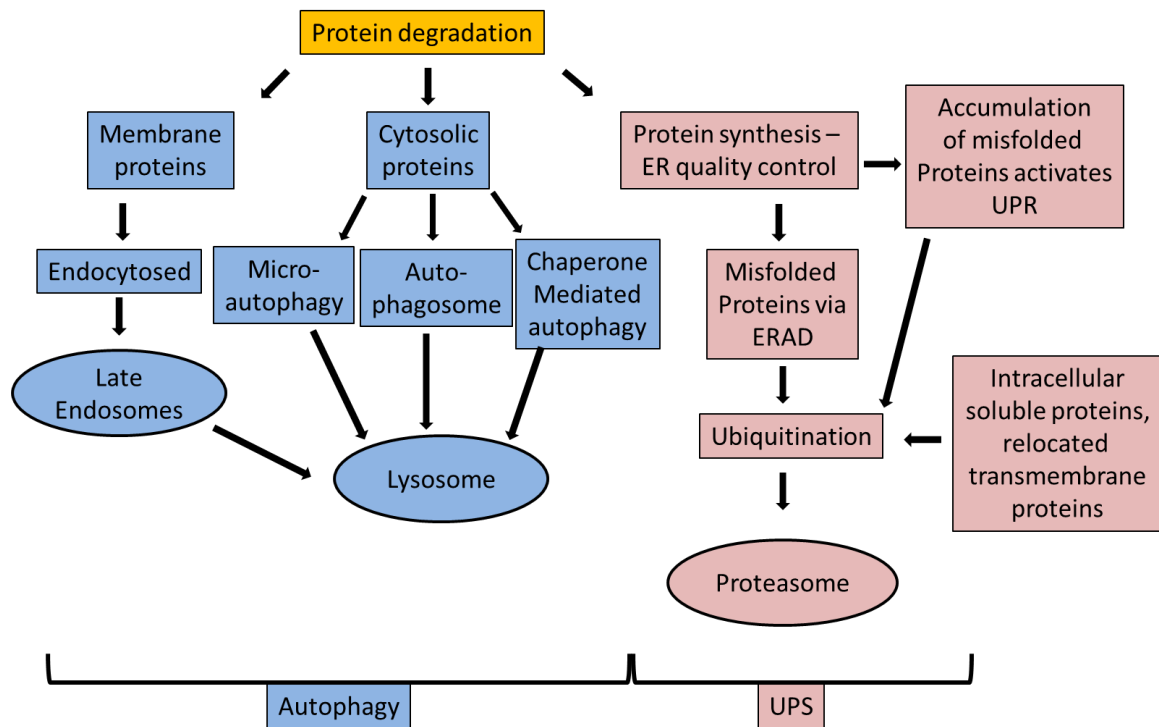


**Figure 77:** Representation of the different protein degradation pathways and their main substrates. ER – endoplasmic reticulum, ERAD – endoplasmic reticulum associated degradation.

The endoplasmic reticulum (ER) is responsible for quality control, meaning that only correctly folded proteins reach their cellular targets. Misfolded proteins are retained and subject to the endoplasmic reticulum associated degradation (ERAD) pathway, where they are marked for degradation by the proteasome. An accumulation of misfolded proteins and disruption of ER homeostasis can lead to a perturbation of function and ER stress which in turn can trigger the unfolded protein response (UPR). This results in decreased levels of protein translation, and increased levels of molecular chaperones, folding enzymes and ERAD, <sup>(405)</sup> resulting in increased protein degradation by UPS (see **Figure 77**).

The UPS consists of the enzymatic proteasome complex itself, and the associated ubiquitination system which is responsible for labelling proteins for degradation. The proteasome complex is known as the 26S proteasome, and consists of the 20S core and one or two 19S regulatory subunits (see **Figure 78**).

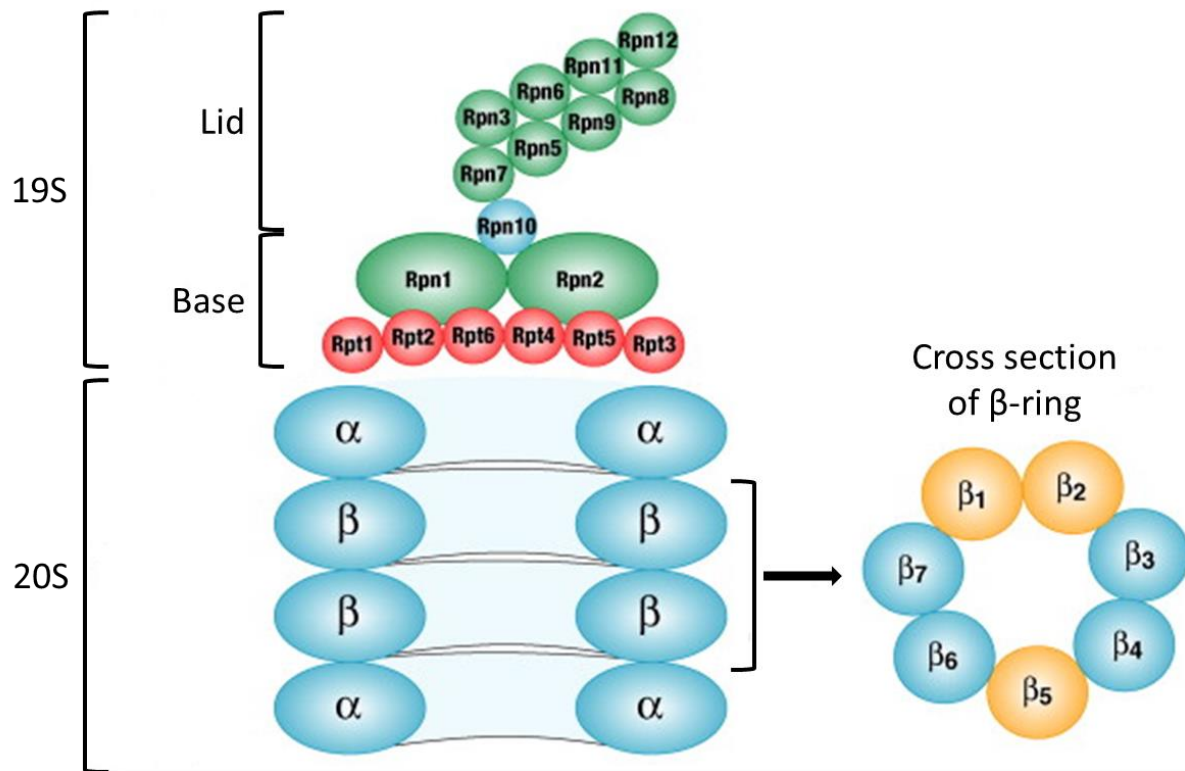


**Figure 78:** Schematic diagram of the 26S proteasome, showing the 20S core and the 19S regulatory particle. Rpt and Rpn indicate subunits of the regulatory particle with or without ATPase activity respectively. Figure adapted from Deriziotis *et al.* <sup>(400)</sup>

The 19S subunit binds and cleaves the polyubiquitin chain, allowing the substrate to be denatured and fed into the proteolytic core. The C-termini of the ATPases dock into the  $\alpha$ -ring of the core particle and open the gate, resulting in substrate hydrolysis. The cross section of the  $\beta$ -ring, as shown in **Figure 78**, shows the core particle subunits and demonstrates the location of the  $\beta$ 1,  $\beta$ 2 and  $\beta$ 5 subunits. These differ in substrate specificity and activity and are responsible for caspase-like, trypsin-like and chymotrypsin-like activities respectively. Protein substrates are degraded into small peptides 3-25 amino acids in length <sup>(406)</sup>

Proteins are marked for degradation with chains of ubiquitin, and the process is modulated by the sequential action of three different enzymes (see **Figure 79**). The ubiquitin activating enzymes (E1) bind ubiquitin and transfer it to the ubiquitin conjugating enzymes (E2). E2 presents the ubiquitin to the ubiquitin protein ligases (E3) which bind to the target protein and, with the help of E2, the ubiquitin molecule is covalently attached. There are a limited number of E2 enzymes but many more E3 enzymes, as the E3 enzymes have highly specific interactions. The E3 ligases have ultimate control over protein stability. <sup>(407)</sup> The polyubiquitinated substrate is then identified by the 19S regulatory subunit as described above.

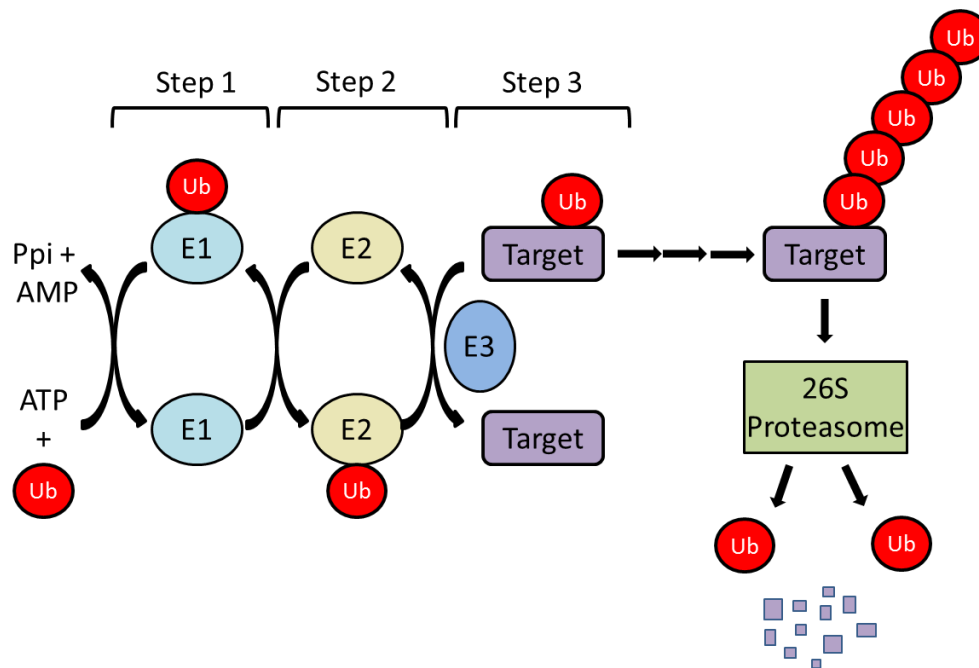


**Figure 79:** The process of labelling targets proteins for degradation *via* ubiquitination. E1 binds ubiquitin and transfers it to E2. The ubiquitin is transferred to E3 which covalently binds it to the target protein. E3 ligases are specific for their target protein. Figure adapted from Adams. <sup>(406)</sup>

Heat shock protein 90 (HSP90) is a molecular chaperone and one of the most abundant proteins in cells. It is upregulated in response to stresses such as heat shock, from which it gets its name. It is involved in a wide range of cellular processes including signal transduction, intracellular transport and protein degradation and is required for the activation and stabilisation of a wide range of client proteins, many of which are involved in important cellular pathways. <sup>(408)</sup> It has been shown to associate with the proteasome, and is thought to participate in regulation as well as assembly and repair of the proteasome complex. <sup>(409)</sup> It has been shown to prevent protein aggregation, <sup>(410)</sup> and acts to keep denatured proteins in a partially folded state so they can be rescued and refolded with the help of the appropriate chaperone. <sup>(409)</sup> HSP90 is required for the degradation of ER membrane proteins, and various E3 ligases, including CHIP, Ubr1 and Cul5 are associated with HSP90. <sup>(408)</sup> Ubr1 is among the upregulated E3 ligases, as is a Cul complex, along with the HSP90 chaperone CDC37. Numerous cell-cycle related kinases are reported to form stable complexes with HSP90 and CDC37 is thought to be involved in directing immature kinase complexes to their final destination. <sup>(409)</sup>

### 6.1.1. Could These Systems be Affected by the I3GA Compounds?

It can be seen in **Table 41** that a significant proportion of the DEGs identified by the microarray as a result of treatment with 3001012 are E3 ubiquitin ligases. This in turn suggests that the SMB cells may be undergoing increased levels of ubiquitination, resulting in an increase in proteasomal activity in treated cells compared to cured cells. Although investigations have not found any effect on ubiquitin levels after treatment with 3001012 it is not known if this would be required for increased ubiquitination *via* up-regulation of the E3 ligases. In theory, up regulation of the proteasomal pathway may allow the cells to clear their burden of PrP<sup>Sc</sup> more efficiently, or at least reduce it to a level where it can be maintained without further conversion. The up-regulation of HSP90 in the microarray, along with one of its chaperones in the proteomics study, suggests that this may play an important role in helping clear the cells of infection.

As previously discussed in sections **1.1.2.5** and **5.3.3**, there is a well- established link between the UPS and prion diseases, <sup>(399)</sup> so in this context it's not surprising that there should be some alterations to this pathway. Inhibition of the UPS has been directly implicated in neurodegeneration, and PrP<sup>Sc</sup> has been shown to inhibit the proteasome. <sup>(181, 182)</sup> There are several compounds that have been reported to work either by redirecting PrP<sup>Sc</sup> to lysosomes for degradation or by upregulating autophagy including cationic dendrimers, <sup>(229, 411)</sup> tyrosine kinase inhibitors, <sup>(237)</sup> chlorpromazine, <sup>(238)</sup> tamoxifen and its metabolites <sup>(239)</sup> and rapamycin, lithium and trehalose. <sup>(259)</sup> Analogues of congo red have also been shown to restore normal proteasomal activity in the persistently infected SMB cells which suffer from chronic proteasomal inhibition, and this was suggested as their mode of anti-prion activity. <sup>(220)</sup> It would appear that this is a potential therapeutic avenue that merits further investigation.

Previous work by Chen *et al* (unpublished data) showed that there is no significant effect of treatment with 3001012 on levels of LC3-II, a commonly used marker of autophagy, and therefore concluded that this compound was not working *via* modulation of autophagic processes. Another of the I3GA compounds, 3001086, was investigated in co-dosing experiments with autophagy inhibitors, with activity found to be unaffected. The same study also found no effect of treatment on ubiquitin levels by western blot. However, no investigations were undertaken into the effect of treatment on the UPS, and from the evidence presented so far it was hypothesised that some function of HSP90, possibly related to its association with the

proteasome, might have a role in the activity of lead compound 3001012. To determine the possible effects of treatment with 3001012 two methods were employed. The first method was to run competition assays in which 3001012 was co-dosed with inhibitors of both the proteasome and of lysosomal proteases. The second method was to probe for HSP90 using western blotting to determine if there was a difference in HSP90 levels between treated and untreated cells. Proteasomal activity was not measured directly, as all work with the SMB cells was required to be carried out within a class II containment lab, containing essential facilities for the direct measurements of proteasomal activity. Unfortunately, these facilities were not available during the life time of this project.

## **6.2. Competition Studies Using Inhibitors of the Proteasome and Lysosomal Proteases**

### **6.2.1. Introduction**

It was hypothesised that if treatment with 3001012 was causing up-regulation of the proteasome, then inhibition of the proteasome should negate the curative properties of the compound. Initially two proteasomal inhibitors were used; one with very specific inhibitory activity on the proteasome and one which affected both the proteasome and lysosomal cysteine proteases (LCPs). The rationale for using two different inhibitors was to show more precisely any pathways which might be affected by 3001012. For example, if 3001012 activity was affected by the general inhibitor but not the specific inhibitor of the proteasome, that would suggest that 3001012 was not targeting the proteasome exclusively. MG132 and lactacystin were chosen for this purpose in the first instance (see **Figure 80**).

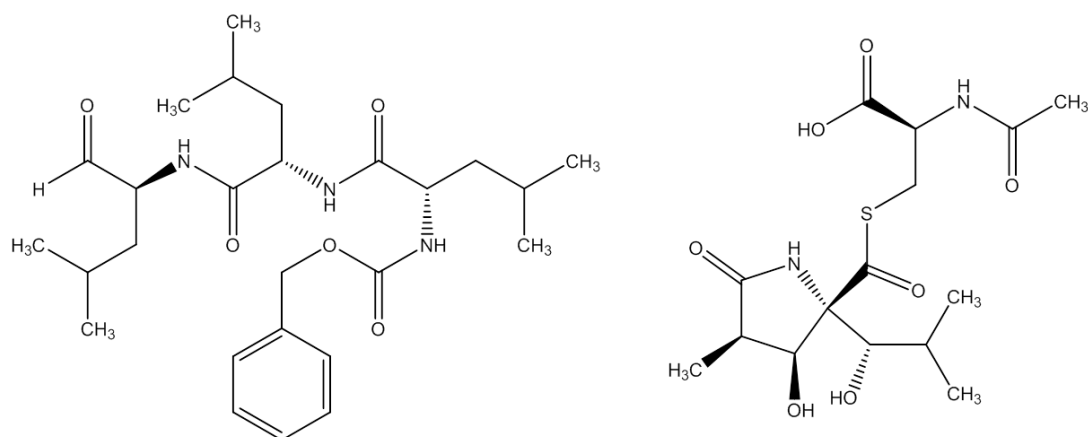


**Figure 80:** Structure of MG132 (left), a general inhibitor of the proteasome and the LCPs, and lactacystin (right), a specific proteasomal inhibitor.

MG132 is a peptide aldehyde and is a well characterised inhibitor of the proteasome. It reversibly blocks the proteolytic activity of the 26S proteasome *via* potent inhibition of its chymotrypsin-like activity. It also inhibits LCPs. <sup>(412)</sup> Lactacystin is a natural microbial product which inhibits the proteasome in a highly specific manner by covalently modifying the N-terminal threonine of certain subunits of the  $\beta$ -ring. <sup>(413)</sup> Both trypsin-like and chymotrypsin-like activities are irreversibly inhibited, with the caspase-like activity inhibited reversibly and at a lower rate. Lactacystin itself does not interact with the proteasome until it undergoes conversion to the active proteasome inhibitor *clasto*-lactacystin  $\beta$ -lactone (see **Figure 81**). <sup>(414)</sup> Unlike lactacystin, *clasto*-lactacystin  $\beta$ -lactone can enter the cells, at which point it either interacts with the proteasome or is converted into an inactive form, known as lactathione, which is structurally and functionally analogous to lactacystin. This can be converted back into *clasto*-lactacystin  $\beta$ -lactone within the cell to be used when required.

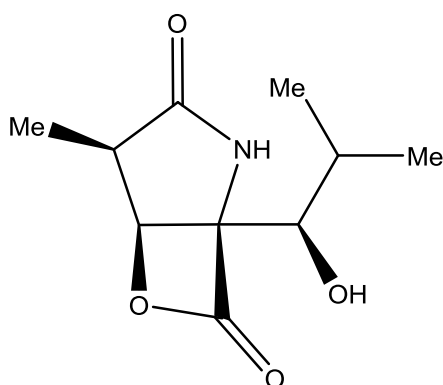


**Figure 81:** Structure of *clasto*-lactacystin  $\beta$ -lactone, the active form of lactacystin.

From a clinical perspective the peptide boronic acids, such as bortezomib, are preferred due to their superior activity and slow dissociation from the proteasome, which gives stable yet reversible inhibition.<sup>(406)</sup> However, from a research perspective MG132 was preferred due to its use in previous studies,<sup>(179)</sup> and also because of price and availability considerations. Due to the high cost, lactacystin was used in a more limited set of experiments and within a pathway validation capacity. Considering MG132's dual effect on both the proteasome and the lysosomal proteases, it was thought important to determine whether selective inhibitors of the lysosomal proteases had the same effect as MG132 to clarify the mechanism behind any observed effects.

Lysosomal cysteine proteases (LCPs) are also known as the cathepsins, with 11 identified so far. They have specific and individual functions that are crucial to normal organism function and are associated with certain pathological events, including neurological disease.<sup>(415)</sup> Two LCP inhibitors with different specificities were used; E64 and Cathepsin inhibitor III (CI3). E64 is an irreversible, selective and highly potent cysteine protease inhibitor. It was chosen for this purpose due to its specificity, low toxicity and availability (Information from supplier MSDS). CI3 selectively inhibits cathepsin B, L, S and papain (Information from supplier MSDS) and was chosen to help determine whether any changes seen might be as a result of inhibition of a specific cathepsin. Structures can be seen in **Figure 82**, and the different targets of all the inhibitors used in this study can be seen in **Figure 83**.

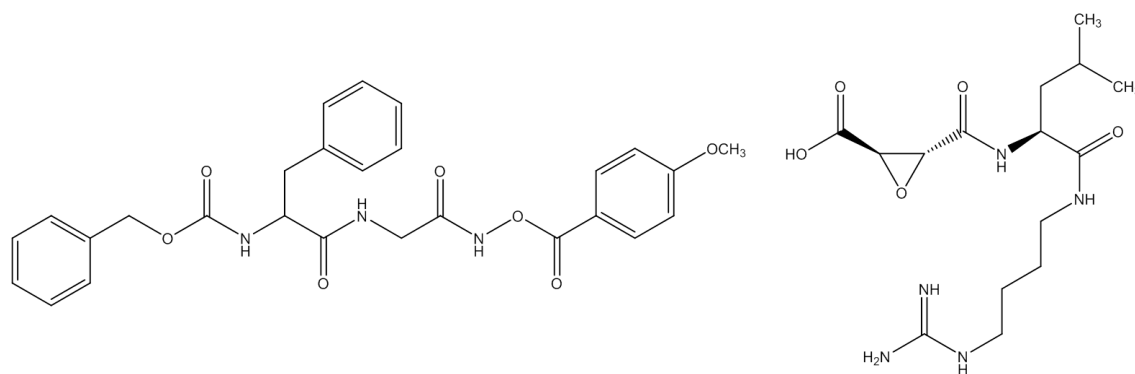


**Figure 82:** Structures of CI3 (left), an inhibitor of cathepsins B, L, S and papain, and E64 (right), a general inhibitor of LCPs.

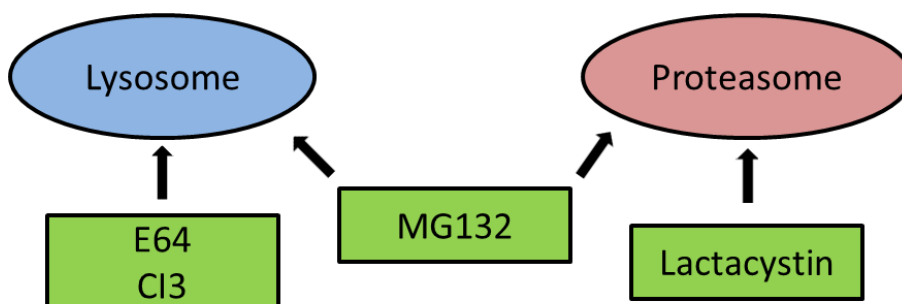


**Figure 83:** Representation of the targets of the different inhibitors used in these experiments.

To assess whether any effect seen was specific to 3001012 or a general feature of the I3GA compounds two other structurally similar I3GA compounds were co-dosed with all the inhibitors where possible. 3001207 was chosen as it was one of the lead compounds, and also because it was also used in the proteomics and microarray studies. No E3 ligases were identified in the microarray and proteomics data for 3001207 and although results showed that there was a link to HSP90 it was found to be down-regulated. It was therefore thought important to also investigate 3001207 for comparative purposes. 3001086 was used as this compound had been investigated previously as part of studies relating to possible effects of the I3GA compounds on autophagy (see section 6.1). Materials and methods for this study are outlined in detail in sections 2.1.4 and 2.2.4.5.

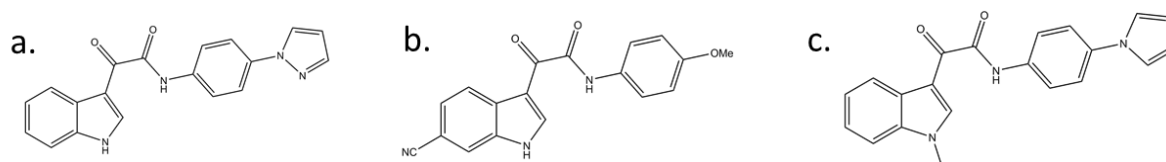


**Figure 84:** Structures of 3001012 (a), 3001207 (b) and 3001086 (c). 3001012 has an  $EC_{50}$  of 1 nM, 3001207 has an  $EC_{50}$  of 1.5 nM (first batch) or 15 nM (second batch) and 3001086 has an  $EC_{50}$  of 180 nM (See section 3.1)

## 6.2.2. Results

### 6.2.2.1. MG132

An initial investigation evaluated the effect of dosing the cells with MG132 on its own to see if it had any effect on PrP<sup>Sc</sup> levels at a range of concentrations.

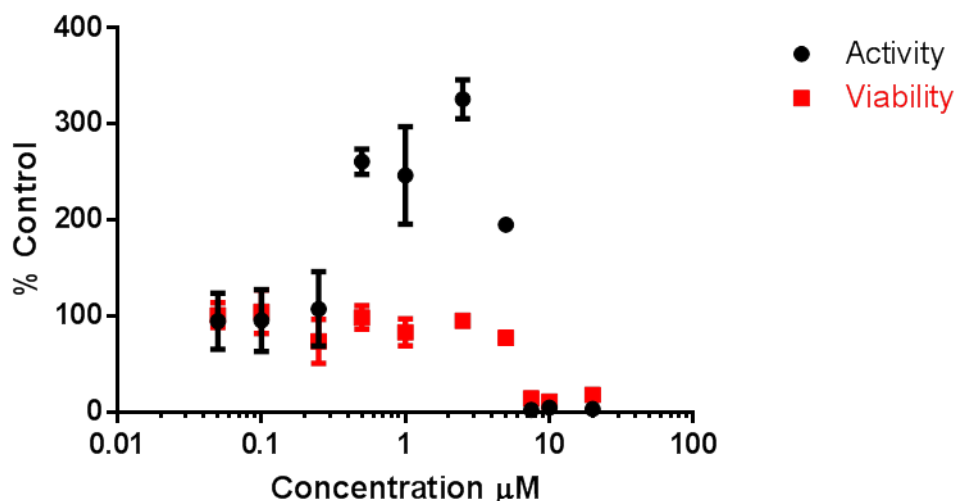


**Figure 85:** PrP<sup>Sc</sup> levels in SMB cells after dosing with MG132 at concentrations ranging from 0.05 µM to 20 µM. 0.5 µM is the lowest concentration to induce an increase in PrP<sup>Sc</sup>, and levels continue to rise in a dose-dependent manner until the amount of PrP<sup>Sc</sup> starts to decrease at 5 µM. Toxicity was observed at concentrations higher than 5 µM. The data points shown represent the mean ± SD values from duplicate experiments where each sample was analysed in triplicate.

It can be seen in **Figure 85** that from concentrations as low as 0.5 µM MG132 caused an increase in PrP<sup>Sc</sup>, with levels increasing to around 3 times that of the untreated control at a concentration of 2.5 µM. The LD<sub>50</sub> was estimated to be around 6 µM, with cell death starting to become obvious at 5 µM. The reported IC<sub>50</sub> for MG132 in cultured cells is around 5 µM, <sup>(412)</sup> so the data here is in agreement with the literature. However, the associated toxicity means that the therapeutic window for this compound is rather small. For all subsequent assays MG132 was used at a concentration of 3 µM to provide the maximum activity without compromising cell viability.

Once the working concentration of MG132 had been established it was co-dosed with 3001012 at a range of concentrations.

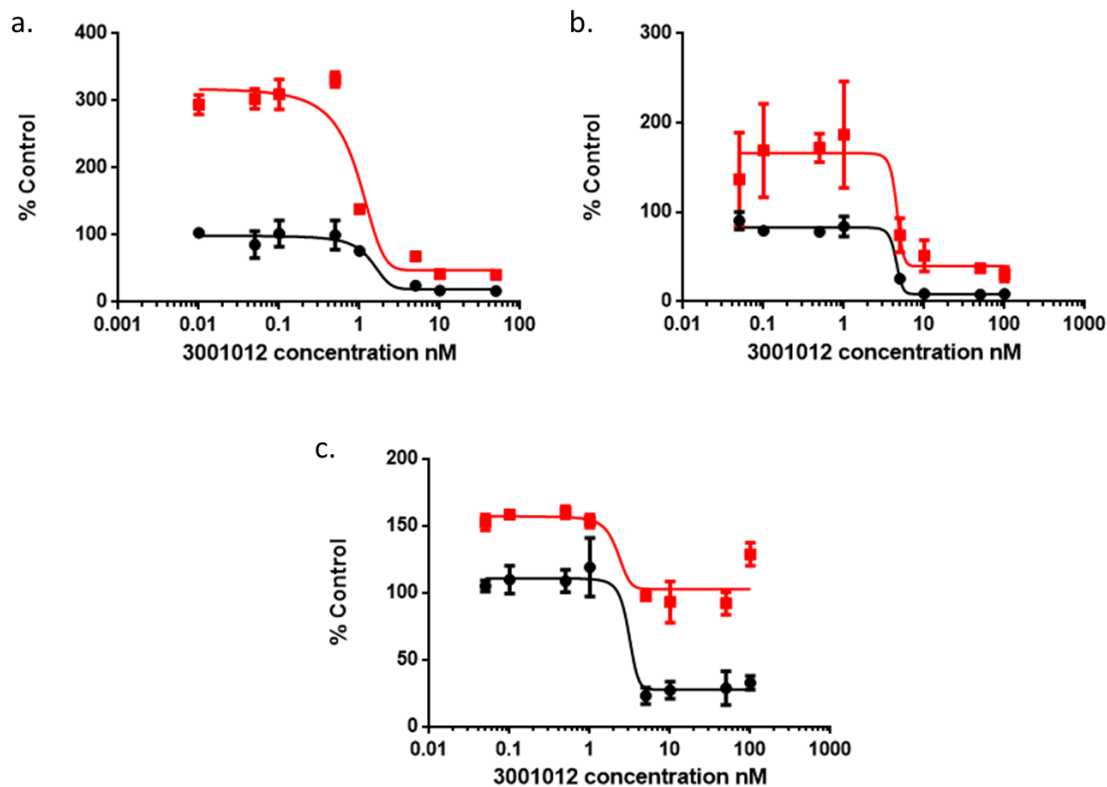


**Figure 86:** Data showing the effect of MG132 on 3001012 activity as measured by PrP<sup>Sc</sup> clearance. The black curve indicates 3001012 on its own at concentrations between 0.001 nM and 100 nM. The red curve indicates 3001012 at the same concentrations but co-dosed with 3 μM MG132. Each graph shows an independent experiment, **Table 42** gives estimated EC<sub>50</sub> values. The data points shown represent the mean ± SD values from a single experiment where each sample was analysed in triplicate.

**Table 42:** EC<sub>50</sub> values for 3001012 on its own or co-dosed with MG132 calculated from the data presented in **Figure 86**.

| Graph | Estimated EC <sub>50</sub> value (nM) |                   |
|-------|---------------------------------------|-------------------|
|       | I3GA only                             | I3GA + 3 μM MG132 |
| a.    | 1                                     | 2.5               |
| b.    | 3                                     | 3                 |
| c.    | 2.5                                   | 2.5               |

The three independent experiments shown in **Figure 86** indicate that 3001012 is less efficient at clearing PrP<sup>Sc</sup> when co-dosed with MG132. In all cases, PrP<sup>Sc</sup> has accumulated at the sub-active concentrations of 3001012 (<5 nM for all experiments), followed by a significant decrease at

active concentrations. The difference between baselines in co-dosed cells and cells dosed with 3001012 only demonstrate a reduction in the efficacy of 3001012, but the extent of this reduction differs between experiments. The reduction of PrP<sup>Sc</sup> levels in co-dosed cells varied between 50 % of the blank (**a.** and **b.**) and 100 % of the blank (**c.**). The extent of PrP<sup>Sc</sup> accumulation as a result of MG132 treatment at sub-active concentrations of 3001012 also varies from 150 % of the blank (**c.**) to 300 % of the blank (**a.**), even though the MG132 concentration is the same. In **b.** and **c.** no change in the EC<sub>50</sub> values is observed (see **Table 42**), although it can be seen that in **a.** the EC<sub>50</sub> has decreased slightly, suggesting that co-dosing with MG132 can actually increase the activity of 3001012.

Data from **Figure 86a** was analysed using multiple t-tests to determine if the differences between 3001012 on its own and 3001012 co-dosed with 3  $\mu$ M MG132 at the higher concentrations of 3001012 were statistically significant.

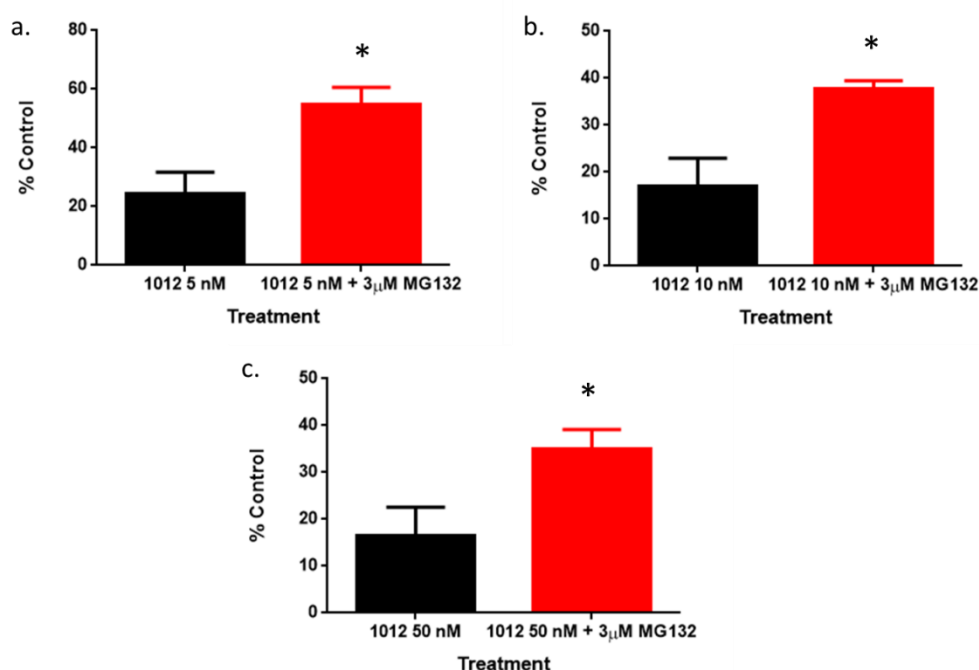


**Figure 87:** Statistical analysis of the data at concentrations of 5 (a), 10 (b) and 50 nM (c), comparing cells treated with 3001012 to cells treated with both 3001012 and MG132. Data from **Figure 86a** above. Statistical analysis using a multiple t-test showed statistically significant differences in all cases with *p*-values as follows; 5 nM *p* = 0.00468012, 10 nM *p* = 0.0041324, 50 nM *p* = 0.0117233. The data points shown represent the mean  $\pm$  SD values from duplicate experiments where each sample was analysed in triplicate.

Statistical analysis of the differences between cells treated with 3001012 and cells treated with both 3001012 and MG132 show that MG132 is causing a statistically significant decrease in the

activity of 3001012 as measured by clearance of PrP<sup>Sc</sup> (see **Figure 87**). This is true for concentrations up to 50 x EC<sub>50</sub> (and up to 100 x EC<sub>50</sub> in some cases) suggesting that even an excess of 3001012 can't fully compensate for the antagonism of MG132. This is to be expected as MG132 is inhibiting the protein degradation systems, rather than 3001012.

A time course assay was carried out to determine how long it took for PrP<sup>Sc</sup> levels to rise after dosing with MG132. This was also carried out for cells which were co-dosed with 10 nM 3001012 and MG132 to determine how co-dosing might alter the time courses of the individual compounds. It was hypothesised that if PrP<sup>Sc</sup> levels rose more quickly than 3001012 was able to reduce PrP<sup>Sc</sup> levels that may explain the reduced clearance seen in the previous experiments, as more PrP<sup>Sc</sup> would have initially been present in the cells. However, if 3001012 was able to reduce PrP<sup>Sc</sup> levels before the MG132 induced increase in levels, 3001012 may be able to mitigate the effects of inhibition. It would also suggest that the decreased clearance efficiency may have resulted from 3001012 being challenged by the effects of MG132.

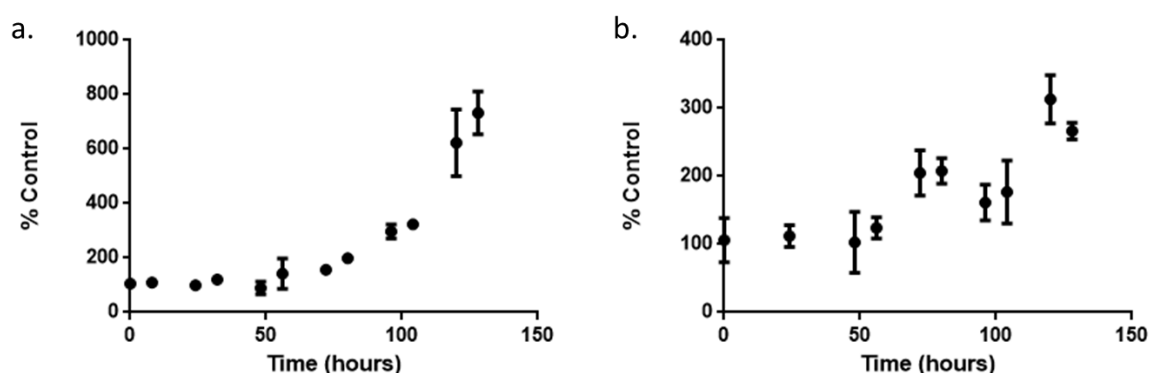


**Figure 88:** Effect on PrP<sup>Sc</sup> levels in SMB cells when dosed with MG132 3 μM over 128 hours (6 days). a. and b. show two independent experiments. PrP<sup>Sc</sup> levels start to rise after 48 hours. Further repeats of the time course showed PrP<sup>Sc</sup> levels beginning to rise at the same time, but the total PrP<sup>Sc</sup> accumulation observed after 128 hours varied between 300 % of control (as seen in b) and 800 % of control (as seen in a). The data points shown represent the mean ± SD values from a single experiment where each sample was analysed in triplicate.

As in the previous experiments it is clear that dosing the SMB cells with 3 μM MG132 causes significant, although not always consistent, rises in the levels of PrP<sup>Sc</sup>, without any associated toxicity (see **Figure 88**). PrP<sup>Sc</sup> does not start to accumulate immediately, with the observed lag phase of around 48 hours suggesting that other systems can compensate for the effects of MG132 inhibition for a limited period. A previous study found a large increase in PrP<sup>Sc</sup> aggregates in ScN2a cells after 16 hours of MG132 treatment, suggesting the SMB cells may be

less sensitive to MG132 inhibition.<sup>(179)</sup> While accompanying MTT assays weren't carried out in this specific instance, no signs of toxicity or imminent cell death were visible by eye before cell lysis. This is in agreement with the low cytotoxicity of MG132 at 3  $\mu$ M (see **Figure 85**).

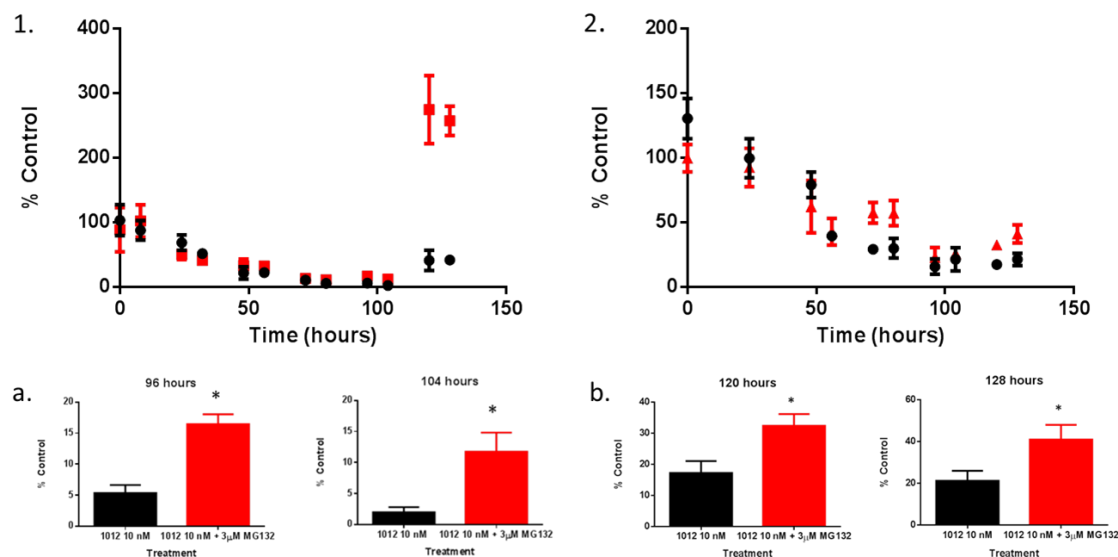


**Figure 89:** Time course effect on PrP<sup>Sc</sup> levels in SMB cells treated with 3001012 at 10 nM co-dosed with MG132 at 3  $\mu$ M. Drug treatment was assessed over a time course of 0 – 128 hours in Experiments 1 and 2. Each data point represents the mean  $\pm$  SD values from a single experiment where each sample was analysed in triplicate. Data points in black show the effect of 3001012 alone; data points in red show the effect of 3001012 co-dosed with MG132. (a) Statistical analysis of Experiment 1 using multiple t-test shows that at the 96 and 104 hour time points the effect of 3001012 alone or 3001012 co-dosed with MG132 is statistically different ( $p < 0.001$  in both cases). (b) Statistical analysis of Experiment 2 using multiple t-test shows that at the 120 hour and 128 hour time points the effect of 3001012 alone or 3001012 co-dosed with MG132 is significantly different ( $p < 0.001$  in both cases).

It can be seen in **Figure 89** that the time course of 3001012 is not affected by co-dosing with MG132. No increase in PrP<sup>Sc</sup> levels above normal was observed, suggesting that 3001012 is able to prevent MG132-induced PrP<sup>Sc</sup> accumulation. The data from experiments one and two in **Figure 89** would seem to suggest that at the final time points the effect of MG132 has more of an inhibitory effect on the activity of 3001012 than it does at earlier time points, with increased MG132 activity and decreased 3001012 efficacy seen from 96 hours in one case and 120 hours in the other.

To determine whether the antagonism of MG132 activity was a feature of all I3GA compounds, or specific to 3001012, MG132 was co-dosed with two other I3GA compounds (3001207 and 3001086) to see if the same pattern was observed. Statistical analysis was also carried out on the

final time points to determine if the differences as a result of the two treatments were significant.

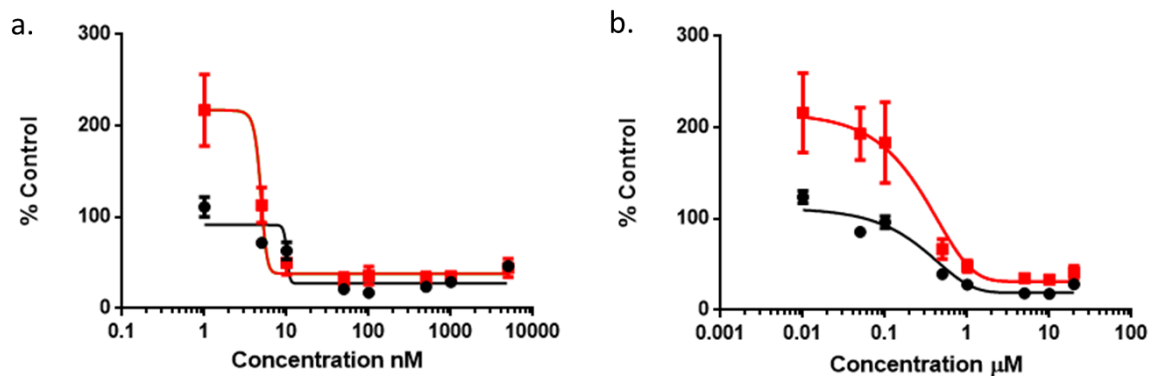


**Figure 90:** Effect on PrP<sup>Sc</sup> levels in SMB cells when treated with a. 3001207 and b. 3001086. Black lines indicates the compound on its own, the red line indicates the compound co-dosed with 3 μM MG132. Cells were dosed for 5 days. The data points shown represent the mean ± SD values from triplicate experiments where each sample was analysed in triplicate.

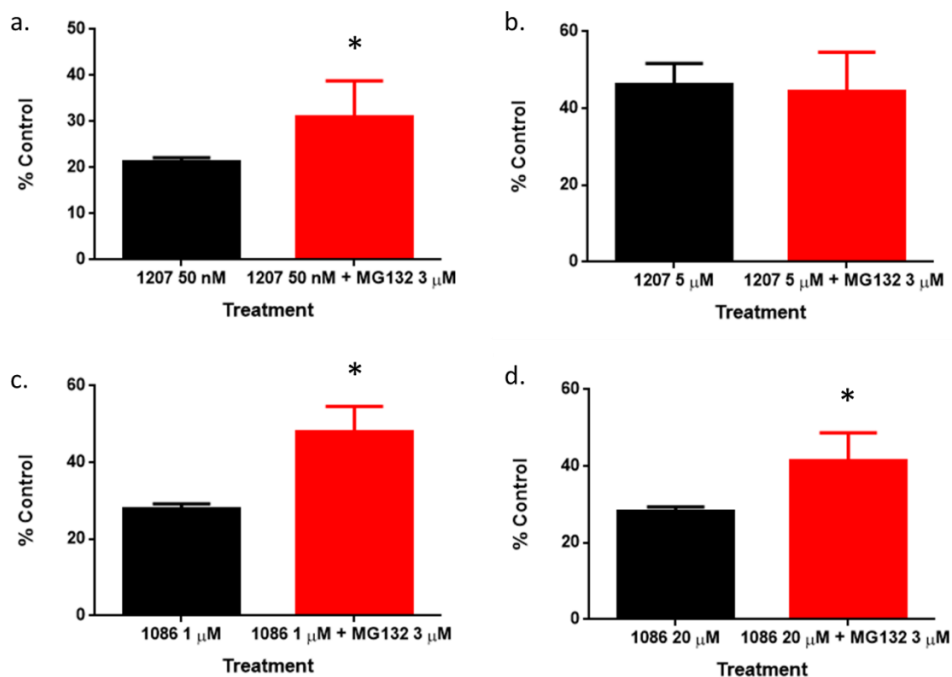


**Figure 91:** Statistical analysis of the data for the lowest and highest active concentrations of 3001207 and 3001086. T-tests were carried out comparing cells dosed with the I3GA on its own to cells co-dosed with MG132 at 3 μM and a concentration gradient of the I3GA. 3001207 only showed a significant difference at 50 nM ( $p = 0.00194683$ ,  $n = 9$ ), while 3001086 showed a significant difference at both 1 μM and 20 μM ( $p < 0.001$ ,  $n = 9$  for both). The data points shown represent the mean ± SD values from triplicate experiments where each sample was analysed in triplicate.

Examination of the data in **Figure 90** and **Figure 91** does suggest that the effect of MG132 on the activity of 3001207 and 3001086 is not as pronounced as it is with 3001012, particularly in comparison to **Figure 86c**. However, the same pattern was seen, with PrP<sup>Sc</sup> levels being significantly higher than normal at sub-active I3GA concentrations, rapidly decreasing around EC<sub>50</sub> concentrations and then plateauing at the higher concentrations at slightly higher than normal levels, with this behaviour suggesting that clearance has been inhibited. Clearance efficiency was also affected to a statistically significant degree in some cases.

These co-dosing experiments were also carried out using a fixed, active concentration of the I3GA compound and a concentration gradient of MG132. MG132 was only used at known sub-toxic concentrations to avoid any toxicity related effects. These experiments were carried out to help elucidate further the mutual antagonism of MG132 and the I3GA compounds.

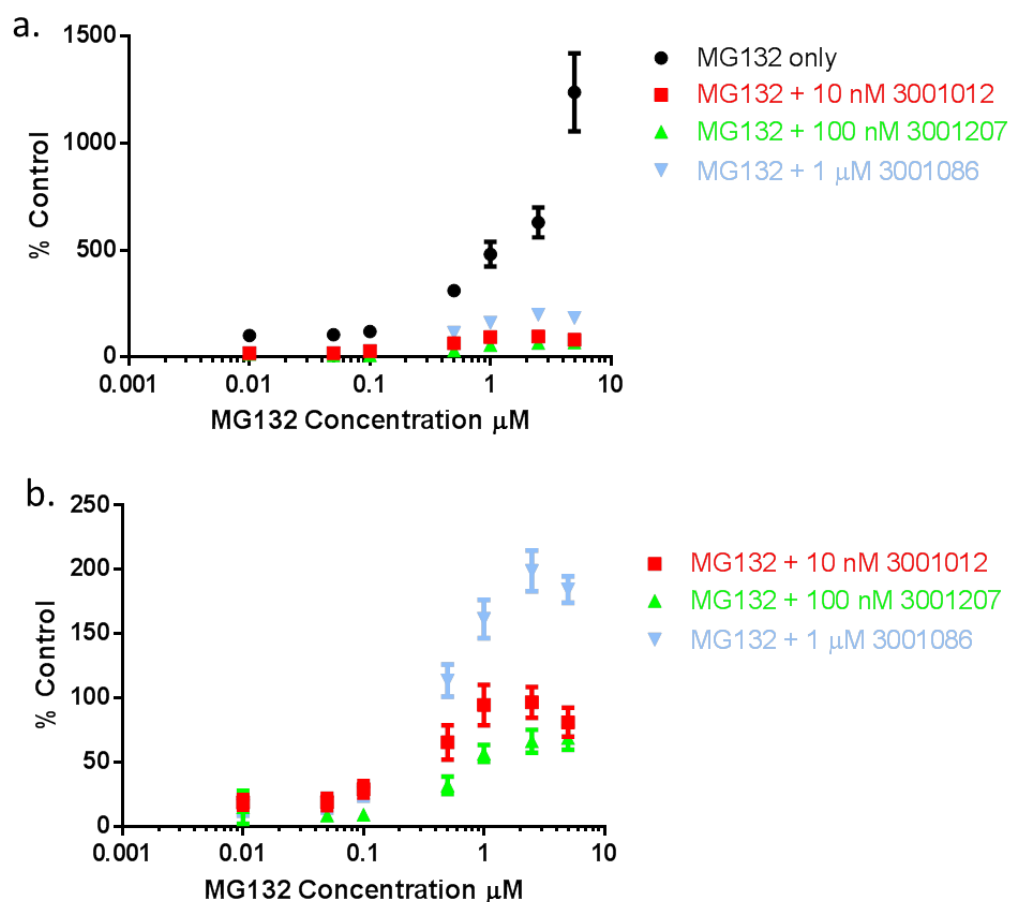


**Figure 92:** Data showing the effect of a fixed concentration of 3001012, 3001207 and 3001086 on MG132 activity; a. shows the co-dosed results in comparison to MG132 on its own, while b. shows the co-dosed results only for greater clarity. The x-axis gives the concentration of MG132. The data points shown represent the mean  $\pm$  SD values from duplicate experiments where each sample was analysed in triplicate.

The data in **Figure 92** clearly show that co-dosing with the I3GA compounds mitigates the accumulation of PrP<sup>Sc</sup> that is observed when the cells are treated with MG132 on its own. Although PrP<sup>Sc</sup> levels are still rising at the active concentrations of MG132 they are not rising to anywhere near the levels seen for MG132 only. This suggests that the I3GAs can compensate for a certain amount of inhibition, but at the higher MG132 concentrations they are less efficient at antagonising the effects of MG132. These data also show that MG132 is able to induce an increase in PrP<sup>Sc</sup> in the presence of the I3GAs, in a dose-dependent manner.

In conclusion, the studies with MG132 have clearly shown that inhibition of the protein degradation systems results in an increase in levels of PrP<sup>Sc</sup>, with associated toxicity being observed at higher concentrations. Co-dosing MG132 with the I3GA compounds mitigates this PrP<sup>Sc</sup> increase, with the I3GA compounds still active at a similar EC<sub>50</sub> to that observed when dosed alone. A decrease in efficacy was noted, with PrP<sup>Sc</sup> being cleared to a lesser extent when co-dosed with MG132. This effect appeared to be more pronounced when 3001012 was the I3GA in question, but statistically significant differences in the clearance of 3001207 and 3001086 when dosed alone or with MG132 were observed. Co-dosing a concentration gradient of MG132 with the I3GAs still resulted in a dose-dependent increase in PrP<sup>Sc</sup> levels, but the extent of the increase was massively reduced compared to MG132 alone. Time course analysis suggests that the I3GAs are able to prevent the PrP<sup>Sc</sup> accumulation induced by MG132 treatment. It can be seen in **Figure 88** that it takes around 56 hours for PrP<sup>Sc</sup> levels to start to rise. This correlates well with the time taken for the I3GAs to reduce PrP<sup>Sc</sup> to a minimum level and it would appear that this is enough to prevent MG132-induced accumulation. The toxicity observed as a result of treatment with MG132 at high concentrations suggests that inhibition of the degradation pathways is dose-dependent, and that a certain amount of inhibition can be tolerated. However, complete inhibition of both the proteasome and LCPs above this level is clearly cytotoxic.

#### **6.2.2.2. Lactacystin**

The co-dosing experiments were subsequently repeated using lactacystin as the inhibitor. Again, this was screened on its own to establish its effect on PrP<sup>Sc</sup> accumulation, and was then co-dosed with the same I3GAs as before to show the effect of proteasomal inhibition on their activity.

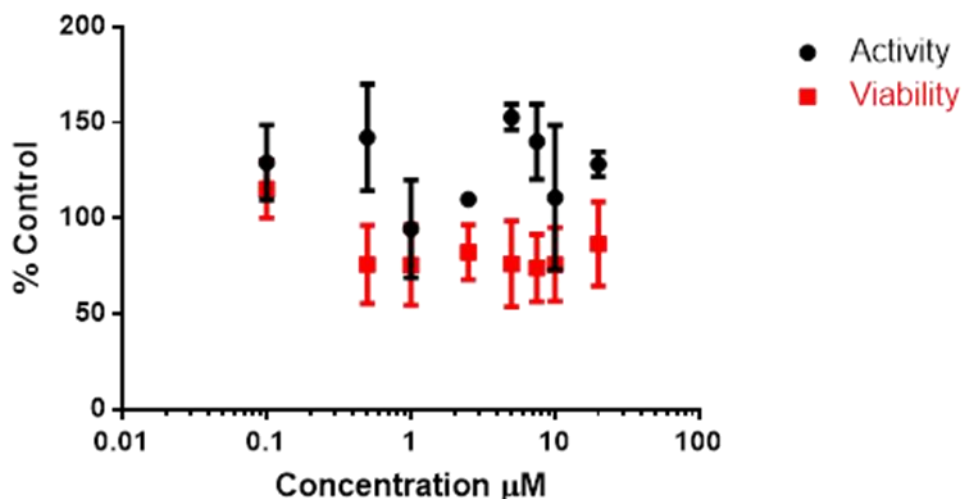


**Figure 93:** PrP<sup>Sc</sup> levels in SMB cells after dosing with lactacystin at concentrations ranging from 0.1 µM to 20 µM. No significant effect was seen on either PrP<sup>Sc</sup> levels or cell viability. The data points shown represent the mean ± SD values from duplicate experiments where each sample was analysed in triplicate.

As can be seen in **Figure 93** lactacystin does not have any effect on PrP<sup>Sc</sup> levels. No toxicity was observed at the highest concentrations. As there was no obvious increase in PrP<sup>Sc</sup> levels it was not possible to estimate active concentrations using the data from lactacystin in isolation. As there was no apparent toxicity at higher concentrations it was decided to use the highest practical concentration, which was 10 µM.

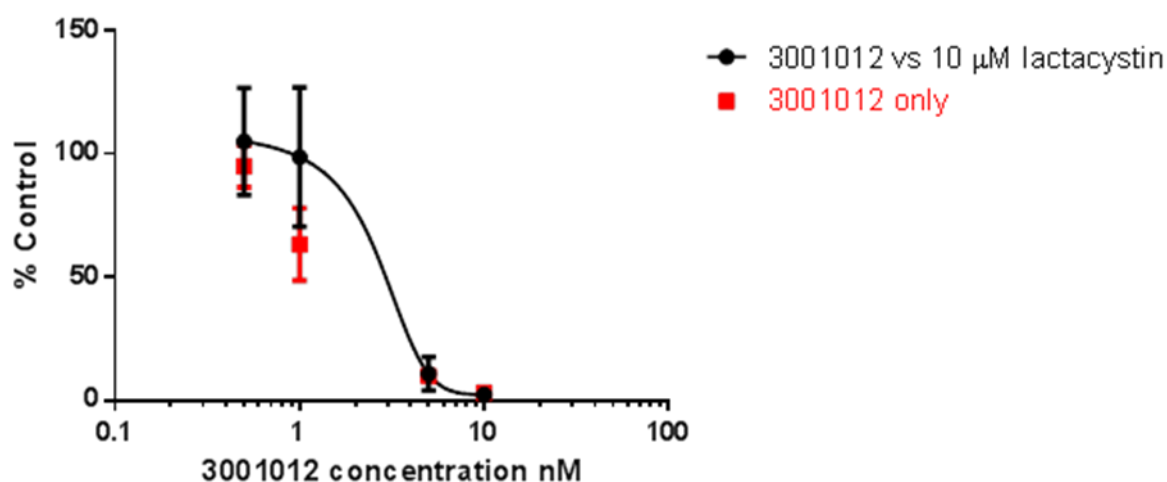


**Figure 94:** Data showing the effect of lactacystin on 3001012 activity as measured by PrP<sup>Sc</sup> clearance. The black curve indicates 3001012 on its own at concentrations between 0.1 nM and 10 nM. The red data indicates 3001012 at the same concentrations but co-dosed with 10 µM lactacystin – a curve could not be fitted to these data. The data points shown represent the mean ± SD values from duplicate experiments where each sample was analysed in triplicate.

Due to compound availability this co-dosing experiment was done at a more limited range of concentrations than normal. However, statistical analysis by t-test of all data points showed no significant difference between any of the data points suggesting no significant effect of lactacystin on 3001012 activity (statistical analysis data not shown).

### 6.2.2.3. E64

As discussed in section 6.2.1, inhibitors of the LCPs were also investigated to clarify whether inhibition of the proteasome or the LCPs was causing the PrP<sup>Sc</sup> increase observed when the cells were dosed with MG132. As direct, specific inhibition of the proteasome using lactacystin had not resulted in PrP<sup>Sc</sup> increases, it was hypothesised that the increases may be due to the inhibition of LCPs, a known effect of MG132. To investigate this further, the effect on PrP<sup>Sc</sup> levels and I3GA activity of two lysosomal protease inhibitors, E64 and Cl3 were investigated. As before, initial studies looked at their effect in isolation, before considering their effect on the activity of the three I3GA compounds.

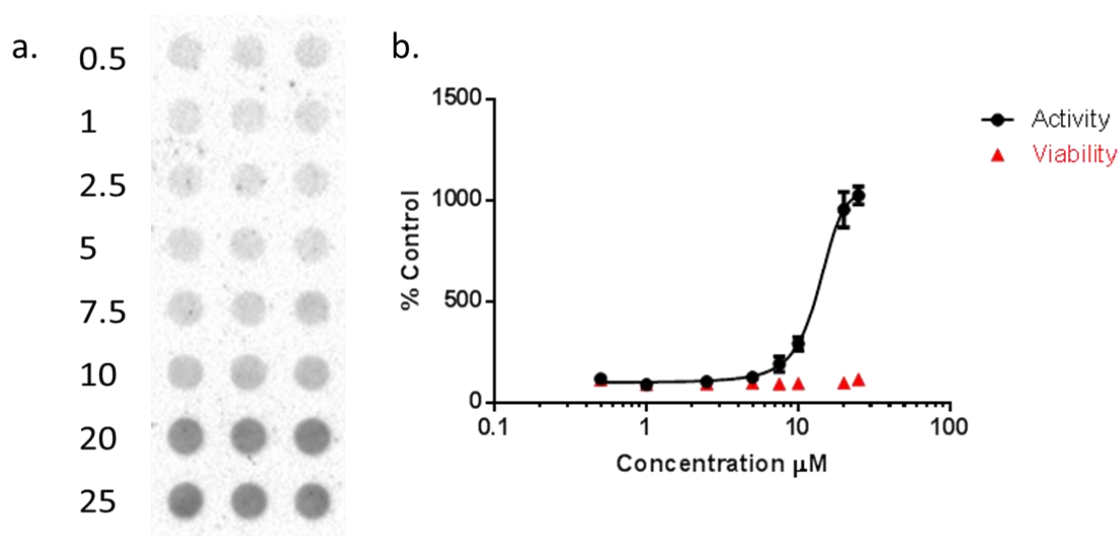


**Figure 95:** PrP<sup>Sc</sup> levels in SMB cells after dosing with E64 at a range of concentrations from 0.5 µM to 25 µM. Each concentration is dosed in triplicate. (a) demonstrates the increased amount of PrP<sup>Sc</sup> as indicated by the darker spots, while (b) shows the IOD values for those spots as a percentage of the untreated control. Figures down the left of (a) indicate the E64 concentration in µM. The data points shown represent the mean ± SD values from duplicate experiments where each sample was analysed in triplicate.

As can be seen in **Figure 95**, E64 caused a large rise in PrP<sup>Sc</sup> at slightly higher concentrations than MG132, with levels starting to rise from around 5µM. Unlike MG132 no toxicity was observed at the higher concentrations. On the basis of this it was decided to run the competition experiments using E64 at both 10 µM and 20 µM to see if different levels of clearance were

observed. E64 at 10  $\mu\text{M}$  caused an increase in PrP<sup>Sc</sup> levels of around 300 %, while E64 at 20  $\mu\text{M}$  caused an increase in PrP<sup>Sc</sup> levels of nearly 1000 %.

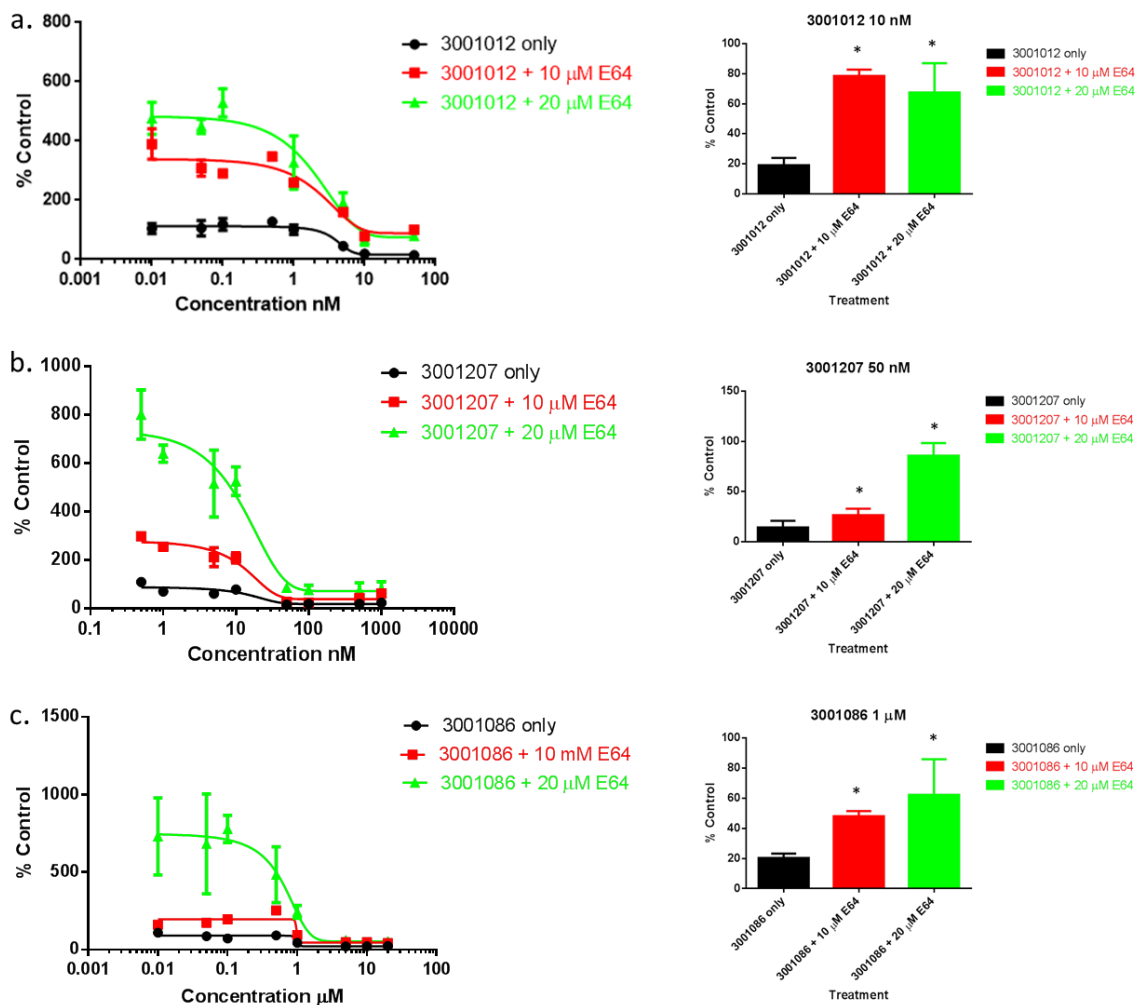


**Figure 96:** The effect of two different concentrations of E64 on the activity of 3001012 (a), 3001207 (b) and 3001086 (c). Bar graphs show the data for the I3GA only, and the I3GA with 10 or 20  $\mu\text{M}$  E64 at the lowest concentration where clearance occurs when the compound is dosed on its own. Stars indicate if the difference in clearance is statistically significant. Apart from 3001207 with 10  $\mu\text{M}$  E64 ( $p = 0.00882755$ ) in all cases  $p = <0.001$ . The data points shown represent the mean  $\pm$  SD values from duplicate experiments where each sample was analysed in triplicate.

**Table 43:** EC<sub>50</sub> values for the I3GAs on their own or co-dosed with two different concentrations of E64 calculated from the data presented in **Figure 96**

| I3GA    | Estimated EC <sub>50</sub> value (nM) |                  |                  |
|---------|---------------------------------------|------------------|------------------|
|         | I3GA only                             | I3GA + 10 μM E64 | I3GA + 20 μM E64 |
| 3001012 | 4                                     | 4                | 3                |
| 3001207 | 25                                    | 25               | 25               |
| 3001086 | 750                                   | 750              | 750              |

It can be seen in **Figure 96** that in all cases co-dosing the I3GAs with E64 results in a statistically significant reduction in clearance efficiency, measured at the lowest concentration at which full clearance occurs. However, this reduced efficiency did not result in a significant reduction in EC<sub>50</sub> values, as can be seen in **Table 43**.

Subsequent experiments co-dosed a concentration gradient of E64 with a fixed concentration of the I3GA compounds.

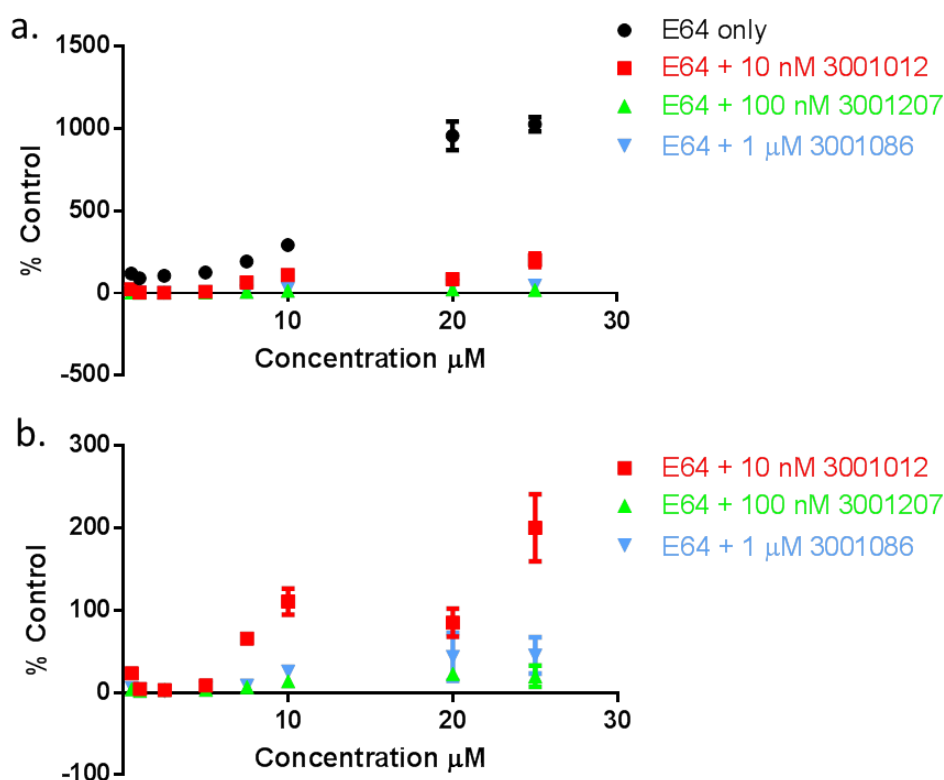


**Figure 97:** The effect of a fixed concentration of 3001012, 3001207 and 3001086 on E64 activity; a. shows the co-dosed results in comparison to E64 on its own, while b. shows the co-dosed results only for greater clarity. The x-axis gives the concentration of E64. All compounds are able to prevent the accumulation of PrP<sup>Sc</sup> induced by E64, with the activity of 3001012 being affected to the greatest degree. The data points shown represent the mean ± SD values from duplicate experiments where each sample was analysed in triplicate.

The data presented in **Figure 97** shows a similar pattern to the MG132 data (see **Figure 92**), with the I3GAs able to mitigate the increases seen as a result of the inhibition, but with clearance efficiency still being reduced in the case of 3001012. Increased concentrations of inhibitor resulted in a dose dependent increase in PrP<sup>Sc</sup> levels, again suggesting that an excess concentration of inhibitor is important. The E64 data presented here suggests that the activity of 3001012 is impaired to a higher degree than the other I3GA compounds, although this is not replicated by the MG132 data.

In conclusion it can be seen that treating the cells with E64 results in a similar pattern to that seen when the cells are dosed with MG132, although there are some notable differences. E64 did not show any associated toxicity, and it was therefore possible to use it at much higher concentrations. Consequently, the PrP<sup>Sc</sup> accumulation that could be induced with E64 was much higher than that induced by the sub-toxic concentrations of MG132. However, MG132 was active at lower concentrations. The I3GA compounds are capable of preventing the accumulation of PrP<sup>Sc</sup> caused by E64, with co-dosing reducing the clearance efficiency of the compounds without affecting the EC<sub>50</sub> values. As with MG132, a dose-response was seen with increasing concentrations of E64 causing increased inhibition of I3GA activity up to a certain point. The reverse was not seen, with an excess of I3GA not resulting in any improvement in clearance efficiency. Comparison of the E64 data presented here with the lactacystin data suggests that the observed increase in PrP<sup>Sc</sup> levels is likely to be induced by inhibition of the LCPs, rather than the proteasome itself.

#### **6.2.2.4. Cathepsin Inhibitor III (CI3)**

The final inhibitor to be used in these co-dosing experiments was CI3, which selectively inhibits cathepsins B, L and S as well as papain. This was used to reveal further information about whether a specific cathepsin might be responsible for the PrP<sup>Sc</sup> accumulation seen as a result of treatment with MG132 and E64. As with the other inhibitors it was first dosed on its own to assess its effect on PrP<sup>Sc</sup> levels, before being co-dosed with the I3GAs.

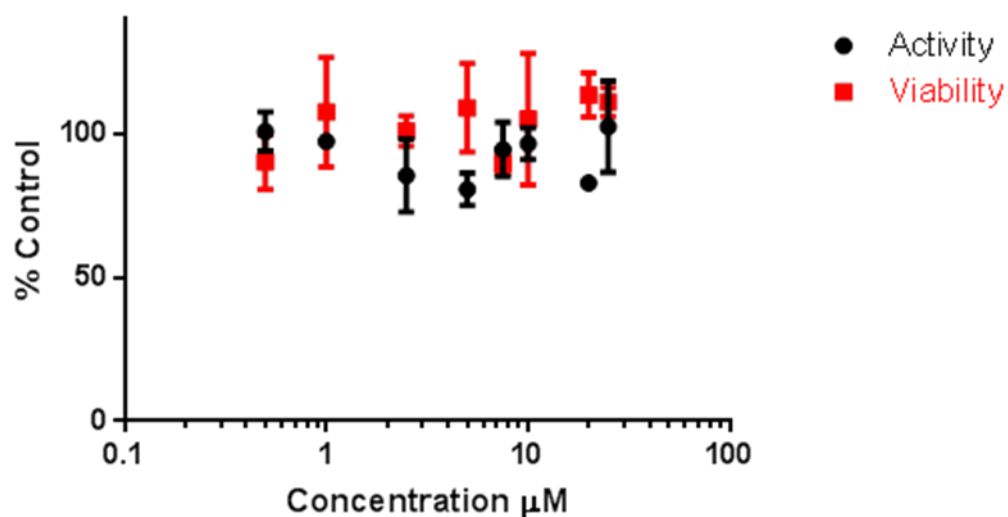


**Figure 98:** PrP<sup>Sc</sup> levels in SMB cells after dosing with CI3 at a range of concentrations from 0.5 μM to 25 μM. No effect was observed on either PrP<sup>Sc</sup> levels (activity) or viability. The data points shown represent the mean ± SD values from duplicate experiments where each sample was analysed in triplicate.

It can be seen in **Figure 98** that, like lactacystin, CI3 did not cause any significant changes in PrP<sup>Sc</sup> levels over the range of concentrations used. This suggests that none of the cathepsins that are inhibited by CI3 have an important role in PrP<sup>Sc</sup> homeostasis. No toxicity was observed at any concentration. As with lactacystin it was not possible to estimate active concentrations using the data from the compound in isolation so again the highest practical concentration, 10 μM, was used.

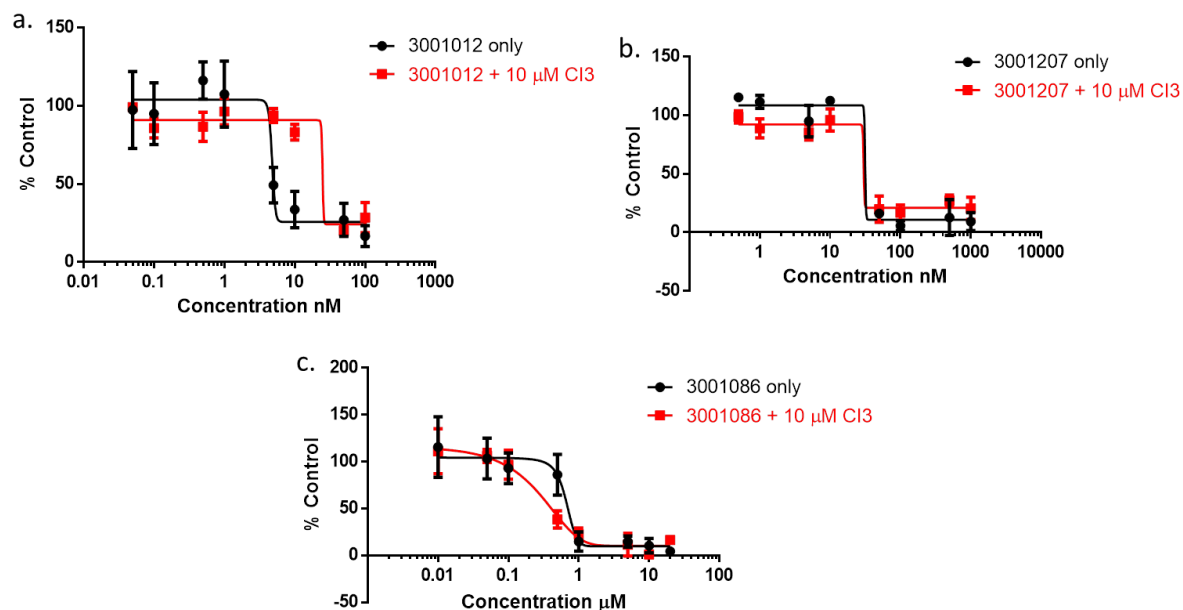


**Figure 99:** The effect of Cl3 at 10 μM on the activity of 3001012 (a), 3001207 (b) and 3001086 (c). Co-dosing with Cl3 results in a decrease of the activity of 3001012 and an improvement in the activity of 3001086, but has no effect on the activity of 3001207. The data, as indicated by PrP<sup>Sc</sup> clearance, is unaffected by treatment. The data points shown represent the mean ± SD values from duplicate experiments where each sample was analysed in triplicate.

**Table 44:** EC<sub>50</sub> values for the I3GAs on their own or co-dosed with Cl3, calculated from the data presented Estimated EC<sub>50</sub> values for the data presented **Figure 99**

| I3GA    | Estimated EC <sub>50</sub> value (nM) |                  |
|---------|---------------------------------------|------------------|
|         | I3GA only                             | I3GA + 10 μM Cl3 |
| 3001012 | 4                                     | 25               |
| 3001207 | 25                                    | 25               |
| 3001086 | 750                                   | 400              |

Even though Cl3 did not have any effect on PrP<sup>Sc</sup> levels it can be seen that there are shifts in the EC<sub>50</sub>s of 3001012 and 3001086 when co-dosed with 10 μM Cl3 (see **Figure 99** and **Table 44**). The EC<sub>50</sub> for 3001012 has increased from approximately 4 nM to 25 nM, and this was found to be a reproducible effect. The EC<sub>50</sub> for 3001086 has decreased slightly, shifting from 0.75 μM to around 0.4 μM, however the small magnitude of the shift and the error observed cast doubt on the significance of this. No change was observed in the EC<sub>50</sub> of 3001207.

Subsequent experiments co-dosed a concentration gradient of CI3 with a fixed concentration of the I3GA compound.

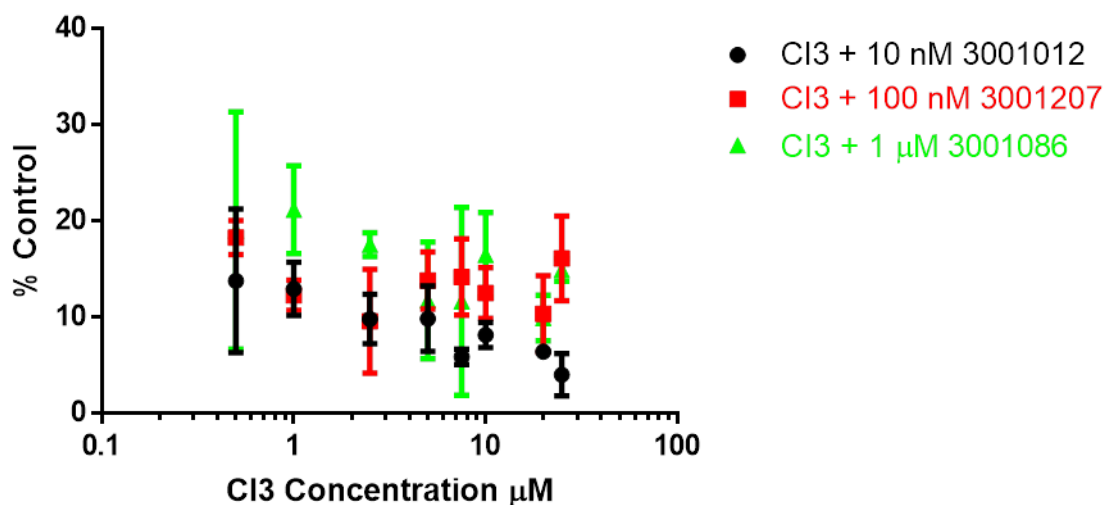


**Figure 100:** The effect of a CI3 concentration gradient on a fixed concentration of 3001012, 3001207 and 3001086. There is no observable change in the activities of the I3GA compounds at their active concentrations. The data points shown represent the mean  $\pm$  SD values from duplicate experiments where each sample was analysed in triplicate.

Co-dosing a fixed concentration of the I3GA compound with a concentration gradient of CI3, as shown in **Figure 100**, had no effect on the activity of the I3GA compounds with clearance comparable to when the compounds are dosed in isolation at these concentrations.

#### 6.2.2.5. Negative Controls

In an attempt to further elucidate the role of the I3GA compounds in antagonising the activity of the inhibitors, the same competition assays were carried out with compounds that had similar effects to either the I3GAs or the inhibitors but without affecting the proteasome or LCPs. During the studies of anti-prion compounds from the literature (see section **4.4.2**), congo red was found to cause a large increase in PrP<sup>Sc</sup> levels at certain concentrations (discussed in **4.4.2.2**). Although analogues of congo red have been shown to work by increasing PrP<sup>Sc</sup> degradation by the proteasome,<sup>(220)</sup> there is no evidence that congo red itself has a direct effect on the proteasome or the LCPs. The I3GA compounds were co-dosed with congo red in place of the inhibitors to see if the rise in PrP<sup>Sc</sup> levels was still diminished. Quinacrine, an anti-prion compound with an established mode of action (see section **4.4.3.2**), was co-dosed with MG132 and E64 to see if a similar effect was observed with a compound not associated with the proteasome or lysosomal proteases.

Experiments were carried out as before, with congo red used at 1  $\mu\text{M}$  (see **Figure 59**) and quinacrine used at 5  $\mu\text{M}$ .

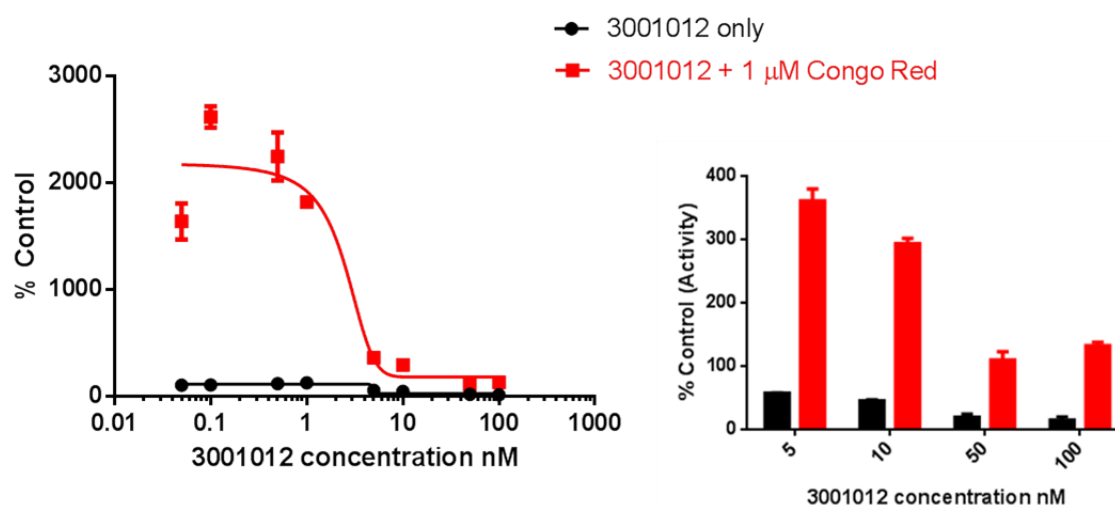


**Figure 101:** PrP<sup>Sc</sup> levels in cells dosed with either 3001012 or co-dosed with 3001012 and 1  $\mu\text{M}$  congo red. At sub-active concentrations of 3001012 (<5 nM in this instance) very high levels of PrP<sup>Sc</sup> are observed, consistent with congo red dosed on its own. This rise in PrP<sup>Sc</sup> levels is reduced at higher levels of 3001012. Bar chart shows the data from the active concentrations of 3001012 for clarity. The data points shown represent the mean  $\pm$  SD values from duplicate experiments where each sample was analysed in triplicate.

The data in **Figure 101** shows a similar pattern to that seen when the I3GAs were co-dosed with E64 and MG132. The biggest difference is that at sub-active I3GA concentrations, the increase in PrP<sup>Sc</sup> seen as a result of congo red treatment is far bigger than seen with either E64 or MG132. The active concentrations of 3001012 are able to mitigate the majority of this increase, but the clearance efficiency is significantly reduced. Even at 50 and 100 nM 3001012, PrP<sup>Sc</sup> levels are only reduced to around 100 % of the control. This suggests that the addition of the I3GA compound is able to counteract the congo red induced accumulation of PrP<sup>Sc</sup>, but is not able to totally cure the cells. It is therefore possible that congo red in some way inhibits the normal mode of action of 3001012, possibly through the direct interaction of congo red with both forms of PrP. It is also possible that the failure of 3001012 to totally mitigate the effects of congo red was simply due to the very high excess levels of PrP<sup>Sc</sup> being produced. An interesting observation is that the cells were seemingly able to tolerate this massive accumulation of PrP<sup>Sc</sup>, as no toxicity was associated with congo red treatment.

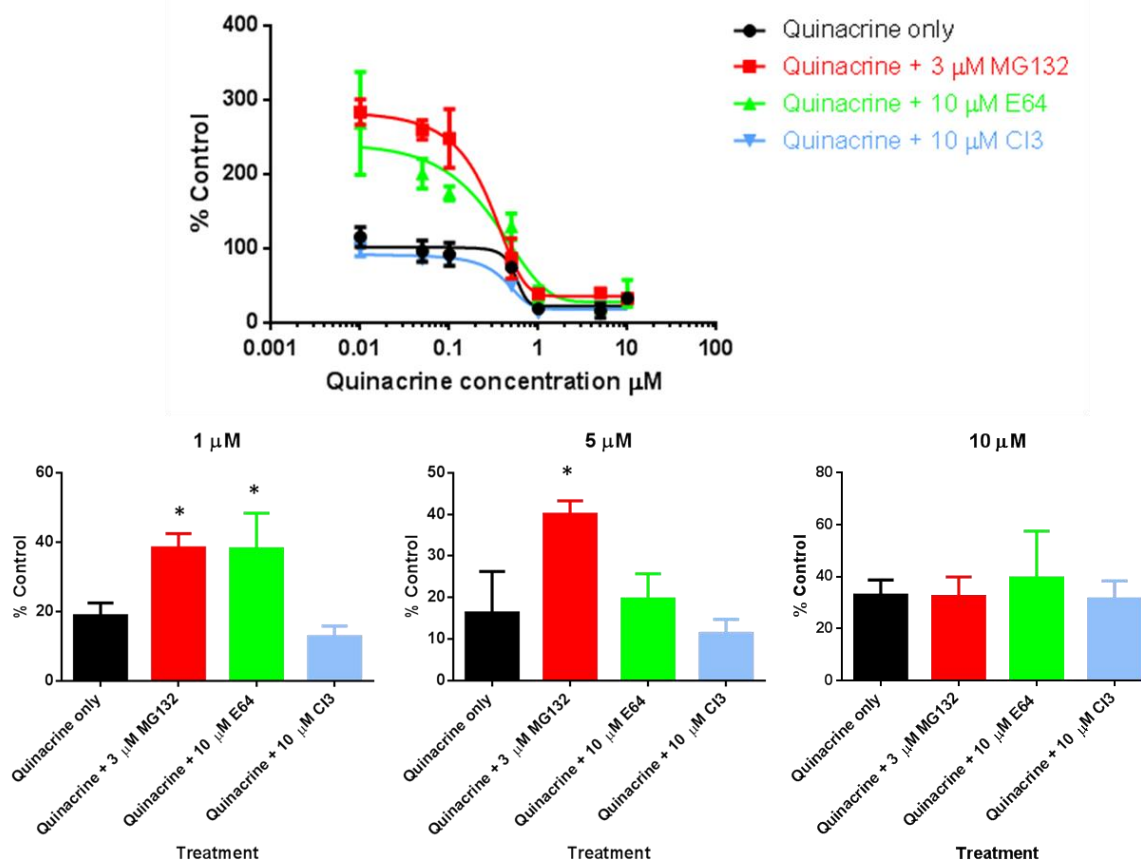


**Figure 102:** Effect on PrP<sup>Sc</sup> levels when a concentration gradient of quinacrine was dosed either on its own or with MG132, E64 or CI3. Bar graphs show data for quinacrine at 1 μM, 5 μM and 10 μM, with stars indicating statistically significant differences from quinacrine on its own. Statistically significant differences were found for quinacrine at 1 μM with MG132 ( $p = 0.000221874$ ) and E64 ( $p = 0.0173923$ ) and for quinacrine at 5 μM with MG132 ( $p = 0.000796993$ ). The data points shown represent the mean  $\pm$  SD values from duplicate experiments where each sample was analysed in triplicate.

**Table 45:** EC<sub>50</sub> values for quinacrine on its own or co-dosed with MG132, E64 or CI3, calculated from the data presented in Figure 102

| Treatment       | Estimated EC <sub>50</sub> value (μM) |
|-----------------|---------------------------------------|
| Quinacrine only | 0.7                                   |
| + 3 μM MG132    | 0.5                                   |
| + 10 μM E64     | 0.4                                   |
| + 10 μM CI3     | 0.4                                   |

The data presented in Figure 102 and Table 45 shows a similar pattern to that seen with the I3GAs. Quinacrine is able to mitigate the increase in PrP<sup>Sc</sup> caused by MG132 and E64, with

clearance efficiency being reduced to a significant degree at 1  $\mu\text{M}$ . Although there was no advantage to increasing the concentration of the I3GAs, statistical analysis suggests that increasing the concentration of quinacrine restores full clearance efficiency, although at 10  $\mu\text{M}$  this would appear to be the result of a slight increase in baseline levels of PrP<sup>Sc</sup> in cells treated with quinacrine only. Treatment with all three inhibitors appears to decrease the EC<sub>50</sub> of quinacrine slightly, although the significance of this remains ambiguous.

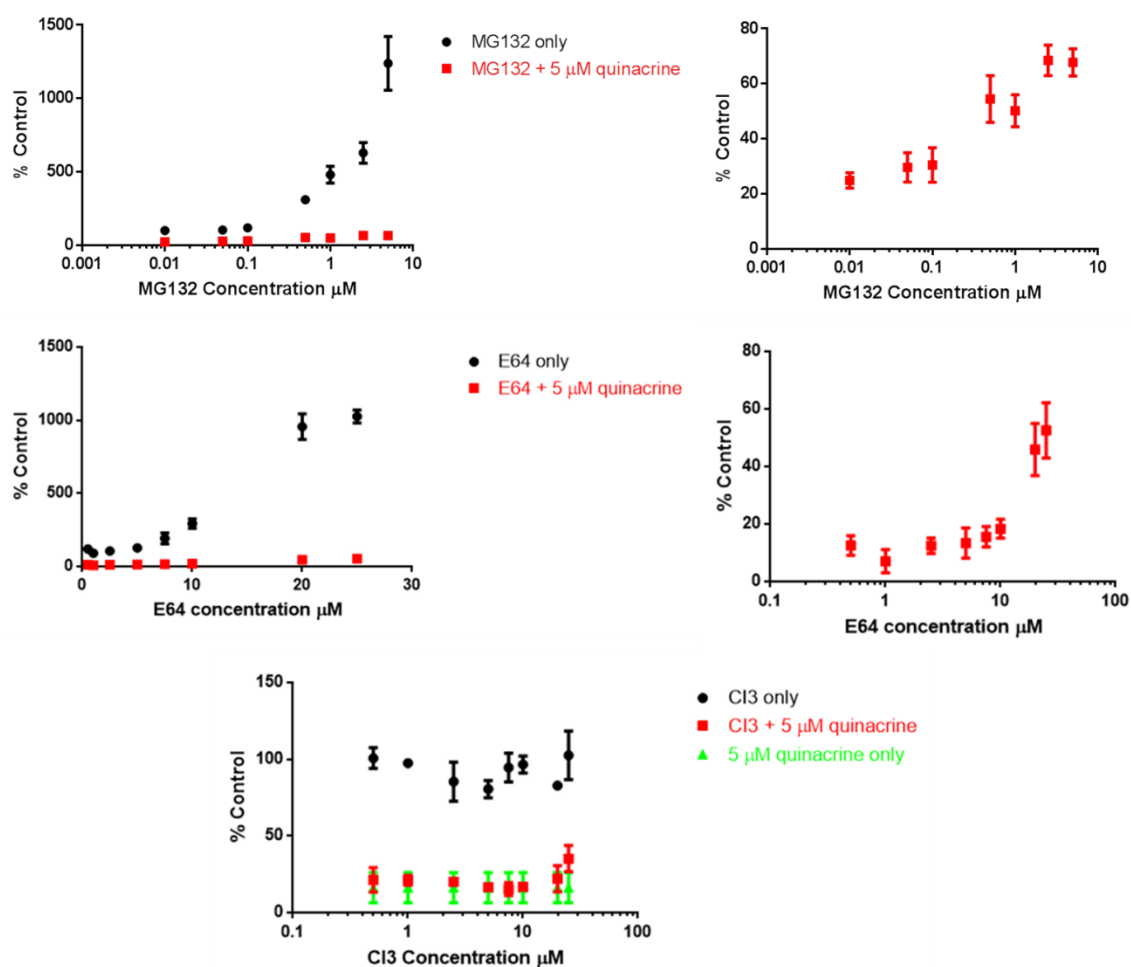


**Figure 103:** Effect on PrP<sup>Sc</sup> levels when MG132 (a), E64 (b) and CI3 (c) were co-dosed with quinacrine. For MG132 and E64 the graph on the right shows the curve for the co-dosed cells only for clarity. The data for CI3 also includes quinacrine on its own at 5  $\mu\text{M}$  for comparison. The difference between quinacrine only and quinacrine with CI3 at 25  $\mu\text{M}$  was not statistically significant (t-test,  $p = 0.0673633$ ). The data points shown represent the mean  $\pm$  SD values from duplicate experiments where each sample was analysed in triplicate.

The effect of co-dosing quinacrine against a concentration gradient of the different inhibitors, as shown in **Figure 103** was similar to that seen with the I3GAs, with the presence of the anti-prion compound dramatically decreasing the magnitude of the increase in PrP<sup>Sc</sup> seen when the

inhibitors were dosed on their own. The slight increase in PrP<sup>Sc</sup> levels as inhibitor concentration increased was also observed. A slight increase in PrP<sup>Sc</sup> levels was observed at the highest concentration of CI3, 25 µM, when a concentration gradient of CI3 was co-dosed with 5 µM quinacrine, but this was not found to be statistically significant.

### 6.2.3. Discussion

In this study 4 different inhibitors of the protein degradation systems were used, and their effect on both steady state levels of PrP<sup>Sc</sup> and the activity of 3 different I3GA compounds was assessed through co-dosing experiments. Negative control experiments were carried out with congo red, which causes PrP<sup>Sc</sup> accumulation *via* a mechanism not associated with protein degradation, and quinacrine, which is known to have a mode of action unrelated to protein degradation.

#### 6.2.3.1. Effects of the Different Inhibitors

MG132 and E64 were the only inhibitors to cause PrP<sup>Sc</sup> accumulation (see **Figure 85** and **Figure 95**), and the correlation between the effects of MG132 and E64 suggest that it is the inhibition of LCPs which results in the increase in PrP<sup>Sc</sup>. This in turn suggests that lysosomal degradation has a crucial role to play in maintaining steady state levels of PrP<sup>Sc</sup> within this system. The lack of increase in PrP<sup>Sc</sup> levels seen as a result of treatment with lactacystin suggests that inhibition of just the proteasome does not have any effect on PrP<sup>Sc</sup> homeostasis although this may be because the proteasome is already inhibited. <sup>(220)</sup> This study by Webb *et al* showed that the proteasomal activity in the SMB cells was reduced by around 50 % compared to cured cells, so although the proteasome was inhibited it did retain some activity. It is possible that other systems, such as the LCPs, are compensating for the partial inhibition of the proteasome under normal circumstances, meaning that specific, total pharmaceutical inhibition of the proteasome by lactacystin is not a challenge to the cells. Partial inhibition of the cathepsins with CI3 was not enough to cause the same effects as total LCP inhibition. It can therefore be concluded that none of the cathepsins inhibited by CI3 are individually responsible for PrP<sup>Sc</sup> homeostasis. It may be that inhibition of some of the cathepsins can be compensated for by those that are unaffected, or that control rests with one (or more) of the uninhibited cathepsins.

It could be hypothesised that if inhibition of the LCPs results in PrP<sup>Sc</sup> accumulation, then their up-regulation may be part of a mechanism by which PrP<sup>Sc</sup> is cleared from the cells. However, the

role of LCPs and lysosomal degradation in prion disease is still ambiguous. Several anti-prion compounds have been shown to work by facilitating the transport of PrP<sup>Sc</sup> to the lysosomes, including cationic dendrimers,<sup>(229, 411)</sup> tyrosine kinase inhibitors,<sup>(237)</sup> chlorpromazine<sup>(238)</sup> and tamoxifen and its metabolites.<sup>(239)</sup> There is direct evidence that the induction of autophagy results in the degradation of PrP<sup>Sc</sup>, with rapamycin, lithium and trehalose, all initiators of autophagy, able to reduce PrP<sup>Sc</sup> *in vitro* and prolong disease incubation times *in vivo*.<sup>(259)</sup> There is also a precedent for MG132 and inhibitors of cathepsins B and L causing increased levels of PrP<sup>Sc</sup>.<sup>(179, 416)</sup> In contradiction to this, there is evidence that the cathepsins are actually involved in disease pathogenesis, with an imbalance of cathepsins being associated with neurodegenerative diseases including Alzheimer's and prion disease.<sup>(417-422)</sup> A study of ScN2a cells found that cathepsins B and L were upregulated in infected compared to uninfected cells, suggesting that they may be involved in PrP<sup>Sc</sup> formation *via* a second autocatalytic route.<sup>(418)</sup> Another study comparing the gene expression profile of infected and uninfected mouse brains found cathepsins S, H, C, D, Z and, to a lesser extent, B and L were upregulated.<sup>(417)</sup> Cathepsins have also been implicated in neuronal death.<sup>(423)</sup> However, despite the evidence above the exact role of cathepsins in prion disease remains to be determined.

From the data presented in section **6.2.2** it is thought likely that the lysosomes have a crucial role in the SMB cells in maintaining PrP<sup>Sc</sup> homeostasis, possibly by degrading a certain amount of the PrP<sup>Sc</sup> that is produced, but without ever being able to totally clear the cells of infection. Whether up-regulation of these processes is part of the mode of action of the I3GA compounds will be discussed in more detail in sections **6.2.3.2** and **6.2.3.3**. The toxicity of MG132 at higher concentrations, the lack of toxicity associated with the LCP inhibitors and lactacystin and the partial inhibition of the proteasome by PrP<sup>Sc</sup> suggest that the cells can withstand inhibition of one or other of the protein degradation pathways but not full inhibition of both. This makes it likely that the two systems may be able to compensate for each other if one is not functioning properly.

#### **6.2.3.2. Inhibitors vs 3001012**

It is clear from the data presented in section **6.2.2.1** that 3001012 is able to mitigate the rise in PrP<sup>Sc</sup> caused by MG132 and E64, although co-dosing with the inhibitors did reduce clearance efficiency without changing the EC<sub>50</sub>. An excess of 3001012 was not found to improve efficiency, while increasing concentrations of the inhibitors were shown to dose-dependently increase PrP<sup>Sc</sup> levels, even when co-dosed with 3001012. Direct inhibition of the proteasome with lactacystin

had no effect on 3001012 activity, while co-dosing with CI3 did shift the  $EC_{50}$ , suggesting that inhibition of certain cathepsins may antagonise the activity of 3001012. The delay observed in the time course analysis suggests that degradation pathways are able to cope with a certain amount of inhibition for a limited period of time. It was hypothesised that the toxicity observed as a result of treatment with MG132 was due to full inhibition of both the degradation pathways, suggesting that some degradative capacity may remain at the concentrations used. Co-dosing with 3001012 totally prevented the rise in PrP<sup>Sc</sup> levels, and it would appear that 3001012 is able to exert its effect before PrP<sup>Sc</sup> levels start to rise. This in turn suggests that the tipping point at which PrP<sup>Sc</sup> starts to accumulate is never reached.

The exact mechanism by which 3001012 is antagonising the effects of LCP inhibition is not clear. The original hypothesis was that 3001012 was upregulating the proteasome, so inhibition of the proteasome should have reduced the activity of 3001012. Evidence presented thus far suggests that it is the lysosomes, rather than the proteasome, which are the important pathway, so it could be suggested that 3001012 is acting by upregulating the LCPs. This would seem to be confirmed in part by the data, as E64 and MG132 do reduce the clearing efficiency of the compound. However, in most cases, 3001012 still retains the majority of its activity, and in all examples except CI3 the  $EC_{50}$  is not affected, suggesting that other pathways are likely to be affected by 3001012 as part of its mode of action. It is also possible that 3001012 has no effect on the LCPs, but compensates for the increases caused by the inhibitors *via* its normal mode of action. The clearance of PrP<sup>Sc</sup> by 3001012 occurs before the hypothetical tipping point at which PrP<sup>Sc</sup> starts to accumulate, suggesting that the presence of 3001012 simply prevents the degradation systems from becoming overwhelmed. The lower efficiency may simply be a consequence of the lowered degradative capacity of the cellular machinery. This possibility was examined further by investigations into other I3GA compounds and also through the use of negative controls with no known connection to the protein degradation pathways.

### **6.2.3.3. Inhibitors vs 3001207 and 3001086**

Two other I3GA compounds, 3001207 and 3001086 were used in co-dosing experiments (see section 6.2.2.1). The data for these compounds followed a similar trend to the 3001012 data, with efficacy affected to a smaller, though sometimes significant degree. Again, an excess of the I3GA was not beneficial, while the inhibitors were able to dose-dependently increase PrP<sup>Sc</sup> levels, even in the presence of the I3GA. As these compounds have a similar time course to

3001012 it is possible they are reducing PrP<sup>Sc</sup> levels to the point where LCP inhibition does not result in the other degradation systems becoming overwhelmed.

It can be seen that the data is not conclusive – although a more limited effect was seen on activity of 3001086 and 3001207, higher concentrations of MG132 in particular caused PrP<sup>Sc</sup> accumulation in the presence of the I3GAs. It is therefore possible that activation of the LCPs are part of the mode of action of all three compounds. The structural similarities between the three compounds (see **Figure 84**), as well as the tight SAR identified for the I3GA compounds, suggests that they should share a mode of action, although this assumption was called into question by the microarray and proteomics data. The hypothesis that the I3GAs work to reduce PrP<sup>Sc</sup> levels *via* a mechanism that is independent of the protein degradation systems, thereby preventing the degradation systems from becoming overwhelmed when inhibited, ties in with the time course data for all compounds. However, an impact on lysosomal function is something that cannot be discounted on the basis of this data, but it is thought unlikely that this would be the only pathway affected by treatment.

#### **6.2.3.4. Negative Control Experiments**

Negative control experiments with quinacrine and congo red were carried out to try and show whether the effects seen were as a result of direct interactions with the LCPs, or due to the anti-prion compounds compensating for PrP<sup>Sc</sup> accumulation *via* a more generic mechanism. Taken as a whole, the data shows a very similar pattern to the data obtained for the I3GAs and inhibitors. Congo red is thought to stimulate PrP<sup>Sc</sup> accumulation by acting as a scaffold for PrP<sup>Sc</sup> formation at low concentrations. <sup>(380)</sup> It therefore causes increases in PrP<sup>Sc</sup> without any effect on the protein degradation systems. 3001012 was shown to counteract this aggregation at active concentrations, although clearance to normal baseline levels was not observed. The mode of action of quinacrine has been investigated and has not been shown to have links to any of the protein degradation systems. However, it was still able to mitigate the accumulation of PrP<sup>Sc</sup> caused by MG132 and E64 with a limited, although in some cases significant, effect on efficacy. Unlike the I3GAs, an increase in quinacrine concentration increased clearance efficiency, again suggesting that quinacrine has a different mode of action to the I3GAs. The data would seem to suggest that the mitigation of the effects of inhibition is not necessarily related to some direct effect on the protein degradation systems, rather that the presence of a compound working to reduce PrP<sup>Sc</sup> levels allows the degradative pathways to continue to function when their activity is impaired or one of them is unable to function.

### **6.2.3.5. Overall Conclusions**

In summary, the data presented here shows the importance of the LCPs in maintaining steady state levels of PrP<sup>Sc</sup>. Direct inhibition of the proteasome does not have any effect on PrP<sup>Sc</sup> levels suggesting a secondary role in PrP<sup>Sc</sup> homeostasis. It is also possible that the inhibition of the proteasome by PrP<sup>Sc</sup>, resulting in a decrease in activity of at least 50 %, renders the inhibition of the proteasome using lactacystin or MG132 redundant. All the anti-prion compounds that were investigated were able to mitigate the effect of inhibition of the protein degradation pathways, and 3001012 was also able to mitigate the PrP<sup>Sc</sup> accumulation induced by congo red. The reduced clearance efficacy shown by 3001012 suggests that the activity of this compound is more sensitive to the presence of LCP inhibitors, and is possibly working in part by upregulating the activity of the lysosomes. However, a less pronounced effect was seen on the activity of the other I3GAs and it is likely that all these compounds share a mode of action. It is thought that if 3001012 is affecting the LCPs then this is likely to be a secondary effect rather than the primary mechanism for clearing the cells of infection. Based on the data presented in section 6.2.2, it would seem likely that the anti-prion compounds are counteracting the inhibitors by reducing PrP<sup>Sc</sup> levels before the alternative degradation systems become overwhelmed, allowing reduced levels of PrP<sup>Sc</sup> to be maintained with a more limited set of cellular machinery and preventing further conversion. The precise mechanism by which the compounds reduce PrP<sup>Sc</sup> remains to be determined, but preventing the tipping point at which the pathways become overwhelmed appears to be key to preventing PrP<sup>Sc</sup> accumulation as a result of inhibition of the protein degradation pathways.

## **6.3. HSP90 Validation**

### **6.3.1. Introduction**

As discussed previously it was hypothesised that the I3GA compounds might be exerting their anti-prion effect through some kind of manipulation of the proteasomal pathway. HSP90 was identified as being upregulated in the microarray after treatment with 3001012 and is known to be associated with the proteasomal activities. It was hoped that by probing for HSP90 levels using western blotting it might be possible to both validate the results of the microarray and

confirm that HSP90 levels, and by extension proteasomal function, are affected by treatment with the I3GAs. Materials and methods for this study are outlined in detail in sections 2.1.5 and 2.2.7.

### 6.3.2. Results

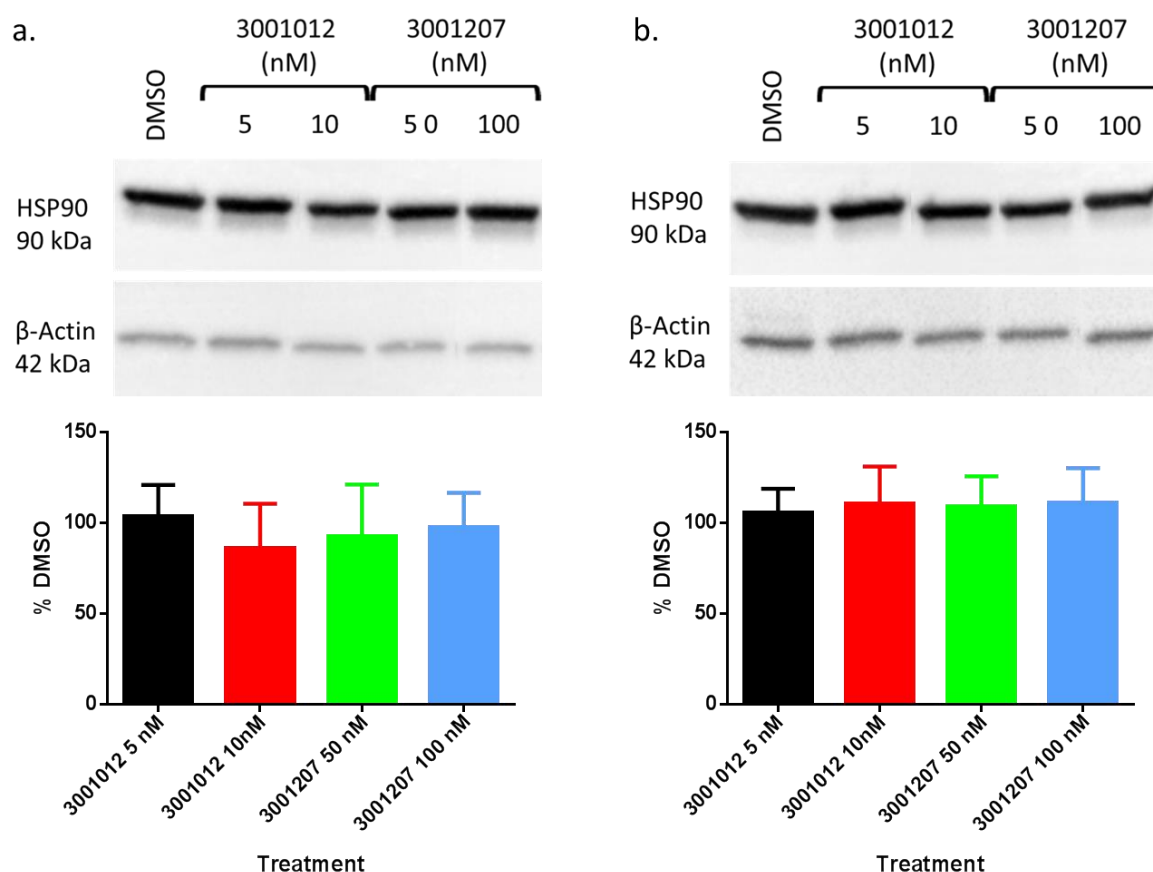


**Figure 104:** Western blots showing expression of HSP90 after a 5 day dose (a) and after a 56 hour dose (b). Graphs show HSP90 levels in treated cells from four biological replicates. Data was adjusted for loading difference and is presented as a percent of the DMSO control.

It is clear from the data in **Figure 104** that treatment with the I3GA compounds does not have any effect on the protein expression of HSP90, with no significant differences being found between the DMSO treated cells and the I3GA treated cells. Dot blots of samples dosed and prepared in the same way were run alongside the western blots and these confirmed that the compounds were reducing PrP<sup>Sc</sup> levels as expected (data not shown). To ensure over-saturation of the signal was not a problem the blots were automatically exposed, allowing the maximum signal to be obtained but without breaching the limits of the detector.

### 6.3.3. Discussion

It can be seen from the data in **Figure 104** that there is no significant change in HSP90 protein expression as a result of treatment with the I3GA compounds. In some ways this is not surprising as although HSP90 was shown to be upregulated at the gene level in the microarray studies, it was not found to be overexpressed in the proteomics study. This suggests that increased gene expression may not directly relate to increased protein levels, or that the change in protein levels was not large enough to be identified through analysis of the proteomics data or detected using this semi-quantitative method. HSP90 is an abundant protein with many different functions so it is possible that the increase in levels required to aid the clearance of PrP<sup>Sc</sup> is not particularly large. As a result the lack of a distinct change in HSP90 levels does not necessarily rule out the involvement of the proteasomal pathway in the mode of action of the I3GA compounds. It is also possible that the signal on the blot was saturated as a result of the loading concentration being too high, meaning that more subtle changes in protein level could not be distinguished. Due to the problems with sensitivity, and the possibly erroneous assumption that up-regulation of gene expression would result in up-regulated protein expression, it is thought that western blotting may not be the optimal technique for validating microarray data. Other studies that have used microarrays to compare uninfected brains with brains infected with TSEs have validated their results using quantitative RT-PCR <sup>(417)</sup> or immunohistochemistry <sup>(424)</sup> and these alternative techniques may be preferable.

## 6.4. Target Identification and Validation using Inverse Docking and Western Blotting

### 6.4.1. Introduction

Inverse docking experiments were carried out by Jorge M Valencia Delgadillo alongside analysis of the microarray and proteomics data to identify potential targets of the I3GA compounds, 3001012 and 3001207. The methods used and the targets suggested by him are outlined in sections **6.4.2** and **6.4.3**. My role in the study was to validate the theoretic mode of action

proposed by him, and to investigate the normal physiological roles of these proteins to determine if and how they may be involved in prion disease and the mode of action of the I3GAs (sections **6.4.3.1** to **6.4.3.4**). The results of this study are outlined and discussed in section **6.4.4**.

The compounds were virtually docked into protein models with the aim of identifying potential interaction partners. Crossover between the top ranked results from the two compounds was then assessed to determine if the compounds might share a target, a hypothesis that was suggested due to the structural similarity of the two compounds (see **Figure 84**). The levels of the identified targets were investigated using western blotting to investigate any possible changes in expression as a result of treatment with the I3GA compounds.

## **6.4.2. Inverse Docking Methods**

Initial work used the set of DEGs identified by Hood *et al.*<sup>(382)</sup> to manually assemble a database of possible target proteins. Where possible a high resolution x-ray model was used, otherwise a homology model was chosen. Homology models have been widely used in high-throughput ligand docking and have been successful in extending the range of ligand docking in the absence of complete protein structures. However, the quality of the model directly affects the accuracy of the results.<sup>(425)</sup> Both 3001012 and 3001207 were tested against this database using the inverse docking protocol established by Hui-fang *et al.*<sup>(426)</sup> A list of 20 possible targets was established for each compound, with the only crossover between the two being Horf6 and catalase HP11, neither of which have any link to prion diseases.

In order to try and further improve the results a second, larger, database of protein targets was used, based on the potential drug target database (PDTD). The PDTD contains 1207 entries covering 841 known and potential drug targets, and focuses on those drug targets with known 3D structures. The structures were prepared for docking by making hydrogens explicit and deleting water molecules, ligands and ions. Using the ChemPLP scoring function, the top 1% of targets was identified, resulting in 12 potential targets for each compound. 6 of the potential targets were found in both lists, although again none of these were found to have any links to prion disease. In order to try and improve the results a calibration set was used, as set out by Santiago *et al.*<sup>(427)</sup> Using this approach Lck and Caspase 7 were identified as potential targets of both the I3GA compounds, with both 3001012 and 3001207 interacting with Lck at the same

residues, namely Gln66, Gln68 and Arg72. As will be discussed further subsequently, Lck does show links to prion disease. Although there is no evidence of the involvement of caspase 7 in prion diseases, there is evidence for the involvement of caspase 12 which shares 85 % homology with caspase 7 but for which no model was available.

### **6.4.3. Target Identification**

Drawing together the results from the inverse docking experiments, as well as analysis of the MetaCore data and results of a literature search, several possible targets of the anti-prion compounds were proposed. These were metal transcription factor 1 (MTF-1), specific protein 1 (sp1), lymphocyte-specific protein tyrosine kinase (lck) and caspase 12. In order to validate the results, and also confirm the validity of inverse docking as a tool to identify the targets of small drug-like molecules, the levels of these proteins in treated cells were probed *via* western blotting and their levels compared to an untreated control to try and establish any differences in expression.

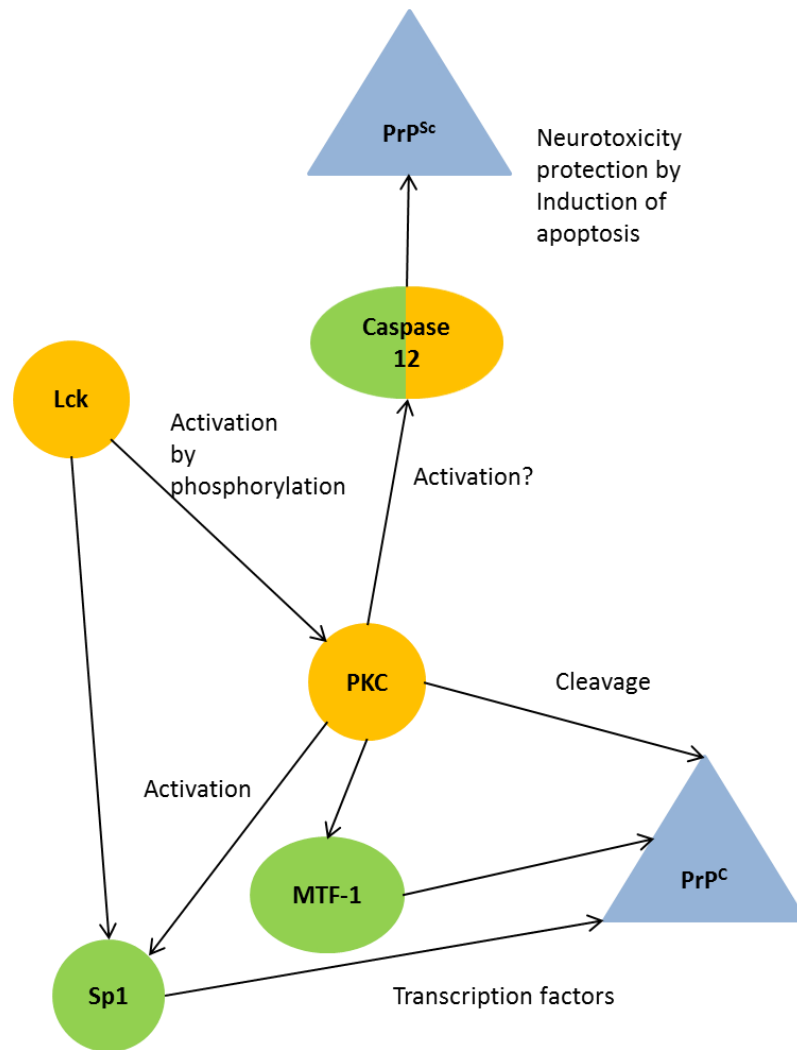


**Figure 105:** Schematic representation of the targets identified and their possible interactions. Targets identified by inverse docking are in orange, targets identified by the microarray are in green and targets identified from a literature search are in blue. PKC was not investigated further in this study but is crucial to understanding the interactions between the other targets. Figure adapted from Jorge M Valencia Delgadillo.

#### 6.4.3.1. MTF-1

MTF-1 encodes a transcription factor which induces the expression of metallothioneins in response to heavy metals such as cadmium, zinc, copper and silver. It is also a known transcription factor for PrP<sup>C</sup>.<sup>(428)</sup> Metallothioneins are a group of proteins with the capacity to bind physiological and xenobiotic heavy metals. They have a diverse range of cellular functions including the inhibition of pro-apoptotic mechanisms and the enhancement of cellular survival and tissue regeneration, and have also been suggested to have a role in neuroprotection and neurodegeneration.<sup>(429)</sup> MTF-1 accumulates in the nucleus in response to heavy metal exposure and binds to promoters containing a metal responsive element. MTF-1 is also a paralog of Gli-3 (see **Figure 73**), meaning that they are related as a result of duplication of the ancestral gene

within the genome. A role for PKC in the activation of MTF-1 in response to metals has been suggested.<sup>(430)</sup>

Metallothioneins exist in four isoforms, known as MT-1 through to MT-4. MT-1 and MT-2 are induced in the liver and are the most widely expressed isoform in mammals, with a diverse range of functions. MT-3 is present in the brain and has specific neuronal growth inhibitory activity.<sup>(431)</sup> MT-4 has been more recently discovered and its function is yet to be revealed, although it resides primarily in the squamous epithelium and may have a function in regulating zinc levels during the differentiation of stratified epithelium.<sup>(432)</sup> MT-1, 2 and 3 have been investigated in relation to prion diseases due to their role in copper homeostasis which may be perturbed during infection due to reductions in PrP<sup>C</sup> activity. Cells in which PrP<sup>C</sup> expression was induced were found to have higher levels of metallothioneins after PrP<sup>C</sup> induction compared to control cells, suggesting that PrP<sup>C</sup> may have a role in protecting against metal-induced toxicity.<sup>(433)</sup> The up-regulation of MT-1 and 2 has been observed in BSE field cases,<sup>(434)</sup> a mouse model of BSE,<sup>(435)</sup> human TSEs,<sup>(436)</sup> and mouse models of scrapie.<sup>(421, 437)</sup> However, knockout of MT-1 and 2 in mice did not have any effect on disease progression.<sup>(438)</sup> Conversely, MT-3 has been shown to be markedly diminished in Alzheimer's brains<sup>(439)</sup> and in patients with long duration CJD.<sup>(436)</sup> It can therefore be seen that there is no simple correlation between metallothionein expression and TSEs.

Given that PrP<sup>C</sup> is thought to have a role in copper binding it is possible that MTF-1 could be upregulated in order to compensate for reduced activity of PrP<sup>C</sup> after infection. It could also be hypothesised that MTF-1 may be upregulated to initiate the proposed neuroprotective properties of metallothioneins, either as a response to infection or as part of the curative mechanism. MTF-1 was found to be down-regulated in treated cells compared to untreated cells in the microarray assay. It's possible that this is a reflection of MTF-1 levels returning to normal baseline levels as a result of treatment. However, another interpretation is that down-regulation of MTF-1 as a result of treatment may result in lower PrP<sup>C</sup> levels *via* its role as a transcription factor for PrP<sup>C</sup>. Less substrate would therefore be available for conversion so this may be a mechanism by which the infectious burden can be cleared.

#### **6.4.3.2. Sp1**

Sp1 is a zinc-finger transcription protein which is involved in many cellular processes including cell differentiation, cell growth, apoptosis, immune responses, responses to DNA damage and

chromatin remodelling. It is a transcription factor and is known to regulate PrP<sup>C</sup> expression, and is involved, along with MTF-1, in the copper dependent regulation of PrP<sup>C</sup>.<sup>(428)</sup> Up-regulation of sp1 has also been shown to be protective against prion-mediated cell death,<sup>(440)</sup> although targeting transcription factors is not a popular therapeutic intervention as they can often promote hundreds of different genes. The risk of unintended side effects is therefore high. Sp1 activation by phosphorylation is regulated by atypical PKC, among other kinases.<sup>(441)</sup> In the microarray both sp1 and MTF-1 were down regulated, with the hypothesis being the same as that proposed for MTF-1. Down-regulation of sp1 would result in lower levels of PrP<sup>C</sup> and therefore reduced substrate for conversion to PrP<sup>Sc</sup>, allowing clearance of the infectious burden.

#### **6.4.3.3. Lck**

Lck is a member of the Src family of protein tyrosine kinases and is crucial in T-cell development and function.<sup>(442-444)</sup> It has a key role in T-cell antigen receptor (TCR) linked signal transduction pathways and contributes to signalling *via* other receptors such as CD2, interleukin-2 and IL-2 receptor  $\beta$ -chain. It is also critical for the selection and maturation of developing T-cells in the thymus.<sup>(445)</sup> Lck has a role in regulating sp1 activity<sup>(446)</sup> and is one of the controls for PrP<sup>C</sup> expression in T-cells which are capable of replicating, but not retaining, PrP<sup>Sc</sup> infection.<sup>(447)</sup> PrP<sup>C</sup> has also been shown to co-localise with Lck in the lipid rafts of human T-cells. An effect of treatment on Lck expression or activity *via* binding (as suggested by the inverse docking results) could therefore affect PrP<sup>C</sup> expression further downstream. Lck could also affect MTF-1 and sp1 *via* interactions with PKC, as Lck can activate PKC *via* phosphorylation.<sup>(448)</sup>

#### **6.4.3.4. Caspase 12**

Caspase-12 is a member of the caspase family of proteins that play an important role in apoptosis. It is linked with the endoplasmic reticulum (ER) which has been proposed as a regulator of cell death, and caspase 12 is a central player in ER-stress induced apoptosis.<sup>(449)</sup> Caspase-12 located at the ER is activated by ER stress and results in cell death, with cleavage of the 55 kDa form into a 42 kDa form resulting in activation.<sup>(450)</sup> ER stress, and the resulting unfolded protein response (UPR), have been implicated in the pathogenesis of prion diseases by both enhancing the accumulation of PrP<sup>C</sup> aggregates<sup>(179)</sup> and by causing a critical decline in the synthesis of key proteins needed for neuronal survival.<sup>(186)</sup> Activation of caspase 12 is at least partially involved in the amyloid-beta neurotoxicity process in cortical neurons<sup>(451)</sup> and stress impairing ER degradation can lead to the accumulation of amyloid-beta and subsequent cell death.<sup>(452)</sup>

Further evidence points to a role for caspase 12 in prion disease, although the precise role remains ambiguous. ScN2a cells treated with purified PrP<sup>Sc</sup> were more susceptible to caspase-12 induced apoptosis, and histological examination of both mouse and human brains infected with scrapie showed the presence of activated caspase 12. <sup>(177)</sup> The same study demonstrated a direct correlation between caspase 12 activation and neuronal loss *in vivo*, with caspase 12 being proteolytically processed and therefore activated in the brains of scrapie infected mice. An increased cellular load of misfolded protein in the ER can trigger caspase dependent cell death, <sup>(453)</sup> and conversely the expression of caspase 12 can sensitise cells to ER stress. <sup>(454)</sup> The above evidence all seems to suggest a role for caspase 12 in the induction of neuronal death *via* ER stress caused by prion infection, and it has been suggested that the inhibition of caspase 12 activation could be a viable therapeutic target as caspase 12 does not seem crucial for normal development or physiological cell death. <sup>(455)</sup> However, a study carried out in mice with caspase 12 knocked out seems to contradict the above body of evidence. Caspase 12 deficient mice were inoculated with RML prions, but no difference in survival, behaviour, pathology or accumulation of PK resistant prions was observed between the knockout and wild type mice. <sup>(456)</sup> The authors concluded that caspase 12 was not required for disease pathogenesis.

It was hypothesised that inhibition of caspase-12 could prevent against neurotoxicity, and may therefore in some way be involved in the action of the I3GAs. The role of PKC in the modulation of caspase 12 is unclear. The activation of PKC has multiple functions in the signalling of the ER and stimulation of PKC can inhibit cleavage of caspase-12 to the active form, <sup>(457)</sup> possibly resulting in decreased neurotoxicity. However, PKC has also been implicated in the activation of caspases, <sup>(458)</sup> rendering its role in the pathway outlined in **Figure 105** ambiguous.

These four targets were investigated further through western blotting with each target being probed for individually. Materials and methods for this study can be found in sections **2.1.5** and **2.2.7**.

## **6.4.4. Target Validation Using Western Blotting**

### **6.4.4.1. Results**

In the time available for these experiments it was not possible to obtain acceptable and reproducible western blots for Sp1 and Lck, meaning no data was obtained for the levels of

these proteins in treated cells. The problems encountered were suspected to be due to low levels of the target proteins in the cell lysate and digestion of the protein by proteases (particularly Lck) even in the presence of protease inhibitors.

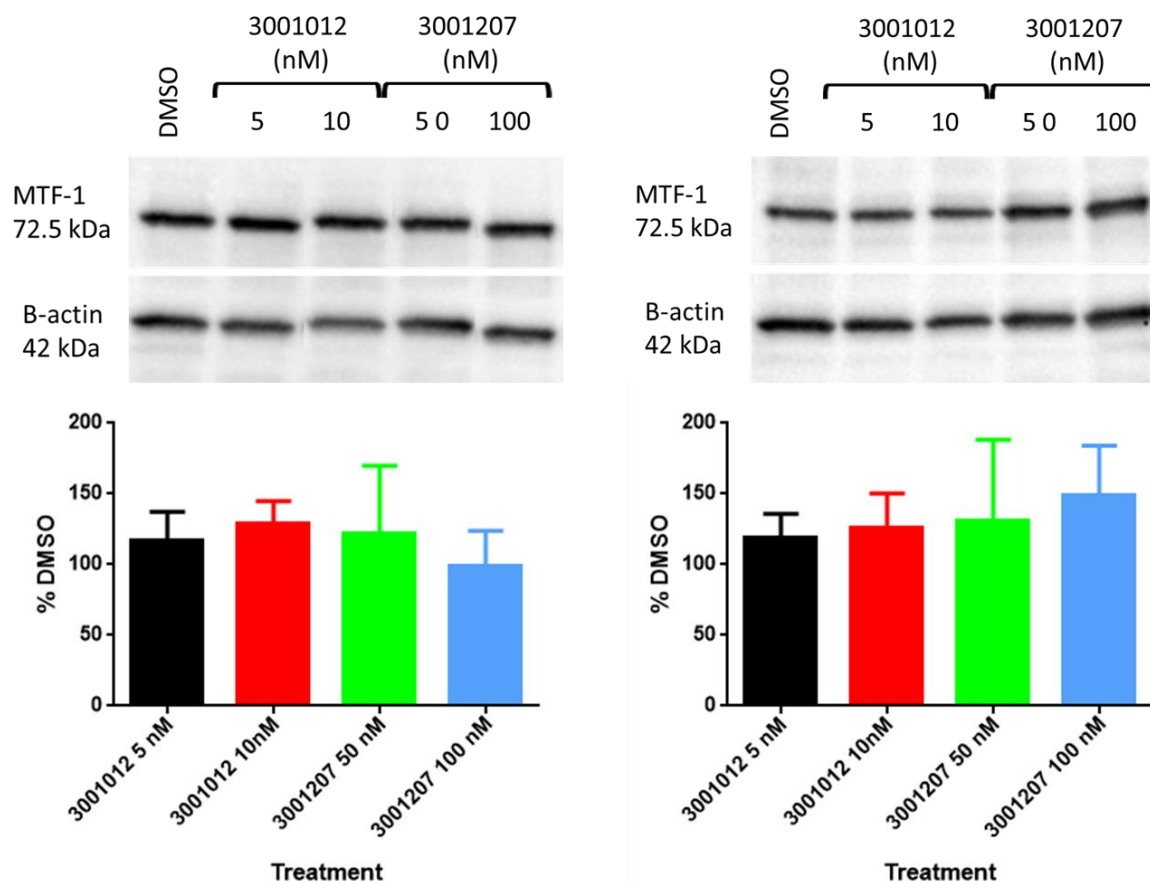


**Figure 106:** Western blots showing expression of MTF-1 after a 5 day dose (a) and after a 56 hour dose (b). Graphs show average MTF-1 levels in treated cells from four biological replicates ( $n = 4$ ), blots shown are representative of all replicates. Data was adjusted for loading difference and is presented as a percent of the DMSO control.

Data in **Figure 106** suggest that after 56 hours the levels of MTF-1 are slightly raised after treatment with the I3GA compounds, although the error in the data casts doubt on the reproducibility and consistency of this effect. The difference in MTF-1 levels between the treated cells and the DMSO control cells was not found to be statistically significant by multiple t-test.

As explained in section **6.4.3.4**, caspase 12 exists as both a full length form, at 55 kDa, and a cleaved form at 42 kDa. Both forms were probed for using the same antibody and the results for both forms are presented here.

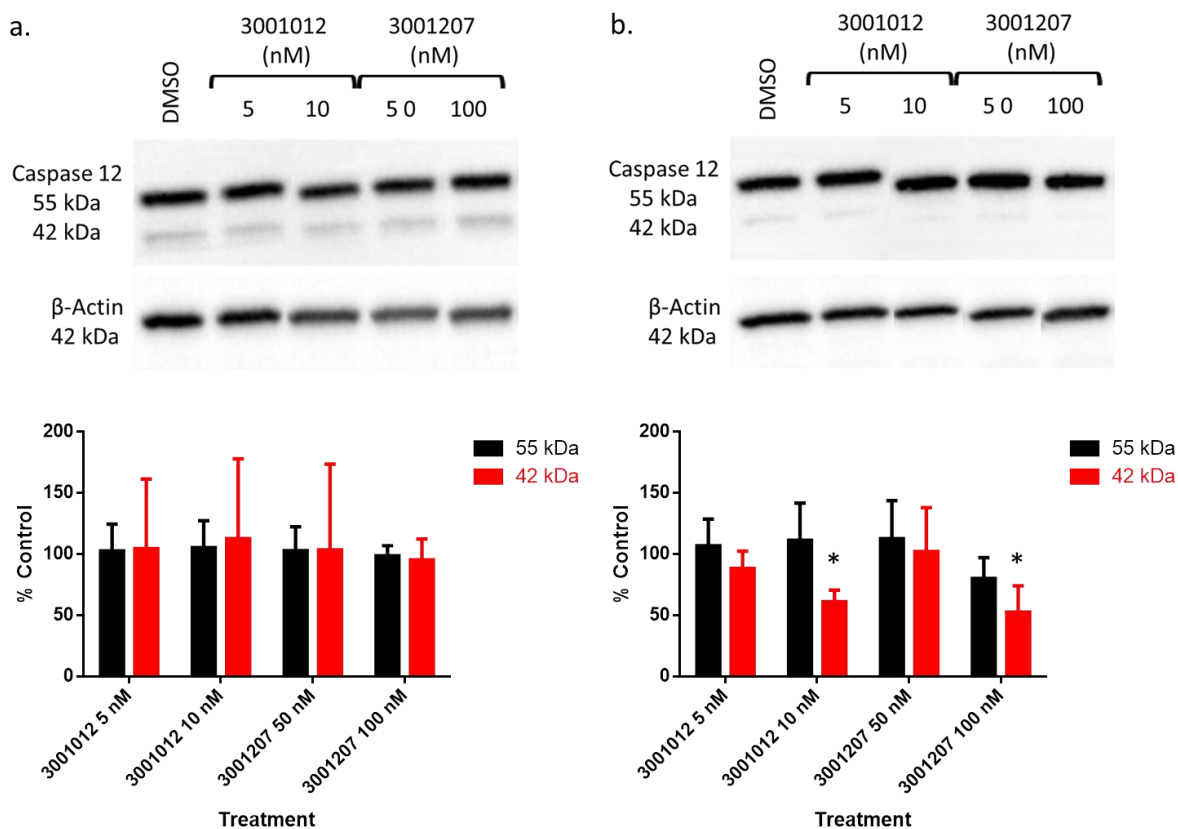


**Figure 107:** Western blots showing expression of both forms of caspase 12 after a 5 day dose (a) and after a 56 hour dose (b). Graphs show average caspase 12 levels in treated cells from four biological replicates ( $n = 4$ ), blots shown are representative of all replicates. Data was adjusted for loading difference and is presented as a percent of the DMSO control. T-tests showed levels of cleaved protein after treatment with high doses of 3001012 and 3001207 were significantly lower than the DMSO control ( $p = 0.00535421$  and  $0.043093$  respectively,  $n = 4$ ).

The data from the 5 day dose (**Figure 107a**) does not show any significant differences between the treated cells and the DMSO control. However, the data from the 56 hour dose (**Figure 107b**) does show significant differences between the amount of the cleaved form of caspase 12, but only at the higher dose for both compounds. There was no significant difference in levels of full length caspase 12 between treated cells and the DMSO control, and these differences were no longer present after five days.

#### 6.4.4.2. Discussion

It can be seen from the data above that no significant effect has been seen on any of the targets identified, with the exception of the cleaved form of caspase 12.

It was hypothesised that MTF-1 might be up-regulated during infection due to the proposed neuroprotective properties of metallothioneins, and also to compensate for a possible reduction

in copper binding and metallothionein induction by PrP<sup>C</sup>. In this case it would be reasonable to assume that once the infection was cleared, MTF-1 expression and metallothionein levels would revert back to normal as extra neuroprotection would no longer be required and PrP<sup>C</sup> would be able to resume its normal physiological roles. As shown in **Figure 106** there was no change in MTF-1 expression levels as a result of treatment with the I3GAs, although PrP<sup>Sc</sup> levels are known to have decreased. Further information could be obtained by comparing MTF-1 levels in infected and uninfected cells, but unfortunately this was not possible.

The down-regulation of MTF-1 and sp1 in the microarray assay were also considered with regards to their shared role as transcription factors for PrP<sup>C</sup>, with the hypothesis being that reduced levels of the transcription factors would result in lower levels of PrP<sup>C</sup> and consequently less substrate being available for conversion. This would allow cells to be cleared of existing PrP<sup>Sc</sup> while limiting the formation of new PrP<sup>Sc</sup> molecules. The lack of change in MTF-1 levels does not preclude this theory, for reasons outlined below, but even if a change had been observed it would have been tenuous at best to draw a direct line between changes in MTF-1 levels and decreased PrP<sup>C</sup> levels as each transcription factor is responsible for the promotion of multiple genes. Further investigation of levels of PrP<sup>C</sup> in treated compared to untreated cells would be useful in helping reveal whether the I3GAs were acting by reducing levels of PrP<sup>C</sup>. However, it would not provide further insights about the mechanism of the reduction in PrP<sup>C</sup> levels or the role of the transcription factors.

As previously discussed, caspase 12 is a key player in ER-stress induced apoptosis. Its role in the UPR, which is implicated in prion disease, suggests that it may have an important role in prion disease pathogenesis, but its exact role is ambiguous (see **6.4.3.4**). Given the conflicting evidence presented above it is difficult to draw any conclusions about the meaning and importance of the finding that the activated form of caspase 12 seems to be down-regulated after 56 hours treatment, although not after 5 days. The literature seems to point to a role for caspase 12 in neuronal death, with inhibition of caspase 12 providing a neuroprotective effect. How this is relevant to our cell model is less clear, especially as treatment does not result in apoptosis or even reductions in growth. It is possible that the down regulation of caspase 12 offers some form of protection from apoptosis, but how this would then translate to a reduction in PrP<sup>Sc</sup> levels is unknown. A more likely explanation would seem to be that the reduction of infection in turn results in lowered ER stress and a resultant decrease in caspase 12 activation. It would be expected, however, that if this was the case then the effect should also be seen in the

cells treated for 5 days, at which point the burden of infection has been significantly reduced for an extra 2 days. It also seems counterintuitive that this effect wasn't seen at the lower concentrations of the I3GA compounds, which were known to clear PrP<sup>Sc</sup> with the same efficiency as the higher concentrations. It is therefore possible that the effect seen is due to some off target effect of the I3GA compounds that is only seen over a limited time frame and at higher concentrations. It is also worth noting that although a significant change was seen in levels of cleaved caspase 12, levels were very low in the first place in comparison to the full length form, meaning that the overall change in the amount of cleaved caspase would be minimal.

There are several unknowns which make drawing meaningful conclusions from the western blotting results difficult. Firstly, there is no uninfected control against which to compare levels of target proteins. For example, it would be useful to know what the levels of activated caspase 12 are in an uninfected equivalent, to help determine the importance of the observed changes. Similarly, being able to identify whether MTF-1 expression was altered as a result of infection would help clarify whether the lack of change seen as a result of treatment was significant. If no difference was observed between infected and uninfected cells it would strengthen the hypothesis that the compounds are not working *via* some effect on PrP<sup>C</sup> transcription factors. It is also important to note that a lack of change in expression does not preclude an interaction between the target and the I3GA, as predicted by the inverse docking. As discussed with reference to the HSP90 data it is possible that western blotting is not a suitable technique for validating these results, as it may not be sensitive enough to detect small changes in protein expression. This is particularly relevant in the case of MTF-1 as it was identified from the microarray data which measured changes in gene expression rather than changes in protein expression, which may not be directly related. It may therefore be desirable to attempt validation of these targets using quantitative RT-PCR, to validate the microarray data, or immunohistochemistry, to validate the proteomics data.

Another consideration, particularly relevant to MTF-1, is the time it would take for MTF-1 levels to return to baseline levels once the cells were cleared, with the 5 day treatment period (including around 64 hours when the majority of PrP<sup>Sc</sup> had been removed from the cells) maybe not long enough for equilibrium to be restored. It is therefore possible that a longer dosing period may have detected more significant changes, although it is not known how likely this scenario is. It is also unlikely that changes observed over a longer time period would be directly

related to the removal of the infectious burden, as the effect would need to be more immediate in order to elicit the observed effects.

Taking the available data at face value an unavoidable conclusion is that treatment with the I3GA compounds doesn't alter expression of MTF-1, making it unlikely that MTF-1 is either involved in, or related to, the mode of action of the I3GA compounds. It seems clear that the levels of activated caspase 12 are significantly lower after treatment for 56 hours, although not after 5 days, which suggests that the down regulation is not simply a result of the cells being cured. The evidence would seem to suggest that the down-regulation was transient, returning to pre-treatment levels after 5 days, and only seen at much higher I3GA concentrations than those required to cure the cells. This all suggests that caspase 12 is not directly responsible for reducing PrP<sup>Sc</sup> in the cells, although an involvement in the process should not be ruled out.

With regards to the hypothetical pathways mapped out in **Figure 105**, the results outlined in section **6.4.4.1** do not provide any evidence for the involvement of any of the identified targets in the mode of action of the I3GAs. For the reasons outlined above, this does not preclude the involvement of one or more of these targets, but the techniques employed were not sensitive enough to provide the information required. Lck and PKC were identified due to their identification as putative binding partners for the I3GAs, which would not necessarily be revealed by western blotting even if these studies had been carried out successfully. The role of PKC in phosphorylation and activation of the targets is key to many of the hypothesised interactions, and again this is not something that could be determined by quantifying levels of PKC due to the number and complexity of PKC's interactions with its substrates, and also the large number of PKC isoforms. Much more work would be required to make clear the possible roles of all these targets in the mode of action of the I3GAs, with investigations into the effect of the I3GAs on PrP<sup>C</sup> levels being key. If PrP<sup>C</sup> levels are unaffected then the involvement of sp1 and MTF-1 would become more unlikely.

## 6.5. Overall conclusions

The fundamental aim of the work carried out within this chapter was to gain further insights into the mode of action of the I3GA compounds. Initial work used a systems biology approach,

combining data from microarray and proteomics studies, to try and narrow down pathways affected by treatment. Based on initial analysis of the MetaCore data an early hypothesis was formulated suggesting that the compounds might be working *via* some form of up-regulation of the protein degradation pathways. These pathways are known to be involved in prion disease pathogenesis, and the presence of a significant number of upregulated E3 ubiquitin ligases in the data set for 3001012 compared to the DMSO control pointed to their possible involvement in the mode of action of the I3GAs.

Investigations were carried out to investigate the effect of proteasomal inhibitors on both PrP<sup>Sc</sup> levels in the cells and on the efficacy of the I3GA compounds. It was found that compounds which inhibited the LCPs more generally, namely MG132 and E64, both caused a significant accumulation of PrP<sup>Sc</sup> within the cells. Neither lactacystin, which is specific for the proteasome, nor Cl3, which selectively inhibits certain cathepsins, caused any change in PrP<sup>Sc</sup> levels. These results suggest that LCPs play a key role in maintaining steady state levels of PrP<sup>Sc</sup> in the SMB cells. Toxicity was only observed after treatment with MG132, which inhibits both the proteasome and the LCPs, suggesting the cells cannot tolerate complete inhibition of both systems at the same time. It is therefore likely that the two systems may act as back up for each other.

All four compounds used in the study (3 I3GAs and quinacrine) were able to counteract the increases in PrP<sup>Sc</sup> caused by LCP inhibition. The efficacy of 3001012 was affected to a larger degree than the efficacy of the other compounds, with PrP<sup>Sc</sup> clearance efficiency compromised even at higher concentrations of 3001012. No significant shift in EC<sub>50</sub> was seen for any of the compounds, with the exception of 3001012 co-dosed with Cl3.

Co-dosing a fixed concentration of the I3GAs with a concentration gradient of MG132 and E64 resulted in a dose-dependent increase in PrP<sup>Sc</sup>. All three compounds were affected by higher concentrations of the inhibitors, suggesting that an excess of the inhibitors is significant. Time course analysis suggested there was a lag phase in PrP<sup>Sc</sup> accumulation of around 48 hours, with PrP<sup>Sc</sup> levels not increasing at all when co-dosed with 3001012. It was therefore hypothesised that alternative systems are able to compensate for the LCP inhibition for a limited period, beyond which a tipping point is reached and accumulation occurs. It was proposed that the I3GAs are antagonising PrP<sup>Sc</sup> accumulation by reducing levels so that this tipping point is never reached and the cells are able to manage with a more limited set of cellular machinery.

Quinacrine was able to antagonise the inhibitors without any documented links to the protein degradation pathways, while 3001012 was able to antagonise the accumulation of PrP<sup>Sc</sup> seen as a result of treatment with 1 µM congo red. This all suggests that the mechanism of antagonism, for the most part, is unrelated to a specific effect of the I3GAs on the LCPs. However, the decreased efficacy seen in 3001012 suggests that this compound may have an effect on the LCPs, but this is not thought to be the primary route by which PrP<sup>Sc</sup> is cleared from the cells. Unfortunately this study was not able to determine the possible role of the upregulated E3 ubiquitin ligases in the I3GA's mode of action.

Levels of HSP90 in treated cells were compared to untreated cells to determine if a difference in expression could be identified *via* western blotting, and also in the hope that it might validate the microarray results. No difference between HSP90 levels could be determined, although it was not clear whether this was due to a lack of sensitivity in the method used. It is also possible that the signal was saturated due to loading concentrations being too high, therefore masking any changes, as the western blots were not carried out at a range of lysate protein concentrations. There was also uncertainty around whether changes in gene expression would directly translate to protein expression. The suitability of western blotting as a mechanism for validating the microarray results was questioned, with quantitative RT-PCR or immunohistochemistry being proposed as alternatives.

Finally, work was carried out to try and validate the results obtained by Chen *et al* from inverse docking experiments. Four targets had been identified through inverse docking, literature searches and interrogation of the microarray and proteomics data, and it was hoped that these results could be validated *via* western blotting. In the end only two of the four proposed targets were blotted successfully, with MTF-1 showing no significant difference in expression between treated and untreated cells over a range of concentrations and dosing periods. The cleaved, activated form of caspase 12 was shown to be significantly reduced after 56 hours of treatment with the highest concentration of both the I3GA compounds, although this was not seen as a result of any of the other treatments or time points. The most likely explanation was that the reduced levels might be due to decreased activation resulting from lowered ER stress after removal of the infectious burden. However, the lack of this effect at the later time points or the lower (but still active) concentrations suggests that this effect may be transitory and secondary to the mechanism by which the cells are cleared of infection. As with validation of the microarray results, the suitability of western blotting for this application is questioned.

Overall, the studies presented here have not resulted in a clearly defined mode of action for the I3GA compounds. It is clear that in the SMB models the lysosomes are essential for maintaining steady state levels of PrP<sup>Sc</sup>, and the correlation between their inhibition and reductions in the efficacy (although not the EC<sub>50</sub>) of 3001012 suggest that this compound may be working, in part, *via* this mechanism. It is thought more likely that the lysosomes are a target of the I3GA compounds than the proteasome. The studies presented here also raise questions as to whether western blotting is a suitable technique for validating the results of *in silico* studies, and it is thought that further validations and investigations need to be carried out before this question can be answered.

## 7. Evaluation of 3D models as high throughput screening models and predictors of *in vivo* activity

The use of 3D cell culture models in drug development has been suggested as a way of evaluating the potential *in vivo* activity of compounds without having to use an animal model. The structures formed in 3D mimic the morphology of cells within the body much more closely than 2D monolayers, and are therefore more representative of *in vivo* conditions (see section 1.3.2 for a detailed review). As discussed in section 1.1.3.1 there has been significant progress in identifying compounds that are capable of reducing PrP<sup>Sc</sup> levels *in vitro*, but in the majority of cases this *in vitro* activity is not reproduced in *in vivo* models. Identifying compounds that are active *in vivo* is therefore crucial in the development of a clinically effective anti-prion compound. Currently, the primary model for determining *in vivo* activity is a rodent model that has been infected with the prion disease of interest. Survival is monitored after dosing with the compound to see if there is any effect on disease pathogenesis. These mouse bioassays are the most powerful method of determining *in vivo* efficacy but they do have drawbacks. The practical constraints associated with working with living animals can make imaging and data acquisition more difficult during experiments.<sup>(311)</sup> Animal stocks are very expensive to maintain and experiments can be very expensive and time consuming to carry out, making the acquisition of statistically significant data more challenging.<sup>(307)</sup> There are also the ethical and regulatory issues associated with animal experimentation to consider.

The challenges associated with carrying out animal studies, as well as the failure of so many anti-prion compounds at this stage, meant that significant *in vitro* and molecular evidence would be required to justify the need for testing the I3GA compounds in an animal model. As this was something that could not be done ourselves, providing justification to potential collaborators of the favourable properties of the compounds would be key. Initial pharmacokinetic studies, discussed in section 4.5, suggested that the compounds had favourable pharmacokinetic properties and could accumulate in the brain, both of which would be required for *in vivo* activity. It was therefore hypothesised that a 3D model could be employed to provide additional evidence of the *in vivo* potential of the I3GAs by demonstrating their anti-prion activity in a

more complex cellular environment. Three different 3D models were established and optimised for testing of the anti-prion activity of the I3GA compounds, and were also assessed for their potential as a high-throughput model for screening anti-prion compounds. If suitable, it could be possible to use one or more of the models for high-throughput screening of anti-prion compounds in the future, allowing the identification of compounds unlikely to be active *in vivo* at an earlier stage of the drug discovery pipeline.

3D models have been used for a variety of applications, with scaffolds most commonly used for tissue engineering<sup>(315)</sup> and spheroids primarily used in the development of anti-tumour drug compounds.<sup>(314)</sup> The validity of the different 3D culture models for these applications has therefore already been tested and verified and as a result the majority of protocols that have been developed and optimised are for looking at cellular proliferation or morphology. However, there is limited evidence in the literature of these models being used to investigate the effect of drug-like molecules on levels of an intracellular target, and as a result detailed methodologies were not available for the testing of the anti-prion compounds. It was for this reason that different systems were trialled.

There are various products on the market which loosely fall into one of two categories: products facilitating the formation of spheroids, or scaffolds that encourage the growth of 3D structures. As part of this study, three different systems, representing both product categories, were trialled: the Biomatrix Perfecta3D® hanging drop plate, Happy Cell® matrix and the Alvetex® polystyrene scaffold. The aim was to establish a model in which the cells could be grown in 3D, dosed with the lead compounds, and then harvested and lysed to allow analysis of PrP<sup>Sc</sup> levels. The Alvetex system has protocols for analysing cell viability *via* MTT and also for harvesting the cells for analysis, but for the other systems there were not established and validated protocols available. If the compounds could be shown to be working in the 3D model then this would give confidence that they may be active *in vivo*, and provide further evidence going forward of the potential of the indole compounds as anti-prion therapeutics.

In order to validate results from the indole compounds a selection of compounds from the literature, with known *in vivo* activity, were also screened in the models. Details of these can be seen in **Table 46**. The EC<sub>50</sub> values are taken from **Table 34**, and more information about this screening can be found in section **4.4.2**.

**Table 46.** Compounds from the literature used in studies of activity in 3D models. Note that not all compounds were used in all studies.

| Compound             | EC <sub>50</sub> in 2D culture | Active <i>in vivo</i> ? | Reference           |
|----------------------|--------------------------------|-------------------------|---------------------|
| Pentosan polysulfate | 0.175 µg/ml                    | Yes                     | (197, 198, 208-210) |
| Dextran sulfate      | 0.5 µg/ml                      | Yes                     | (215, 216)          |
| Heparin              | 5 µg/ml                        | Unknown                 |                     |
| Amphotericin B       | 6.25 µM                        | Yes                     | (209, 459)          |
| Quinacrine           | 0.5 µM                         | No                      | (1, 233, 460)       |
| Curcumin             | 0.7 µM                         | Yes                     | (267)               |

The compounds from the literature were included to provide validation of the ability of the models to predict *in vivo* activity. If the *in vivo* activity of these well characterised compounds could be accurately predicted, then it was hypothesised that the same models could be used to predict the *in vivo* activity of the I3GAs. Good activity in the 3D models could therefore help justify screening these compounds in a genuine *in vivo* model, as well as providing confidence that they would be active.

## 7.1. The Hanging Drop Model

### 7.1.1. Introduction

The hanging drop assay was originally developed as a way of growing homogenous spheroids without requiring an external scaffold.

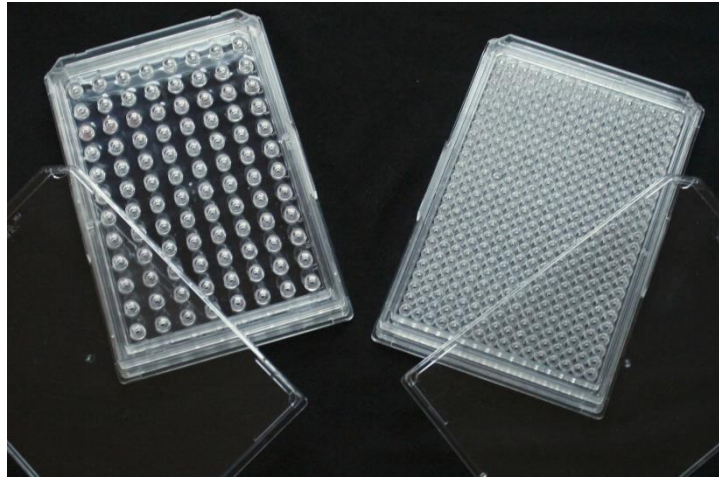


**Figure 108:** Picture of the Perfecta3D<sup>®</sup> hanging drop plate. The 96 well plate is on the left, and the 384 well plate is on the right. The top of the plate can be separated from the bottom to allow the water reservoirs to be filled and replenished. Image taken from [www.3dbiomatrix.com](http://www.3dbiomatrix.com)

The hanging drop plates are made up of two layers, with the top layer holding the drops and the bottom layer enclosing them. Both layers have reservoirs for water round the plate edge to help reduce evaporation from the drops. The cell suspension is pipetted into the top of the well and forms a hanging drop of medium underneath the plate. Cells aggregate at the bottom of the drop and form homogenous spheroids that are all approximately the same size (see **Figure 109**). Spheroid size can be controlled through initial seeding density. The Perfecta3D<sup>®</sup> plate has been developed for use in high throughput screening systems, and is available in both 384 and 96 well formats.

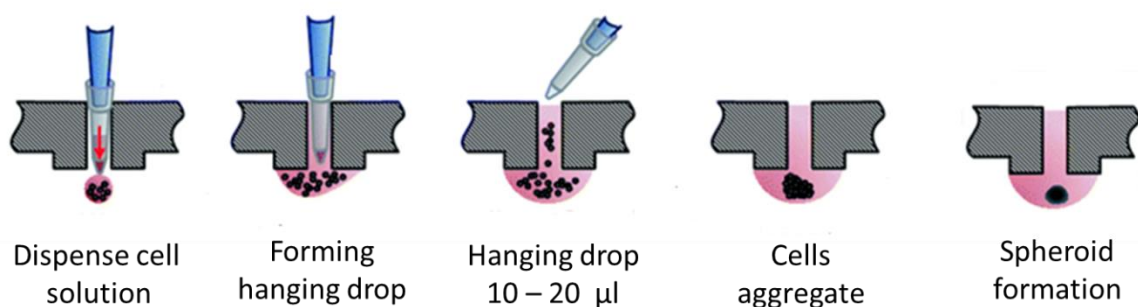


**Figure 109:** Formation of hanging drop spheroids; a diagram depicting the method of formation. A cell suspension is pipetted through the access hole to form a drop on the bottom of the plate. The cells aggregate at the bottom of the drop, forming a spheroid after around 1 day.<sup>(321)</sup>

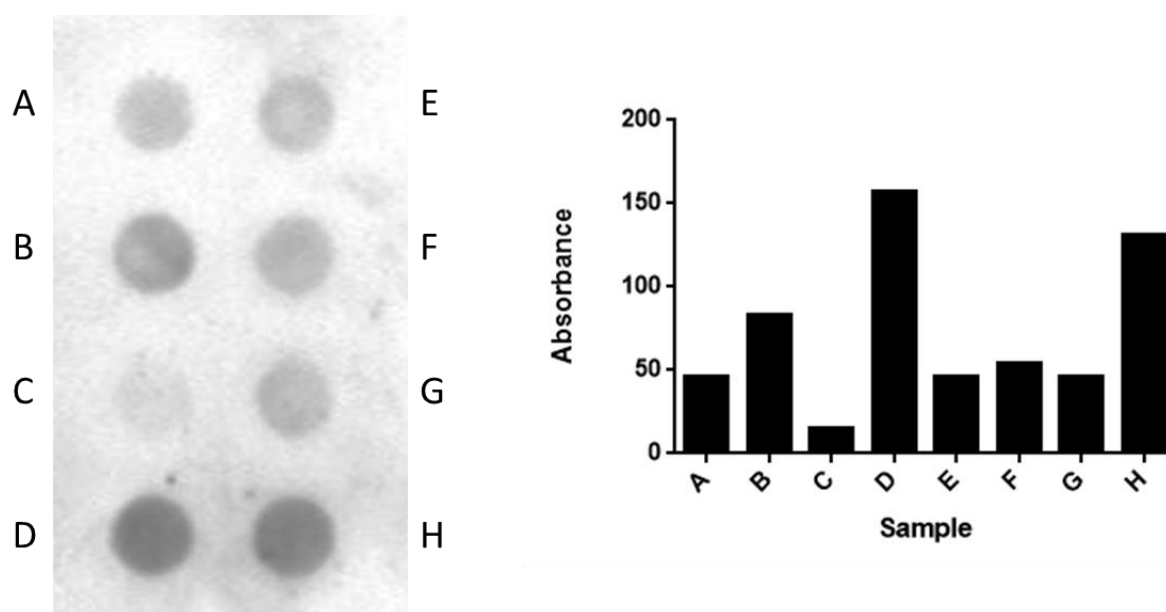
This technique has been used with multiple cell types, including breast and colon cancer cell lines, kidney cell lines, various carcinomas, osteoblasts, endothelial cells and murine embryonic stem cells (information from <https://3dbiomatrix.com/cells/>). However, there is no evidence

that this model has been used in the study of neurodegenerative diseases - or that the SMB cells being grown in this format - in the literature. Consequently, optimisation of growth and seeding conditions was necessary before the model was ready to be dosed with our compounds. Materials and methods for this study are outlined in detail in sections **2.1.6**, **2.2.8.1** and **2.2.8.4**.

## 7.1.2. Results

### 7.1.2.1. Optimisation

Attempts had been made to harvest the spheroids from the 384 well plates with limited success as it was very hard to tell if the spheroid had been retrieved or not. Initial attempts to lyse and blot the spheroids were also unsuccessful. Investigations were continued using the 96 well plates, where it was hoped that the larger spheroids would give an improved signal on the blot without using any additional lysis methods. See **Figure 110** for results.

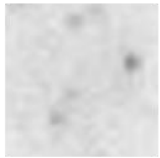
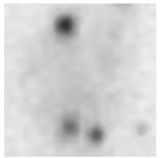
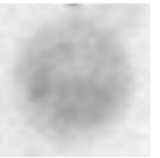
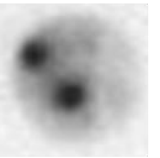
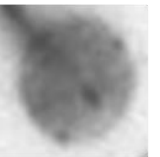
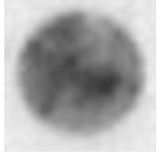
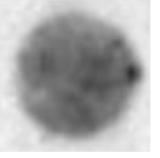
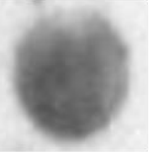


**Figure 110:** Dot blot of PrP<sup>Sc</sup> levels in spheroids grown under optimised conditions in 96 well plates. Each dot represents 1 spheroid. The PrP<sup>Sc</sup> levels can be seen to vary between spheroids, as demonstrated by the differing intensities of the dots and variation in absorbance levels as measured using Bio-Rad Quantity One software. This variation was attributed to problems with the efficiency of spheroid lysis, rather than genuine differences in the level of PrP<sup>Sc</sup> between spheroids.

It can be clearly seen in **Figure 110** that the signal for each spheroid is not consistent, even though all spheroids should have been homogenous in size, and appeared this way under the

microscope. The inconsistent signal was attributed to the ongoing problems with lysing the spheroids, although in this case a signal from the intact spheroids is not visible. All the spheroids were formed from the same number of SMB cells from the same passage, and for this reason it was thought unlikely that the variation in the signal was due to genuine differences in PrP<sup>Sc</sup> levels. In order to confirm this it was necessary to optimise the lysis conditions to obtain a more consistent signal.

Further investigations were undertaken to determine the optimum conditions for the blot in terms of numbers of cells per spheroid, and numbers of spheroids per sample. It was hoped that the production of larger spheroids may result in only one being required per sample, therefore allowing for higher throughput of samples. If this was not the case then it was hoped to identify the minimum number and size of spheroid required for maximum signal. Results can be seen in **Figure 111**.

| Cells/ $\mu$ l | Spheroids per sample  |   |  |   |
|----------------|---|---|--|---|
|                | 1   | 2   | 3  | 4   |
| 500            |  |  |  |  |
| 750            |  |  |  |  |
| 1,000          |  |  |  |  |

**Figure 111:** Optimisation of samples for dot blotting analysis. The table shows PrP<sup>Sc</sup> levels in samples prepared from lysed spheroids. Spheroids were seeded at concentrations of 500, 750 or 1,000 cells/ $\mu$ l in 40  $\mu$ l medium. They were harvested after 4 days and lysed in RIPA buffer. Spheroids were pooled together so that each sample contained either 1, 2, 3 or 4 spheroids, formed from an initial seeding density of 500, 750 and 1,000 cells/ $\mu$ l. Each sample was analysed using dot blot analysis to determine PrP<sup>Sc</sup> levels and the strength of the signal. Seeding cells at 1,000 cells/ $\mu$ l, and using two of these spheroids in each sample, was found to give the best signal.

As a result of these optimisations, subsequent experiments were all carried out with spheroids seeded at 1,000 cells/ $\mu\text{l}$  in 40  $\mu\text{l}$  medium, with 2 spheroids being pooled together for each sample. From the data presented here it does not appear that there is any advantage to having more than two spheroids in each sample, as there is not a proportional increase in signal above this number. The reason for this is not clear as the signal was not saturated.

Before carrying out any dosing experiments, attempts were made to make spheroid lysis more consistent and reliable. This was essential to identify if dosing the spheroids had any detectable and reproducible effect on PrP<sup>Sc</sup> levels. Different methods of lysis were investigated, as well as the possibility of improving lysis by harvesting the spheroids at different time points. It was hypothesised that if the cells were still dividing, with the spheroids becoming denser, then that in turn would make the spheroids harder to lyse. It would therefore be easier to lyse the spheroids shortly after they had formed, rather than when they were well established.

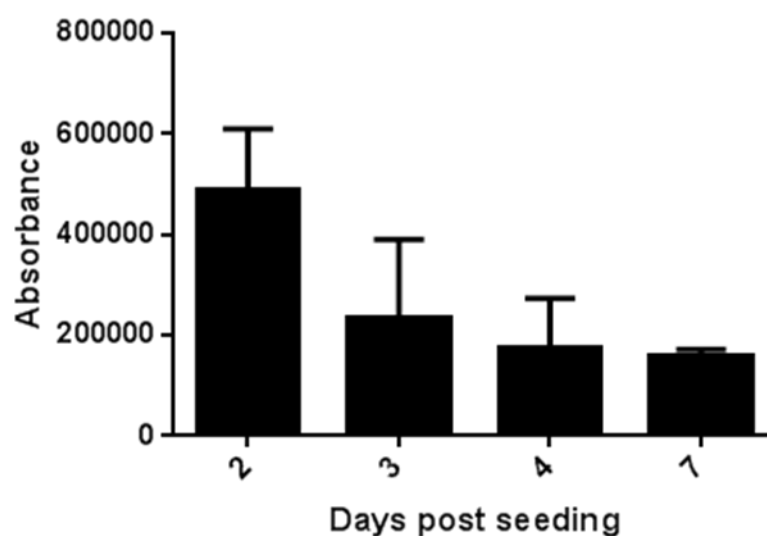


**Figure 112:** Average PrP<sup>Sc</sup> signal from a sample containing 3 spheroids after lysis at different time points. Spheroids were lysed by the addition of RIPA, followed by shaking, at 2, 3, 4 or 7 days after seeding and the strength (as measured by the absorbance) and consistency (as measured by the error) of the PrP<sup>Sc</sup> signal compared. Spheroids lysed shortly after seeding gave a better signal than those harvested after a longer time period, although the signal was less consistent, as indicated by the error. Spheroids harvested and lysed after 7 days gave the weakest yet most consistent signal.

As can be seen in **Figure 112** the most consistent signal was achieved after 7 days incubation. It therefore seemed desirable to attempt to increase the signal from spheroids harvested between 4 and 7 days after lysis. This would also allow screening in the spheroids to be carried out over

the same time frame as the 2D screens, which were dosed for 5 days. To try and improve lysis further, 4 different lysis methods were investigated to try and improve the signal on the dot blot. Six samples, each containing two spheroids that had been treated with 0.5 % DMSO only, were subjected to one of the four lysis methods to see which would produce the strongest and most consistent PrP<sup>Sc</sup> signal on the blot. The results can be seen in **Figure 113**.

Shaking

Heating

Freeze-thaw

Needle

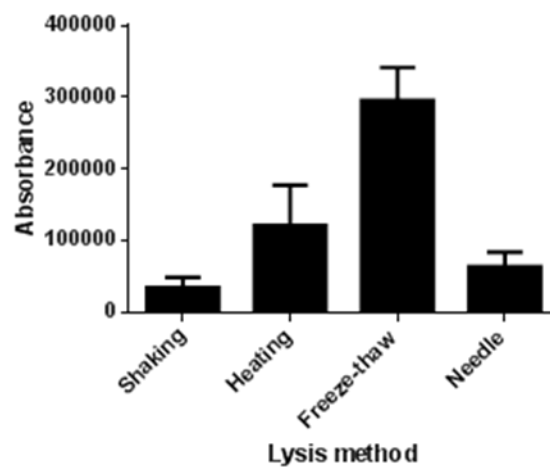
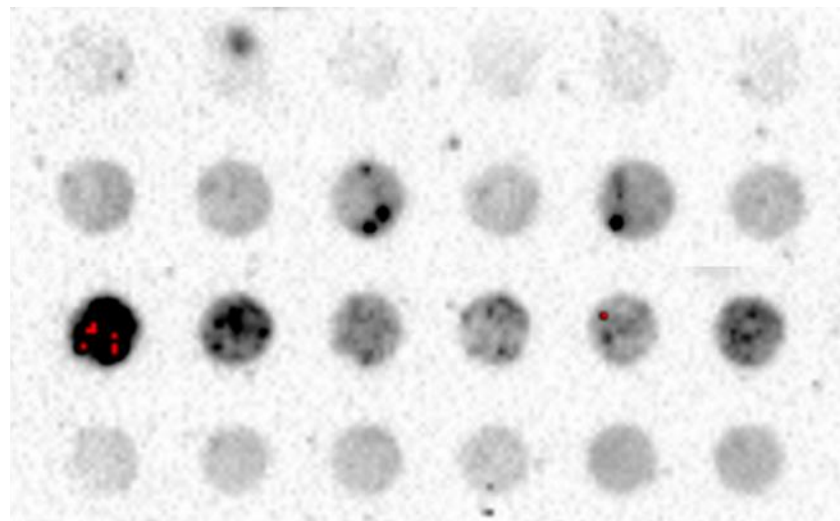


**Figure 113:** Results from the spheroid lysis optimisation. PrP<sup>Sc</sup> levels were analysed by dot blot in spheroids subjected to different lysis conditions to determine the optimum lysis method. Spheroids were treated with 0.5 % DMSO and then subjected to different lysis conditions. Six replicates are presented for each treatment, and each replicate represents a sample containing 2 spheroids, lysed using the method indicated. The data in the bar chart represents the average intensity of the 6 replicates, and the standard deviation is used as a measure of the consistency of the treatment. Data is expressed as the absorbance of the signal on the blot as measured by Quantity One software (Bio-Rad). It can be clearly seen that subjecting the spheroids to freeze-thaw cycles produces the strongest, although not the most consistent, signal.

It is clear from the data in **Figure 113** that by far the strongest signal was obtained after the spheroids were subjected to repeated freeze-thaw cycles. Freeze-thaw cycles cause cells to swell and break due to the formation of ice crystals during the freezing process, so it is possible in this case that the freeze-thaw cycles are disrupting the integrity of the spheroid as well as lysing the individual cells. It can be seen from the blot that lysis still isn't as consistent as might be desired – dark spots suggest that parts of the spheroid may not have been completely lysed. However, it is possible that this method could be used in conjunction with another method, such as passing the spheroids through a small gauge needle after the freeze-thaw cycles, to allow the spheroid to be fully lysed.

In addition to the lysis methods outlined above the use of collagenase to dissociate the spheroid before lysis was investigated. Again, there was no precedent in the literature for this procedure so all parameters had to be optimised. Collagenase is an enzyme which cleaves the main helical polypeptide chains of collagen. It exists in various forms, with the most potent form being the 'crude' collagenase obtained from *Clostridium histolyticum*.<sup>(461)</sup> Because of its ability to cleave collagen it is widely used in the isolation of cells from tissue, and as such it was thought it could potentially be useful in improving the lysis of the spheroids.

Initial results from the collagenase digestions suggested that using 1 mg/ml collagenase in high calcium TESCA was optimal as, by eye, this was the lowest concentration at which effective digestion was observed. Problems were encountered with removing the spheroids by centrifugation as the collagenase also came out of solution and it was very hard to separate the two to avoid interference with downstream analysis. Instead of spinning the spheroids down in the collagenase solution, the spheroids were removed and put straight into lysis buffer. When the lysis buffer was aspirated with a pipette it could be observed that the spheroid was disintegrating and was no longer visible in the lysis buffer, and the subsequent blot showed a much better and more consistent signal (see **Figure 114**). However, the signal was still very weak and was not as good or as consistent as the signal from the spheroids treated with freeze-thaw cycles, or the signal from the cells grown in 2D.

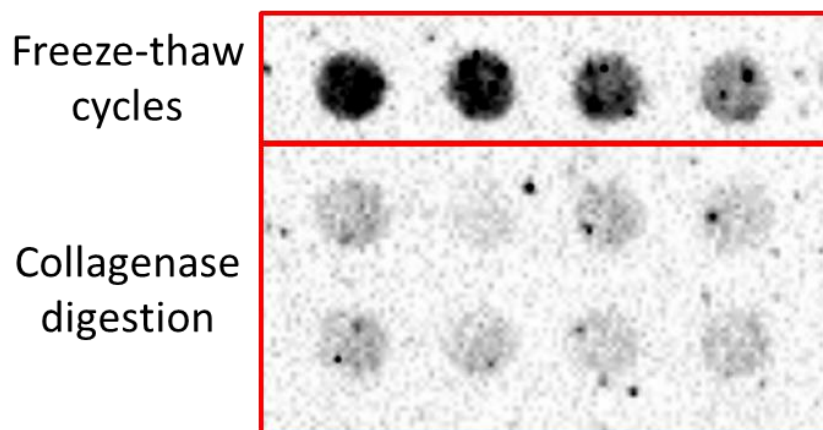


**Figure 114:** Dot blot showing PrP<sup>Sc</sup> levels in spheroids lysed using either multiple freeze-thaw cycles (top row) or digestion with collagenase (bottom two rows). Four samples were lysed with freeze-thaw cycles, 8 samples were lysed using collagenase, and each sample contained 2 spheroids. The strength of the signal was used as a measure of the successfulness of the lysis method.

After these rounds of optimisation it was concluded that subjecting the spheroids to freeze-thaw cycles was the most consistent method of spheroid lysis. Although the collagenase had been proved successful it was a more labour intensive process that resulted in a weaker signal, and it was necessary to consider the potential hazards of working with a substance such as collagenase. At this point a new piece of equipment called a bioruptor (made by Diagenode) was purchased which allowed the sonication of samples sealed in microcentrifuge tubes, and which was effective on samples as small as 100 µl. This proved to be a much better instrument for sonicating the spheroids – the sealed tubes meant there was no risk of the sample contaminating the sonicator and the small volumes that could be used meant that the sample wouldn't be too dilute. 5 cycles of 30 seconds each with 30 seconds in between was found to give a good reproducible signal, although two spheroids per sample were still required to get a decent signal (see **Figure 115**). From this point forward the sonicator was used to lyse the spheroids and all subsequent results are using spheroids prepped in this way.

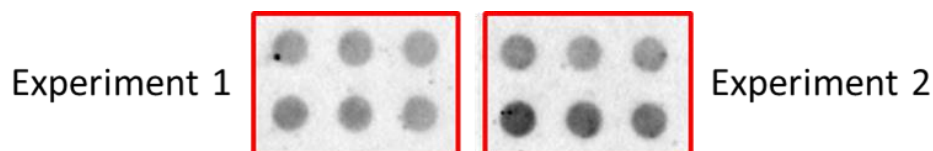


**Figure 115.** Example dot blots of PrP<sup>Sc</sup> levels in spheroids dosed with 0.5 % DMSO and sonicated using the Bioruptor. Blots show results from two separate experiments. The signal is much clearer and more consistent. The blots shown in each experiment represent 6 different samples, each containing two of the DMSO treated spheroids. All samples were the same, with both blots being presented to demonstrate the consistency associated with lysing the spheroids in the Bioruptor.

#### **7.1.2.2. Compound screening**

As the ultimate aim of the development of this model was to be able to use it as a high throughput screening model for identifying anti-prion compounds that may be effective *in vivo* the next step was to dose the cells. Initial experiments looking at optimising the spheroid lysis also looked to see if a difference in PrP<sup>Sc</sup> levels could be detected *via* any of the lysis methods when the spheroids were dosed with curcumin which is known to be active *in vivo*.<sup>(267)</sup>

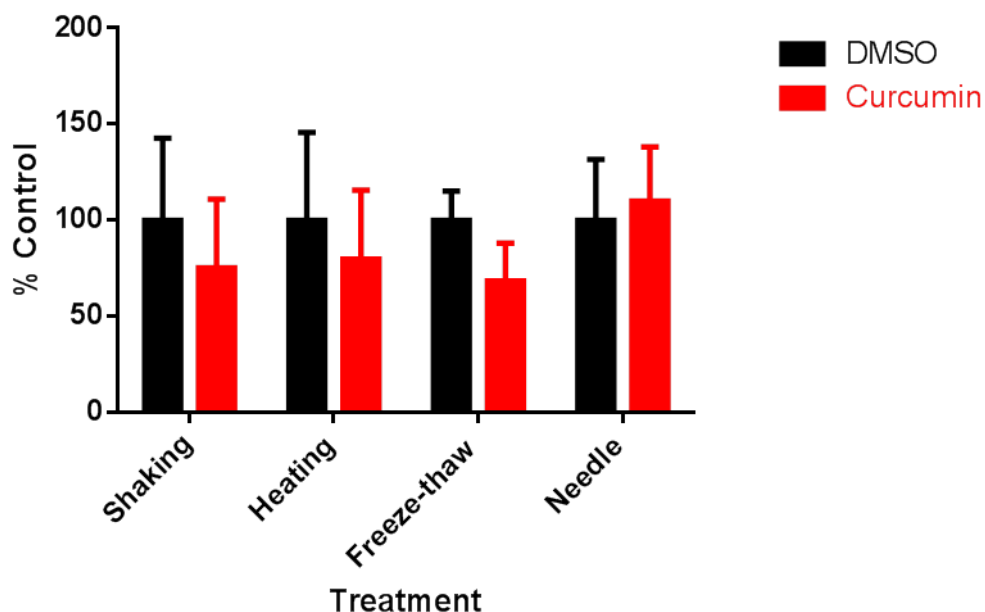
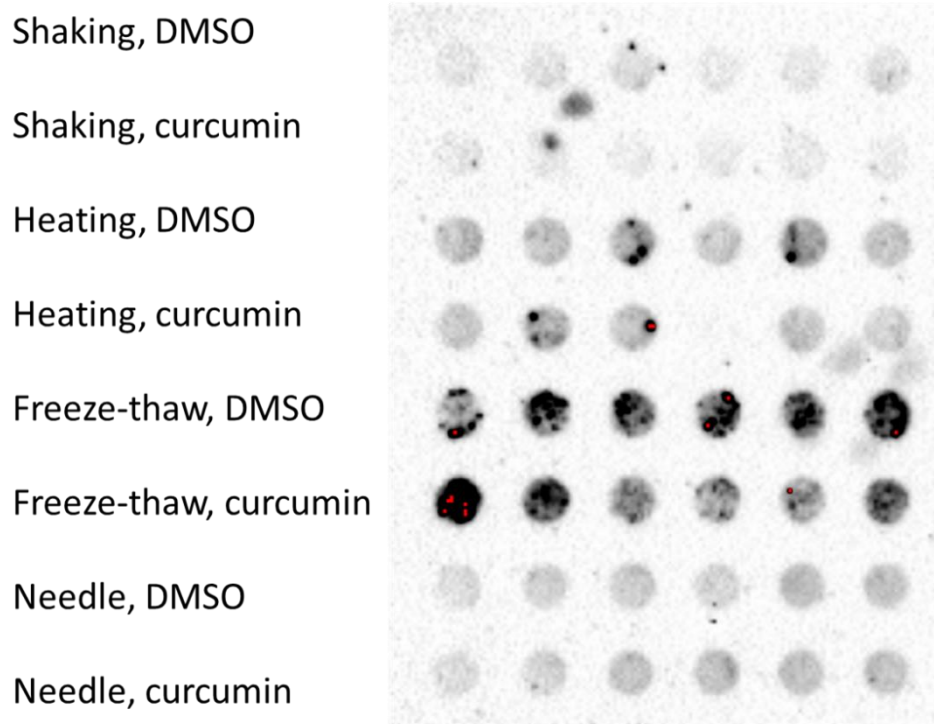


**Figure 116:** PrP<sup>Sc</sup> levels for the spheroids treated with curcumin expressed as % of the DMSO treated spheroids subjected to the same lysis conditions. Only the freeze-thaw treated samples showed PrP<sup>Sc</sup> levels of less than 70% of the DMSO control (the limit for activity), and this was also the only treatment that showed a significant difference (t-test) between the DMSO treated spheroids and the curcumin treated spheroids ( $p = 0.014749$ ,  $n = 6$ ). Differences between the DMSO treated spheroids and the curcumin treated spheroids for all other treatments were non-significant. Six replicate samples were used for each lysis treatment, with each sample containing 2 spheroids treated with either 0.5 % DMSO or curcumin.

The lack of a significant reduction in PrP<sup>Sc</sup> levels to below 70 % of the control for 3 out of the 4 lysis methods (see **Figure 116**) suggests that the reduction seen in the spheroids subjected to freeze thaw cycles may not be a real effect. This experiment was not repeated and therefore the results were not validated as the decision was made to use the bioruptor instead. Due to the lack of activity shown by curcumin, other anti-prion compounds from the literature with known *in vivo* activity (see **Table 46**) were screened in this model. It was hoped that if these compounds caused a reduction in PrP<sup>Sc</sup> in the spheroids then it would act as a proof of concept that this model could be used to correctly identify compounds with and without *in vivo* anti-prion activity.

Spheroids were dosed with both the I3GAs compounds and the compounds from the literature. The effect of 0.5 % DMSO on spheroid formation was investigated and found to have no effect on spheroid formation or stability (data not shown). Results for the literature compounds and the I3GAs can be seen in **Figure 117** and **Figure 118**.

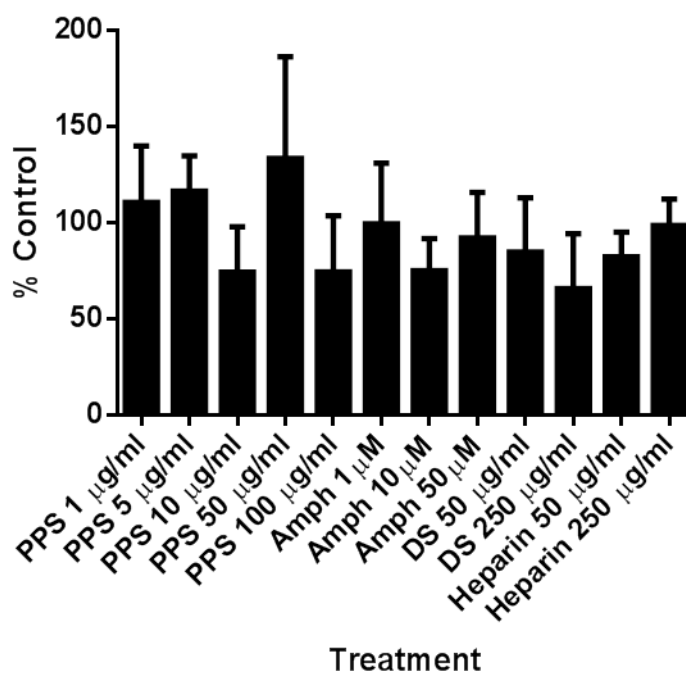


**Figure 117:** PrP<sup>Sc</sup> levels as a % of the DMSO control in spheroids treated with different compounds from the literature at a range of concentrations. PPS; Pentosan polysulfate, Amph; Amphotericin B, DS; Dextran sulfate. The data points shown represent the mean ± SD values from duplicate experiments where each sample was analysed in triplicate. Each sample contains 2 spheroids.

**Figure 117** shows that the literature compounds did not show any significant evidence of activity at concentrations much greater than their EC<sub>50</sub> in the 2D cell model, with the only treatment

reducing PrP<sup>Sc</sup> levels below the standard cut off point of 70 % being dextran sulfate (65.71 % average). The reduction in PrP<sup>Sc</sup> levels was found to be statistically significant using a multiple t-test ( $p = 0.0277763$ ).

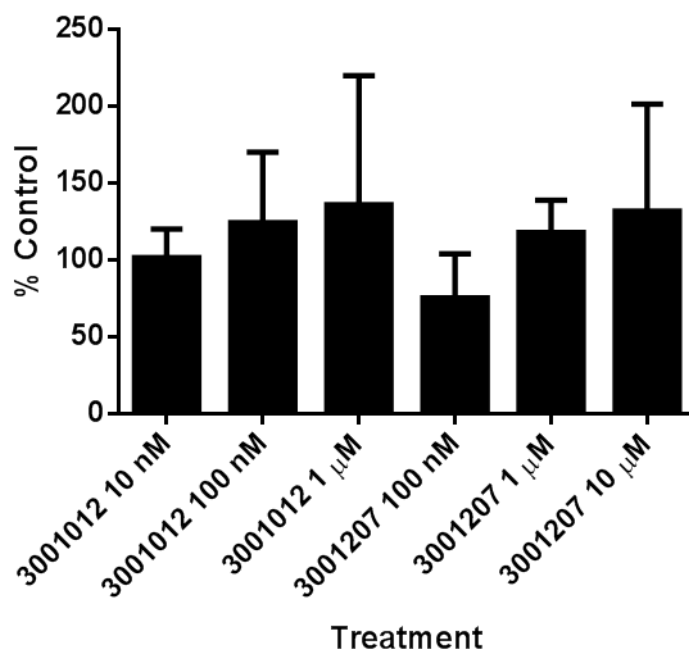


**Figure 118:** PrP<sup>Sc</sup> levels as a % of the DMSO control in spheroids treated with the indole compounds 3001012 and 3001207 at a range of concentrations up 1000 x EC<sub>50</sub> in the 2D cell model. The data points shown represent the mean ± SD values from duplicate experiments where each sample was analysed in triplicate for all treatments except 3001012 at 100 nM and 1 μM and 3001207 at 10 μM where the data points shown represent the mean ± SD values from 4 experiments where each sample was analysed in triplicate.

None of the indole compounds showed any reduction of PrP<sup>Sc</sup> below the 70 % cut-off (see **Figure 118**), with the only treatment showing anything near this being 3001207 at 100 nM. This was not found to be a statistically significant reduction in PrP<sup>Sc</sup> levels compared to the untreated control (multiple t-test,  $p = 0.0656629$ ).

### 7.1.2.3. Further Elucidation of Spheroid Morphology

During the observations of the spheroids it was noted that after the initial formation period of around two days the spheroids did not appear to increase in size. It was not possible to monitor the growth of the spheroids using standard proliferation assays due to containment issues, so each day a spheroid was removed from the plate and photographed. Direct comparison of these pictures shows that, as suspected, the spheroids don't appear to be growing in size (see **Figure 119**). In the 2D model the cells double in number approximately every three days.

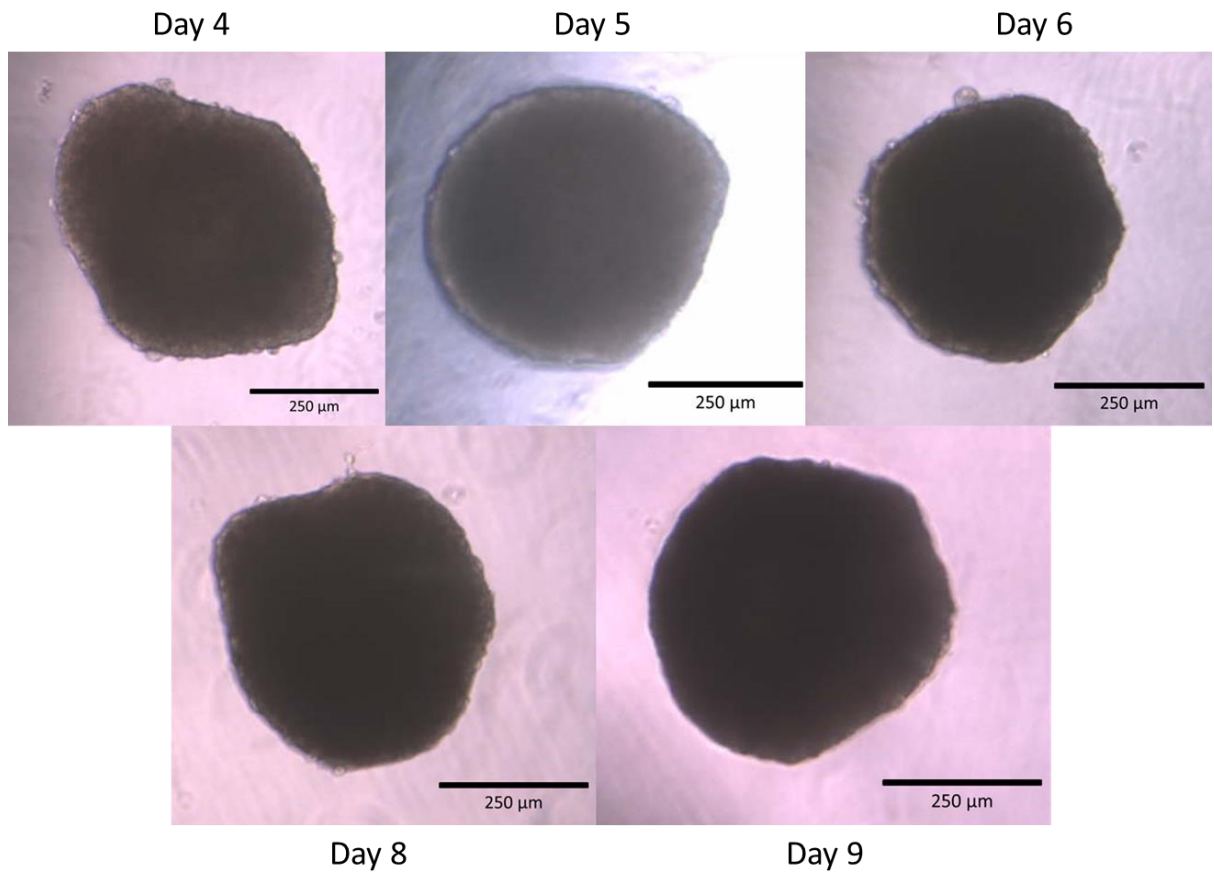


**Figure 119:** Images of spheroids taken over a number of days after seeding. Comparison of the images shows that they do not appear to be increasing in size.

At this stage it was not known whether the cells were alive or not. It was hypothesised that they may be alive but no longer growing, or they may still be growing with the spheroids becoming more and more compact as the days go by. A necrotic core is a feature of spheroids larger than 500nm used in cancer models, <sup>(334)</sup> so another possibility was that it was only the cells on the outside that were dividing, with this not being enough to causes the spheroid to increase in size. An image was obtained using confocal microscopy to further reveal the structure and morphology of the spheroid.

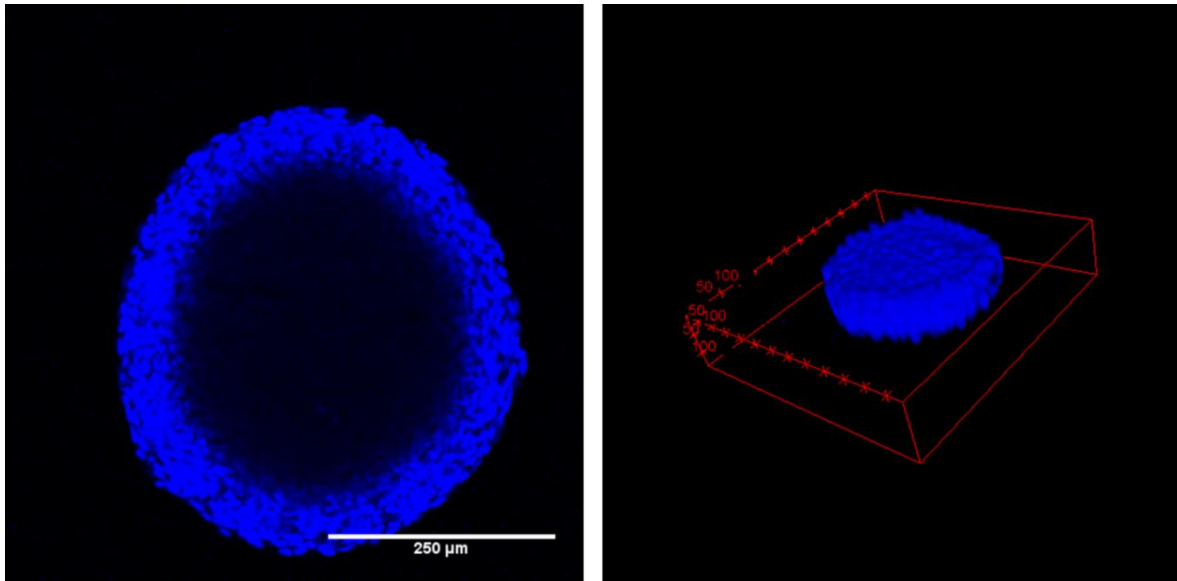


**Figure 120:** Confocal microscope image at 20 x magnification of a spheroid formed in a hanging drop plate and stained with DAPI.

The image in **Figure 120** shows the cells round the edge of the spheroid have been stained with DAPI. The blank space in the middle of the spheroid may be the necrotic core or it may be that this area of the spheroid cannot be visualised using this technique. The flattened morphology observed in the 3D visualisation (right) is thought to be a result of spheroid flattening due to mounting.

In order to investigate spheroid viability further, experiments were carried out to determine what would happen if the spheroids were seeded into a different environment, specifically a tissue culture treated 96 well plate with or without a pre-established SMB cell monolayer. It was hypothesised that if the cells were still alive they would attach to the bottom of the plate and spread out, although the extent to which this might occur was unknown.

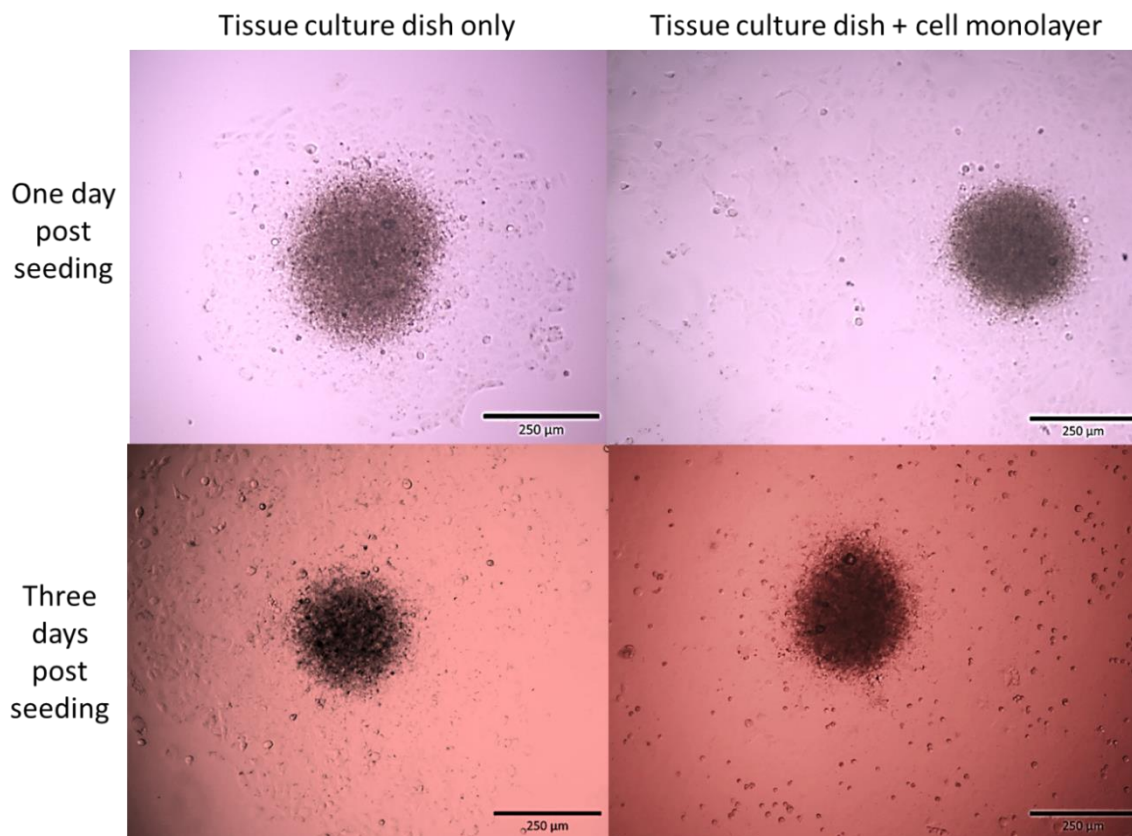


**Figure 121:** Pictures demonstrating the attachment and spread of spheroids when transplanted into a 96 well plate either with or without a cell monolayer. Spread and growth of the cells from the spheroids can be clearly seen on the blank surface of the plate. Distinguishing cells from the plate from cells in the monolayer is more challenging.

It can be seen from the pictures in **Figure 121** that initial suspicions that the cells were dead are probably unfounded, and this was subsequently investigated further using an MTT assay. It is still theoretically possible that the cells at the centre of the spheroid are no longer alive but it is clear that those around the periphery, at least, are alive and have attached and spread out on the surface of the plate. The presence or absence of a cell monolayer doesn't appear to make much of a difference to the spread of the spheroids.

Finally, an attempt was made to carry out an MTT assay on the spheroids to determine if they were still alive, with cell death being a possible explanation for the observed lack of growth. The spheroids were obviously purple, indicating the presence of the conversion product, but after solubilisation only gave a very weak signal. One well of a 96 well plate, containing a monolayer of approximately 20,000 cells would give a signal of around 0.1 absorbance units (AU). The spheroids, which contained 40,000 cells when seeded, gave a signal of between 0.015 and 0.03 AU.

Although the MTT assay only gave a very weak signal it was enough to show that formation of the conversion product was happening, indicating that at least some of the cells in the spheroid were still alive. The weak signal, despite a larger number of cells in the spheroid than in the monolayer, could be explained either by the presence of a necrotic core or by problems with either MTT penetration or final solubilisation. It was apparent from the work carried out that at least a proportion of the cells within the spheroid were alive, and due to the problems with solubilisation and visualisation no attempt was made to assess the live/dead ratio of the cells through any other method.

### 7.1.3. Discussion

The first and most obvious conclusion that can be drawn is that the SMB cells will aggregate to form spheroids when cultured in the hanging drop format. This was observed in both the 384 and 96 well plate formats, with the spheroids being stable for up to 9 days. Unfortunately from this point on there is a lot of uncertainty associated with this model.

The literature around this spheroid model primarily focusses on the application of the technique for studying anti-cancer drugs, with protocols available for using these spheroids in proliferative assays. There was no literature available at the time of writing about using this model for monitoring the effect of drugs on intracellular proteins, and therefore there were no standard protocols available for lysing the spheroids and analysing the lysate *via* immunoblotting. For this reason an extensive period of lysis optimisation was required. Advice from the manufacturer did not extend beyond using a more stringent lysis buffer and using a sonicator if possible so a search of the literature revealed some other options for homogenising tissue samples including mechanical techniques and enzymatic digestion using collagenase. The most promising of these techniques was subjecting the spheroids to repeated freeze-thaw cycles but sonication using the bioruptor was found to be much more efficient.

Once lysis was optimised it was possible to dose the spheroids with a range of compounds to see if any change in PrP<sup>Sc</sup> levels could be observed. As can be seen from the data (**Figure 117** and **Figure 118**) the majority of the treatments didn't result in any reduction of PrP<sup>Sc</sup> below the 70 % cut off. Even the compounds that are reported to work *in vivo* showed no activity, with the only exception being dextran sulfate at 250 µg/ml. Much variation was observed even with the

optimised lysis conditions, with the large error being testament to the inconsistency of results between runs. The lack of activity from the compounds with known *in vivo* activity means that no conclusions can be drawn from this model about the potential *in vivo* activity of the indoles. The exact reason behind the failure of the compounds to exert their anti-prion effect in this model is not known, but various reasons have been hypothesised. It was observed early on in the study that once the spheroids had formed they did not appear to be increasing in size. Questions were therefore raised about whether cells within the spheroid were still alive and whether this may be a reason for the lack of activity seen from the anti-prion compounds. Studies were carried out to try and make this clear, with the cells round the edge of the spheroid appearing to be alive as they attached to the surface of a tissue culture plate when transferred to a 96 well plate. Preliminary MTT data also suggested that the cells in the spheroids were still alive, but due to the weak signal it was not possible to quantify this accurately. Due to containment issues it was not possible at this time to pursue this investigation using a different proliferation assay, but this would be something to be considered if this model were to be investigated further.

The possible lack of growth was proposed as another reason why the compounds might not be working. In curative assays conducted with quinacrine it was found that when growth was arrested (in a 2D model), PrP<sup>Sc</sup> reappeared within three days, much more quickly than when the cells were allowed to proliferate as normal.<sup>(377)</sup> Cell division has also been shown to contribute to the reduction of PrP<sup>Sc</sup> levels to a steady state level, although not to total clearance.<sup>(110)</sup> It is therefore possible that cell division may have a role to play in the mode of action of one, if not all of these compounds, where if the cells within the spheroid are no longer dividing then the compound's action may be compromised. As discussed previously, larger spheroids tend to have a necrotic core, which may contribute to this effect. Once again, a better measure of proliferation may help determine this further.

Another suggestion was that the way the cells are tightly packed into the spheroid may be preventing the compounds from accessing the cells within the spheroid. If penetration was limited then the potential effect of the compounds would also be limited. The main attraction of this hanging drop model was the manufacturer's claim that the spheroids represented *in vivo* condition closely, and some of the compounds used in this study have been shown to have *in vivo* activity. Despite the evidence of its efficacy in a mouse model of prion disease, curcumin has been shown to have poor bioavailability in humans, with reasons given including poor

absorption, rapid metabolism and rapid systemic elimination.<sup>(462)</sup> It may be that these unfavourable pharmacokinetic properties are a reason why curcumin does not appear to be as active as might have been expected in this model. However, this is not thought to be the case with PPS and DS, and initial studies on the pharmacokinetic properties of the I3GAs found them to be present in mouse brains at concentrations above the cellular EC<sub>50</sub> (see section 4.5). While unfavourable pharmacokinetic properties may have a role to play in the lack of observed activity from the indole compounds, possibly due to their poor solubility, it is thought unlikely that this is the only factor preventing the compounds from working.

The image of the spheroid obtained using confocal microscopy appears to show a region in the middle of the spheroid that is devoid of DNA, which may represent the necrotic core that exists in multicellular tumour spheroids. However, it has been suggested that confocal microscopy is not a suitable technique for imaging the central region of spheroids, with two photon excitation microscopy suggested as an alternative.<sup>(463)</sup> Other work has suggested that optimisation of the experiment parameters can result in imaging depth increasing from 100 µm to 320 µm.<sup>(464)</sup> The key parameters for optimisation were suggested to be the use of a water immersion lens and careful modulation of laser output as a function of depth. It may be that optimising one or other of these parameters may help elucidate the image of the spheroid further. All images presented here were obtained using oil immersion objectives, and the water immersion objectives have been suggested as being preferable as water more closely matches the refractive index of most living biological systems.<sup>(465)</sup>

Overall there are advantages to this model which would, in theory, make it ideal for use as a high-throughput model for screening anti-prion compounds. It's low cost and easy to use without any specialised equipment, and results in the formation of spheroids that are homogenous in size and shape. However, the total lack of activity seen from any of the compounds investigated raises questions about the suitability of this model for this specific application. It is thought that further investigation would be required to get to the bottom of why the compounds are not working, with the crucial bit of information being about whether the cells are proliferating. It was not possible to monitor this by MTT but there are other assays available that could be tried, and it is thought that this should be the first step if the spheroid model is going to be pursued any further.

## 7.2. The Alvetex Scaffold Model

### 7.2.1. Introduction

The use of scaffolds to culture cells in 3D is a well-established technique, with a variety of different materials, both natural and synthetic, being used as the basis of the scaffold. Scaffolds are designed to encourage cells to maintain their natural, rounded morphology, rather than being flattened as they are in 2D culture, as well as encouraging the formation of tissue like structures and cell-cell interactions.

For the purposes of this study the Alvetex scaffold system was trialed. The Alvetex scaffold is a highly porous polystyrene scaffold which is 200  $\mu\text{m}$  thick.

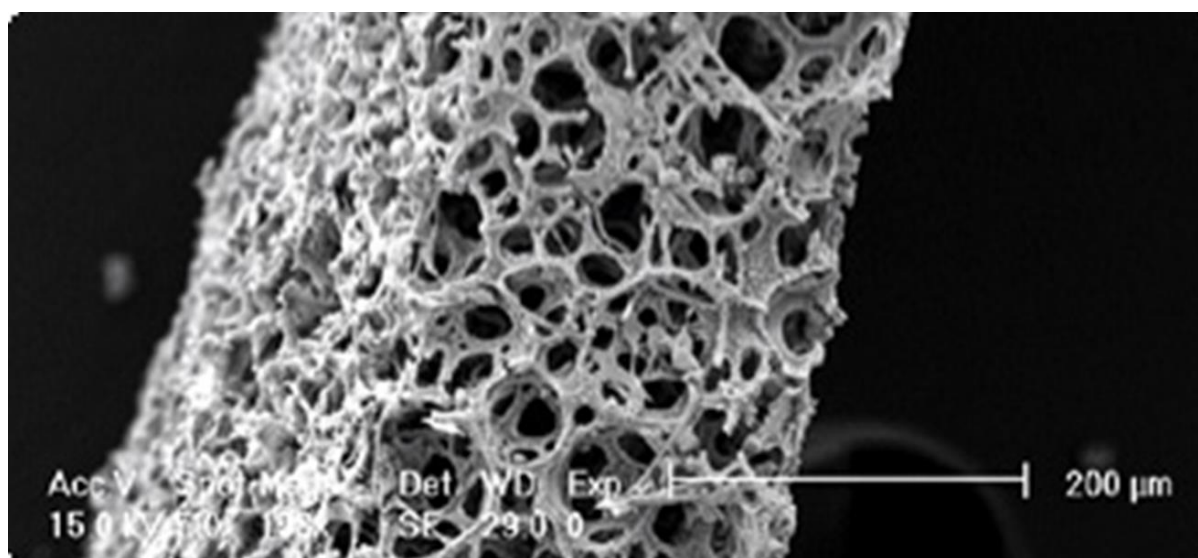


**Figure 122:** Scanning electron microscopy image showing the edge of an Alvetex Scaffold (image from [www.amsbio.com](http://www.amsbio.com), suppliers of Alvetex scaffold).

A significant advantage of the Alvetex platform was that it was available in a 96 well format which, in theory, could be used without the need for any significant optimisation or changes to culture conditions. The only optimisation that was needed was to check initial seeding densities. It was also available as 12 and 24 well plates, as well as inserts. The other advantage with this system, as stated earlier, was that detailed protocols existed for monitoring growth using an

MTT assay and also for lysing cells and retrieving the intact cells for analysis. Materials and methods for this study are outlined in detail in sections 2.1.6, 2.2.8.2 and 2.2.8.4.

## 7.2.2. Results

### 7.2.2.1. Growth Curve and Seeding Density Optimisation

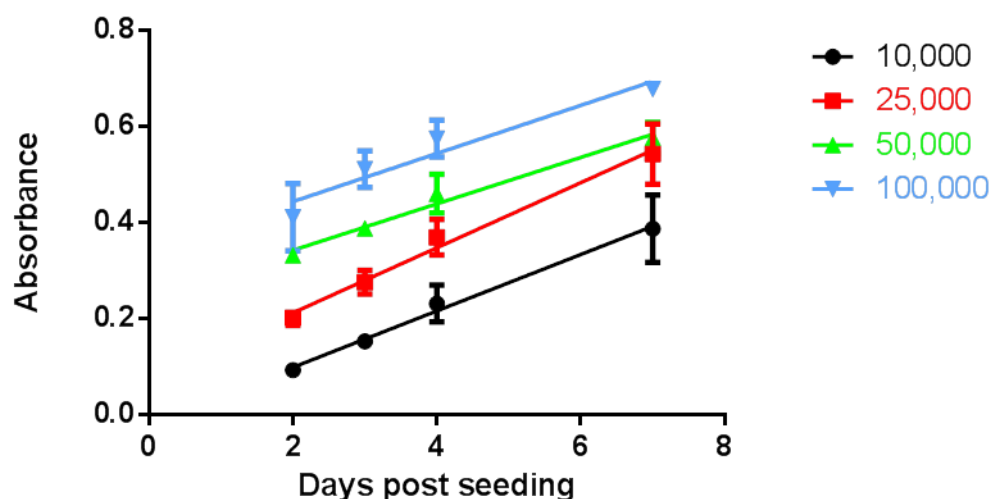


**Figure 123:** MTT results for SMB cells seeded onto the scaffold at densities ranging from 10,000 cells/well to 100,000 cells/well. Increased metabolic activity, suggesting increased cell numbers, can be seen for all groups. The data points shown represent the mean  $\pm$  SD values from duplicate experiments where each sample was analysed in triplicate.

The results of the MTT assay, shown in **Figure 123**, strongly suggest that the cells were alive and proliferating within the scaffold over the 5 day period that was routinely used for compound screening.

### 7.2.2.2. Cell Visualisation

It was not possible to visualise the cells within the scaffold using brightfield microscopy, so attempts were made to visualise the cells by employing neutral red staining. Staining was carried out three days after seeding at 50,000 cells/well.

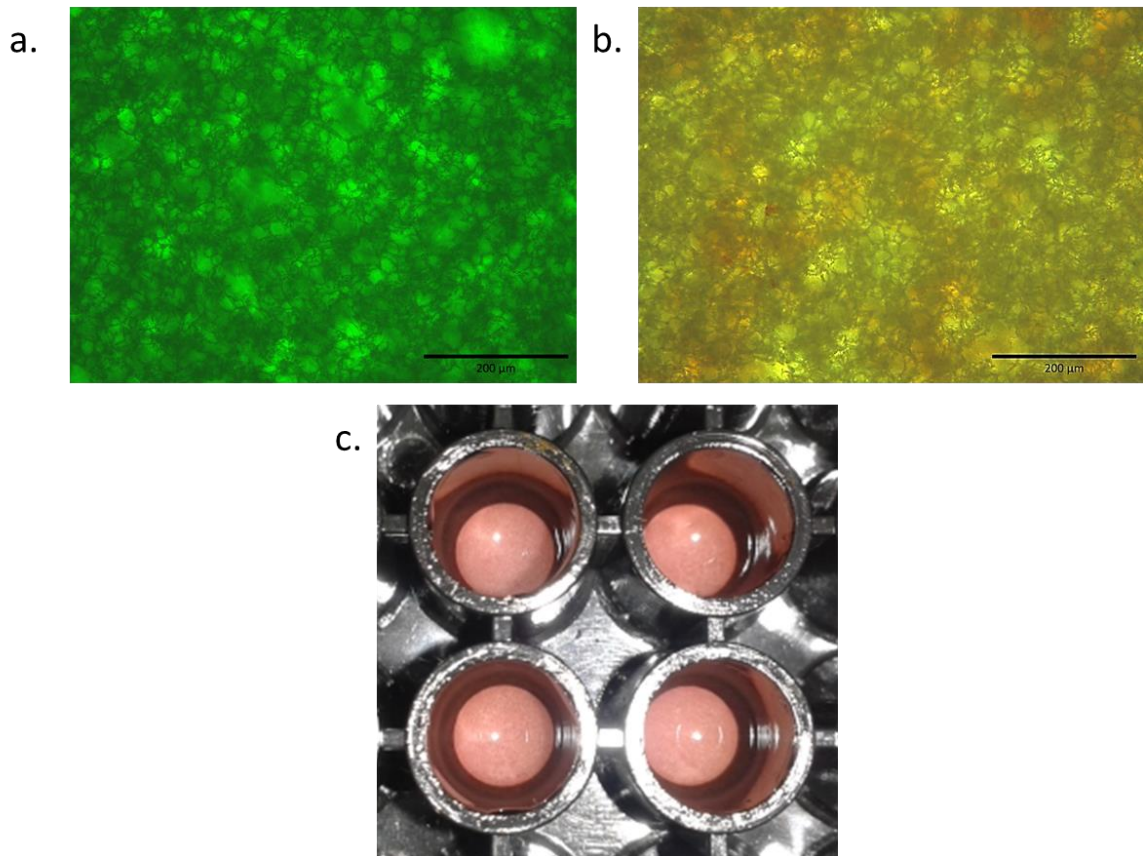


**Figure 124:** Images of the Alvetex scaffold under the brightfield microscope. a. shows the scaffold containing cells at 20 x magnification. b. shows the scaffold containing cells that have been stained with neutral red, also at 20 x magnification. Although a red colour can be seen it is not possible to identify individual cells. c. shows the appearance of the wells to the naked eye with the red staining clearly visible, showing the presence of living cells within the scaffold. Staining was carried out three days after seeding, with initial seeding densities of 50,000 cells/well.

It can clearly be seen in **Figure 124c** that neutral red staining was successful and the cells are alive and embedded within the scaffold, but this did not give any more information than the MTT assay. However, the lack of resolution under the brightfield microscope meant it was still not possible to identify individual cells under the microscope, as was the case in the 2D model.

### 7.2.2.3. Cell Visualisation Continued – Confocal Microscopy

Due to the lack of resolution available using the normal brightfield microscopes (see **Figure 124**) it was necessary to look at other options for visualising the cells. Protocols were available for fixing and mounting the scaffolds for use in a confocal microscope so this was explored further. It was hoped that the higher resolution afforded by the confocal microscope would help visualise the cells and confirm their 3D conformation within the scaffold.

In order to visualise the cells and the scaffold, different dyes were used. 4'-6-diamidino-2-phenylindole (DAPI), which produces a blue fluorescence when bound to DNA, was used to visualise the nuclei of the cells. Nile red, a lipophilic dye which fluoresces red was used to stain and visualise the scaffold, both with and without cells present. An acti-stain phalloidin, which fluoresces green, was used to stain actin, a protein found in the cytoplasm and gain further insights into the orientation of the cells within the scaffold and cell-cell contacts.

Initial studies visualised the nuclei of the cells to confirm the 3D conformation that was expected. Images of the scaffold were obtained, both when empty and when seeded with cells. Cells were visualised either as nuclei or as nuclei surrounded by the cytoskeleton.

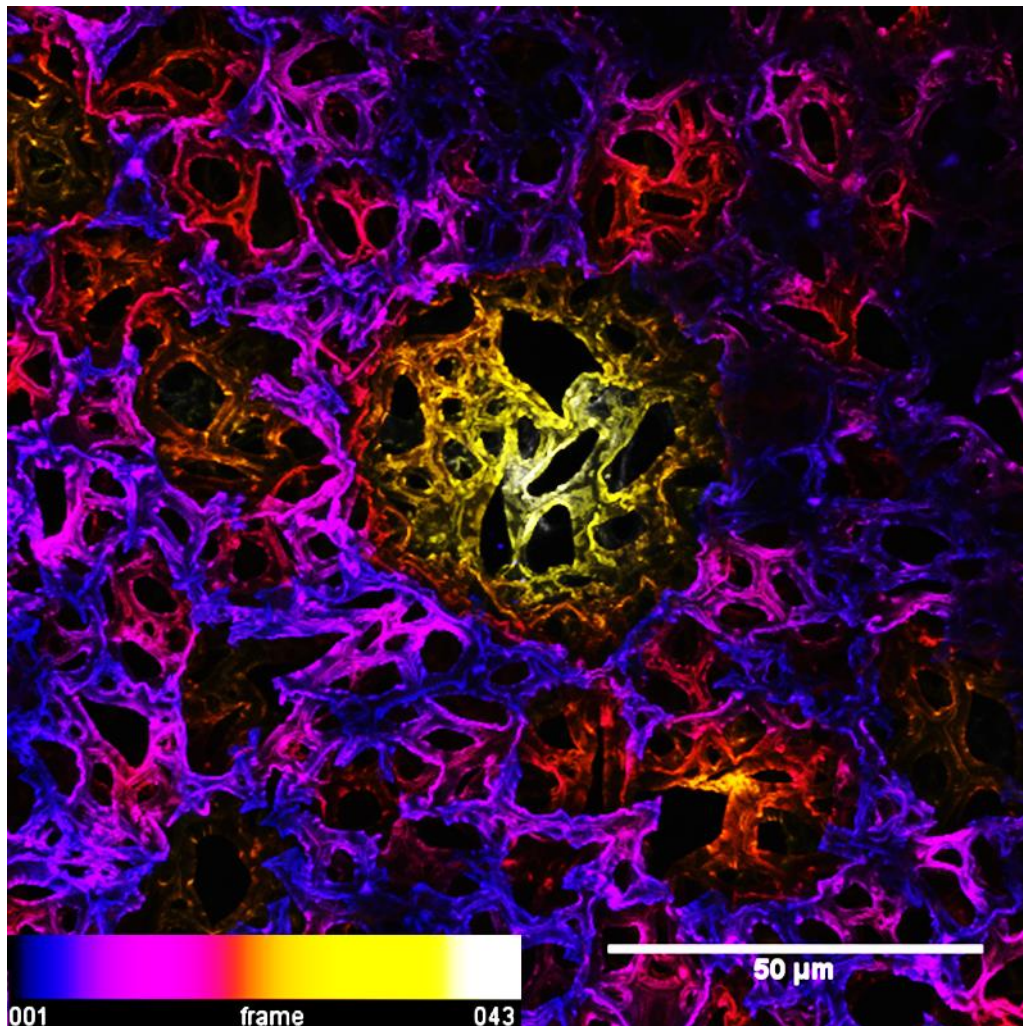


**Figure 125:** Depth colour coded z-stack of cell free Alvetex scaffold at 40 x magnification. Frame 1 represents the top of the scaffold, frame 43 represents the bottom. Total depth is around 120 μm with each frame 2.8 μm apart.

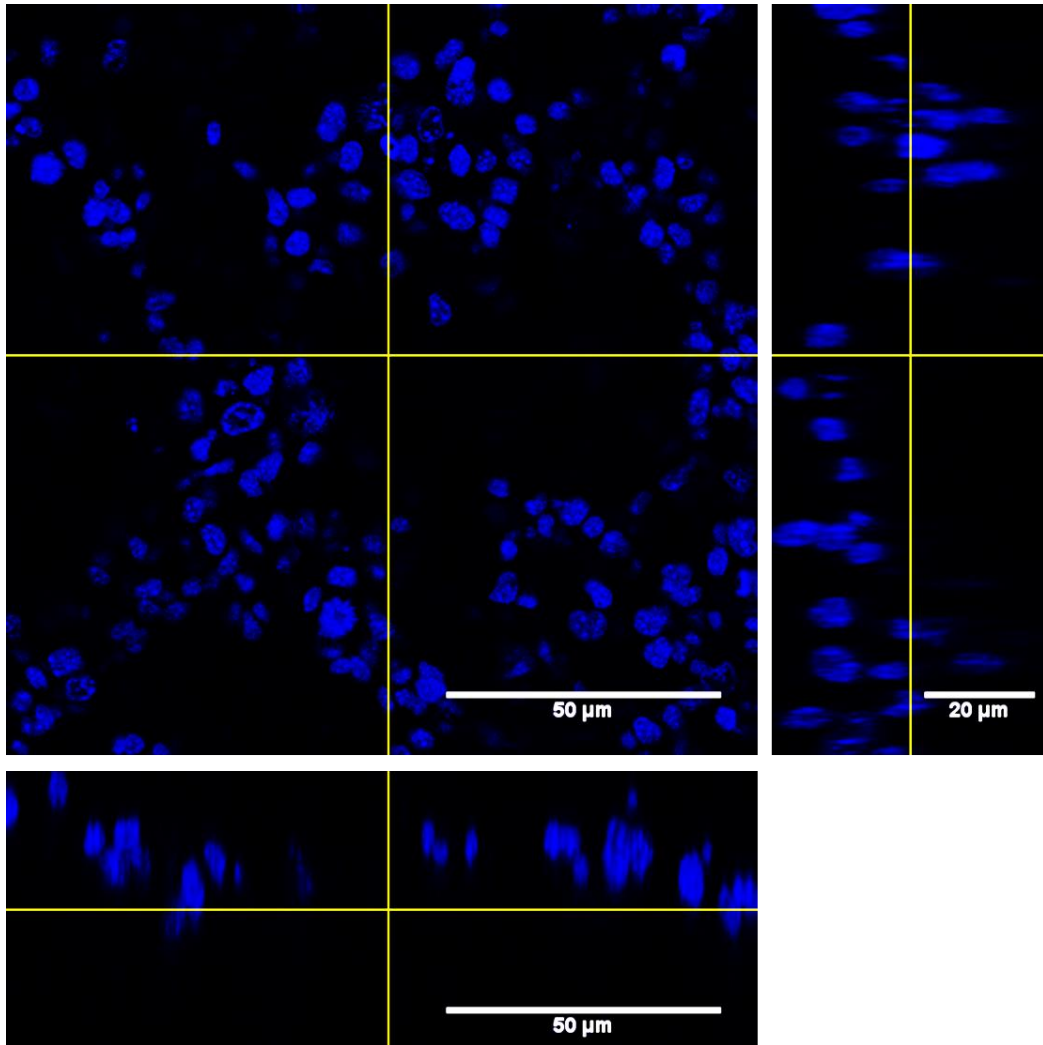


**Figure 126:** Orthogonal view of a z-stack image at 40 times magnification of the Alvetex scaffold from a 12 well plate seeded with cells at an initial seeding density of 500,000 cells. Cells are stained with DAPI to visualise the nucleus, and have penetrated the scaffold to a depth of 50  $\mu\text{m}$ .

It can clearly be seen in **Figure 126** that the cell nuclei are in a 3D conformation, and also that the cells had penetrated into the scaffold rather than just settling on the top. Once it was established that the cells were showing the expected rounded morphology further investigations were carried out, using scaffolds harvested at different time points to visualise the proliferation of the cells.

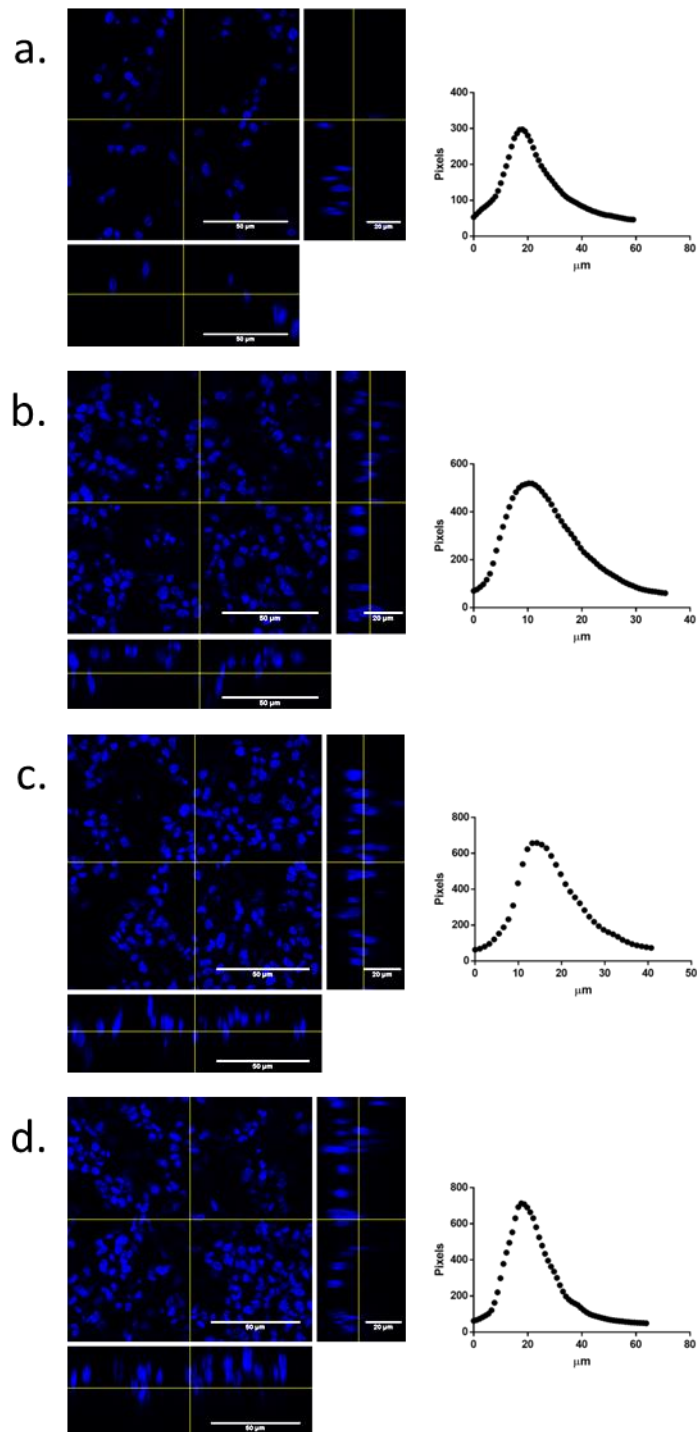


**Figure 127:** Orthogonal views of z-stack images from scaffolds harvested at different time points; 2 days (a), 4 days (b), 6 days (c) and 8 days (d). Graphs show the number of pixels in each slice of the z-stack, representing the distribution of the cells within the scaffold and the depth to which they have penetrated, which did not change much between time points.

The time course represented in **Figure 127** confirmed the proliferation of the cells within the scaffold, and also validated the results from the MTT assay and the validity of using this technique for measuring cell growth in this model. The cells do not appear to be penetrating

further into the scaffold over time, suggesting that migration through the scaffold may not be a dynamic process.

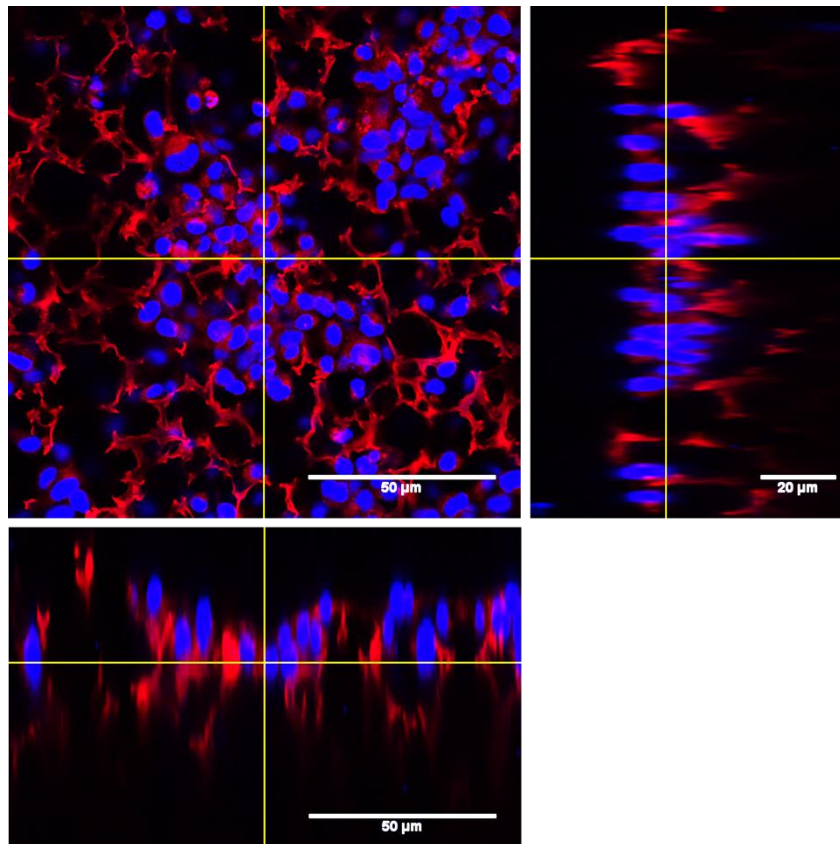


**Figure 128:** Orthogonal view of a z-stack image at 40 x magnification where the cells and the scaffold were stained with DAPI and Nile red respectively and imaged at different wavelengths. Total depth of the image is around 100 μm.

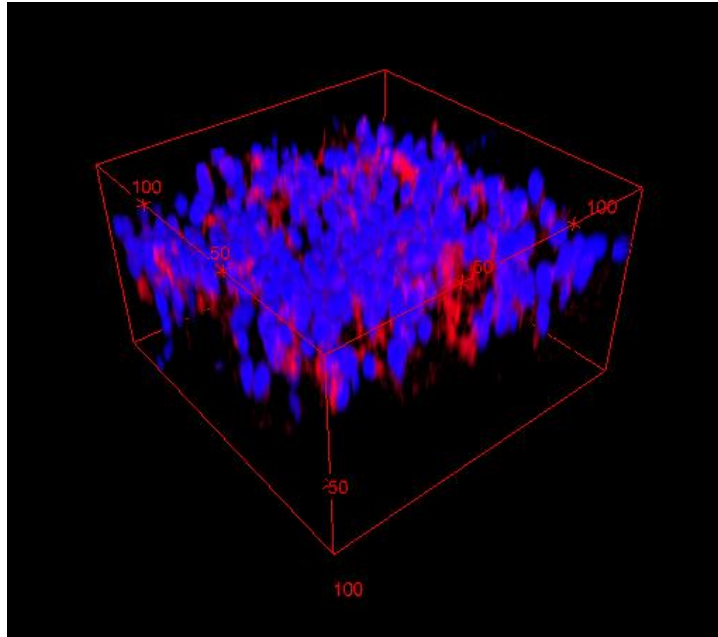


**Figure 129:** 3D representation of the z-stack shown above in **Figure 128**. Numbers are in  $\mu\text{m}$  and represent the dimensions of the section.

It can be seen from the images in **Figure 128** and **Figure 129** that the cells are embedded into the scaffold. The majority of the cells appear to be towards the top of the scaffold, although there is evidence of the cells migrating through it.

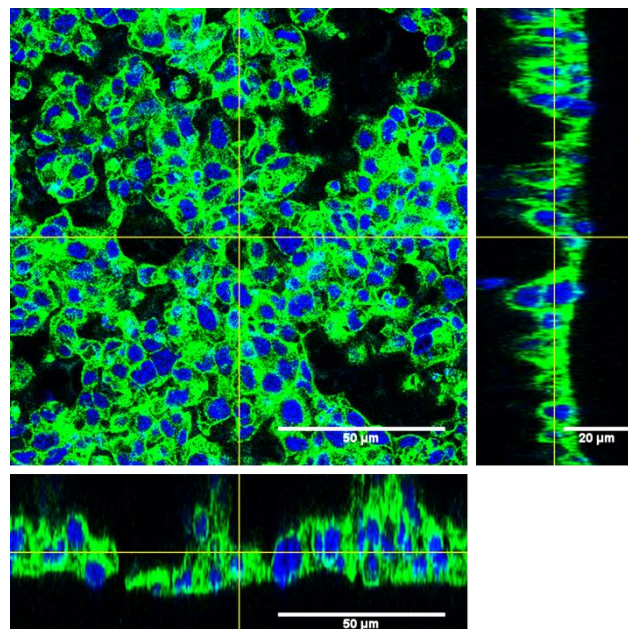


**Figure 130:** Orthogonal view of a z-stack image at 40 x magnification. Cell nuclei are stained with DAPI (blue), actin in the cytoskeleton is stained with phalloidin acti-stain 488 (green). The cell-cell contacts and 3D structure can be observed in all sections.

Staining of the cells with both DAPI and acti-stain as in **Figure 130** allowed the cell-cell contacts to be visualised. The increased level of cell-cell contact is something that is key to the 3D model's ability to replicate *in vivo* conditions and therefore being able to visualise this was a key finding. Further evidence of the cell-cell contact, and the cell's orientation within the scaffold, can be seen in **Figure 131** and **Figure 133**.

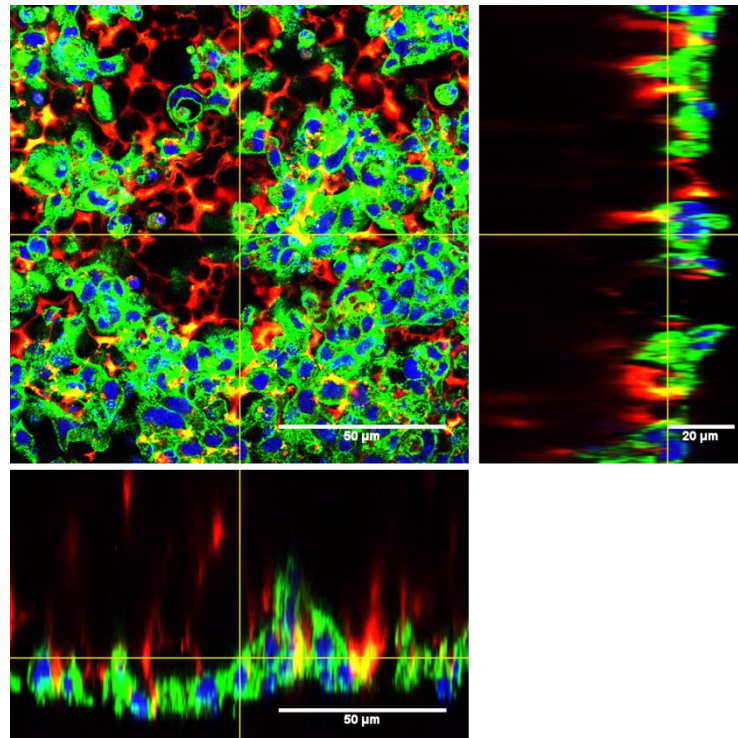


**Figure 131:** Orthogonal view of a z-stack image at 40 x magnification. Cell nuclei are stained with DAPI (blue), actin in the cytoskeleton is stained with phalloidin acti-stain 488 (green) and the scaffold is stained with Nile red (red). The red signal has slightly bled into the green channel, resulting in the yellow signal from some points of the scaffold. However, the cell nuclei, surrounded by the cytoskeleton, can be clearly seen.

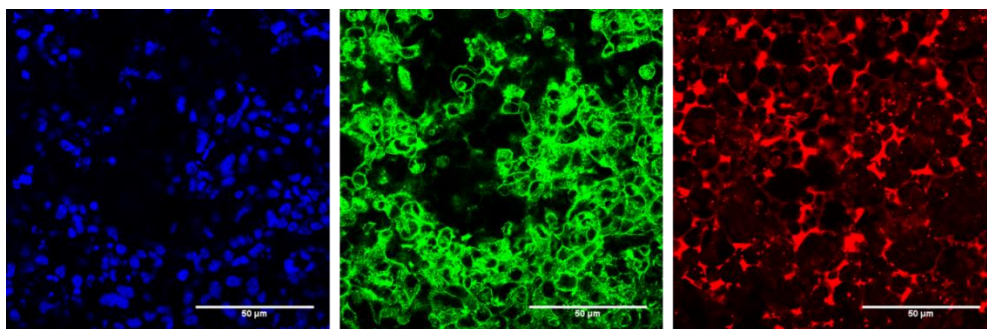


**Figure 132:** Deconstruction of **Figure 131** above. Pictures represent either cell nuclei stained with DAPI (left), actin stained green, along with bleed through from the red channel (middle) and the scaffold stained red (right).

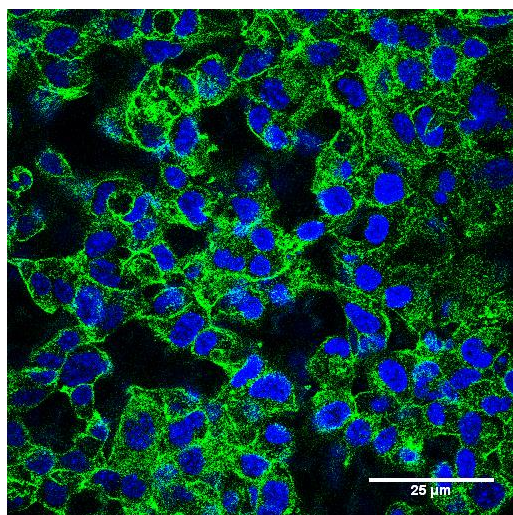


**Figure 133:** Image taken at 60 x magnification of scaffolds stained with DAPI and acti-stain.

It can be seen in **Figure 133** that imaging at 60 times magnification does not provide a significant amount of extra detail, therefore validating the decision to do the majority of the imaging at 40 times magnification.

#### **7.2.2.4. Compound Screening**

Initial dosing trials were carried out to see if any activity could be seen from the I3GAs. Cells were dosed with HBSS, 0.5% DMSO, 10 μM curcumin or 10 nM 3001012. For this trial the lysis was repeated, with both sets of lysate being analysed to assess the effect of treatment on PrP<sup>Sc</sup> levels.

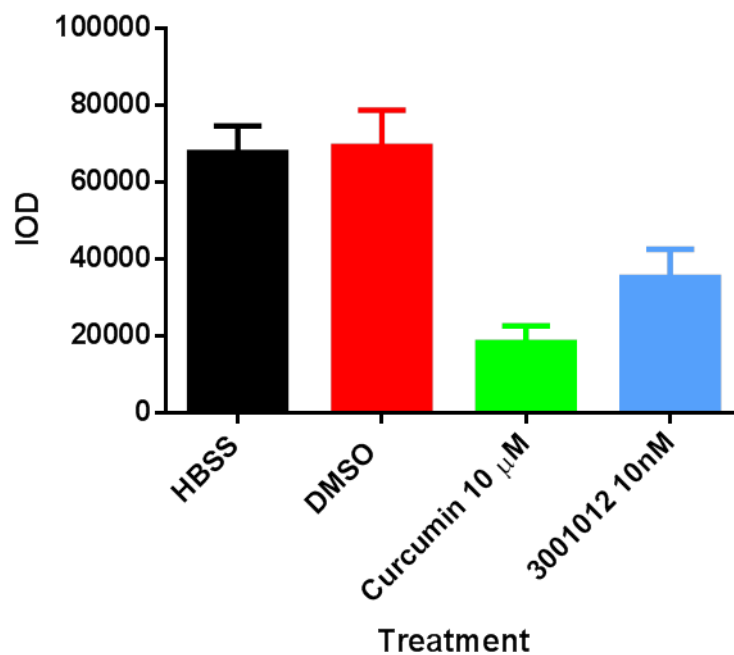


**Figure 134:** Results of initial dosing trial on cells grown in 3D within the Alvetex scaffold. PrP<sup>Sc</sup> levels are directly proportional to the integrated optical density (IOD) of the dots on the blot, as measured by Bio-Rad Quantity One software. It can clearly be seen that curcumin and 3001012 are causing reductions in the levels of PrP<sup>Sc</sup> in treated cells, although with slightly reduced efficacy compared to results in the monolayer. The results were also fairly consistent over different wells. The data points shown represent the mean  $\pm$  SD values from duplicate experiments where each sample was analysed 4 times.

The data in **Figure 134** was thought to be extremely promising, as they show that the Alvetex scaffold can be used for this application, and also that the compounds seem to be capable of reducing PrP<sup>Sc</sup> in this model, even if the efficiency compared to the 2D model does appear to be reduced.

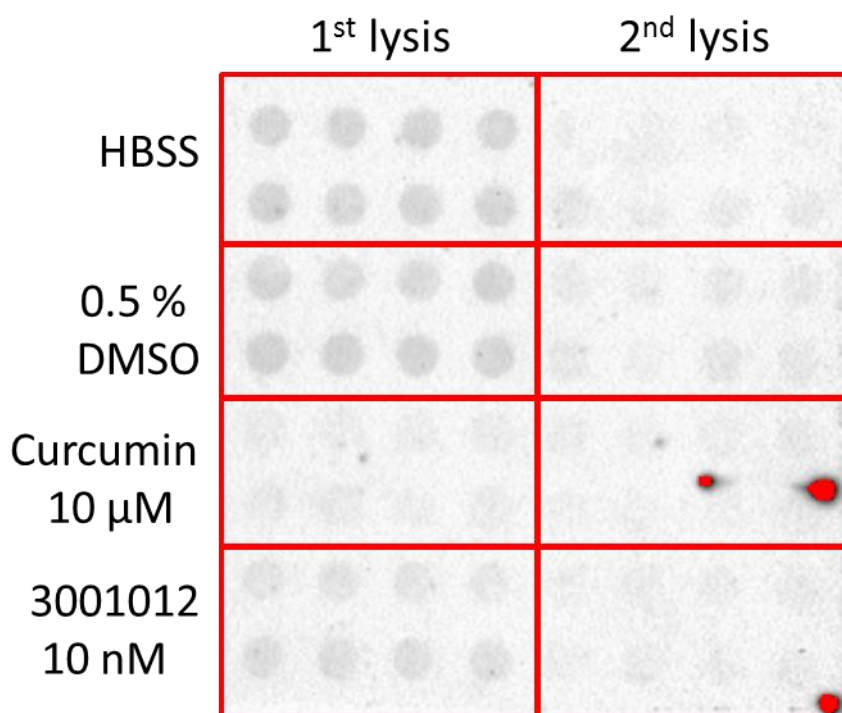


**Figure 135:** Comparison of the PrP<sup>Sc</sup> levels, as denoted by the signal on the dot blot, after treatment with different compounds and either 1 or 2 rounds of lysis. Two rows of an alvetex plate were treated with either HBSS, 0.5 % DMSO, curcumin or 3001012. Eight replicate wells, comprising 2 rows and 4 columns, were used for each treatment. Cells were lysed using RIPA buffer within the Alvetex scaffold, the lysate removed (lysis 1), and a second aliquot of RIPA buffer added to lyse any remaining cells (lysis 2). The faint signal from the second set of lysates suggests that the majority of the cells are being lysed in the initial lysis. This figure also demonstrates the activity of both curcumin and 3001012 in this model as shown by the decreased signal compared to the HBSS and DMSO control. This is more obvious in the results from the first lysis.

An interesting observation from the blot pictured in **Figure 135** was that the PrP<sup>Sc</sup> levels in the Alvetex lysate, as denoted by the signal on the dot blot were much lower than had been expected, even though the low signal from the second lysis suggests that all the cells are being lysed. The signal from the MTT assay was much stronger than that from the 2D model, and given the higher initial seeding densities (50,000 cells/well in 3D, 10,000 cells in 2D) as well as the proliferation observed in both the MTT study and the confocal microscopy images it would be expected that higher levels of PrP<sup>Sc</sup>, and a much stronger signal than normal, should be seen on the blot. Blots done at the same time, using the same antibody but with cells grown in 2D, gave a signal consistent with what is normally expected, suggesting the weak signal was not down to problems with the blotting protocol.

After this initial trial, further 96 well plates were purchased in order to obtain EC<sub>50</sub> values for each of the compounds, allowing a direct comparison with activity in the 2D models. Cells were dosed with two I3GA compounds as well as compounds from the literature with known *in vivo* activity (see **Table 46**) and were seeded and harvested as previously, although in this case only one round of lysis was carried out. Compounds were dosed at a range of concentrations based on their EC<sub>50</sub> in the 2D model. MTT assays were also carried out, using the highest concentrations of the compound used in the activity screen. For logistical reasons these were carried out in 24 well Alvetex plates, with each compound being dosed in duplicate, and each well analysed in triplicate. Compounds were screened in both 96 and 24 well plates and harvested as described in section **2.2.8.2**. Results shown below are a combination of both sets of results. Results shown below represent at least three separate experiments.

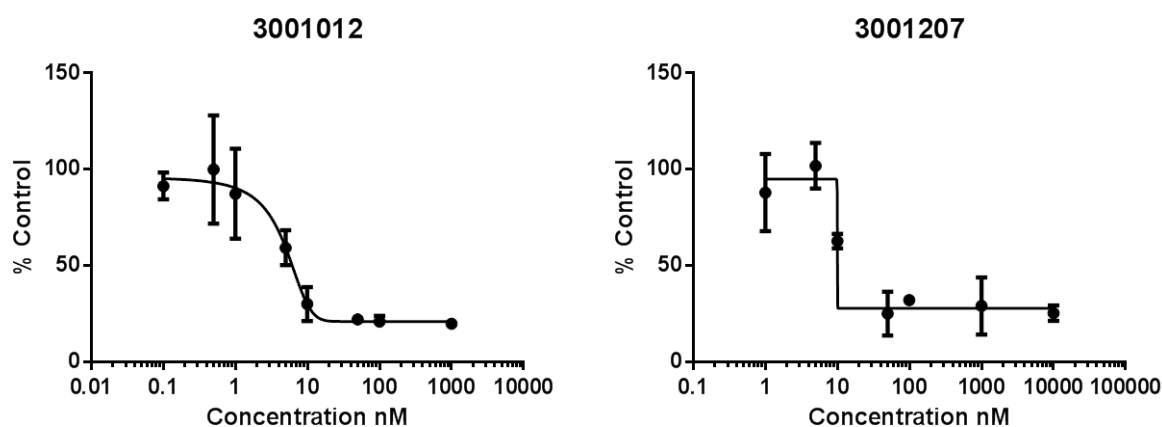


**Figure 136:** PrP<sup>Sc</sup> levels in cells grown in Alvetex scaffolds and treated with the I3GA compounds that have not been tested *in vivo*. Both compounds can be seen to reduce PrP<sup>Sc</sup> levels at concentrations similar to their EC<sub>50</sub>s in the 2D cellular model. The data points shown represent the mean  $\pm$  SD values from duplicate experiments where each sample was analysed in triplicate.

It is clear from the curves presented in **Figure 136** that both 3001012 and 3001207 are active in the Alvetex model with EC<sub>50</sub>s of 5 nM and 10 nM respectively.

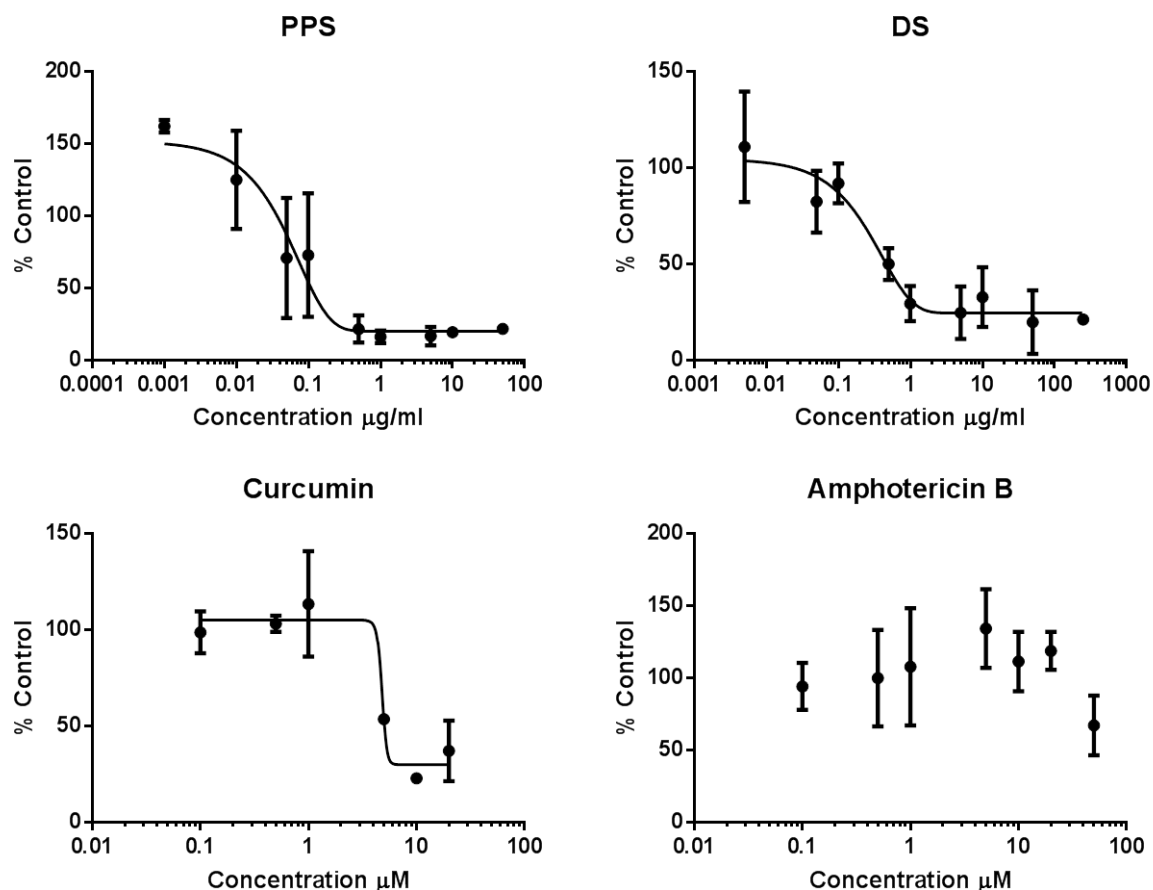


**Figure 137:** PrP<sup>Sc</sup> levels in cells grown in Alvetex scaffolds and treated with compounds known to have *in vivo* activity (see **Table 46** for references). All compounds except amphotericin B were shown to be active. The data points shown represent the mean  $\pm$  SD values from duplicate experiments where each sample was analysed in triplicate.

The data in **Figure 137** demonstrates that both PPS and DS retain excellent activity in the Alvetex model with EC<sub>50</sub>s of 0.25 µg/ml and 0.3 µg/ml respectively, as would be expected given their well-established *in vivo* activity. Curcumin retains some activity, with an EC<sub>50</sub> of 4 µM, although it is not as active as it is in the 2D model. Surprisingly, amphotericin B did not show any activity, and this is thought to be due to the concentrations used in this screen not being high enough.

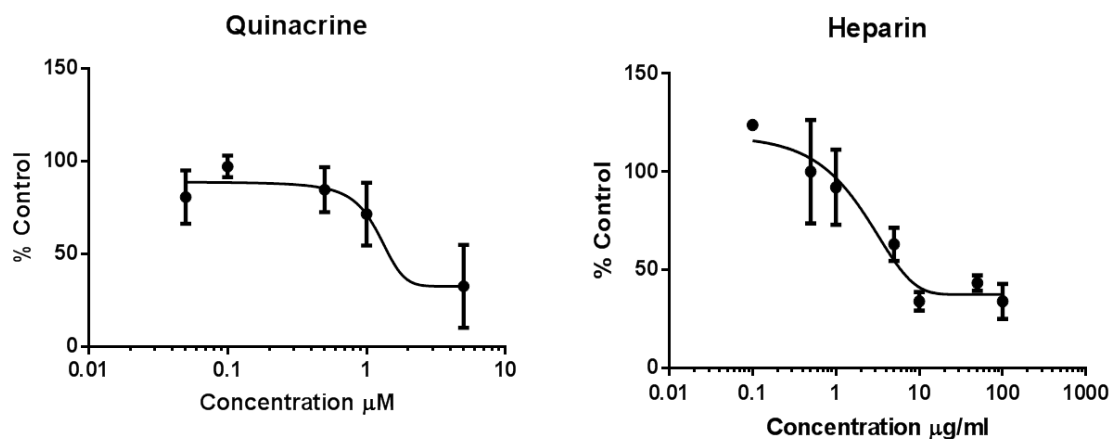


**Figure 138:** PrP<sup>Sc</sup> levels in cells grown in Alvetex scaffolds and treated with quinacrine and heparin. Quinacrine has been shown to be ineffective *in vivo*, while heparin has not been tested. (see **Table 46** for references). Both compounds showed activity, although in the case of quinacrine activity was reduced compared to activity in the 2D model. The data points shown represent the mean  $\pm$  SD values from duplicate experiments where each sample was analysed in triplicate.

**Figure 138** shows that quinacrine showed some activity, with an EC<sub>50</sub> of 2.5 μM although it was much more active in the 2D model. The efficiency of quinacrine is also reduced, with clearance at the higher concentrations being much reduced compared to the 2D model and the transition from inactive to active concentrations not being as sharp as that observed in the 2D model. Heparin retains all its activity compared to the 2D screen, with an EC<sub>50</sub> of 3 μg/ml No information was available in the literature at the time of writing about the activity of heparin *in vivo* but the data presented here would suggest that it has the potential to be active.

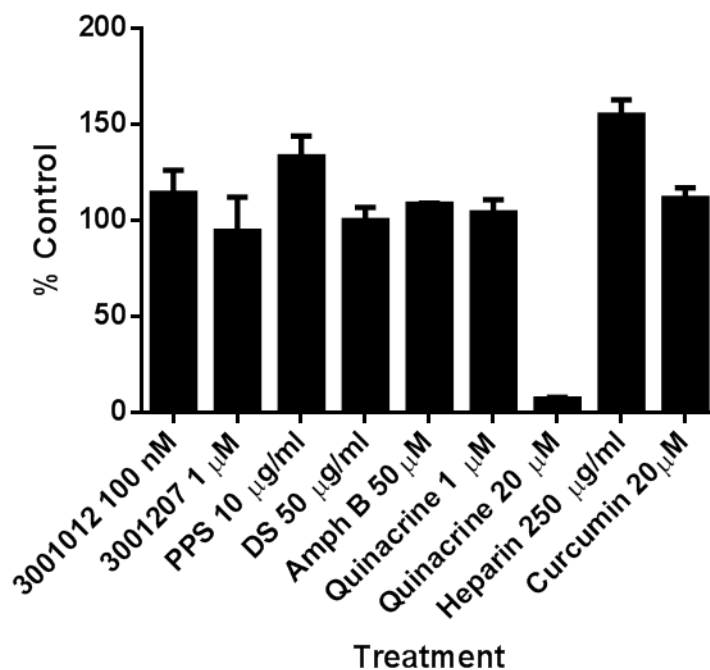


**Figure 139:** MTT viability data for cells grown in scaffolds and treated with the highest concentrations of the compounds used in the activity screening. All compounds apart from quinacrine were non-toxic at their highest concentrations. The data points shown represent the mean  $\pm$  SD values from duplicate experiments where each sample was analysed in triplicate.

It can be seen from the data in **Figure 139** that quinacrine at 20  $\mu$ M was highly toxic, as it is in the 2D models, but was non-toxic at 1  $\mu$ M. PPS and heparin showed increased signal compared to the DMSO treated control, something that had also been observed in the 2D culture (see **Figure 64**).

### 7.2.3. Discussion

In some respects the Alvetex model was found to be ideal for the purposes required. It was available in a 96 well format, ideal for high-throughput screening. Protocols were available for the visualisation of the cells using both brightfield and confocal microscopes, monitoring viability *via* MTT, lysing the cells for protein retrieval and using a trypsin-EDTA digestion to harvest the cells from the scaffold. The availability of these protocols made optimisation much easier and also gave confidence that this model could be used for the desired application.

Initial studies were encouraging with linear growth, as measured by MTT, being observed at 4 different seeding densities (see **Figure 123**). Initial studies using curcumin and 3001012 also showed that both compounds were active, and that an adequate signal could be obtained on the blot using the lysis methods advised by the manufacturer (see **Figure 134**). The problems with visualising the cells under the brightfield microscope were solved through the use of confocal microscopy, which confirmed that the cells were in the correct 3D conformation. An actin stain was employed to allow visualisation of the cell-cell contacts which are a key feature of 3D models, and confirmed that the cells are in contact with each other in 3 dimensions.

Seeding, dosing, lysing and harvesting the cells were all straightforward, with the only drawback being that the plates could be quite time consuming to prepare if several were being seeded at the same time. A very large number of cells were also required for the preparation of several plates. However, it was possible to obtain a good signal on the dot blot without too much optimisation. It is worth noting that removal of the cells from the scaffold, either by direct lysis or trypsin-EDTA digestion, was a very inefficient process. The MTT data (**Figure 123**) suggested a population doubling time of 4 days, so maybe 120,000 cells would be present in the scaffold. This compares to a doubling time of approximately 3 days in 2D, and an approximate final cell number of 40,000 cells/well. However, the signal on the blot was similar to that obtained from one well of a 96 well plate monolayer, even though 3 times as many cells were thought to be present. Although the signal was adequate, it is thought that further optimisation of lysis methods to increase efficiency might be desirable. Removal of the cells from the scaffold using trypsin was also a very time consuming process that only released a small proportion of the cells thought to be within the scaffold. The 96 well plate was also affected by evaporation from the outer wells, and for this reason only the inner wells could be used which limited the number of compounds that could be screened on each plate.

The results from the Alvetex screening are very encouraging, with PPS, DS and the I3GAs all showing excellent activity in the model, with EC<sub>50</sub> values equivalent to, or lower, than their 2D counterparts (see **Figure 136** and **Figure 137**). The activity shown by the I3GAs is extremely promising, with no loss of activity observed in the 3D system. Heparin was also shown to be active at low concentrations suggesting that it has the potential to be active *in vivo* (see **Figure 138**). This is not surprising given its structural similarity to PPS and DS, and its well established role as an anticoagulant suggests favourable pharmacokinetic properties.<sup>(466)</sup> Surprisingly, given its reported *in vivo* activity and activity in the 2D cell culture, amphotericin B was not active in

this model (see **Figure 137**). The suggestion had been made that it might be active against the hamster scrapie agent but not the mouse scrapie agent,<sup>(467)</sup> however this does not explain why it was still found to be active in the 2D model. It's possible that unfavourable pharmacokinetic properties have hampered its activity, or that sufficient concentration were not reached in this study, but both things would require further investigation. Curcumin also showed reduced efficacy when it is known to be active *in vivo* (see **Figure 137**). As discussed in section 7.1.3, this may be due to its reported poor bioavailability.<sup>(462)</sup> Quinacrine, known not to be active *in vivo*, displayed reduced activity, with an increase in EC<sub>50</sub> as well as a reduction in clearance efficiency at the higher concentrations (see **Figure 138**). All the data suggests that the Alvetex model is capable of predicting *in vivo* activity in this context, and that the activity shown by the I3GAs is very promising in terms of their potential *in vivo* activity.

In conclusion, the Alvetex model has many properties that would make it ideal for high-throughput screening. The 96 well format is easy to use, and it is possible to get an adequate signal on the blot from one well. The Alvetex model has provided valuable information on the potential activity of the indole compounds, providing evidence that they may be active *in vivo* due to their activity and low concentrations in this model. The relevance of these results is backed up by the very good activity shown by PPS and DS, and the reduced efficiency of quinacrine. Despite this there are some drawbacks. Not being able to visualise the cells under a brightfield microscope makes it difficult to perform routine checks on the cells, and the expense of the plates may render it too expensive to be used on a large scale.

## 7.3. The Happy Cell Model

### 7.3.1. Introduction

The final system to be trialled was the Happy Cell system. Like the Alvetex scaffold this is based on the concept of using a supportive matrix to allow the cells to grow in 3D, but in this case the matrix is not a solid scaffold but an advanced suspension medium. Instead of attaching to, and migrating within, a polystyrene scaffold the cells are suspended in a special formulation of medium, allowing the formation of colonies of cells with a spheroid-like morphology. The

hypothesis was that within this system the cells would be able to develop distinct 3D structures that weren't as tightly formed as the spheroids, allowing easier lysis and analysis. Materials and methods for this study are outlined in sections **2.1.6**, **2.2.8.3** and **2.2.8.4**.

## 7.3.2. Results

### 7.3.2.1. Spheroid formation

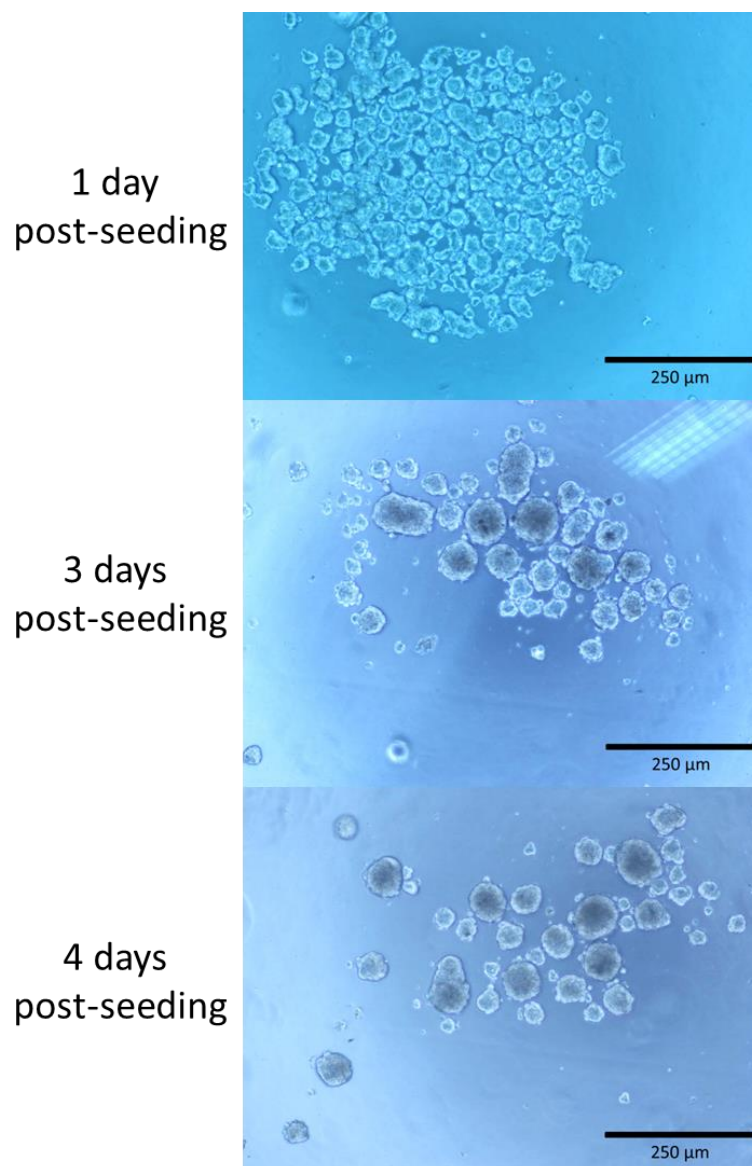


**Figure 140:** Pictures showing the formation of colonies and spheroid-like structures over time when SMB cells are cultured in Happy Cell matrix. Cells were seeded at 5,000 cells/well and monitored over 4 days.

It can be seen in **Figure 140** that spheroids were forming within the Happy Cell medium, although it was not clear whether the cells were proliferating or simply aggregating together to form spheroids.

In order to gain further insights into the morphology of the spheroids they were examined by confocal microscopy after staining with DAPI.

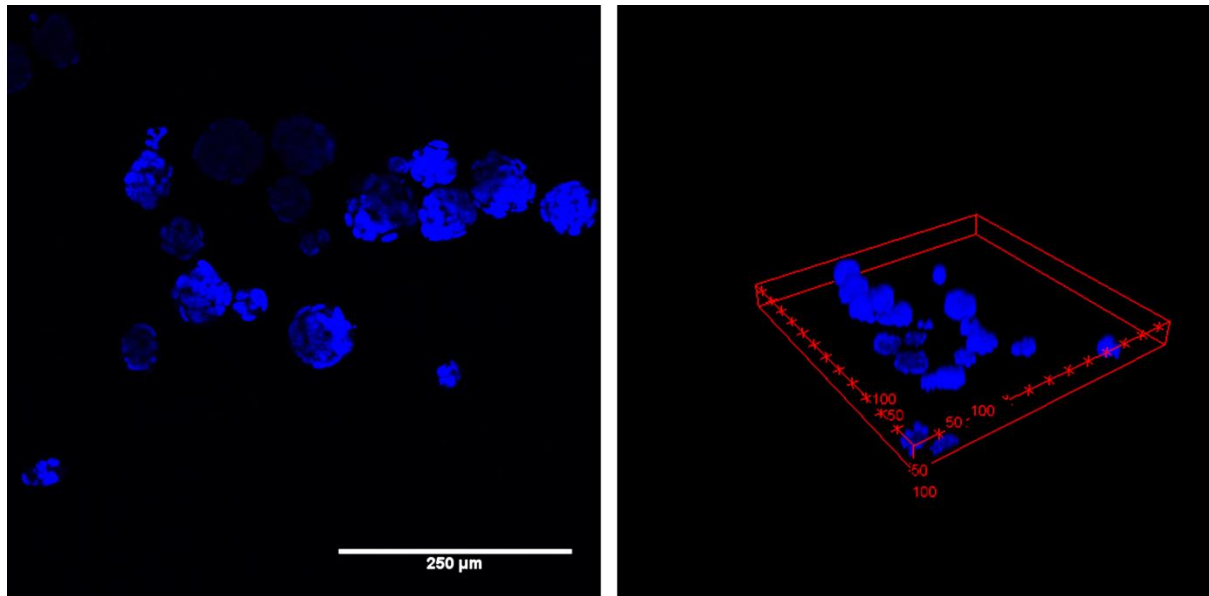


**Figure 141:** Confocal image of the spheroids after transferal to a microscope slide and staining with DAPI. The right hand image shows a 3D representation of the left hand image. A strong signal can be seen from some of the spheroids, while some show a very weak signal.

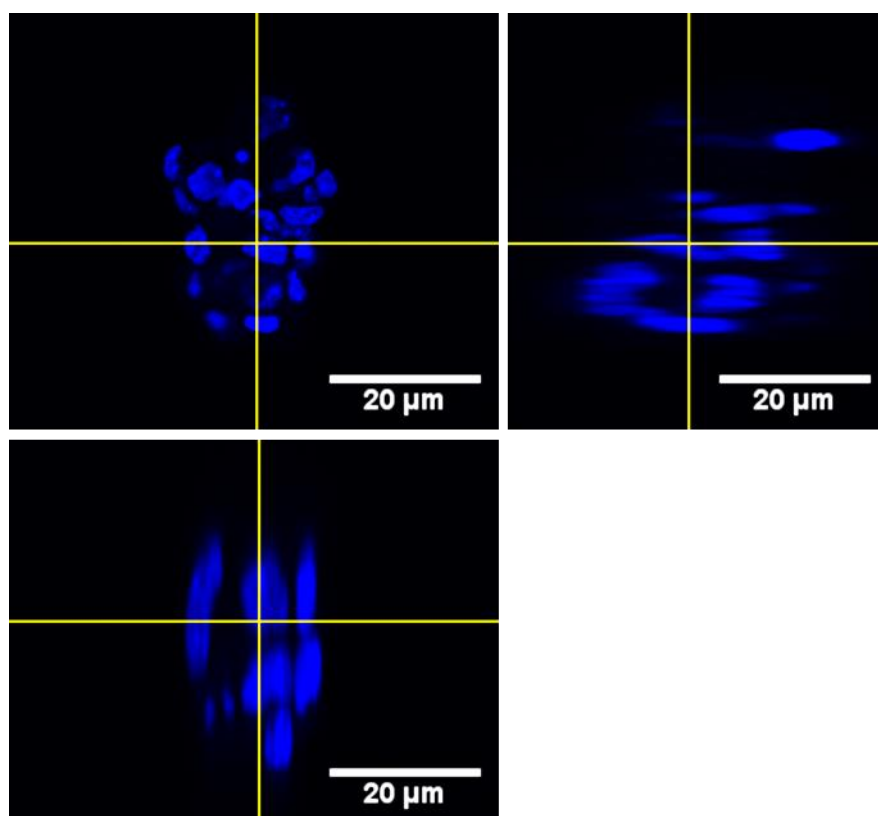


**Figure 142:** Orthogonal view of a z-stack of a spheroid formed in the Happy Cell model.

The images in **Figure 141** and **Figure 142** demonstrate that each of the spheroids is composed of multiple cells, although the DAPI signal does vary between cells. However, these images do show the 3D structure of the cells within the spheroid, validating the 3D conformation of the cells. It was not possible to determine any possible interactions between the spheroids as they had to be removed from the matrix for analysis, and therefore separated into individual units. However, it is thought that the majority of cell-cell interactions would take place within the spheroid rather than between spheroids.

### **7.3.2.2. Compound Screening**

Spheroids were seeded and grown as before, with an initial seeding density of 5,000 cells/well. They were dosed with a selection of the compounds used in the Alvetex and hanging drop studies, namely 3001012, 3001207, PPS, DS and quinacrine.

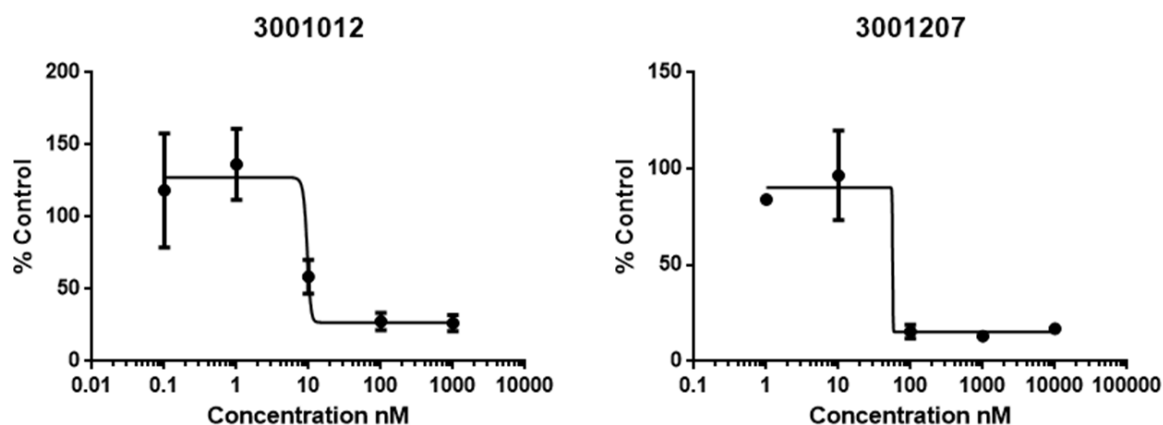


**Figure 143:** PrP<sup>Sc</sup> levels in cells grown in Happy Cell matrix and treated with compounds that have not been tested *in vivo*. Both compounds can be seen to be active. The data points shown represent the mean  $\pm$  SD values from duplicate experiments where each sample was analysed in triplicate.

It can be seen in **Figure 143** that both 3001012 are active in the Happy Cell model, with EC<sub>50</sub>s of 10 nM and 50 nM respectively.

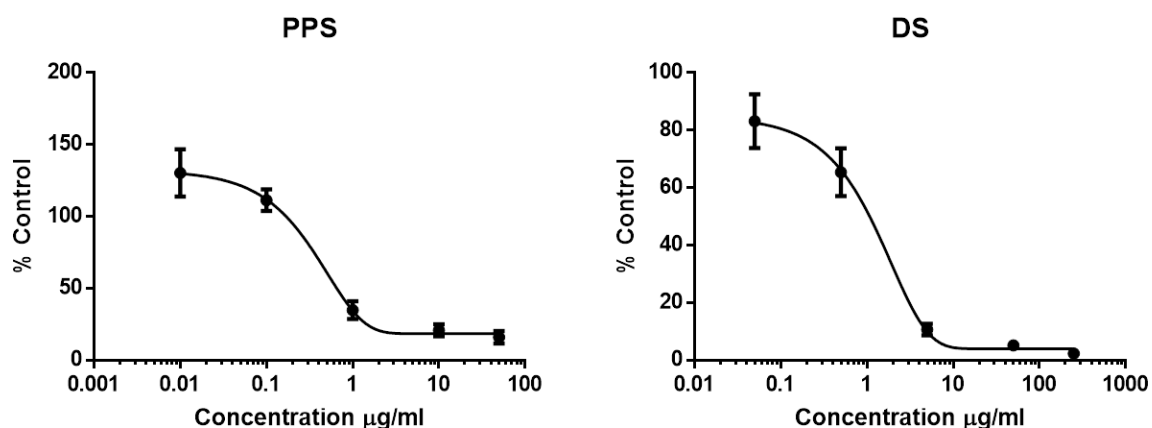


**Figure 144:** PrP<sup>Sc</sup> levels in cells grown in Happy Cell matrix and treated with compounds known to have *in vivo* activity (see **Table 46** for references). Both compounds were shown to be active. The data points shown represent the mean  $\pm$  SD values from duplicate experiments where each sample was analysed in triplicate.

Again, the data in **Figure 144** shows that both PPS and DS retain excellent activity in the Happy Cell model, with EC<sub>50</sub>s of 0.5 µg/ml and 1 µg/ml. For both these compounds and the I3GAs in **Figure 143**, the EC<sub>50</sub> values are slightly higher than those seen in 2D and in the Alvetex model.

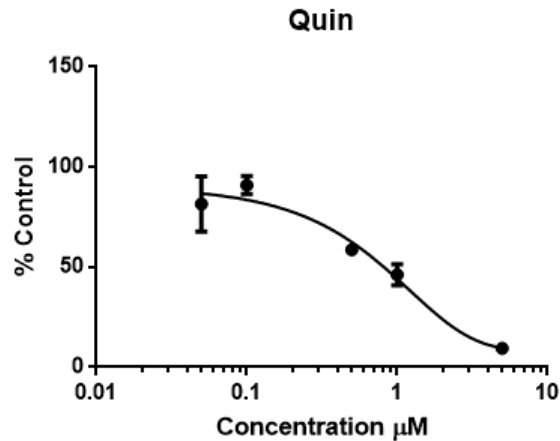


**Figure 145:** PrP<sup>Sc</sup> levels in cells grown in Happy Cell matrix and treated with quinacrine, which is known not to be active *in vivo* (see **Table 46**). Quinacrine retained some activity but this was reduced compared to activity in the 2D model. The data points shown represent the mean  $\pm$  SD values from duplicate experiments where each sample was analysed in triplicate.

The quinacrine data, as shown in **Figure 145**, shows a similar pattern to the data from the Alvetex model. The activity of quinacrine is reduced, both in terms of its EC<sub>50</sub> (1  $\mu$ M in this model) and in terms of the efficiency, with the transition from inactive to active concentrations being much slower.

Unfortunately it was only possible to do the EC<sub>50</sub> screens once, due to the limited amount of inactivation solution that was available. However, each concentration was done in triplicate and it is thought that the low error associated with the majority of points provides confidence that the results are meaningful.

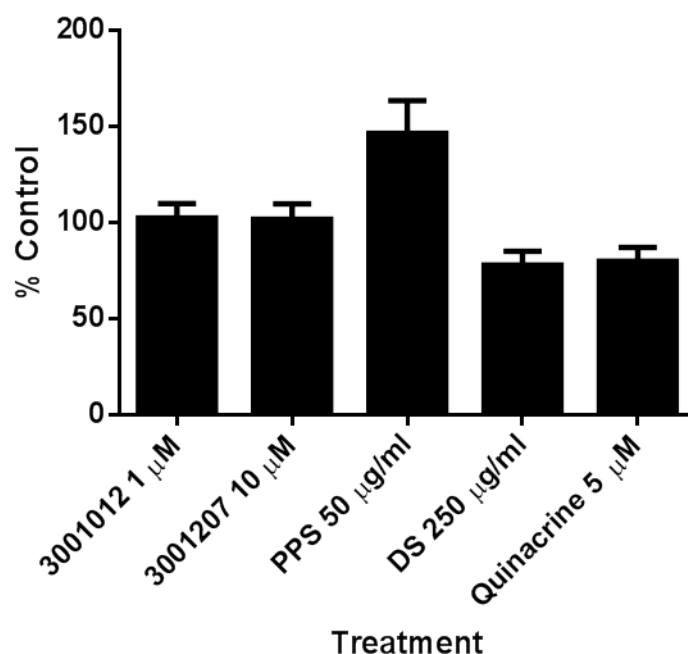


**Figure 146:** MTT viability data for cells grown in Happy Cell matrix and treated with the highest concentrations of the compounds used in the activity screening. The data points shown represent the mean  $\pm$  SD values from duplicate experiments where each sample was analysed in triplicate.

The data in **Figure 146** demonstrates that none of the compounds were toxic at the concentrations used in the Happy Cell screening. As observed in the Alvetex model (see **Figure 139**), PPS increased the signal compared to the untreated control. Quinacrine was used at lower concentrations in this study after the observation in previous studies that it was toxic at higher concentrations – there was a clearly visible degradation of the spheroids. This study took place before the inactivation solution had been obtained so it was not possible to retrieve the spheroids for further analysis and quantify this degradation.

### 7.3.2.3. Growth Curve Analysis

Growth curve analysis using MTT assays was undertaken to demonstrate whether or not the cells were proliferating within the Happy Cell matrix. The cells were also dosed with compounds at active concentrations to see if they had any effect on growth.

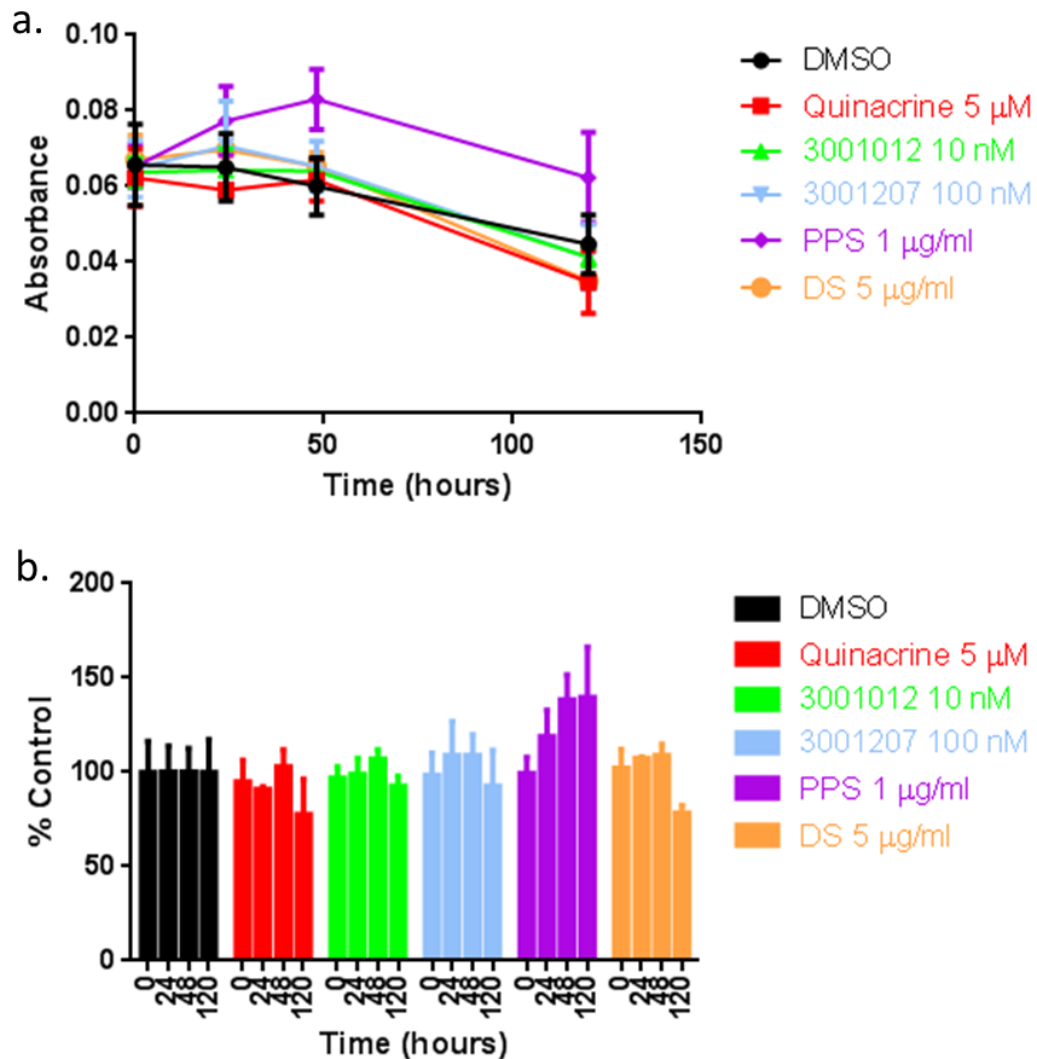


**Figure 147:** Cell growth within the Happy Cell medium as measured using MTT. Graph a. shows the cell numbers, as measured by absorbance levels, over time. Graph b. shows the absorbance as a factor of the control, demonstrating the effect of the different treatments on growth. The data points shown represent the mean  $\pm$  SD values from duplicate experiments where each sample was analysed in triplicate.

It can be seen from the data in **Figure 147** that the cells don't appear to be proliferating within the Happy Cell medium, conversely numbers actually seem to decrease towards the end of the time course. The data showing the effect of the different treatments also validates the data shown in **Figure 146** that suggest that treatment with PPS results in a higher MTT signal. Given the lack of proliferation observed from the other treatments it is not possible to say whether this is as a result of the effect of PPS on growth, or some other interference within the MTT assay.

### 7.3.3. Discussion

The Happy Cell system was trialled in this investigation as a half-way point between the rigid, physical scaffold of the Alvetex system, and the total lack of scaffold as demonstrated in the hanging drop model. The support provided by the matrix allowed the formation of spheroids which then appeared to aggregate together, although the individual spheroids were still distinct from each other. The spheroids formed in this model were much smaller than those formed in the hanging drop model, which was to be expected given the much lower initial seeding density (5,000 cells/well in the hanging drop model compared to 40,000 cells/well in the hanging drop model) and also the fact that one single spheroid formed in the hanging drop model, whereas the Happy Cell model resulted in the formation of many smaller, heterogeneous spheroids.

In terms of its suitability as a high throughput model for screening, there are certainly advantages to this system. Culturing the cells was very easy and not too time consuming – apart from the extra step of combining the Happy Cell medium with the DMEM it was no more trouble than seeding cells into the 2D model. A big advantage was that all assays were able to be completed without lengthy optimisation, something that wasn't achievable with the other systems. However, retrieving the spheroids for further analysis was time consuming and problematic, with the potential to lose all the spheroids if enough care and attention wasn't applied. The edge effect was also found to be particularly pronounced in this model, limiting the amount of compounds that could be run on each plate. Despite this, in terms of the results achieved from the screening, it was possible to obtain a good signal on the blot without any optimisation, not something forthcoming in the other models. It may also be possible that, with more time and experience, the protocol could be refined in order to make it more user-friendly. The further application of this system would also depend on the inactivation solution being commercially available, which it is not at the time of writing.

The activity shown by both the I3GAs was very promising, especially when compared to the decreased efficacy shown by quinacrine in this model. An interesting observation was that, as measured by the MTT assay, the cells did not appear to be proliferating. This raises the potentially interesting question of how the compounds are working as cell division is thought to be crucial for the maintenance of steady state PrP<sup>Sc</sup> levels.<sup>(110)</sup> It would be interesting to see if an accumulation of PrP<sup>Sc</sup> was observed within the spheroids over time as a consequence of the lack of proliferation. As all the compounds were active it suggests that the reduction of PrP<sup>Sc</sup>

levels without cell growth is common to all compounds, rather than a specific feature of the mode of action of the indoles.

The confocal data also raised questions due to the weak signal shown by some of the spheroids. The reason behind this is unclear – it may be that a proportion of the cells are dead, however it would be expected that dead cells would actually give a stronger signal as the DAPI would be able to enter the cells more easily due to increased membrane permeability. A more likely explanation is that the sample preparation and microscopy conditions were not properly optimised – as discussed in section **7.1.3** the acquisition of good confocal images of spheroids may require more optimisation than was possible here. Ideally the cells would be imaged while still within the matrix, something that was not possible at the time of writing. It can be seen in **Figure 142** that the spheroid imaged here shows a distinct 3D structure, with the individual cells visible. However, the relevance of these spheroids to *in vivo* conditions is perhaps questionable, as although spheroids are formed they are limited in size and therefore don't represent the pharmacokinetic challenge that would be presented *in vivo*. However, from a practical perspective these smaller spheroids are much easier to work with and the aggregation of spheroids that is observed may help to more closely replicate *in vivo* conditions.

## 7.4. Results Summary

A summary of the screening results can be seen below in **Table 47**. The hanging drop results are not included as no activity was seen from any of the compounds and therefore the validity of the results is questionable, as discussed in section **7.1.3**. A summary of the properties of the different models, with specific reference to the anti-prion screening, can be seen in **Table 48**.

**Table 47:** Summary of the EC<sub>50</sub> results from screening in the different 3D models. 2D results are from screens carried out alongside the 3D screens

| Compound              | EC <sub>50</sub> |            |            |
|-----------------------|------------------|------------|------------|
|                       | 2D culture       | Alvetex    | Happy Cell |
| 3001012               | 5 nM             | 5 nM       | 10 nM      |
| 3001207               | 20 nM            | 10 nM      | 50 nM      |
| Pentosan polysulphate | 0.175 µg/ml      | 0.25 µg/ml | 0.5 µg/ml  |
| Dextran sulphate      | 0.5 µg/ml        | 0.3 µg/ml  | 1 µg/ml    |
| Heparin               | 5 µg/ml          | 3 µg/ml    | n/a        |
| Amphotericin B        | 6.25 µM          | Inactive   | n/a        |
| Quinacrine            | 0.5 µM           | 2.5 µM     | 1 µM       |
| Curcumin              | 0.7 µM           | 4 µM       | n/a        |

Alvetex results represent an EC<sub>50</sub> calculated from the combination of at least three different sets of experiments. As discussed previously the Happy Cell EC<sub>50</sub> screens were carried out once, and the 2D screens were only carried out once as they were simply for conformation.

**Table 48:** Advantages and disadvantages of the different 3D models with relation to their potential as high-throughput drug screening systems.

| System       | Advantages   | Disadvantages   |
|--------------|--|---|
| Hanging drop | Easy to use (once experienced) for growing and harvesting spheroids<br>Enabled growth of homogenous spheroids  | No existing protocols for this kind of application<br>Lysis of spheroids requires specialist equipment or time consuming methods.<br>No proliferation observed.<br>Not compatible with existing viability assay.<br>Lack of activity from any of the compounds is concerning. |
| Alvetex      | Cells show good proliferation<br>Easy to visualise with confocal microscopy<br>Easy to use existing assays<br>Wide range of protocols available for all elements of this application | Cell seeding is time consuming<br>Unable to visualise cells under a brightfield microscope<br>Inefficient cell lysis and retrieval.   |
| Happy Cell   | Easy to set up<br>Little optimisation required for any element of the application<br>Gives a good signal on the blot   | Harvesting the cells is fiddly and inefficient.<br>Inactivation solution not commercially available.<br>Protocols available from the manufacturer but much still in development.  |

## 7.5. Discussion

The results shown in this chapter demonstrate the successful establishment of three different models of 3D culture with the aims of both testing the potential of the I3GA compounds to be active *in vivo* and evaluating the suitability of the different models to be used for the high-throughput screening of anti-prion compounds. A summary of the advantages and disadvantages of each system, with specific reference to the anti-prion screening can be seen in **Table 48**.

The first of the stated aims of this study was to determine whether the I3GA compounds were active in the 3D models, and therefore determine their potential suitability for screening them in

an animal model of prion disease. It is clear that in the two models in which screens were successfully carried out, both the I3GA compounds used in the study retained good activity, albeit with EC<sub>50</sub> values that were slightly higher than in the 2D model. Interestingly, 3001012 was active at concentrations lower than 16 nM, the concentration found in the brains of mice during the pharmacokinetic investigations. The retention of good activity, and the correlation between results from the different models suggests that these compounds may be active *in vivo*. These findings are further validated by the results from the screens of the anti-prion compounds identified from the literature. PPS and DS have been reported to be effective *in vivo*, and retained their activities in the 3D model comparable to their activity in the 2D model. Amphotericin B showed no activity in the Alvetex model, possibly due to insufficiently high concentrations, while curcumin showed reduced activity, a finding attributed to its reported poor bioavailability.<sup>(462)</sup> The activity of quinacrine was assessed in both the Alvetex and the Happy Cell models as this compound has been shown to be ineffective *in vivo*.<sup>(1, 194, 233, 460)</sup> Quinacrine showed a much reduced efficacy in the 3D models, as demonstrated by both a reduction in the EC<sub>50</sub> value and also a change in the shape of the clearance curve. The correlation between the reported activities of these compounds and the activities seen in the 3D model supports the hypothesis that the 3D model is a more realistic screening system than the 2D model, further strengthening the case for testing the I3GAs in an animal model of prion disease.

It can be seen in **Table 48** that all of the systems that were used have advantages and disadvantages. The hanging drop model was excluded from consideration due to the lack of activity shown by any of the anti-prion compounds. The reason for this lack of activity was unclear, with explanations including the lack of growth shown by the spheroids, the presence of a necrotic core and possible pharmacokinetic and bioavailability problems being suggested. Although it does have several advantages in terms of ease of use it is clearly not suitable for this application. The Alvetex scaffold model was easy to use and assay development was facilitated by the wide range of protocols that were available for different applications. It would, however, be quite time consuming and require a lot of cells to set up several plates at the same time, as would be required for high-throughput screening. The inefficient lysis and retrieval of the cells is also something that would need to be optimised. The inability to visualise the cells under a brightfield microscope is potentially disadvantageous as it is not possible to monitor the health of the cells without staining or fixing for visualisation under the confocal microscope. However, this does not preclude the Alvetex model from being used in a high-throughput capacity. The

Happy Cell model also demonstrated potential as a high-throughput model. It was easy and cheap to set up, and allowed the culturing of spheroids that could be easily lysed and visualised under a brightfield microscope. Again, though, problems were encountered. Retrieving and processing the spheroids for downstream analysis was problematic, and only possible with the use of an inactivation solution that, at the time of writing, was not available commercially. The small size of the spheroids and the lack of insight into inter-spheroid interactions mean that more work is required to determine the relevance of this model to the *in vivo* situation. It is thought, however, that despite the problems outlined here both the Alvetex model and the Happy Cell model have the potential to be used as platforms for high-throughput screening of anti-prion compounds, although further optimisation would be required in both cases. The cost of these models is significantly higher than the cost of the 2D screening but in the context of the expense associated with animal experiments they are thought to represent good value for money.

In summary, the data presented within this chapter investigated three different 3D models of cell culture as potential high-throughput screening systems. All three systems were found to have advantages and disadvantages, but the hanging drop system was discounted due to the problems with lysis and the lack of activity shown by any of the compounds. Evaluation of the three different systems concluded that both the Happy Cell system and the Alvetex system had the potential to be used as high-throughput models in future. The activity of several compounds was evaluated in the Happy Cell and Alvetex models, with good correlation found between the *in vivo* activity of a compound and its activity in the 3D model. Both the indole compounds used in this study were found to be active in the 3D model, with EC<sub>50</sub> values only slightly higher than those found in the 2D model. This provides further evidence that these compounds may be active *in vivo*, again reinforcing their potential as anti-prion compounds.

## 8. Discussion and Future Work

The data presented within this thesis outlines the development of a group of I3GA compounds with potent anti-prion activity and a tightly defined structure-activity relationship (SAR). Their pharmacokinetic and pharmacodynamic properties have been investigated, along with studies designed to gain insights into their mode of action. The potential of these compounds to be effective *in vivo* has been investigated using 3D cell culture models, and these models, in turn, have been assessed to determine whether they would be suitable for use in routine high-throughput screening in future.

The identification of a group of small molecule anti-prion compounds with a well-defined SAR and nanomolar activities is outlined in chapter 2. Optimal activity was conferred by the presence of the following structural motifs:

- No substitutions on the indole
- An aromatic amine
- Substitution at the para-position
- Both carbonyl groups

The optimised lead structure can be seen in **Figure 148**. It contains an unsubstituted indole, both carbonyl groups and an N-linked heterocycle at the para-position of the phenyl ring

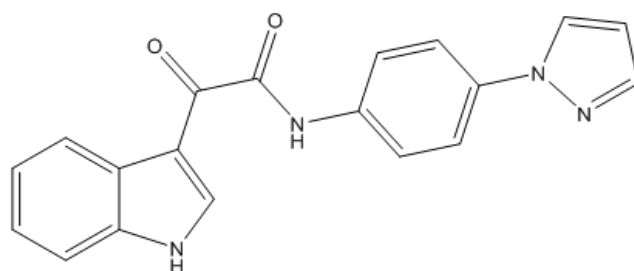


**Figure 148:** Structure of 3001012, the lead compound.

At the time the work was carried out, the I3GAs were unique in the literature both in terms of activity and in the specificity of the structural features required for activity. Extensive SAR investigations have been carried out with other structural groups that have demonstrated anti-prion activity. However, despite all the investigations, to be discussed in more detail subsequently, a cure for prion diseases is still out of reach. The further investigation of the I3GAs

to obtain insights into their mode of action was therefore thought to be crucial in the continuing search for small molecule therapeutics for prion disease.

In order to gain further insights into the pharmacodynamic properties of the compounds, time course and curative assays were carried out as well as binding studies using SPR. A series of compounds from the literature were also screened to validate the techniques being used. A large number of the I3GA compounds were screened to evaluate their binding to PrP<sup>C</sup>, with none of the I3GAs showing significant binding even at much higher concentrations than their cellular EC<sub>50</sub>. Direct interaction with PrP was therefore thought unlikely to be a possible mode of action. Time course studies showed that the I3GAs reduced PrP<sup>Sc</sup> levels within 56 hours at concentrations of 3 and 10 times EC<sub>50</sub>, while the curative assay showed that one treatment of lead compound 3001012 at a concentration of 10 times EC<sub>50</sub> could cure the cells of infection for at least 76 days. The I3GA compounds were also found to have favourable pharmacokinetic properties, showing good microsomal stability and reaching concentrations higher than the cellular EC<sub>50</sub> in mouse brains. Toxicity studies using zebrafish found no evidence of toxicity *in vivo*. Good correlation was found between compound activity in the SMB cell line and the ScN2a cell line, showing that the compounds are active in a neuronal model, as well as the non-neuronal SMB model. Good correlation was also found between the reported EC<sub>50</sub> values for the literature compounds in a variety of cell lines, and the EC<sub>50</sub> calculated from the SMB model, validating this technique as a model for screening compounds with unknown anti-prion activity. The only exception to this was congo red, which showed no reduction of PrP<sup>Sc</sup>. Conversely, at certain concentrations it caused a very large increase in PrP<sup>Sc</sup> levels. The reason for the increase in PrP<sup>Sc</sup> at lower concentrations was thought to be due to congo red in its monomeric form acting as a template for conversion. The reasons behind the lack of activity at higher concentrations are unknown.

Initial mode of action studies aimed to show whether the compounds might be affecting cell growth or protein aggregation by using MTT assays. Neither growth nor aggregation was found to be affected using these techniques. An interesting observation from the SPR, time course and MTT-FE assays was that in all cases quinacrine showed a markedly different effect to the I3GAs. Reproducible binding of quinacrine to PrP was observed in the SPR assay, and a quinacrine-specific pattern of MTT exocytosis was observed during the MTT-FE assay, as well as increases in TS-MTT independent of total MTT. In contrast to the I3GAs, the reduction of PrP<sup>Sc</sup> over time was dependent on quinacrine concentration, with treatment at 5 µM clearing PrP<sup>Sc</sup> within 24 hours,

while treatment with 1.5  $\mu$ M took 48 hours. The ability of quinacrine to bind to PrP, unlike the I3GAs, may explain these differences at least in part. Quinacrine has been proposed to act by binding to PrP<sup>C</sup> and therefore rendering it less susceptible to transformation into the abnormal isoform, <sup>(223)</sup> which would correlate with increased efficacy at higher concentrations. The MTT-FE results could also be explained in this context, with the effect seen due to the prevention of continued conversion and aggregation. Quinacrine was originally synthesised as an anti-malarial drug, and has also been used for other applications, so it is perhaps not surprising that it has demonstrated different pharmacodynamic properties.

The elucidation of the quinacrine results underline one of the main problems associated with this study. While the quinacrine data can be explained in terms of what is already known about the mode of action, this background information is not available for the I3GA compounds. Indole derivatives have been shown to prevent the aggregation of both hen egg white lysosome <sup>(468)</sup> and amyloid beta <sup>(469-471)</sup> with the mode of action generally suggested to be interaction of the indole with the native form of the protein, preventing aggregation. However, the lack of binding seen with PrP<sup>C</sup> suggests that this is not how the compounds investigated here are working. Similarly, the SAR described here does not correlate with the SAR described for other modes of action for related indoles, for example as tubulin polymerisation inhibitors. <sup>(365-367)</sup> The absence of any clues as to the mode of action of the I3GA compounds makes it particularly difficult to draw meaningful conclusions from the pharmacodynamic and mode of action data presented in chapter 3. This is a common problem in the development of anti-prion compounds – the existence of a wide variety of compounds with little apparent commonality in their mode of action suggests that prion metabolism is a complex process, making development of an effective therapeutic more problematic. <sup>(207)</sup>

In an attempt to confront the lack of knowledge around the possible mode of action of the I3GAs a top-down approach was used. The hope was to identify pathways affected by treatment with the I3GA compounds, and use this information to draw conclusions about the areas involved in the anti-prion effect. Fasano *et al* used this approach to identify targets of quinacrine in cured mouse neuronal cells <sup>(383)</sup> and quinacrine was included in the study presented here to validate the technique for this application. The combination of the microarray and proteomics studies produced vast amounts of data that was analysed using MetaCore software.

Various conclusions were reached as a result of these studies, which are summarised below;

- The results of the Fasano study could not be replicated.
- However, up-regulation of fatty acid synthesis correlates with the suggestion that quinacrine works by increasing cholesterol recycling.
- Limited crossover between the individual targets identified by the microarray and proteomics studies suggests that, in this case, gene expression does not directly translate to protein expression.
- Where the data set was large enough, affected pathways could be identified from the combined data sets, suggesting that analysing both genomic and proteomic changes was advantageous.
- Pathways identified for the I3GA compounds do not appear to have any relevance to prion disease, suggesting possible new areas of investigation. The up-regulation of hedgehog signalling as a result of treatment with 3001012 may suggest a potential anti-cancer role for 3001012.
- Analysis of pathway components suggests a role for either the proteasomal pathway, *via* up-regulation of E3 ligases, or the prion protein transcription factor, sp1.
- 3001012 and 3001207 don't appear to share a mode of action.

In order to assess the relevance of the above findings it was necessary to validate the results, and this was done using western blotting. As can be seen in chapter 5, no difference was seen in levels of HSP90 or MTF-1. Small changes were observed in the amount of cleaved caspase-12, but this was not thought to be of great relevance due to the very low levels of cleaved caspase-12 present in the sample, as well as the lack of change observed at other concentrations and time points. The suitability of western blotting for this application was questioned due to its semi-quantitative nature, with the suggestion that it may not be sensitive enough to identify any changes in protein expression. MTF-1, like sp1, is a known transcription factor for PrP<sup>C</sup>, and the lack of change in MTF-1 levels casts doubt on the hypothesis that the compounds are working *via* direct modulation of PrP<sup>C</sup> transcription factors. Unfortunately it was not possible to obtain any direct measure of sp1 levels, and this would be essential for more concrete conclusions to be drawn.

Studies using inhibitors of the protein degradation pathways produced some insights into the role of the different degradation pathways in the maintenance of steady state PrP<sup>Sc</sup> levels in the SMB cells. Broad inhibition of the LCPs resulted in accumulation of PrP<sup>Sc</sup> to levels well above normal, something that was not observed with specific inhibition of either the proteasome or

particular cathepsins. Time course analysis of the PrP<sup>Sc</sup> accumulation showed a lag phase of around two days before accumulation was seen, suggesting that alternative cellular systems were able to compensate for the inhibition of the LCPs for a limited amount of time. PrP<sup>Sc</sup> accumulation was shown to increase in a dose-dependent manner, with increasing concentrations resulting in increased accumulation. MG132, which inhibits both the proteasome and the cathepsins, was toxic at high concentrations suggesting that a certain level of inhibition of both systems can be tolerated by the cells, but results in cell death above a certain point. The accumulation of large amounts of PrP<sup>Sc</sup> without any associated toxicity, as observed after treatment with inhibitors and also congo red, suggests that the PrP<sup>Sc</sup> aggregation in itself is not toxic to the cells in the short term.

All the compounds tested in conjunction with the inhibitors were found to mitigate the worst of the PrP<sup>Sc</sup> aggregation. It appeared that the decrease in PrP<sup>Sc</sup> levels as a result of treatment meant that the tipping point above which the other cellular machinery was overwhelmed was never reached, with the cured baseline remaining steady for the duration of the experiment. The clearance efficiency of 3001012 was shown to be reduced when co-dosed with the inhibitors, suggesting that 3001012 may work, in part, by some effect on lysosomal degradation. Several compounds have been reported to work by facilitating transport to the lysosomes, <sup>(229, 237-239, 411)</sup> so there is a precedent for compounds working this way. However, the majority of activity was maintained and there was no decrease in EC<sub>50</sub>, suggesting that any effect on lysosomal degradation is unlikely to be the primary mode of action.

The findings regarding the central role of the LCPs, and lysosomal degradation in general, correlate well with the literature. Protein aggregates are known to accumulate in cells when protein quality systems become overwhelmed, <sup>(472)</sup> and other studies have reported increases in PrP<sup>Sc</sup> as a result of treatment with E64, one of the inhibitors used in this study. <sup>(144, 473)</sup> It has been suggested that the proteasome cannot degrade protein aggregates as their size means that entry into the catalytic chamber is not possible, which may explain the lack of effect of proteasomal inhibition. <sup>(474)</sup> This could also be explained by the finding that PrP<sup>Sc</sup> can cause partial inhibition of the proteasome, <sup>(181, 182)</sup> a phenomena that has been demonstrated in the SMB cells. <sup>(220)</sup> In addition, ubiquitination of PrP<sup>Sc</sup> has been shown to be limited, with highly sensitive techniques required for detection of ubiquitinated PrP<sup>Sc</sup> *in vivo*. <sup>(475, 476)</sup> The apparent lack of effect on the proteasome and the explanation above calls into question the original rationale for investigating the proteasomal degradation systems i.e. the identification of several

up-regulated E3 ubiquitin ligases. It may be that they are up-regulated as a result of treatment, without a concomitant up-regulation of proteasome activity. No change in ubiquitin levels was observed as a result of treatment with the I3GAs suggesting that up-regulation of E3 ligases may not correlate with increased ubiquitination and proteasomal degradation. Similarly, studies into autophagy carried out by other members of the group suggest that autophagy is not affected as a result of treatment with the I3GA compounds and therefore that any lysosomal effect may not be related to the autophagy pathway.

One of the aims of the mode of action studies was to test the hypothesis that the I3GAs shared a mode of action. This was suggested due to the structural similarity between the I3GA compounds, as well as the tightly defined SAR. This hypothesis was contradicted by the microarray and proteomics data, as well as the more pronounced effect of LCP inhibition on 3001012 activity. However, it seems unlikely that the compounds have entirely separate modes of action. The more pronounced effect of LCP inhibition on 3001012 activity is thought to represent either an off-target effect unrelated to the anti-prion activity, or a small part of a more significant effect which is shared with the other I3GAs.

The I3GAs are part of a large and ever growing number of compounds, with a wide range of mode of actions, that have been identified as having anti-prion properties. The variety observed among therapeutic molecules and the pathways by which they exert their anti-prion effects means that generating a hypothesis about compounds with an as yet unidentified mode of action is challenging.

Therapeutic interventions can broadly be divided into four categories:

1. Interfering directly with conversion through interaction with PrP<sup>C</sup>, PrP<sup>Sc</sup>, or co-factors necessary for conversion.
2. Reduction of substrate for conversion through reductions in PrP<sup>C</sup> levels.
3. Modification of cellular pathways to prevent conversion or increase PrP<sup>Sc</sup> degradation.
4. Other miscellaneous strategies.

The I3GAs are a group of compounds which, despite the extensive investigations outlined above, do not have a defined mode of action. It has been shown that they do not bind to recombinant PrP, suggesting that they do not exert their anti-prion effect through direct interaction with either PrP<sup>C</sup> or PrP<sup>Sc</sup> (therapeutic intervention number 1). Binding to PrP<sup>C</sup> by glycosaminoglycans

(GAGs) such as PPS, DS and heparin sulfate can reduce conversion by competing for binding with endogenous GAGs that have a role in conversion, and also by reducing the amount of PrP<sup>C</sup> available for interaction with PrP<sup>Sc</sup>.<sup>(211, 212, 214)</sup> Congo red has been shown to interact with PrP<sup>C</sup>,<sup>(221, 222)</sup> compete with endogenous GAGs for binding<sup>(213)</sup> and stabilise PrP<sup>Sc</sup>, preventing further conversion.<sup>(224)</sup> Conversely, however, it has also been shown to induce the formation of PrP<sup>Sc</sup> at low concentrations.<sup>(190, 217, 225)</sup> Analogues of congo red have been synthesised and a structure activity relationship determined,<sup>(217-220)</sup> with the mode of action thought to be prevention of conversion of PrP<sup>C</sup> to PrP<sup>Sc</sup><sup>(190, 218, 225)</sup> or increased degradation of aggregates by reversing proteasomal inhibition.<sup>(220)</sup> The compounds suramin and curcumin, which are structurally similar to each other and to congo red, have been shown to be active anti-prion compounds<sup>(208, 226, 266)</sup> and while curcumin has been shown to bind to PrP<sup>C</sup>, sharing a binding site with congo red,<sup>(268)</sup> suramin is thought to work by re-routing PrP<sup>C</sup> away from the cell surface.<sup>(226)</sup>

Quinacrine and related compounds have been studied intensively, and quinacrine is thought to work by either direct binding to PrP<sup>C</sup>,<sup>(223, 233)</sup> inhibition of the PrP<sup>C</sup>-GAG interaction through activity in the lysosomes<sup>(209)</sup> or destabilisation of the cell membrane.<sup>(245)</sup> It can therefore be seen that the proposed modes of action for quinacrine fall into the first three categories mentioned above. Quinacrine has been shown to be ineffective *in vivo*<sup>(194, 233)</sup> and has also been shown to induce the formation of drug resistant prions,<sup>(377)</sup> suggesting that it does not have the required properties to be used as an effective therapeutic. Analogues of quinacrine, known as fluphenazine and trimipramine, have been shown to be active *in vivo*,<sup>(477)</sup> and quinacrine has been synergistically dosed with statins resulting in more than additive activities.<sup>(245, 246)</sup> Quinpramine, a chimeric molecule composed of the acridine scaffold of quinacrine linked to the iminodibenzyl scaffold of despiramine was found to have 5 times higher activity than quinacrine, suggesting that the combination of two different molecules may be advantageous.<sup>(245, 478)</sup>

Other compounds thought to work by preventing the conversion of PrP<sup>C</sup> to PrP<sup>Sc</sup> include a group of small molecules that were designed to block the site on PrP<sup>C</sup> reserved for physiological ligands that are important for conversion. The pyridine dicarbonitriles were the first rationally designed group of anti-prion compounds and were developed to fit the putative protein-X binding site.<sup>(264)</sup> Other groups thought to work by blocking this binding site include anionic cyclic tetrapyrroles, sulfonated dyes, phosphorothioated oligonucleotides and sulfated glycans.<sup>(199)</sup> Antibodies have been shown to prevent conversion by binding to PrP<sup>C</sup>,<sup>(250-252)</sup> and concealing the epitope of the 6H4 antibody, at residues 144-152, also blocks conversion.<sup>(479)</sup> The C1 cleavage

fragment of PrP<sup>C</sup> has been suggested as a dominant negative inhibitor of conversion, working by competing with PrP<sup>Sc</sup> for binding sites on PrP<sup>C</sup>.<sup>(152)</sup> An alternative route to preventing conversion is reducing the number of seeds by stabilising PrP<sup>Sc</sup> aggregates. As mentioned above this has been suggested as part of the mode of action of congo red, and RNA aptamer D reduces the *de novo* formation of PrP<sup>Sc</sup> through its incorporation into PrP<sup>Sc</sup> aggregates.<sup>(265)</sup>

A related, but functionally distinct, strategy is to modulate the amount of PrP<sup>C</sup> available as a substrate for conversion. It was shown that mice lacking PrP<sup>C</sup> were resistant to scrapie infection<sup>(24)</sup> and this has subsequently been explored in a therapeutic context. The effect of the I3GAs on PrP<sup>C</sup> levels was not assessed, and this is a potential mode of action that could be explored. Depleting neuronal PrP<sup>C</sup> in mice was shown to increase survival and reverse early stages of disease pathogenesis, despite the accumulation of PrP<sup>Sc</sup>.<sup>(161, 162)</sup> Silencing of PrP<sup>C</sup> expression using RNAi and shRNA has also been shown to be beneficial *in vivo*.<sup>(247, 248)</sup> Removing PrP<sup>C</sup> from the cell surface has been shown to be an effective therapeutic strategy as the amount of PrP<sup>C</sup> available for conversion is reduced. Interference with cholesterol synthesis, recycling and raft formation counteracted PrP<sup>Sc</sup> formation,<sup>(132, 241, 243, 244)</sup> and polyene antibiotics such as amphotericin B are thought to work by modifying lipid raft composition.<sup>(242)</sup> Tacrolimus, an immunosuppressant drug, was shown to reduce PrP<sup>C</sup> levels *in vitro* and inhibit prion replication<sup>(480)</sup> although the anti-prion activity of tacrolimus has also been attributed to its role as an inhibitor of calcineurin, a calcium dependent phosphatase that has been linked to prion induced neurodegeneration.<sup>(481)</sup>

The modification of existing cellular pathways and cell signalling has also been explored. The effect on protein degradation systems was hypothesised to be part of the mode of action of the I3GAs, although subsequent investigations failed to provide any unambiguous evidence in support of this hypothesis. A key finding, however, was that the LCPs appear to be crucial to PrP<sup>Sc</sup> homeostasis, and several compounds are thought to work by increasing lysosomal degradation. Chlorpromazine,<sup>(238)</sup> tamoxifen<sup>(239)</sup> and tyrosine kinase inhibitors<sup>(131, 237)</sup> are thought to work by rerouting PrP<sup>Sc</sup> to the lysosomes where it is degraded. Branched polyamines accumulate in the lysosomes, where the acidic environment facilitates their degradation of PrP<sup>Sc</sup>. They are thought to work by causing fibre breakage and the capping of elongated fibres.<sup>(227-230)</sup> Induction of autophagy can cause a reduction in the burden of PrP<sup>Sc</sup>, and this has been demonstrated using compounds such as trehalose,<sup>(260)</sup> rapamycin<sup>(261)</sup> and lithium and imatinib.<sup>(259)</sup> Reversal of PrP<sup>Sc</sup> induced proteasomal inhibition can lead to a reduction in PrP<sup>Sc</sup>,<sup>(194)</sup> and

disruption of processes affecting apoptosis can alter disease progression.<sup>(262)</sup> Targeting the unfolded protein response (UPR), and specifically the inhibition of global protein synthesis *via* activation of the PERK/eIF-2 $\alpha$  branch of the UPR, has proved beneficial. Restoration of the synthesis of synaptic proteins as a result of inhibition of the PERK/eIF-2 $\alpha$  pathway has been shown to prevent neurodegeneration.<sup>(184-186)</sup> The targeting of a cellular pathway, rather than a prion disease-specific target, means that this approach could also be applied to a number of different protein misfolding diseases.

Outside of these three therapeutic avenues a wide number of additional approaches have also been reported. The range of strategies outlined here demonstrate, for the most part, known compounds or techniques with a defined mode of action being applied to the prion disease model. As mentioned before, no insights into the mode of action of the I3GAs have been revealed from their mode of action in other therapeutic applications, and the existing mode of action of the I3GAs was not part of the original rationale for investigating these compounds as anti-prion therapeutics. Oligomer modulators that inhibit oligomer formation were found to inhibit neuronal degeneration and disease progression *in vivo*, as well as having excellent oral bioavailability and BBB penetration, making it another candidate for treatment of different protein misfolding diseases.<sup>(482)</sup> Conversely, the induction of oligomerisation has been shown to trap prion infectivity *in vitro*.<sup>(483)</sup> Stem cell therapies have recently been trialled in the treatment of prion disease, with injection of both wild type and PrP knockout stem cells into mice 100 d.p.i resulting in increases in both incubation time and survival.<sup>(484)</sup> The mechanism behind this curative effect is unknown, but is thought to involve the release of trophic factors or other neuroprotective components. The hypothesis that disease could result from a loss of the proposed anti-oxidant effect of PrP<sup>C</sup><sup>(34)</sup> led to the investigation of anti-oxidant compounds as possible therapeutics with some success,<sup>(485, 486)</sup> although the anti-oxidant effect is not always thought to be the primary mode of action.<sup>(485)</sup> The nonpsychoactive cannabis constituent cannabidiol (CBD) has been shown to be effective as an anti-prion compound both *in vitro* and *in vivo*, although the mode of action is ambiguous.<sup>(487)</sup> It has no effect on cell free conversion, PrP<sup>C</sup> expression or PrP<sup>Sc</sup> stability, so the authors suggest that it may be working by blocking microglial activation or antagonising the N-methyl-D-aspartate (NMDA) receptor, whose overactivation has been implicated in neurodegeneration. Flupirtine, a trimainopyridine analgesic, has been shown to improve cognitive function in CJD patients *via* upregulation of the proto-oncogene Bcl-2 and normalisation of glutathione levels.<sup>(488)</sup>

In addition to the compounds outlined above there are also a significant group of anti-prion compounds, generally identified through phenotypic screening, that do not have a defined mode of action. This group of course includes the I3GAs. Investigations into 2-aminothiazoles (2-AMTs) have so far been very promising, as they have excellent pharmacokinetic properties and are able to double the survival time in mice.<sup>(274, 489)</sup> However, the mode of action is unknown and, like quinacrine, the 2-AMTs were able to induce the formation of drug resistant prions.<sup>(489, 490)</sup> Other compounds include biaryl amides and hydrazones,<sup>(491)</sup> piperazine derivatives,<sup>(492)</sup> diphenylpyrazole derivatives,<sup>(493)</sup> diarylthiazoles<sup>(276, 277)</sup> and 6-aminophenanthridines<sup>(494)</sup> and none of these have a known mode of action.

The lack of conclusive evidence regarding the mode of action of the I3GAs means it is hard to say where the I3GAs fit in to the vast array of compounds shown to have anti-prion activity. It is unlikely that they exert their effect through direct interaction with PrP<sup>C</sup> or PrP<sup>Sc</sup>, even though the original rationale for investigating the I3GAs was based on their proposed ability to bind PrP<sup>C</sup>. It is possible that they are working *via* modulation of PrP<sup>C</sup> levels but this is something that requires further investigation. The results of the studies using the LCP inhibitors suggest that the I3GAs may be targeting cellular processes rather than the PrP<sup>C</sup>-PrP<sup>Sc</sup> interaction itself, making their inclusion into the third category the most well supported hypothesis. Despite this, the microarray and proteomics studies have suggested the intriguing possibility of a completely novel mode of action, perhaps *via* modulation of the notch or hedgehog signalling pathways. It is therefore conceivable that the I3GAs could open up an as yet unexplored avenue for the treatment of prion diseases.

The use of 3D cellular models is something that has been widely used in the study of anti-cancer drugs and in tissue engineering. The use of these models to study the potential *in vivo* activity of anti-prion compounds is a novel application, although their use as models for Alzheimer's disease is becoming increasingly popular.<sup>(328, 337, 338)</sup> The observed activity of the compounds in the different models is summarised in **Table 47**, and the pros and cons of each model are outlined in **Table 48**. The lack of success thus far in identifying anti-prion compounds that are active *in vivo* has been a major barrier to the development of clinical therapeutics. The hope was therefore that these 3D models could be used to provide more information on the potential *in vivo* activities of anti-prion compounds, and identify those with unfavourable properties without the use of animal models.

It can be seen from the data presented that there was a correlation between the efficacy of compounds in the 3D models and their known *in vivo* activity. Although the EC<sub>50</sub> for the I3GA compounds was slightly reduced, the compounds were still shown to be active at very low concentrations, which is extremely promising. The reduced efficacy shown by quinacrine suggests that compounds which are unlikely to be active *in vivo* could be identified earlier in the drug discovery pipeline by using these 3D models. An interesting observation was that while the cells in the Alvetex model were shown to be proliferating, the cells in the Happy Cell model did not appear to be. Given that cell division has been suggested to be crucial in speeding up the clearance of PrP<sup>Sc</sup> from cells after treatment,<sup>(110, 377)</sup> the ability of all the compounds to clear PrP<sup>Sc</sup> from both models with a similar efficiency and within the same time frame is surprising and requires further investigation. Both the Alvetex and the Happy Cell models would require further optimisation before they could be used in a high-throughput capacity, and the cost of these models, particularly the Alvetex scaffold, may be prohibitive. However, from the evidence presented here, and compared to the cost and ethical considerations of animal studies, it is thought that there is potential for these models to become a valuable tool in the arsenal of the medicinal chemist researching anti-prion compounds.

The excellent activity demonstrated in the 3D models by the I3GAs has provided confidence that these compounds have the potential to work *in vivo*. The next step would therefore be to determine the optimal animal model to use for further investigation of these compounds. As described in section 4.5 the compounds have already been tested in a zebrafish model and were found to have no effect on zebra fish survival, suggesting low *in vivo* toxicity. The zebrafish model has been shown to be an accurate representation of rodent toxicity and can be used to predict LD<sub>50</sub>s with good accuracy.<sup>(495, 496)</sup> However, although they are a useful and cost-effective model, and have been used to investigate the function of PrP<sup>C</sup>,<sup>(497, 498)</sup> there is currently no infected model to be used in the testing of therapeutics. The presence of three different forms of PrP in zebra fish would also make interpreting any results from an infected model more challenging.<sup>(499)</sup> Alternatively, PrP transgenic *Drosophila*, which are a tractable animal model of transmissible mammalian prion disease, could be used to test the *in vivo* effectiveness of the I3GA compounds.

Animal models were initially used in order to prove that the disease-causing agent was infective. After the original outbreak of scrapie, the disease was successfully transferred to mice,<sup>(58)</sup> and subsequently kuru<sup>(59)</sup> and CJD<sup>(500)</sup> were inoculated into chimpanzees. Animal models were

therefore key to initially establishing the properties of this unusual pathogen. Animal models have continued to play a vital role, both in the testing of therapeutics and in elucidating the processes associated with prion disease pathogenesis and neurodegeneration. The most widely used model is the rodent model, both for practical reasons and also because they allow the discrimination between and characterisation of different prion strains.<sup>(283)</sup> Prion knockout mice enabled investigations into the cellular role of PrP<sup>C</sup>, and have provided crucial insights into the role of the normal isoform of the protein in disease pathogenesis.<sup>(23, 24)</sup> Transgenic mouse models have allowed the development of mice expressing human prions which can faithfully replicate all the key features of human disease, and these mice have made a vital contribution to the understanding of human prion disease pathogenesis and aetiology.<sup>(501)</sup> Both normal and transgenic mice have played key roles in elucidating the mysteries of prion biology, as well as allowing the analysis of the activity of potential therapeutic compounds *in vivo*.<sup>(283, 502-504)</sup> Highly susceptible transgenic mice that overexpress PrP<sup>C</sup> have allowed very sensitive detection of infectivity in prion preparations, helping provide the first evidence that infectious prions could be formed *in vitro*.<sup>(70)</sup> As well as mice, Syrian hamsters have also been used as a model for prion diseases due to their increased susceptibility and decreased incubation times.<sup>(15)</sup> Bank vole models have also become of interest as the bank vole is uniquely susceptible to a wide range of prions from different species.<sup>(505)</sup>

Although there are a range of other animal models that can be used in the continuing research into prion diseases it is thought that the optimal route for the I3GAs would be to test them in a mouse model of prion disease. At the most basic level this would involve normal mice, infected with scrapie and dosed with the I3GAs to determine if there is any effect on disease progression and survival. It is thought that the evidence presented in this thesis would provide a compelling justification for these experiments to be carried out. Another approach, which has been discussed with collaborators, would be to screen the compounds in a cell line infected with CJD prions. This would test the compounds against human prions and, if the I3GAs were active, would provide further evidence that they could be used in clinical trials. This is something that is under development at the moment and will hopefully be available for screening in the near future.

It can be seen from the discussion above that even though a large amount of information has been gained from the studies outlined above there are still many questions that need answering:

**Do the cells retain infectivity after treatment?** It can be seen that in all of the experiments carried out here, PrP<sup>Sc</sup> levels are generally not lowered to zero, suggesting that residual amounts of PrP<sup>Sc</sup> still remain in the 'cured' cells. Although the data from the curative assays suggest that levels do not return to normal in the short term, it would be interesting to see if the cells still contain enough of the infective agent to infect other cells. In the absence of a readily available mouse model, establishing an uninfected cell line that was susceptible to infection, and exposing them to lysate from treated cells may help determine if residual infectivity remains. Cell based infectivity assays have been reported in the literature, suggesting that this approach is valid. (294, 295)

**How is compound activity affected by cell replication?** A study by Ghaemmaghami *et al* that reported the results of a curative assay similar to the one outlined in this thesis found that the curative effect of quinacrine was drastically reduced when cell growth was arrested using sodium butyrate or dibutyl cAMP. (377) This was not investigated here at the time but may help to provide insights into the pharmacodynamic properties of the I3GAs, as well as providing further comparison with published quinacrine data. Analysis of the cell cycle using fluorescent-activated cell sorting (FACS) may also provide further insights into any effect of treatment on cell cycle. Investigations into cell growth and cell cycle may also help reveal what is happening in the Happy Cell model, where anti-prion activity was observed without any apparent cell growth.

**Can the results of the microarray and proteomics studies be validated?** Other studies had used quantitative RT-PCR (417) or immunohistochemistry (424) to validate the results of microarray studies and further work along these lines would be required to extrapolate the relevance or otherwise of the lack of change observed in the targets investigated by western blotting. Validation of the results is essential to understanding whether the approach taken in this study is suitable for deconvoluting the targets of small molecule anti-prion compounds.

**Are the proteasome and lysosomes directly affected by treatment with the I3GA compounds?** The studies undertaken so far suggest that the I3GAs may be affecting some function of the lysosomes, whether that is the trafficking pathways that deliver PrP<sup>Sc</sup> for degradation or degradation itself. However, neither this nor the effect on proteasomal activity has been measured directly due to containment issues. This is something that would be necessary to either validate or exclude an effect on the proteasomal degradation systems as part of the mode of action of the I3GAs. Direct measurement of proteasomal activity in the SMB cells under

steady state conditions would also determine the extent of proteasomal inhibition by PrP<sup>Sc</sup>, allowing clarification of the results of pharmacological proteasome inhibition.

**Is PrP<sup>C</sup> affected by treatment?** The reduction of PrP<sup>C</sup> levels, resulting in decreased substrate for conversion, was suggested as a mode of action of the compounds due to the down regulation of sp1 in the microarray assay. As well as direct validation of sp1 down-regulation, investigations into the effect of treatment on PrP<sup>C</sup> levels would validate or exclude an effect on PrP<sup>C</sup> levels as part of the mode of action of the I3GAs. Western blotting of cell lysates has been carried out by other members of the group to validate the dot blot approach that is used routinely, and this is something that could perhaps be employed to investigate PrP<sup>C</sup> levels.

**Do the I3GAs share a mode of action?** As discussed earlier this is still ambiguous, although it is thought that there should be at least some crossover in the mode of action of the different I3GAs. Establishing whether all the I3GAs are working in the same way relies on the identification of a mode of action for at least one of these compounds. Structurally similar compounds could then be investigated to determine if they are working in the same way.

**What exactly is going on in the 3D screening models?** The results presented within this thesis are the result of very limited investigations into the 3D screening models, with the focus on whether or not the anti-prion compounds show activity. Further investigations would be required to discover why PrP<sup>Sc</sup> levels within the hanging drops were not affected by treatment with anti-prion compounds known to be active *in vivo*. The priority would be elucidating whether the spheroids are proliferating, and whether this has affected the activity of the compounds. Similarly, further investigations would be required to clarify the apparent lack of proliferation observed in the Happy Cell model, with alternative measures of proliferation being required to confirm the MTT results presented here. Further optimisation of the Alvetex model would be required to enable more efficient lysis and/or retrieval of the cells, allowing analysis to be carried out in a more reliable and less time consuming manner. Improved harvesting and mounting of both hanging drop and Happy Cell spheroids for analysis by confocal microscopy may also provide insights into their structural morphology.

In summary, it can be seen that the I3GA compounds represent a novel group of anti-prion compounds with a mode of action that is yet to be fully determined. Further work may confirm that they are working by one of the mechanisms outlined here, or it may be that they are

working by a mechanism which is, as yet, unknown among existing anti-prion compounds. The possibility that these compounds represent a novel mode of action suggests that they may have promise as either a stand-alone treatment or as part of a multifaceted therapeutic intervention. Assessment of the *in vivo* activity of these compounds in mouse models is, at this point, essential in determining whether they have the potential to be used as therapeutics in a real life setting. However, the development of 3D models as outlined here suggests that the information which at the moment can only be obtained from animal models might, at some point, be available using *in vitro* methods.

## 9. References

1. Collinge J. Prion diseases of humans and animals: their causes and molecular basis. *Annu Rev Neurosci.* 2001;24:519-50.
2. Gambetti P, Dong Z, Yuan J, Xiao X, Zheng M, Alshekhlee A, et al. A novel human disease with abnormal prion protein sensitive to protease. *Ann Neurol.* 2008 Jun;63(6):697-708.
3. Brown DA, Bruce ME, Fraser JR. Comparison of the neuropathological characteristics of bovine spongiform encephalopathy (BSE) and variant Creutzfeldt-Jakob disease (vCJD) in mice. *Neuropathol Appl Neurobiol.* 2003 Jun;29(3):262-72.
4. Bruce ME. TSE strain variation. *Br Med Bull.* 2003;66:99-108.
5. Bruce ME, Will RG, Ironside JW, McConnell I, Drummond D, Suttie A, et al. Transmissions to mice indicate that 'new variant' CJD is caused by the BSE agent. *Nature.* 1997 Oct 2;389(6650):498-501.
6. Ritchie DL, Boyle A, McConnell I, Head MW, Ironside JW, Bruce ME. Transmissions of variant Creutzfeldt-Jakob disease from brain and lymphoreticular tissue show uniform and conserved bovine spongiform encephalopathy-related phenotypic properties on primary and secondary passage in wild-type mice. *J Gen Virol.* 2009 Dec;90(Pt 12):3075-82.
7. Hill AF, Desbruslais M, Joiner S, Sidle KC, Gowland I, Collinge J, et al. The same prion strain causes vCJD and BSE. *Nature.* 1997 Oct 2;389(6650):448-50, 526.
8. Diack AB, Head MW, McCutcheon S, Boyle A, Knight R, Ironside JW, et al. Variant CJD. 18 years of research and surveillance. *Prion.* 2014;8(4):286-95.
9. Collinge J, Sidle KC, Meads J, Ironside J, Hill AF. Molecular analysis of prion strain variation and the aetiology of 'new variant' CJD. *Nature.* 1996 Oct 24;383(6602):685-90.
10. Collinge J, Palmer MS, Dryden AJ. Genetic predisposition to iatrogenic Creutzfeldt-Jakob disease. *Lancet.* 1991 Jun 15;337(8755):1441-2.
11. Prusiner SB. Novel proteinaceous infectious particles cause scrapie. *Science.* 1982 Apr 9;216(4542):136-44.
12. Colby DW, Prusiner SB. Prions. *Cold Spring Harb Perspect Biol.* 2011 Jan;3(1):a006833.
13. Aguzzi A, Baumann F, Bremer J. The prion's elusive reason for being. *Annu Rev Neurosci.* 2008;31:439-77.
14. Linden R, Martins VR, Prado MA, Cammarota M, Izquierdo I, Brentani RR. Physiology of the prion protein. *Physiol Rev.* 2008 Apr;88(2):673-728.
15. Prusiner SB. Prions. *Proc Natl Acad Sci U S A.* 1998 Nov 10;95(23):13363-83.
16. Hegde RS, Mastrianni JA, Scott MR, DeFea KA, Tremblay P, Torchia M, et al. A transmembrane form of the prion protein in neurodegenerative disease. *Science.* 1998 Feb 6;279(5352):827-34.
17. Gabriel JM, Oesch B, Kretzschmar H, Scott M, Prusiner SB. Molecular cloning of a candidate chicken prion protein. *Proc Natl Acad Sci U S A.* 1992 Oct 1;89(19):9097-101.
18. Simonic T, Duga S, Strumbo B, Asselta R, Cecilian F, Ronchi S. cDNA cloning of turtle prion protein. *FEBS Lett.* 2000 Mar 3;469(1):33-8.
19. Strumbo B, Ronchi S, Bolis LC, Simonic T. Molecular cloning of the cDNA coding for *Xenopus laevis* prion protein. *FEBS Lett.* 2001 Nov 16;508(2):170-4.
20. Harrison CF, Lawson VA, Coleman BM, Kim YS, Masters CL, Cappai R, et al. Conservation of a glycine-rich region in the prion protein is required for uptake of prion infectivity. *J Biol Chem.* 2010 Jun 25;285(26):20213-23.
21. Manson JC, Clarke AR, Hooper ML, Aitchison L, McConnell I, Hope J. 129/Ola mice carrying a null mutation in PrP that abolishes mRNA production are developmentally normal. *Mol Neurobiol.* 1994 Apr-Jun;8(2-3):121-7.

22. Bueler H, Fischer M, Lang Y, Bluethmann H, Lipp HP, DeArmond SJ, et al. Normal development and behaviour of mice lacking the neuronal cell-surface PrP protein. *Nature*. 1992 Apr 16;356(6370):577-82.
23. Steele AD, Lindquist S, Aguzzi A. The prion protein knockout mouse: a phenotype under challenge. *Prion*. 2007 Apr-Jun;1(2):83-93.
24. Bueler H, Aguzzi A, Sailer A, Greiner RA, Autenried P, Aguet M, et al. Mice devoid of PrP are resistant to scrapie. *Cell*. 1993 Jul 2;73(7):1339-47.
25. Le Pichon CE, Valley MT, Polymenidou M, Chesler AT, Sagdullaev BT, Aguzzi A, et al. Olfactory behavior and physiology are disrupted in prion protein knockout mice. *Nat Neurosci*. 2009 Jan;12(1):60-9.
26. Singh A, Kong Q, Luo X, Petersen RB, Meyerson H, Singh N. Prion protein (PrP) knock-out mice show altered iron metabolism: a functional role for PrP in iron uptake and transport. *PLoS One*. 2009;4(7):e6115.
27. Zhang Y, Kim SO, Opsahl-Vital S, Ho SP, Souron JB, Kim C, et al. Multiple effects of the cellular prion protein on tooth development. *Int J Dev Biol*. 2011;55(10-12):953-60.
28. Strom A, Wang GS, Scott FW. Impaired glucose tolerance in mice lacking cellular prion protein. *Pancreas*. 2011 Mar;40(2):229-32.
29. Stella R, Massimino ML, Sandri M, Sorgato MC, Bertoli A. Cellular prion protein promotes regeneration of adult muscle tissue. *Mol Cell Biol*. 2010 Oct;30(20):4864-76.
30. Gourdain P, Ballerini C, Nicot AB, Carnaud C. Exacerbation of experimental autoimmune encephalomyelitis in prion protein (PrPc)-null mice: evidence for a critical role of the central nervous system. *J Neuroinflammation*. 2012;9:25.
31. Hu W, Nessler S, Hemmer B, Eagar TN, Kane LP, Leliveld SR, et al. Pharmacological prion protein silencing accelerates central nervous system autoimmune disease via T cell receptor signalling. *Brain*. 2010 Feb;133(Pt 2):375-88.
32. Nico PB, de-Paris F, Vinade ER, Amaral OB, Rockenbach I, Soares BL, et al. Altered behavioural response to acute stress in mice lacking cellular prion protein. *Behav Brain Res*. 2005 Jul 30;162(2):173-81.
33. Bounhar Y, Zhang Y, Goodyer CG, LeBlanc A. Prion protein protects human neurons against Bax-mediated apoptosis. *J Biol Chem*. 2001 Oct 19;276(42):39145-9.
34. Milhavet O, Lehmann S. Oxidative stress and the prion protein in transmissible spongiform encephalopathies. *Brain Res Brain Res Rev*. 2002 Feb;38(3):328-39.
35. Brown DR, Qin K, Herms JW, Madlung A, Manson J, Strome R, et al. The cellular prion protein binds copper in vivo. *Nature*. 1997 Dec 18-25;390(6661):684-7.
36. Brown DR, Clive C, Haswell SJ. Antioxidant activity related to copper binding of native prion protein. *J Neurochem*. 2001 Jan;76(1):69-76.
37. Brown DR, Schmidt B, Kretzschmar HA. Effects of oxidative stress on prion protein expression in PC12 cells. *Int J Dev Neurosci*. 1997 Dec;15(8):961-72.
38. Brown DR, Schulz-Schaeffer WJ, Schmidt B, Kretzschmar HA. Prion protein-deficient cells show altered response to oxidative stress due to decreased SOD-1 activity. *Exp Neurol*. 1997 Jul;146(1):104-12.
39. Brown DR, Wong BS, Hafiz F, Clive C, Haswell SJ, Jones IM. Normal prion protein has an activity like that of superoxide dismutase. *Biochem J*. 1999 Nov 15;344 Pt 1:1-5.
40. Jones S, Batchelor M, Bhelt D, Clarke AR, Collinge J, Jackson GS. Recombinant prion protein does not possess SOD-1 activity. *Biochem J*. 2005 Dec 1;392(Pt 2):309-12.
41. Hutter G, Heppner FL, Aguzzi A. No superoxide dismutase activity of cellular prion protein in vivo. *Biol Chem*. 2003 Sep;384(9):1279-85.
42. Zocche Soprana H, Canes Souza L, Debbas V, Martins Laurindo FR. Cellular prion protein (PrP(C)) and superoxide dismutase (SOD) in vascular cells under oxidative stress. *Exp Toxicol Pathol*. 2011 Mar;63(3):229-36.

43. Encalada SE, Moya KL, Lehmann S, Zahn R. The role of the prion protein in the molecular basis for synaptic plasticity and nervous system development. *J Mol Neurosci*. 2008;34(1):9-15.
44. Nicolas O, Gavin R, del Rio JA. New insights into cellular prion protein (PrP<sup>c</sup>) functions: the "ying and yang" of a relevant protein. *Brain Res Rev*. 2009 Oct;61(2):170-84.
45. Bremer J, Baumann F, Tiberi C, Wessig C, Fischer H, Schwarz P, et al. Axonal prion protein is required for peripheral myelin maintenance. *Nat Neurosci*. 2010 Mar;13(3):310-8.
46. Malaga-Trillo E, Solis GP, Schrock Y, Geiss C, Luncz L, Thomanetz V, et al. Regulation of embryonic cell adhesion by the prion protein. *PLoS Biol*. 2009 Mar 10;7(3):e55.
47. Watts JC, Huo H, Bai Y, Ehsani S, Jeon AH, Shi T, et al. Interactome analyses identify ties of PrP and its mammalian paralogs to oligomannosidic N-glycans and endoplasmic reticulum-derived chaperones. *PLoS Pathog*. 2009 Oct;5(10):e1000608.
48. Zhang CC, Steele AD, Lindquist S, Lodish HF. Prion protein is expressed on long-term repopulating hematopoietic stem cells and is important for their self-renewal. *Proc Natl Acad Sci U S A*. 2006 Feb 14;103(7):2184-9.
49. Hu W, Kieseier B, Frohman E, Eagar TN, Rosenberg RN, Hartung HP, et al. Prion proteins: physiological functions and role in neurological disorders. *J Neurol Sci*. 2008 Jan 15;264(1-2):1-8.
50. Isaacs JD, Jackson GS, Altmann DM. The role of the cellular prion protein in the immune system. *Clin Exp Immunol*. 2006 Oct;146(1):1-8.
51. Walker LC, LeVine H, 3rd. Corruption and spread of pathogenic proteins in neurodegenerative diseases. *J Biol Chem*. 2012 Sep 28;287(40):33109-15.
52. Jucker M, Walker LC. Pathogenic protein seeding in Alzheimer disease and other neurodegenerative disorders. *Ann Neurol*. 2011 Oct;70(4):532-40.
53. Jucker M, Walker LC. Self-propagation of pathogenic protein aggregates in neurodegenerative diseases. *Nature*. 2013 Sep 5;501(7465):45-51.
54. Prusiner SB. Cell biology. A unifying role for prions in neurodegenerative diseases. *Science*. 2012 Jun 22;336(6088):1511-3.
55. Collinge J. Molecular neurology of prion disease. *J Neurol Neurosurg Psychiatry*. 2005 Jul;76(7):906-19.
56. Pattison IH. Experiments with scrapie with special reference to the nature of the agent and the pathology of the disease. Slow, latent and temperate virus infections. 1965;NINDB Monograph 2:249-57.
57. Soto C, Castilla J. The controversial protein-only hypothesis of prion propagation. *Nat Med*. 2004 Jul;10 Suppl:S63-7.
58. Chandler RL. Encephalopathy in mice produced by inoculation with scrapie brain material. *Lancet*. 1961 Jun 24;1(7191):1378-9.
59. Gajdusek DC, Gibbs CJ, Alpers M. Experimental transmission of a Kuru-like syndrome to chimpanzees. *Nature*. 1966 Feb 19;209(5025):794-6.
60. Cho HJ. Is the scrapie agent a virus? *Nature*. 1976 Jul 29;262(5567):411-2.
61. Alper T, Cramp WA, Haig DA, Clarke MC. Does the agent of scrapie replicate without nucleic acid? *Nature*. 1967 May 20;214(5090):764-6.
62. Griffith JS. Self-replication and scrapie. *Nature*. 1967 Sep 2;215(5105):1043-4.
63. Bolton DC, McKinley MP, Prusiner SB. Identification of a protein that purifies with the scrapie prion. *Science*. 1982 Dec 24;218(4579):1309-11.
64. Gabizon R, McKinley MP, Groth D, Prusiner SB. Immunoaffinity purification and neutralization of scrapie prion infectivity. *Proc Natl Acad Sci U S A*. 1988 Sep;85(18):6617-21.
65. Chesebro B, Race R, Wehrly K, Nishio J, Bloom M, Lechner D, et al. Identification of scrapie prion protein-specific mRNA in scrapie-infected and uninfected brain. *Nature*. 1985 May 23-29;315(6017):331-3.
66. Rubenstein R, Carp RI, Callahan SM. In vitro replication of scrapie agent in a neuronal model: infection of PC12 cells. *J Gen Virol*. 1984 Dec;65 ( Pt 12):2191-8.

67. Race RE, Fadness LH, Chesebro B. Characterization of scrapie infection in mouse neuroblastoma cells. *J Gen Virol*. 1987 May;68 ( Pt 5):1391-9.
68. Kocisko DA, Come JH, Priola SA, Chesebro B, Raymond GJ, Lansbury PT, et al. Cell-free formation of protease-resistant prion protein. *Nature*. 1994 Aug 11;370(6489):471-4.
69. Saborio GP, Permanne B, Soto C. Sensitive detection of pathological prion protein by cyclic amplification of protein misfolding. *Nature*. 2001 Jun 14;411(6839):810-3.
70. Legname G, Baskakov IV, Nguyen HO, Riesner D, Cohen FE, DeArmond SJ, et al. Synthetic mammalian prions. *Science*. 2004 Jul 30;305(5684):673-6.
71. Castilla J, Saa P, Hetz C, Soto C. In vitro generation of infectious scrapie prions. *Cell*. 2005 Apr 22;121(2):195-206.
72. Deleault NR, Harris BT, Rees JR, Supattapone S. Formation of native prions from minimal components in vitro. *Proc Natl Acad Sci U S A*. 2007 Jun 5;104(23):9741-6.
73. Barria MA, Mukherjee A, Gonzalez-Romero D, Morales R, Soto C. De novo generation of infectious prions in vitro produces a new disease phenotype. *PLoS Pathog*. 2009 May;5(5):e1000421.
74. Wang F, Wang X, Yuan CG, Ma J. Generating a prion with bacterially expressed recombinant prion protein. *Science*. 2010 Feb 26;327(5969):1132-5.
75. Zhang Z, Zhang Y, Wang F, Wang X, Xu Y, Yang H, et al. De novo generation of infectious prions with bacterially expressed recombinant prion protein. *FASEB J*. 2013 Dec;27(12):4768-75.
76. Yuan Z, Yang L, Chen B, Zhu T, Hassan MF, Yin X, et al. Protein misfolding cyclic amplification induces the conversion of recombinant prion protein to PrP oligomers causing neuronal apoptosis. *J Neurochem*. 2015 Jun;133(5):722-9.
77. Soto C. Prion hypothesis: the end of the controversy? *Trends Biochem Sci*. 2011 Mar;36(3):151-8.
78. Supattapone S. Synthesis of high titer infectious prions with cofactor molecules. *J Biol Chem*. 2014 Jul 18;289(29):19850-4.
79. Morales R, Abid K, Soto C. The prion strain phenomenon: molecular basis and unprecedented features. *Biochim Biophys Acta*. 2007 Jun;1772(6):681-91.
80. Bessen RA, Kocisko DA, Raymond GJ, Nandan S, Lansbury PT, Caughey B. Non-genetic propagation of strain-specific properties of scrapie prion protein. *Nature*. 1995 Jun 22;375(6533):698-700.
81. Safar J, Wille H, Itri V, Groth D, Serban H, Torchia M, et al. Eight prion strains have PrP(Sc) molecules with different conformations. *Nat Med*. 1998 Oct;4(10):1157-65.
82. Telling GC, Parchi P, DeArmond SJ, Cortelli P, Montagna P, Gabizon R, et al. Evidence for the conformation of the pathologic isoform of the prion protein enciphering and propagating prion diversity. *Science*. 1996 Dec 20;274(5295):2079-82.
83. Aguzzi A, Calella AM. Prions: protein aggregation and infectious diseases. *Physiol Rev*. 2009 Oct;89(4):1105-52.
84. Sigurdson CJ, Nilsson KP, Hornemann S, Manco G, Polymenidou M, Schwarz P, et al. Prion strain discrimination using luminescent conjugated polymers. *Nat Methods*. 2007 Dec;4(12):1023-30.
85. Castilla J, Morales R, Saa P, Barria M, Gambetti P, Soto C. Cell-free propagation of prion strains. *EMBO J*. 2008 Oct 8;27(19):2557-66.
86. Walker LC, Jucker M. Neurodegenerative Diseases: Expanding the Prion Concept. *Annu Rev Neurosci*. 2015 Mar 30.
87. Bossers A, Belt P, Raymond GJ, Caughey B, de Vries R, Smits MA. Scrapie susceptibility-linked polymorphisms modulate the in vitro conversion of sheep prion protein to protease-resistant forms. *Proc Natl Acad Sci U S A*. 1997 May 13;94(10):4931-6.
88. Horiuchi M, Priola SA, Chabry J, Caughey B. Interactions between heterologous forms of prion protein: binding, inhibition of conversion, and species barriers. *Proc Natl Acad Sci U S A*. 2000 May 23;97(11):5836-41.

89. Kocisko DA, Priola SA, Raymond GJ, Chesebro B, Lansbury PT, Jr., Caughey B. Species specificity in the cell-free conversion of prion protein to protease-resistant forms: a model for the scrapie species barrier. *Proc Natl Acad Sci U S A*. 1995 Apr 25;92(9):3923-7.
90. Raymond GJ, Hope J, Kocisko DA, Priola SA, Raymond LD, Bossers A, et al. Molecular assessment of the potential transmissibilities of BSE and scrapie to humans. *Nature*. 1997 Jul 17;388(6639):285-8.
91. Priola SA, Caughey B, Race RE, Chesebro B. Heterologous PrP molecules interfere with accumulation of protease-resistant PrP in scrapie-infected murine neuroblastoma cells. *J Virol*. 1994 Aug;68(8):4873-8.
92. Priola SA, Chesebro B. A single hamster PrP amino acid blocks conversion to protease-resistant PrP in scrapie-infected mouse neuroblastoma cells. *J Virol*. 1995 Dec;69(12):7754-8.
93. Scott MR, Kohler R, Foster D, Prusiner SB. Chimeric prion protein expression in cultured cells and transgenic mice. *Protein Sci*. 1992 Aug;1(8):986-97.
94. Schatzl HM, Da Costa M, Taylor L, Cohen FE, Prusiner SB. Prion protein gene variation among primates. *J Mol Biol*. 1995 Jan 27;245(4):362-74.
95. Collinge J, Clarke AR. A general model of prion strains and their pathogenicity. *Science*. 2007 Nov 9;318(5852):930-6.
96. Heppner FL, Christ AD, Klein MA, Prinz M, Fried M, Kraehenbuhl JP, et al. Transepithelial prion transport by M cells. *Nat Med*. 2001 Sep;7(9):976-7.
97. Fraser H, Dickinson AG. Pathogenesis of scrapie in the mouse: the role of the spleen. *Nature*. 1970 May 2;226(5244):462-3.
98. Lasmezas CI, Cesbron JY, Deslys JP, Demaimay R, Adjou KT, Rioux R, et al. Immune system-dependent and -independent replication of the scrapie agent. *J Virol*. 1996 Feb;70(2):1292-5.
99. Flores-Langarica A, Sebti Y, Mitchell DA, Sim RB, MacPherson GG. Scrapie pathogenesis: the role of complement C1q in scrapie agent uptake by conventional dendritic cells. *J Immunol*. 2009 Feb 1;182(3):1305-13.
100. Mabbott NA, Mackay F, Minns F, Bruce ME. Temporary inactivation of follicular dendritic cells delays neuroinvasion of scrapie. *Nat Med*. 2000 Jul;6(7):719-20.
101. Klein MA, Frigg R, Flechsig E, Raeber AJ, Kalinke U, Bluethmann H, et al. A crucial role for B cells in neuroinvasive scrapie. *Nature*. 1997 Dec 18-25;390(6661):687-90.
102. Beekes M, Baldauf E, Diringer H. Sequential appearance and accumulation of pathognomonic markers in the central nervous system of hamsters orally infected with scrapie. *J Gen Virol*. 1996 Aug;77 ( Pt 8):1925-34.
103. Aguzzi A, Falsig J. Prion propagation, toxicity and degradation. *Nat Neurosci*. 2012 Jul;15(7):936-9.
104. Gousset K, Schiff E, Langevin C, Marijanovic Z, Caputo A, Browman DT, et al. Prions hijack tunnelling nanotubes for intercellular spread. *Nat Cell Biol*. 2009 Mar;11(3):328-36.
105. Gousset K, Zurzolo C. Tunnelling nanotubes: a highway for prion spreading? *Prion*. 2009 Apr-Jun;3(2):94-8.
106. Silveira JR, Raymond GJ, Hughson AG, Race RE, Sim VL, Hayes SF, et al. The most infectious prion protein particles. *Nature*. 2005 Sep 8;437(7056):257-61.
107. Tixador P, Herzog L, Reine F, Jaumain E, Chapuis J, Le Dur A, et al. The physical relationship between infectivity and prion protein aggregates is strain-dependent. *PLoS Pathog*. 2010 Apr;6(4):e1000859.
108. Krauss S, Vorberg I. Prions Ex Vivo: What Cell Culture Models Tell Us about Infectious Proteins. *Int J Cell Biol*. 2013;2013:704546.
109. Greil CS, Vorberg IM, Ward AE, Meade-White KD, Harris DA, Priola SA. Acute cellular uptake of abnormal prion protein is cell type and scrapie-strain independent. *Virology*. 2008 Sep 30;379(2):284-93.

110. Ghaemmaghami S, Phuan PW, Perkins B, Ullman J, May BC, Cohen FE, et al. Cell division modulates prion accumulation in cultured cells. *Proc Natl Acad Sci U S A*. 2007 Nov 13;104(46):17971-6.
111. Fevrier B, Vilette D, Archer F, Loew D, Faigle W, Vidal M, et al. Cells release prions in association with exosomes. *Proc Natl Acad Sci U S A*. 2004 Jun 29;101(26):9683-8.
112. Alais S, Simoes S, Baas D, Lehmann S, Raposo G, Darlix JL, et al. Mouse neuroblastoma cells release prion infectivity associated with exosomal vesicles. *Biol Cell*. 2008 Oct;100(10):603-15.
113. Paquet S, Langevin C, Chapuis J, Jackson GS, Laude H, Vilette D. Efficient dissemination of prions through preferential transmission to nearby cells. *J Gen Virol*. 2007 Feb;88(Pt 2):706-13.
114. Caughey B, Raymond GJ, Ernst D, Race RE. N-terminal truncation of the scrapie-associated form of PrP by lysosomal protease(s): implications regarding the site of conversion of PrP to the protease-resistant state. *J Virol*. 1991 Dec;65(12):6597-603.
115. Riesner D. Biochemistry and structure of PrP(C) and PrP(Sc). *Br Med Bull*. 2003;66:21-33.
116. Huang Z, Prusiner SB, Cohen FE. Scrapie prions: a three-dimensional model of an infectious fragment. *Fold Des*. 1995;1(1):13-9.
117. Diaz-Espinoza R, Soto C. High-resolution structure of infectious prion protein: the final frontier. *Nat Struct Mol Biol*. 2012 Apr;19(4):370-7.
118. Govaerts C, Wille H, Prusiner SB, Cohen FE. Evidence for assembly of prions with left-handed beta-helices into trimers. *Proc Natl Acad Sci U S A*. 2004 Jun 1;101(22):8342-7.
119. DeMarco ML, Daggett V. From conversion to aggregation: protofibril formation of the prion protein. *Proc Natl Acad Sci U S A*. 2004 Feb 24;101(8):2293-8.
120. Cobb NJ, Sonnichsen FD, McHaourab H, Surewicz WK. Molecular architecture of human prion protein amyloid: a parallel, in-register beta-structure. *Proc Natl Acad Sci U S A*. 2007 Nov 27;104(48):18946-51.
121. Smirnovas V, Baron GS, Offerdahl DK, Raymond GJ, Caughey B, Surewicz WK. Structural organization of brain-derived mammalian prions examined by hydrogen-deuterium exchange. *Nat Struct Mol Biol*. 2011 Apr;18(4):504-6.
122. Cronier S, Gros N, Tattum MH, Jackson GS, Clarke AR, Collinge J, et al. Detection and characterization of proteinase K-sensitive disease-related prion protein with thermolysin. *Biochem J*. 2008 Dec 1;416(2):297-305.
123. Meier P, Genoud N, Prinz M, Maissen M, Rulicke T, Zurbriggen A, et al. Soluble dimeric prion protein binds PrP(Sc) in vivo and antagonizes prion disease. *Cell*. 2003 Apr 4;113(1):49-60.
124. Aguzzi A, Sigurdson C, Heikenwaelder M. Molecular mechanisms of prion pathogenesis. *Annu Rev Pathol*. 2008;3:11-40.
125. Telling GC, Scott M, Mastrianni J, Gabizon R, Torchia M, Cohen FE, et al. Prion propagation in mice expressing human and chimeric PrP transgenes implicates the interaction of cellular PrP with another protein. *Cell*. 1995 Oct 6;83(1):79-90.
126. Kaneko K, Zulianello L, Scott M, Cooper CM, Wallace AC, James TL, et al. Evidence for protein X binding to a discontinuous epitope on the cellular prion protein during scrapie prion propagation. *Proc Natl Acad Sci U S A*. 1997 Sep 16;94(19):10069-74.
127. Geoghegan JC, Miller MB, Kwak AH, Harris BT, Supattapone S. Trans-dominant inhibition of prion propagation in vitro is not mediated by an accessory cofactor. *PLoS Pathog*. 2009 Jul;5(7):e1000535.
128. Weissmann C. The state of the prion. *Nat Rev Microbiol*. 2004 Nov;2(11):861-71.
129. Cobb NJ, Surewicz WK. Prion diseases and their biochemical mechanisms. *Biochemistry*. 2009 Mar 31;48(12):2574-85.
130. Birkmann E, Riesner D. Prion infection: seeded fibrillization or more? *Prion*. 2008 Apr-Jun;2(2):67-72.

131. Gilch S, Nunziante M, Ertmer A, Schatzl HM. Strategies for eliminating PrP(c) as substrate for prion conversion and for enhancing PrP(Sc) degradation. *Vet Microbiol.* 2007 Aug 31;123(4):377-86.
132. Taraboulos A, Scott M, Semenov A, Avrahami D, Laszlo L, Prusiner SB. Cholesterol depletion and modification of COOH-terminal targeting sequence of the prion protein inhibit formation of the scrapie isoform. *J Cell Biol.* 1995 Apr;129(1):121-32.
133. Gorodinsky A, Harris DA. Glycolipid-anchored proteins in neuroblastoma cells form detergent-resistant complexes without caveolin. *J Cell Biol.* 1995 May;129(3):619-27.
134. Sarnataro D, Paladino S, Campana V, Grassi J, Nitsch L, Zurzolo C. PrPC is sorted to the basolateral membrane of epithelial cells independently of its association with rafts. *Traffic.* 2002 Nov;3(11):810-21.
135. Vey M, Pilkuhn S, Wille H, Nixon R, DeArmond SJ, Smart EJ, et al. Subcellular colocalization of the cellular and scrapie prion proteins in caveolae-like membranous domains. *Proc Natl Acad Sci U S A.* 1996 Dec 10;93(25):14945-9.
136. Caughey B, Raymond GJ. The scrapie-associated form of PrP is made from a cell surface precursor that is both protease- and phospholipase-sensitive. *J Biol Chem.* 1991 Sep 25;266(27):18217-23.
137. Borchelt DR, Scott M, Taraboulos A, Stahl N, Prusiner SB. Scrapie and cellular prion proteins differ in their kinetics of synthesis and topology in cultured cells. *J Cell Biol.* 1990 Mar;110(3):743-52.
138. Caughey B, Race RE, Ernst D, Buchmeier MJ, Chesebro B. Prion protein biosynthesis in scrapie-infected and uninfected neuroblastoma cells. *J Virol.* 1989 Jan;63(1):175-81.
139. Prusiner SB, Scott MR, DeArmond SJ, Cohen FE. Prion protein biology. *Cell.* 1998 May 1;93(3):337-48.
140. Taylor DR, Hooper NM. The prion protein and lipid rafts. *Mol Membr Biol.* 2006 Jan-Feb;23(1):89-99.
141. Hannaoui S, Shim SY, Cheng YC, Corda E, Gilch S. Cholesterol balance in prion diseases and Alzheimer's disease. *Viruses.* 2014 Nov;6(11):4505-35.
142. Jeffrey M, McGovern G, Goodsir CM, Brown KL, Bruce ME. Sites of prion protein accumulation in scrapie-infected mouse spleen revealed by immuno-electron microscopy. *J Pathol.* 2000 Jul;191(3):323-32.
143. Marijanovic Z, Caputo A, Campana V, Zurzolo C. Identification of an intracellular site of prion conversion. *PLoS Pathog.* 2009 May;5(5):e1000426.
144. Goold R, McKinnon C, Rabbanian S, Collinge J, Schiavo G, Tabrizi SJ. Alternative fates of newly formed PrP<sup>Sc</sup> upon prion conversion on the plasma membrane. *J Cell Sci.* 2013 Aug 15;126(Pt 16):3552-62.
145. Goold R, Rabbanian S, Sutton L, Andre R, Arora P, Moonga J, et al. Rapid cell-surface prion protein conversion revealed using a novel cell system. *Nat Commun.* 2011;2:281.
146. Grassmann A, Wolf H, Hofmann J, Graham J, Vorberg I. Cellular aspects of prion replication in vitro. *Viruses.* 2013 Jan;5(1):374-405.
147. Bate C, Tayebi M, Williams A. The glycosylphosphatidylinositol anchor is a major determinant of prion binding and replication. *Biochem J.* 2010 May 15;428(1):95-101.
148. Kimura T, Ishikawa K, Sakasegawa Y, Teruya K, Sata T, Schatzl H, et al. GABAA receptor subunit beta1 is involved in the formation of protease-resistant prion protein in prion-infected neuroblastoma cells. *FEBS Lett.* 2010 Mar 19;584(6):1193-8.
149. Taylor DR, Whitehouse IJ, Hooper NM. Glypican-1 mediates both prion protein lipid raft association and disease isoform formation. *PLoS Pathog.* 2009 Nov;5(11):e1000666.
150. Radulescu RT, Brenig B. Infectious nucleic acids in prion disease: halfway there. *Trends Biochem Sci.* 2009 Jan;34(1):4-5; author reply 6.

151. Yadavalli R, Guttman RP, Seward T, Centers AP, Williamson RA, Telling GC. Calpain-dependent endoproteolytic cleavage of PrP<sup>Sc</sup> modulates scrapie prion propagation. *J Biol Chem*. 2004 May 21;279(21):21948-56.
152. Westergard L, Turnbaugh JA, Harris DA. A naturally occurring C-terminal fragment of the prion protein (PrP) delays disease and acts as a dominant-negative inhibitor of PrP<sup>Sc</sup> formation. *J Biol Chem*. 2011 Dec 23;286(51):44234-42.
153. Kovacs GG, Budka H. Molecular pathology of human prion diseases. *Int J Mol Sci*. 2009 Mar;10(3):976-99.
154. Flechsig E, Shmerling D, Hegyi I, Raeber AJ, Fischer M, Cozzio A, et al. Prion protein devoid of the octapeptide repeat region restores susceptibility to scrapie in PrP knockout mice. *Neuron*. 2000 Aug;27(2):399-408.
155. Lasmez C, Deslys JP, Robain O, Jaegly A, Beringue V, Peyrin JM, et al. Transmission of the BSE agent to mice in the absence of detectable abnormal prion protein. *Science*. 1997 Jan 17;275(5298):402-5.
156. Manson JC, Jamieson E, Baybutt H, Tuzi NL, Barron R, McConnell I, et al. A single amino acid alteration (101L) introduced into murine PrP dramatically alters incubation time of transmissible spongiform encephalopathy. *EMBO J*. 1999 Dec 1;18(23):6855-64.
157. Race R, Raines A, Raymond GJ, Caughey B, Chesebro B. Long-term subclinical carrier state precedes scrapie replication and adaptation in a resistant species: analogies to bovine spongiform encephalopathy and variant Creutzfeldt-Jakob disease in humans. *J Virol*. 2001 Nov;75(21):10106-12.
158. Hill AF, Joiner S, Linehan J, Desbruslais M, Lantos PL, Collinge J. Species-barrier-independent prion replication in apparently resistant species. *Proc Natl Acad Sci U S A*. 2000 Aug 29;97(18):10248-53.
159. Brandner S, Isenmann S, Raeber A, Fischer M, Sailer A, Kobayashi Y, et al. Normal host prion protein necessary for scrapie-induced neurotoxicity. *Nature*. 1996 Jan 25;379(6563):339-43.
160. Manson JC, Clarke AR, McBride PA, McConnell I, Hope J. PrP gene dosage determines the timing but not the final intensity or distribution of lesions in scrapie pathology. *Neurodegeneration*. 1994 Dec;3(4):331-40.
161. Mallucci G, Dickinson A, Linehan J, Klohn PC, Brandner S, Collinge J. Depleting neuronal PrP in prion infection prevents disease and reverses spongiosis. *Science*. 2003 Oct 31;302(5646):871-4.
162. Mallucci GR, White MD, Farmer M, Dickinson A, Khatun H, Powell AD, et al. Targeting cellular prion protein reverses early cognitive deficits and neurophysiological dysfunction in prion-infected mice. *Neuron*. 2007 Feb 1;53(3):325-35.
163. Hill AF, Collinge J. Subclinical prion infection. *Trends Microbiol*. 2003 Dec;11(12):578-84.
164. Huang P, Lian F, Wen Y, Guo C, Lin D. Prion protein oligomer and its neurotoxicity. *Acta Biochim Biophys Sin (Shanghai)*. 2013 Jun;45(6):442-51.
165. Sandberg MK, Al-Doujaily H, Sharps B, Clarke AR, Collinge J. Prion propagation and toxicity in vivo occur in two distinct mechanistic phases. *Nature*. 2011 Feb 24;470(7335):540-2.
166. Solomon IH, Schepker JA, Harris DA. Prion neurotoxicity: insights from prion protein mutants. *Curr Issues Mol Biol*. 2010;12(2):51-61.
167. Peretz D, Williamson RA, Matsunaga Y, Serban H, Pinilla C, Bastidas RB, et al. A conformational transition at the N terminus of the prion protein features in formation of the scrapie isoform. *J Mol Biol*. 1997 Oct 31;273(3):614-22.
168. Brown DR, Herms J, Kretschmar HA. Mouse cortical cells lacking cellular PrP survive in culture with a neurotoxic PrP fragment. *Neuroreport*. 1994 Oct 27;5(16):2057-60.
169. Fioriti L, Quaglio E, Massignan T, Colombo L, Stewart RS, Salmona M, et al. The neurotoxicity of prion protein (PrP) peptide 106-126 is independent of the expression level of PrP and is not mediated by abnormal PrP species. *Mol Cell Neurosci*. 2005 Jan;28(1):165-76.

170. Forloni G, Angeretti N, Chiesa R, Monzani E, Salmona M, Bugiani O, et al. Neurotoxicity of a prion protein fragment. *Nature*. 1993 Apr 8;362(6420):543-6.
171. Solfrosi L, Criado JR, McGavern DB, Wirz S, Sanchez-Alavez M, Sugama S, et al. Cross-linking cellular prion protein triggers neuronal apoptosis in vivo. *Science*. 2004 Mar 5;303(5663):1514-6.
172. Ma J, Lindquist S. Conversion of PrP to a self-perpetuating PrPSc-like conformation in the cytosol. *Science*. 2002 Nov 29;298(5599):1785-8.
173. Chakrabarti O, Hegde RS. Functional depletion of mahogunin by cytosolically exposed prion protein contributes to neurodegeneration. *Cell*. 2009 Jun 12;137(6):1136-47.
174. Drisaldi B, Stewart RS, Adles C, Stewart LR, Quaglio E, Biasini E, et al. Mutant PrP is delayed in its exit from the endoplasmic reticulum, but neither wild-type nor mutant PrP undergoes retrotranslocation prior to proteasomal degradation. *J Biol Chem*. 2003 Jun 13;278(24):21732-43.
175. Fioriti L, Dossena S, Stewart LR, Stewart RS, Harris DA, Forloni G, et al. Cytosolic prion protein (PrP) is not toxic in N2a cells and primary neurons expressing pathogenic PrP mutations. *J Biol Chem*. 2005 Mar 25;280(12):11320-8.
176. Hetz CA, Soto C. Stressing out the ER: a role of the unfolded protein response in prion-related disorders. *Curr Mol Med*. 2006 Feb;6(1):37-43.
177. Hetz C, Russelakis-Carneiro M, Maundrell K, Castilla J, Soto C. Caspase-12 and endoplasmic reticulum stress mediate neurotoxicity of pathological prion protein. *EMBO J*. 2003 Oct 15;22(20):5435-45.
178. Rane NS, Kang SW, Chakrabarti O, Feigenbaum L, Hegde RS. Reduced translocation of nascent prion protein during ER stress contributes to neurodegeneration. *Dev Cell*. 2008 Sep;15(3):359-70.
179. Nunziante M, Ackermann K, Dietrich K, Wolf H, Gadtke L, Gilch S, et al. Proteasomal dysfunction and endoplasmic reticulum stress enhance trafficking of prion protein aggregates through the secretory pathway and increase accumulation of pathologic prion protein. *J Biol Chem*. 2011 Sep 30;286(39):33942-53.
180. Kristiansen M, Messenger MJ, Klohn PC, Brandner S, Wadsworth JD, Collinge J, et al. Disease-related prion protein forms aggregates in neuronal cells leading to caspase activation and apoptosis. *J Biol Chem*. 2005 Nov 18;280(46):38851-61.
181. Kristiansen M, Deriziotis P, Dimcheff DE, Jackson GS, Ovaa H, Naumann H, et al. Disease-associated prion protein oligomers inhibit the 26S proteasome. *Mol Cell*. 2007 Apr 27;26(2):175-88.
182. Deriziotis P, Andre R, Smith DM, Goold R, Kinghorn KJ, Kristiansen M, et al. Misfolded PrP impairs the UPS by interaction with the 20S proteasome and inhibition of substrate entry. *EMBO J*. 2011 Aug 3;30(15):3065-77.
183. Solomon IH, Biasini E, Harris DA. Ion channels induced by the prion protein: mediators of neurotoxicity. *Prion*. 2012 Jan-Mar;6(1):40-5.
184. Halliday M, Radford H, Mallucci GR. Prions: generation and spread versus neurotoxicity. *J Biol Chem*. 2014 Jul 18;289(29):19862-8.
185. Moreno JA, Radford H, Peretti D, Steinert JR, Verity N, Martin MG, et al. Sustained translational repression by eIF2alpha-P mediates prion neurodegeneration. *Nature*. 2012 May 24;485(7399):507-11.
186. Moreno JA, Halliday M, Molloy C, Radford H, Verity N, Axten JM, et al. Oral treatment targeting the unfolded protein response prevents neurodegeneration and clinical disease in prion-infected mice. *Sci Transl Med*. 2013 Oct 9;5(206):206ra138.
187. Senatore A, Colleoni S, Verderio C, Restelli E, Morini R, Condliffe SB, et al. Mutant PrP suppresses glutamatergic neurotransmission in cerebellar granule neurons by impairing membrane delivery of VGCC alpha(2)delta-1 Subunit. *Neuron*. 2012 Apr 26;74(2):300-13.

188. Caughey B. Prion protein interconversions. *Philos Trans R Soc Lond B Biol Sci.* 2001 Feb 28;356(1406):197-200; discussion -2.
189. Nunziante M, Gilch S, Schatzl HM. Prion diseases: from molecular biology to intervention strategies. *Chembiochem.* 2003 Dec 5;4(12):1268-84.
190. Kirby L, Birkett CR, Rudyk H, Gilbert IH, Hope J. In vitro cell-free conversion of bacterial recombinant PrP to PrPres as a model for conversion. *J Gen Virol.* 2003 Apr;84(Pt 4):1013-20.
191. Supattapone S. Prion protein conversion in vitro. *J Mol Med (Berl).* 2004 Jun;82(6):348-56.
192. Butler DA, Scott MR, Bockman JM, Borchelt DR, Taraboulos A, Hsiao KK, et al. Scrapie-infected murine neuroblastoma cells produce protease-resistant prion proteins. *J Virol.* 1988 May;62(5):1558-64.
193. Schatzl HM, Laszlo L, Holtzman DM, Tatzelt J, DeArmond SJ, Weiner RI, et al. A hypothalamic neuronal cell line persistently infected with scrapie prions exhibits apoptosis. *J Virol.* 1997 Nov;71(11):8821-31.
194. Collinge J, Gorham M, Hudson F, Kennedy A, Keogh G, Pal S, et al. Safety and efficacy of quinacrine in human prion disease (PRION-1 study): a patient-preference trial. *Lancet Neurol.* 2009 Apr;8(4):334-44.
195. Rainov NG, Tsuboi Y, Krolak-Salmon P, Vighetto A, Doh-Ura K. Experimental treatments for human transmissible spongiform encephalopathies: is there a role for pentosan polysulfate? *Expert Opin Biol Ther.* 2007 May;7(5):713-26.
196. Tsuboi Y, Doh-Ura K, Yamada T. Continuous intraventricular infusion of pentosan polysulfate: clinical trial against prion diseases. *Neuropathology.* 2009 Oct;29(5):632-6.
197. Newman PK, Todd NV, Scoones D, Mead S, Knight RS, Will RG, et al. Postmortem findings in a case of variant Creutzfeldt-Jakob disease treated with intraventricular pentosan polysulfate. *J Neurol Neurosurg Psychiatry.* 2014 Aug;85(8):921-4.
198. Honda H, Sasaki K, Minaki H, Masui K, Suzuki SO, Doh-Ura K, et al. Protease-resistant PrP and PrP oligomers in the brain in human prion diseases after intraventricular pentosan polysulfate infusion. *Neuropathology.* 2012 Apr;32(2):124-32.
199. Caughey B, Caughey WS, Kocisko DA, Lee KS, Silveira JR, Morrey JD. Prions and transmissible spongiform encephalopathy (TSE) chemotherapeutics: A common mechanism for anti-TSE compounds? *Acc Chem Res.* 2006 Sep;39(9):646-53.
200. Cashman NR, Caughey B. Prion diseases--close to effective therapy? *Nat Rev Drug Discov.* 2004 Oct;3(10):874-84.
201. Klein MA, Kaeser PS, Schwarz P, Weyd H, Xenarios I, Zinkernagel RM, et al. Complement facilitates early prion pathogenesis. *Nat Med.* 2001 Apr;7(4):488-92.
202. Brown KL, Stewart K, Ritchie DL, Mabbott NA, Williams A, Fraser H, et al. Scrapie replication in lymphoid tissues depends on prion protein-expressing follicular dendritic cells. *Nat Med.* 1999 Nov;5(11):1308-12.
203. Kitamoto T, Muramoto T, Mohri S, Doh-Ura K, Tateishi J. Abnormal isoform of prion protein accumulates in follicular dendritic cells in mice with Creutzfeldt-Jakob disease. *J Virol.* 1991 Nov;65(11):6292-5.
204. Mabbott NA, Bruce ME, Botto M, Walport MJ, Pepys MB. Temporary depletion of complement component C3 or genetic deficiency of C1q significantly delays onset of scrapie. *Nat Med.* 2001 Apr;7(4):485-7.
205. Kocisko DA, Baron GS, Rubenstein R, Chen J, Kuizon S, Caughey B. New inhibitors of scrapie-associated prion protein formation in a library of 2000 drugs and natural products. *J Virol.* 2003 Oct;77(19):10288-94.
206. Kocisko DA, Engel AL, Harbuck K, Arnold KM, Olsen EA, Raymond LD, et al. Comparison of protease-resistant prion protein inhibitors in cell cultures infected with two strains of mouse and sheep scrapie. *Neurosci Lett.* 2005 Nov 11;388(2):106-11.

207. Trevitt CR, Collinge J. A systematic review of prion therapeutics in experimental models. *Brain*. 2006 Sep;129(Pt 9):2241-65.
208. Ladogana A, Casaccia P, Ingrosso L, Cibati M, Salvatore M, Xi YG, et al. Sulphate polyanions prolong the incubation period of scrapie-infected hamsters. *J Gen Virol*. 1992 Mar;73 ( Pt 3):661-5.
209. Doh-ura K, Ishikawa K, Murakami-Kubo I, Sasaki K, Mohri S, Race R, et al. Treatment of transmissible spongiform encephalopathy by intraventricular drug infusion in animal models. *J Virol*. 2004 May;78(10):4999-5006.
210. Diringer H, Ehlers B. Chemoprophylaxis of scrapie in mice. *J Gen Virol*. 1991 Feb;72 ( Pt 2):457-60.
211. Kamatari YO, Hayano Y, Yamaguchi K, Hosokawa-Muto J, Kuwata K. Characterizing antiprion compounds based on their binding properties to prion proteins: implications as medical chaperones. *Protein Sci*. 2013 Jan;22(1):22-34.
212. Shyng SL, Lehmann S, Moulder KL, Harris DA. Sulfated glycans stimulate endocytosis of the cellular isoform of the prion protein, PrP<sup>C</sup>, in cultured cells. *J Biol Chem*. 1995 Dec 15;270(50):30221-9.
213. Caughey B, Brown K, Raymond GJ, Katzenstein GE, Thresher W. Binding of the protease-sensitive form of PrP (prion protein) to sulfated glycosaminoglycan and congo red [corrected]. *J Virol*. 1994 Apr;68(4):2135-41.
214. Caughey B, Raymond GJ. Sulfated polyanion inhibition of scrapie-associated PrP accumulation in cultured cells. *J Virol*. 1993 Feb;67(2):643-50.
215. Farquhar CF, Dickinson AG. Prolongation of scrapie incubation period by an injection of dextran sulphate 500 within the month before or after infection. *J Gen Virol*. 1986 Mar;67 ( Pt 3):463-73.
216. Ehlers B, Diringer H. Dextran sulphate 500 delays and prevents mouse scrapie by impairment of agent replication in spleen. *J Gen Virol*. 1984 Aug;65 ( Pt 8):1325-30.
217. Rudyk H, Vasiljevic S, Hennion RM, Birkett CR, Hope J, Gilbert IH. Screening Congo Red and its analogues for their ability to prevent the formation of PrP<sup>res</sup> in scrapie-infected cells. *J Gen Virol*. 2000 Apr;81(Pt 4):1155-64.
218. Sellarajah S, Lekishvili T, Bowring C, Thompsett AR, Rudyk H, Birkett CR, et al. Synthesis of analogues of Congo red and evaluation of their anti-prion activity. *J Med Chem*. 2004 Oct 21;47(22):5515-34.
219. Rudyk H, Knaggs MH, Vasiljevic S, Hope J, Birkett C, Gilbert IH. Synthesis and evaluation of analogues of Congo red as potential compounds against transmissible spongiform encephalopathies. *Eur J Med Chem*. 2003 Jun;38(6):567-79.
220. Webb S, Lekishvili T, Loeschner C, Sellarajah S, Prelli F, Wisniewski T, et al. Mechanistic insights into the cure of prion disease by novel antiprion compounds. *J Virol*. 2007 Oct;81(19):10729-41.
221. Touil F, Pratt S, Mutter R, Chen B. Screening a library of potential prion therapeutics against cellular prion proteins and insights into their mode of biological activities by surface plasmon resonance. *J Pharm Biomed Anal*. 2006 Mar 3;40(4):822-32.
222. Kawatake S, Nishimura Y, Sakaguchi S, Iwaki T, Doh-ura K. Surface plasmon resonance analysis for the screening of anti-prion compounds. *Biol Pharm Bull*. 2006 May;29(5):927-32.
223. Georgieva D, Schwark D, von Bergen M, Redecke L, Genov N, Betzel C. Interactions of recombinant prions with compounds of therapeutical significance. *Biochem Biophys Res Commun*. 2006 Jun 2;344(2):463-70.
224. Caspi S, Halimi M, Yanai A, Sasson SB, Taraboulos A, Gabizon R. The anti-prion activity of Congo red. Putative mechanism. *J Biol Chem*. 1998 Feb 6;273(6):3484-9.
225. Demaimay R, Harper J, Gordon H, Weaver D, Chesebro B, Caughey B. Structural aspects of Congo red as an inhibitor of protease-resistant prion protein formation. *J Neurochem*. 1998 Dec;71(6):2534-41.

226. Gilch S, Winklhofer KF, Groschup MH, Nunziante M, Lucassen R, Spielhauer C, et al. Intracellular re-routing of prion protein prevents propagation of PrP(Sc) and delays onset of prion disease. *EMBO J*. 2001 Aug 1;20(15):3957-66.
227. Supattapone S, Nguyen HO, Cohen FE, Prusiner SB, Scott MR. Elimination of prions by branched polyamines and implications for therapeutics. *Proc Natl Acad Sci U S A*. 1999 Dec 7;96(25):14529-34.
228. Supattapone S, Piro JR, Rees JR. Complex polyamines: unique prion disaggregating compounds. *CNS Neurol Disord Drug Targets*. 2009 Nov;8(5):323-8.
229. Supattapone S, Wille H, Uyechi L, Safar J, Tremblay P, Szoka FC, et al. Branched polyamines cure prion-infected neuroblastoma cells. *J Virol*. 2001 Apr;75(7):3453-61.
230. Winklhofer KF, Tatzelt J. Cationic lipopolyamines induce degradation of PrPSc in scrapie-infected mouse neuroblastoma cells. *Biol Chem*. 2000 May-Jun;381(5-6):463-9.
231. McKinley MP, Taraboulos A, Kenaga L, Serban D, Stieber A, DeArmond SJ, et al. Ultrastructural localization of scrapie prion proteins in cytoplasmic vesicles of infected cultured cells. *Lab Invest*. 1991 Dec;65(6):622-30.
232. Korth C, May BC, Cohen FE, Prusiner SB. Acridine and phenothiazine derivatives as pharmacotherapeutics for prion disease. *Proc Natl Acad Sci U S A*. 2001 Aug 14;98(17):9836-41.
233. Barret A, Tagliavini F, Forloni G, Bate C, Salmona M, Colombo L, et al. Evaluation of quinacrine treatment for prion diseases. *J Virol*. 2003 Aug;77(15):8462-9.
234. Yung L, Huang Y, Lessard P, Legname G, Lin ET, Baldwin M, et al. Pharmacokinetics of quinacrine in the treatment of prion disease. *BMC Infect Dis*. 2004 Nov 29;4:53.
235. Gayraud V, Picard-Hagen N, Viguie C, Laroute V, Androletti O, Toutain PL. A possible pharmacological explanation for quinacrine failure to treat prion diseases: pharmacokinetic investigations in a ovine model of scrapie. *Br J Pharmacol*. 2005 Feb;144(3):386-93.
236. Doh-Ura K, Iwaki T, Caughey B. Lysosomotropic agents and cysteine protease inhibitors inhibit scrapie-associated prion protein accumulation. *J Virol*. 2000 May;74(10):4894-7.
237. Ertmer A, Gilch S, Yun SW, Flechsig E, Klebl B, Stein-Gerlach M, et al. The tyrosine kinase inhibitor STI571 induces cellular clearance of PrPSc in prion-infected cells. *J Biol Chem*. 2004 Oct 1;279(40):41918-27.
238. Yamasaki T, Suzuki A, Hasebe R, Horiuchi M. Comparison of the Anti-Prion Mechanism of Four Different Anti-Prion Compounds, Anti-PrP Monoclonal Antibody 44B1, Pentosan Polysulfate, Chlorpromazine, and U18666A, in Prion-Infected Mouse Neuroblastoma Cells. *PLoS One*. 2014;9(9):e106516.
239. Marzo L, Marijanovic Z, Browman D, Chamoun Z, Caputo A, Zurzolo C. 4-hydroxytamoxifen leads to PrPSc clearance by conveying both PrPC and PrPSc to lysosomes independently of autophagy. *J Cell Sci*. 2013 Mar 15;126(Pt 6):1345-54.
240. Westergaard L, Christensen HM, Harris DA. The cellular prion protein (PrP(C)): its physiological function and role in disease. *Biochim Biophys Acta*. 2007 Jun;1772(6):629-44.
241. Bate C, Reid S, Williams A. Phospholipase A2 inhibitors or platelet-activating factor antagonists prevent prion replication. *J Biol Chem*. 2004 Aug 27;279(35):36405-11.
242. Mange A, Nishida N, Milhavet O, McMahon HE, Casanova D, Lehmann S. Amphotericin B inhibits the generation of the scrapie isoform of the prion protein in infected cultures. *J Virol*. 2000 Apr;74(7):3135-40.
243. Gilch S, Kehler C, Schatzl HM. The prion protein requires cholesterol for cell surface localization. *Mol Cell Neurosci*. 2006 Feb;31(2):346-53.
244. Gilch S, Bach C, Lutzny G, Vorberg I, Schatzl HM. Inhibition of cholesterol recycling impairs cellular PrP(Sc) propagation. *Cell Mol Life Sci*. 2009 Dec;66(24):3979-91.
245. Klingenstein R, Lober S, Kujala P, Godsave S, Leliveld SR, Gmeiner P, et al. Tricyclic antidepressants, quinacrine and a novel, synthetic chimera thereof clear prions by destabilizing detergent-resistant membrane compartments. *J Neurochem*. 2006 Aug;98(3):748-59.

246. Orru CD, Cannas MD, Vascellari S, Angius F, Cocco PL, Norfo C, et al. In vitro synergistic anti-prion effect of cholesterol ester modulators in combination with chlorpromazine and quinacrine. *Central European Journal of Biology*. 2010 Apr;5(2):151-65.
247. White MD, Farmer M, Mirabile I, Brandner S, Collinge J, Mallucci GR. Single treatment with RNAi against prion protein rescues early neuronal dysfunction and prolongs survival in mice with prion disease. *Proc Natl Acad Sci U S A*. 2008 Jul 22;105(29):10238-43.
248. Biasini E, Harris DA. Targeting the cellular prion protein to treat neurodegeneration. *Future Med Chem*. 2012 Sep;4(13):1655-8.
249. Verity NC, Mallucci GR. Rescuing neurons in prion disease. *Biochem J*. 2011 Jan 1;433(1):19-29.
250. Heppner FL, Musahl C, Arrighi I, Klein MA, Rulicke T, Oesch B, et al. Prevention of scrapie pathogenesis by transgenic expression of anti-prion protein antibodies. *Science*. 2001 Oct 5;294(5540):178-82.
251. Peretz D, Williamson RA, Kaneko K, Vergara J, Leclerc E, Schmitt-Ulms G, et al. Antibodies inhibit prion propagation and clear cell cultures of prion infectivity. *Nature*. 2001 Aug 16;412(6848):739-43.
252. White AR, Enever P, Tayebi M, Mushens R, Linehan J, Brandner S, et al. Monoclonal antibodies inhibit prion replication and delay the development of prion disease. *Nature*. 2003 Mar 6;422(6927):80-3.
253. Krammer C, Vorberg I, Schatzl HM, Gilch S. Therapy in prion diseases: from molecular and cellular biology to therapeutic targets. *Infect Disord Drug Targets*. 2009 Feb;9(1):3-14.
254. Gilch S, Wopfner F, Renner-Muller I, Kremmer E, Bauer C, Wolf E, et al. Polyclonal anti-PrP auto-antibodies induced with dimeric PrP interfere efficiently with PrPSc propagation in prion-infected cells. *J Biol Chem*. 2003 May 16;278(20):18524-31.
255. Alexandrenne C, Hanoux V, Dkhissi F, Boquet D, Couraud JY, Wijkhuisen A. Curative properties of antibodies against prion protein: a comparative in vitro study of monovalent fragments and divalent antibodies. *J Neuroimmunol*. 2009 Apr 30;209(1-2):50-6.
256. Aguzzi A, O'Connor T. Protein aggregation diseases: pathogenicity and therapeutic perspectives. *Nat Rev Drug Discov*. 2010 Mar;9(3):237-48.
257. Mabbott NA, Young J, McConnell I, Bruce ME. Follicular dendritic cell dedifferentiation by treatment with an inhibitor of the lymphotoxin pathway dramatically reduces scrapie susceptibility. *J Virol*. 2003 Jun;77(12):6845-54.
258. Nicoll AJ, Collinge J. Preventing prion pathogenicity by targeting the cellular prion protein. *Infect Disord Drug Targets*. 2009 Feb;9(1):48-57.
259. Heiseke A, Aguib Y, Schatzl HM. Autophagy, prion infection and their mutual interactions. *Curr Issues Mol Biol*. 2010;12(2):87-97.
260. Aguib Y, Heiseke A, Gilch S, Riemer C, Baier M, Schatzl HM, et al. Autophagy induction by trehalose counteracts cellular prion infection. *Autophagy*. 2009 Apr;5(3):361-9.
261. Cortes CJ, Qin K, Cook J, Solanki A, Mastrianni JA. Rapamycin delays disease onset and prevents PrP plaque deposition in a mouse model of Gerstmann-Straussler-Scheinker disease. *J Neurosci*. 2012 Sep 5;32(36):12396-405.
262. Kranich J, Krautler NJ, Falsig J, Ballmer B, Li S, Hutter G, et al. Engulfment of cerebral apoptotic bodies controls the course of prion disease in a mouse strain-dependent manner. *J Exp Med*. 2010 Sep 27;207(10):2271-81.
263. Corsaro A, Thellung S, Chiovitti K, Villa V, Simi A, Raggi F, et al. Dual modulation of ERK1/2 and p38 MAP kinase activities induced by minocycline reverses the neurotoxic effects of the prion protein fragment 90-231. *Neurotox Res*. 2009 Feb;15(2):138-54.
264. Perrier V, Wallace AC, Kaneko K, Safar J, Prusiner SB, Cohen FE. Mimicking dominant negative inhibition of prion replication through structure-based drug design. *Proc Natl Acad Sci U S A*. 2000 May 23;97(11):6073-8.

265. Proske D, Gilch S, Wopfner F, Schatzl HM, Winnacker EL, Famulok M. Prion-protein-specific aptamer reduces PrP<sup>Sc</sup> formation. *Chembiochem*. 2002 Aug 2;3(8):717-25.
266. Caughey B, Raymond LD, Raymond GJ, Maxson L, Silveira J, Baron GS. Inhibition of protease-resistant prion protein accumulation in vitro by curcumin. *J Virol*. 2003 May;77(9):5499-502.
267. Riemer C, Burwinkel M, Schwarz A, Gultner S, Mok SW, Heise I, et al. Evaluation of drugs for treatment of prion infections of the central nervous system. *J Gen Virol*. 2008 Feb;89(Pt 2):594-7.
268. Hafner-Bratkovic I, Gaspersic J, Smid LM, Bresjanac M, Jerala R. Curcumin binds to the alpha-helical intermediate and to the amyloid form of prion protein - a new mechanism for the inhibition of PrP(Sc) accumulation. *J Neurochem*. 2008 Mar;104(6):1553-64.
269. Shaked GM, Engelstein R, Avraham I, Kahana E, Gabizon R. Dimethyl sulfoxide delays PrP<sup>Sc</sup> accumulation and disease symptoms in prion-infected hamsters. *Brain Res*. 2003 Sep 5;983(1-2):137-43.
270. Xiao CQ, Feng BY, Ge YS, Fan XY, Jiang FL, Xiao G, et al. Comprehensive study of the interaction between a potential antiprion cationic porphyrin and human prion protein at different pH by using multiple spectroscopic methods. *J Pharm Sci*. 2013 Mar;102(3):1076-85.
271. Bolognesi ML, Ai Tran HN, Staderini M, Monaco A, Lopez-Cobenas A, Bongarzone S, et al. Discovery of a class of diketopiperazines as antiprion compounds. *ChemMedChem*. 2010 Aug 2;5(8):1324-34.
272. Iwamaru Y, Takenouchi T, Murayama Y, Okada H, Imamura M, Shimizu Y, et al. Anti-prion activity of Brilliant Blue G. *PLoS One*. 2012;7(5):e37896.
273. Stanton JB, Schneider DA, Dinkel KD, Balmer BF, Baszler TV, Mathison BA, et al. Discovery of a novel, monocationic, small-molecule inhibitor of scrapie prion accumulation in cultured sheep microglia and Rov cells. *PLoS One*. 2012;7(11):e51173.
274. Li Z, Silber BM, Rao S, Gever JR, Bryant C, Gallardo-Godoy A, et al. 2-Aminothiazoles with improved pharmacotherapeutic properties for treatment of prion disease. *ChemMedChem*. 2013 May;8(5):847-57.
275. Gallardo-Godoy A, Gever J, Fife KL, Silber BM, Prusiner SB, Renslo AR. 2-Aminothiazoles as therapeutic leads for prion diseases. *J Med Chem*. 2011 Feb 24;54(4):1010-21.
276. Thompson MJ, Louth JC, Greenwood GK, Sorrell FJ, Knight SG, Adams NB, et al. Improved 2,4-diarylthiazole-based antiprion agents: switching the sense of the amide group at C5 leads to an increase in potency. *ChemMedChem*. 2010 Sep 3;5(9):1476-88.
277. Thompson MJ, Louth JC, Little SM, Chen B, Coldham I. 2,4-diarylthiazole antiprion compounds as a novel structural class of antimalarial leads. *Bioorg Med Chem Lett*. 2011 Jun 15;21(12):3644-7.
278. Thompson MJ, Louth JC, Ferrara S, Sorrell FJ, Irving BJ, Cochrane EJ, et al. Structure-activity relationship refinement and further assessment of indole-3-glyoxylamides as a lead series against prion disease. *ChemMedChem*. 2011 Jan 3;6(1):115-30.
279. Thompson MJ, Louth JC, Ferrara S, Jackson MP, Sorrell FJ, Cochrane EJ, et al. Discovery of 6-substituted indole-3-glyoxylamides as lead antiprion agents with enhanced cell line activity, improved microsomal stability and low toxicity. *Eur J Med Chem*. 2011 Sep;46(9):4125-32.
280. Thompson MJ, Borsenberger V, Louth JC, Judd KE, Chen B. Design, synthesis, and structure-activity relationship of indole-3-glyoxylamide libraries possessing highly potent activity in a cell line model of prion disease. *J Med Chem*. 2009 Dec 10;52(23):7503-11.
281. Brazier MW, Doctrow SR, Masters CL, Collins SJ. A manganese-superoxide dismutase/catalase mimetic extends survival in a mouse model of human prion disease. *Free Radic Biol Med*. 2008 Jul 15;45(2):184-92.
282. Taraboulos A, Scott M, Semenov A, Avrahami D, Prusiner SB. Biosynthesis of the prion proteins in scrapie-infected cells in culture. *Braz J Med Biol Res*. 1994 Feb;27(2):303-7.

283. Groschup MH, Buschmann A. Rodent models for prion diseases. *Vet Res.* 2008 Jul-Aug;39(4):32.
284. Solassol J, Crozet C, Lehmann S. Prion propagation in cultured cells. *Br Med Bull.* 2003;66:87-97.
285. Vilette D. Cell models of prion infection. *Vet Res.* 2008 Jul-Aug;39(4):10.
286. Clarke MC, Haig DA. Evidence for the multiplication of scrapie agent in cell culture. *Nature.* 1970 Jan 3;225(5227):100-1.
287. Birkett CR, Hennion RM, Bembridge DA, Clarke MC, Chree A, Bruce ME, et al. Scrapie strains maintain biological phenotypes on propagation in a cell line in culture. *EMBO J.* 2001 Jul 2;20(13):3351-8.
288. Vilette D, Andreoletti O, Archer F, Madelaine MF, Vilotte JL, Lehmann S, et al. Ex vivo propagation of infectious sheep scrapie agent in heterologous epithelial cells expressing ovine prion protein. *Proc Natl Acad Sci U S A.* 2001 Mar 27;98(7):4055-9.
289. Bosque PJ, Prusiner SB. Cultured cell sublines highly susceptible to prion infection. *J Virol.* 2000 May;74(9):4377-86.
290. Nishida N, Harris DA, Vilette D, Laude H, Frobert Y, Grassi J, et al. Successful transmission of three mouse-adapted scrapie strains to murine neuroblastoma cell lines overexpressing wild-type mouse prion protein. *J Virol.* 2000 Jan;74(1):320-5.
291. Archer F, Bachelin C, Andreoletti O, Besnard N, Perrot G, Langevin C, et al. Cultured peripheral neuroglial cells are highly permissive to sheep prion infection. *J Virol.* 2004 Jan;78(1):482-90.
292. Cronier S, Laude H, Peyrin JM. Prions can infect primary cultured neurons and astrocytes and promote neuronal cell death. *Proc Natl Acad Sci U S A.* 2004 Aug 17;101(33):12271-6.
293. Geissen M, Leidel F, Eiden M, Hirschberger T, Fast C, Bertsch U, et al. From high-throughput cell culture screening to mouse model: identification of new inhibitor classes against prion disease. *ChemMedChem.* 2011 Oct 4;6(10):1928-37.
294. Liu Y, Sun R, Chakrabarty T, Manuelidis L. A rapid accurate culture assay for infectivity in Transmissible Encephalopathies. *J Neurovirol.* 2008 Oct;14(5):352-61.
295. Klohn PC, Stoltze L, Flechsig E, Enari M, Weissmann C. A quantitative, highly sensitive cell-based infectivity assay for mouse scrapie prions. *Proc Natl Acad Sci U S A.* 2003 Sep 30;100(20):11666-71.
296. Milhavet O, McMahon HE, Rachidi W, Nishida N, Katamine S, Mange A, et al. Prion infection impairs the cellular response to oxidative stress. *Proc Natl Acad Sci U S A.* 2000 Dec 5;97(25):13937-42.
297. Sim VL. Prion disease: chemotherapeutic strategies. *Infect Disord Drug Targets.* 2012 Apr;12(2):144-60.
298. Stocks M, Alcaraz, M, Griffen E. *On Medicinal Chemistry.*
299. Wade RC, Goodford PJ. The role of hydrogen-bonds in drug binding. *Prog Clin Biol Res.* 1989;289:433-44.
300. Priest BT, Bell IM, Garcia ML. Role of hERG potassium channel assays in drug development. *Channels (Austin).* 2008 Mar-Apr;2(2):87-93.
301. Gabrielsson J, Green AR. Quantitative pharmacology or pharmacokinetic pharmacodynamic integration should be a vital component in integrative pharmacology. *J Pharmacol Exp Ther.* 2009 Dec;331(3):767-74.
302. Ganesan A. Recent developments in combinatorial organic synthesis. *Drug Discov Today.* 2002 Jan 1;7(1):47-55.
303. Myers S, Baker A. Drug discovery--an operating model for a new era. *Nat Biotechnol.* 2001 Aug;19(8):727-30.
304. Giese K, Kaufmann J, Pronk GJ, Klippel A. Unravelling novel intracellular pathways in cell-based assays. *Drug Discov Today.* 2002 Feb 1;7(3):179-86.

305. Breslin S, O'Driscoll L. Three-dimensional cell culture: the missing link in drug discovery. *Drug Discov Today*. 2013 Mar;18(5-6):240-9.
306. Schmeichel KL, Bissell MJ. Modeling tissue-specific signaling and organ function in three dimensions. *J Cell Sci*. 2003 Jun 15;116(Pt 12):2377-88.
307. Page H, Flood P, Reynaud EG. Three-dimensional tissue cultures: current trends and beyond. *Cell Tissue Res*. 2013 Apr;352(1):123-31.
308. Maltman DJ, Przyborski SA. Developments in three-dimensional cell culture technology aimed at improving the accuracy of in vitro analyses. *Biochem Soc Trans*. 2010 Aug;38(4):1072-5.
309. Kleinman HK, Philp D, Hoffman MP. Role of the extracellular matrix in morphogenesis. *Curr Opin Biotechnol*. 2003 Oct;14(5):526-32.
310. Bissell MJ, Radisky DC, Rizki A, Weaver VM, Petersen OW. The organizing principle: microenvironmental influences in the normal and malignant breast. *Differentiation*. 2002 Dec;70(9-10):537-46.
311. Pampaloni F, Reynaud EG, Stelzer EH. The third dimension bridges the gap between cell culture and live tissue. *Nat Rev Mol Cell Biol*. 2007 Oct;8(10):839-45.
312. Bissell MJ, Hall HG, Parry G. How does the extracellular matrix direct gene expression? *J Theor Biol*. 1982 Nov 7;99(1):31-68.
313. Bhadriraju K, Chen CS. Engineering cellular microenvironments to improve cell-based drug testing. *Drug Discov Today*. 2002 Jun 1;7(11):612-20.
314. Mueller-Klieser W. Three-dimensional cell cultures: from molecular mechanisms to clinical applications. *Am J Physiol*. 1997 Oct;273(4 Pt 1):C1109-23.
315. Ma W, Fitzgerald W, Liu QY, O'Shaughnessy TJ, Maric D, Lin HJ, et al. CNS stem and progenitor cell differentiation into functional neuronal circuits in three-dimensional collagen gels. *Exp Neurol*. 2004 Dec;190(2):276-88.
316. Kim JB. Three-dimensional tissue culture models in cancer biology. *Semin Cancer Biol*. 2005 Oct;15(5):365-77.
317. Lin RZ, Chang HY. Recent advances in three-dimensional multicellular spheroid culture for biomedical research. *Biotechnol J*. 2008 Oct;3(9-10):1172-84.
318. Hirschhaeuser F, Leidig T, Rodday B, Lindemann C, Mueller-Klieser W. Test system for trifunctional antibodies in 3D MCTS culture. *J Biomol Screen*. 2009 Sep;14(8):980-90.
319. Keller GM. In vitro differentiation of embryonic stem cells. *Curr Opin Cell Biol*. 1995 Dec;7(6):862-9.
320. Kelm JM, Timmins NE, Brown CJ, Fussenegger M, Nielsen LK. Method for generation of homogeneous multicellular tumor spheroids applicable to a wide variety of cell types. *Biotechnol Bioeng*. 2003 Jul 20;83(2):173-80.
321. Tung YC, Hsiao AY, Allen SG, Torisawa YS, Ho M, Takayama S. High-throughput 3D spheroid culture and drug testing using a 384 hanging drop array. *Analyst*. 2011 Feb 7;136(3):473-8.
322. Bell E. Strategy for the selection of scaffolds for tissue engineering. *Tissue Eng*. 1995 Summer;1(2):163-79.
323. Hosseinkhani H. 3D in vitro technology for drug discovery. *Curr Drug Saf*. 2012 Feb;7(1):37-43.
324. Levenberg S, Huang NF, Lavik E, Rogers AB, Itskovitz-Eldor J, Langer R. Differentiation of human embryonic stem cells on three-dimensional polymer scaffolds. *Proc Natl Acad Sci U S A*. 2003 Oct 28;100(22):12741-6.
325. van Wezel AL. Growth of cell-strains and primary cells on micro-carriers in homogeneous culture. *Nature*. 1967 Oct 7;216(5110):64-5.
326. Johns RA, Tichotsky A, Muro M, Spaeth JP, Le Cras TD, Rengasamy A. Halothane and isoflurane inhibit endothelium-derived relaxing factor-dependent cyclic guanosine monophosphate accumulation in endothelial cell-vascular smooth muscle co-cultures independent of an effect on guanylyl cyclase activation. *Anesthesiology*. 1995 Oct;83(4):823-34.

327. Toh YC, Zhang C, Zhang J, Khong YM, Chang S, Samper VD, et al. A novel 3D mammalian cell perfusion-culture system in microfluidic channels. *Lab Chip*. 2007 Mar;7(3):302-9.
328. Park J, Lee BK, Jeong GS, Hyun JK, Lee CJ, Lee SH. Three-dimensional brain-on-a-chip with an interstitial level of flow and its application as an in vitro model of Alzheimer's disease. *Lab Chip*. 2015 Jan 7;15(1):141-50.
329. Andrei G. Three-dimensional culture models for human viral diseases and antiviral drug development. *Antiviral Res*. 2006 Sep;71(2-3):96-107.
330. Shamir ER, Ewald AJ. Three-dimensional organotypic culture: experimental models of mammalian biology and disease. *Nat Rev Mol Cell Biol*. 2014 Oct;15(10):647-64.
331. Lebonvallet N, Jeanmaire C, Danoux L, Sibille P, Pauly G, Misery L. The evolution and use of skin explants: potential and limitations for dermatological research. *Eur J Dermatol*. 2010 Nov-Dec;20(6):671-84.
332. Randall KJ, Turton J, Foster JR. Explant culture of gastrointestinal tissue: a review of methods and applications. *Cell Biol Toxicol*. 2011 Aug;27(4):267-84.
333. Sutherland RM, McCredie JA, Inch WR. Growth of multicell spheroids in tissue culture as a model of nodular carcinomas. *J Natl Cancer Inst*. 1971 Jan;46(1):113-20.
334. Kunz-Schughart LA, Freyer JP, Hofstaedter F, Ebner R. The use of 3-D cultures for high-throughput screening: the multicellular spheroid model. *J Biomol Screen*. 2004 Jun;9(4):273-85.
335. Kimlin LC, Casagrande G, Virador VM. In vitro three-dimensional (3D) models in cancer research: an update. *Mol Carcinog*. 2013 Mar;52(3):167-82.
336. Elliott NT, Yuan F. A review of three-dimensional in vitro tissue models for drug discovery and transport studies. *J Pharm Sci*. 2011 Jan;100(1):59-74.
337. Choi SH, Kim YH, Hebisch M, Sliwinski C, Lee S, D'Avanzo C, et al. A three-dimensional human neural cell culture model of Alzheimer's disease. *Nature*. 2014 Nov 13;515(7526):274-8.
338. Zhang D, Pekkanen-Mattila M, Shahsavani M, Falk A, Teixeira AI, Herland A. A 3D Alzheimer's disease culture model and the induction of P21-activated kinase mediated sensing in iPSC derived neurons. *Biomaterials*. 2014 Feb;35(5):1420-8.
339. Falsig J, Sonati T, Herrmann US, Saban D, Li B, Arroyo K, et al. Prion pathogenesis is faithfully reproduced in cerebellar organotypic slice cultures. *PLoS Pathog*. 2012;8(11):e1002985.
340. Campeau JL, Wu G, Bell JR, Rasmussen J, Sim VL. Early increase and late decrease of purkinje cell dendritic spine density in prion-infected organotypic mouse cerebellar cultures. *PLoS One*. 2013;8(12):e81776.
341. Falsig J, Aguzzi A. The prion organotypic slice culture assay--POSCA. *Nat Protoc*. 2008;3(4):555-62.
342. Falsig J, Julius C, Margalith I, Schwarz P, Heppner FL, Aguzzi A. A versatile prion replication assay in organotypic brain slices. *Nat Neurosci*. 2008 Jan;11(1):109-17.
343. Roth A, Singer T. The application of 3D cell models to support drug safety assessment: Opportunities & challenges. *Adv Drug Deliv Rev*. 2013 Dec 27.
344. Seiler AE, Spielmann H. The validated embryonic stem cell test to predict embryotoxicity in vitro. *Nat Protoc*. 2011 Jul;6(7):961-78.
345. DesRochers TM, Suter L, Roth A, Kaplan DL. Bioengineered 3D human kidney tissue, a platform for the determination of nephrotoxicity. *PLoS One*. 2013;8(3):e59219.
346. Huh D, Torisawa YS, Hamilton GA, Kim HJ, Ingber DE. Microengineered physiological biomimicry: organs-on-chips. *Lab Chip*. 2012 Jun 21;12(12):2156-64.
347. Vogtherr M, Grimme S, Elshorst B, Jacobs DM, Fiebig K, Griesinger C, et al. Antimalarial drug quinacrine binds to C-terminal helix of cellular prion protein. *J Med Chem*. 2003 Aug 14;46(17):3563-4.
348. Hong HS, Maezawa I, Yao N, Xu B, Diaz-Avalos R, Rana S, et al. Combining the rapid MTT formazan exocytosis assay and the MC65 protection assay led to the discovery of carbazole analogs as small molecule inhibitors of Abeta oligomer-induced cytotoxicity. *Brain Res*. 2007 Jan 26;1130(1):223-34.

349. Benjamini YH, Y. Controlling the false discovery rate - a practical and powerful approach to multiple testing. *Journal of the Royal Statistical Society Series B - Methodological*. 1995;57(1):289-300.
350. Dlakic WM, Grigg E, Bessen RA. Prion infection of muscle cells in vitro. *J Virol*. 2007 May;81(9):4615-24.
351. Reddy TR, Mutter R, Heal W, Guo K, Gillet VJ, Pratt S, et al. Library design, synthesis, and screening: pyridine dicarbonitriles as potential prion disease therapeutics. *J Med Chem*. 2006 Jan 26;49(2):607-15.
352. Zahn R, Liu A, Luhrs T, Riek R, von Schroetter C, Lopez Garcia F, et al. NMR solution structure of the human prion protein. *Proc Natl Acad Sci U S A*. 2000 Jan 4;97(1):145-50.
353. Cope H, Mutter R, Heal W, Pascoe C, Brown P, Pratt S, et al. Synthesis and SAR study of acridine, 2-methylquinoline and 2-phenylquinazoline analogues as anti-prion agents. *Eur J Med Chem*. 2006 Oct;41(10):1124-43.
354. Guo K, Mutter R, Heal W, Reddy TR, Cope H, Pratt S, et al. Synthesis and evaluation of a focused library of pyridine dicarbonitriles against prion disease. *Eur J Med Chem*. 2008 Jan;43(1):93-106.
355. Heal W, Thompson MJ, Mutter R, Cope H, Louth JC, Chen B. Library synthesis and screening: 2,4-diphenylthiazoles and 2,4-diphenyloxazoles as potential novel prion disease therapeutics. *J Med Chem*. 2007 Mar 22;50(6):1347-53.
356. Rosenson RS, Hislop C, Elliott M, Stasiv Y, Goulder M, Waters D. Effects of varespladib methyl on biomarkers and major cardiovascular events in acute coronary syndrome patients. *J Am Coll Cardiol*. 2010 Sep 28;56(14):1079-88.
357. Rosenson RS, Hislop C, McConnell D, Elliott M, Stasiv Y, Wang N, et al. Effects of 1-H-indole-3-glyoxamide (A-002) on concentration of secretory phospholipase A2 (PLASMA study): a phase II double-blind, randomised, placebo-controlled trial. *Lancet*. 2009 Feb 21;373(9664):649-58.
358. Hui DY, Cope MJ, Labonte ED, Chang HT, Shao J, Goka E, et al. The phospholipase A(2) inhibitor methyl indoxam suppresses diet-induced obesity and glucose intolerance in mice. *Br J Pharmacol*. 2009 Aug;157(7):1263-9.
359. Bradley JD, Dmitrienko AA, Kivitz AJ, Gluck OS, Weaver AL, Wiesenhutter C, et al. A randomized, double-blinded, placebo-controlled clinical trial of LY333013, a selective inhibitor of group II secretory phospholipase A2, in the treatment of rheumatoid arthritis. *J Rheumatol*. 2005 Mar;32(3):417-23.
360. Takhi M, Singh G, Murugan C, Thaplyyal N, Maitra S, Bhaskarreddy KM, et al. Novel and potent oxazolidinone antibacterials featuring 3-indolylglyoxamide substituents. *Bioorg Med Chem Lett*. 2008 Sep 15;18(18):5150-5.
361. Genovese MC, Cohen SB, Wofsy D, Weinblatt ME, Firestein GS, Brahn E, et al. A 24-week, randomized, double-blind, placebo-controlled, parallel group study of the efficacy of oral SCIO-469, a p38 mitogen-activated protein kinase inhibitor, in patients with active rheumatoid arthritis. *J Rheumatol*. 2011 May;38(5):846-54.
362. Siegel DS, Krishnan A, Lonial S, Chatta G, Alsina M, Jagannath S, et al. Phase II trial of SCIO-469 as monotherapy (M) or in combination with bortezomib (MB) in relapsed refractory multiple myeloma (MM). *Blood*. 2006 Nov 16;108(11):1022a-a.
363. Cottrell JA, Meyenhofer M, Medicherla S, Higgins L, O'Connor JP. Analgesic effects of p38 kinase inhibitor treatment on bone fracture healing. *Pain*. 2009 Mar;142(1-2):116-26.
364. Medicherla S, Wadsworth S, Cullen B, Silcock D, Ma JY, Mangadu R, et al. p38 MAPK inhibition reduces diabetes-induced impairment of wound healing. *Diabetes Metab Syndr Obes*. 2009;2:91-100.
365. De Martino G, Edler MC, La Regina G, Coluccia A, Barbera MC, Barrow D, et al. New arylthioindoles: potent inhibitors of tubulin polymerization. 2. Structure-activity relationships and molecular modeling studies. *J Med Chem*. 2006 Feb 9;49(3):947-54.

366. La Regina G, Edler MC, Brancale A, Kandil S, Coluccia A, Piscitelli F, et al. Arylthioindole inhibitors of tubulin polymerization. 3. Biological evaluation, structure-activity relationships and molecular modeling studies. *J Med Chem*. 2007 Jun 14;50(12):2865-74.
367. Brancale A, Silvestri R. Indole, a core nucleus for potent inhibitors of tubulin polymerization. *Med Res Rev*. 2007 Mar;27(2):209-38.
368. Wang T, Yin Z, Zhang Z, Bender JA, Yang Z, Johnson G, et al. Inhibitors of human immunodeficiency virus type 1 (HIV-1) attachment. 5. An evolution from indole to azaindoles leading to the discovery of 1-(4-benzoylpiperazin-1-yl)-2-(4,7-dimethoxy-1H-pyrrolo[2,3-c]pyridin-3-yl)ethane -1,2-dione (BMS-488043), a drug candidate that demonstrates antiviral activity in HIV-1-infected subjects. *J Med Chem*. 2009 Dec 10;52(23):7778-87.
369. Mosmann T. Rapid colorimetric assay for cellular growth and survival: application to proliferation and cytotoxicity assays. *J Immunol Methods*. 1983 Dec 16;65(1-2):55-63.
370. Bradford MM. A rapid and sensitive method for the quantitation of microgram quantities of protein utilizing the principle of protein-dye binding. *Anal Biochem*. 1976 May 7;72:248-54.
371. Ghaemmaghami S, May BC, Renslo AR, Prusiner SB. Discovery of 2-aminothiazoles as potent antiprion compounds. *J Virol*. 2010 Apr;84(7):3408-12.
372. Pattnaik P. Surface plasmon resonance: applications in understanding receptor-ligand interaction. *Appl Biochem Biotechnol*. 2005 Aug;126(2):79-92.
373. Cooper MA. Optical biosensors in drug discovery. *Nat Rev Drug Discov*. 2002 Jul;1(7):515-28.
374. Warner RG, Hundt C, Weiss S, Turnbull JE. Identification of the heparan sulfate binding sites in the cellular prion protein. *J Biol Chem*. 2002 May 24;277(21):18421-30.
375. Shoichet BK. Screening in a spirit haunted world. *Drug Discov Today*. 2006 Jul;11(13-14):607-15.
376. Fiorino F, Eiden M, Giese A, Severino B, Esposito A, Groschup MH, et al. Synthesis of benzamide derivatives and their evaluation as antiprion agents. *Bioorg Med Chem*. 2012 Aug 15;20(16):5001-11.
377. Ghaemmaghami S, Ahn M, Lessard P, Giles K, Legname G, DeArmond SJ, et al. Continuous quinacrine treatment results in the formation of drug-resistant prions. *PLoS Pathog*. 2009 Nov;5(11):e1000673.
378. Rambold AS, Miesbauer M, Olschewski D, Seidel R, Riemer C, Smale L, et al. Green tea extracts interfere with the stress-protective activity of PrP and the formation of PrP. *J Neurochem*. 2008 Oct;107(1):218-29.
379. Edwards RA, Woody RW. Spectroscopic studies of Cibacron Blue and Congo Red bound to dehydrogenases and kinases. Evaluation of dyes as probes of the dinucleotide fold. *Biochemistry*. 1979 Nov 13;18(23):5197-204.
380. Stopa B, Gorny M, Konieczny L, Piekarska B, Rybarska J, Skowronek M, et al. Supramolecular ligands: monomer structure and protein ligation capability. *Biochimie*. 1998 Dec;80(12):963-8.
381. Kitano H. Systems biology: a brief overview. *Science*. 2002 Mar 1;295(5560):1662-4.
382. Hwang D, Lee IY, Yoo H, Gehlenborg N, Cho JH, Petritis B, et al. A systems approach to prion disease. *Mol Syst Biol*. 2009;5:252.
383. Fasano C, Campana V, Griffiths B, Kelly G, Schiavo G, Zurzolo C. Gene expression profile of quinacrine-cured prion-infected mouse neuronal cells. *J Neurochem*. 2008 Apr;105(1):239-50.
384. Farrelly PV, Kenna BL, Laohachai KL, Bahadi R, Salmona M, Forloni G, et al. Quinacrine blocks PrP (106-126)-formed channels. *J Neurosci Res*. 2003 Dec 15;74(6):934-41.
385. Bourdon JC. p53 and its isoforms in cancer. *Br J Cancer*. 2007 Aug 6;97(3):277-82.
386. Killick R, Niklison-Chirou M, Tomasini R, Bano D, Rufini A, Grespi F, et al. p73: a multifunctional protein in neurobiology. *Mol Neurobiol*. 2011 Apr;43(2):139-46.

387. Cullen SP, Brunet M, Martin SJ. Granzymes in cancer and immunity. *Cell Death Differ.* 2010 Apr;17(4):616-23.
388. Ehsanian R, Van Waes C, Feller SM. Beyond DNA binding - a review of the potential mechanisms mediating quinacrine's therapeutic activities in parasitic infections, inflammation, and cancers. *Cell Commun Signal.* 2011;9:13.
389. Boucher JG, Boudreau A, Atlas E. Bisphenol A induces differentiation of human preadipocytes in the absence of glucocorticoid and is inhibited by an estrogen-receptor antagonist. *Nutr Diabetes.* 2014;4:e102.
390. van Leeuwen LAG, Hoozemans JJM. Physiological and pathophysiological functions of cell cycle proteins in post-mitotic neurons: implications for Alzheimer's disease. *Acta Neuropathol.* 2015 Apr;129(4):511-25.
391. Raina AK, Hochman A, Zhu X, Rottkamp CA, Nunomura A, Siedlak SL, et al. Abortive apoptosis in Alzheimer's disease. *Acta Neuropathol.* 2001 Apr;101(4):305-10.
392. Varjosalo M, Taipale J. Hedgehog: functions and mechanisms. *Genes Dev.* 2008 Sep 15;22(18):2454-72.
393. Jeong SY, Seol DW. The role of mitochondria in apoptosis. *BMB Rep.* 2008 Jan 31;41(1):11-22.
394. Fiskum G. Mitochondrial participation in ischemic and traumatic neural cell death. *J Neurotrauma.* 2000 Oct;17(10):843-55.
395. Brustovetsky N, Brustovetsky T, Jemmerson R, Dubinsky JM. Calcium-induced cytochrome c release from CNS mitochondria is associated with the permeability transition and rupture of the outer membrane. *J Neurochem.* 2002 Jan;80(2):207-18.
396. Deniaud A, Sharaf el dein O, Maillier E, Poncet D, Kroemer G, Lemaire C, et al. Endoplasmic reticulum stress induces calcium-dependent permeability transition, mitochondrial outer membrane permeabilization and apoptosis. *Oncogene.* 2008 Jan 10;27(3):285-99.
397. Reddy PV, Rao KV, Norenberg MD. The mitochondrial permeability transition, and oxidative and nitrosative stress in the mechanism of copper toxicity in cultured neurons and astrocytes. *Lab Invest.* 2008 Aug;88(8):816-30.
398. Buki A, Okonkwo DO, Wang KK, Povlishock JT. Cytochrome c release and caspase activation in traumatic axonal injury. *J Neurosci.* 2000 Apr 15;20(8):2825-34.
399. Lin Z, Zhao D, Yang L. Interaction between misfolded PrP and the ubiquitin-proteasome system in prion-mediated neurodegeneration. *Acta Biochim Biophys Sin (Shanghai).* 2013 Jun;45(6):477-84.
400. Deriziotis P, Tabrizi SJ. Prions and the proteasome. *Biochim Biophys Acta.* 2008 Dec;1782(12):713-22.
401. Allocati N, Di Ilio C, De Laurenzi V. p63/p73 in the control of cell cycle and cell death. *Exp Cell Res.* 2012 Jul 1;318(11):1285-90.
402. Ables JL, Breunig JJ, Eisch AJ, Rakic P. Not(ch) just development: Notch signalling in the adult brain. *Nat Rev Neurosci.* 2011 May;12(5):269-83.
403. De Strooper B, Iwatsubo T, Wolfe MS. Presenilins and gamma-secretase: structure, function, and role in Alzheimer Disease. *Cold Spring Harb Perspect Med.* 2012 Jan;2(1):a006304.
404. Nedelsky NB, Todd PK, Taylor JP. Autophagy and the ubiquitin-proteasome system: collaborators in neuroprotection. *Biochim Biophys Acta.* 2008 Dec;1782(12):691-9.
405. Ellgaard L, Molinari M, Helenius A. Setting the standards: quality control in the secretory pathway. *Science.* 1999 Dec 3;286(5446):1882-8.
406. Adams J. The proteasome: structure, function, and role in the cell. *Cancer Treat Rev.* 2003 May;29 Suppl 1:3-9.
407. Bedford L, Paine S, Sheppard PW, Mayer RJ, Roelofs J. Assembly, structure, and function of the 26S proteasome. *Trends Cell Biol.* 2010 Jul;20(7):391-401.
408. Li J, Buchner J. Structure, function and regulation of the hsp90 machinery. *Biomed J.* 2013 May-Jun;36(3):106-17.

409. Csermely P, Schnaider T, Soti C, Prohaszka Z, Nardai G. The 90-kDa molecular chaperone family: structure, function, and clinical applications. A comprehensive review. *Pharmacol Ther.* 1998 Aug;79(2):129-68.
410. Johnson JL, Craig EA. Protein folding in vivo: unraveling complex pathways. *Cell.* 1997 Jul 25;90(2):201-4.
411. Okemoto-Nakamura Y, Yamakawa Y, Hanada K, Tanaka K, Miura M, Tanida I, et al. Synthetic fibril peptide promotes clearance of scrapie prion protein by lysosomal degradation. *Microbiol Immunol.* 2008 Jul;52(7):357-65.
412. Lee DH, Goldberg AL. Proteasome inhibitors: valuable new tools for cell biologists. *Trends Cell Biol.* 1998 Oct;8(10):397-403.
413. Fenteany G, Standaert RF, Lane WS, Choi S, Corey EJ, Schreiber SL. Inhibition of proteasome activities and subunit-specific amino-terminal threonine modification by lactacystin. *Science.* 1995 May 5;268(5211):726-31.
414. Dick LR, Cruikshank AA, Destree AT, Grenier L, McCormack TA, Melandri FD, et al. Mechanistic studies on the inactivation of the proteasome by lactacystin in cultured cells. *J Biol Chem.* 1997 Jan 3;272(1):182-8.
415. Turk V, Turk B, Turk D. Lysosomal cysteine proteases: facts and opportunities. *EMBO J.* 2001 Sep 3;20(17):4629-33.
416. Luhr KM, Nordstrom EK, Low P, Kristensson K. Cathepsin B and L are involved in degradation of prions in GT1-1 neuronal cells. *Neuroreport.* 2004 Jul 19;15(10):1663-7.
417. Xiang W, Windl O, Wunsch G, Dugas M, Kohlmann A, Dierkes N, et al. Identification of differentially expressed genes in scrapie-infected mouse brains by using global gene expression technology. *J Virol.* 2004 Oct;78(20):11051-60.
418. Zhang Y, Spiess E, Groschup MH, Burkle A. Up-regulation of cathepsin B and cathepsin L activities in scrapie-infected mouse Neuro2a cells. *J Gen Virol.* 2003 Aug;84(Pt 8):2279-83.
419. Baker CA, Manuelidis L. Unique inflammatory RNA profiles of microglia in Creutzfeldt-Jakob disease. *Proc Natl Acad Sci U S A.* 2003 Jan 21;100(2):675-9.
420. Combarros O, Alvarez-Arcaya A, Sanchez-Guerra M, Infante J, Berciano J. Candidate gene association studies in sporadic Alzheimer's disease. *Dement Geriatr Cogn Disord.* 2002;14(1):41-54.
421. Dandoy-Dron F, Guillo F, Benboudjema L, Deslys JP, Lasmezas C, Dormont D, et al. Gene expression in scrapie. Cloning of a new scrapie-responsive gene and the identification of increased levels of seven other mRNA transcripts. *J Biol Chem.* 1998 Mar 27;273(13):7691-7.
422. Diedrich JF, Minnigan H, Carp RI, Whitaker JN, Race R, Frey W, 2nd, et al. Neuropathological changes in scrapie and Alzheimer's disease are associated with increased expression of apolipoprotein E and cathepsin D in astrocytes. *J Virol.* 1991 Sep;65(9):4759-68.
423. Nakanishi H. Neuronal and microglial cathepsins in aging and age-related diseases. *Ageing Res Rev.* 2003 Oct;2(4):367-81.
424. Vidal E, Tortosa R, Marco P, Fondevila D, Rabanal RM, Torres JM, et al. Late stage cathepsin C, CXCL13 and Ki-67 overexpression correlate with regional neuropathology in a BSE transgenic murine model. *J Comp Pathol.* 2013 Jan;148(1):22-32.
425. Cavasotto CN. Homology models in docking and high-throughput docking. *Curr Top Med Chem.* 2011;11(12):1528-34.
426. Hui-fang L, Qing S, Jian Z, Wei F. Evaluation of various inverse docking schemes in multiple targets identification. *J Mol Graph Model.* 2010 Nov;29(3):326-30.
427. Santiago DN, Pevzner Y, Durand AA, Tran M, Scheerer RR, Daniel K, et al. Virtual target screening: validation using kinase inhibitors. *J Chem Inf Model.* 2012 Aug 27;52(8):2192-203.
428. Bellingham SA, Coleman LA, Masters CL, Camakaris J, Hill AF. Regulation of prion gene expression by transcription factors SP1 and metal transcription factor-1. *J Biol Chem.* 2009 Jan 9;284(2):1291-301.

429. Santos CR, Martinho A, Quintela T, Goncalves I. Neuroprotective and neuroregenerative properties of metallothioneins. *IUBMB Life*. 2012 Feb;64(2):126-35.
430. LaRoche O, Gagne V, Charron J, Soh JW, Seguin C. Phosphorylation is involved in the activation of metal-regulatory transcription factor 1 in response to metal ions. *J Biol Chem*. 2001 Nov 9;276(45):41879-88.
431. Coyle P, Philcox JC, Carey LC, Roife AM. Metallothionein: the multipurpose protein. *Cell Mol Life Sci*. 2002 Apr;59(4):627-47.
432. Vasak M, Meloni G. Chemistry and biology of mammalian metallothioneins. *J Biol Inorg Chem*. 2011 Oct;16(7):1067-78.
433. Rachidi W, Chimienti F, Aouffen M, Senator A, Guiraud P, Seve M, et al. Prion protein protects against zinc-mediated cytotoxicity by modifying intracellular exchangeable zinc and inducing metallothionein expression. *J Trace Elem Med Biol*. 2009;23(3):214-23.
434. Hanlon J, Monks E, Hughes C, Weavers E, Rogers M. Metallothionein in bovine spongiform encephalopathy. *J Comp Pathol*. 2002 Nov;127(4):280-9.
435. Tortosa R, Vidal E, Costa C, Alamillo E, Torres JM, Ferrer I, et al. Stress response in the central nervous system of a transgenic mouse model of bovine spongiform encephalopathy. *Vet J*. 2008 Oct;178(1):126-9.
436. Kawashima T, Doh-ura K, Torisu M, Uchida Y, Furuta A, Iwaki T. Differential expression of metallothioneins in human prion diseases. *Dement Geriatr Cogn Disord*. 2000 Sep-Oct;11(5):251-62.
437. Duguid JR, Rohwer RG, Seed B. Isolation of cDNAs of scrapie-modulated RNAs by subtractive hybridization of a cDNA library. *Proc Natl Acad Sci U S A*. 1988 Aug;85(15):5738-42.
438. Vidal E, Tortosa R, Marquez M, Serafin A, Hidalgo J, Pumarola M. Infection of metallothionein 1+2 knockout mice with Rocky Mountain Laboratory scrapie. *Brain Res*. 2008 Feb 27;1196:140-50.
439. Hozumi I. Roles and therapeutic potential of metallothioneins in neurodegenerative diseases. *Curr Pharm Biotechnol*. 2013 Mar;14(4):408-13.
440. Jeong JK, Park SY. Transcriptional regulation of specific protein 1 (SP1) by hypoxia-inducible factor 1 alpha (HIF-1alpha) leads to PRNP expression and neuroprotection from toxic prion peptide. *Biochem Biophys Res Commun*. 2012 Dec 7;429(1-2):93-8.
441. Newton AC. Protein kinase C: structure, function, and regulation. *J Biol Chem*. 1995 Dec 1;270(48):28495-8.
442. Sefton BM. The lck tyrosine protein kinase. *Oncogene*. 1991 May;6(5):683-6.
443. Straus DB, Weiss A. Genetic evidence for the involvement of the lck tyrosine kinase in signal transduction through the T cell antigen receptor. *Cell*. 1992 Aug 21;70(4):585-93.
444. Anderson SJ, Levin SD, Perlmutter RM. Involvement of the protein tyrosine kinase p56lck in T cell signaling and thymocyte development. *Adv Immunol*. 1994;56:151-78.
445. Isakov N, Biesinger B. Lck protein tyrosine kinase is a key regulator of T-cell activation and a target for signal intervention by Herpesvirus saimiri and other viral gene products. *Eur J Biochem*. 2000 Jun;267(12):3413-21.
446. Chakraborty G, Rangaswami H, Jain S, Kundu GC. Hypoxia regulates cross-talk between Syk and Lck leading to breast cancer progression and angiogenesis. *J Biol Chem*. 2006 Apr 21;281(16):11322-31.
447. Raeber AJ, Sailer A, Hegyi I, Klein MA, Rulicke T, Fischer M, et al. Ectopic expression of prion protein (PrP) in T lymphocytes or hepatocytes of PrP knockout mice is insufficient to sustain prion replication. *Proc Natl Acad Sci U S A*. 1999 Mar 30;96(7):3987-92.
448. Liu Y, Witte S, Liu YC, Doyle M, Elly C, Altman A. Regulation of protein kinase Ctheta function during T cell activation by Lck-mediated tyrosine phosphorylation. *J Biol Chem*. 2000 Feb 4;275(5):3603-9.
449. Szegezdi E, Fitzgerald U, Samali A. Caspase-12 and ER-stress-mediated apoptosis: the story so far. *Ann N Y Acad Sci*. 2003 Dec;1010:186-94.

450. Momoi T. Caspases involved in ER stress-mediated cell death. *J Chem Neuroanat.* 2004 Sep;28(1-2):101-5.
451. Nakagawa T, Zhu H, Morishima N, Li E, Xu J, Yankner BA, et al. Caspase-12 mediates endoplasmic-reticulum-specific apoptosis and cytotoxicity by amyloid-beta. *Nature.* 2000 Jan 6;403(6765):98-103.
452. Viana RJ, Nunes AF, Rodrigues CM. Endoplasmic reticulum enrollment in Alzheimer's disease. *Mol Neurobiol.* 2012 Oct;46(2):522-34.
453. Hetz C, Bernasconi P, Fisher J, Lee AH, Bassik MC, Antonsson B, et al. Proapoptotic BAX and BAK modulate the unfolded protein response by a direct interaction with IRE1alpha. *Science.* 2006 Apr 28;312(5773):572-6.
454. Hitomi J, Katayama T, Taniguchi M, Honda A, Imaizumi K, Tohyama M. Apoptosis induced by endoplasmic reticulum stress depends on activation of caspase-3 via caspase-12. *Neurosci Lett.* 2004 Mar 4;357(2):127-30.
455. Mehmet H. Caspases find a new place to hide. *Nature.* 2000 Jan 6;403(6765):29-30.
456. Steele AD, Hetz C, Yi CH, Jackson WS, Borkowski AW, Yuan J, et al. Prion pathogenesis is independent of caspase-12. *Prion.* 2007 Oct-Dec;1(4):243-7.
457. Lee W, Kim DH, Boo JH, Kim YH, Park IS, Mook-Jung I. ER stress-induced caspase-12 activation is inhibited by PKC in neuronal cells. *Apoptosis.* 2005 Mar;10(2):407-15.
458. Denning MF, Wang Y, Tibudan S, Alkan S, Nickoloff BJ, Qin JZ. Caspase activation and disruption of mitochondrial membrane potential during UV radiation-induced apoptosis of human keratinocytes requires activation of protein kinase C. *Cell Death Differ.* 2002 Jan;9(1):40-52.
459. Pocchiari M, Schmittinger S, Masullo C. Amphotericin B delays the incubation period of scrapie in intracerebrally inoculated hamsters. *J Gen Virol.* 1987 Jan;68 ( Pt 1):219-23.
460. Geschwind MD, Kuo AL, Wong KS, Haman A, Devereux G, Raudabaugh BJ, et al. Quinacrine treatment trial for sporadic Creutzfeldt-Jakob disease. *Neurology.* 2013 Dec 3;81(23):2015-23.
461. Harper E. Collagenases. *Annu Rev Biochem.* 1980;49:1063-78.
462. Anand P, Kunnumakkara AB, Newman RA, Aggarwal BB. Bioavailability of curcumin: problems and promises. *Mol Pharm.* 2007 Nov-Dec;4(6):807-18.
463. Indovina P, Collini M, Chirico G, Santini MT. Three-dimensional cell organization leads to almost immediate HRE activity as demonstrated by molecular imaging of MG-63 spheroids using two-photon excitation microscopy. *FEBS Lett.* 2007 Feb 20;581(4):719-26.
464. le Roux L, Volgin A, Maxwell D, Ishihara K, Gelovani J, Schellingerhout D. Optimizing imaging of three-dimensional multicellular tumor spheroids with fluorescent reporter proteins using confocal microscopy. *Mol Imaging.* 2008 Sep-Oct;7(5):214-21.
465. Sheppard CRJT, P. Effects of specimen refractive index on confocal imaging. *J Microsc.* 1997;185(3):366-74.
466. Gandhi NS, Mancera RL. Heparin/heparan sulphate-based drugs. *Drug Discov Today.* 2010 Dec;15(23-24):1058-69.
467. Demaimay R, Adjou K, Lasmezas C, Lazarini F, Cherifi K, Seman M, et al. Pharmacological studies of a new derivative of amphotericin B, MS-8209, in mouse and hamster scrapie. *J Gen Virol.* 1994 Sep;75 ( Pt 9):2499-503.
468. Morshedi D, Rezaei-Ghaleh N, Ebrahim-Habibi A, Ahmadian S, Nemat-Gorgani M. Inhibition of amyloid fibrillation of lysozyme by indole derivatives--possible mechanism of action. *FEBS J.* 2007 Dec;274(24):6415-25.
469. Cohen T, Frydman-Marom A, Rechter M, Gazit E. Inhibition of amyloid fibril formation and cytotoxicity by hydroxyindole derivatives. *Biochemistry.* 2006 Apr 18;45(15):4727-35.
470. Bendheim PE, Poeggeler B, Neria E, Ziv V, Pappolla MA, Chain DG. Development of indole-3-propionic acid (OXIGON) for Alzheimer's disease. *J Mol Neurosci.* 2002 Aug-Oct;19(1-2):213-7.

471. Torok M, Abid M, Mhadgut SC, Torok B. Organofluorine inhibitors of amyloid fibrillogenesis. *Biochemistry*. 2006 Apr 25;45(16):5377-83.
472. Goold R, McKinnon C, Tabrizi SJ. Prion degradation pathways: Potential for therapeutic intervention. *Mol Cell Neurosci*. 2015 Jan 10.
473. Luhr KM, Nordstrom EK, Low P, Ljunggren HG, Taraboulos A, Kristensson K. Scrapie protein degradation by cysteine proteases in CD11c+ dendritic cells and GT1-1 neuronal cells. *J Virol*. 2004 May;78(9):4776-82.
474. Scotter EL, Vance C, Nishimura AL, Lee YB, Chen HJ, Urwin H, et al. Differential roles of the ubiquitin proteasome system and autophagy in the clearance of soluble and aggregated TDP-43 species. *J Cell Sci*. 2014 Mar 15;127(Pt 6):1263-78.
475. Kang SC, Brown DR, Whiteman M, Li R, Pan T, Perry G, et al. Prion protein is ubiquitinated after developing protease resistance in the brains of scrapie-infected mice. *J Pathol*. 2004 May;203(1):603-8.
476. Kovacs GG, Preusser M, Strohschneider M, Budka H. Subcellular localization of disease-associated prion protein in the human brain. *Am J Pathol*. 2005 Jan;166(1):287-94.
477. Chung E, Prelli F, Dealler S, Lee WS, Chang YT, Wisniewski T. Styryl-based and tricyclic compounds as potential anti-prion agents. *PLoS One*. 2011;6(9):e24844.
478. Meyer zu Horste G, Mausberg AK, Korth C, Stuve O, Kieseier BC. Quinpramine--a promising compound for treating immune-mediated demyelination of the nervous system. *Drug News Perspect*. 2010 Jun;23(5):287-94.
479. Zhou X, Bi H, Wong J, Shimoji M, Wang Y, Yuan J, et al. Alkylating antitumor drug mechlorethamine conceals a structured PrP domain and inhibits in vitro prion amplification. *J Toxicol Environ Health A*. 2011;74(22-24):1493-503.
480. Karapetyan YE, Sferrazza GF, Zhou M, Ottenberg G, Spicer T, Chase P, et al. Unique drug screening approach for prion diseases identifies tacrolimus and astemizole as anti-prion agents. *Proc Natl Acad Sci U S A*. 2013 Apr 23;110(17):7044-9.
481. Mukherjee A, Morales-Scheihing D, Gonzalez-Romero D, Green K, Tagliatalata G, Soto C. Calcineurin inhibition at the clinical phase of prion disease reduces neurodegeneration, improves behavioral alterations and increases animal survival. *PLoS Pathog*. 2010;6(10):e1001138.
482. Wagner J, Ryazanov S, Leonov A, Levin J, Shi S, Schmidt F, et al. Anle138b: a novel oligomer modulator for disease-modifying therapy of neurodegenerative diseases such as prion and Parkinson's disease. *Acta Neuropathol*. 2013 Jun;125(6):795-813.
483. Imberdis T, Ayrolles-Torro A, Verdier JM, Perrier V. Thienyl pyrimidine derivatives with PrP(Sc) oligomer-inducing activity are a promising tool to study prions. *Curr Top Med Chem*. 2013;13(19):2477-83.
484. Relano-Gines A, Lehmann S, Bencsik A, Herva ME, Torres JM, Crozet CA. Stem cell therapy extends incubation and survival time in prion-infected mice in a time window-dependant manner. *J Infect Dis*. 2011 Oct 1;204(7):1038-45.
485. Muyrers J, Klingenstein R, Stitz L, Korth C. Structure-activity relationship of tocopherol derivatives suggesting a novel non-antioxidant mechanism in anti-prion potency. *Neurosci Lett*. 2010 Jan 18;469(1):122-6.
486. Drisko JA. The use of antioxidants in transmissible spongiform encephalopathies: a case report. *J Am Coll Nutr*. 2002 Feb;21(1):22-5.
487. Dirikoc S, Priola SA, Marella M, Zsurger N, Chabry J. Nonpsychoactive cannabidiol prevents prion accumulation and protects neurons against prion toxicity. *J Neurosci*. 2007 Sep 5;27(36):9537-44.
488. Otto M, Cepek L, Ratzka P, Doehlinger S, Boekhoff I, Wiltfang J, et al. Efficacy of flupirtine on cognitive function in patients with CJD: A double-blind study. *Neurology*. 2004 Mar 9;62(5):714-8.
489. Berry DB, Lu D, Geva M, Watts JC, Bhardwaj S, Oehler A, et al. Drug resistance confounding prion therapeutics. *Proc Natl Acad Sci U S A*. 2013 Oct 29;110(44):E4160-9.

490. Ghaemmaghami S, Russo M, Renslo AR. Successes and challenges in phenotype-based lead discovery for prion diseases. *J Med Chem*. 2014 Aug 28;57(16):6919-29.
491. Lu D, Giles K, Li Z, Rao S, Dolgih E, Gever JR, et al. Biaryl amides and hydrazones as therapeutics for prion disease in transgenic mice. *J Pharmacol Exp Ther*. 2013 Nov;347(2):325-38.
492. Leidel F, Eiden M, Geissen M, Hirschberger T, Tavan P, Giese A, et al. Piperazine derivatives inhibit PrP/PrP(res) propagation in vitro and in vivo. *Biochem Biophys Res Commun*. 2014 Feb 28;445(1):23-9.
493. Leidel F, Eiden M, Geissen M, Kretzschmar HA, Giese A, Hirschberger T, et al. Diphenylpyrazole-derived compounds increase survival time of mice after prion infection. *Antimicrob Agents Chemother*. 2011 Oct;55(10):4774-81.
494. Nguyen P, Oumata N, Soubigou F, Evrard J, Desban N, Lemoine P, et al. Evaluation of the antiprion activity of 6-aminophenanthridines and related heterocycles. *Eur J Med Chem*. 2014 Jul 23;82:363-71.
495. Ali S, van Mil HG, Richardson MK. Large-scale assessment of the zebrafish embryo as a possible predictive model in toxicity testing. *PLoS One*. 2011;6(6):e21076.
496. Zon LI, Peterson RT. In vivo drug discovery in the zebrafish. *Nat Rev Drug Discov*. 2005 Jan;4(1):35-44.
497. Malaga-Trillo E, Salta E, Figueras A, Panagiotidis C, Sklaviadis T. Fish models in prion biology: underwater issues. *Biochim Biophys Acta*. 2011 Mar;1812(3):402-14.
498. Halliez S, Passet B, Martin-Lannere S, Hernandez-Rapp J, Laude H, Mouillet-Richard S, et al. To develop with or without the prion protein. *Front Cell Dev Biol*. 2014;2:58.
499. Cotto E, Andre M, Forgue J, Fleury HJ, Babin PJ. Molecular characterization, phylogenetic relationships, and developmental expression patterns of prion genes in zebrafish (*Danio rerio*). *FEBS J*. 2005 Jan;272(2):500-13.
500. Gibbs CJ, Jr., Gajdusek DC, Asher DM, Alpers MP, Beck E, Daniel PM, et al. Creutzfeldt-Jakob disease (spongiform encephalopathy): transmission to the chimpanzee. *Science*. 1968 Jul 26;161(3839):388-9.
501. Wadsworth JD, Asante EA, Collinge J. Review: contribution of transgenic models to understanding human prion disease. *Neuropathol Appl Neurobiol*. 2010 Dec;36(7):576-97.
502. Watts JC, Prusiner SB. Mouse models for studying the formation and propagation of prions. *J Biol Chem*. 2014 Jul 18;289(29):19841-9.
503. Aguzzi A, Brandner S, Marino S, Steinbach JP. Transgenic and knockout mice in the study of neurodegenerative diseases. *J Mol Med (Berl)*. 1996 Mar;74(3):111-26.
504. Jankowsky JL, Savonenko A, Schilling G, Wang J, Xu G, Borchelt DR. Transgenic mouse models of neurodegenerative disease: opportunities for therapeutic development. *Curr Neurol Neurosci Rep*. 2002 Sep;2(5):457-64.
505. Watts JC, Giles K, Patel S, Oehler A, DeArmond SJ, Prusiner SB. Evidence that bank vole PrP is a universal acceptor for prions. *PLoS Pathog*. 2014 Apr;10(4):e1003990.